

Department of Applied Geology

**High-resolution Sequence Stratigraphy of the Arab-D Reservoir, Khurais Field,
Saudi Arabia**

Saad Fahd Al-Awwad

**This thesis is presented for the Degree of
Doctor of Philosophy
of
Curtin University**

August 2013

Declaration

To the best of my knowledge and belief this thesis contains no material previously published by any other person except where due acknowledgment has been made.

This thesis contains no material which has been accepted for the award of any other degree or diploma in any university.

Saad Fahd Al-Awwad

Signature:

Date:

Copyright Statement

This thesis was supported by Saudi Aramco and Curtin University of Technology. As the author of this thesis I bear responsibility for the scientific content and findings presented herein. As such, all copyrights of this thesis are reserved by the author, Saad Fahd Al-Awwad. Reproduction or retransmission of this thesis, in whole or in part, in any manner, without the prior written consent of the copyright holder is a violation of copyright law.

© Copyright by Saad Fahd Al-Awwad, 2013

All Rights Reserved

Saad Fahd Al-Awwad

Signature:

Date:

Professor Lindsay B. Collins (Supervisor)

Signature:

Date:

List of Publications

This dissertation presents a collection of papers that were composed in the course of this research project. These papers are either in press or in review. The way the different papers interplay and contribute to achieving the research goals is explained in the introduction. The research results are summarised in the conclusion.

The following papers are presented in this thesis:

Al-Awwad, S. & Collins, L. B. (2013a). Arabian carbonate reservoirs: A depositional model of the Arab-D reservoir in Khurais Field, Saudi Arabia. *AAPG Bulletin*, 97(7), 1099–1119.

Al-Awwad, S. & Collins, L. B. (in-review). Stacked high-frequency carbonate reservoir sequences in the Arab-D, Khurais Field, Saudi Arabia. *Marine and Petroleum Geology*.

Al-Awwad, S. & Collins, L. B. (2013b). Carbonate platform scale correlation of stacked high frequency sequences in the Arab-D Reservoir, Saudi Arabia. *Sedimentary Geology*, 294, 205–2018.

Sections such as methodology and geologic background in the above papers share commonalities, as each paper has been presented as a stand-alone publication.

The following conference presentation was delivered in the course of this research project:

Alawwad, S. F. & Collins L. B. A giant within a giant: depositional model of the Arab-D reservoir in Khurais Field, Saudi Arabia [abstract]. In 34th International Geologic Congress; 5-10 August 2012; Brisbane, Australia. Australian Geoscience Council, Canberra, Australia. p 154. Abstract nr 2041.

Permissions

I warrant that I have obtained, where necessary, permission from the copyright owners to use any third-party copyright material reproduced in the thesis (e.g. questionnaires, artwork, unpublished letters), or to use any of my own published work (e.g. journal articles) in which the copyright is held by another party (e.g. publisher, co-author).

Saad Fahd Al-Awwad

Signature:

Date:

Dedication



القصص (24)

'Then he [Moses] turned back to shade, and said: "My Lord! truly, I am in need of whatever good that You bestow on me!"'
The Holy Quran, Chapter 28, Verse 24.

الى من ضحت كثيرا حتى ترى هذه الرسالة النور.. الى من أعطت كثيرا ولم تأخذ حتى القليل
الى من أدين لها بكل شئٍ حققته أو أنجزته أو نلتته في حياتي.. إلى الهواء الذي أتوق أن أملاً به رأيتي.. إلى النبض
الذي يُنشِده قلبي كل يوم فيدفع الدم في ثنايا عروقي.. إلى سحابة الودق العذب الزلال التي لا تفتن أن تروي صحراء
ظمني.. إلى سيدتي ومولاتي التي ملكت علي قلبي.. إلى التاج فوق رأسي، لا بل المرجان فوق التاج، لا بل الجواهر
والمرجان والتاج والرأس...
الى أمي الغالية
السيدة خولة المشاري

To the one person who sacrificed the most for me. To the one person who knows all too well how to give, but never understood how to take. To the one person to whom I owe every accomplishment, achievement or gain in my entire life. To the air in my lungs, to the blood in my veins, to the pulse of my heart, to the absolute crown jewel ornamenting my head; to my mother, Mrs. Khawlah Al-Mishary.

Acknowledgements

Professor Lindsay B. Collins' much-needed availability, insightful guidance, boundless patience and tireless commitment are nothing short of awe-inspiring, and I shall be forever in his debt.

My deepest gratitude goes to the sponsorship of Saudi Aramco and their endorsement of my research project. I would especially like to thank Dr. Aus Al-Tawil, Reservoir Characterisation Manager; Mr. Hussain Al-Otaibi, Exploration Technical Services Manager; Mr. Ahmed Al-Otaibi, Geological Technical Services Chief Geologist; and Mrs. Najwa Eszaimie from the Exploration Planning and Support Division. Their commitment, efforts, support and investment in my project were extraordinary to say the least.

In particular, words of gratitude, no matter how big, will remain dwarfed by the dedication, zeal and patronage of Dr. Aus Al-Tawil. In short, this study would have not been accomplished had it not been for his visionary leadership and continuous support.

The comments and critiques that I was lucky enough to receive from Professor Luis Pomar, University de les Illes Balears, Spain, have significantly enriched the findings of the study. It was a remarkable opportunity to interact with a person with such an impressive command of carbonate geology.

Robert Lindsay, Saudi Aramco, Saudi Arabia; Langhorne Smith, New York State Museum, USA; and Wyn Hughes, Saudi Aramco, Saudi Arabia shared many essential insights, for which I am profoundly thankful.

I am also thankful, in the truest sense of the word, to my dear friend and colleague Najim Al-Qahtani for his substantial efforts in the review and approval process that preceded the publication of this study.

I am grateful to my colleagues Abdullah Al-Moejel, Aiman Bakhorji and Emad Busbait for their sincere and heartfelt help, advocacy and support throughout the course of this study.

Lastly, I would like to thank the coffee man at Curtin University's cafeteria for his magnificent lattes; they were the elixir that kept me awake through many long, sleepless nights.

Contents

Declaration	ii
Copyright Statement	iii
List of Publications	iv
Permissions	v
Dedication	vi
Acknowledgements	vii
Contents	ix
List of Figures	xiv
List of Tables	xviii
List of Enclosures	xix
List of Abbreviations	xx
Abstract	xxi
Introduction	1
Geologic Controversy	2
Objectives	5
Dissertation Structure	6
Materials and Methods	6
Facilities and Resources.....	9
Chapter 1: Literature Review—Economic Importance and Exploration History	10
1.1 Economic Importance.....	10
1.2 Exploration History	11
1.2.1 Saudi Arabia: The Second Attempt.....	13
1.2.2 The Discovery	15
1.2.3 Discovering Ghawar Field.....	16
1.2.4 Evolution of Saudi Aramco	18
Chapter 2: Literature Review—Evolution of the Arabian Platform’s Jurassic System	19
2.1 Tectonic Setting.....	19
2.1.1 The Paleo-Tethys Ocean	19

2.1.2 The Neo-Tethys Ocean.....	20
2.1.3 The Pan-African Orogeny	24
2.2 Eustasy	29
2.2.1 Focusing on the Jurassic Period.....	33
2.3 Jurassic Climate	36
2.3.1 Late Jurassic Climate	39
2.4 Evolution of Depositional Environments	45
2.4.1 Overview of the Jurassic Depositional Systems	46
2.4.2 Early Jurassic Environments	47
2.4.3 Middle Jurassic Environments.....	48
2.4.4 Late Jurassic Environments	56
2.5 Facies Depositional Models	60
2.6 Sequence-stratigraphic Hierarchy	70
2.6.1 Early and Middle Jurassic of Saudi Arabia	74
2.6.1.1. <i>Minjur Sandstone</i>	74
2.6.1.2. <i>Marrat Formation</i>	74
2.6.1.3. <i>Dhurma Formation</i>	74
2.6.1.4. <i>Tuwaiq Mountain Limestone</i>	75
2.6.2 Late Jurassic.....	75
2.6.2.1. <i>The Early Oxfordian Pre-Hanifa Sequence Boundary</i>	75
2.6.2.2. <i>Hanifa Formation</i>	76
2.6.2.3. <i>Jubaila Formation</i>	77
2.6.2.4. <i>Arab Formation</i>	77
2.6.2.5. <i>Arab-A Member and Hith Formation</i>	79
2.6.3 Sequence Hierarchy of the Arab-D Reservoir	80
2.7 Implications: Regional and Local Correlations of the Reservoir	82
Chapter 3: Arabian Carbonate Reservoirs: A Depositional Model of the Arab-D Reservoir in	
Khurais Field, Saudi Arabia	90
3.1 Abstract.....	90
3.2 Introduction and History.....	91
3.3 Regional Setting.....	93
3.4 Lithofacies	97

3.4.1 Anhydrite Lithofacies	97
3.4.2 Cryptomicrobial Lithofacies	98
3.4.3 Oolitic Lithofacies	98
3.4.4 Peloidal Lithofacies	100
3.4.5 <i>Cladocoropsis</i> Lithofacies	100
3.4.6 Dasycladacean algae Lithofacies	102
3.4.7 Stromatoporoid Lithofacies	102
3.4.8 Pelletal Lithofacies	103
3.4.9 Intraclastic Lithofacies	103
3.4.10 Lime Mud Lithofacies	107
3.4.11 Dolomite Lithofacies	109
3.5 Depositional Model	109
3.5.1 Intraclastic and Lime Mud Lithofacies	112
3.5.2 Pelletal Lithofacies	114
3.5.3 Stromatoporoid Lithofacies	114
3.5.4 Dasycladacean algae Lithofacies	117
3.5.5 <i>Cladocoropsis</i> Lithofacies	117
3.5.6 Peloidal Lithofacies	118
3.5.7 Oolitic Lithofacies	118
3.5.8 Cryptomicrobial Lithofacies	119
3.5.9 Anhydrite Lithofacies	119
3.6 Accommodation and Physical versus Ecological Process	119
3.7 Conclusions	120
3.8 Acknowledgments	121
3.9 References	122
Chapter 4: Stacked High Frequency Carbonate Reservoir Sequences in the Arab-D	
Reservoir, Khurais Field, Saudi Arabia	128
4.1 Abstract.....	128
4.2 Introduction	129
4.3 Terminology	132
4.4 Geologic and Stratigraphic Setting.....	134
4.5 Focusing on the Kimmeridgian of Saudi Arabia	141

4.5.1 Jubaila Formation	142
4.5.2 Arab Formation.....	143
4.6 Arab-D Reservoir Cyclic Hierarchy.....	145
4.6.1 Small-Scale Cycles	145
4.6.1.1. Basin Cycles.....	145
4.6.1.2. Reef Cycles	147
4.6.1.3. Lagoon Cycles	148
4.6.1.4. Sand-sheets Cycles	149
4.6.1.5. Peritidal Cycles.....	151
4.6.2 Cycle and Parasequence Sets, and High-Frequency Sequences	151
4.6.2.1. Basinal Cycle Sets and High Frequency Sequences	153
4.6.2.2. Shelfal Cycle Sets and High Frequency Sequences.....	153
4.6.3 Composite Sequences.....	155
4.7 Discussion and Implications	159
4.8 Conclusions	161
4.9 Acknowledgements	163
4.10 References.....	164
Chapter 5: Carbonate-Platform Scale Correlation of Stacked High-Frequency Sequences in the Arab-D Reservoir, Saudi Arabia	175
5.1 Abstract.....	175
5.2 Introduction	176
5.3 Regional and Structural Settings	179
5.4 Methodology	182
5.5 Regional Correlation	183
5.5.1 Shelfal Lithofacies Correlated from West to East	186
5.5.2 Basinal Lithofacies Correlated from West to East.....	187
5.5.3 North to South Correlation	189
5.6 Discussion.....	189
5.7 The Timelines Dilemma	196
5.8 Reservoir Quality	199
5.9 Conclusions	201
5.10 Acknowledgments	201

5.11 References.....	202
Conclusions.....	208
Bibliography	213
Appendices	254
Appendix A: Supervisor and Co-author Statement.....	255
Appendix B: AAPG Bulletin Permission to Reprint “Arabian Carbonate Reservoirs: A Depositional Model of the Arab-D Reservoir in Khurais Field, Saudi Arabia”	257
Appendix C: Arabian Carbonate Reservoirs: A Depositional Model of the Arab-D Reservoir in Khurais Field, Saudi Arabia	259
Appendix D: Sedimentary Geology Permission to Reprint “Carbonate-platform scale correlation of stacked high-frequency sequences in the Arab-D reservoir, Saudi Arabia”	281
Appendix E: Carbonate-platform scale correlation of stacked high-frequency sequences in the Arab-D reservoir, Saudi Arabia	283
Appendix F: Sample of semi-quantitative petrography data from Arab-D reservoir, Khurais Field.....	298
Appendix G: Representative Photomicrographs of the Arab-D reservoir lithofacies from Khurais Field	304
Appendix H: Representative Core Photographs of the Arab-D reservoir lithofacies from Khurais Field	307
Appendix I: Foldout of Enclosure 3.1	309
Appendix J: Foldouts of Enclosures 5.1 and 5.2	310

List of Figures

Figure 1: A typical coarsening-upward cycle from the upper part of the reservoir....	4
Figure 12: A typical fining-upward cycle from the lower part of the reservoir.	4
Figure 3: Embry and Klovan's (1971) modification of Dunham's (1962) classification.	8
Figure 14: Charts of visual percentage estimation.	9
Figure 1.1: At the Khurais Field production facilities, a worker covers his face to protect it from the sand.	11
Figure 1.2: Major Frank Holmes.	12
Figure 1.3: From left, Dick Bramkamp, Dick Kerr, Max Steineke and Fred Davies in Jubail in the early 1940s.	13
Figure 1.4: Harry St. John Bridger Philby.	14
Figure 1.5: L. N. Hamilton and Abdullah al-Sulaiman signing the concession, 29 May 1933.	14
Figure 1.6: Max Steineke.	15
Figure 1.7: The tanker D. G. Scofield offshore Ras Tanura, 1 May 1939.	16
Figure 1.8: The size of Ghawar Field compared to the state of Louisiana, USA	17
Figure 2.1: Early Permian Paleo-Tethys Ocean before the rifting of the Cimmerian plate.	19
Figure 2.2: Permian-Triassic-boundary northward drift of the Cimmerian plate, which closed the Paleo-Tethys Ocean and opened the Neo-Tethys Ocean.	20
Figure 2.3: Paleotectonic map of Arabia and North Africa in the Callovian.	22
Figure 2.4: Profile of the evolution of the Arabian plate from the Carboniferous onwards.	23
Figure 2.5: Pan-African Orogeny belts across a reconstruction of Gondwana at the end of the Neoproterozoic (<i>ca.</i> 540 Myr).	24
Figure 2.6: Evolution of the Arabian-Nubian Shield.	25
Figure 2.7: The different terranes that compose the Arabian Shield.	27
Figure 2.8: Jurassic cycle chart of the Arabian platform juxtaposed next to the global cycle chart.	31
Figure 2.9: Schematic chronostratigraphic column of the Jurassic.	32
Figure 2.10: Palaeogeographic reconstruction of the earth in the Kimmeridgian/Tithonian.	

.....	34
Figure 2.11: Humid and arid continental belts in the Early Jurassic and Late Jurassic.	37
Figure 2.12: Late Jurassic distribution of coals, evaporates and eolian deposits.	40
Figure 2.13: Modelled annual precipitation minus evaporation during the Kimmeridgian-Tithonian.	42
Figure 2.14: Climatic belt distribution during the Late Jurassic.	42
Figure 2.15: Late Jurassic modelled surface air temperature (°C).	43
Figure 2.16: Simulated Kimmeridgian-Tithonian cyclone season	44
Figure 2.17: Jurassic reservoirs of Saudi Arabia.	47
Figure 2.18: Structural map of the Arabian plate.	49
Figure 2.19: Triassic-to-Jurassic-Transition Palaeofacies.	50
Figure 2.20: Early Jurassic Palaeofacies.	51
Figure 2.21: Middle Jurassic Palaeofacies.	52
Figure 2.22: Environments of deposition from late Oxfordian to early Kimmeridgian.	53
Figure 2.23: Jurassic oil and gas generation zones with respect to the location of major fields in the Arabian Gulf area.	55
Figure 2.24: Jurassic distribution of source rocks, reservoirs and seal in the Arabian Gulf countries.	55
Figure 2.25: Late Jurassic Palaeofacies.	57
Figure 2.26: Suggested location of a grain shoal on the Rimthan Arch and suggested southward progradation from there into the Arabian basin.	58
Figure 2.27: Schematic depositional model of the Arab-D reservoir, interpreting it as a ramp complex with a stromatoporoid patch reef.	65
Figure 2.28: Schematic depositional model of the Arab-D reservoir interpreting a grainy shoal at Rimthan Arch flanked by ramps to the north and south.	67
Figure 2.29: Depositional model of the Arab-D reservoir interpreting it as a ramp with a grain shoal (red) and a stromatoporoid biostromes (green).	68
Figure 2.30: Schematic distribution of biocomponents from the Middle to Late Jurassic of Saudi Arabia.	69
Figure 2.31: Jurassic-Cretaceous schematic chronostratigraphic chart.	71
Figure 2.32: Late Triassic-Jurassic chronostratigraphy of Saudi Arabia with the GTS 2004 and AROS dates.	72

Figure 2.33: Lithostratigraphic column from the Upper Triassic to Early Cretaceous in central Saudi Arabia.	73
Figure 2.34: Schematic E–W section designating position of the Callovian and Oxfordian source rocks.	82
Figure 2.35: Murriss’s (1980) E–W cross-section of the Middle-Upper Jurassic in the Arabian Gulf region.....	83
Figure 2.36: Suggested northward and southward progradation of the Arab-D reservoir.	83
Figure 2.37: Environments of deposition and sequence-stratigraphic architecture of the Arab-D reservoir from Dukhan Field, Qatar.....	84
Figure 2.38: Cross-section of the Arab and Hith formation correlated from Yemen to Saudi Arabia and Kuwait, datumed atop the Hith Formation.....	86
Figure 2.39: W–E cross-section correlating the Arab and Hith formations in central Abu Dhabi, datumed atop the Hith Formation	87
Figure 2.40: Depositional model of the Arab Formation in Qatar.....	88
Figure 2.41: An E–W cross-section across Ghawar Field, Saudi Arabia of the upper part of the Arab-D reservoir.	89
Figure 3.1: Saudi Arabia’s Jurassic reservoir stratigraphy and lithology	91
Figure 3.2: Location map of Khurais Field.	95
Figure 3.3 (next page): Characterisation of Arab-D reservoir core from well Aramco KHKH Khurais, Khurais Field.....	95
Figure 3.4: Anhydrite, cryptomicrobial and oolitic lithofacies.	99
Figure 3.5: Peloidal, <i>Cladocoropsis</i> and dasycladacean algae lithofacies.	101
Figure 3.6: Stromatoporoid, pelletal and dolomite lithofacies.	104
Figure 3.7: Intraclastic and lime mud lithofacies.....	105
Figure 3.8: The thicknesses of 110 described intraclastic beds plotted against their occurrence depth in the lower part of the Arab-D reservoir core, Aramco HKHK Khurais	107
Figure 3.9: Aramco HKHK Khurais—typical type-CCC turbidite.	108
Figure 3.10: Schematic depositional model.	110
Figure 4.1: Location map of Khurais Field.	130
Figure 4.2: Saudi Arabia’s Jurassic succession.....	131
Figure 4.3: Characterisation of the Arab-D reservoir core, Aramco KHKH Khurais.	133

Figure 4.4: Sequence stratigraphic hierarchy.....	134
Figure 4.5 (previous page): A schematic depositional model of a prograding frequently storm-abraded, gently sloping, shallow, arid, stromatoporoid-reef-rimmed shelf	136
Figure 4.6: Offshore to offshore-transition basin cycles.....	146
Figure 4.7: A reef parasequence that coarsens upward from the pelletal lithofacies to the stromatoporoid lithofacies.	147
Figure 4.8: Upper shoreface lagoon parasequence.....	149
Figure 4.9: Foreshore sand-sheet parasequence.	150
Figure 4.10: Backshore supratidal parasequence.....	152
Figure 4.11: A plot of intraclastic bed thickness in the lower part of the reservoir shown against the core description and gamma log.....	154
Figure 4.12 (previous page): An idealised Arab-D reservoir cored section and the interpreted sequence-stratigraphic framework.	158
Figure 5.1: Jurassic succession of Saudi Arabia.	177
Figure 5.2: Location map of Khurais Field and schematic structural model.	181
Figure 5.3 (previous page): An idealised Arab-D reservoir core with the interpreted sequence-stratigraphic framework and a schematic depositional model.	186
Figure 5.4: A west–east cross-section of the Arab-D reservoir correlating its outcrop south of Riyadh to its subsurface in Ghawar Field.....	188
Figure 5.5: A north-south cross-section of the Arab-D reservoir correlating it in the subsurface from the Safaniya area to south Khurais Field.	190
Figure 5.6: A fence diagram showing the intersection of Figures 5.4 and 5.5 at Khurais HKHK.	192
Figure 5.7: Hypothesised timelines superimposed on dip section presented in Figure 5.4.	198
Figure 5.8: Stratigraphic thickness model.	200
Figure 5: A typical coarsening-upward cycle from the upper part of the reservoir.	211
Figure 6: Typical fining-upward cycles from the lower part of the reservoir.	212

List of Tables

Table 2.1: Major tectonic events that controlled sedimentation on the Arabian platform throughout the Phanerozoic.	30
Table 2.2: Suggested Arab-D reservoir progradation directions.	59
Table 2.3: Characteristics of the Arab-D reservoir lithofacies.	62
Table 2.4: Characteristics and environmental interpretation of the Arab-D reservoir lithofacies.	63
Table 4.1: Summary of Arab-D lithofacies and their deduced environmental setting.	138

List of Enclosures

Enclosure 3.1: Characterisation of Arab-D reservoir core, Aramco KHKH Khurais, Khurais Field.....	309
Enclosure 5.1: A west–east cross-section of the Arab-D reservoir correlating its outcrop south of Riyadh to its subsurface in Ghawar Field.	310
Enclosure 5.2: A north-south cross-section of the Arab-D reservoir correlating it in the subsurface from the Safaniya area to south Khurais Field.	310

List of Abbreviations

AROS	Arabian Orbital Stratigraphy
Bapco	Bahrain Petroleum Company
c	coral
Casoc	California Arabian Standard Oil Company
F	floatstone
FWWB	fair weather wave base
G	grainstone
GTS	geological time scale
HCS	hummocky cross stratification
HFS	high-frequency sequences
HST	highstand systems tract
Kyr	thousand years
LST	lowstand systems tract
M	mudstone
m	mudclast
MFS	maximum flooding surfaces
Myr	million years
o	oncolid
P	packstone
R	rudstone
s	stromatoporoid
Socal	Standard Oil of California
SWB	storm wave base
TMS	tectonostratigraphic megasequences
TST	transgressive systems tract
Type-CCC turbidites	turbidites with climbing ripples, convolutions and rip-up clasts
W	wackestone

Abstract

The Late Jurassic Arab Formation contains four of the world's best oil reservoirs stacked in shallowing-upward cycles of carbonates capped by nonpermeable anhydrites. The subject of analysis in this study is the most prolific of these reservoirs, the Arab-D reservoir in Khurais Field, which is one of the world's largest oil fields. The study conducted high-resolution lithofacies analysis (10 cm-scaled) of the Arab-D reservoir from 32 cored wells in Khurais Field to construct a high-resolution depositional cyclicity model that deciphers the architectural distribution of the reservoir's lithofacies and allows the mapping of the reservoir's porosity-permeability distribution.

The reservoir has been classified into 11 lithofacies, which are, from deepest to shallowest: 1) hardground-capped skeletal wackestone and lime mudstone; 2) intraclast floatstone and rudstone; 3) pelletal wackestone and packstone; 4) stromatoporoid wackestone, packstone and floatstone; 5) *Cladocoropsis* wackestone, packstone and floatstone; 6) *Clypeina* and *Thaumatoporella* wackestone and packstone; 7) peloidal packstone and grainstone; 8) ooid grainstone; 9) cryptomicrobial laminites; 10) evaporites; and 11) stratigraphically reoccurring dolomite. These lithofacies are interpreted to have been deposited in an array of shallowing-upward depositional environments, which from deepest to shallowest are: offshore submarine turbidity fans (lithofacies 1 and 2); lower shoreface settings (lithofacies 3); stromatoporoid reef (lithofacies 4); lagoon (lithofacies 5 and 6); shallow subtidal settings (lithofacies 7 and 8); peritidal settings (lithofacies 9); and sabkhas and salinas (lithofacies 10). These facies and environments are interpreted to reflect a prograding, shallow-marine, reef-rimmed, arid carbonate shelf with turbidites generated by frequent storm action.

The reservoir's lithofacies preserve an upper part of a third-order composite sequence overlain by another, almost complete, third-order composite sequence. These composite sequences are segmented into six high-frequency, fourth-order sequences, with 12 parasequence and cycle sets; superimposed over which are many fifth-order parasequences and parasequence-scale cycles.

The study also presents a correlation model that suggests a regional progradation and clinoforming eastward from the shallow Late Jurassic epeiric shelf and downlapping into the relatively deep Arabian intrashelf basin. This model explains the drastic thickening and downward descent of the reservoir's lithofacies that is observed between its outcrops and its subsurface successions. The model predicts a regional eastward porosity improvement in the upper part of the reservoir, accompanied by a porosity reduction in the lower part.

Introduction

The Jurassic Period is probably most famous as being a time when dinosaurs roamed the Earth's continents. Movies, television programmes and news coverage of dinosaur excavations all contributed to arousing public interest in dinosaurs, and to some extent in the Jurassic. While the Jurassic rocks of the Arabian Peninsula have not yielded many dinosaur fossils, these rocks are of utmost economic significance to the peninsula's people, who inhabit one of the world's most prolific petroleum regions. This remarkable petroleum system was constructed by the interplay of a multitude of geological factors before, during and after the Jurassic period, which will be thoroughly discussed in this thesis.

Regional palaeogeographic reconstructions have concluded that the Jurassic Arabian platform was a broad, shallow stable shelf, circa 1,000 km wide, which was located between 10–15° south latitude and encompassed a few intrashelf basins. The platform was bounded by passive continental margins and the Neo-Tethys to the east, northeast and southeast, and by a complex of Precambrian igneous and metamorphic rocks, the Arabian Shield, to the west (Al-Husseini, 1997; Alsharhan & Kendall, 1986; Alsharhan & Magara, 1994; Alsharhan, Whittle, Clerke & Buiting, 1995; Ayres et al., 1982; Grabowski & Norton, 1995; Le Nindre, Manivit & Vaslet, 1987; Mitchell, Lehmann, Cantrell, Al-Jallal & Al-Thagafy, 1988; Murriss, 1980; J. Wilson, 1975). Carbonate deposition dominated the Arabian platform in the Jurassic Period; and in Saudi Arabia, the Jurassic carbonates contain 13 reservoir intervals that have been chronostratigraphically assigned by macrofossils' correlation with their outcrop-equivalents west of the Saudi capital Riyadh (Powers, 1962; Powers, Ramirez, Redmond & Elberg, 1966; Steineke & Bramkamp, 1952). Of these reservoirs, those of the Arab Formation are the most economically significant, and they are composed of four anhydrite-capped carbonate cycles that reflect the high-frequency cyclicity of late Kimmeridgian sea-level (Handford, Cantrell & Keith, 2002). The carbonates of these cycles host remarkable reservoir-quality units: the

Arab-D, -C, and -B reservoirs are each capped by a nonpermeable anhydrite layer, and the uppermost carbonate unit, the Arab-A reservoir, is capped by the thick Hith Formation anhydrites. The Arab-D reservoir is the most prolific in the Arab Formation and has been discovered in many fields in the Arabian Gulf region, including Ghawar Field, the largest oil field on the planet.

Large compressional anticlines, which were formed during the Precambrian accretion of the Arabian plate, constituted frames that shaped huge structural traps (100's km by 10's km in scale) containing oil, such as the Ghawar and Khurais Fields in Saudi Arabia. The oil is sourced from the organic-rich, anoxic shales that were deposited in the relatively deep intrashelf basins (Ayres et al., 1982; Droste, 1990; M. A. Ziegler, 2001). The carbonates are sealed by overlying anhydrites; the thick, uppermost Hith Anhydrite forms the ultimate seal of the Arab reservoirs.

Geologic Controversy

Long standing, unpublished, in-house exploration and reservoir-characterisation studies have been conducted by various workers in Saudi Aramco on the Arab-D reservoir. Relevant results from these studies can only be discussed in general terms in this open-format thesis. Specific environmental information deduced from these studies has led to the division of the reservoir's lime mudstones and wackestones into upper and lower units based on their biotic components. The upper mudstones and wackestones have been interpreted to represent a shallow lagoonal environment, while the lower ones represent a deep basinal environment. One weakness of this interpretation, however, is that it does not explain the lack of expected slope and lack of clinofolding trends (a typical pattern of a sedimentologic/stratigraphic prograding system), which characterised the reservoir's regional correlation studies, which were compiled in a north-south direction on Ghawar and other fields in the area. In other words, if the platform appears to be flat, based on the 'layer-cake' correlation studies, then that contradicts the presence of basinal and lagoonal mudstones at different bathymetries at the same time. Another approach has conceived the flatness

reflected in the reservoir correlation studies as evidence that the system aggraded, which would separate the upper and lower mudstones and wackestone temporally. Consequently, differences between the faunas of mudstones and wackestones are interpreted to reflect different oxygenation levels. In other words, the Arabian platform is interpreted to have acted as a 'dinner plate' during the Late Jurassic; the bottom of the plate formed a silled, isolated and oxygen-deprived platform, while the top of the plate was more open to marine circulation and oxygenated. While this view seems to explain the 'layer-cake' correlation studies, it contradicts the presence of the following biotic components that characterise Arab-D's lower mudstones and wackestones and indicate deep marine setting rather than differential oxygenation: ammonites (*Perisphinctes*), nautiloids (*Paracenoceras*), coccoliths, ichnofossils *Zoophycos* and *Rhizocorallium* (G. W. Hughes, personal communication, 3 August 2011).

This rather academic-sounding controversy bears profoundly on the reservoir modelling and development, as it dictates the philosophy of interpreting reservoir cyclicity (Figures 1 and 2), which in turn impacts the reservoir's correlation criteria. For example, the former interpretation dictates a progradational scenario in which the characteristic coarsening-upward cycles of the upper part of the reservoir are interpreted as shallowing-upward cycles capped by 'grainier' lithofacies (Figure 1a). Conversely, the latter interpretation dictates an aggradational scenario, where a rise in the sea-level is expected to cause an increase in energy in the silled platform and thus deposit 'grainier' lithofacies, while a fall in sea-level would cause a decrease in energy within the silled platform and thus deposit muddier lithofacies (Figure 1b). For the fining-upward cycles that characterize the lower part of the reservoir, the former interpretation sees them, again, as shallowing-upward cycles, attributing the 'grainier' lithofacies to sea-level falls and the muddier lithofacies to sea-level rises (Figure 2a). The latter interpretation however, explains the 'grainier' lithofacies to be deposited during sea-level rises, which cause energy increase in the silled platform; and explains the muddier lithofacies as being deposited during sea-level falls, which cause energy decrease within the silled platform (Figure 2b).

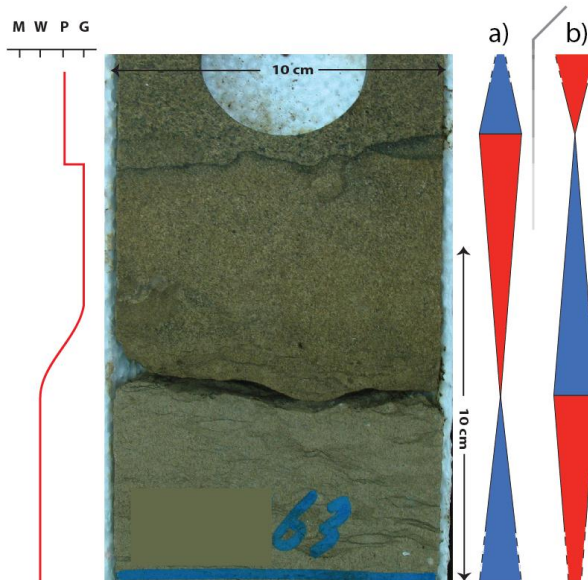


Figure 1: A typical coarsening-upward cycle from the upper part of the reservoir.

a) The cyclicity interpretation adopted by a hypothesized progradational scenario in an open shelf. b) The cyclicity interpretation adopted by a hypothesized aggradational scenario in a silled platform.

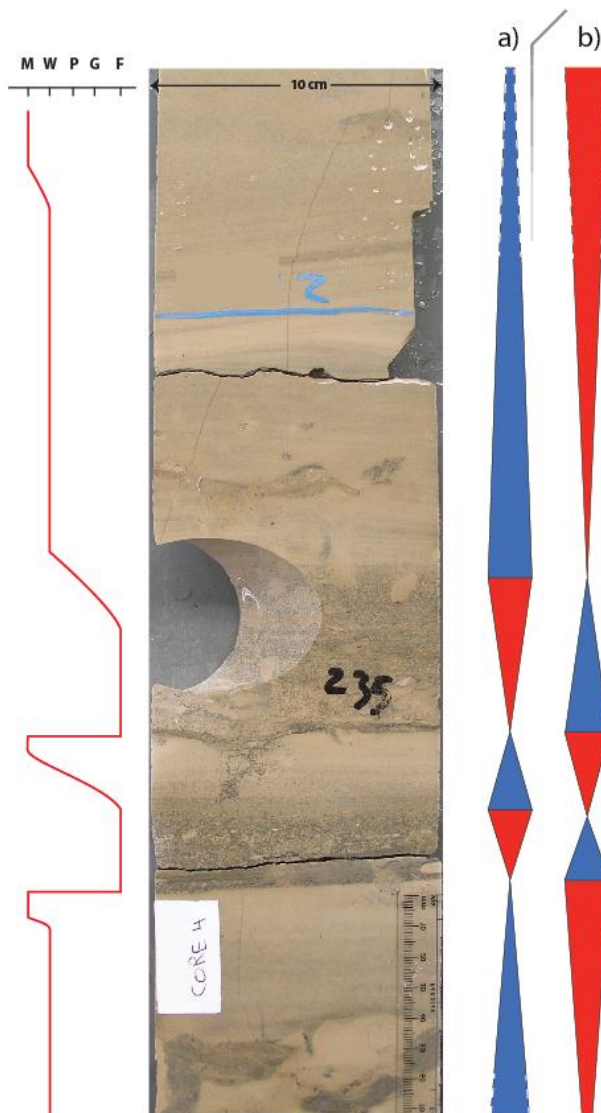


Figure 12: A typical fining-upward cycle from the lower part of the reservoir.

a) The cyclicity interpretation adopted by a hypothesized progradational scenario in an open shelf. b) The cyclicity interpretation adopted by a hypothesized aggradational scenario in a silled platform.

This thesis addresses the above controversy in a twofold approach. First, it characterises reservoir facies in meticulous detail, which allows accurate deduction of depositional environments and sheds insight on the hierarchical arrangements of these environments into vertical Waltherian successions. Second, the thesis puts these environmental and sequence-stratigraphic interpretations to the test by examining reservoir facies and cycle correlation across broad regions of the depositional basin and in orthogonal lines of section to envisage the regional strike and dip directions of the reservoir.

Objectives

A grasp of the geologic factors, their relative significance, and how they interplayed to control the palaeoenvironments of the Arabian platform is essential for the mapping of the prolific porosity-permeability systems that characterise the Jurassic carbonates of Saudi Arabia. Detecting subtle lithofacies variations and deciphering what they disclose in terms of changes introduced to the depositional environments could potentially provide a proxy for relative sea-level fluctuations, which would assist in constructing reservoir architectural models. This criterion has been implemented in this study of the Kimmeridgian Arab-D reservoir, which is comprised of the carbonates of the Arab-D Member of the Arab Formation and the upper part of the Jubaila Formation. The study aims to unfold the distribution of reservoir facies into a high-resolution depositional cyclicity model that can predict lateral and vertical heterogeneities and architectural arrangements of reservoir facies in Khurais Field, Saudi Arabia, one of the world's largest oil fields. This would be instrumental for the management and production of the field by guiding prediction of future 3-D spatial distribution of porosity, permeability, diagenetic, structural and other petrophysical parameters within the reservoir and how they dictate the architecture of fluid flow and baffle units.

Dissertation Structure

This dissertation is structured in two parts. The first part comprises a literature review that summaries the broad picture of the development of the Arabian oil system under the umbrella of the Jurassic Period. It begins with the economic significance of the reservoir and the history of oil discovery in the region, discussed in chapter 1. Then chapter 2 reviews the evolution of the Arabian platform's Jurassic system in terms of tectonic setting, eustasy, climate setting, depositional environments, depositional and sequence-stratigraphic hierarchy models of the reservoir, and the regional and local correlations of the reservoir. The second part of the dissertation comprises the original work accomplished in this thesis. First, chapter 3 details an architectural depositional model of the reservoir, which has been presented at the International Geologic Conference in Brisbane, Australia, 2012; and published in the *American Association of Petroleum Geologists Bulletin*, Volume 97, no. 7, July 2013, Pages 1099–1119. Chapter 4 lays out the distribution of the reservoir lithofacies into high-resolution sequences, sequence sets, high-frequency sequences and composite sequences; this was submitted as a paper to *Marine and Petroleum Geology* on 11 July 2013 and is currently in review. Last, chapter 5 presents an application of the proposed depositional and sequence-stratigraphic models by correlating the reservoir regionally in two sections, north-south and east-west; this was published in *Sedimentary Geology*, Volume 294, 15 August 2013, Pages 205–218.

Materials and Methods

This study conducted a detailed (10-cm-scale) sedimentological characterisation of the Arab-D reservoir from 32 cored Khurais wells, and 500 thin-sections covering more than 1,900 m of subsurface section.

The data base for the study is lodged in the Saudi Aramco's Core Handling and Well Samples Laboratory in Dhahran, Saudi Arabia. Core description and thin section work was mentored by Dr. Aus Al-Tawil, Saudi Aramco, Dhahran, Saudi Arabia, and

Dr. Langhorne Smith, New York State Museum, New York, USA. Confidentiality requirements restrict the disclosure of well locations, well names (coded well names are used) and the studied field outline both in this thesis and in publications.

Cores were restored, depth-marked, plugged and slabbed by Saudi Aramco's Core Handling and Well Samples Laboratory staff. The author etched the cores with 10% hydrochloric acid for 10 seconds before examining them under a stereo microscope and photographing them. Core characterization was logged on Saudi Aramco's standard core logging sheet (Enclosure 3.1) and utilised Embry and Klovan's (1971) modification of Dunham's (1962) classification of depositional textures (Figure 3). Mineral composition was estimated using comparison charts for visual percentage estimation (Figure 4, Terry and Chilingar, 1955). Other parameters that were logged include sedimentary structures, unconformities, and bed boundaries; porosity amount and type percentage (Choquette & Pray, 1970; Lucia, 1995); fractures, faults, stylolites; and hydrocarbon shows. Besides this, the logging recorded abiotic constituents; fossils (logged as common (20-30%), designated by grey rectangles, or dominant (> 30%), designated by black rectangles, Enclosure 3.1); grain and crystal sizes (also logged also as common or dominant); and layering hierarchy in terms of beds, cycles, parasequences, parasequence sets, and high frequency sequences.

Thin sections were prepared by Saudi Aramco's Core Handling and Well Samples Laboratory staff. Cores were sampled every 1 ft (3.28 m)—or 6 inches (0.5 m) in some wells— and samples were vacuum impregnated with blue-dyed epoxy for porosity recognition. Samples were then cut into 30 μm thick slices and epoxied to standard 26 mm x 46 mm glass slides without cover slips. The author half-stained the thin sections for 30 to 60 seconds in alizarin red-S for calcite versus dolomite recognition (Dickson, 1966). After that, the sections were gently rinsed with distilled water and stacked vertically to drain before examining them under a petrographic microscope and photomicrographing them. 200 thin-sections were used in conjunction with the core characterization. Semi-quantitative petrography was conducted on another 300 thin-sections using comparison charts for visual percentage estimation (Figure 4, Terry and Chilingar, 1955). The following

parameters were recorded into spread sheets and plotted against thin-sections' depths: abundance of different fossil types (using Hughes, 2004 b; 2009), abundance of different abiotic constituents, mineral types, abundance of different porosity types relative to total visible porosity, and amounts of different types of cements. Only a sample of the data collected from the semi-quantitative petrography characterization is included in appendices F, G and H, as it is the author's intention to publish these results in a separate paper.

Other approaches adopted in this thesis include measuring the intraclastic beds' thickness present in the lower part of the reservoir, cumulating the thicknesses into bins of < 0.5 ft, 0.5 to < 1 ft, 1 to < 2 ft, 2 to < 3 ft, 3 to < 5 ft and \geq 5 ft, and plotting the bin values against the beds' occurrence depths to visualize the thickness variance with depth as detailed in section 3.4.9.

In addition, noticing lithofacies components, repetitive motifs of lithofacies stacking patterns, retrogradational, aggradational and progradational modulations,

Allochthonous limestone original components not organically bound during deposition					Autochthonous limestone original components organically bound during deposition				
Less than 10% >2 mm components				Greater than 10% >2 mm components		Boundstone			
Contains lime mud (<0.02 mm)			No lime mud		Matrix supported	>2 mm component supported	By organisms which act as barriers	By organisms which encrust and bind	By organisms which build a rigid framework
Mud supported		Grain supported							
Less than 10% grains (>0.02 mm to <2 mm)	Greater than 10% grains								
Mudstone	Wackestone	Packstone	Grainstone	Floatstone	Rudstone	Bafflestone	Bindstone	Framestone	

Figure3: Embry and Klovan's (1971) modification of Dunham's (1962) classification.

Source: Embry and Klovan (1971).

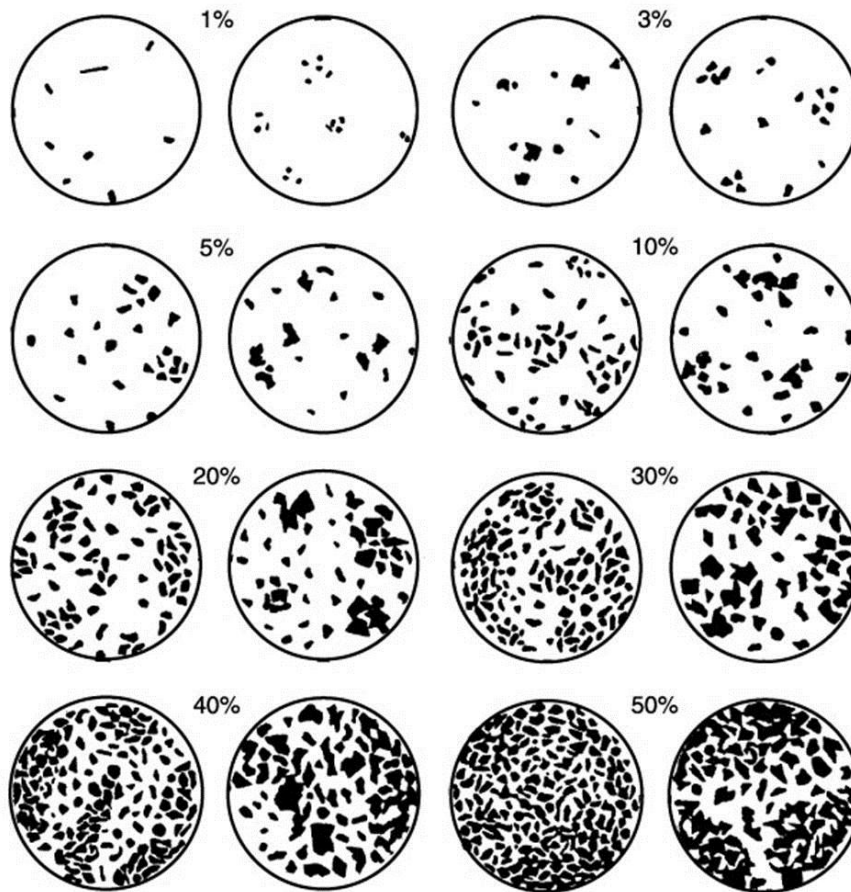


Figure 14: Charts of visual percentage estimation. Source: Terry and Chilingar, (1955).

vertical thickening versus thinning trends, upward fining versus coarsening and/or shallowing versus deepening trends was used in one-dimensional sequence stratigraphic analysis that was conducted on the 32 cored wells. This was integrated with the analysis and core-to-log matching of 40 wireline logs, and utilised in correlating the reservoir's lithofacies on local (across Khurais Field) and regional (across the eastern part of Saudi Arabia) scales.

Facilities and Resources

This research has been funded by Saudi Aramco. Most of the data collection was completed in Saudi Aramco's Core Handling and Well Samples Laboratory in Dhahran, Saudi Arabia. The data analysis and composition of this dissertation were conducted under the supervision of Professor Lindsay B. Collins in the Western Australian School of Mines, Department of Applied Geology, Curtin University, Australia.

Chapter 1: Literature Review—Economic Importance and Exploration History

1.1 Economic Importance

Saudi Arabia's stature as an unrivalled leader in the world's oil market came by its tremendous production and exportation capabilities in addition to its possession of a quarter of the world's known oil reserves (Our company, 2013). Oil was discovered in Saudi Arabia in the Upper Jurassic Arab Formation, the world's most prolific oil-bearing interval, in 1938 (Barger, 1984; Sorkhabi, 2008; Stegner, 2007). It took a few more years of continued exploration and discovery to grasp the sheer magnitude of the world's largest known oil field, Ghawar, discovered in 1948 (Barger, 2000; Bates, 1973; Durham, 2005; Keith, 2005). Sixty years after its discovery, Ghawar, the super-giant that stretches for 174 miles and occupies an area of 1.3 million acres, remains the most prolific oil field on the planet (Durham, 2005; Fischbuch & Soremi, 2008).

The Late Jurassic clean grainstones of the Arab-D limestone form the major oil-producing reservoir in Ghawar (Durham, 2005). The excellent porosities and permeabilities of the Arab-D are sandwiched between organic-rich mudstones of the Jurassic Hanifa and Tuwaiq Mountain formations below and the tight anhydrites of the Arab and Hith Formations above (Durham, 2005). The remarkable lateral extent of the Jurassic source-reservoir-seal sandwich, over and across Ghawar, is what makes this system unequalled (Sorkhabi, 2010). The Arabian Jurassic oils are harvested into expansive structural traps, such as the anticlines of the Ghawar and Khurais fields, which are proficient in draining extensive areas of source rock (Alsharhan, 1993; Sorkhabi, 2011). These structures are also characterised by gentle dips, which make them less susceptible to fracturing and render the capping anhydrites even more effective (Alsharhan, 1993; Alsharhan, & Kendall, 1986).

The Arab-D oil was discovered in Saudi Arabia's second largest onshore oil field, Khurais Field in 1957 (Al-Mulhim, Al-Ajmi, Al-Shehab & Pham, 2010). Further delineation drilling proved that the Qirdi Field, discovered south of Khurais in 1973, is also part of the huge Khurais oil accumulation (Al-Mulhim, et al., 2010). In 2009, Saudi Aramco's investment of US\$60 billion over five years culminated with the successful completion of the largest-ever oil expansion project, known as the Khurais Mega Project (Al-Ghamdi, Tello, Al-Bain & Swadi, 2008; Al-Mulhim et al., 2010). For this project, the Kingdom of Saudi Arabia utilised a task force of 28,000 employees and relocated and rebuilt a village of 25,000 people to make room for the gigantic production and processing facilities required to make the field's tremendous resources available to energise the world (Al-Ghamdi et al., 2008; Al-Mulhim et al., 2010). The project orchestrated the drilling of 168 horizontal wells, each totalling 12,000 ft (3,658 m) of measured depth, producing 1.2 million barrels a day from Khurais and adjacent satellite fields (Al-Ghamdi et al., 2008; Al-Mulhim et al., 2010; Mouawad, 2010). This means that Khurais yields roughly 1.5 per cent of the global daily demand of oil, mainly from the 100-m-thick Arab-D reservoir.

1.2 Exploration History

For mile after mile, there is nothing but flat and unrelenting sand on every side, with a few black camels wandering in the desert glare. Then, suddenly, it rises into view, like some vast industrial mirage. The Khurais oil field's processing plant resembles nothing so much as an oversize Erector Set... gleaming in the sun. (Worth, 2008)



It all began in 1922, with a man pointing to his nose and saying confidently, 'This is my geologist!' (Sorkhabi, 2008). The man with the 'geologist nose' was the British-New

Figure 1.1: At the Khurais Field production facilities, a worker covers his face to protect it from the sand.

Source: Worth (2008)

Zealander, Major Frank Holmes, who worked in gold mining as a mining engineer and joined the British navy in World War I (Sorkhabi, 2008, 2010).

Holmes, who was later given the Arabic epithet 'Abu Naft' or 'father of oil', was convinced that the Middle East sat on untold oil fortunes, and he was determined



Figure 1.2: Major Frank Holmes.
Source: 'Prelude to discovery' (2007)

to harvest it, hence the proud claiming of a nose with geologist-like capabilities (Sorkhabi, 2008).

The first oil well in the Middle East was drilled on 25 May 1908 by a British millionaire, William Knox D'Arcy, who struck oil at the Persian natural oil seepage area of Masjid-i-suliman ('A Red Line', 2007). This was followed by the discovery of the first Iraqi oil field, Kirkuk, in 1927 (Sorkhabi, 2008).

Negotiation between Holmes and King Abdul Aziz Ibn Saud of Saudi Arabia started in 1922.

With the recommendations of Ameen Rihani, an American-Lebanese writer, intellectual and friend of the king, a concession for exploration was awarded to Holmes' company, Eastern and General Syndicate, for a rental payment of £2,500 a year, in 1923 (Sorkhabi, 2008). After exploration began, the company hired a Swiss geologist, Arnold Albert Heim, who submitted a report in 1926 discouraging the drilling in Saudi Arabia; subsequently Holmes halted his exploration activities in 1927 (Sorkhabi, 2008).

In 1925, Sheikh Hamad al-Khalifa awarded concession rights in Bahrain to Holmes in return for several artesian water wells that Holmes had drilled there (Sorkhabi, 2008). After facing financial troubles, Holmes equipped himself with an attractive geological report and Bahraini oil-dripping rocks and embarked on a trip to find an investor (Sorkhabi, 2008). Gulf Oil Corporation purchased Holmes' concession rights in 1927 based on the recommendations of their geologist, Ralph Rhoades (Sorkhabi,

2008). Fifteen years earlier, in 1912, a coalition of British-Dutch groups, including German and French investors, formed the Turkish Petroleum Company, which later became the Iraq Petroleum Company, to control the Iraqi oil wealth ('A Red Line', 2007). The coalition drew an almost arbitrary red line on the region's map defining the borders of the Ottoman Empire and agreed to only seek exploration concessions within these borders through the Iraq Petroleum Company ('A Red Line', 2007). The 'red line' included Turkey, Iraq and Saudi Arabia, but excluded Iran and Kuwait. Due to its commitments to the Iraq Petroleum Company, Gulf Oil was forced to sell its Bahrain concession for US \$50,000 to Standard Oil of California (Socal) in 1929, which established the Bahrain Petroleum Company (Bapco) (Sorkhabi, 2008). Socal, which later became Chevron, together with other companies, had emerged earlier from an anti-trust ruling by the United States Supreme Court in 1911 that led to the dissolution of John D. Rockefeller's Standard Oil conglomerate into 33 smaller companies ('A Red Line', 2007).

1.2.1 Saudi Arabia: The Second Attempt

Saudi Arabia was destined for a return of the oil companies when Fred A. Davies, a Socal geologist, came up with the visionary idea of finding the reservoir rocks producing in Bahrain 32 km across the gulf in Saudi Arabia; and he convinced his superiors back in San Francisco of the merits of his idea (Sorkhabi, 2008).



Figure 1.3: From left, Dick Bramkamp, Dick Kerr, Max Steineke and Fred Davies in Jubail in the early 1940s.
Source: Shirley (2008)

Harry St. John Bridger Philby, an Arabist, explorer, writer, and British colonial officer

who had converted to Islam and was given the name Shaikh Abdullah by King Abdul Aziz of Saudi Arabia, persuaded the King to exploit the country's hidden oil wealth.



Figure 1.4: Harry St. John Bridger Philby.
Source: 'Prelude to Discovery' (2007)

Upon Philby's recommendation, the American plumbing tycoon Charles Crane was invited by King Abudl Aziz to Jeddah ('A Red Line', 2007). Crane was overwhelmed with the king's graciousness and gift of swords, horses and carpets, and decided to return the favour by dispatching his mining engineer, Karl Twitchell, to look for artesian water in Saudi Arabia ('A Red Line', 2007). Twitchill arrived in 1931, and after some time, he concluded in his report that although there was no water, the geology of Al-Hasa in eastern Saudi Arabia resembled that of Bahrain ('A Red Line', 2007). If Socal had

found oil in Bahrain, then the possibilities of finding it in abundance in Al-Hasa were intriguing, Twitchell's report concluded ('A Red Line', 2007).

After his findings, Twitchill went to the United States and returned with Socal's lawyer, Lloyd Hamilton ('A Red Line', 2007). A concession agreement was signed on 29 May 1933 by Hamilton and Saudi Finance Minister Abdullah al-Sulaiman al-

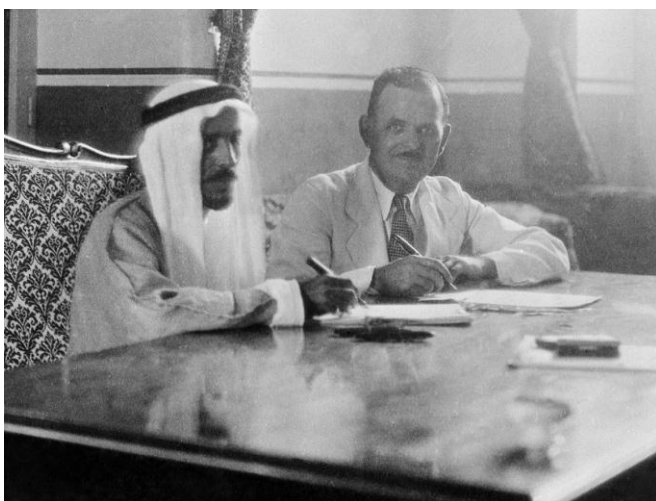


Figure 1.5: L. N. Hamilton and Abdullah al-Sulaiman signing the concession, 29 May 1933.
Source: 'Saudi Aramco: 80 Years' (2013)

Hamdan, who was advised by the king: 'Put your trust in God and sign' (Sorkhabi, 2008). In 1933, Socal founded the California Arabian Standard Oil Company (Casoc) as its subsidiary to operate the concession in Saudi Arabia

('Saudi Aramco', 2008; Sorkhabi, 2008).

1.2.2 The Discovery

In the fall of 1934, Max Steineke, a Social geologist, crossed the Persian Gulf from Bahrain on an Al Gosaibi Brothers dhow, arriving at Jubail to join the pioneer geologists in Saudi Arabia ('Max Steineke', 1952). The geologists identified an anticline structure, Jabal Dhahran, which became known later as the Dammam Field, but not much success was encountered by the 10 wells drilled there (Lindsay et al., 2006; Sorkhabi, 2008). In fact, Dammam Dome's first wildcat was spudded on 30 April 1935, but it had encountered only minor hydrocarbon shows by the time it penetrated the section that was producing in Bahrain (Lindsay et al., 2006; 'Saudi Aramco', 2008; Sorkhabi, 2008). After this geologic disappointment, Steineke embarked on a field trip roaming the Arabian Peninsula from Jiddah to the Dhana desert, observing and recording strikes and dips in 1937 (Barger, 1984; 'Max Steineke', 1952). To Steineke, finding oil in Arabia was a matter of when rather than if; yet his optimism was not matched by the Board of Social, who disputed whether to continue (Barger, 1984). Steineke insisted, 'Dig a bit deeper'. A decision was made to deepen Dammam Well Number 7 to see if hydrocarbons resided below the producing strata in Bahrain (Barger, 1984; Sorkhabi, 2008). It turned out that a mere 200 feet of rock stood in the way between the long-awaited 'Saudi black gold' and the surface. On 4 March 1938, the well produced 1,585 barrels, which rose to 3,690 barrels three days later; it was completed at 1441 m deep in the Upper Jurassic Arab zone, yielding 34–35° API gravity oil with 1.5 per cent sulphur content (Barger,



Figure 1.6: Max Steineke.
Source: Norton (1988)

1984; 'A Red Line', 2007; 'Saudi Aramco', 2008; Sorkhabi, 2008). Forty-five years after its spud, Dammam Well Number 7 was shut in 1982, having produced 32 million barrels of oil and averaging about 2,000 barrels of oil per day ('Saudi Aramco', 2008; Sorkhabi, 2008).



On 1 May 1939, the first crude oil ever to be exported from Saudi Arabia was loaded aboard tanker D. G. Scofield., which was named after Demetrius G. Scofield, the first president of Socal ('Giant of the Sea', 1962; 'Oil Pioneer', 1917; 'Saudi Aramco', 2008).

Figure 1.7: The tanker D. G. Scofield offshore Ras Tanura, 1 May 1939.

Source: 'Saudi Aramco: 80 years' (2013)

1.2.3 Discovering Ghawar Field

A major problem that faced the pioneers was that differential solution of the lower Eocene Rus evaporites caused false surficial structures. These structures were drilled in Ma'agala and El Alat and found to be dry (Durham, 2005; Lindsay et al., 2006). Therefore, a grid of shallow, 300 m deep structural-stratigraphic wells, situated to penetrate the top of the Cretaceous section, was established by Max Steineke. The aim of that grid was to map the subsurface stratigraphy and collect pre-Neogene information that would help in distinguishing true from false structures. As a result of the shallow drilling program, Abqaiq Field was discovered in 1940 and produced oil from the porous carbonates of the Arab Formation (Durham, 2005; Lindsay et al., 2006; Sorkhabi, 2008, 2011).

While mapping Miocene and Pliocene rocks, Max Steineke and Tom Kock detected the presence of the En Nala (an Arabic word for 'slipper') anticline, which hosted



Figure 1.8: The size of Ghawar Field compared to the state of Louisiana, USA

Source: Durham (2005)

Ghawar Field in 1935 ('Ghawar Oil Field', 1959; Sorkhabi, 2008, 2011). In 1940, Ernie Berg noted during field mapping that an east–west trending wadi, Wadi Sahaba, suddenly changed course to trend to the south near Abqaiq Field and interpreted that to be a result of a north-south trending

subsurface anticline; Steineke agreed (Lindsay et al., 2006; Sorkhabi, 2008, 2011). Further to the south, a large, broad, low-relief dome was revealed by dip measurements taken by Ernie Berg and was called the 'Haradh feature' (Durham, 2005; Lindsay et al., 2006). This low-relief dome formed the southern tip of the large En Nala anticline (Lindsay et al., 2006).

In 1941, Steinke's shallow drilling programme, together with gravity and magnetic surveys, had confirmed the existence of the En Nala anticline, a 280-km long and 30-km wide whaleback anticline with six humps: Fazran, Ain Dar, Shedgum, Uthmaniyah, Hawiyah and Haradh, from north to south ('Ghawar Oil Field', 1959; Fischbuch & Soremi, 2008; Sorkhabi, 2008, 2011).

In 1948, Ain Dar 1 produced from the D member of the Arab Formation and the Jubaila Formation and brought to attention the possibility of oil entrapment throughout the En Nala anticline. In 1949, a second wildcat was drilled 200 km to the south of Ain Dar-1 at Haradh Number 1; and when it struck oil, the possibility of these fields being connected was significantly substantiated (Fischbuch & Soremi, 2008; Lindsay et al., 2006). By 1953, the name Ghawar was applied to denote the

largest field of the world (Sorkhabi, 2008, 2011).

1.2.4 Evolution of Saudi Aramco

In 1936, Texaco bought 50 per cent interest in Casoc's concession ('Saudi Aramco', 2008; Sorkhabi, 2008). In 1944, the company's name changed to Arabian American Oil Company (Aramco) ('Saudi Aramco', 2008; Sorkhabi, 2008). In 1948, Standard Oil of New Jersey and Socony-Vacuum (both now Exxon Mobil) bought interests in Aramco, and the company headquarters moved from San Francisco to New York and later, in 1952, to Dhahran, Saudi Arabia ('Saudi Aramco', 2008; Sorkhabi, 2008). In 1959, Hafidh Wahba, the Saudi ambassador to Britain, and Abdullah Al-Turaiqi, the first Saudi Oil Minister, were elected to be the first Saudis on Aramco's Board of Directors ('Saudi Aramco', 2008). In 1980, the Saudi government completed the phased purchase of Aramco's assets, which began with 25 per cent in 1973 and increased to 60 per cent in 1974 ('Saudi Aramco', 2008). In 1983 Ali I. Naimi, the then Saudi Oil Minister, was elected as the first Saudi President of the company, and in 1988 the Saudi Arabian Oil Company (Saudi Aramco) was established ('Saudi Aramco', 2008; Sorkhabi, 2008).

Chapter 2: Literature Review—Evolution of the Arabian Platform’s Jurassic System

This chapter discusses the most relevant conclusions from the literature on the Jurassic Period in terms of tectonic and climatic settings, eustatic fluctuations and evolution of depositional environments, stratigraphy and correlation, focusing whenever possible on the southern Tethyan realm, the Arabian plate and the Late Jurassic system of Saudi Arabia.

2.1 Tectonic Setting

2.1.1 The Paleo-Tethys Ocean

Pangea’s formation as a supercontinent resulted from the collision of Gondwana and Laurussia in the Late Devonian to Permian Hercynian Orogeny, which yielded a



Figure 2.1: Early Permian Paleo-Tethys Ocean before the rifting of the Cimmerian plate.

Source: Dezes (1999)

2006; Von Raumer & Stampfli, 2001).

huge mountain range that spread across a number of today’s continents. An embayment was also configured by the supercontinent’s formation and it was occupied by the Paleo-Tethys’s ocean basin, which opened from Late Ordovician to Early Devonian (Figure 2.1) (Golonka, 2004; Leveridge & Hartley,

To the north of the Paleo-Tethys was Laurussia, composed of today's northern Europe, North America, Siberia and Baltica, and to the south was Gondwana, composed of Arabia, Africa, Lut and Iranian terranes (Figure 2.1) (Golonka, 2004; Sengor & Natal'in, 1996). Most of Pangea was south of the equator during the Pennsylvanian to the late Permian (Parrish, 1985; Scotese & Golonka, 1992).

2.1.2 The Neo-Tethys Ocean

Focusing on the southern Tethyan realm (Frizon de Lamotte et al., 2011), the northern margin of the Paleo-Tethys hosted north-dipping subduction in the Late Devonian, which largely drove the plates' movement in the realm while the Gondwanan margin experienced multiple phases of rifting from Carboniferous to Triassic (Golonka, 2004; Stampfli, Marcoux & Baud, 1991). Due to the pull of the Paleo-Tethys subduction, the Cimmerian microplate, which was composed of parts of today's Turkey, Iran, Afghanistan, Tibet, Indochina and Malaya, rifted from the



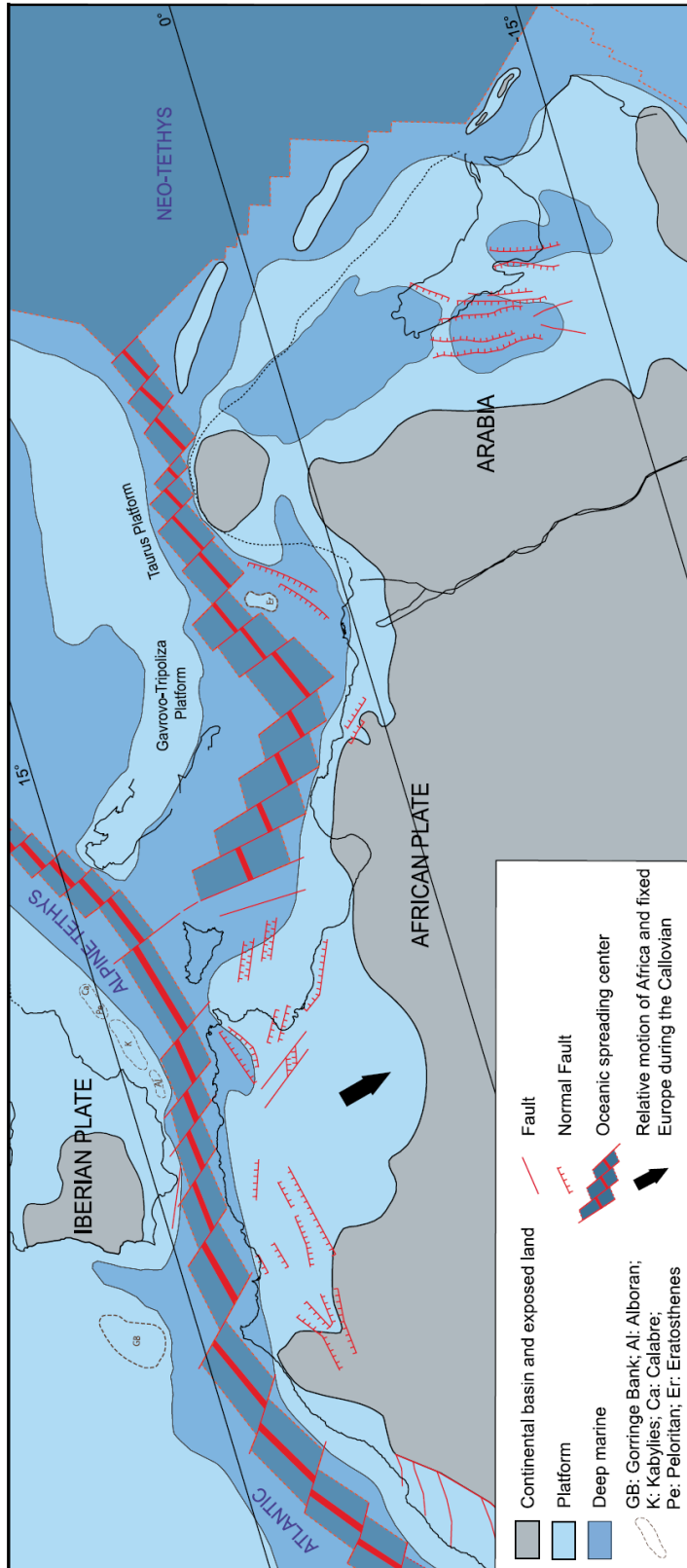
Figure 2.2: Permian-Triassic-boundary northward drift of the Cimmerian plate, which closed the Paleo-Tethys Ocean and opened the Neo-Tethys Ocean.

Source: Dezes (1999)

continental shelf of the Gondwanan branch of Pangea and moved northward in the Permian (Figure 2.2) (Dercourt, Cotiereau & Vrielynck, 1993; Golonka, 2004; Golonka & Bocharova, 2000; Golonka, Ross & Scotese, 1994; Sengor & Natal'in, 1996). Progressive drifting of the Cimmerian continent yielded opening of the Neo-Tethys at the expense of the Paleo-Tethys, whose oceanic

crust was consumed in the subduction zone (Figure 2.2) (Frizon de Lamotte et al., 2011; Golonka, 2004). This eventually led to a diachronous west-to-east closure of the Paleo-Tethys, which finished in the Middle-Late Triassic, creating in the process the Cimmerian Orogeny (Golonka, 2004; Stampfli, Mosar et al., 2001). Thus, the Neo-Tethys, which formed from Pennsylvanian to early Permian, separated Arabia and the Cimmerian microplate. A new north dipping subduction zone formed south of the sutured Cimmerian microplate, leading to slab-pull and rifting of new terranes from the passive margin of Gondwana in the Early Jurassic (Favre & Stampfli, 1992; Frizon de Lamotte et al., 2011; Golonka, 2002; Sengor, 1979; Stampfli & Borel, 2004; Stampfli, Mosar et al., 2001; Stocklin, 1974). Pangea became almost symmetrical about the equator in the Triassic and Early Jurassic (Parrish, 1985; Scotese & Golonka, 1992). The Neo-Tethys branched to the southwest, yielding the East Mediterranean in the Late Triassic–Early Jurassic, which later connected with the Alpine Tethys that rifted open in Europe in the Jurassic (Stampfli & Borel, 2002) east of Sicily in the Late Jurassic (Figure 2.3) (Frizon de Lamotte et al., 2011). Epeiric seas formed and expanded due to Jurassic sea-level rise (Parrish, 1992). The Alpine Tethys connected with the Middle Atlantic ridge as Eurasia separated from Gondwana during the Pangean breakup (Golonka, 2004).

In the Late Cretaceous, opening of the South Atlantic ocean and the northward drifting and anticlockwise rotation of Africa-Arabia led to closure of the Neo-Tethys's west side (Figure 2.4). This was manifested by structural growth of east Arabia's giant anticlines as discussed in section 2.1.3 below. The Neo-Tethys's east was narrowed by India's northward drift and convergence with Eurasia, which led to the opening of the Indian Ocean in the Cretaceous (Frizon de Lamotte et al., 2011; Golonka, Ross & Scotese, 1994). Remnants of the Neo-Tethys, which have not been subducted or obducted, still exist today and are represented by the East Mediterranean basin and Gulf of Oman, while the Alpine Tethys is completely sutured (Frizon de Lamotte et al., 2011; Stampfli & Borel, 2004; Stampfli et al., 1991; Stampfli, Borel et al., 2001). Finally, the African-Eurasian convergence marked the transition of the eastern Arabian margin from passive to foredeep settings from the Late Cretaceous onward, characterised by flysch-like deposits that pinch out



from Iran to the Arabian platform (Dercourt et al., 1993; Guiraud & Bellion, 1996; Homke et al., 2009; Robertson, Searle & Ries, 1990; Sengor & Natal'in, 1996). This evolution of the Neo-Tethys largely controlled the Phanerozoic succession of the Arabian plate. The Proterozoic basement of the plate, however, was controlled by the Pan-African Orogeny.

Figure 2.3: Paleotectonic map of Arabia and North Africa in the Callovian.
 Source: Frizon de Lamotte et al. (2011)

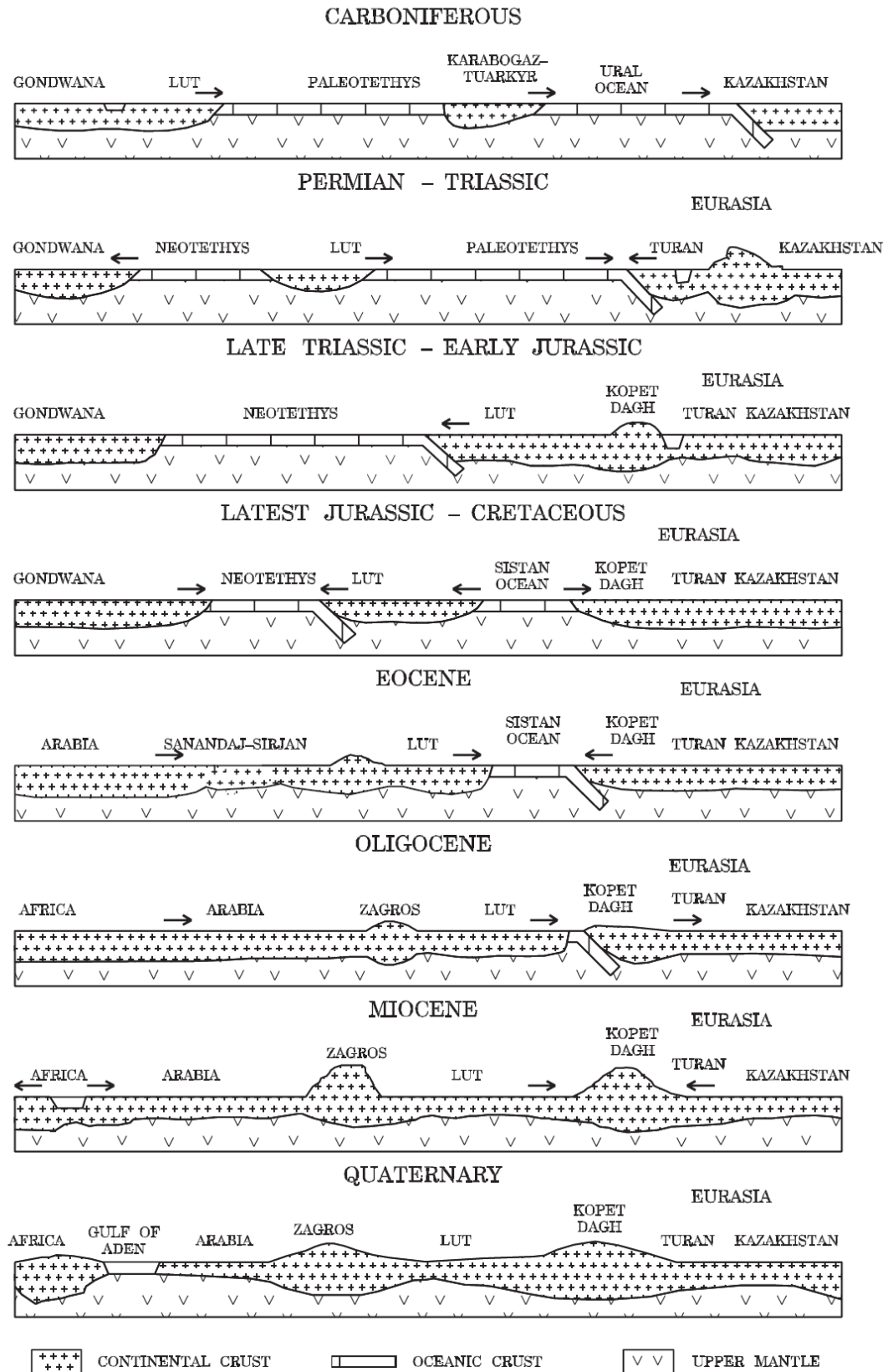


Figure 2.4: Profile of the evolution of the Arabian plate from the Carboniferous onwards.
Note: For palaeolocations of the African and Eurasian plates, see Figures 2.2 and 2.3.
Source: Golonka (2004)

2.1.3 The Pan-African Orogeny

The term 'Pan-African' was originally coined by WQ Kennedy in 1964, and diverged from its original use to designate Neoproterozoic to earliest Palaeozoic tectonic, magmatic, and metamorphic activities associated with rifting, collision and accretion events that culminated with the formation of Gondwana (Figure 2.5) (Kroener & Stern, 2005).

The Arabian-Nubian Shield is part of the Pan-African orogenic belt and extends 3000 km north to south and more than 1000 km east to west from the Nile River to Central Saudi Arabia and from northern Kenya to Sinai and Jordan (Abdelsalam & Dawoud, 1991; Johnson & Stewart, 1995; Vail, 1988). East Gondwana, which was composed of today's Australia, Antarctica and Southern India, and West Gondwana, which was composed of today's Africa and South America (Figure 2.5) converged 630–310 Myr ago and crushed the arcs, back arc basins and terranes of the Mozambique Ocean which existed between 870–630 Myr (Figure 2.6) (Kroener & Stern, 2005).

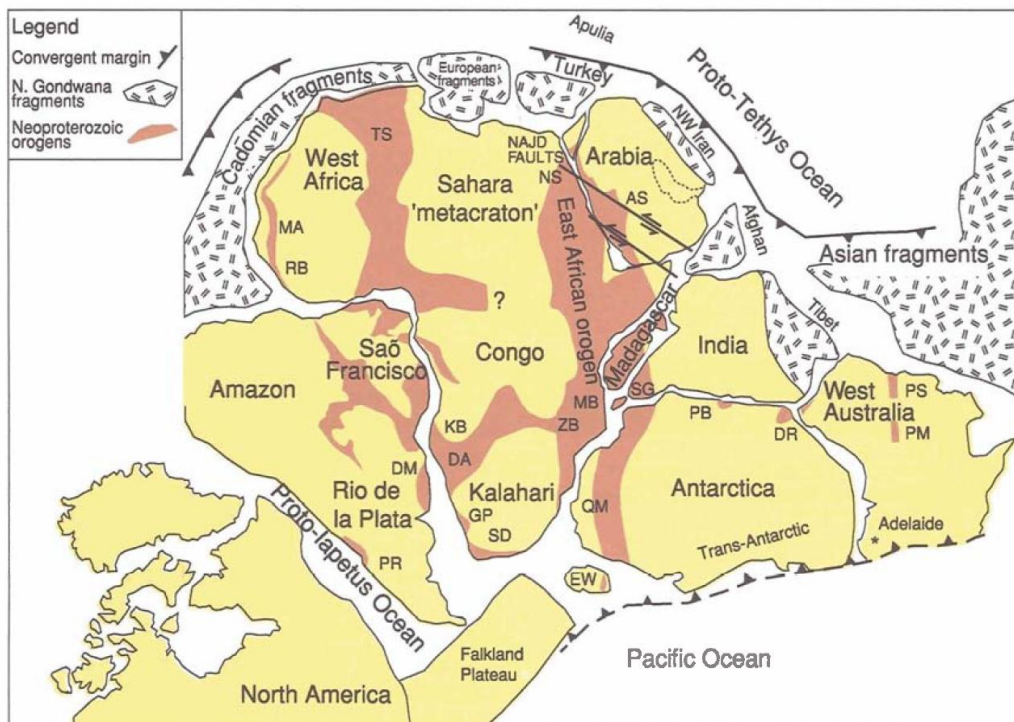


Figure 2.5: Pan-African Orogeny belts across a reconstruction of Gondwana at the end of the Neoproterozoic (ca. 540 Myr).

Note: Belts are shown in red.
Source: Kusky et al. (2003)

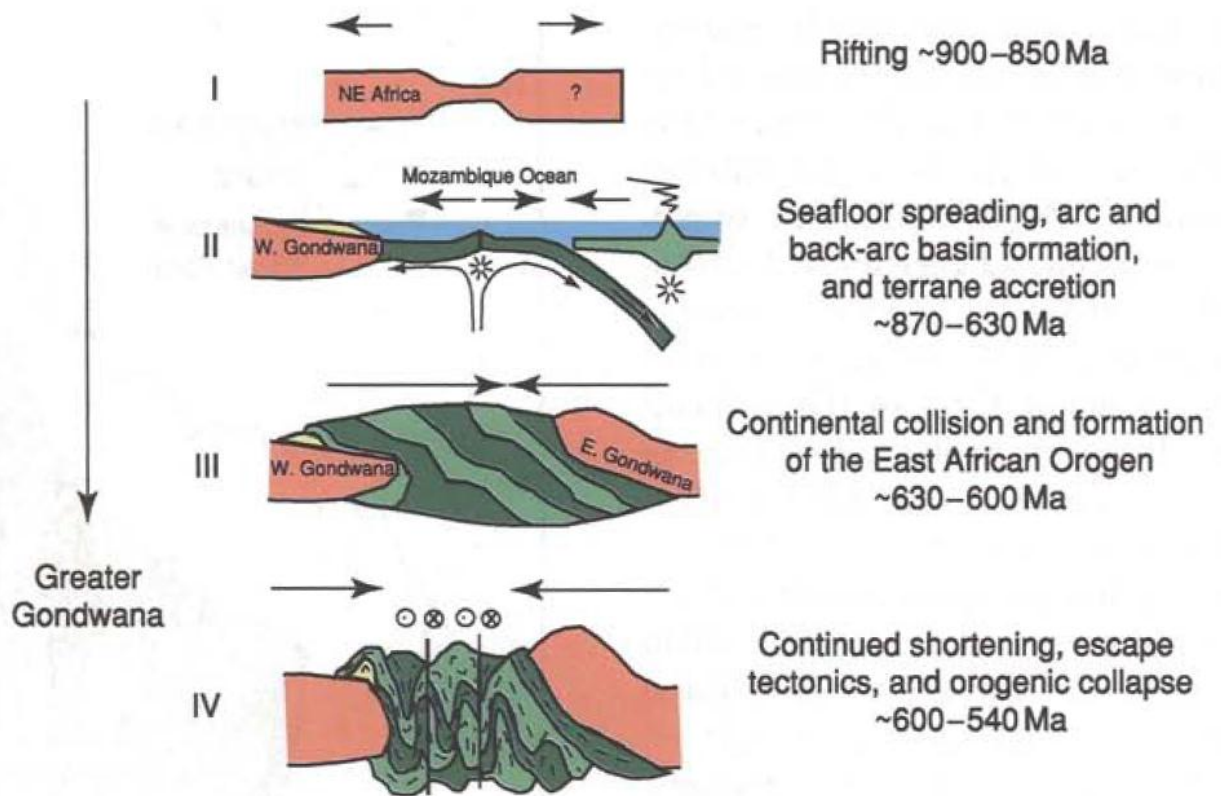


Figure 2.6: Evolution of the Arabian-Nubian Shield.

Note: For palaeolocation of the diverging continents, see Figure 2.5.

Source: Kroener & Stern (2005)

The Arabian-Nubian Shield records multiple orogenic cycles, where intra-oceanic convergent plate boundaries generated juvenile crust that together with older continental crust fused into complex terranes (Kroener & Stern, 2005). The shield also contains island-arcs and ophiolites, is characterised by relatively low grade metamorphism and was exposed during the Red Sea associated rifting and uplift in the Cenozoic (Johnson & Stewart, 1995; Kroener & Stern, 2005; Pollastro, Karshbaum & Viger, 1999).

On the Arabian plate, the Shield extends from the plate's western margin to the escarpments of central Arabia, where Palaeozoic to Tertiary rocks, as inferred from magnetic data, unconformably cover the basement, dip eastward and are buried by mostly flat Tertiary to Pliocene sediments (Johnson & Stewart, 1995; Kroener & Stern, 2005; Powers, 1968; Powers et al., 1966).

Figure 2.7 shows Midyan, Hijaz, and Asir terranes of the Arabian Shield, which were accreted to the northeastern edge of the African plate before 715 Myr and were separated from the Afif Terrane by the Nabitah Sea (Stoeser & Camp, 1985). Between 680–640 Myr, the Nabitah collision between the Afif Terrane on one side and Midyan, Hijaz and Asir terranes on the other consumed the Nabitah Sea into the Nabitah Suture. At 670 Myr ago, an east-dipping subduction commenced below the Amar Arc, consuming the Amar Sea, and culminated with the fusion of the Rayn terrane, which is composed of eastern and central Arabia, and the Afif Terrane.

This fusion, known as the Amar collision, took place between 640–620 Myr and yielded the obducted N-trending thrust slices of ophiolites known as the Amar Suture (Figure 2.7) (Al-Husseini, 2000; Stoeser & Camp, 1985). The Amar collision also generated EW-trending compressional stresses that propagated through the Arabian plate and formed uniformly aligned, N-oriented Rayn anticlines, namely the En Nala Anticline, the Khurais-Burgan Anticline, the Summan Platform and the Qatar Arch, over which Mesozoic and Cenozoic rocks flex in eastern Arabia (Figure 2.7), (Al-Husseini, 2000; Brown, Schmidt & Huffman, 1989; Johnson & Stewart, 1995; Konert et al., 2001; Powers, 1968; Stoeser & Camp, 1985). It is upon these anticlines that some of the world's largest oil fields such as the Ghawar, Safaniya, Khurais and Burgan fields are situated (Al-Husseini, 2000). The collision also yielded two orthogonal, strike-slip faults, the NE-trending Wadi Batin Fault and NW-trending Abu Jifan Fault, which bind the Rayn anticlines and intersect near the Amar Suture (Figure 2.7). In addition, drilling and seismic data show evidence of an extensive network of faults trending N, NW and NE that cut through the Precambrian basement, and form rigid unstable basement blocks, which propagated upward movement through the Phanerozoic succession controlling subsequent deposition and structures through structural growth, drape folding, subsidence and hydrocarbon migration (Al-Husseini, 2000; Ayres et al., 1982; Konert et al., 2001).

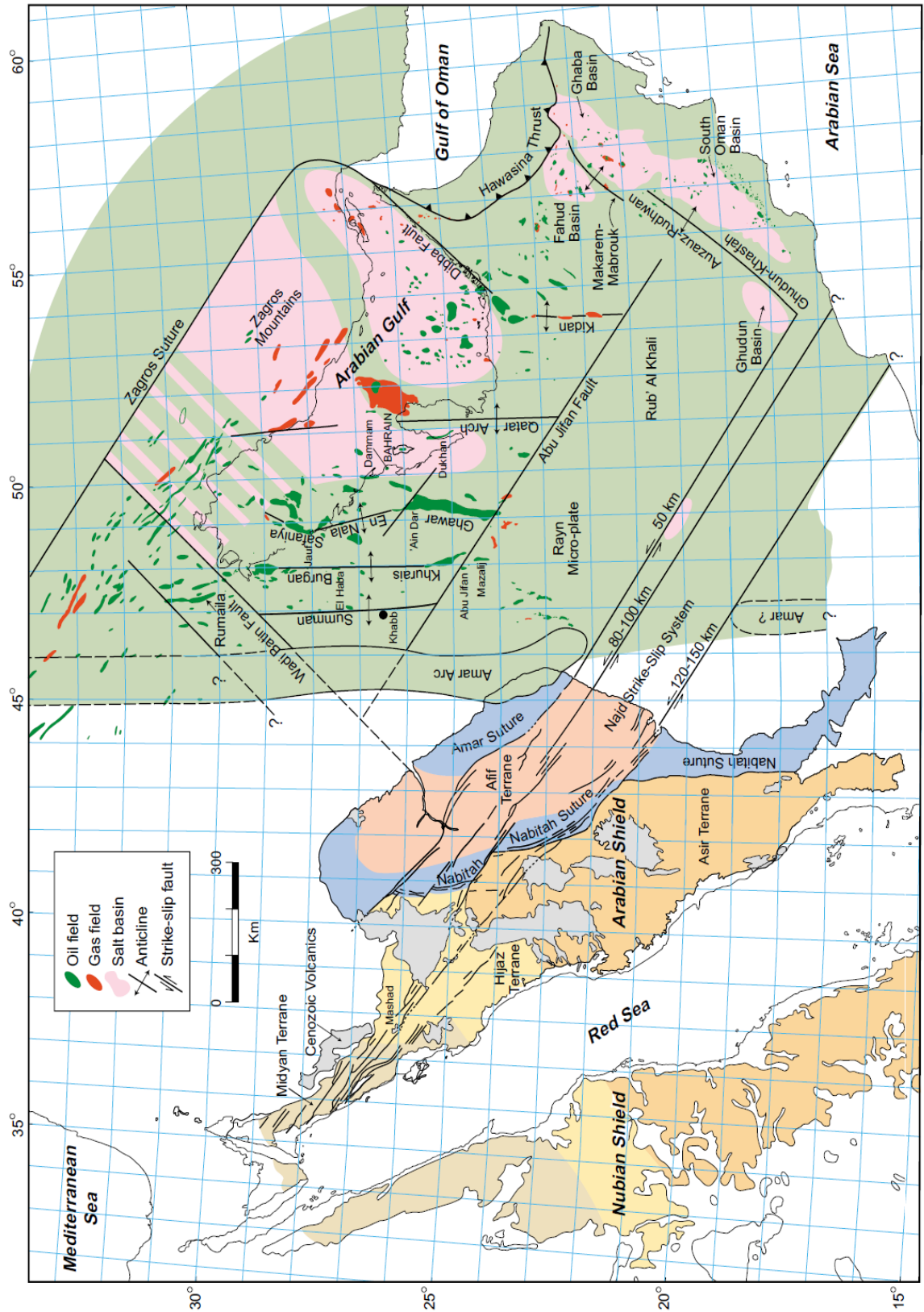


Figure 2.7: The different terranes that compose the Arabian Shield.
 Source: Al-Husseini (2000)

The collision between east and west Gondwana caused shortening, deformation, metamorphism, orogenic uplift and collapse, and escape tectonism marked by the development of the sinistral Najd Fault System. This fault system was initiated as transcurrent shear zones at 650–615 Ma; then evolved to pull-apart structures at 620–608 Ma, and lastly became a system of normal faults and associated rift basins as post-collision extensional tectonism peaked at 600 – 530 Ma, leading to the collapse of the Arabian-Nubian Shield (Agar, 1987; Blasband, White, Brooijmans, De Boorder & Visser, 2000; Cole & Hedge, 1986; Genna, Vaslet, Janjou, Le Metour & Halawani, 2000; Hussein, 1989; Hussein & Hussein, 1990; Johnson & Stewart, 1995; Kroener & Stern, 2005). The Najd Fault System (Figure 2.7) comprises three northwest-striking, parallel fault zones, that collectively extend over 1,100 km of length and 300 km of width, and individually are 5 to 10 km wide (Brown, 1972; Brown & Jackson, 1960; Brown et al., 1989; Howland, 1979). The fault system had dislocated the 680–640 Myr N-trending Nabitah Suture laterally by *ca.* 300 km (Brown, 1972; Brown & Jackson, 1960; Brown et al., 1989; Cole & Hedge, 1986; Johnson & Stewart, 1995; Howland, 1979; J. M. Moore, Allen, Wells & Howland, 1979). Magnetic data suggest that the Najd fault system cuts across terranes and intrusive complexes within the Arabian Shield and extends below the Phanerozoic section (Johnson & Stewart, 1995). The post-collision extensional phase caused the Rayn anticlines to become uplifted horsts bounded by normal faults and subsiding grabens (Al-Husseini, 2000; Haq & Al-Qahtani, 2005). Another episode of uplift encountered the Rayn anticlines during the Hercynian Orogeny, which rotated the Arabian plate, uplifted and tilted central Arabia towards the east and eroded several kilometres of sediments creating a hiatus (Al-Husseini, 2000; Haq & Al-Qahtani, 2005). Finally, the Rayn anticlines show evidence of continued growth especially in the Late Cretaceous in conjunction with the Neo-Tethys closure compression, and as recent as the Miocene–Pliocene in conjunction with Zagros suture subduction (Beydoun, 1991; Glennie, 2000; Nicholson, 2000, 2002).

2.2 Eustasy

The eustatic sea-level curve (Haq, Hardenbol & Vail, 1988) represents a mean global model of long-term trends of transgression and regression on continental margins and flooding or exposure of epeiric seas. Concurrence of local sea-level curves with the global one reflects tectonic dormancy and hence eustatic control of sedimentation, while tectonic upheaval is reflected by discordance (Haq & Al-Qahtani, 2005). The great width of the buoyant Arabian plate continental crust (more than 1,500 km between the pre-Red Sea margin to the Zagros suture from the Permian onward) had likely caused very low subsidence rates (Bishop & Jones, 1995; Sharland et al., 2001). This would have resulted in eustatic control over accommodation and hence similar sedimentary trends across wide areas of the plate except where tectonism affected subsidence (Sharland et al., 2001). Regional tectonic unconformities are known to extend across the Arabian platform signifying second- and third-order sequences through shifting of rates and loci of subsidence and controlling of accommodation production or destruction (Grabowski & Norton, 1995; Haq & Al-Qahtani, 2005; see Table 2.1). The quiescent periods that intervened between these tectonic unconformities witnessed eustatic control on the development of sedimentary sequences (Haq & Al-Qahtani, 2005).

Haq and Al-Qahtani (2005) constructed an Arabian plate-wide cycle chart that shows regional onlap and relative sea-level curves of the plate (Figure 2.8). This chart depended on Sharland's et al. (2001) identified regional maximum flooding surfaces (MFS), whose dating was fraught with copious uncertainties inherited by inaccuracies of biostratigraphic dating and calibration to the absolute time scales; and thus these uncertainties are in turn inherent in the Arabian plate cycle chart (Figure 2.9).

Although Hughes (2004) depicted upward tiering faunal assemblages on the scale of 3 m to represent sea-level shallowing of possibly 20 m, Haq and Qahtani (2005) stated that this and other methods such as coastal aggradation during highstands, marine inundation extent, lowstands' incision depths and ice-volume fluctuations

inferred from oxygen-isotopic variations carry large error ranges that reflect considerable uncertainties in determining absolute scale of sea-level fluctuations, and hence published their Arabian plate cycle chart to show relative rather than absolute scale of coastal onlap (Figure 2.8).

Table 2.1: Major tectonic events that controlled sedimentation on the Arabian platform throughout the Phanerozoic.

Source: Grabowski & Norton (1995) and Sharland et al. (2001)

System/Series	Tectonic Event	Subsequent Arabian Plate Effects
Late Precambrian	Najd shear-zone-related rifting begins	Development of rift salt basins to be filled with continental clastics
Early Cambrian	Subsidence starts after peneplanation	Transgressions of the Platform in Late Cambrian and Early Ordovician
Latest Ordovician	Hinterland is uplifted	Major hiatus and down-cutting on Platform
Latest Devonian	'Hercynian' Orogeny begins on Arabian Plate	Multiple phases of compression and block faulting. Widespread inversion, erosion of several km of sediments on the Platform
Latest Carboniferous	End of 'Hercynian' Orogeny on Arabian Plate	Plate tilts gently to the northeast
Late Permian	Neo-Tethys opens and the NE passive margin begins to subside	Transgression and beginning of dominantly carbonate sedimentation over the Platform
Early Jurassic	Rifting of India from Africa/Arabia begins	India separates from Gondwana by Late Jurassic. Plate tilts toward north.
Late Early Jurassic	Rifting starts in eastern Mediterranean and western margin of Plate	Uplift of western margin of the Plate, beginning of a passive margin along northwestern margin of the Plate
Early Cretaceous	South Atlantic begins to open	Plate tilts more to the east and dominant sediment transport is now from west to east.
Mid Cretaceous	Mediterranean begins to open	Sub-basins form on Arabian Platform
Late Cretaceous	Ophiolite obduction along NE margin begins	Fault reactivation and uplift of NE margin of Platform
Early Paleocene	Ophiolite obduction ends	Erosion along NE margin of Platform
Late Eocene	Closure of Tethys Seaway	Arabian Plate begins its collision with Asia and tilts again to the northeast
Late Oligocene	Gulf of Aden and Red Sea starts to open	Eastern branch of Tethys closed by this time

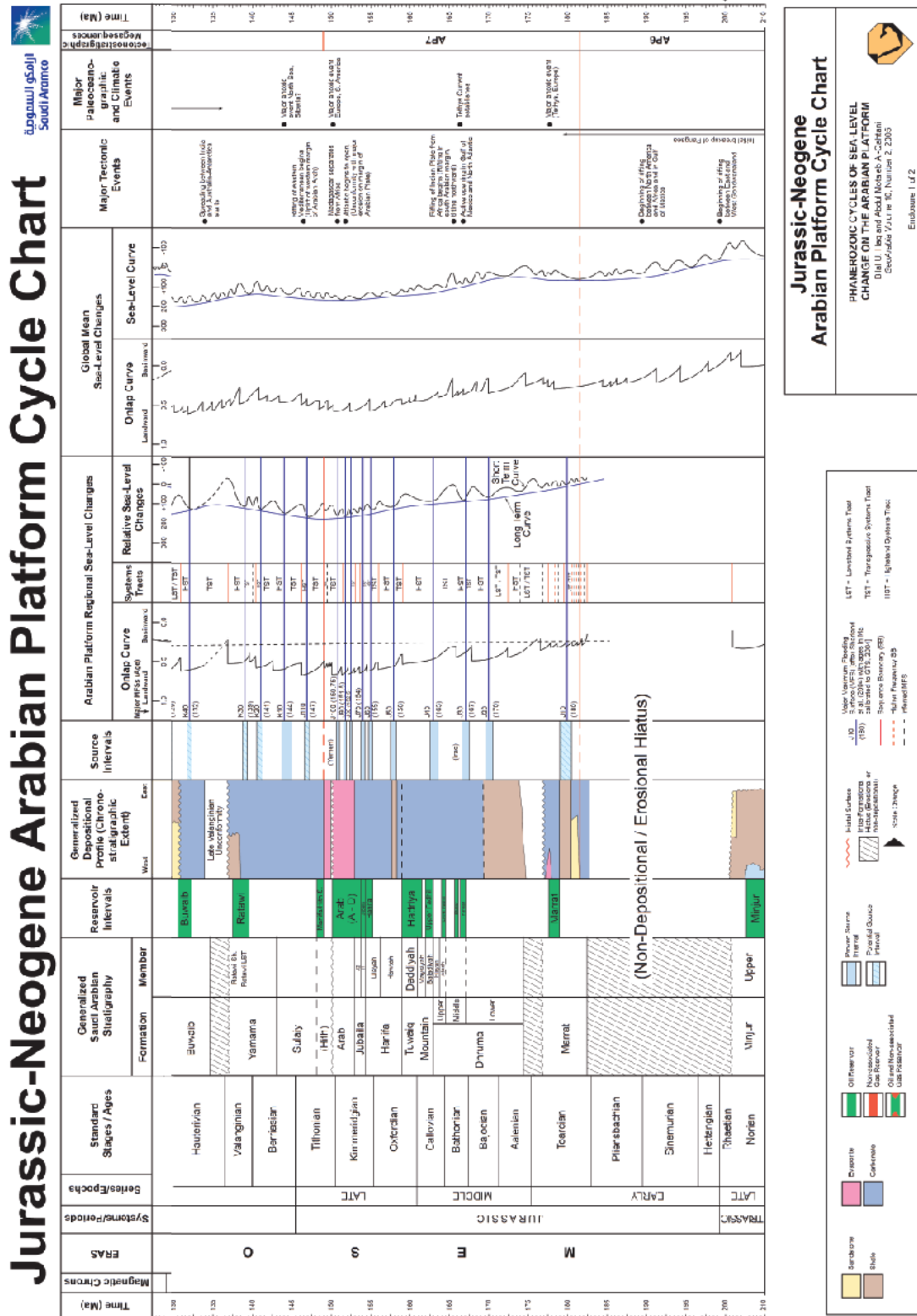


Figure 2.8: Jurassic cycle chart of the Arabian platform juxtaposed next to the global cycle chart.
Source: Haq and Al-Qahtani (2005)

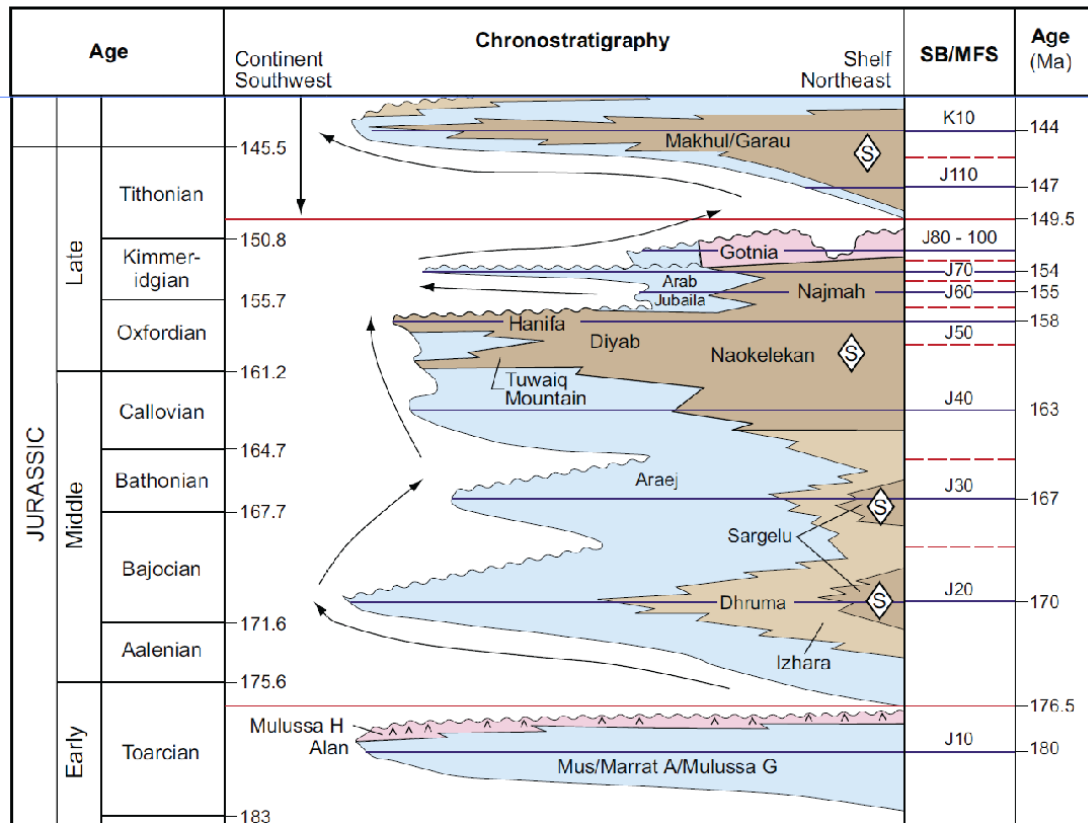


Figure 2.9: Schematic chronostratigraphic column of the Jurassic.

Notes: Sequence boundaries (red lines) and maximum flooding surfaces (blue lines) are shown on the right. Curved arrows denote transgressive-regressive cycles. Colour scheme is similar to that of Figure 2.8.

Source: Modified from Haq and Al-Qahtani (2005) and Sharland et al. (2001)

Based on the resemblance of the regional Arabian plate sea-level cyclicity to the global one, the Phanerozoic succession of the Arabian plate can be divided into periods of tectonic dormancy or activity. The Cambrian through early Silurian gentle subsidence of the Arabian platform led to eustatic control on sedimentation, which is reflected as long-term trend agreement between the global and regional sea-level curves (Haq & Al-Qahtani, 2005). Active tectonism obscured the eustatic signal from the late Silurian through Mississippian, which is reflected as disagreement between the two curves (Haq & Al-Qahtani, 2005). A 25 Myr Carboniferous hiatus associated with erosion of several kilometres of sediments from the Arabian platform is linked to the compression and deformation associated with the Hercynian Orogeny (Haq & Al-Qahtani, 2005). Neo-Tethys rifting and related crustal extension of the Arabian plate denotes discordance between the two curves during the early Permian (Haq & Al-Qahtani, 2005).

In the late Permian through Triassic, the Arabian plate moved into equatorial latitudes, which is reflected by accordance of the regional curve with the global one (Haq & Al-Qahtani, 2005). Gondwana's breakup and separation of India from Arabia and Africa, coupled with the central Mediterranean rifting, caused another 20 Myr hiatus from latest Triassic through Early Jurassic, which tilted Arabia northward (Grabowski & Norton, 1995; Haq & Al-Qahtani, 2005). From Middle Jurassic through Palaeogene, the patterns of the two curves are largely in agreement, indicating the dominance of eustatic control on sedimentation (Haq & Al-Qahtani, 2005; Le Nindre, Manivit & Vaslet, 1990). This agrees with the conclusion of attributing the sequence-stratigraphic rhythm preserved in the Arab-D succession to eustatic sea-level fluctuations, which is discussed in detail in Chapters 3 and 4. The Oligocene closure of the eastern limb of the Neo-Tethys created a 10 Myr hiatus (Haq & Al-Qahtani, 2005). The tectonics of the closure of the Neo-Tethys and emergence of Zagros Mountains reflect a reduced number of third-order cycles on the regional curve as compared to the global one from late Palaeogene to Neogene (Grabowski & Norton, 1995; Haq & Al-Qahtani, 2005).

2.2.1 Focusing on the Jurassic Period

Rates of seafloor spreading together with the shapes and lengths of the spreading centres have been suggested as causes of long-term fluctuations of eustatic sea-level (Hayes & Pitman, 1973; Kennedy, 1964; Pitman, 1978; Valentine & Moores, 1972). Palaeogeographic reconstruction of the Kimmeridgian/Tithonian (Figure 2.10) shows that the Neo-Tethys had three propagating rifts that eventually trisected Pangea into North American, Gondwana (of which the Arabian plate occupied the northeastern edge) and Eurasia (Scotese, 1991; P. A. Ziegler, 1988). Throughout the Jurassic, hastened spreading associated with the breakdown of Pangea caused a eustatic sea-level rise that peaked in the Kimmeridgian, causing flooding of continental margins and formation of epicontinental seas, such as the one that covered the eastern part of the Arabian plate and dominated it with carbonate and evaporite deposition (Hallam, 1988; Haq et al., 1988; Sharland et al., 2001).

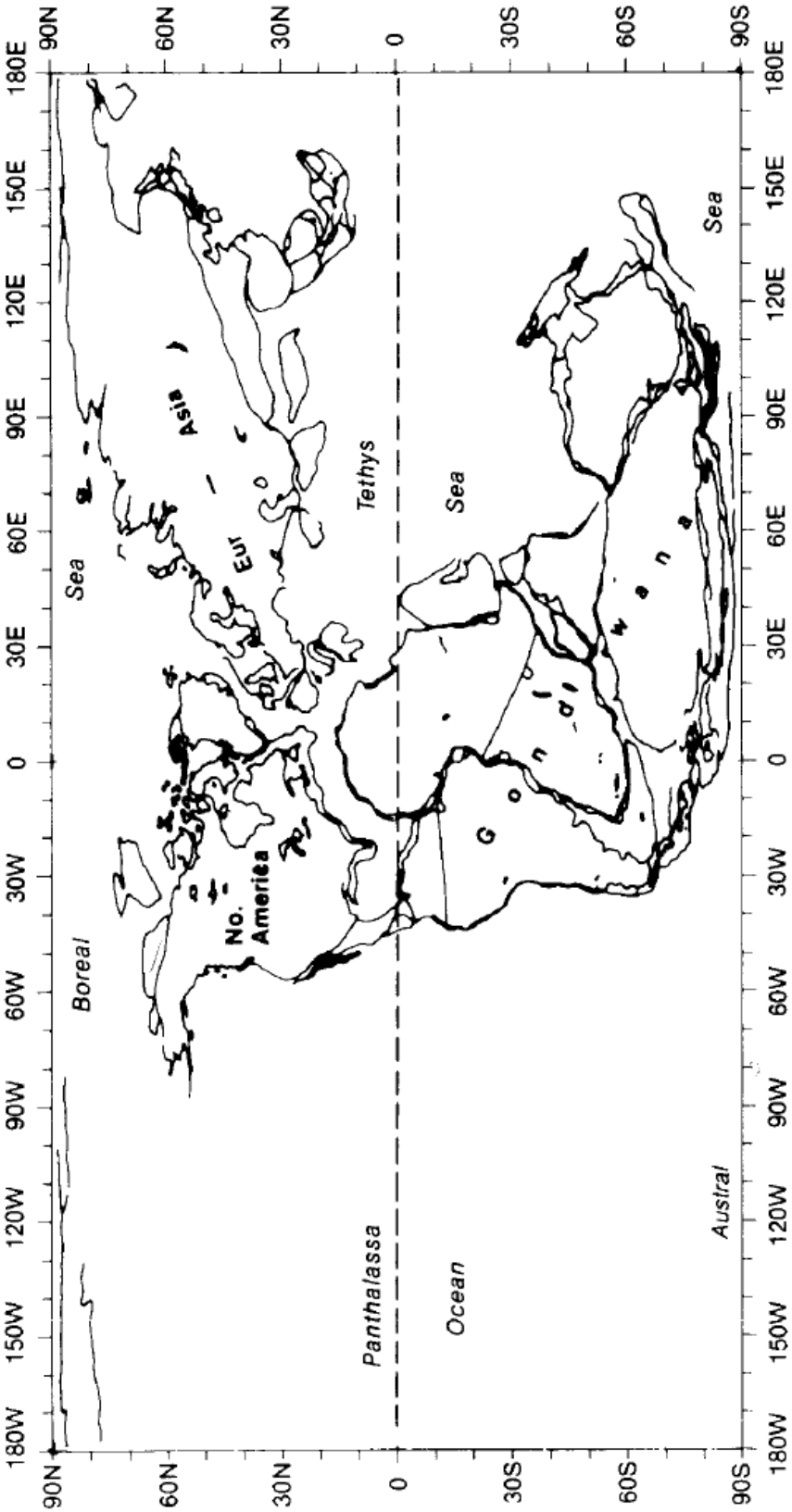


Figure 2.10: Palaeogeographic reconstruction of the earth in the Kimmeridgian/Tithonian.
Source: G. T. Moore et al. (1992)

Hallam (1982, 1993) argued that the global expansion of limestone deposition during the Jurassic denotes the expansion of epicontinental seas rather than temperature increase. Slow subsidence, which characterised the Arabian plate as mentioned earlier, has substantiated the carbonate's ability to fill accommodation created by slow sea-level rises. Thus, plate-wide flooding, which came from the Neo-Tethys to the north and east (Ross & Ross, 1983), is attributed to rapid relative-sea-level rises (Sharland et al., 2001). Furthermore, the slow subsidence rate is linked to keeping the accommodation filled with sediment at or close to sea-level, which yielded horizontal substrate and a flat-layered succession, except at plate margins (Sharland et al., 2001). This flat epeiric setting of the Arabian plate could have meant an enhanced sensitivity to sea-level fluctuations, as they were likely to cause widespread facies shifts or lead to substantial lateral exposure or flooding across the plate (Sharland et al., 2001).

The flat carbonate substrate of the Arabian plate is likely to reflect high order sub-aerial exposure surfaces, where significant non-depositional time—beyond the biostratigraphic resolution—resides during highstands and relative lowstands (de Matos, 1977; Sharland et al., 2001). These exposure surfaces did not yield significant erosion due to lack of structural hinterland—the Arabian Shield was not significantly uplifted until the Neogene—to supply energy to surface runoff. Therefore, palaeosols are more likely to form instead of deep penetrating karsts, which would make their identification more difficult (Sharland et al., 2001). This agrees with Haq and Al-Qahtani (2005), who stated that lowstand deposits were limited to incised valleys on the Arabian plate, which made separating the lowstand systems tract (LST) from transgressive systems tract (TST) difficult in most instances; and hence the authors lumped the two together below easier-to-identify MFSs. Thus, it can be said that the effects of sea-level cyclicity on a 'table top', such as the Arabian plate had been, is 'layer cake stratigraphy' on the third-order level; but progradational and/or retrogradational trends can be preserved on the fourth- and/or fifth-order cyclicity level, especially at plate margins (Haq & Al-Qahtani, 2005). This 'layer cake stratigraphy' seems to be reflected in the Arab-D succession, as mentioned earlier and as discussed in Chapter 5.

2.3 Jurassic Climate

The earth's climatic belts remained largely fixed with respect to the latitudes from Permian to present due to Hadley cell circulation (A. M. Ziegler, Eshel, Rees, Rothfus, Rowley, & Sunderlin, 2007). Pangea's vast continental extent and its position—being split by the equator—had disrupted zonal circulation, where equatorial easterlies carried warm moisture to release rainfall on land, by the megamonsoon, which is characterised by strongly seasonal rainfall at low-latitudes (Kutzbach & Gallimore, 1989; Parrish, 1993). This Pangean megamonsoon started in the Pennsylvanian and peaked in the Triassic (Parrish, 1993). As Pangea commenced disintegrating, the Early Jurassic reflects weakened seasonality that transitioned to zonal climatic conditions in the Middle Jurassic and completely reverted back to zonal conditions in the Late Jurassic (Parrish, 1993). Thus, the cessation of the megamonsoon upon Pangea's breakup stopped moisture transport to low and mid-latitudes, increased aridity and led to evaporite deposition (Parrish, 1993). This increased aridity and consequent evaporite deposition are reflected in the succession of the Arab Formation, as discussed in Chapter 3.

The Jurassic climate is characterised by expansion of the tropical-subtropical conditions into the present-day temperate climatic belts, which in turn expanded into the polar zones (Hallam, 1982, 1993). Thus, desert or seasonally wet-conditions dominated low latitudes, warm temperate conditions dominated mid-latitudes, and cool temperate conditions dominated high latitudes (Rees, Noto, J. M. Parrish & J. T. Parrish, 2004). The Jurassic climate is also characterised by being much more equable, as it lacks extremes, although harsh arid conditions prevailed in the interiors of the expansive Jurassic continents (Crowley & North, 1991; Sloan & Barron, 1990) with gentler equator-to-pole climatic gradients compared to present-day figures (Hallam, 1985). Continents almost completely lacked ice, and polar ice caps were minimal and probably seasonal, if present, which translated into higher sea levels compared to those of today; and this probably further enhanced the climate equability (Christie-Blick, 1982; Crowell & Frakes, 1970; Frakes, 1979; Frakes, Kemp, & Crowell, 1975; Hallam, 1982, 1985, 1993; Parrish, Ziegler &

Scotese, 1982; Valdes & Sellwood, 1992).

Widespread global distribution of bauxites, evaporates and eolian deposits, and the existence of extensive varieties of thermophilic organisms across broad ranges of latitudes all indicate significant warmer Jurassic temperatures compared to the

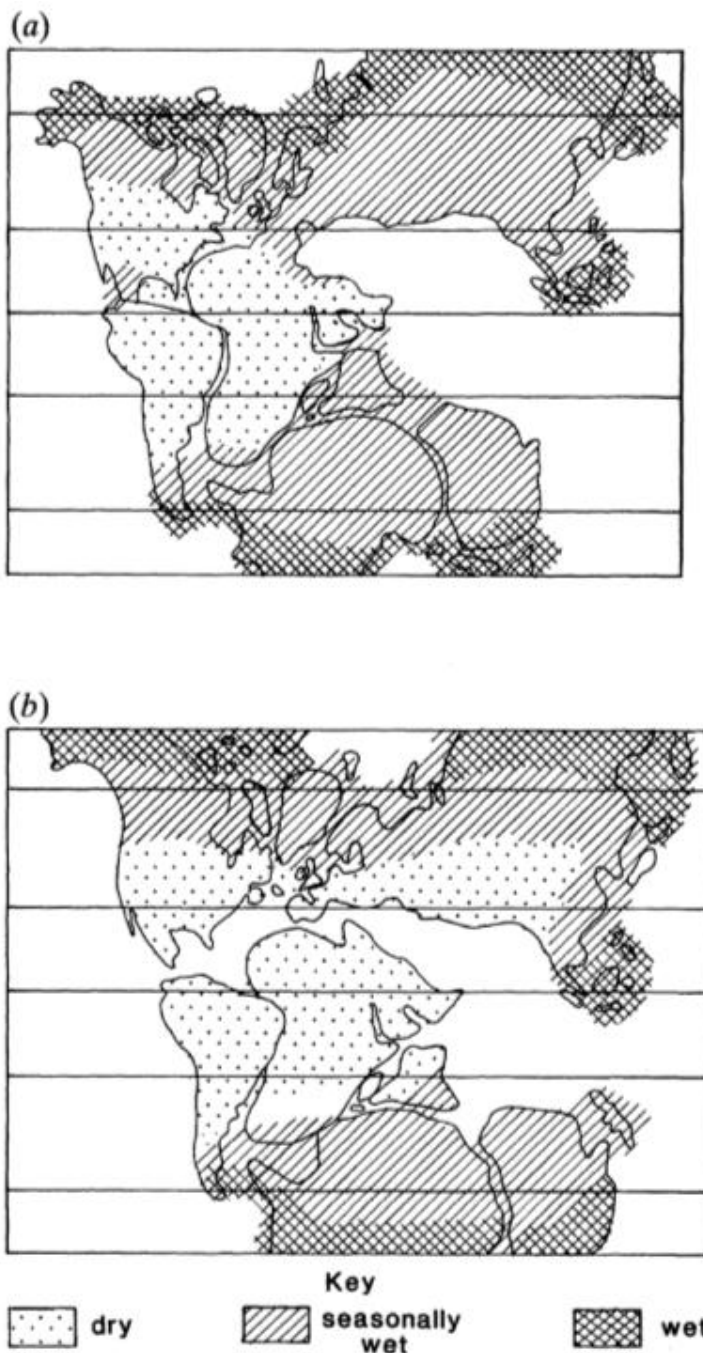


Figure 2.11: Humid and arid continental belts in the Early Jurassic and Late Jurassic.

Notes: (a) Early Jurassic (b) Late Jurassic.

Source: Hallam (1985)

present (Figure 2.11) (Fluigel & Fluigel-Kahler, 1992; Frakes 1979; Habicht, 1979; Hallam, 1985; Huber, MacLeod, & Wing, 1999; Sellwood & Price, 1994; Vakhrameev, 1991).

Jurassic evaporites ranged from 45° N to 45° S, covering an area surpassed only by the evaporites of the Triassic period and geographically distributed in a similar manner to the present day (Gordon, 1975; Hallam, 1993). There is also a trend of increased aridity, which is reflected throughout the Jurassic and into the Cretaceous, based on evaporite distribution (Frakes, 1979; Vakhrameev, 1964).

Coals were concentrated at mid- and high latitudes. The high-latitude coals are attributed to monsoonal circulations, which can move heat and moisture towards the poles and in the process increase the rainfall there (Hallam, 1993; Manabe & Wetherald 1980; Rees et al., 2004).

Jurassic warm, equable marine conditions are substantiated by the broad global dispersal of invertebrates, in addition to the documenting of reef-building corals in as far as 60° N palaeolatitude, as opposed to the 30° current limit (Hallam, 1982, 1993).

Further, many Jurassic bivalve genera are spread across a broad latitudinal range and reflect mild diversity reductions as they depart from the equator (Hallam, 1982, 1993). Ceratodontid lungfish, whose modern relatives are tropical-sub-tropical limited, also show latitudinal expansion (Schaeffer, 1971).

Jurassic sea water temperatures are estimated to be about 20°C as suggested by the presence of reef-building corals to as far as 60° N palaeolatitude (Hallam, 1982, 1993). This is supported by Jurassic oxygen isotope values indicating palaeowater temperatures in the range of 12–20°C (Anderson, Popp, Williams, Ho & Hudson, 1994; Hudson & Martill, 1991). More specifically, oxygen isotope values reflect the Oxfordian to early Kimmeridgian cooling that was followed by warming from the Kimmeridgian to the earliest Cretaceous (Weissert & Erba, 2004). Other authors have suggested that the diagenetic alterations, thermohaline-circulation induced depletions and fresh-water runoff at mid-latitudes limit the utility of oxygen isotope ratios in Jurassic climate interpretations (Pearson et al., 2001; Price & Sellwood, 1997; Williams et al., 2005).

Terrestrially, Jurassic ferns, whose modern relatives are intolerant of cold conditions, and gymnosperm floras were widely distributed and found in the poles, further supporting a warm and equable climate (Barnard, 1973). Based on terrestrial plant distribution in Laurasia, warming is inferred throughout the Jurassic

and into the Cretaceous, and Siberian temperatures are concluded to have never fallen below 0°C (Vakhrameev, 1964). Furthermore, *Classopolis*, a conifer pollen indicative of aridity, was found to be most abundant in the Late Jurassic, indicating that aridity increased throughout the period (Vakhramcev, 1981).

In addition, since annual growth rings in tree trunks are indicative of the seasonal climate that interrupts their growth rate, Creber and Chaloner (1984) documented absences of these rings from the Jurassic record at latitudes spanning between 30°N and 30°S, and concluded that there had been an expansive equatorial, seasonless zone within that range (Hallam, 1993). On the other hand, seasonal climate prevailed at higher latitudes, based on the development of growth rings in tree trunks, suggesting broad temporal belts that pushed into the polar realms (Creber & Chaloner; 1984; Epshteyn, 1978). Based on climate models and floral distribution, the Late Jurassic probably lacked everwet biome; and diverse forests populated the warm temperate belts, which occupied mid and high-latitudes, with vegetation of highest diversity in mid-latitudes and those of lowest diversity in the equator and poles (Rees, Ziegler & Valdes, 2000). Dinosaur records reflect an expansive latitudinal domain between 45° N and S of the equator, which, if dinosaurs had been ectothermic like today's reptiles, supports the notion of a warm equable Jurassic (Charig, 1973; Colbert, 1964).

2.3.1 Late Jurassic Climate

The low Middle-Late Jurassic $^{87}\text{Sr}/^{86}\text{Sr}$ signal has been attributed to the high eustatic sea-level, which reduces rubidium- and strontium weathering from igneous and metamorphic rocks, increased oceanic volcanism associated with the Pangean breakup and reduced continental runoff caused by low precipitation-to-evaporation rates (Hallam, 1984; Haq et al., 1988). Distribution of arid and humid climatic belts in the Late Jurassic is shown in Figure 2.12 from Hallam (1984), which illustrates the geographic distribution of evaporites and eolian sands, indicating elevated temperatures and arid conditions; and coals, indicating swampy humid conditions, (Christie-Blick, 1982; Crowell & Frakes, 1970; Frakes 1979; Hallam 1982, 1985, 1993;

Leeder & Zeidan, 1977; Parrish et al., 1982).

Jurassic atmospheric CO₂ estimates vary from 400 ppm to 2100 ppm as compared to today's, pre-industrial, 280 ppm (Berner, 1990; Budyko, Ronov, & Ianshin, 1985). G. T. Moore et al. (1992) and Sellwood and Valdes (2008) used General Circulation Models simulating the Late Jurassic palaeoclimate, and produced 90-day seasonal-average maps. They used 1120 ppm CO₂, which amounts to a fourfold increase of the pre-industrial levels; this led to simulations mimicking biologic and lithologic data from the Late Jurassic and indicated a strong greenhouse effect at the time (G. T. Moore et al., 1992; Sellwood & Valdes, 2008).

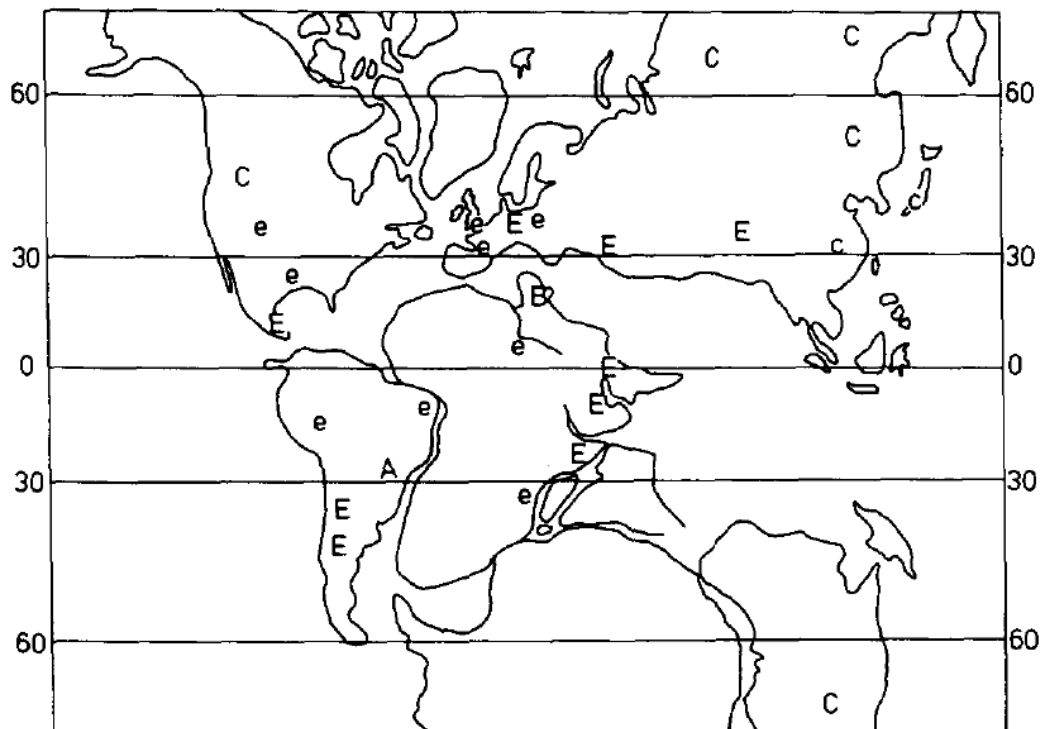


Figure 2.12: Late Jurassic distribution of coals, evaporates and eolian deposits.
Notes: Coals (C-major, c-minor), evaporates (E-major, e-minor), eolian deposits (A).
Source: Hallam (1984)

Limitations of Jurassic General Circulation Models of climate include their divergence from plant data at high-latitudes as they reflect cooler temperatures than the plants' (Rees et al., 2000, 2004), and their blunt reflection of small-scale local climatic controllers such as mountain ranges or volcanoes (Sellwood & Valdes, 2008).

The modelled precipitation minus evaporation with the palaeolocation of the Arabian plate enclosed in a green square is shown in Figure 2.13 (G. T. Moore et al., 1992). Continents between 30°-40° north and 30°-40° south were dry and hot with evaporation exceeding precipitation, while wetlands were located at mid-to-high latitudes, where precipitation exceeded evaporation, with cold winters and warm summers (Figure 2.14) (G. T. Moore et al., 1992; Scotese, 2000; Sellwood & Valdes, 2008). Much of the Jurassic rains were brought by the trade winds and fell over the Neo-Tethys; and hence drought spread on continents (Sellwood & Valdes, 2008). The simulations also show heavy precipitation in northwestern Gondwana and southeastern Asia (G. T. Moore et al., 1992). The palaeoposition of the Arabian plate falls out of these high precipitation areas, and into a net-evaporation area (Figure 2.13). The simulations show an equatorial net-precipitation belt that divides a wider mid-litudinal net-evaporation belt which extends between about 40° north and south of the equator, with high evaporation rates at the margins of the Neo-Tethys and at high precipitation areas on continents (G. T. Moore et al., 1992).

The modelled air's surface temperature and the oceans' surface and deep-water temperatures were much higher than today's (Figure 2.15); most of the warming effect was concentrated in the sub-polar and polar latitudes, where sea ice disappears from the southern hemisphere, and thins in the northern hemisphere (G. T. Moore et al., 1992). As cyclones (wind velocity > 32 m/s) need sea-surface temperatures in excess of 27°C, the warm sea-surface temperatures of the Late Jurassic could have meant longer, or even continuous, cyclone seasons (G. T. Moore et al., 1992). Cyclone paths are subject to subtropical highs' position, strength and size (Anthes, 1982; Barron, Hay & Thompson, 1989). G. T. Moore et al.'s (1992) simulation reflects sea-surface temperatures in excess of 30°C, and subtropical highs near 30°N that would have allowed development of immense cyclones, due to the vast fetch length over the Panthalassa Ocean, to fall over northeastern Gondwana and move inland (G. T. Moore et al., 1992). Thus they predict the upper Jurassic of northeastern Gondwana to contain tempestites, which agrees with our conclusions regarding the lower intraclastic lithofacies of the Arab-D reservoir,

discussed in Chapter 3. According to the G. T. Moore et al.'s (1992) model, surface wind vectors and cyclone paths during the Kimmeridgian were oriented east–west at the palaeolocation of the Arabian plate (Figure 2.16). This also agrees with our conclusion of the Arab-D shelf being subjected to storms coming from the east that collided with the reef rim of the shelf causing turbidity avalanches to propagate westward towards the basin (Chapters 3 and 5).

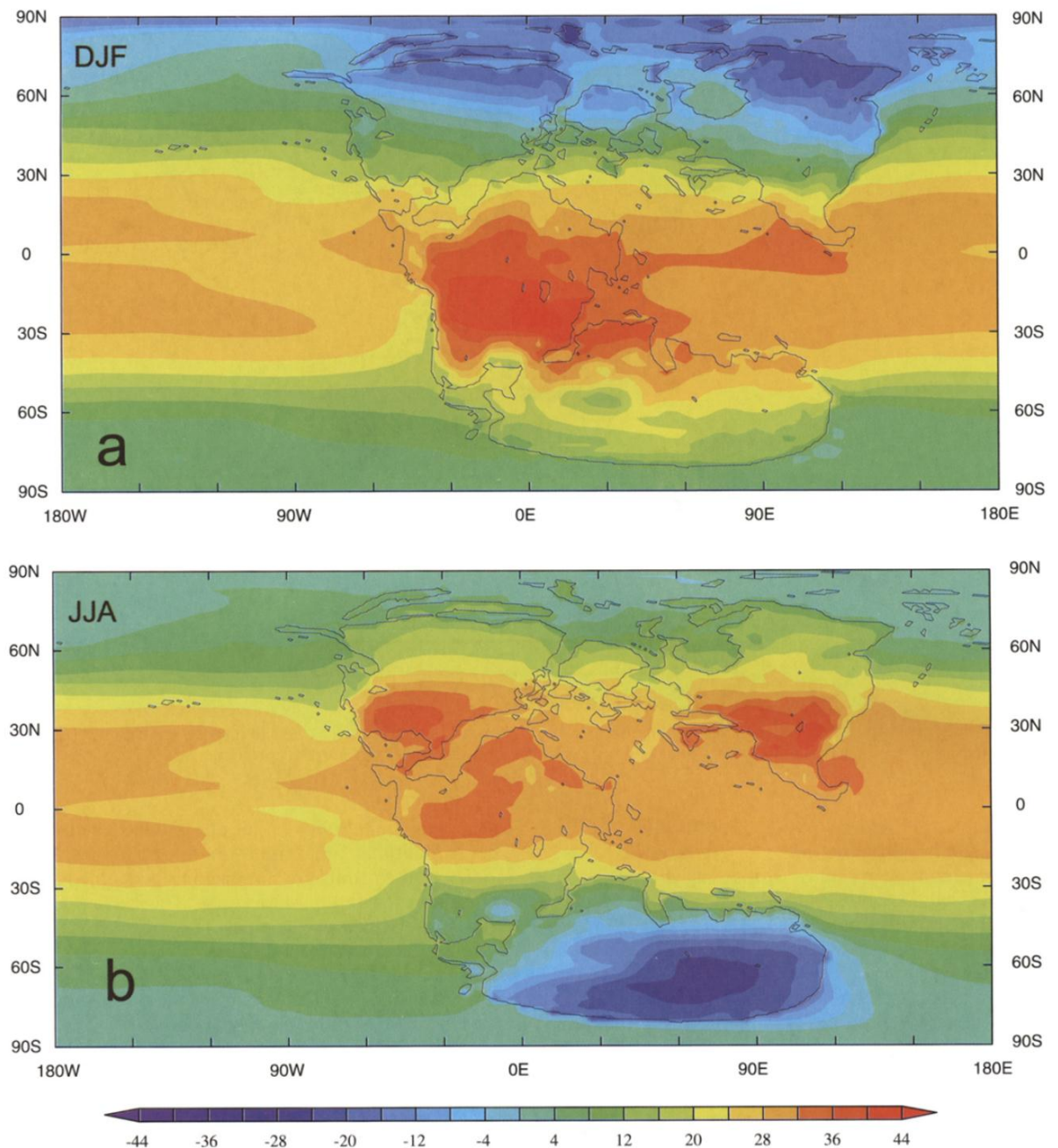


Figure 2.15: Late Jurassic modelled surface air temperature (°C).

Notes: (a) December–January–February (b) June–July–August. Contour interval is 4°C and the black outline denotes palaeolocation of continents.

Source: After Sellwood and Valdes (2008)

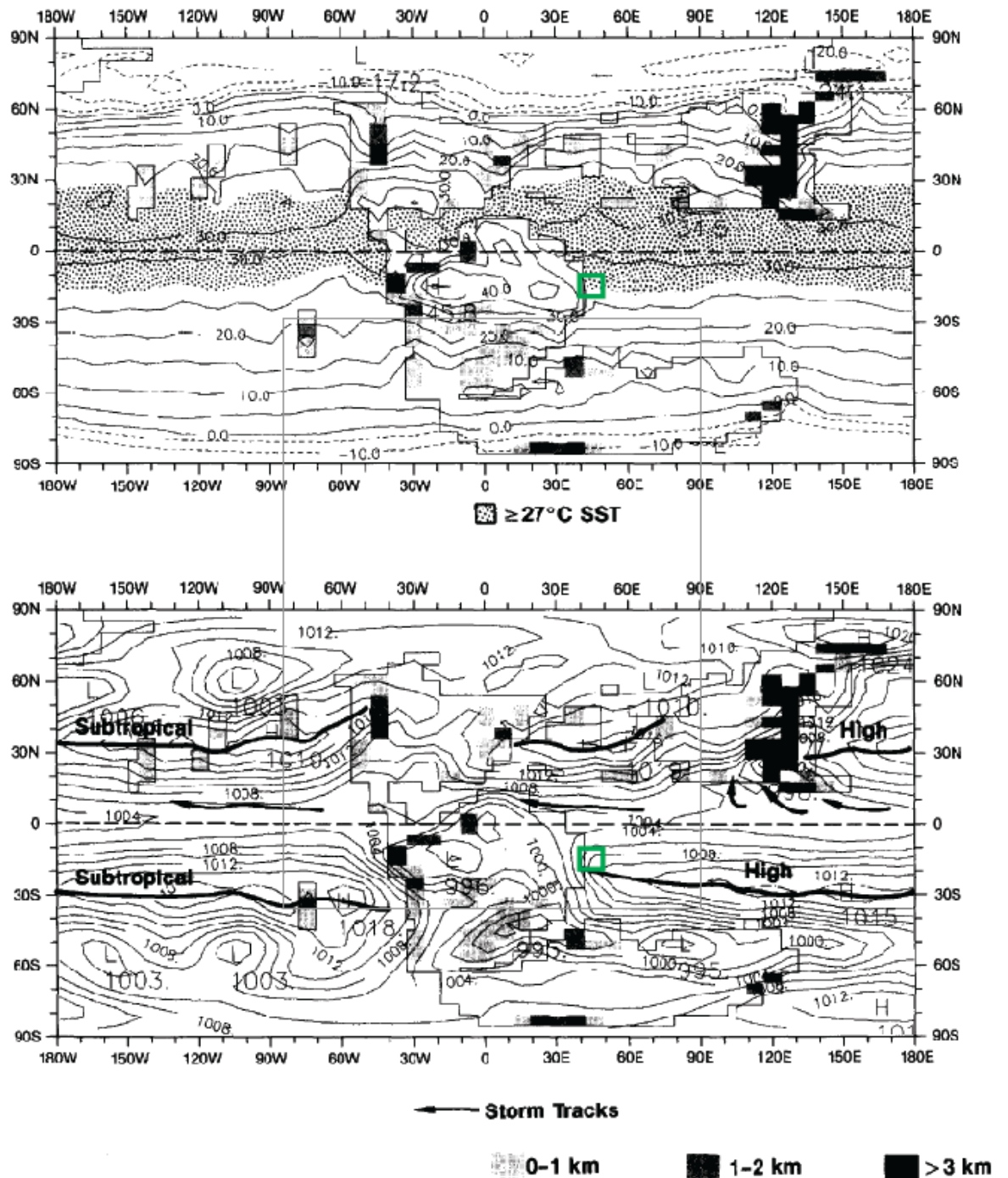


Figure 2.16: Simulated Kimmeridgian-Tithonian cyclone season

Notes: The dotted pattern on top map denotes sea-surface temperature in excess of 27 °C; the arrows on bottom map denote cyclone tracks on a sea-level pressure (mb) map; the green square denotes palaeolocation of the eastern part of the Arabian plate.

Source: Modified from G. T. Moore et al. (1992)

2.4 Evolution of Depositional Environments

The Arabian platform formed a continental margin of Gondwana that accumulated terrestrial and shallow-marine sediments throughout the Palaeozoic, and marine carbonates and evaporites from the Pennsylvanian to Miocene (Alsharhan & Magara, 1994; Murriss, 1980). The platform has been situated in tropical to subtropical latitudes since the Permian and its deposits reflect alternating periods of aridity and humidity (Murriss, 1980). The stability of the Arabian platform during the Mesozoic caused the deposited rock-stratigraphic units to approximate time-stratigraphic units (Ayres et al., 1982). Murriss (1980) differentiated the shallow carbonates of the Arabian plate into ramps and shelves based on depositional patterns. Deposition on ramps coincided with increased clastic influx and is characterised by cyclic appearance of argillaceous units that are correlatable over hundreds of kilometres, both parallel and perpendicular to depositional strike. These cyclic units show consistent to gradual change in thicknesses and lithologies. Carbonate ramp deposits, such as the Middle Jurassic Dhurma Formation, coincided with sea-level lowstands and included reservoirs of moderate quality composed of peloidal packstones and less common oolitic grainstones and seals of marls and argillaceous limestones with limited sealing capacity over gentle structures (Murriss, 1980).

Deposition on a carbonate shelf, such as the Late Jurassic Tuwaiq Mountain, Hanifa, Jubaila and Arab formations, coincided with periods of highstands of sea-level, when clastic influx was inhibited, and is characterised by less consistency in thickness and lithology compared to ramps. Deposits on the shallow parts of the shelves typically included algal-foraminiferal wackestones and packstones and oolitic and peloidal packstones and grainstones, which formed good reservoirs. Deeper parts of the shelves were starved and typically contained marl and lime mud deposited in anoxic conditions, which formed excellent source rocks (Murriss, 1980). Effective seals developed during sea-level highstands in arid conditions, which allowed for development of widespread anhydrites and salts (Murriss, 1980). Off-shelf, open marine conditions were not favourable for development of reservoirs or

sources rocks and shale seals were moderately effective (Murriss, 1980). The difference of reaction to a 10-m-fall in sea-level in a ramp versus a shelf is that such a drop would cause extensive lateral exposure on a rimmed shelf but would cause a lowstand platform in a ramp, as deeper parts of it would be brought to shallow conditions and initiate shallow carbonate production (Sharland et al., 2001). In Chapters 3 and 5 of this thesis, the Arab-D reservoir is interpreted to represent deposition on a rimmed shelf, as no lowstand deposits are depicted and laterally extensive flooding events are noted within the reservoir, which agrees with the above notions of Murriss (1980) and Sharland et al. (2001).

2.4.1 Overview of the Jurassic Depositional Systems

The major initial transgression of the Jurassic, coupled with the Arabian plate's stability led to the shelf-carbonate deposition of the Toarcian Marrat Formation. The formation comprises sandstone, red shale and limestone, which suggests that the shoreline was not pushed very far westward from its current position (Alsharhan & Magara, 1994). The transgression led to the formation of a shallow shelf that sloped gently towards the northeast (Alsharhan & Magara, 1994; Murriss, 1980). The shelf then transitioned into ramp deposition, characterised by wide spread lithologic units, such as the Middle Jurassic Dhurma Formation (Alsharhan & Magara, 1994). During the Middle Jurassic, intrashelf basins developed on the platform and harboured euxinic conditions, leading to deposition of laminated bituminous lime muds which later sourced the oil of the Upper Jurassic reservoirs (Alsharhan & Magara, 1994). The intrashelf basins were separated from the open marine by shallow grainy limestone facies (Alsharhan & Magara, 1994). Another major transgression marked the Callovian, causing the plate to become a shallow epeiric shelf differentiated with shallow basins and pushed the shore line further westward; meanwhile carbonates kept up with the rising sea level and deposited the shallow carbonate facies of the Arab Formation. This epeiric sea was shallow, overheated, vertically stratified and probably cut off from open water circulation of the Neo-Tethys and hence, it was nutrient deprived (Alsharhan & Sadooni, 2003; Leinfelder et al., 2005; G. T. Moore et al., 1992; Sellwood, Valdes & Price, 2000).

Finally, widespread Arab and Hith evaporites formed the cap rocks over the Jurassic reservoirs. Maturation of the source rocks and migration out of them occurred in the Palaeogene (Ayres et al., 1982, Murriss, 1980). This evolution of depositional environments resulted in the triplet of Tuwaiq Mountain and Hanifa source, Arab reservoirs and Hith seal, which comprises the world’s richest known oil accumulation (Alsharhan & Magara, 1994; see Figure 2.17).

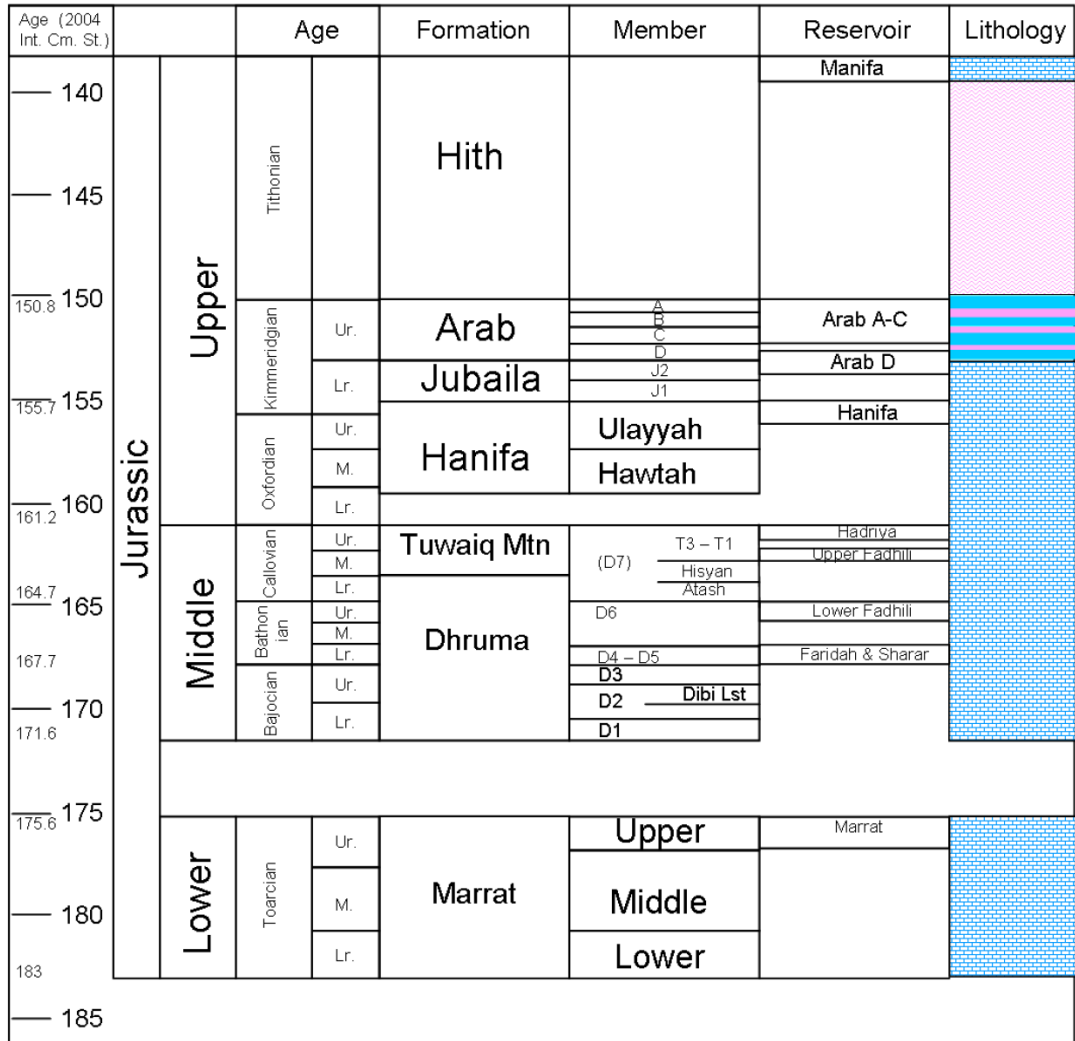


Figure 2.17: Jurassic reservoirs of Saudi Arabia.
Notes: In the lithology column, blue denotes carbonates and purple denotes anhydrites.
Source: Hughes (2009)

2.4.2 Early Jurassic Environments

A combination of a sea-level lowstand and tectonic uplift of the Arabian plate, associated with Mediterranean rifting, led to erosion and non-deposition of most of the Hettangian and Rhaetian age rocks (Haq et al., 1988; M. A. Ziegler, 2001). In

Saudi Arabia, the transition period between the Triassic and Jurassic witnessed the deposition of the upper Minjur Formation as mixed carbonates and shallow-marine shales and spillover sands, sourced from the Arabian Shield, (Figures 2.18 and 2.19) (M. A. Ziegler, 2001). The Early Jurassic witnessed subsidence of the Summan platform, which together with the northwestern passive margin created by the opening of the eastern Mediterranean led to an expansion in carbonate deposition as a vast shallow-marine shelf occupied most of the peninsula. As a result, the Marrat Formation, composed of carbonate to clastic sequences, was deposited (Énay, 1993; Le Nindre et al., 1987; Murris, 1980; Pollastro et al., 1999; M. A. Ziegler, 2001; see Figure 2.20). The climate continued to become more humid and in effect reduced evaporite deposition throughout the end of the Early Jurassic (Murris, 1980).

2.4.3 Middle Jurassic Environments

Ramp carbonates of coral-algal and bioclastic shallow lime sands dominated broad areas of the platform during the Middle Jurassic; and they are characterised by wide spread alternating units of peloidal and oolitic packstones and grainstones and argillaceous peloidal and bioclastic mudstones and wackestones (Alsharhan & Kendall, 1986). Eustatic sea-level rose in this period and the transgression pushed the shoreline to the west reducing clastic run-off, which came from the southwestern hinterlands (Figure 2.21) (M. A. Ziegler, 2001).

The sea-level rise also caused the continental margin that separated the platform from the Neo-Tethys to erode back westward (Figure 2.22). On nearshore areas, coastal sands were deposited and transitioned into shallow-marine shales and detrital carbonates (Figure 2.21). In Saudi Arabia, the Middle Jurassic Dhurma Formation contains the oil producing Fadhili reservoir, which is present in Fadhili, Khurais and Qatif fields (Alsharhan & Kendall, 1986; Powers et al., 1966; Steineke, Bramkamp & Sander, 1958; A. O. Wilson, 1985).

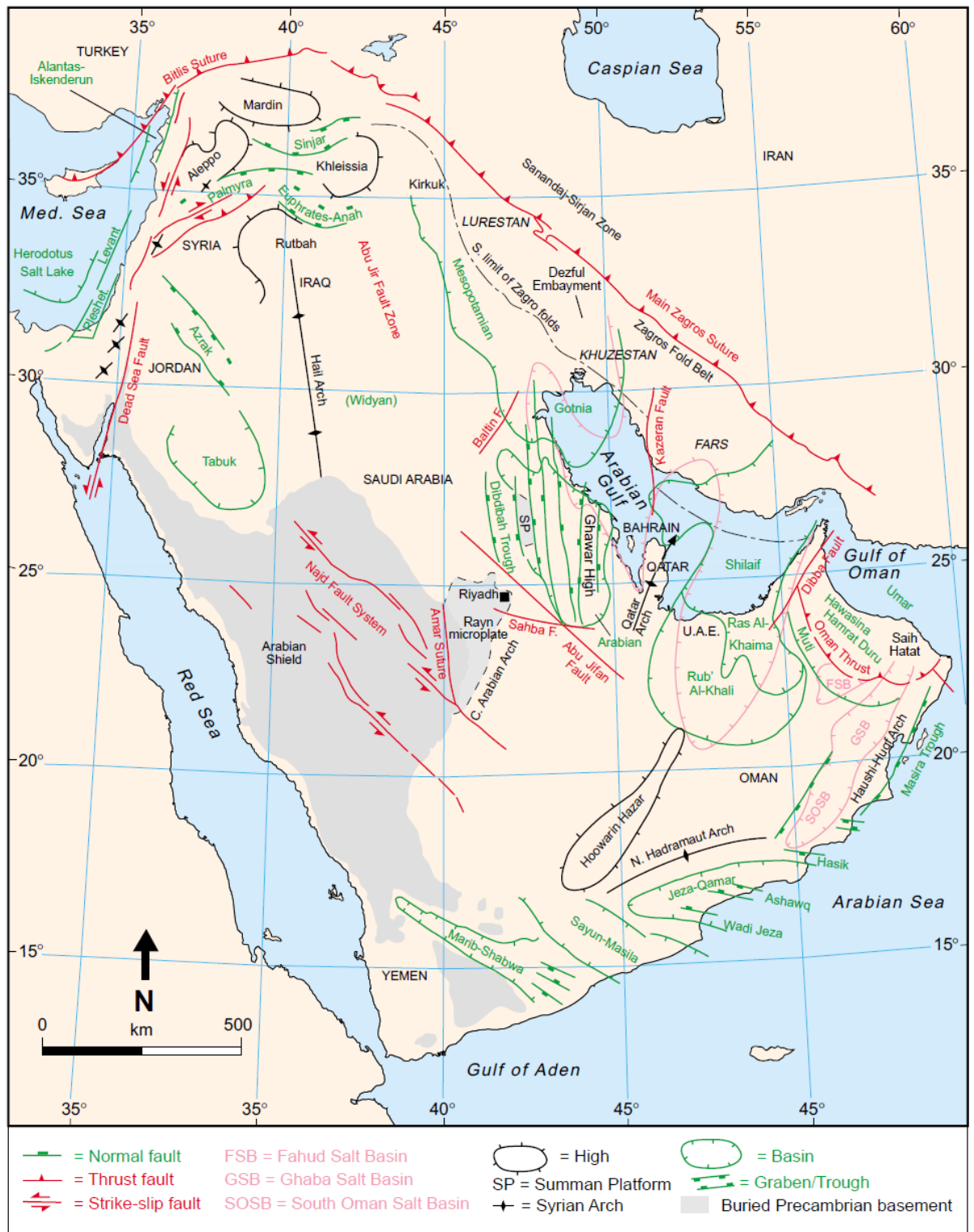


Figure 2.18: Structural map of the Arabian plate.
Source: M. A. Ziegler (2001)

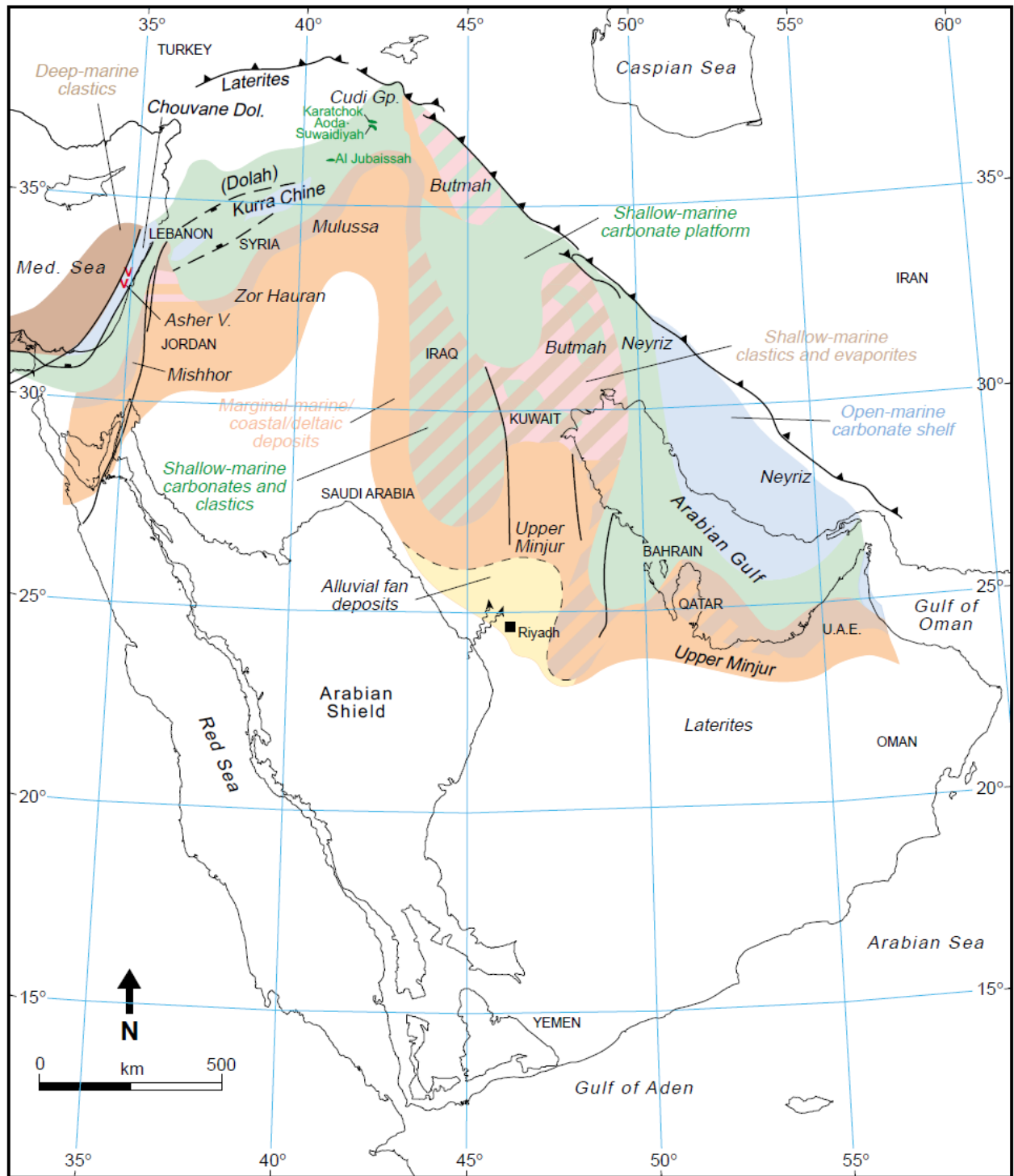


Figure 2.19: Triassic-to-Jurassic-Transition Palaeofacies.
Source: M. A. Ziegler (2001)

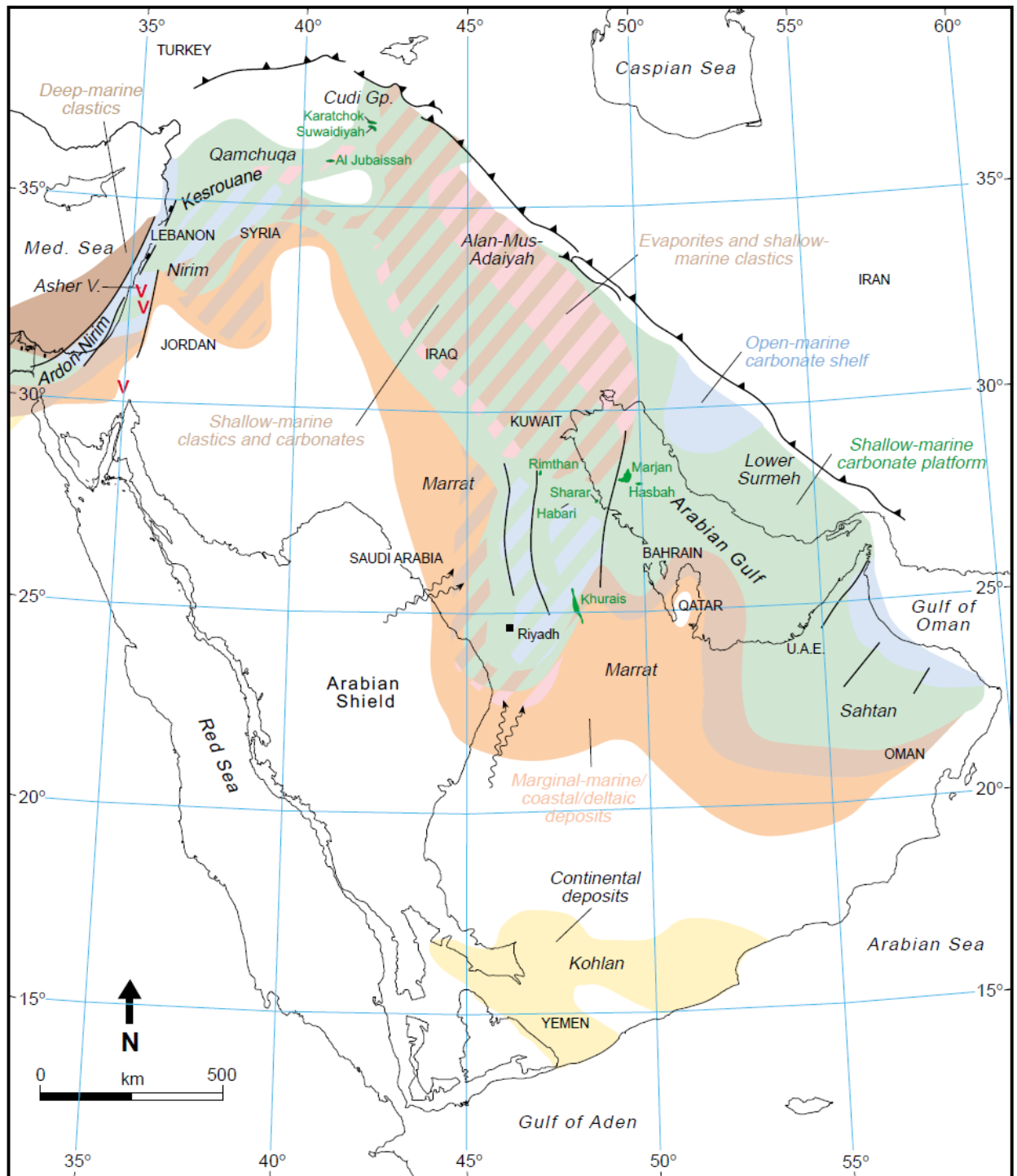


Figure 2.20: Early Jurassic Palaeofacies.
Source: M. A. Ziegler (2001)

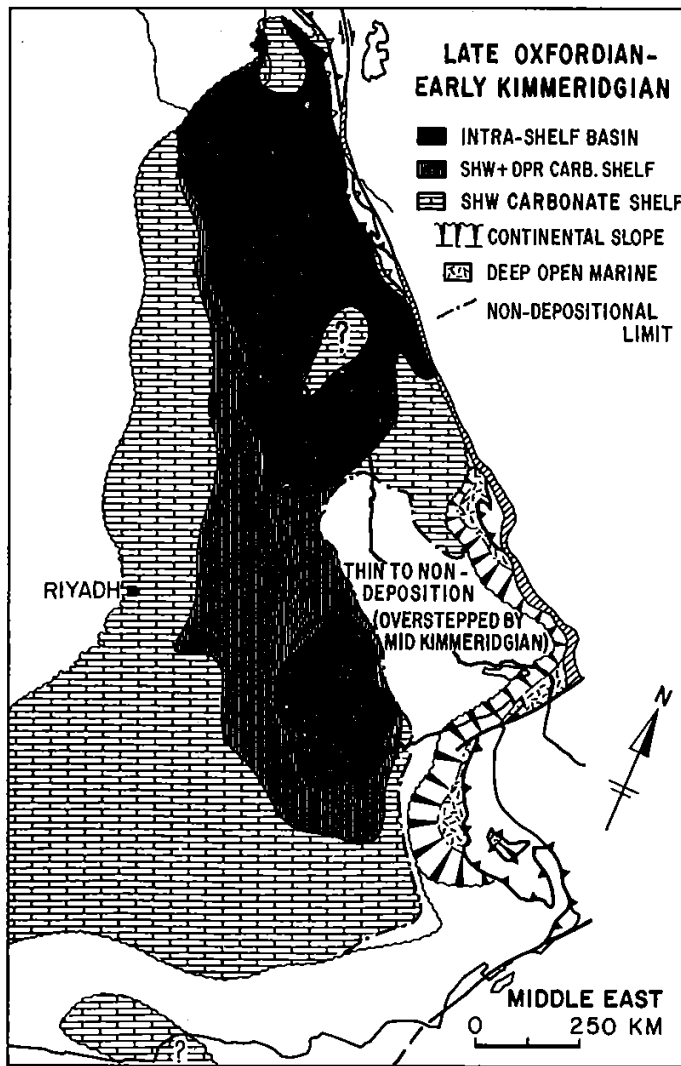


Figure 2.22: Environments of deposition from late Oxfordian to early Kimmeridgian.

Note the position of the continental slope on the eastern margin of the Arabian plate.

From the Middle Jurassic through the Late Cretaceous, development of intrashelf basins due to epeirogenic downwarp broke up the shallow carbonate continuum. These intrashelf basins are the Arabian and Gotnia basins, separated by the Rimthan Arch, Rub' Al-Khali and Ras Al Khaima basins (Figure 2.18) (Alsharhan & Kendall, 1986; Murriss, 1980; M. A. Ziegler, 2001).

Significant volumes of organic-rich anoxic shales and carbonates were deposited in the intrashelf basins contemporaneously with the sea-level rise and later sourced the oils of the Arab reservoirs (Ayres et al., 1982; Droste, 1990; M. A. Ziegler, 2001). These source rocks possess up to 3–5 wt. % organic content; are conspicuous on logs with high resistivity, low sonic velocity and high but variable gamma response; and are tight with 3–5 % porosity (Figures 2.23 and 2.24) (Ayres et al., 1982). The source rocks are composed mainly of thinly laminated peloidal carbonates where the organic matter is concentrated in dark 0.3–5 mm thick laminae. The fine peloids, horizontal burrows, flat and undulating laminations, coccoliths, ammonites, spicules, richness in organic matter and lateral continuity that characterise the

source rocks suggest a deep-water setting; yet some components such as miliolid and agglutinated foraminifera and accessory anhydrite suggest shallower water settings (Ayres et al., 1982). Still, richness in biocomponents suggests that bottom conditions were not toxic to various organisms (Ayres et al., 1982). Because the thickness of the source rock units is only slightly greater in the intrashelf basins compared to the shallow platform parts, Ayres et al. (1982) concluded that the difference between subsidence and deposition rates was little.

Amorphous organic matter in the source rocks suggests that algae may have grown as films covering the sediments at the seafloor of the intrashelf basins; in addition fungi and phytoplankton were probably present (Ayres et al., 1982). This restricts the ambiguous depth of the source rocks to be within the photic zone. High salinity within the intrashelf basins is indicated by development of discrete anhydrite laminae; the elevated salinity likely restrained flourishing of species and hence led to preservation of organic matter (Ayres et al., 1982). Kerogens of the source rocks are of Type II, sourced from cyanobacteria, and capable of generating large quantities of oil (Ayres et al., 1982). Based on carbon isotope ratios, the Callovian-Oxfordian source rocks are interpreted to have supplied the oils in the Arab, Hanifa, Hadriya and Fadhili reservoirs (Figure 2.17); this means that the oil migrated through 1000 ft (338 m) of vertical succession to reach the Arab reservoirs. Carbonates deposited on the shallow parts of the platform were probably able to keep up with sea-level rise, and in the process built shoals surrounding the intrashelf basins that sheltered them and kept them mostly calm (Ayres et al., 1982). The intrashelf basins formed antecedent palaeotopography that dictated the deposition of the subsequent Jubaila, Arab and Hith formations, which is manifested by the changes in lithofacies, thickness and composition of these formations over the basins (Lindsay et al., 2006; M. A. Ziegler, 2001). An unconformity caps the Callovian Tuwaiq Mountain Limestone and is overlapped by late Oxfordian shales of the base of Hanifa Formation (M. A. Ziegler, 2001). G. Wilson put the transition from ramp carbonates to shelf carbonates at the Tuwaiq Mountain Formation (see Alsharhan & Kendall, 1986, p. 997).

2.4.4 Late Jurassic Environments

Central Arabia remained stable during the Late Jurassic, and although sea-level kept rising throughout most of the period, shallow carbonates were deposited due to their ability to keep up with the rising sea-level (Murriss, 1980; M. A. Ziegler, 2001). Shales were deposited in place of the clastics that circumscribed the Arabian Shield, and continental rifting of Afro-Arabia and India created a passive margin to the southeast of the Arabian plate (Haq & Al-Qahtani, 2005; M. A. Ziegler, 2001; see Figure 2.25).

The shallow-water carbonates of the Hanifa Formation reflect deposition on the shelf, while its kerogenous micrites and shales reflect deposition in the relatively deep euxinic intrashelf basins (Ayres et al., 1982; Murriss, 1980). Overlying the Hanifa is the Jubaila Formation which comprises deeper water argillaceous carbonates that shoaled into the Arab-D shallow subtidal grainstones, which in turn shallowed up into supratidal sabkha anhydrites (Alsharhan & Kendall, 1986). The Arab-D Member and its capping anhydrite form the first of four Kimmeridgian-Tithonian shallowing-upward carbonate cycles each capped by anhydrites (Alsharhan & Kendall, 1986; Ayres et al., 1982; Powers, 1962). The grainy facies within these carbonates contain the Arab-A, -B, -C, and -D reservoirs in Saudi Arabia (Alsharhan & Kendall, 1986; Ayres et al., 1982; Powers, 1962; Steineke et al., 1958; M. A. Ziegler, 2001). The Arab and Hith formations' four shallowing-upward cycles are likely caused by eustasy due to their extensive distribution across the plate (Alsharhan & Magara, 1994). The Arab-D reservoir contains the largest oil accumulation amongst the Arab reservoirs, retains most of its original porosity due to minimal pore-filling diagenesis, and does not seem to be effected by early structural growth in Ghawar Field as its facies show only gradual changes in texture from crest to flanks (Ayres et al., 1982).

Shelf marginal carbonates of the Hanifa, Jubaila, Arab formations and Manifa Member prograded, downlapped and thinned or wedged out onto the Arabian and Rub' Al-Khali intrashelf basins transitioning into argillaceous deep-water deposits (M. A. Ziegler, 2001). Contrary to this notion, other workers proposed that the intrashelf basins were completely filled by the Kimmeridgian and interpreted the Arab-D to show a broad 'layer-cake' aggradation (Ayres et al., 1982; A. O. Wilson, 1985). Controversy also exists on the interpretation of the depositional environment of the Jubaila and Arab Formations. While Steineke et al. (1958) and Powers (1968) interpreted them as current- and wave-washed shoals in shallow

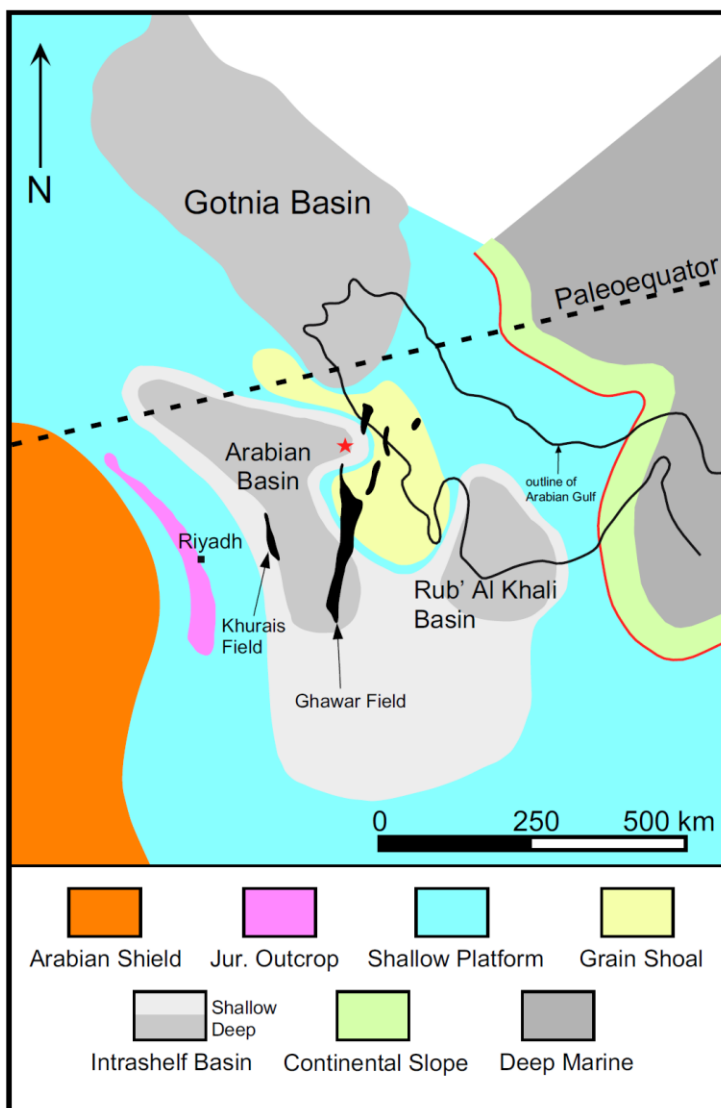


Figure 2.26: Suggested location of a grain shoal on the Rimthan Arch and suggested southward progradation from there into the Arabian basin.

Source: Handford et al. (2002)

water at wave base; G.

Wilson, cited in Alsharhan and Kendall (1986), interpreted them as shoaling-upward lagoonal to tidal-flat sequences (p. 998).

With respect to the progradational direction of the Arab-D reservoir, opinions also differ (Table 2.2). The reservoir has been suggested to prograde southward from the Rimthan Arch into the Arabian basin (Figure 2.26) (Handford et al., 2002; Handford, Keith, Mueller & Dommissse, 2003; Lindsay et al., 2006). A northward progradation has also been

suggested, interpreting the northern margin of the Arabian basin to be deeper than its southern one (Mitchell et al., 1988). A westward progradation has been suggested based on hypothesizing a reef barrier in the Zagros area from which carbonate prograded to the Arabian basin (Al-Saad and Sadooni, 2001). An eastward progradation direction has been suggested from the western hinterlands to the Arabian basin (Al-Awwad & Collins, 2013a, b; Meyer & Price, 1993). Chapter 5 of this thesis presents ample and detailed evidence that the progradation happened from west to east.

Table 2.2: Suggested Arab-D reservoir progradation directions.

Suggested Progradation	Comments	Author
Southward	From the Rimtham Arch situated north of the Arabian basin	Handford et al., (2002; 003) and Lindsay et al., (2006)
Northward	Interpreting the northern margin of the Arabian basin to be deeper than its southern one	Mitchell et al., (1988)
Westward	Based on a hypothetical reef barrier in the Zagros area	Al-Saad and Sadooni (2001)
Eastward	From the western hinterlands to the Arabian basin	Al-Awwad & Collins (2013a, b) and Meyer & Price (1993)

Aridity increase in the Tithonian led to expansive evaporite deposition across the platform and the intrashelf basins making the ultimate seals over the world's richest oil reservoirs (Alsharhan & Kendall, 1986; Ayres et al., 1982; Murriss, 1980; Powers, 1968).

The Hith Formation anhydrite is 180 m thick west of Abu Dhabi; is thickest over the Arabian intrashelf basin, and thins over the Gotnia intrashelf basin where it is overlain by organic-rich, argillaceous, thinly bedded micrites interpreted to have formed due to continuous subsidence of the Gotnia basin (M. A. Ziegler, 2001). Marine replenishment from the Neo-Tethys to the intrashelf basins has been interpreted to have come from the north (M. A. Ziegler, 2001) or from the east (Al-Husseini, 1997). The extent of the spread of the Hith anhydrite is shown by the dash line in Figure 2.25 (M. A. Ziegler, 2001). The top of the Hith Formation comprises a

porous oil-bearing unit, the Manifa reservoir, which produces in the Manifa Field in Saudi Arabia (Powers, 1968). The Manifa reservoir was interpreted by G. Wilson to reflect the beginning of the Early Cretaceous transgressions (as cited in Alsharhan & Kendall, 1986, p. 998). Late Tithonian hiatus surfaces that reflect sea-level lowstand are conspicuous on the Summan Platform as described in Rimthan Field (M. A. Ziegler, 1982). At the end of the Rayazanian or end Portlandian continental uplift caused a major sequence boundary marked by a 1000 m thick pervasive near-subaerial diagenetic dolomitisation event on the Fuwaris trend (an anticlinal structure located between Kuwait and Saudi Arabia; M. A. Ziegler, 2001). The Early Cretaceous witnessed a gradual increase in humidity associated with the disappearance of evaporites. This coincided with a sea-level drop that led to ramp carbonate deposition, which was followed by increased clastic influx (Murriss, 1980).

The Arabian plate oil habitats aggregate in these intrashelf basins because the source, reservoir, seal and closure conditions align well over them (Lindsay et al., 2006; M. A. Ziegler, 2001). What makes the Arabian plate oil habitats exceptional is not their vertical extent, which is average, but rather their horizontal extent. The platform was 2000 to 3000 km wide and 4000–6000 km long in the Mesozoic and marked by extensive and continuous lithologic units that facilitated horizontal migration of hydrocarbons (Murriss, 1980). This advantageously coalesced with the broad gently-dipping- and hence less susceptible to fracturing- structures that characterised the plate. These structures are effective in draining large areas of source rocks and can have more than 1000 square kilometre of closure (Murriss, 1980).

2.5 Facies Depositional Models

Past studies of the Arab-D reservoir in Saudi Arabia primarily focused on Ghawar Field and different depositional models were conceived. Mitchell et al. (1988) divided the Arab-D carbonates into micritic limestones and dolomites, bivalve-coated grain-intraclast limestones, stromatoporoid-red algae-coral limestones, *Cladocoropsis* limestones and dolomites, skeletal-oolitic limestones and dolomites,

sealing anhydrite and diagenetic dolomite. Lindsay et al. (2006) used the same classification scheme of Mitchell et al. (1988) and characteristics of these classified lithofacies are summarised in Table 2.3 (Lindsay et al., 2006). Meyer and Price (1993) slightly modified Mitchell et al.'s (1988) lithofacies and listed the following types: micritic, bivalve-coated grain-intraclast, Stromatoporoid, burrowed skeletal-peloidal, *Cladocoropsis*, fragmented *Cladocoropsis*, foraminiferal, mixed skeletal-peloidal, oolite and anhydrite. Handford et al. (2002) modified Mitchell et al.'s (1988) classification scheme using Dunham's (1962) and Embry and Klovan's (1971) textures and listed the following lithofacies: lime mudstone-wackestone, burrowed skeletal-peloidal wackestone-packstone, intraclast rudstone and oncoid rudstone, coral stromatoporoid wackestone-packstone to boundstone and floatstone, burrowed to stratified *Cladocoropsis* wackestone grainstone and boundstone (bafflestone), stratified foram-peloid packstone-grainstone; ooid-coated-grain packstone and grainstone; evaporite association of peloidal-ostracod dolowackestone-packstone, gastropod dolopackstone and dolomudstone, palaeosol breccias and rooted wackestones and bedded nodular to massive anhydrite; characteristics of these lithofacies are summarised in Table 2.4 (Handford et al., 2002).

The analysis of the lithofacies of the same reservoir in Khurais Field is detailed in Chapter 3 of this thesis (Al-Awwad & Collins, 2013a). These facies in ascending order are skeletal wackestones and lime mudstones, skeletal-oncolitic-intraclastic mud-dominated packstones to floatstones, skeletal-pelletal wackestones to grain-dominated packstones, skeletal-stromatoporoid wackestones to floatstones, skeletal-peloidal-*Cladocoropsis* wackestones to floatstones, *Thaumatoporella-Clypeina* wackestones and mud-dominated packstones, skeletal-peloidal mud-dominated packstones to grainstones, skeletal-oolitic grainstones and grain-dominated packstone, oolitic-skeletal-cryptomicrobial laminated wackestones to grainstones, anhydrite and dolomite.

Table 2.3: Characteristics of the Arab-D reservoir lithofacies.
Source: Lindsay et al. (2006)

Lithofacies	Skeletal-Oolitic	<i>Cladocoropsis</i>	Stromatoporoid Red Algae-coral	Bivalve-coated grain-intraclast	Micritic	Dolomite
Depositional types	Grainstone, mud-lean packstone, packstone	Mud-lean packstone, grainstone, packstone,	Mud-lean packstone, grainstone, packstone, boundstone	Packstone, mud-lean packstone, grainstone, wackestone	Wackestone, mudstone, packstone	Indeterminate
Major Grain types	Micritized grains, foraminifera (including miliolids), dasycladacean algae, ooids, bivalves	Micritized grains, <i>Cladocoropsis</i> , dasycladacean algae, foraminifera (including miliolids)	Micritized grains, stromatoporoids, corals, foraminifera (including miliolids)	Micritized grains, bivalves, coated grains, intraclasts, foraminifera	Micritized grains, bivalves, foraminifera (including <i>kurnubia</i>), intraclasts	Anhedral to euhedral dolomite rhombs
Minor Grain types	Echinoderms, stromatoporoids, corals, <i>cladocoropsis</i> , gastropods, composite grains, intraclasts, ostracods, red algae, brachiopods	Stromatoporoids, echinoderms, bivalves, corals, ooids, gastropods, brachiopods, composite grains, red algae	<i>Cladocoropsis</i> , bivalves, echinoderms, dasycladacean algae, intraclasts, coated grains, composite grains, gastropods	Miliolid foraminifera, corals, stromatoporoids, dasycladacean algae, echinoderms, gastropods, <i>Cladocoropsis</i>	Coated grains, miliolid foraminifera, dasycladacean algae, intraclasts, ostracods, echinoderms, gastropods, stromatoporoids, corals	Relict and leached bivalves, <i>Cladocoropsis</i> , stromatoporoids, intraclasts, echinoderms, ind. grains
Sedimentary structures	Cross-bedding, burrows, hardgrounds, fining-upward graded beds, borings, horizontal laminae	Burrows, hardgrounds, cross-bedding, horizontal laminae	Burrows, borings, hardgrounds, fining-upward graded beds, cross-bedding	Burrows, hardgrounds, borings, fining-upward graded beds, cross-bedding	Burrows, hardgrounds, wavy laminae, horizontal laminae, borings, fining-upward graded beds,	Relict burrows?, hardgrounds?, carbonaceous? laminae
Pore types	Interparticle, moldic, intraparticle, intercrystalline, fracture	Interparticle, intraparticle, moldic, intercrystalline	Interparticle, moldic, intraparticle, intercrystalline, fracture	Interparticle, moldic, intraparticle, intercrystalline, fracture	Interparticle, (within burrow fills), intraparticle, moldic, intercrystalline, fracture, vug?	Intercrystalline, moldic, fracture
Diagenetic modification	Leaching and recrystallization, isopachous bladed calcite cement, dolomitization, physical compaction, stylolitization, equant calcite cement, kaolinite emplacement, anhydrite emplacement / replacement, silicification	Leaching and recrystallization, dolomitization, equant calcite cement, stylolitization, anhydrite emplacement, silicification	Leaching and recrystallization, dolomitization, anhydrite emplacement, stylolitization, isopachous bladed calcite cement, equant calcite cement, pyrite, dedolomitization	Leaching and recrystallization, dolomitization, stylolitization, equant calcite cement, anhydrite emplacement, isopachous bladed calcite cement, pyrite	Leaching and recrystallization, dolomitization, stylolitization, anhydrite Emplacement, pyrite, silicification, equant calcite cement, kaolinite	Dolomitization, leaching anhydrite emplacement, equant calcite cement, stylolitization, kaolinite dedolomitization
Distribution (zone)	1, 2A, 2B, 3A, 3B	2A, 2B	2A, 2B, 3A, 3B, Jubaila	2B, 3A, 3B, Jubaila	1, 2A, 2B, 3A, 3B, Jubaila	1, 2A, 2B, 3A

Table 2.4: Characteristics and environmental interpretation of the Arab-D reservoir lithofacies.
Source: Handford et al. (2002)

Lithofacies	Grain Types	Sedimentary Structures	Depositional Processes and Environments
1. Lime mudstone-wackestone (varying dolomite content)	Absent to rare peloids, forams, echinoderms, spicules, bivalves, etc. Locally abundant calcispheres. Miliolids sometimes present.	Structureless, burrowed (<i>Thalassinoides</i> , <i>Chondrites</i>) to finely laminated. Capped by <i>Glossifungites</i> firmgrounds with <i>Thalassinoides</i> and mm-diameter <i>Trypanites?</i> , and possibly solution voids. Burrows filled with lithofacies 3 grains. Numerous, fungal hyphae at firmgrounds. Rare nodular bedding (few inches thick), stylolite seams. Tan to cream color except where nodular bedded (gray). Stylolites (horizontal and vertical)	Low-energy, oxygenated outer ramp setting. Water depths up to 100 ft. Some mud may also record tidal-channel-fill and overbank deposition. Fine laminae record rapid suspension settling from tidal flows or storm waves/currents. Muds also record normal background suspension settling. Firmground surfaces record submarine lithification and possibly starved sedimentation. Some surfaces may have been altered by subaerial exposure. Rare nodular bedding suggests slow sedimentation rates.
2. Burrowed, skeletal, peloidal wackestone-packstone (varying dolomite content)	Peloids, bivalves, rare intraclasts, echinoderms, and rare to abundant forams.	Abundant burrows (<i>Thalassinoides</i>), wispy or faint, horizontal to irregular, or partially bioturbated laminae with stylolites. Fining- and coarsening-upward units	Low- to moderate-energy, middle-ramp setting. Suspension settling of mud and <i>in-situ</i> production and deposition of mud and skeletal debris. Minor current/wave reworking during storms. Low to moderate energy. Dense burrowing. Aerobic bottom, muddy skeletal bank, low relief (<10 ft). Water depth 15–30 ft.
3. Intraclast rudstone and oncoid rudstone	Intraclasts and oncoids up to 5 cm in diameter, peloids or small intraclasts and micritized skeletal grains, brachiopods and bivalves, forams, oncoids, abraded corals and stromatoporoids, and echinoderms. Forams include <i>Textularia</i> , <i>Kurnubia</i> , and miliolids.	Sharp, basal contacts, mostly structureless to crudely bedded. Coarse-tail grading. Minor parallel laminae in upper part. Units usually fine upward into coarse packstones and eventually mudstone.	High-energy tidal channels, gravel sheet-lobes, and gravelly upper shoreface with water depths of 20–50 ft for intraclast rudstones. Storm processes and tidal flows dominant in channels. Wave processes dominant in upper shoreface, where oncolites were deposited in depths of < 20 ft.
4. Coral, stromatoporoid wackestone-packstone to boundstone (minor dolomite). Many rocks can also be classified as floatstones.	Bulbous, laminar, and encrusting stromatoporoids, corals, peloids, abundant forams, bivalves, echinoderms, and some <i>Cladocoropsis</i> .	Mostly burrowed with minor current and wave stratification. Stylolites	Open, well-circulated marine shelf 15–30 ft water depth). Muddy packstone and wackestone deposited below fair-weather wave base. Packstone and boundstone above fair-weather wave base. Formed sheets and local buildups (10–20 ft of relief).
5. Burrowed to stratified <i>Cladocoropsis</i> facies. Mud- to grain-dominated. Wackestone-grainstone and boundstone (bafflestone)	Whole or nearly whole to highly abraded and worn <i>Cladocoropsis</i> . Also peloids, forams, bivalves, corals, stromatoporoids, echinoderms, intraclasts	Burrows in and parallel stratification and cross-stratification. Fining- and coarsening-upward units.	Open, well-circulated marine shelf. Accumulation at or just below fair-weather wave base for muddy packstones (15–25 ft water depth) and upper shoreface to foreshore (0–15 ft) for highly abraded packstones and grainstones. Deposited generally shelfward of stromatoporoid facies, in prograding banks.
6. Stratified foram, peloid packstone-grainstone (minor dolomite)	Peloids, abundant forams, intraclasts, bivalves, and echinoderms.	Minor burrowing (<i>Ophiomorpha</i>), parallel stratification and cross stratification. Hardground surfaces. Fining- and coarsening-upward units.	Relatively high energy, current- or wave-generated structures. Mobile substrate except where hardgrounds formed. Lower energy where burrowed. Very shallow subtidal to intertidal zone. 0–10 ft water depth.

continued on next page

7. Ooid, coated-grain packstone and grainstone (fabric-preserving dolomite)	Ooids, coated grains, forams, intraclasts, bivalves, gastropods.	Commonly structureless or burrowed. Also parallel stratification and cross-stratification. Hardground surfaces are common.	Relatively high-energy, current- and wave-generated structures. Mobile substrate. Small grain shoals located in very shallow subtidal to intertidal zone. 0-10 ft water depth.
8. Evaporite association of peloidal, ostracod dolowackestone-packstone, gastropod dolopackstone, and dolomudstone (commonly dolomitized)	Peloids, ostracods, gastropods, intraclasts, and minor forams	Structureless or wispy bedded to thin, parallel laminae, including some algal laminae. Rare hemispheroids.	Moderately low-energy with minor wave/current activity for grain-supported carbonates. Suspension settling for mudstone. Highly restrictive, hypersaline environment. Shallow subtidal to intertidal. Pond-like environment associated with evaporite salina. 0–5 ft water depth
9. Paleosol breccias and rooted wackestones	Intraclasts and breccia clasts, and peloids	Laminae, sediment- and cement-filled vugs, small rootlets.	Subaerial exposure and pedogenic alteration. Above sea-level.
10. Bedded nodular to massive anhydrite	None	Discrete, isolated nodules surrounded by dolomite or packed nodules separated by thin partings. Vague laminae and dolomitic layers separate nodular beds. Some intervals contain vertically elongate nodules.	Subaqueous precipitation and displacive growth in evaporite salina. 0–10 ft water depth.

The stratigraphic hierarchy of the recognised lithofacies of the Arab-D reservoir reflect an overall upward-shallowing succession caused by high frequency eustatic changes. The interpretation by Mitchell et al. (1988) of the depositional environments starts at the bottom of the succession with low energy micrites, followed upsection by possible storm deposited intraclasts; these shallow up to stromatoporoid buildups or mounds, which shallow to low energy *Cladocoropsis* lagoon facies; these are overlain by subtidal to intertidal oolitic shoals and tidal deltas that shallow up into sabkha anhydrites followed by subaqueous anhydrites. Meyer and Price (1993) and Meyer et al. (1996b) interpreted the reservoir lithofacies to reflect a ramp (Figure 2.27) that spans the following depositional environments in ascending order: turbidites comprised of rhythmic micrites and Intraclastic rudstones, stromatoporoid and *Cladocoropsis* ‘thicket’, beach complex with shoreface oolitic and peloidal sands and backshore skeletal-peloidal sands that shallow up into evaporitic flat anhydrites.

The Handford et al. (2002) depositional model is shown in Figure 2.28 and it interprets the reservoir as a ramp where grain shoals formed on the Rimthan Arch to the northwest of the Arabian intrashelf basin and prograded southeast laying down the reservoir grainy facies over the position of Ghawar Field (Figure 2.26).

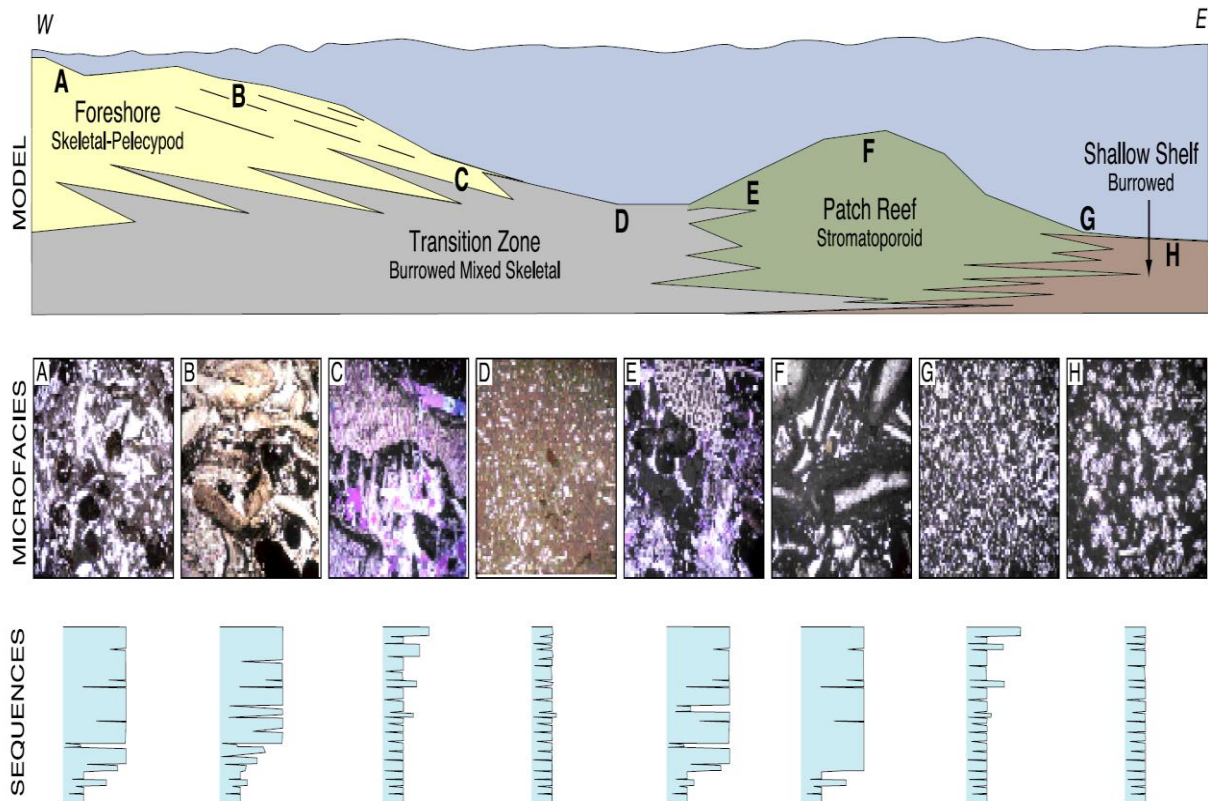


Figure 2.27: Schematic depositional model of the Arab-D reservoir, interpreting it as a ramp complex with a stromatoporoid patch reef.

Note: Letters on the model designate respective positions of photomicrographs. Sequences show variance in grain size.

Source: Meyer et al. (1996)

They interpret the lime mudstones as oxygenated outer ramp deposits that shallow up to middle-ramp wackestones and packstones. The Intraclastic rudstones are interpreted as tidal channel splays overlain by stromatoporoid biostromes and low-relief buildups that shallow into *Cladocoropsis* shoals. These in turn are overlain by shallow subtidal to intertidal peloidal shoals that shallow up into high-energy oolitic shoals and ultimately into salina evaporites (Handford et al., 2002).

The Lindsay et al. (2006) depositional model is shown in Figure 2.29; and it distributes the reservoir's lithofacies into the following ascending environments: outer ramp with sub-storm-effect micrites, distal middle ramp with sub-fair-weather-wave-base storm derived rudstones and floatstones, proximal middle ramp with stromatoporoid biostromes and mounds and sheltered *Cladocoropsis* within intermound areas, very shallow subtidal to intertidal ramp crest oolitic and peloidal shoals, inner ramp lagoon protected by a grain shoal and comprised of wackestones

to grainstones, inner ramp tidal flat, and finally salina.

Based on biotic components detected in outcrop, Ghawar and Khurais fields, Hughes (2004 b; 2009) interpreted the palaeoenvironment of the Arab-D to be a deep lagoon with normal salinity setting characterized by the presence of *Kurnubia palastiniensis*, *Nautiloculina oolithica*, laminated stromatoporoids, *Cladocoropsis mirabilis*, *Clypeina sulcata* and *Thaumatoporella parvovesiculifer*. These shallowed up into shallower lagoon subtidal setting marked by “*Pfenderina salernitana*”, *Mangashtia viennoti*, *Trocholina alpina* and undifferentiated simple miliolids. Finally, a hypersaline, intertidal environment is inferred from the presence of undifferentiated simple miliolids, costate, cerithid-like gastropods, bivalve and brachiopod debris, and algal laminae (Figure 2.30; Hughes, 2004 b).

Chapter 3 lays out ample discussion of what the lithofacies analysis in Khurais field implies with respect to the depositional environments, spells out points of agreement and disagreement with the above authors and others, and concludes a depositional model of the reservoir shown in Figure 3.9, Chapter 3 (Al-Awwad & Collins, 2013a). Our depositional model is of a prograding, gently sloping, arid, shallow, reef-rimmed carbonate shelf, which was subjected to frequent storm ‘shaving’ that triggered turbidity avalanches. The shallow epeiric shelf carbonates and evaporites prograded into the relatively deep, Late Jurassic Arabian intrashelf basin. In ascending order the depositional environments reflected by the reservoir lithofacies are offshore submarine turbidite fans comprised of interbedded intraclastic rudstones and lime mudstones that either draped the turbidites and/or transgressed over them as pelagic rain, followed shoreward by lower shoreface pelletal sands and silts deposited at or near the fair-weather-wave-base (FWWB). These shallowed up into a rim densely populated by small-scale stromatopore reefs that protected, shoreward of it, a *Cladocoropsis* and dasycladacean algae lagoon. Shoreward of these laid shallow subtidal peloidal and oolitic shore-attached sand sheets, followed by supratidal stromatolites and finally sabkha evaporitic flats and salina (Al-Awwad & Collins, 2013a).

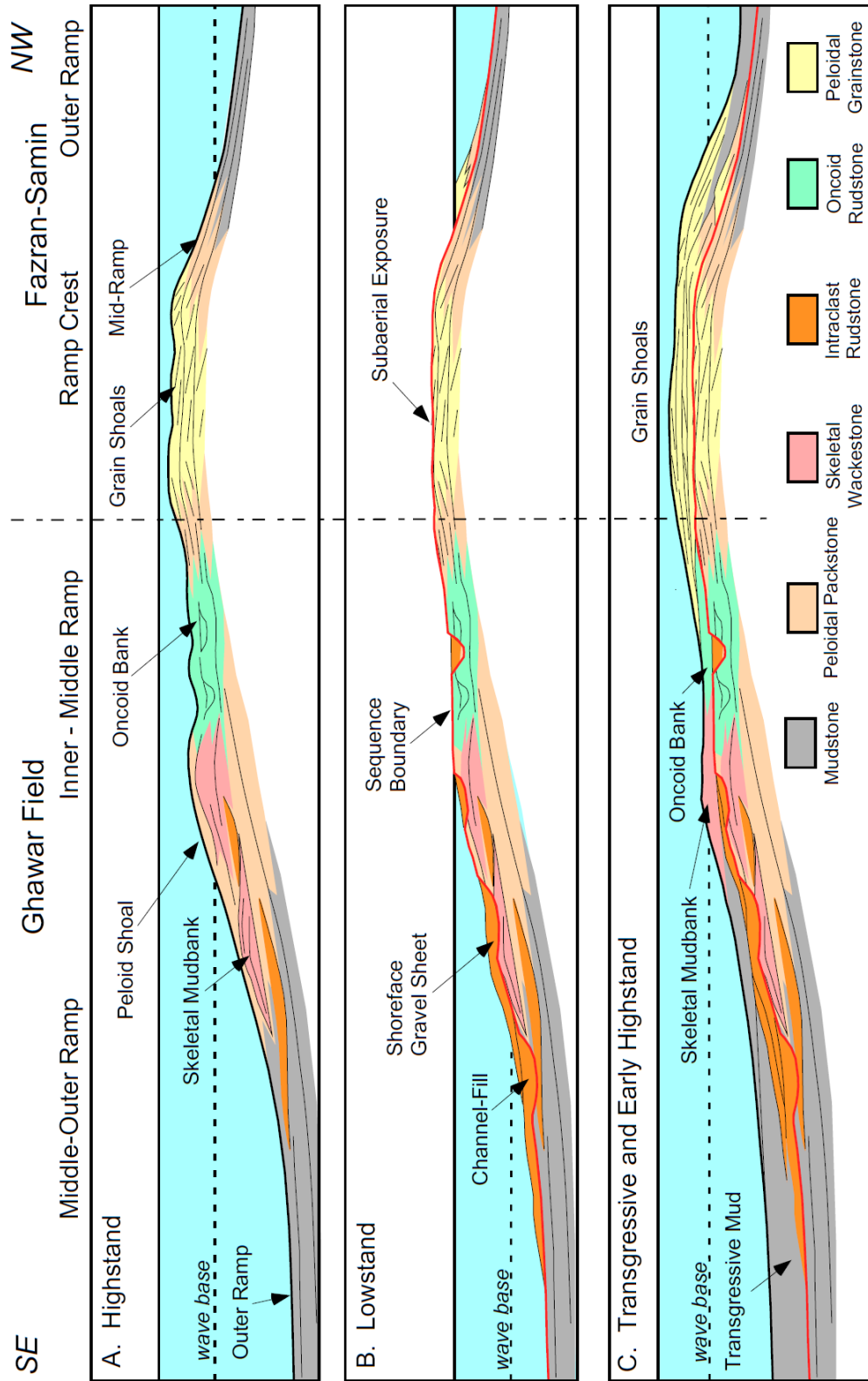


Figure 2.28: Schematic depositional model of the Arab-D reservoir interpreting a grainy shoal at Rimthan Arch flanked by ramps to the north and south.
 Source: Handford et al. (2002)

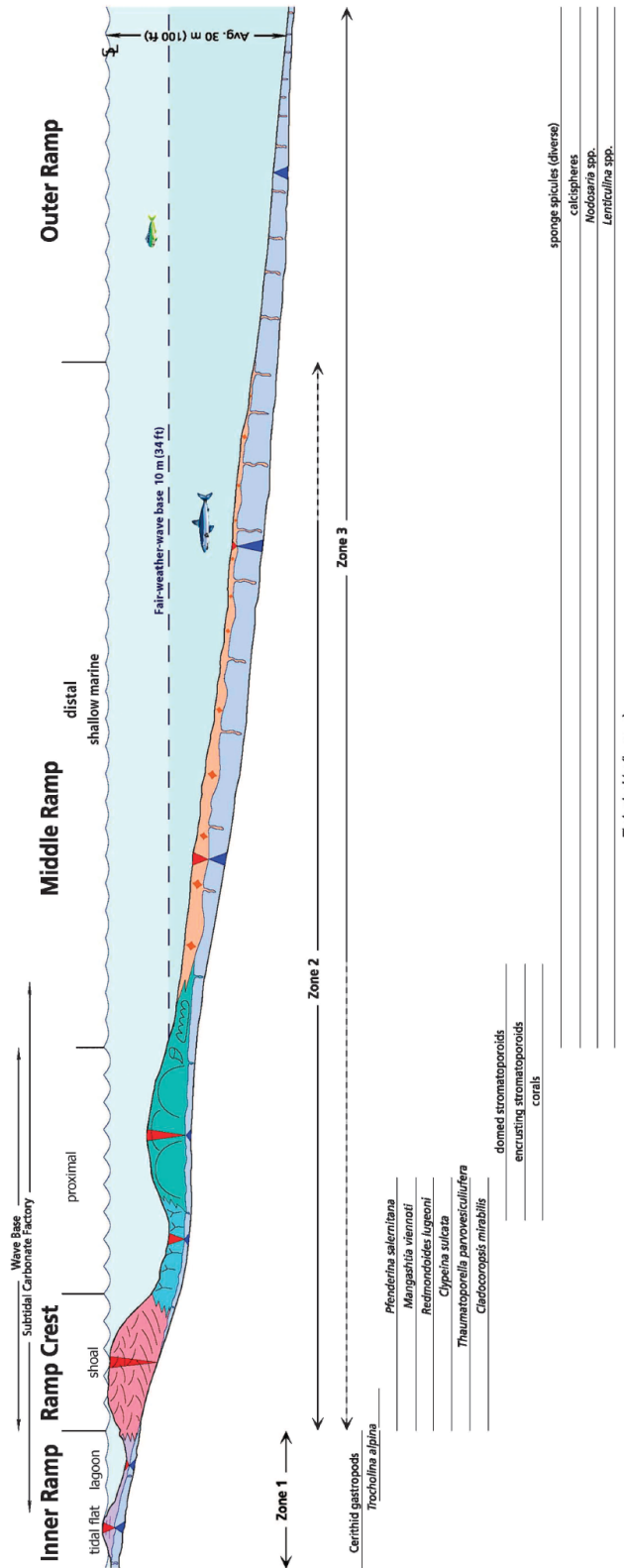


Figure 2.29: Depositional model of the Arab-D reservoir interpreting it as a ramp with a grain shoal (red) and a stromatoporoid biostromes (green). Source: Lindsay et al. (2006)

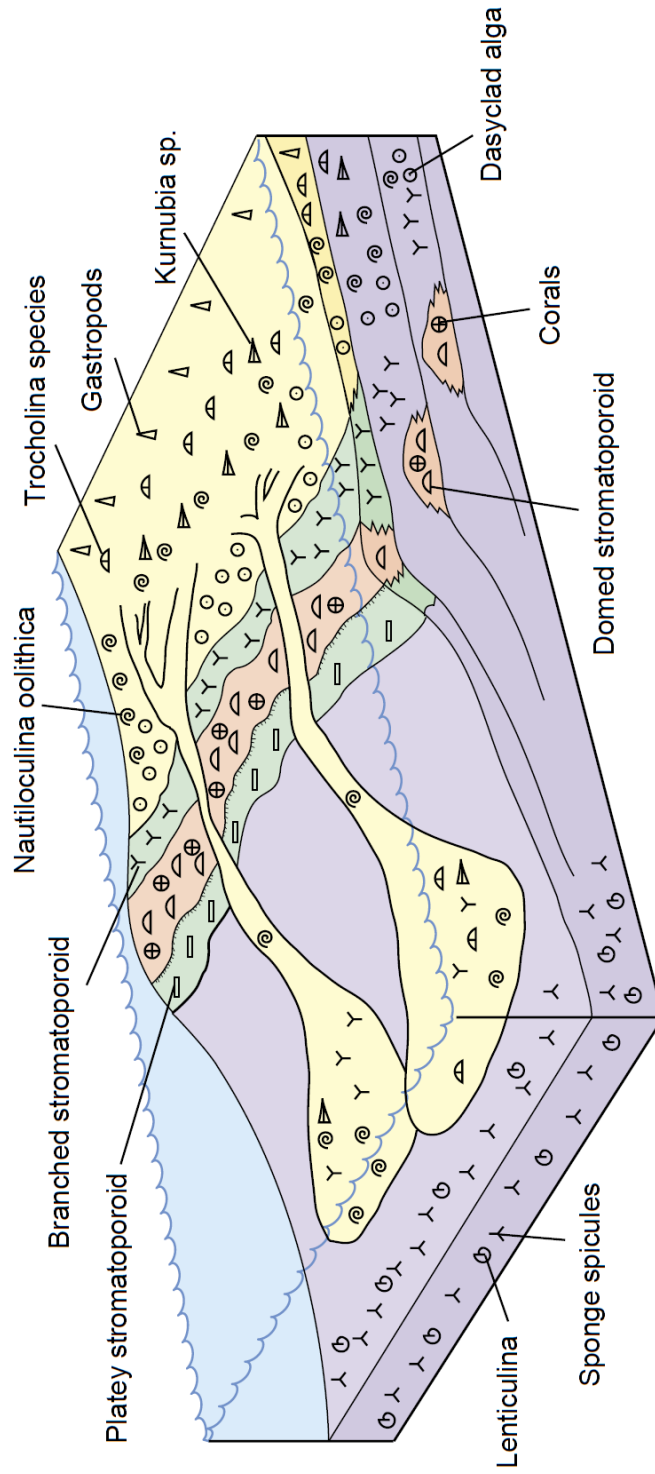


Figure 2.30: Schematic distribution of biocomponents from the Middle to Late Jurassic of Saudi Arabia.

Source: Hughes (2004 b)

2.6 Sequence-stratigraphic Hierarchy

Haq and Al-Qahtani (2005) listed major hiatuses that pervaded the Arabian platform succession. These were mentioned earlier in this chapter and briefly include a 25 Myr long Carboniferous hiatus, a 20 Myr long latest Triassic through Early Jurassic hiatus, an Eocene hiatus, a 10 Myr long Oligocene hiatus. Haq and Al-Qahtani (2005) also separated the Arabian Phanerozoic succession into periods of dominance of eustatic control over sedimentation and others of subordination as mentioned earlier (Figure 2.8). Using the genetic stratigraphic sequences sensu Galloway (1989), Sharland et al. (2001) divided the late Precambrian and Phanerozoic of the Arabian plate into 11 tectonostratigraphic megasequences (TMS); and identified, dated and correlated MFSs that extend across the plate and are likely eustatic in origin (Figure 2.31). Nevertheless, the Arabian platform succession suffers from incompleteness and significant inaccuracies, which led Al-Husseini and Matthews (2005a) to use an orbital-forcing model, the Arabian Orbital Stratigraphy Project (AROS), as an alternative to the biostratigraphic-radiometric time scale (Figure 2.32). They modelled 38 second-order sequences and correlated 34 of them, mostly by stratigraphic positioning, to Arabian regional stratigraphic discontinuities. Each of the modelled second-order sequences (DS^2) spans for 14.58 Myr, and comprise six third-order sequences (DS^3) of 2.43 ± 0.405 Myr, which in turn are each composed of six fourth-order sequences (DS^4) of 0.405 Myr (Al-Husseini & Matthews, 2005a).

The following is a brief description of the lithologies, geological time scale (GTS 2004) (Gradstein et al., 2004) dates and AROS (Al-Husseini & Matthews, 2008) dates of the key formations and members of the Jurassic Shaqra' Group of Saudi Arabia (Figure 2.33).

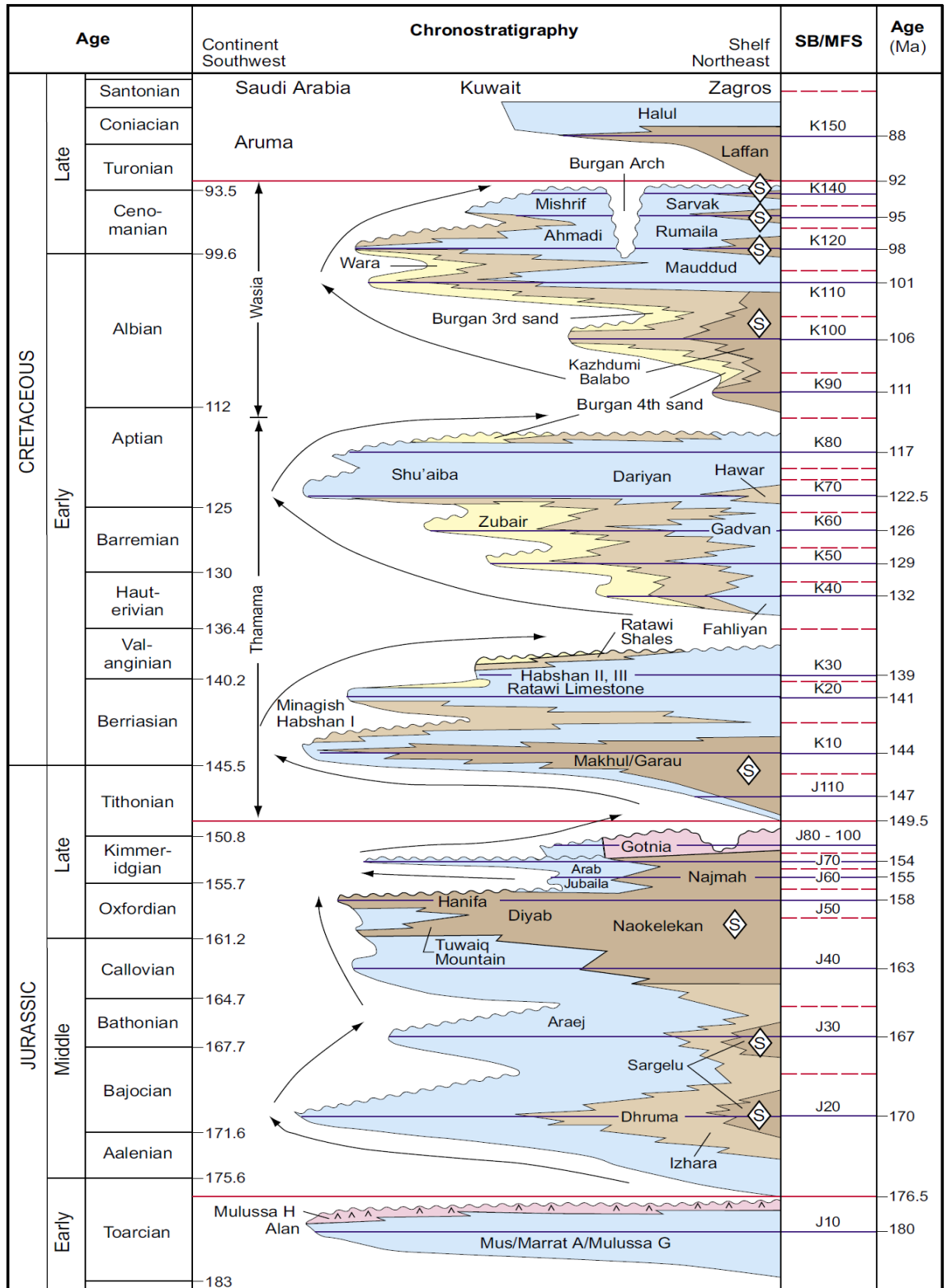


Figure 2.31: Jurassic-Cretaceous schematic chronostratigraphic chart.
 Source: Sharland et al. (2001) and Haq and Al-Qahtani (2005)

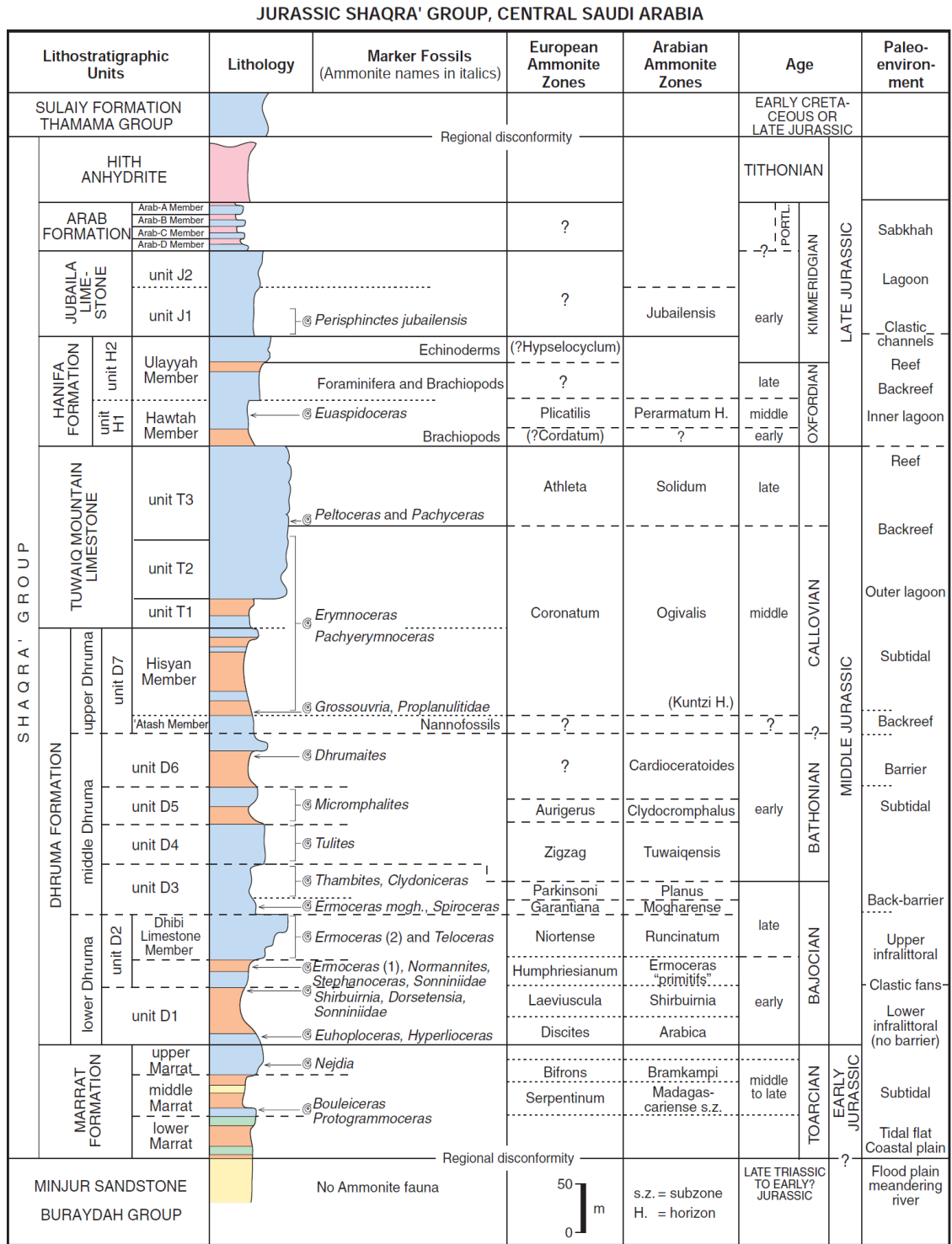


Figure 2.33: Lithostratigraphic column from the Upper Triassic to Early Cretaceous in central Saudi Arabia.

Source: Haq and Al-Qahtani (2005)

2.6.1 Early and Middle Jurassic of Saudi Arabia

2.6.1.1. *Minjur Sandstone*

The Late Triassic Minjur sandstone has been interpreted to comprise two fining upward sequences, the lower of which is *ca.* 137 m thick, beginning with cross-bedded gravel and ending with medium-grained, well-bedded sandstone. The upper sequence is *ca.* 90 m thick, starting with conglomeratic sand and grading up into medium-to-fine sandstone. These sequences are correlated to AROS's modelled sequence DS³ 14.1 and 14.2, and dated between 205.6 and 200.8 Myr (Al-Husseini, 2009). The Triassic-Jurassic boundary is placed in GTS 2004 at 199.6 ± 0.6 Myr (Figure 2.32).

2.6.1.2. *Marrat Formation*

The Early Jurassic (Toarcian) Marrat Formation lies unconformably over the Minjur Sandstone and is composed in outcrop of 126 m of mostly limestone in addition to shale and sandstone (Manivit et al., 1985). The Marrat Formation has been divided into three members; the lower two compose a sequence and the upper one composes a separate sequence (Al-Husseini, 2009). In AROS, these sequences have been correlated to DS³ 13.5 and 13.6, dated between 181.3 and 176.5 Myr. In GTS 2004, Marrat deposition is placed between 183.0 ± 1.5 and 175.6 ± 2.0 Myr (Al-Husseini, 2009).

2.6.1.3. *Dhruma Formation*

The Middle Jurassic (Bajocian to Callovian) Dhruma Formation unconformably overlies the Marrat Formation. It is 447 m thick in outcrop and comprises siliciclastics, carbonates and claystones. Dhruma members have been correlated to AROS's modelled sequence DS³ 12.3, 12.4 and 12.5 dated by AROS between 171.6 and 164.3 Myr, and by GTS 2004 at 171.6 ± 3.0 and 162.5 Myr (Al-Husseini, 2009).

2.6.1.4. *Tuwaiq Mountain Limestone*

The Middle Jurassic (middle to upper Callovian) Tuwaiq Mountain Limestone lies unconformably over Dhurma rocks and is overlain by another unconformity that precedes the Hanifa Formation. It is 203 m thick in outcrop and composed of calcarenitic limestone and marls, which transition up into coral-bearing limestone. It has been correlated to modelled sequences 12.5 and 12.6 spanning between 166.7 and 161.9 Myr in AROS and between 166.3 to 161.2 Myr in GTS 2004 (Al-Husseini, 2009).

2.6.2 Late Jurassic

Al-Husseini and Matthews (2005a, 2008) found that the Late Jurassic, except for the late Tithonian, represents a complete, modelled second-order sequence, DS² 11, which consists of the Hanifa, Jubaila, Arab Formations and the Hith Anhydrite beneath the Manifa reservoir and spans *ca.* 14.6 Myr. The lower sequence boundary of DS² 11 implies the Callovian-Oxfordian polar glaciations, while the upper one implies the Tithonian glaciations (Al-Husseini, 2009; Dromart et al., 2003; Palike et al., 2006). The modelled DS² 11 has been divided into six third-order modelled sequences, referred to as DS³ 11.1 to of DS³ 11.6 (Al-Husseini, 2009; Al-Husseini & Matthews, 2005b, 2008).

2.6.2.1. *The Early Oxfordian Pre-Hanifa Sequence Boundary*

The Hanifa-Tuwaiq Mountain Boundary (Figure 2.32) in outcrop has been placed by Powers (1968) at the disconformable contact between coral-bearing limestone and calcareous shale. This outcrop boundary correlates with the pre-Hanifa unconformity in the subsurface (Al-Husseini & Matthews, 2005b); has been dated as early Oxfordian, 161.2 ± 4.0 Myr (Fischer et al., 2001); and extends for *ca.* 1,000 km (Al-Husseini & Matthews, 2005a).

2.6.2.2. Hanifa Formation

In outcrop, the Hanifa Formation is 113.3 to 180 m thick, composed of lower shales, that form part of the Jurassic source rocks, and upper limestones, which form the Hanifa reservoir (Al-Husseini, 1997). The Hanifa Formation is dated as middle Oxfordian and early Kimmeridgian (Énay, Le Nindre, Mangold, Manivit & Vaslet, 1987; Vaslet et al., 1991), and has been divided into two members, the lower Hawtah and the upper Ulayyah (Vaslet et al., 1991).

2.6.2.2.1. Hawtah Member

The 66 m thick, lower and middle Oxfordian Hawtah Member forms a 3rd order sequence (Al-Husseini, 2009; Al-Husseini, Matthews & Mattner, 2006; Hughes et al., 2008; Mattner & Al-Husseini, 2002; Vaslet et al., 1991). Sharland et al. (2001) placed a lower Oxfordian, 159.0 Myr, 'MFS J50' in the Hawtah Member (Al-Husseini, 2007; Simmons, Sharland, Casey, Davies & Sutcliffe, 2007). Al-Husseini et al. (2006) correlated the Hawtah sequence to 'DS³ 11.1' with a depositional age of 161.9–159.9 Myr, and dated its MFS as 160.9 Myr.

2.6.2.2.2. Ulayyah Member

The 74 m thick, late Oxfordian to possibly early Kimmeridgian, Ulayyah Member is a third-order sequence (Al-Husseini, 2009; Al-Husseini et al., 2006; Hughes et al., 2008; Mattner & Al-Husseini, 2002; Vaslet et al., 1991). Sharland et al. (2001) placed an upper Oxfordian, 155.25 Myr, 'MFS J60' in the Ulayyah (Simmons et al., 2007). Al-Husseini et al. (2006) correlated the Ulayyah Sequence to 'DS³ 11.2' with a depositional age of 159.9 to 157.0 Myr, and dated its MFS at *ca.* 158.4 Myr.

A late Oxfordian-Kimmeridgian and early Kimmeridgian, 1.5 Myr, hiatus separates the Hanifa from the overlying Jubaila Formations (Al-Husseini & Matthews, 2006; Énay et al., 1987; Vaslet et al., 1991). A disconformable contact between the uppermost Hanifa and the overlying, Jubaila Formation has been identified to be at

the contact between underlying oncolites and overlying reworked coral-bearing beds (Hughes, 2004; Meyer & Hughes, 2000; Meyer, Hughes & Al-Ghamdi, 2000).

The Jubaila and Arab formations are discussed in more detail in Chapter 4 and briefly mentioned below.

2.6.2.3. Jubaila Formation

In outcrop, the Jubaila is 130 m thick, and is composed of a lower part, named informally J1, of mudstones and intraclastic, peloidal packstones and wackestones, with multiple hardgrounds; and an upper part, named informally J2, that becomes increasingly rich in allocthonous sclerosponges and corals (Bramkamp & Steineke, 1952; Énay et al., 1987; Hughes, 2004b; Manivit et al., 1985; Meyer et al., 2000; Powers, 1968; Powers et al., 1966).

The Jubaila is dated as Kimmeridgian based on nautiloids *Paracenoceras wepferi* and *P. ex gr. moreausum* (Tintant, 1987) and endemic ammonites *Perisphinctes jubailensis* (Al-Husseini, 2009; Arkell, 1952; Énay et al., 1987; Fischer et al., 2001; Hughes, 2004b, 2006) and is interpreted as a discrete third-order transgressive-regressive sequence (Al-Husseini, 2009; Sharland et al., 2001). The Jurassic sea level (Haq et al., 1988) peaked in late Kimmeridgian and deposited the (*ca.* 152.25 Myr) 'MFS J70' within the Jubaila's lower unit, J1 (Al-Husseini, 2009; Sharland et al., 2001; Simmons et al., 2007). Al-Husseini (2009) correlated the Jubaila to AROS DS³ 11.3 sequence (Figure 2.32), which brackets it between 157.0 and 154.6 Myr, and puts the Jubaila MFS at *c.* 155.8 Myr (Al-Husseini, 2009).

2.6.2.4. Arab Formation

The Arab Formation is dominantly a highstand systems tract (HST) because global sea level was lowered after the deposition of the upper Jubaila (Sharland et al., 2001). The Arab Formation is about 54 m thick in outcrop, and around 100–180 m thick in the subsurface (Al-Husseini, 2009; Powers, 1968; Powers et al., 1966;

Steineke & Bramkamp, 1952; Steineke et al., 1958). The Arab Formation is Kimmeridgian to Tithonian based on microfaunal components (de Matos, 1995; Fischer, Manivit & Vaslet, 2001; Hughes, 1997, 2006; Hughes, Dhubeeb, Varol, Lindsay, & Mueller, (2004; Le Nindre et al., 1990).

2.6.2.4.1. Arab-D Member

The Arab-D Member contains a lower carbonate unit and an overlying anhydrite (Figures 2.32 and 2.33). The following benthic foraminifera have been detected in the Arab-D: *Alveosepta jaccardi*, *Kurnubia palastiniensis*, *Mangashtia viennoti*, *Trocholina palastiniensis*, *Everticyclammina hedbergi/virguliana*, *Nautiloculina oolithica* and *Pfenderina salernitana* and taken to indicate an undifferentiated Kimmeridgian age (Hughes, 2004 b; 2006; 2009; Hughes et al., 2004; Lindsay et al., 2006; Sharland et al., 2001). In the outcrop, the base of the Arab-D was mapped at the uppermost occurrence of stromatoporoids (Hughes et al., 2004 b). The Arab-D is recognised as a third-order sequence (Le Nindre et al., 1990), yet it does not have a regionally correlatable MFS (Sharland et al., 2001). Al-Husseini (2009) correlated the Arab-D to the modelled DS³ 11.4 sequence (Figure 2.32), which brackets it between 154.6 and 152.2 Myr, and put an Arab-D Member MFS at 153.4 Myr.

2.6.2.4.2. Arab-C and Arab-B Members

The early Kimmeridgian (Sharland et al., 2001) to Tithonian (Hughes, 2006) Arab-C and -B members are interpreted each as fourth-order sequences, as each member contains a carbonate unit and a sealing anhydrite above it. Both fourth-order sequences combine to make a third-order sequence. The regionally correlatable MFS J80 (151.75 Ma), MFS J90 (151.25 Ma) are located in the lower carbonates of Arab-C, and B respectively (Al-Husseini, 2009; Sharland et al., 2001).

AROS's modelled 3rd order sequence DS³ 11.5 (Figure 2.32) has been correlated to the Arab-C and B, which brackets them between 152.2 and 150.1 Myr, and puts the

main fourth-order MFS in the Arab-C carbonate at c.151.6 Myr, while the other fourth-order MFS of the Arab-B is put at *ca.* 150.8 Myr (Al-Husseini, 2009).

2.6.2.5. Arab-A Member and Hith Formation

The Main Hith Anhydrite (Figures 2.3 and 2.33) forms the regional caprock of the Arab reservoirs and combines with the Arab-A carbonate to make a 3rd order sequence (Al-Husseini, 2009). The Hith Formation has been dated by stratigraphic position only as Tithonian by Powers (1968). More recently however, it has been dated as early to mid-Tithonian based on strontium-isotope analysis by G. Grabowski (Al-Husseini, 2009; Al-Husseini & Matthews, 2005a). The Arab- A is dated as late Kimmeridgian by Sharland et al. (2001), while Hughes (2006) puts it as possibly Tithonian.

Sharland et al. (2001) placed the regionally correlatable MFS J100 (150.75 Myr) near the base of the Arab-A carbonate. Al-Husseini (2009) correlated the Arab-A and Main Hith Anhydrite sequence to AROS's 3rd order modelled sequence, DS³ 11.6 (Figure 2.32), which brackets them between 150.1 and 147.3 Myr, and puts a third-order MFS at *ca.* 148.5 Myr within the Hith. The regional MFS J100 was picked based on the model within the Arab-A carbonate at *ca.* 149.9 as a fourth-order MFS (Al-Husseini, 2009).

2.6.2.5.1. Manifa Member and Sulaiy-Hith Boundary

In Saudi Arabia, the second-order Jurassic-Cretaceous boundary is placed at the contact between the Hith and Sulaiy formations, which passes from brecciated limestones up to evenly bedded oolitic calcarenite in outcrop (Al-Husseini, 2009; Powers, 1968). This boundary has been dated by stratigraphic positioning only as Tithonian by Powers (1968), and Late Jurassic by Vaslet et al. (1991).

Sharland et al. (2001) positioned the regionally correlatable middle Tithonian MFS

J110 in the Manifa Reservoir with an age of 147.0 Myr, and considered the Manifa Member as the first third-order MFS above the Sulaiy/Hith second-order sequence boundary, which they dated at 149 Myr. Al-Husseini (2009) considered the Manifa Member to represent the first transgressive fourth-order sequence correlating its base to that of the modelled second-order sequence DS² 10, which he dated at 147.3 Myr. He estimated the age of the Manifa's MFS to be *ca.* 147.1 Myr (Al-Husseini, 2009).

2.6.3 Sequence Hierarchy of the Arab-D Reservoir

The overall shallowing-upward trend preserved in the stratigraphy of the Arab-D reservoir was caused by a long-term fall in base-level during the Late Jurassic (Handford et al., 2002; Haq & Al-Qahtani, 2005; Meyer & Price, 1993; Mitchell et al., 1988; Sharland et al., 2001) (Figure 2.8). This upward-shallowing trend is intermittent at multiple scales with cycles that are discussed in detail in chapter 4. The Arab-D Member of the Arab Formation is largely established in the literature as a discrete third-order composite sequence bound by a lower third-order composite sequence represented by the Jubaila Formation and an upper third-order composite sequence represented by the Arab-C and Arab-B Members (Al-Husseini, 2009; Le Nindre et al., 1990; McGuire et al., 1993; Sharland et al., 2001).

Powers et al. (1966) redefined time-stratigraphic units of the Arab-D, C and B so that the capping anhydrites are lumped with their underlying carbonates in the same sequences. Al-Husseini (1997, 2009) placed the Arab anhydrites and that of the Hith as late HST deposits, as the Arab carbonates as LST, TST and early HST deposits. Le Nindre et al. (1990) also interpreted the Arab members' anhydrites and that of the Hith as highstand deposits. McGuire et al. (1993) placed the anhydrites of the Arab members as lowstand wedges and transgressive system tracts, and the carbonates as highstand system tracts separating the two by a sequence boundary, which is supported by the findings of Lindsay et al. (2006).

In Chapter 4, evidence is documented from the Khurais cores studied that suggest that the upper sequence boundary of the Arab-D reservoir's composite sequence is at the transition between the sabkha and massive subaqueous anhydrites, as the latter represent a sea-level transition from a fall to a rise. In Chapter 4, two composite sequences are recognised; these are divided by a sequence boundary that separates the upper Jubaila Member from the overlying Arab-D Member, which agrees with Lindsay et al. (2006) and Mitchell et al. (1988). However, it disagrees with Meyer et al. (1996) and Meyer and Price (1993), who interpreted the reservoir as preserving one shallowing-upward genetic depositional sequence, and with Handford et al. (2002), who placed a composite sequence boundary within the Arab-D Member's carbonate. As mentioned earlier, in the Geologic Controversy section, the consequences of these stratigraphic interpretations are important for deciphering the reservoir's cyclicity, which would impact its correlation models and in turn its development strategies.

2.7 Implications: Regional and Local Correlations of the Reservoir

It has been proposed that the intrashelf basins that were scattered on the Arabian platform were completely filled by Kimmeridgian time and that the Arab-D reservoir represents a broad layer-cake aggradational trend (Ayres et al., 1982; A. O. Wilson, 1985; see Figure 2.34).

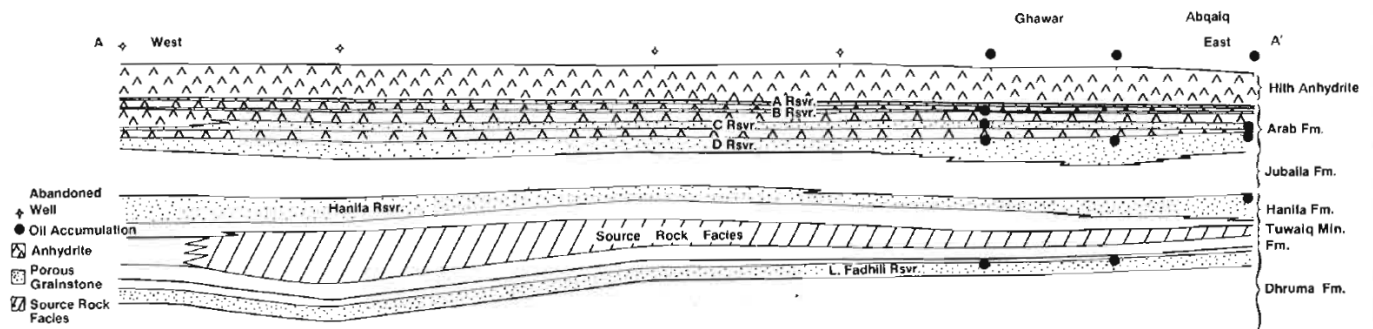


Figure 2.34: Schematic E–W section designating position of the Callovian and Oxfordian source rocks.

Source: Ayres et al. (1982)

Other workers, however, concluded that the reservoir's inherent upward-shallowing trend is manifested horizontally by a regional progradational trend, although disagreements over the direction of progradation exist (Figure 2.35). Mitchell et al. (1988) noted that the volume of the reservoir's grainstones in Ghawar Field diminishes southward, and that carbonates in general thin, while evaporites thicken in the same direction. Mitchell et al. (1988) and Meyer and Price (1993) interpreted these trends to manifest shallow-water carbonates and coeval sabkha evaporite progradation from the shallower, more restricted southern part of the basin to the deeper, more open northern part (Figure 2.36A). Conversely, Handford et al. (2002) interpreted the trend to reflect shallow carbonate progradation from the Rimtham arch, which framed the northern part of the Arabian intrashelf basin, to the deeper southern part of the basin where salina evaporites thicken as they consume the remainder of accommodation during the subsequent lowstand and transgression (Figure 2.36B). Lindsay et al. (2006) suggested that southward progradation happened in the southern 80 per cent of Ghawar Field, and northward in its northern 20 per cent. Stephens, Puls, Albotrous, Al-Ansi & Fahad

(2009) deduced that the Arab-D prograded to the north based on a stratigraphic study conducted on Dukhan Field in Qatar (Figure 2.37).

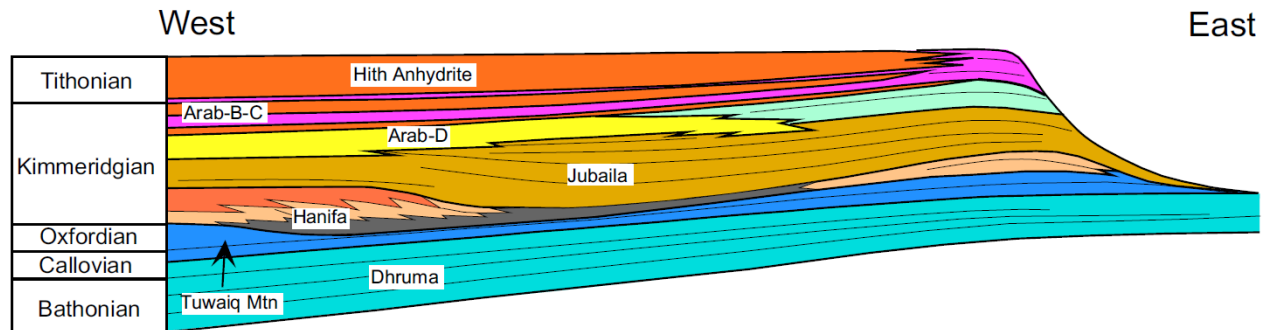


Figure 2.35: Murriss's (1980) E-W cross-section of the Middle-Upper Jurassic in the Arabian Gulf region.

Source: Handford et al. (2002)

It should be noted here that while some of the above conceptions are based on anhydrite thinning, it has been documented that a pinch out of the Arab-D carbonate and the top Arab-D anhydrite occurs to the east of Ruwais, which is located west of Abu Dhabi (Figure 2.38) (Al-Silwadi, Kirkham, Simmons, & Twombly, 1996; de Matos & Hulstrand, 1995; Simmons, 1994). Furthermore, and Peebles (1995) showed significant thinning and pinch out of the Hith Anhydrite and the Arab-C member in the area offshore of Abu Dhabi, from west to east (Figure 2.39).

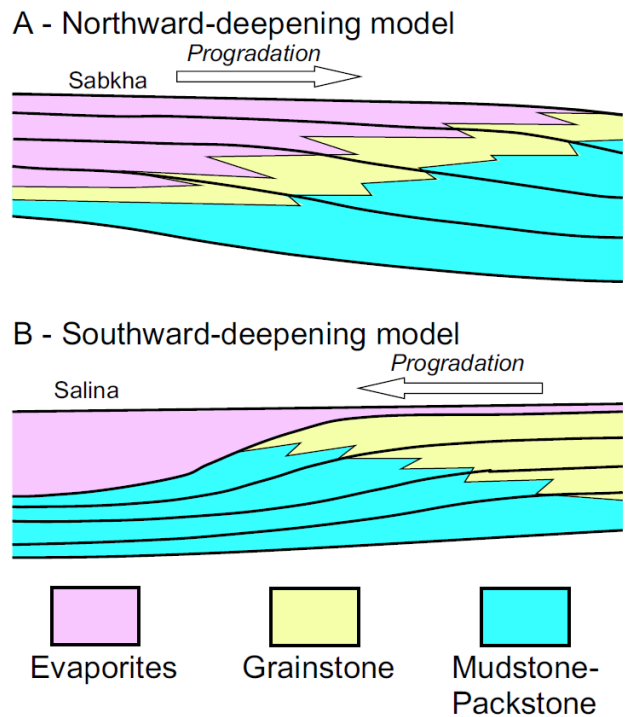


Figure 2.36: Suggested northward and southward progradation of the Arab-D reservoir.

Notes: (A) interprets the anhydrites as coeval sabkha deposits as per Mitchell et al., (1988); (B) interprets the anhydrites as subsequent salina deposits as per Handford et al. (2002).

Source: Handford et al. (2002) and Weber, Albertin & Lehrmann (1997)

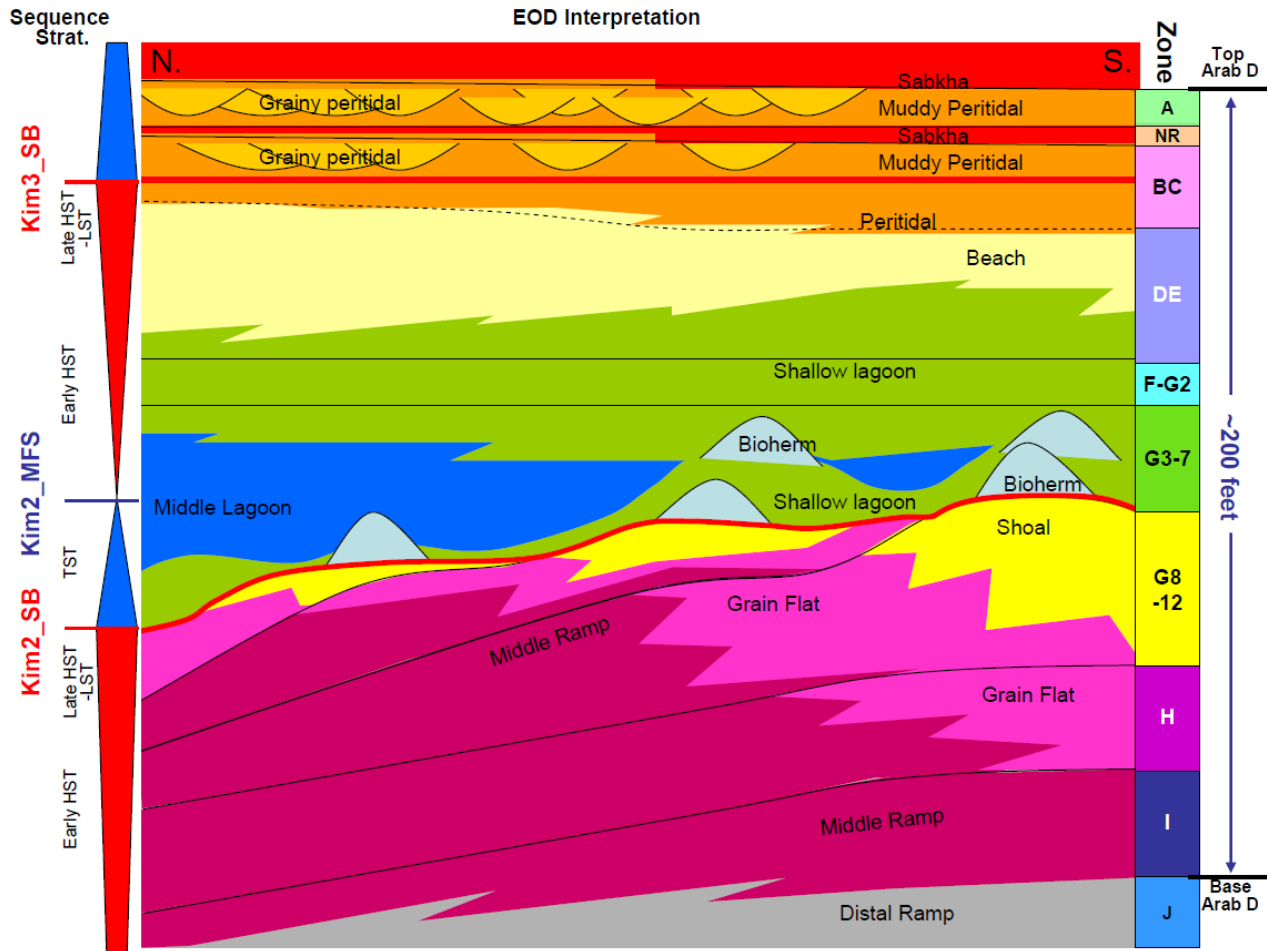


Figure 2.37: Environments of deposition and sequence-stratigraphic architecture of the Arab-D reservoir from Dukhan Field, Qatar.

Notes: 3rd order sequence boundaries are represented by thick red lines; 4th order sequence boundaries are represented by black lines.

Source: Stephens et al. (2009)

Al-Saad and Sadooni (2001) found fallacies in the previous Arab Formation depositional models in that they do not explain the unusual thickness of the Arab cycles, which are tens of meters thick compared to the 2-5 m-scaled typical thickness of cycles deposited in a “greenhouse” time such as was the Jurassic (Read and Horbury, 1993). They also found that the existing models fail to explain the Arab Formation lateral progradation on such a flat-topped platform such as was the Arabian platform. Consequently, they hypothesized the existence of a reef barrier in the current Zagros Mountains area, which protected the intrashelf basins and made them, essentially, relatively deep lagoons. This hypothesized barrier is also interpreted to have stationed westward prograding carbonate wedges that were deposited whenever the Neo-Tethys waters overcame the hypothetical barrier

(Figure 2.40; Al-Saad and Sadooni, 2001).

Meyer and Price (1993), in addition to agreeing with the interpretation by Mitchell et al. (1988), also interpreted a progradation element from west to east based on eastward thickening of the entire reservoir across Ghawar Field (Figure 2.41). In Chapter 5 of this thesis, the reservoir is correlated regionally outside Khurais Field boundaries in two cross-sections; one extends from the Arab-D outcrops south of the Saudi capital Riyadh to Ghawar Field across a distance of 413 km (Figures 5.2 and 5.4); and a N-S cross-section that extends from the Safaniya area down to south Khurais along a 397 km (Figures 5.2 and 5.5). The chapter presents evidence of a west to east progradation and bridges the correlational gap between the reservoirs' outcrop sections and its subsurface succession in Ghawar Field. In addition it is concluded that the majority of the top Arab-D anhydrite represents salina deposits, which could indicate that local anhydrite thickening trends on the plate could simply denote locations of palaeodepressions that received more replenishing waters from the open ocean during transgressions and thus accumulated thicker anhydrite columns.

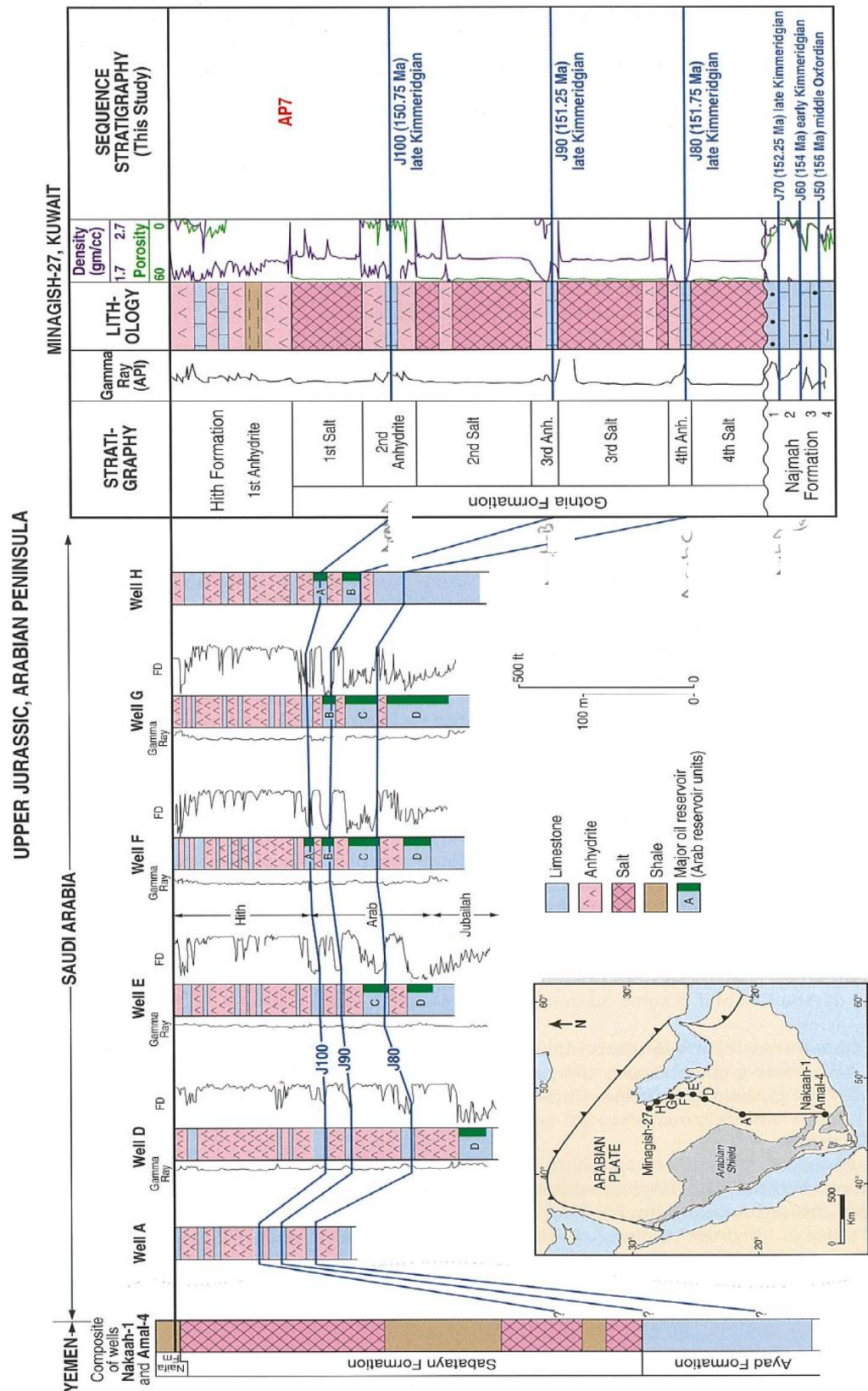


Figure 2.38: Cross-section of the Arab and Hith formation correlated from Yemen to Saudi Arabia and Kuwait, datumed atop the Hith Formation. Note the pinch out of the top Arab-D Anhydrite in the eastern most well, Well H. Source: Sharland et al. (2001)

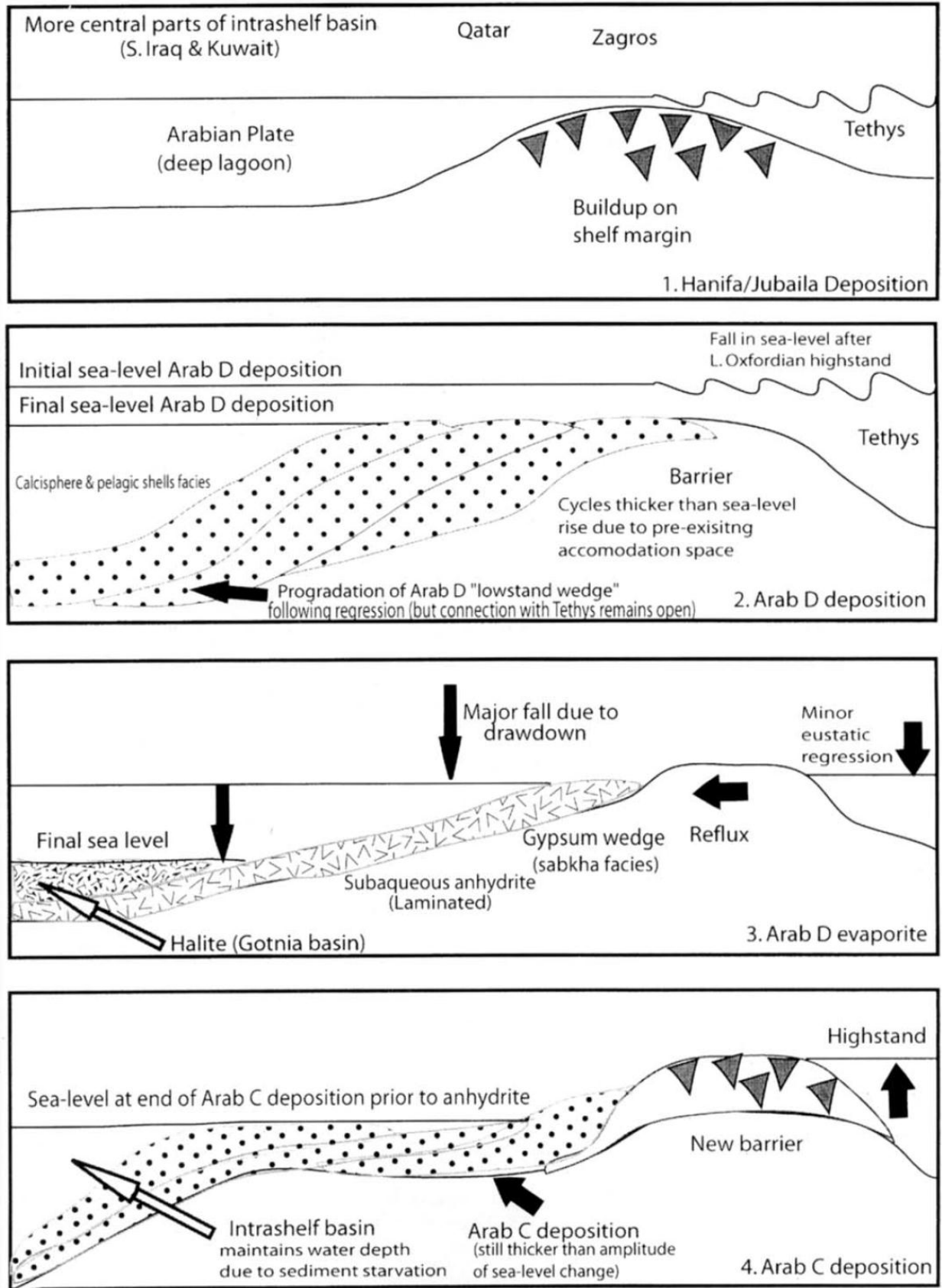


Figure 2.40: Depositional model of the Arab Formation in Qatar.

Notes: Progradation happened from the Neo-Tethys to the east, at the current Zagros Mountains location, onto the Arabian plate to the west.

Source: Al-Saad and Sadooni (2001)

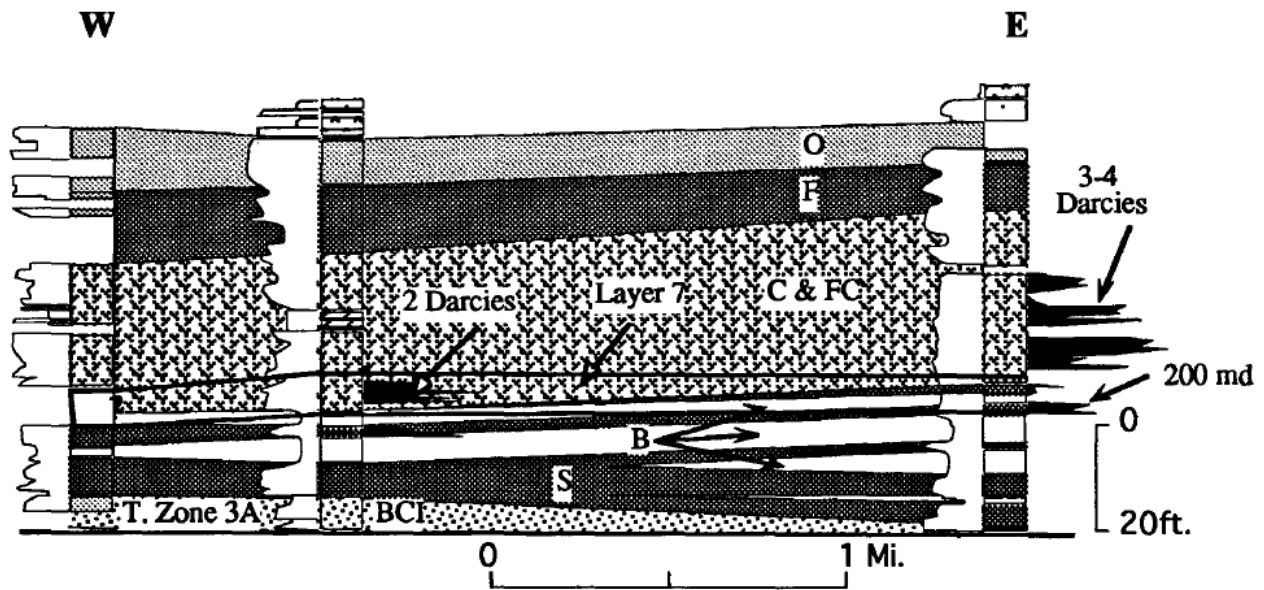


Figure 2.41: An E–W cross-section across Ghawar Field, Saudi Arabia of the upper part of the Arab-D reservoir.

Notes: The section shows facies progradation and aggradation eastward; BCI = bivalve-coated grain-intraclast; S = stromatoporoid; B = burrowed mixed skeletal-peloidal; C and FC = *Cladocoropsis* and fragmented *Cladocoropsis*; F = oolitic.

Source: Meyer and Price (1993)

This review of the Jurassic of the Arabian platform commenced with the broadscale evolutionary processes that controlled the detailed facies development patterns that led to deposition of one of the Earth's most prolific carbonate petroleum reservoirs, the Arab-D reservoir, as a prograding arid-region shelf system. Succeeding sections focus on the reservoir's facies evolution on the scale of the giant petroleum field, Khurais, and on a regional scale across the Arabian platform.

Chapter 3: Arabian Carbonate Reservoirs: A Depositional Model of the Arab-D Reservoir in Khurais Field, Saudi Arabia¹

3.1 Abstract

The Late Jurassic Arab Formation, the world's most prolific oil-bearing interval in the Arabian Peninsula, is a succession of interbedded thick carbonates and evaporites that are defined stratigraphically upsection as the Arab-D, Arab-C, Arab-B, and Arab-A. The Arab-D reservoir is the main reservoir in Khurais field, one of the Saudi Kingdom's largest onshore oil fields.

In Khurais Field, the Arab-D reservoir is comprised of the overlying evaporitic Arab-D Member of the Arab Formation and the underlying upper part of the Jubaila Formation. It contains 11 lithofacies that, from deepest to shallowest, are the following 1) hardground-capped skeletal wackestone and lime mudstone; 2) intraclast floatstone and rudstone; 3) pelletal wackestone and packstone; 4) stromatoporoid wackestone, packstone and floatstone; 5) *Cladocoropsis* wackestone, packstone and floatstone; 6) *Clypeina* and *Thaumatoporella* wackestone and packstone; 7) peloidal packstone and grainstone; 8) ooid grainstone; 9) cryptomicrobial laminites; 10) evaporites; and 11) stratigraphically reoccurring dolomite.

The Arab-D reservoir lithofacies succession represents shallowing-upward deposition, which from deepest to shallowest reflects the following depositional environments: offshore submarine turbidite fans (lithofacies 1 and 2); lower shoreface settings (lithofacies 3); stromatoporoid reef (lithofacies 4); lagoon (lithofacies 5 and 6); shallow subtidal settings (lithofacies 8 and 9); peritidal settings (lithofacies 9); and sabkhas and salinas (lithofacies 10). The depositional succession

¹ This chapter has been published in the *AAPG Bulletin*, Volume 97, no. 7, July 2013, Pages 1099–1119. See appendices B and C for further details and permissions.

of the reservoir represents a prograding, shallow-marine, reef-rimmed carbonate shelf that was subjected to frequent storm abrasion, which triggered turbidity currents and deposited turbidites.

3.2 Introduction and History

The Late Jurassic Arab Formation, the world's most prolific oil-bearing interval (Barger, 1984; Sorkhabi, 2008; Stegner, 2007), is composed of a series of excellent reservoir-quality carbonates, namely the Arab-D, C, B, and A members. Each member is capped by a nonpermeable anhydrite layer, while the uppermost member is capped by the Hith Formation anhydrite (Figure 3.1). Previous work done

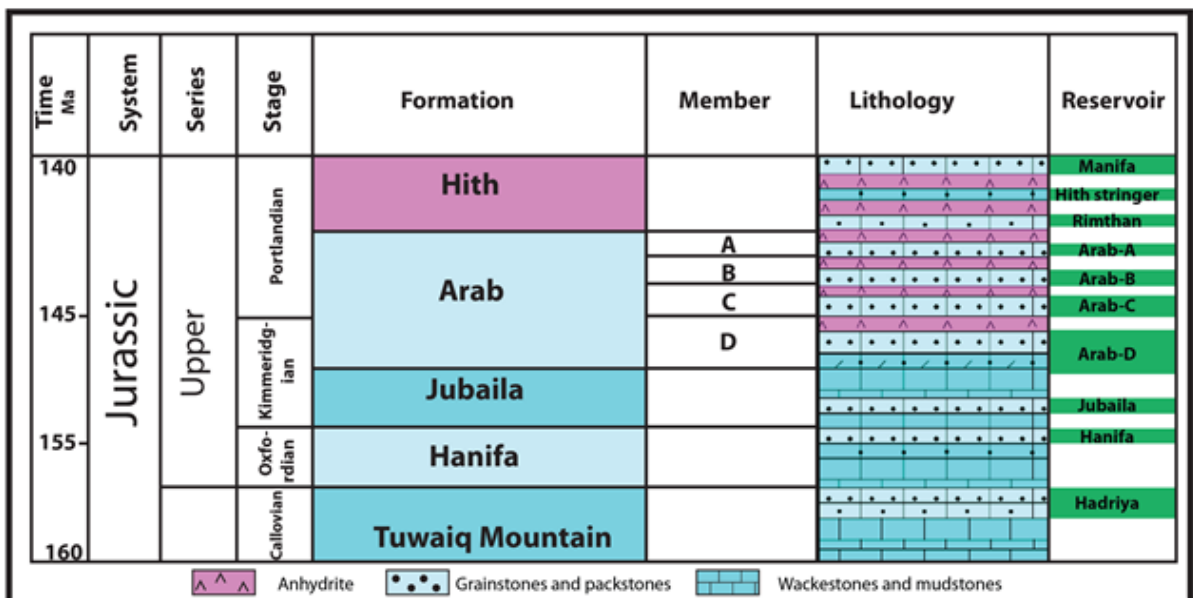


Figure 3.1: Saudi Arabia's Jurassic reservoir stratigraphy and lithology

Notes: There is no biostratigraphic control on the age of the Arab and Hith formations (Hughes, 2004). Note that the Arab-D reservoir extends from the carbonates of the Arab-D Member of the Arab Formation to the upper part of Jubaila Formation.

Source: Modified from Powers (1968)

on the Arab-D reservoir focused primarily on Ghawar Field and different depositional models were developed. Mitchell et al. (1988) divided the Arab-D carbonates into skeletal-oolitic limestones and dolomites, *Cladocoropsis* limestones and dolomites, stromatoporoid-red algae-coral limestones, bivalve-coated grain-intraclast limestones, micritic limestones and dolomites, and diagenetic dolomite, in

addition to the sealing anhydrite.

Lindsay et al. (2006) used the same classification scheme of Mitchell et al. (1988). Meyer and Price (1993) slightly modified Mitchell et al. (1988) lithofacies and listed the following types: micritic, bivalve-coated grain-intraclast, Stromatoporoid, burrowed skeletal-peloidal, *Cladocoropsis*, fragmented *Cladocoropsis*, foraminiferal, mixed skeletal-peloidal, oolite, and anhydrite. Handford et al. (2002) modified Mitchell's et al. (1988) classification scheme using Dunham's (1962) and Embry and Klovan's (1971) textures and listed the following lithofacies: lime mudstone-wackestone, burrowed skeletal-peloidal wackestone-packstone, intraclast rudstone and oncolite rudstone, coral stromatoporoid wackestone-packstone to boundstone and floatstone, burrowed to stratified *Cladocoropsis* wackestone grainstone and boundstone (bafflestone), stratified foram-peloid packstone-grainstone; ooid-coated-grain packstone and grainstone; evaporite association of peloidal-ostracod dolowackestone-packstone gastropod dolopackstone and dolomudstone, palaeosol breccias and rooted wackestones, bedded nodular to massive anhydrite.

In 1957, the Arab-D oil was discovered in Saudi Arabia's second largest onshore oil field, Khurais Field, using surface and gravity mapping (Figure 3.2a) (Al-Mulhim et al., 2010). Further delineation drilling proved that the Qirdi Field, discovered south of Khurais in 1973, is also part of the huge Khurais oil accumulation. The field occupies an asymmetric NW-SE trending anticline with 2° of dip on its east flank and 8.7° of dip on its west flank (Figure 3.2a) (Al-Afalge, Al-Garni, Rahmeh & Al-Towailib, 2002; hydrocarbons-technology.com, 2011). In the summer of 2009, Saudi Aramco successfully completed the largest oil expansion project in history, bringing to production a nationally significant rate from Khurais and adjacent satellite fields in what became known as the Khurais Mega Project (Al-Mulhim et al., 2010; Mouawad, 2010). This paper is the first to address the sedimentology of the Arab-D in Khurais Field. The paper focuses on the analysis of thirty-two cored Khurais wells and over 500 thin-sections, and proposes a different depositional model to currently accepted models. The study was carried out in Saudi Aramco's Exploration Core Laboratories and Curtin University. The core from the Aramco HKHK Khurais

well (coded name) has been chosen as a representative example due to its substantial vertical coverage (Figure 3.3) and the continuity of its lithofacies across the field. The results of this study provide evidence that the Arab-D is a prograding, upward-shallowing reservoir, and this paper presents a new depositional model that can be used in predicting the architectural heterogeneities of the reservoir lithofacies.

3.3 Regional Setting

Approximately 640–620 Myr ago, the Amal Collision between the Rayn plate and the Arabian-Nubian Craton created a north trending horst-graben system on the Precambrian basement east of the Arabian Shield (a complex of Precambrian igneous and metamorphic rocks; Figure 3.2a (Blasband, White, Brooijmans, De Boorder & Visser, 2000). This fault system acted as an architectural mould that controlled subsequent deposition and shaped subsequent structures, including the Khurais Field anticline (Figure 3.2a) (Al-Husseini, 2000; Al-Mulhim et al., 2010; Ayres et al., 1982; Konert et al., 2001). During the late Palaeozoic, the Hercynian orogeny event rotated the Arabian Plate 90° anticlockwise, uplifted central Arabia, tilted it towards the east and eroded it. Following the Hercynian orogeny event, the Neo-Tethys commenced rifting and spreading during the late Permian along the Zagros Suture and Gulf of Oman (Figure 3.2a and b) creating a passive margin with Arabia (Powers et al., 1966; M. A. Ziegler, 2001). The Early Jurassic witnessed the opening of the eastern Mediterranean, which resulted in another passive margin development along Arabia's northern edge. As a result of this Early Jurassic development, a vast shallow-marine shelf occupied most of the Arabian Peninsula, possibly extending all the way to the present-day Arabian Shield, and dominated the plate with shallow-shelf carbonate and evaporites deposition (Énay, 1993; Le Nindre et al., 1990; Murriss, 1980). Epeirogenic downwarp during the Middle Jurassic led to the development of four intrashelf basins on the Arabian Craton, namely, the Rub' Al-Khali, the Ras al Khaimah, the Arabian, and the Gotnia basins; the latter two separated by the Rimtham Arch (Figure 3.2) (Alsharhan & Kendall, 1986; Murriss, 1980; M. A. Ziegler, 2001). Organic-rich, anoxic shales (Hanifa and Tuwaiq Mountain

formations; Figure 3.1) were deposited in the intrashelf basins and later sourced the oils of the Arab reservoirs (Ayres et al., 1982; Droste, 1990; M. A. Ziegler, 2001). The intrashelf basins provided antecedent palaeotopography that dictated the later deposition of the Jubaila, Arab and Hith formations; as evident in changes in lithofacies, thickness and composition of these formations over the intrashelf basins (Lindsay et al., 2006; M. A. Ziegler, 2001). Since the source-reservoir-seal-enclosure requirements were spectacularly met in these intrashelf basins, the Arabian oil fields were concentrated around them (Lindsay et al., 2006; M. A. Ziegler, 2001). During the Late Jurassic, Central Arabia remained stable and carbonates progressively filled the intrashelf basins with repetitive cycles of shoaling-upward carbonate sediments that were capped with evaporitic flat facies; whereas the Afro-Arabian and Indian plates rifted along Southern Oman creating another passive margin to the south of Arabia. The Neo-Tethys closing did not commence until the Late Cretaceous, causing the obduction of the Oman ophiolites during the Arabian-Eurasian plates (Alsharhan & Kendall, 1986; M. A. Ziegler, 2001) compression.

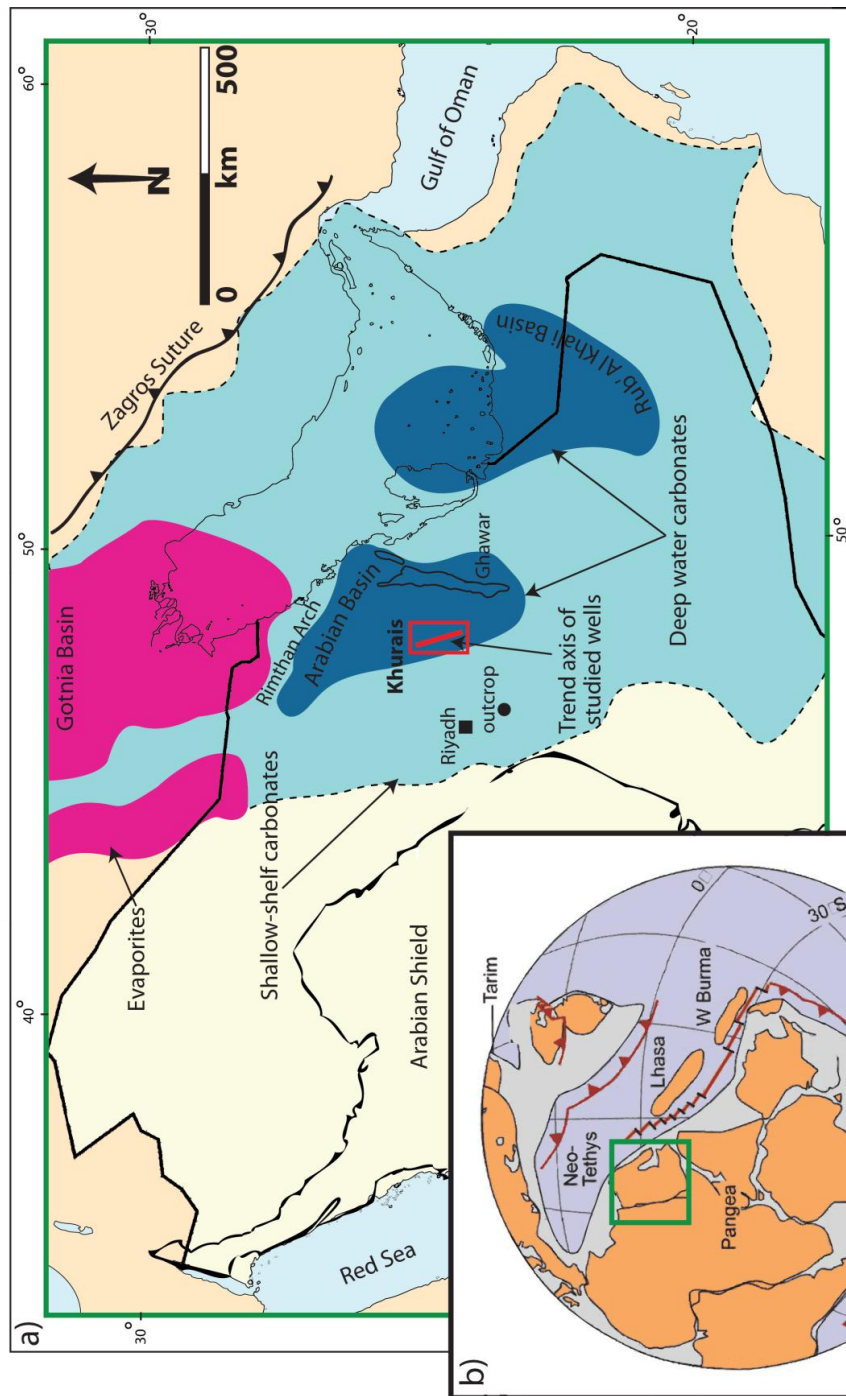


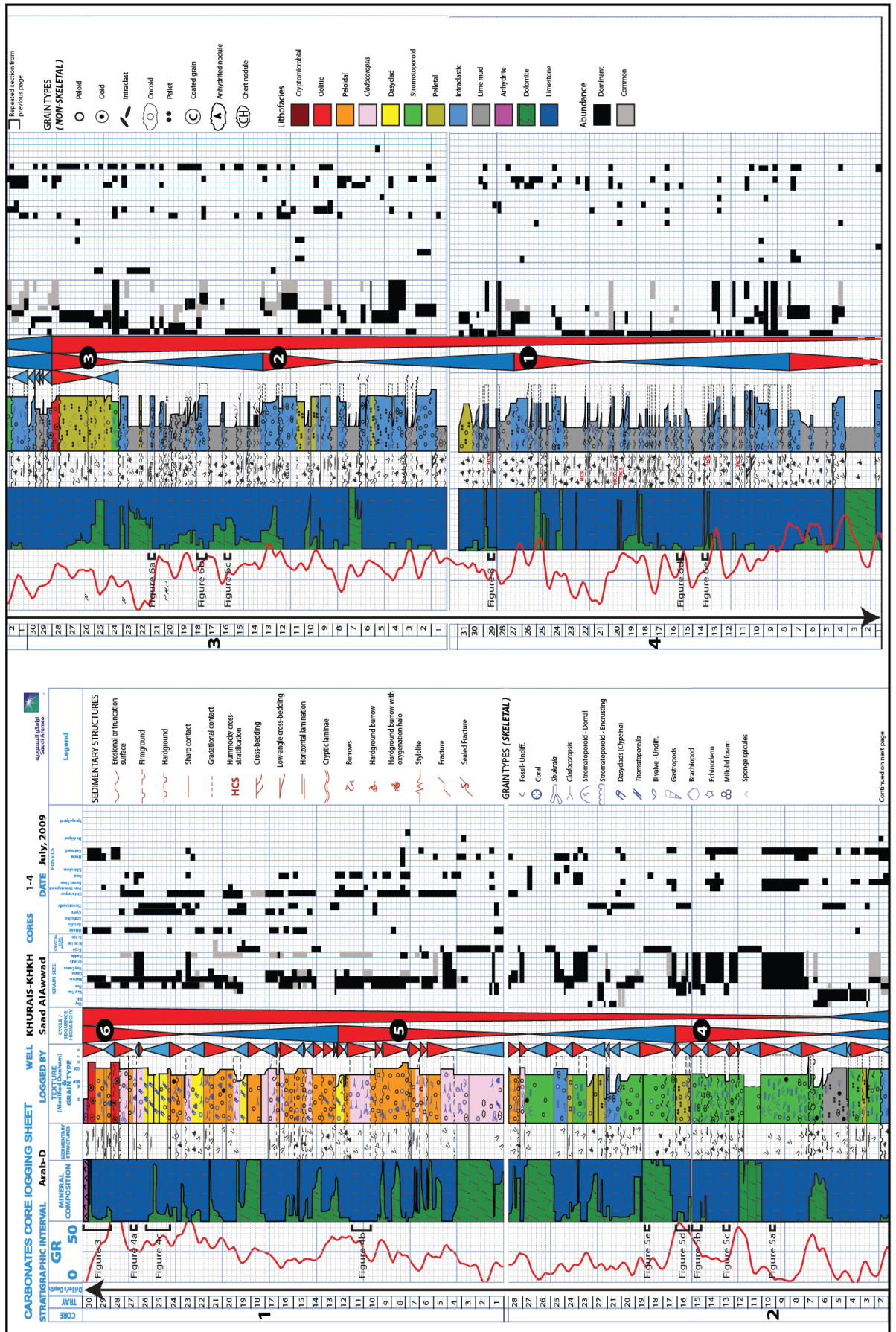
Figure 3.2: Location map of Khurais Field.

Notes: a) Trend axis of studied Arab-D cores is shown by the red line.; the outlined dark blue areas depict intrashelf basins where deposition of deep water carbonates took place; the outlined light blue area depicts shallow-shelf carbonate deposition. Note the location of Late Jurassic outcrops south of the capital Riyadh. b) Li and Powell's (2005) palaeogeographic configuration during the Jurassic, with the Arabian Plate position enclosed in the green square; orange, pale blue and purple areas depict emergent continents above present sea-level, oceanic areas and mafic volcanic rocks respectively. Note that the location of the paleo-equator is controversial (Stampfli et al., 2001; Golonka, 2002).

Source: Modified from M. A. Ziegler (2001) and Li and Powell (2001)

Figure 3.3 (next page): Characterisation of Arab-D reservoir core from well Aramco KHKH Khurais, Khurais Field.

Note that only high frequency sequences are picked in the monotonously interbedded lower part of the reservoir based on upward thickness increase of the intraclastic beds (see text for more details); a 1 inch = 10 ft scaled enclosure (Enclosure 3.1) is appended at the back of the thesis.



3.4 Lithofacies

Detailed (4 in-scaled [10 cm]) analysis of the Arab-D reservoir from thirty-two cored Khurais wells has resulted in recognition of the following eleven lithofacies (Figure 3.3):

1. Anhydrite Lithofacies;
2. Oolitic-skeletal-cryptomicrobial laminated wackestones to grainstones (referred to as Cryptomicrobial lithofacies hereafter);
3. Skeletal-oolitic grainstones and grain-dominated packstone (Oolitic lithofacies);
4. Skeletal-peloidal mud-dominated packstones to grainstones (Peloidal lithofacies);
5. *Thaumatoporella-Clypeina* wackestones and mud-dominated packstones (Dasycladacean algae lithofacies);
6. Skeletal-peloidal-*Cladocoropsis* wackestones to floatstones (*Cladocoropsis* lithofacies);
7. Skeletal-stromatoporoid wackestones to floatstones (Stromatoporoid lithofacies);
8. Skeletal-pelletal wackestones to grain-dominated packstones (Pelletal lithofacies);
9. Skeletal-oncolitic-intraclastic mud-dominated packstones to floatstones (Intraclastic lithofacies);
10. Skeletal wackestones and lime mudstones (Lime-mud lithofacies);
11. Dolomite Lithofacies.

3.4.1 Anhydrite Lithofacies

The anhydrite lithofacies (Figure 3.4a and b) provides the non-porous, vertical seal for the Arab-D reservoir and although rarely cored, it can be easily identified from its conspicuous gamma and density log character. The anhydrite contact with underlying carbonates varies from gradational to sharp. Typically, at gradational

boundaries, anhydrites start out as displacive nodules that grew at the expense of the limestone and dolomite sediments, increase upward into bedded nodular fabrics and ultimately became (apparently) massive.

The anhydrite lithofacies is interbedded with several dolomite stringers, where the lower most of these, which was described by the first author in a few Khurais cores, ranges in thickness from 1 to 4 ft (0.3–1.2 m) and contains fabric-mimetic to semi-mimetic dolomites of what appears to have been originally oolitic grainstones.

A substantial thickness of anhydrite covers the Arab-D reservoir in Khurais Field and provides an excellent vertical seal.

3.4.2 Cryptomicrobial Lithofacies

The oolitic-bivalve-cryptomicrobial laminated mudstone to grainstone, the cryptomicrobial lithofacies (Figure 3.4c), caps the reservoir just below the anhydrite seal. The faunal composition is restricted and consists of cerithiid gastropods and bivalves. Beds are thin, about 1 ft (0.3 m) thick, usually with gradational upper and lower contacts. The microbial laminae are millimetres in scale and are undulatory and/or domed. Mouldic porosity is the most common porosity type in this lithofacies.

3.4.3 Oolitic Lithofacies

The skeletal-oolitic grainstone and grain-dominated packstone, the oolitic lithofacies (Figure 3.4d), is present in the upper part of the reservoir and is composed of very well-sorted, well-rounded, medium-grained ooids, bivalves, and foraminifera. The beds are usually 0.5 to 1 ft (0.2–0.3 m) thick and amalgamate into 2 to 3 ft (0.6–1 m) thick intervals below the cryptomicrobial lithofacies. Sharp, hardground or firmground, contacts characterise this lithofacies. High and low angle cross stratification and horizontal laminations are the dominant sedimentary structures present. Porosity types are mostly interparticle and mouldic.

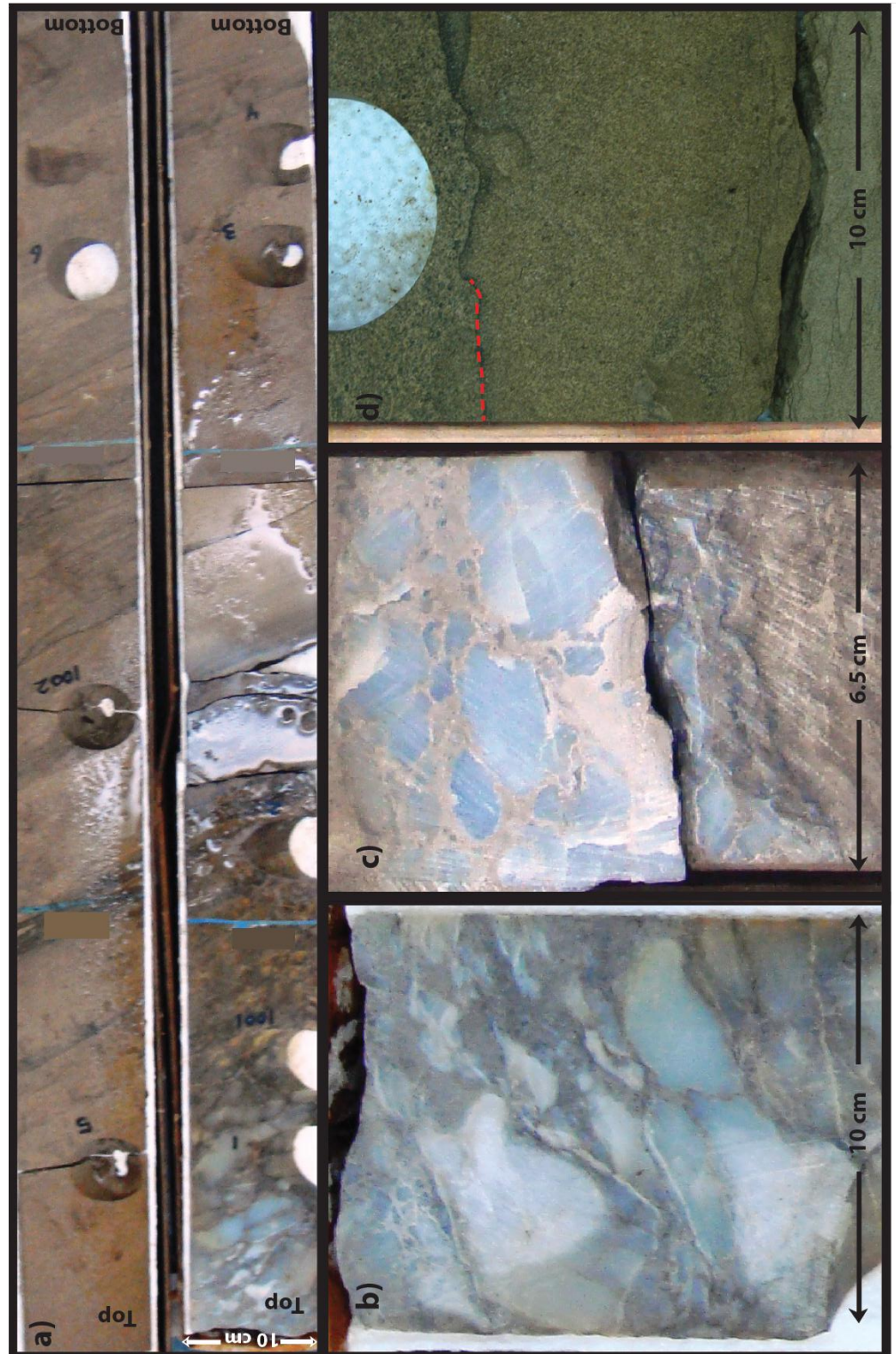


Figure 3.4: Anhydrite, cryptomicrobial and oolitic lithofacies.

Notes: a) The upper two trays of the Aramco HKHK Khurais core, showing a continuum through the Anhydrite, Cryptomicrobial and Oolitic lithofacies; b) Anhydrite; c) Millimetre-scale cryptomicrobial laminae below the anhydrite; d) Oolitic lithofacies with well-sorted and well-rounded ooids and a hardground marked in red. Photographs are located on Aramco HKHK Khurais core description, Figure 3.2 and Enclosure 3.1.

3.4.4 Peloidal Lithofacies

The peloidal lithofacies (Figure 3.5a) is located in the upper part of the reservoir, stratigraphically beneath the oolitic lithofacies, and is composed of well-sorted, well-rounded to rounded, fine to medium-grained skeletal-peloidal mud-dominated packstone, grain-dominated packstone, and grainstone. Bivalve fragments, fragmented micritised *Cladocoropsis*, and foraminifera are among the components present in this lithofacies. Bed thickness ranges from 1 to 6 ft (0.3–1.8 m) with both sharp and gradational boundaries. In addition to massive unstratified beds, horizontal lamination, low angle cross stratification, bioturbation and graded bedding with muddier caps characterise this lithofacies. Porosity is mostly interparticle with some mouldic and intraparticle pores.

3.4.5 *Cladocoropsis* Lithofacies

The skeletal-peloidal-*Cladocoropsis* wackestone to floatstone, the *Cladocoropsis* lithofacies (Figure 3.5b), is present in the upper part of the Arab-D reservoir. It is located below, and mixed with, the peloidal lithofacies. It is composed of nodular and dendroid *Cladocoropsis* (calcified sponge) mud-dominated packstones and wackestones in addition to floatstones and rudstones with mud-dominated packstone to grain-dominated packstone matrices. Bed thickness ranges from 1 to 5 ft (0.3–1.5 m) and contacts can be gradational or sharp. The components of this lithofacies are poorly sorted and subrounded, and consist of *Cladocoropsis* stems (broken but unfragmented, Figure 3.5b), *Cladocoropsis* fragments (see description of the peloidal lithofacies above), *Shuqraia* (a *Cladocoropsis* relative), foraminifera, corals (Figure 3.5b), bivalves, peloids, *Clypeina* (dasycladacean algae), and *Thaumatoporella* (considered to be related to the calcareous green algae by De Castro, 1990). Bioturbation, horizontal laminations and firmgrounds are the

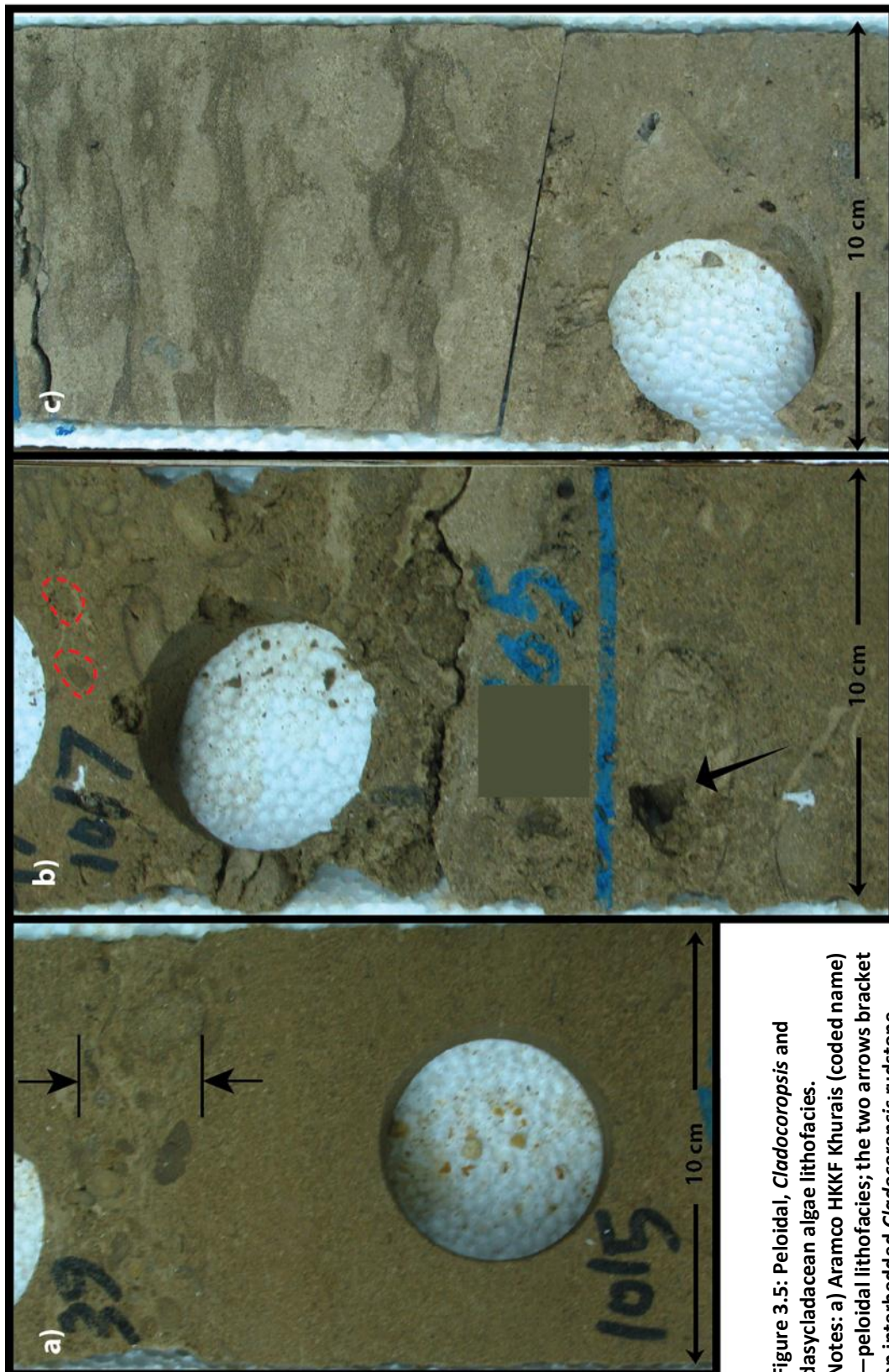


Figure 3.5: Peloidal, *Cladocoropsis* and dasycladacean algae lithofacies.
 Notes: a) Aramco HKKF Khurais (coded name) — peloidal lithofacies; the two arrows bracket an interbedded *Cladocoropsis* rudstone.
 b) Aramco HKKF Khurais — *Cladocoropsis* lithofacies; cross sectional cuts of *Cladocoropsis* stems are enclosed in dashed red ovals. Note the poor sorting and coral dissolution causing vugular porosity (black arrow). c) Aramco HKKF Khurais — dasycladacean algae lithofacies; note the heavy bioturbation. Photographs are projected from correlated lithofacies onto Aramco HKKF Khurais core description, Figure 3.2 and Enclosure 3.1.

dominant sedimentary structures present in this lithofacies. Porosity types in order of abundance are: interparticle, intraparticle, mouldic and vugular.

3.4.6 Dasycladacean algae Lithofacies

The *Thaumatoporella-Clypeina* wackestone and mud-dominated packstone, the dasycladacean algae lithofacies (Figure 3.5c), is intermixed with the *Cladocoropsis* and the peloidal lithofacies, but is limited stratigraphically to the interval above the stromatoporoid lithofacies. Components present in this lithofacies are *Clypeina*, predominantly miliolid foraminifera, *Kurnubia*, *Thaumatoporella*, bivalves and peloids. This lithofacies forms 1 to 3 ft (0.3–0.9 m) thick beds, gradationally caps the stromatoporoid and *Cladocoropsis* lithofacies and is capped by sharp or gradational upper contacts. Sedimentary structures present in this lithofacies include bioturbation, wispy laminations, and some firmgrounds that, when present, commonly cap this lithofacies. Porosity types include mouldic and intraparticle porosities.

3.4.7 Stromatoporoid Lithofacies

The skeletal-stromatoporoid (calcified sponge) wackestone to floatstone, the stromatoporoid lithofacies (Figure 3.6a), is present in the middle part of the Arab-D reservoir and is composed of floatstones and rudstones with matrix textures ranging from wackestone to grain-dominated packstone. The components of this lithofacies are very poorly sorted with a wide range of grain sizes ranging from fine sands to pebbles. The components include mostly displaced domal and encrusting stromatoporoids – a few centimetres to a decimetre across (Figure 3.6a), corals – a few centimetres to a decimetre across (Figure 3.6b), microbial encrustations, foraminifera, bivalves (including up to 2 in (5 cm) width gastropods; Figure 3.6c), pellets, peloids, oncoids and intraclasts. Thick bedding – up to 9 ft (2.7 m) in the illustrated Khurais core (Figure 3.3) and up to 18 ft (5.5 m) in another Khurais core characterise this lithofacies. This latter bed may have had its boundaries obliterated

by diagenesis. Sharp bases, commonly hardgrounds or firmgrounds, and gradational upper contacts into the pelletal lithofacies discussed below mark this lithofacies. Heavy bioturbation is very common in addition to borings, occurring mostly in the stromatoporoids. Vugular (due to dissolution of aragonitic corals; Figure 3.6a), mouldic and intraparticle porosities are the dominant pore types.

3.4.8 Pelletal Lithofacies

The skeletal-pelletal wackestone to grain-dominated packstone, the pelletal lithofacies (Figure 3.6d), is present in the middle part of the Arab-D reservoir. The components of this lithofacies range in size from clay to very fine sand, and are moderately sorted pellets, bivalve fragments, foraminifera and lime mud. The beds are 0.5 to 4 ft (0.2–1.2 m) thick and have sharp, firmground, contacts with the underlying lime-mud lithofacies. The upper contacts of this lithofacies can be gradational or sharp with the overlying stromatoporoid lithofacies. Bioturbation, horizontal laminations, firmgrounds and hardgrounds are the common sedimentary structures characterising this lithofacies. Porosity types present are mostly mouldic and microporosity

3.4.9 Intraclastic Lithofacies

The skeletal-oncolitic-intraclastic mud-dominated packstone to floatstone, the intraclastic lithofacies (Figures 3.7a and b), is present in the middle and lower parts of the Arab-D reservoir, and is composed of oncolitic and/or intraclastic rudstones and floatstones with matrix textures ranging from wackestone to grain-dominated packstone. The components in this lithofacies are extremely poorly sorted and include angular to sub-rounded intraclasts, oncoids (marked by coating development around intraclasts and skeletal fragments), bivalves, reworked stromatoporoid and coral fragments (Figure 3.7b), foraminifera, pellets, peloids, and rare *Cladocoropsis* fragments. Bed thickness varies from 0.1 to 4 ft (.03–1.6 m) with sharp hardground or firmground bases that were often scoured, and sharp to .

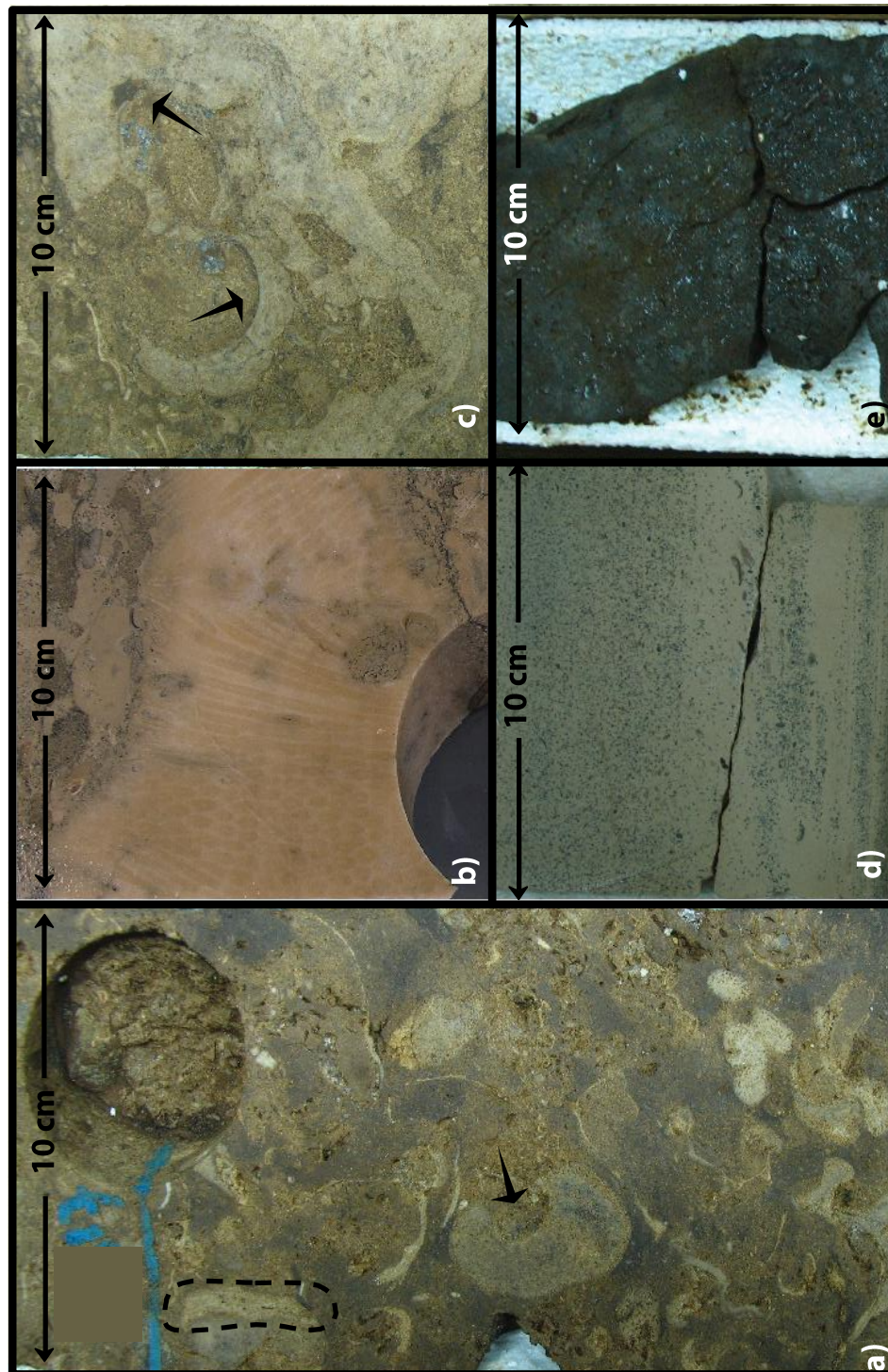


Figure 3.6: Stromatoporoid, pelletal and dolomite lithofacies.

Notes: a) Aramco HKHK Khurais—stromatoporoid lithofacies, domal (arrow) and laminar (oval) forms. Note leaching mostly of corals making vugular porosity (shown by the rugged breakage surface of the plug cut (upper right corner). b) Aramco NAN Khurais (coded name)—coral in stromatoporoid lithofacies. c) Aramco HKHK Khurais—gastropods encrusted by stromatoporoids (arrows) in stromatoporoid lithofacies. d) Aramco Khurais-HKKF—pelletal lithofacies showing dark coloured silt and very fine sand pellets. e) Aramco HKHK Khurais—dolomite lithofacies, black due to oil staining. Photographs are located or projected from correlated lithofacies onto Aramco HKHK Khurais core description, Figure 3.2 and Enclosure 3.1.

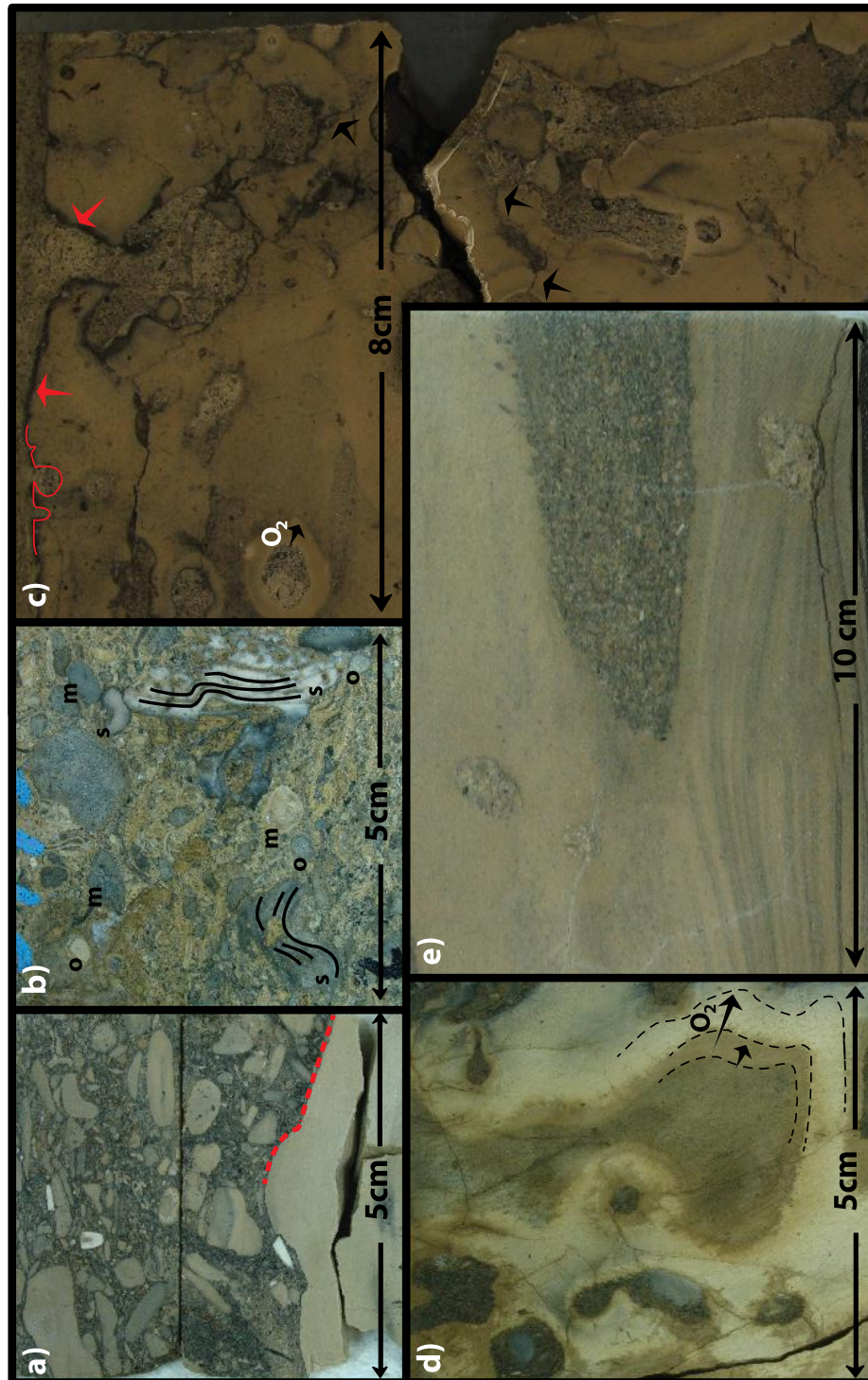


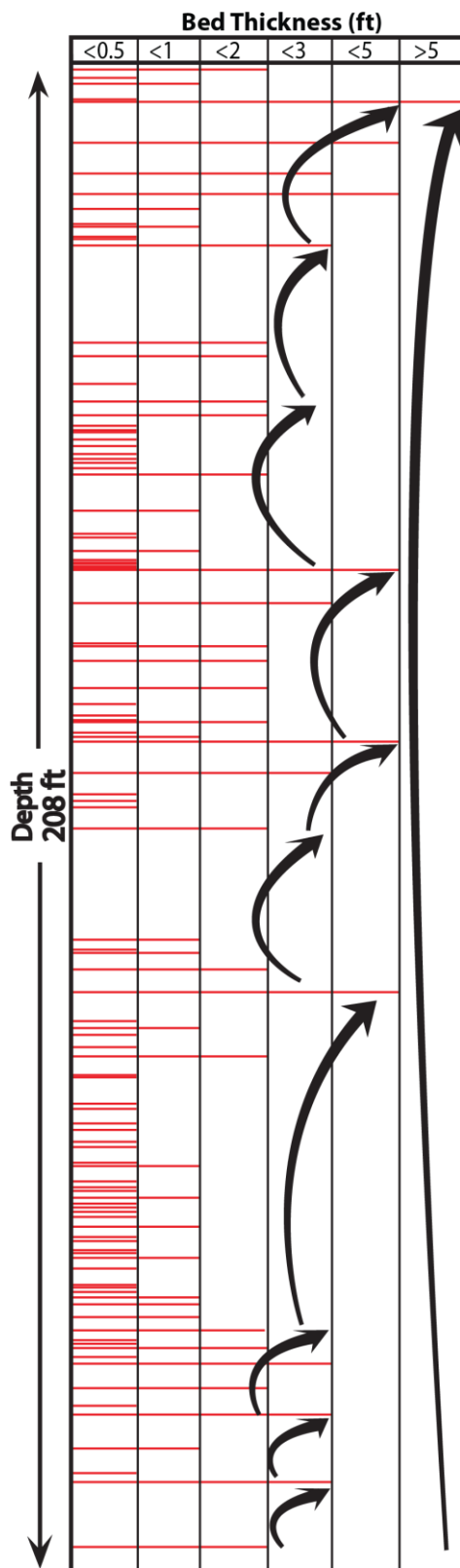
Figure 3.7: Intraclastic and lime mud lithofacies.

a) Aramco HKKF Khurais—intraclastic and lime mud lithofacies separated by a scour mark (red line). b) Aramco HKKF Khurais—different components of the Intraclastic lithofacies, stromatoporoids (S)-black lines mark internal lamina-mixed with mudclasts (m) and oncoids (o). c) Aramco NAN Khurais—hardground with organic marks separating a lower lime mud bed from an upper Intraclastic bed;. Note borings (red line) and phosphatisation at hardground surface (red arrows); oxygenation halos (O₂) and fractures connecting burrows (black arrows). d) Aramco HKHK Khurais—oil staining spreading out from hardground burrows. Note staining in interconnecting fractures, oxygenation halos (O₂) and dolomitisation in burrows. e) Aramco HKKF Khurais—hummocky cross stratification (HCS) in lime mud. Photographs are located or projected from correlated lithofacies onto Aramco HKHK Khurais core description, Figure 3.2 and Enclosure 3.1.

often gradational upper contacts, showing graded bedding into muddier and/or finer sediments. These beds are numerous, up to one bed every 2 inches in the lower part of the reservoir as shown in Figure 3.8, which is a plot of intraclastic bed thicknesses against their occurrence depth. The figure was constructed by measuring the thicknesses of 110 intraclastic beds in the lower part of the reservoir and aggregating these thickness values into bins of < 0.5 ft, 0.5 to < 1 ft, 1 to < 2 ft, 2 to < 3 ft, 3 to < 5 ft and ≥ 5 ft. Each bed thickness was then plotted as a bin value, represented on the X-axis, against its occurrence depth, represented by the Y-axis. This technique allowed for visualizing the frequency distribution of the bed thicknesses, as well as their variance with depth.

The hardgrounds that underline almost every single intraclastic bed correlates one-for-one with conspicuous increase (hot) gamma-log spikes that mark the lower Arab-D reservoir. Hardgrounds are marked by colour alteration and/or blackening, possibly attributed to phosphatisation (Bodenbender, Wilson & Palmer, 1989; Palmer, 1982) that extends down from the hardground surface, and/or borings (Figure 3.7c). The firmgrounds are characterised by colour alterations and terminated burrow tops against the firmground surface. Angular to subangular mudclasts rest on top of the hardgrounds (Figure 3.7a), whereas subrounded ones cap some firmgrounds. Scour marks (made by a scouring current, Figure 3.7a) and organic marks (made by burrowing organisms and filled with the intraclastic lithofacies, Figure 3.7c) characterise the hardgrounds and firmgrounds underlying this lithofacies. Other sedimentary structures include burrowing, graded bedding, horizontal laminations and rare hummocky and/or swaley cross stratification. The porosity types present in this lithofacies are interparticle, intraparticle and microporosity.

3.4.10 Lime Mud Lithofacies



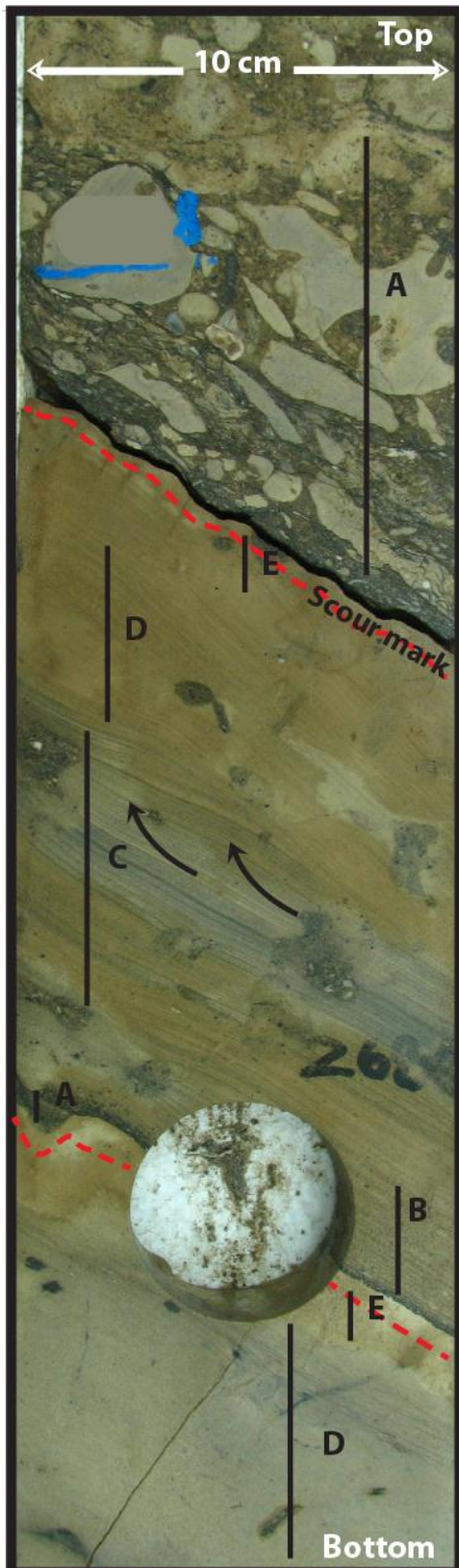
The skeletal wackestone and lime mudstone, the lime mud lithofacies (Figures 3.7a and e), is present in the lower part of the Arab-D reservoir. In addition to lime mud, the components of this lithofacies include micritised pellets, bivalves, brachiopods, foraminifera, particularly *Lenticulina spp.*, echinoderms, and rare blackened and/or reddened peloids and/or pellets.

Bed thickness varies from 0.2 to 4 ft (0.06–1.2 m) with mostly sharp hardground or firmground caps (these make up the base of the intraclastic lithofacies as discussed above) and transitional bases. This lithofacies is characterised by heavy bioturbation that, generally, churns the sediment and becomes more distinct, filled with grainier sediment infills and preferentially dolomitised toward the hardground caps (Figure 3.7c). These distinct burrows, associated with hardgrounds, are subsequently referred to as hardground burrows.

The hardground burrows are outlined with oxygenation halos, dolomitised and/or have dolomitised outer rims in some cases (Figures 3.7c and d). Commonly oil staining intensifies around the hardground burrows (Figure 3.7d). When this lithofacies is not interrupted by

Figure 3.8: The thicknesses of 110 described intraclastic beds plotted against their occurrence depth in the lower part of the Arab-D reservoir core, Aramco HKHK Khurais
Notes: Cyclicity is indicated by the thick curved arrows and is depicted by bed thickness increase up each cycle; note the overall thickness increase up the entire interval (large curved arrow).

bioturbation, original horizontal to slightly inclined to undulated laminations, commonly attributed to the size difference between mud and micro-pellets, are preserved. Rare hummocky cross stratification (HCS) to swaley bedding marks this



lithofacies (Figure 3.7e), in addition to rare slumps. Fractures commonly interconnect these hardground burrows, fracture the overlying mudclasts of the intraclastic lithofacies and range from completely sealed with blocky calcite cement to partially open to completely open, in addition to solution enhanced fractures (Figure 3.7c).

The pore types are mostly micropores and to a lesser extent mouldic and intraparticle pores. Some interparticle and intercrystal porosity can be observed in the grainy infills of the hardground burrows, and usually contain higher porosities than the surrounding lime muds.

Figure 3.9 shows a typical continuum through the

Figure 3.9: Aramco HKHK Khurais—typical type-CCC turbidite.

Notes: This turbidite is indicative of deposition on a submarine channel levee and distinguished by the presence of climbing-ripple laminations, convolutions and rip-up clasts (Walker, 1985) with a full Bouma sequence (Bouma, 1962) preserved. Division A of the sequence above the scour marks is structureless, consists of clasts up to 5 cm across, and represents highest energy conditions. Division A grades up into the horizontally laminated sands of division B, which represent current energy fall to upper flow regime, then follows the current ripples of division C that form climbing ripples (indicated by curved arrows) as more sediments deposit from suspension. These are followed by the parallel-laminated silts and muds of division D. Finally, pellets and muds of division E (t) are deposited and they represent the final decay of the current energy. E (h) muds and pellets, if present, are hemipelagic sediments sourced from the turbidity current but deposited directly from the sea water (i.e., no current movement is involved). Position marked on Enclosure 3.1; vertical scale is same as horizontal scale.

intraclastic and lime mud lithofacies in the lower part of the Arab-D reservoir; the following observations can be made:

1. The lower Arab-D is composed of monotonous interbedded couplets of these two lithofacies;
2. The bases of the intraclastic lithofacies separating it from the underlying lime mud lithofacies are almost invariably sharp;
3. These sharp bases are marked with scour marks or organic marks (Figures 3.9, 3.7a and 3.7c) as previously discussed;
4. The couplets show preserved Bouma sequences, some with all divisions A, B, C, D, and E (Figure 3.9).

3.4.11 Dolomite Lithofacies

The Dolomite lithofacies (Figure 3.6e) is composed of sucrosic or mosaic, fine to medium sized dolomite crystals that occur as distinctive beds, commonly with sharp top and bottom boundaries, ranging in thickness from 0.2 to 8 ft (0.06–2.4 m). These beds are not specific to any of the aforementioned lithofacies and occur throughout the reservoir, commonly obliterating original fabrics. Porosity types are mostly intercrystal and to a lesser extent mouldic.

3.5 Depositional Model

Figure 3.10 illustrates our proposed depositional model of the Arab-D reservoir in Khurais field. This model was constructed by defining the recognized lithofacies components, their stratigraphic positions in core, the nature of their boundaries and sedimentary structures, their bedding thickness trends, in addition to being integrated with Hughes' (2004b, 2009) published micropalaeontological analysis of Arab-D samples. This model is of a prograding, gently sloping, arid, shallow, rimmed carbonate shelf, which was subjected to frequent storm 'shaving' that deposited turbidites. The following points summarise key aspects pertaining to the model:

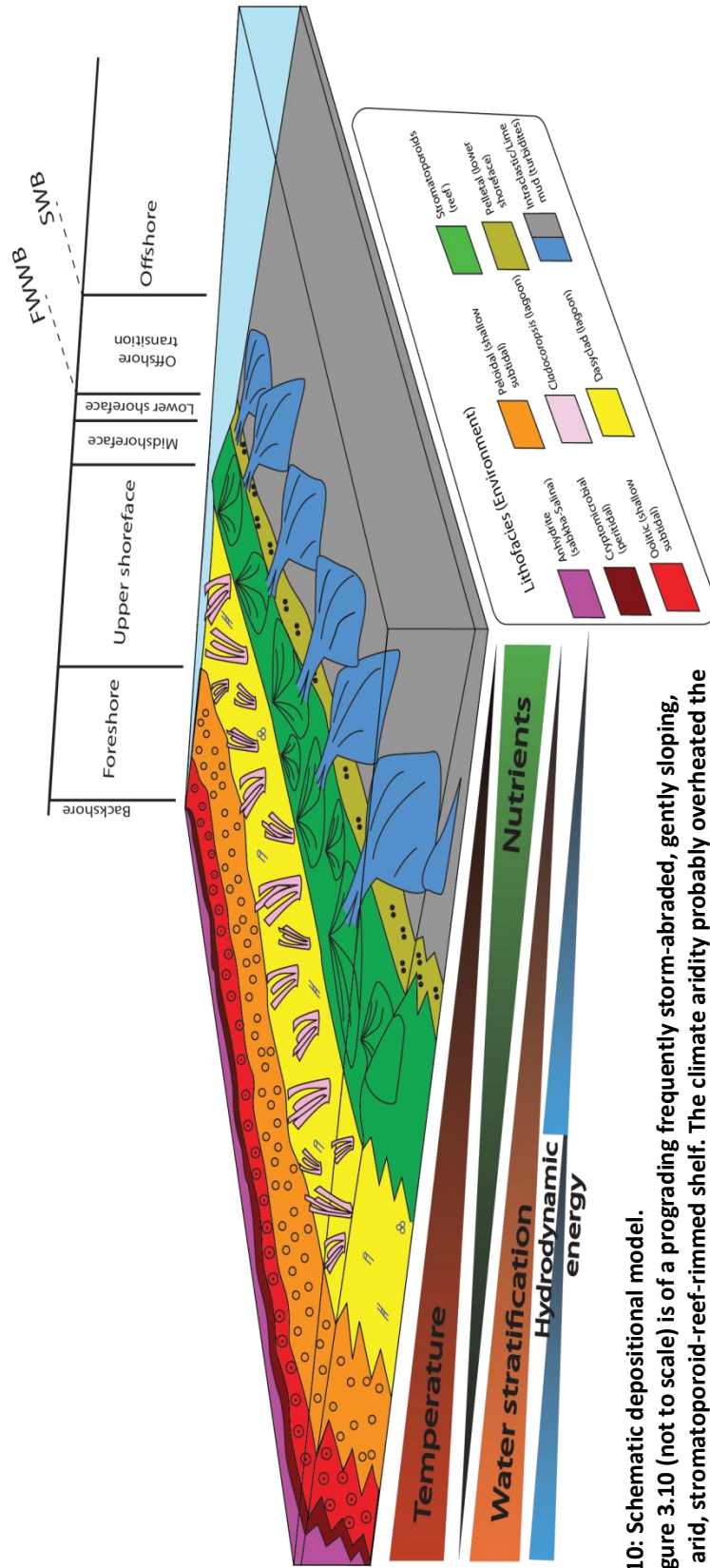


Figure 3.10: Schematic depositional model.

Notes: Figure 3.10 (not to scale) is of a prograding frequently storm-abraded, gently sloping, shallow, arid, stromatoporoid-reef-rimmed shelf. The climate aridity probably overheated the nearshore waters as shown by the temperature gradient. This overheating inflicted a corresponding vertical water stratification gradient. The enormous width and shallow depth of the shelf probably cut off water circulation with the Neo-Tethys and caused nutrients to decrease landward. The hydrodynamic energy increased up to the reef, decreased by reef resistance to waves in the lagoon, and increased back up to the shoreface. The salina and sabkha environment was followed basinward by peritidal settings, with stromatolites, and shallow subtidal settings, with ooids and peloids deposited as shore-attached sand sheets. These were followed by a *Cladocoropsis* and *Dasycladacean* algae lagoon that was protected by a rim densely populated by small-scale stromatoporoid reefs. These were succeeded by lower shoreface environment characterised by pelletal sands and silts at or near the FWWB. Storms mainly reworked the reefs generating turbidites, which are shown (cross sectional view) to represent wedging out basinward. Finally, lime muds draped the turbidites (E(t) and E(h) divisions of Bourma Sequence) and/or transgressed over the turbidites as pelagic rain. SWB is storm wave base. The entire platform was ~ 1000 km wide (Figure 3-2); the vertical cored section (Enclosure 1) is ~ 100 m long.

- Progradation took place from the shallow epeiric shelf into the relatively deep Arabian intrashelf basin (Figure 3.2) (Leinfelder et al., 2005; M. A. Ziegler, 2001);
- The epeiric sea waters were probably overheated as suggested by palaeoclimatic modelling (Alsharhan & Sadooni, 2003; Moore, Sloan, Hayashida & Umrigar, 1992; Sellwood et al., 2000);
- Palaeogeographic reconstruction and proximity to palaeoequator (Figure 3.2) (Li & Powell, 2001) also suggest overheating of the waters;
- Evaporites that are characterized by chicken wire fabrics and cap the succession, and presence of miliolid foraminifera and *Clypeina* suggested water shallowness;
- The water probably cooled and caused a vertical water stratification (Leinfelder et al., 2005) towards the intrashelf basin (Figure 3.10);
- The enormous width and shallow depth of the shelf (M. A. Ziegler, 2001) probably led to cutting the water circulation off with the Neo-Tethys and yielded a decrease in nutrient supply landward (Figure 3.10) (Leinfelder et al., 2005);
- The gulf's present-day bathymetry of 33 ft (10 m) FWWB, and 164 ft (50 m) storm wave base (SWB) (Hughes, Varol, & Al-Dhubeeb, 2004; Lindsay et al., 2006), can be thought of, with caution, as a proxy for the Arab-D-time (Handford et al., 2002; Kinsman & Park, 1976; Moore et al., 1992; Sellwood et al., 2000).

The stratigraphic position of the recognized lithofacies represent an overall upward-shallowing succession (see discussion below), that is punctuated by parasequences and parasequence sets (Figure 3.3) caused by high frequency eustatic changes. This interpretation is in agreement with the micropalaeontological tiering observed by Hughes (2004), where he deduced that upward tiering faunal assemblages on the scale of 10 ft (3 m) represent sea level shallowing of possibly 66 ft (20 m).

3.5.1 Intraclastic and Lime Mud Lithofacies

Starting at the bottom of Aramco HKHK Khurais core (Figure 3.3), the complexity of the lower intraclastic and lime mud lithofacies dictates that we reiterate some of the pertinent facts associated with them. First, these two lithofacies occur monotonously interbedded. Second, both lithofacies are characterised by the presence of HCS, swaley bedding, Bouma sequences, and type-CCC turbidites characterised by the presence of rip-up clasts, convolutions and climbing ripples (Figures 3.7e and 3.9) (Bouma, 1962; Walker, 1985b). Third, the contact between a lime mud bed and an overlying intraclastic bed is almost consistently marked by a sharp hardground or firmground. Fourth, the lime muds show oxygenation halos around hardground burrows. Fifth, the lime mud lithofacies is interpreted to represent the deepest Arab-D lithofacies by Hughes (1996b, 2004), who described the foraminifera *Lenticulina spp.* in this lithofacies, which together with monaxon and tetraxon sponge spicules and juvenile costate brachiopods represent normal marine conditions. This succession in the outcrop uniquely contains ammonites and deep marine trace fossils (Hughes, personal communication, 3 August 2011). Sixth, plotting the thickness of the intraclastic beds against their occurrence depth (Figure 3.8) shows a cyclic pattern that bundles the beds in thickening upward sets, and depicts an overall increase in thickness throughout the lower part of the reservoir.

With the above facts in mind, we think that separating the lime mud lithofacies genetically from the intraclastic lithofacies is not warranted in all cases. Close attention must be paid to the nature of the transition from an intraclastic bed and an overlying lime mud bed. In the less common cases where the transitions are abrupt, it is most likely that the lime muds represent transgression of deep pelagic muds over the intraclastic lithofacies. More commonly however, the transitions are gradational and exhibit Bouma sequences indicating that the two lithofacies are genetically related, which leads to interpreting them as turbidite couplets, placing them by definition below FWWB; (Figure 3.10); (Walker, 1984). In these latter cases, it is conceivable that the turbidity currents avalanched down the slope and into the basin (see stromatoporoids discussion below), scoured surfaces, ripped up clasts,

and arranged sediments into Bouma sequences. Thus, the lime mud blankets that gradually drape the intraclastic beds are mere Bouma's E(t) divisions (settled down as the turbidity current's energy dwindled to null) and E(h) divisions (turbidity-sourced, hemipelagic muds deposited directly from sea water, where no current movement is involved) (Figure 3.9) (Church, Coniglio, Hardie & Longstaffe, 2003; Walker & James, 1992). This deduction explains the apparent coincidence of the intraclastic beds being consistently situated on hardgrounds that cap the lime mud beds. Had the lime mud been deposited by continuous, slow, deep-water sourced pelagic rain, it would be rather inexplicable to assume that the pelagic "rain" stopped conveniently before every turbidity commencement to allow for the lime muds to cement up and form hardgrounds! The more likely scenario is that every intraclastic and lime mud couplet represents a geologic "instant" of time when a turbidity current avalanched. All of the remaining time subsequent to the turbidity "instant" had probably been consumed in cementing up the deposits and forming a hardground that would be scoured and ripped up by the next turbidity current. Meyer and Price used this geologic "instant" concept of the turbidites to correlate across Ghawar field as discussed further below (F. O. Meyer & Price, 1993).

The HCS that in some cases mark the couplets points out a storm origin and a specific bathymetry between FWWB and SWB; (Walker & James, 1992). This coupled with the cyclicity depicted in Figure 3.8 eliminates tectonic-driven seismic activities as the triggering mechanism of the turbidites. Rather, we interpret the turbidites to be triggered by frequent storms as their wave bases are affected by the cyclic fluctuations of sea level. In other words, as the sea level dropped, it lowered SWB allowing higher levels of energy to strike the reef (see stromatoporoids discussion below), and generating thicker turbidites.

In cases where the turbidites were deposited between FWWB and SWB, the upper divisions of their Bouma sequences (divisions C, D, and E) were likely reworked by storm waves into HCS, whereas full preservation of Bouma sequences was probably attained when the turbidites were deposited below SWB. In the latter case, submarine fans would have been likely to form where channel-levee complexes

would develop in their suprafans yielding type-CCC turbidites, like the one shown in Figure 3.9 (Walker, 1985a).

Thus, the preserved vertical succession of the turbidite couplets represents shallowing-upward from thin incomplete Bouma sequences deposited below SWB in the lower fan, to thicker type-CCC turbidites deposited below SWB in the mid-fan, to even thicker – and probably amalgamated – HCS to swaley bedded stratified couplets deposited between FWWB and SWB.

Finally, the oxygenation halos marking the hardground burrows in the lime muds suggest that they were deposited in anoxic conditions; a phenomenon known to happen in basins separated from the open ocean by shallow sills (Leeder, 2011), which is the case of the Arabian intrashelf basin being separated from the Neo-Tethys (M. A. Ziegler, 2001).

3.5.2 Pelletal Lithofacies

Landward from the interpreted turbidites, the pelletal lithofacies is characterised by silt and very-fine-sand-sized particles, moderate sorting, bioturbation, and horizontal lamination. These features represent a low energy environment where physical processes are still in play; because of this, we position this lithofacies in the lower shoreface, above or near FWWB (Figure 3.10).

3.5.3 Stromatoporoid Lithofacies

Further landward the stromatoporoid lithofacies is deposited. The observed gregarious laminar and domical stromatoporoid growth forms and the presence of microbial encrustations, characterized by micritized microbial fibers and few lamina coating stromatoporoid heads, in this lithofacies are interpreted as a reef (Figure 3.10) in the sense of (Wood, 1999): “a discrete carbonate structure formed by in situ or bound organic components that develops topographic relief upon the sea floor” (p. 5). The fact that the stromatoporoids in this lithofacies are mostly

reworked is taken in light of the findings of Blanchon, Jones, & Kalbfleisch (1997); Hubbard (1992); Hubbard, Miller, & Scaturro (1990); Montaggioni, (2005); and R. A. Wood, (1995, 2001), who concluded that the interlocked, in place, framework requirements in the literature for defining reefs are difficult to demonstrate in modern and ancient examples. In fact Hubbard goes as far as describing the term 'framework' in reef terminology and definition as 'troublesome,' as he demonstrates that up to 90% of his studied reefs are composed of detritus (reworked reef components and bioeroded sediments that were reincorporated in reef accretion) and voids (Hubbard, 1992; Hubbard et al., 1990; R. A. Wood, 2001). Moreover, we think that Arab-D stromatoporoids reefs, were probably kept from being overwhelmed by detrital sediments by the storm reworking, as was demonstrated by Hubbard's (1992) and Hubbard et al.'s (1990) results. Leinfelder et al. (2005), documented that about 20% of the Upper Jurassic reefs have significant stromatoporoids with corals; and another 10% are dominated by stromatoporoids, especially in the southern Neo-Tethys and Intra-Neo-Tethys areas.

Based on the stratigraphic position of life assemblages of the stromatoporoids in beach-capped, shoaling-up sequences, they have been determined to live in mid-to-upper shoreface environments at palaeowater depths of less than 10 m (see Toland, 1994). Stromatoporoids are also absent from *Lithocodium*-dominated facies which have an estimated palaeowater depth of 15–60 m (Banner, Finch & Simmons, 1990; Toland, 1994; R. A. Wood, 1987). This coupled with the stromatoporoid's reworked nature suggests that they were able to build wave-resistant reefs, as their reworking and displacement is highly unlikely to be the result of fair-weather waves, but rather storm waves. With this in mind, interpreting the stromatoporoid lithofacies as reefs explains the apparent discrepancy between the heterogeneous, muddy nature of its matrix and the high energy of its hydrodynamic position in the mid-to-upper shoreface, simply by reef resistance to wave energy. This conclusion contrasts with Meyer and Price (1993), who positioned the stromatoporoids at FWWB and attribute the matrix muddiness to low hydrodynamic energy.

The fact that the stromatoporoids are stratigraphically limited to the middle interval

of the Arab-D reservoir (Figure 3.3), suggests a palaeoenvironmental control on their ecological niches. Salinity could be a control, as they are absent from the hypersaline waters that are transitional to deposition of the anhydrite caps; yet stromatoporoids are tolerant to slight hypersalinity as they dominate in echinoderm-free intervals of the Arab-D (Leinfelder et al., 2005). On the other hand, the absence of stromatoporoids in *Lithocodium*-dominated sediments and their limitation to pure carbonates (as opposed to argillaceous carbonates or siliciclastics) suggests a dependence on well-lit waters, which could be explained by a bacterial-photosymbiotic feeding habit in addition to their filter-feeding one (Leinfelder et al., 2005). It is likely that the well-lit, slightly hypersaline water requirements for stromatoporoids were only met at the rims of the intrashelf basins, hence limiting stromatoporoids to this narrow geographic niche; this conforms with Powers et al.'s (1966) and Le Nindre et al.'s (1990) conclusions. The position of the stromatoporoid reefs at the intrashelf basin rims probably increased the slope into the basin, and thus gave more momentum to the interpreted turbidity currents (see discussion above). This deduction is supported by Meyer and Price (1993), who used the turbidites to correlate across Ghawar field, and showed that the stromatoporoid and shallower lithofacies dip at a gentler angle than the intraclastic and lime mud lithofacies.

Although the stromatoporoid reefal buildups were insignificant in height, 10–16 ft (3–5 m) high and 98 ft (30 m) wide (Hughes et al., 2004; Hughes et al., 2004; Hughes, 2004; Meyer et al., 1996a, 1996b), their relief would have been accentuated by the gentle nature of the shelf behind it (F. O. Meyer, 2000). This configuration probably contributed to the composition of the interpreted turbidites in two ways. First, although the shelf's carbonate factory extended from the stromatoporoid reef all the way upslope to the cryptomicrobial lithofacies, for the most part, only the reefs sourced sediments to the turbidites, as they were the highest points facing abrasion by storms coming towards the shoreline. Second, the reefs, being elevated barriers, prevented storm transportation of sediments from the back-reefal area down slope. Both of these interpretations are supported by the facts that reworked stromatoporoids contribute substantially to the makeup of the

lower turbidites (Figure 3.7f), and the paucity of shallower than stromatoporoid components in the turbidites.

Last, based on our preliminary stratigraphic correlation of several cores across Khurais field, and by Hughes (2004) and Meyer et al. (1996) outcrop observation, we think that these stromatoporoid reefs were not laterally continuous; yet they were probably rather abundant in the mid-to-upper shoreface of the Arab-D shelf, as illustrated in Figure 3.10.

3.5.4 Dasycladacean algae Lithofacies

The stromatoporoid reefal buildups, as interpreted above, would have facilitated the deposition of mud-dominated textures in the upper shoreface, in a lagoon behind the stromatoporoid reef, by hindering wave energy. The dasycladacean algae lithofacies is interpreted as being deposited in this upper-shoreface lagoon (Figure 3.10). This interpretation accords with the lack of stratification, abundance of bioturbation and wispy lamination in the dasycladacean algae lithofacies, which reflects a reduced energy setting where biologic rather than physical processes are the determinant factor. This interpretation is also in line with Hughes' (2004) interpretation of the foraminiferal assemblages associated with this lithofacies as lagoonal.

3.5.5 *Cladocoropsis* Lithofacies

The *Cladocoropsis* lithofacies is stratigraphically mixed with the dasycladacean algae lithofacies. This suggests that it probably existed as bush-like aggregates, or a meadow within the lagoon (Figure 3.10). In fact, the *Cladocoropsis* presence behind the reef could have further reduced energy and enhanced mud deposition as its dendroid form would have baffled wave energy. Storm activity in the lagoon is manifested in the *Cladocoropsis* dendritic or branching form, which is a morphologic adaptation known to flourish in abrasive settings, and it is capable of substantial sediment shedding and is beneficial in keeping up with high sedimentation rate

(Toland, 1994). Storm activity is also evident by the frequent reworking of the *Cladocoropsis*, which generally leaves them out of growth position. Worthy of notice is that *Cladocoropsis* floatstones and the rudstones base the peloidal lithofacies in fining upward sequences (Figure 3.3, upper part of Figure 3.5a), suggesting that the *Cladocoropsis* were transported up-dip, probably by storms. In other words, when storms struck, they probably winnowed the lagoonal sediments from the muds, carried the bigger grains, the *Cladocoropsis* stems, up-dip and concentrated them in thin sheets that were later capped by the peloidal lithofacies. Lastly, the fact that the *Cladocoropsis* and dasycladacean algae lithofacies intermix and variably overlie the stromatoporoid lithofacies suggests a random distribution of the *Cladocoropsis* within the lagoon rather than occurrence in a specific zone or belt as suggested by Lindsay et al. (2006) and Hughes (2004).

3.5.6 Peloidal Lithofacies

Further landward, the low angle cross stratification, rounded, sorted and winnowed components that are characteristics of the peloidal lithofacies indicate an increase in hydrodynamic energy, and an increase in sorting and abrasion ability as the lithofacies belts continue shallowing toward the shoreline. Therefore, we interpret this lithofacies as a peloidal sand sheet in the wave dominated foreshore area (Figure 3.10).

3.5.7 Oolitic Lithofacies

The oolitic lithofacies' well-rounded, well-sorted, well-winnowed depositional texture, and its cross-bedded structure suggests a further increase in hydrodynamic energy, as the lithofacies belts continue shallowing to agitated-water conditions. Due to the absence of muddy lagoonal sediments separating the oolitic lithofacies from the overlying Cryptomicrobial lithofacies, we interpret it as a foreshore oolitic sand sheet fringing the Arab-D-time shoreline (Figure 3. 10), as opposed to an oolitic shoal as suggested by Lindsay et al. (2006).

3.5.8 Cryptomicrobial Lithofacies

The microbial laminae in the cryptomicrobial lithofacies together with its restricted fauna, dominated by cerithiid gastropods, and stratigraphic position right below the anhydrites represent hypersaline, peritidal stromatolites deposited in the backshore area (Figure 3.10). This conclusion is in line with the microfaunal assemblage recognized by Hughes (2004) in this lithofacies.

3.5.9 Anhydrite Lithofacies

Further backshore, the anhydrite lithofacies represents deposition in a sabkha type environment, at least in its lower interval. This is evident by the chicken wire fabrics that characterise the lower interval of the anhydrites and its displacive nature, together with its stratigraphic position right above the cryptomicrobial lithofacies. The change from the chicken wire fabric to the bedded nodular and ultimately massive fabrics could be interpreted as a change from a sabkha to a salina environment, where evaporites were produced subaqueously, allowing accommodation for the deposition of the thick (*ca.* 164 ft/50 m) anhydrite seal, and indicating a possible transgressive expansion of the salina.

3.6 Accommodation and Physical versus Ecological Process

The whole Arab-D succession can be divided in terms of dominance of physical and ecological process into three realms. The first realm spans from the peloidal sand sheet upward, plus the pelletal lithofacies (Figure 3.3). Fair-weather waves are the dominant controller of sorting, sediment dispersal, and sedimentary structures in this shallow realm; except for the storm-wave effected, normally graded, shallowing-upward cycles of *Cladocoropsis* bases and peloidal caps (Figure 3.3 and Figure 3.5a). The second realm is the reef and the lagoon protected by it, where

ecological processes, namely, stromatoporoid-reef resistance and *Cladocoropsis* baffling to wave energy, control sediment size, sorting and dispersal. The third realm represents the intrashelf basin and includes the intraclastic and lime mud lithofacies, where storm abrasion and reworking and turbidity currents are the controlling factors on the sorting, grain size shape and composition, sediment dispersal, and sedimentary structures. In terms of accommodation space, the presence of the reefal framework above FWFB, and its resistance to wave energy, allowed for ecologically-driven accommodation above the wave base “razor” (Figure 3.10) (Pomar & Kendall, 2008).

3.7 Conclusions

The world’s largest oil reservoir, the Arab-D, is present in one of Saudi Arabia’s largest onshore oil fields, Khurais. Detailed (4 in-scaled (10 cm)) core analysis of the Arab-D reservoir in Khurais Field led to the recognition of eleven lithofacies that begin with, at the bottom of the reservoir, monotonously interbedded units of intraclastic floatstone and rudstone that abruptly overlie hardground-capped skeletal wackestone and lime mudstone. These lower lithofacies are overlain by pelletal wackestone and packstone units that pass up into stromatoporoid wackestone, packstone and floatstone units. Overlying these are *Cladocoropsis* wackestone, packstone and floatstone, dasycladacean algae wackestone and packstone, and peloidal packstone and grainstone units. Ooid grainstone units cap the succession and are in turn capped by cryptomicrobial laminites and ultimately evaporites.

This depositional succession represents shallow epeiric carbonate and evaporite lithofacies that prograded across the Late Jurassic Arabian shelf and into the relatively deep Arabian intrashelf basin.

The depositional model interpreted here is of a gently sloping, shallow, arid, reef-rimmed carbonate shelf, which was subjected to frequent storm “shaving” that

triggered turbidity avalanches. The lithofacies are interpreted to have been deposited in the following environment in ascending order: submarine turbidite fans shallowing up into FWWB pelletal silts and sands, stromatoporoid reefs, *Cladocoropsis* and *Clypeina* lagoon, peloidal and oolitic sand sheets, supratidal stromatolites, and finally evaporitic flats and salina.

3.8 Acknowledgments

We would like to thank Saudi Aramco for granting permission to publish this study. Our appreciation is also extended to Aus Al-Tawil of Saudi Aramco for his continuous support and tireless commitment. The comments and critique we received from Luis Pomar, University de les Illes Balears, Spain, Robert Lindsay and Wyn Hughes of Saudi Aramco, Langhorne Smith, New York State Museum, USA and Jerry Lucia, University of Texas at Austin, USA were as insightful as they were essential.

3.9 References

- Al-Afalge, N. I., S. Al-Garni, B. Rahmeh, and A. Al-Towailib, 2002, Successful integration of sparsely distributed core and well test derived permeability data in a viable model of a giant carbonate reservoir: Society of Petroleum Engineers Annual Technical Conference and Exhibition, San Antonio, Texas, SPE Paper 77743, p. 1–8, doi:10.2118/77743-MS.
- Al-Husseini, M. I., 2000, Origin of the Arabian plate structures: Amar collision and Najd rift: *GeoArabia* (Manama), v. 5, p. 527–542.
- Al-Mulhim, W. A., F. A. Al-Ajmi, M. A. Al-Shehab, and T. R. Pham, 2010, Khureis complex: Part 1. Field development required best practices, leveraged technology: *Oil & Gas Journal*, v. 108, p. 37–38, 40–42.
- Alsharhan, A. S., and C. G. S. C. Kendall, 1986, Precambrian to Jurassic rocks of Arabian Gulf and adjacent areas: Their facies, depositional setting, and hydrocarbon habitat: *AAPG Bulletin*, v. 70, p. 977–1002.
- Alsharhan, A. S., and F. N. Sadooni, 2003, Eustatic overprints on the diagenetic evolution of Mesozoic platform carbonates from the Arabian plate: *AAPG Annual Meeting Expanded Abstracts*, v. 12, p. 5.
- Ayres, M. G., M. Bilal, R. W. Jones, L. W. Slentz, M. Tartir, and A. O. Wilson, 1982, Hydrocarbon habitat in main producing areas, Saudi Arabia: *AAPG Bulletin*, v. 66, p. 1–9.
- Banner, F. T., E. M. Finch, and M. D. Simmons, 1990, On *Lithocodium Elliott* (calcareous algae): Its paleobiological and stratigraphical significance: *Journal of Micropalaeontology*, v. 9, p. 21–35, doi:10.1144/jm.9.1.21.
- Barger, T. C., 1984, Birth of a dream: Saudi Aramco world: Houston, Texas, Aramco Services Company, p. 34–41.
- Blanchon, P., B. Jones, and W. Kalbfleisch, 1997, Anatomy of a fringing reef around Grand Cayman: Storm rubble, not coral framework: *Journal of Sedimentary Research*, v. 67, p. 1–16.
- Blasband, B., S. White, P. Brooijmans, H. De Boorder, and W. Visser, 2000, Late Proterozoic extensional collapse in the Arabian-Nubian shield: *Journal of the*

- Geological Society, v. 157, p. 615–628, doi:10.1144/jgs.157.3 .615.
- Bodenbender, B. E., M. A. Wilson, and T. J. Palmer, 1989, Paleocology of Sphenothallus on an Upper Ordovician hardground: *Lethaia*, v. 22, p. 217–225, doi:10.1111/j .1502-3931.1989.tb01685.x.
- Bouma, A. H., 1962, *Sedimentology of some flysch deposits: A graphic approach to facies interpretation*: Amsterdam, Elsevier Publishing Company, 168 p.
- Church, M., M. Coniglio, L. A. Hardie, and F. J. Longstaffe, 2003, Encyclopedia of sediments and sedimentary rocks, in G. V. Middleton, ed., *Encyclopedia of Earth sciences series*: Dordrecht, Netherlands, Springer, p. 928.
- De Castro, P., 1990, Thaumatoporelle: Conoscenze attuali e approccio all'interpretazione: *Bollettino della Societa Paleontologica Italiana*, v. 29, p. 179–206.
- Droste, H., 1990, Depositional cycles and source rock development in an epeiric intraplateau basin: The Hanifa Formation of the Arabian Peninsula: *Sedimentary Geology*, v. 69, p. 281–296, doi:10.1016/0037-0738(90)90054-W.
- Dunham, R. J., 1962, Classification of carbonate rocks according to depositional texture, in W. E. Ham, ed., *Classification of carbonate rocks: Memoir 1*, p. 108–121.
- Embry III, A. F., and J. E. Klovan, 1971, A late Devonian reef tract on northeastern Banks Island, N.W.T: *Bulletin of Canadian Petroleum Geology*, v. 19, p. 730–781.
- Enay, R., 1993, Les apports sud-Tethysiens parmi les faunes jurassiques Nord-Ouest Europeennes: Interpretation paleobiogeographique: *Comptes Rendus de l'Academie des Sciences Serie 2*, v. 317, p. 115–121.
- Golonka, J., 2002, Plate-tectonic maps of the Phanerozoic: *Society for Sedimentary Geology Special Publication 72*, p. 21–75.
- Handford, C. R., D. L. Cantrell, and T. H. Keith, 2002, Regional facies relationships and sequence stratigraphy of a super-giant reservoir (Arab-DMember), Saudi Arabia: *Society of Economic Paleontologists Gulf Coast Section Research Conference Program and Abstracts 22*, p. 539–563.
- Hubbard, D. K., 1992, Hurricane-induced sediment transport in open-shelf tropical systems: An example from St. Croix, U.S. Virgin Islands: *Journal of*

- Sedimentary Research, v. 62, p. 946–960.
- Hubbard, D. K., A. I. Miller, and D. Scaturro, 1990, Production and cycling of calcium carbonate in a shelf-edge reef system (St. Croix, U.S. Virgin Islands): Applications to the nature of reef systems in the fossil record: *Journal of Sedimentary Research*, v. 60, p. 335–360.
- Hughes, G. W., 1996, A new bioevent stratigraphy of Late Jurassic Arab-D carbonates of Saudi Arabia: *GeoArabia (Manama)*, v. 1, p. 417–434.
- Hughes, G. W. A. G., 2004, Middle to Upper Jurassic Saudi Arabian carbonate petroleum reservoirs: Biostratigraphy, micropaleontology and paleoenvironments: *GeoArabia (Manama)*, v. 9, p. 79–114.
- Hughes, G. W. A. G., 2009, Using Jurassic micropaleontology to determine Saudi Arabian carbonate paleoenvironments: *Society for Sedimentary Geology Special Publication 93*, p. 127–152.
- Hughes, G. W., A. G. Dhubeeb, O. Varol, R. F. Lindsay, H. Mueller, and Anonymous, 2004a, The Arab-D biofacies of Saudi Arabia: Their paleoenvironment and new biozonation: *GeoArabia (Manama)*, v. 9, p. 79–80.
- Hughes, G. W., O. Varol, A. Al-Dhubeeb, and Anonymous, 2004b, Biofacies and paleoenvironments of Late Jurassic carbonates of Saudi Arabia: *Congres Geologique International Resumes*, v. 32, part 2, p. 893.
- Kinsman, D. J. J., and R. K. Park, 1976, Algal belt and coastal sabkha evolution, Trucial Coast, Persian Gulf: *Stromatolites*: Amsterdam, Elsevier Science Publishing Company, p. 421–433.
- Konert, G., A. M. Afifi, S. A. Al-Hajri, K. de Groot, A. A. Al Naim, and H. J. Droste, 2001, Paleozoic stratigraphy and hydrocarbon habitat of the Arabian plate: *AAPG Memoir 74*, p. 483–515.
- Leeder, M., 2011, *Sedimentology and sedimentary basins: From turbulence to tectonics*: Oxford, United Kingdom, Wiley-Blackwell, 768 p.
- Leinfelder, R. R., F. Schlagintweit, W. Werner, O. Ebli, M. Nose, D. U. Schmid, and G.W. Hughes, 2005, Significance of stromatoporoids in Jurassic reefs and carbonate platforms: Concepts and implications: *Facies*, v. 51, p. 299–337, doi:10.1007/s10347-005-0055-8.
- Le Nindre, Y. M., J. Manivit, and D. Vaslet, 1990, *Stratigraphie sequentielle du*

- Jurassique et du cretace en Arabie Saoudite: Societe Geologique de France Bulletin, Paris, v. 6, p. 1025–1035.
- Li, Z.-X., and C. M. Powell, 2001, An outline of the paleogeographic evolution of the Australasian region since the beginning of the Neoproterozoic: *Earth-Science Reviews*, v. 53, p. 237–277, doi:10.1016/S0012-8252(00)00021-0.
- Lindsay, R. F., D. L. Cantrell, G. W. Hughes, T. H. Keith, H. W. Mueller III, and D. Russell, 2006, Ghawar Arab-D reservoir: Widespread porosity in shoaling-upward carbonate cycles, Saudi Arabia: *AAPG Memoir* 88, p. 97–138.
- Meyer, F., 2000, Carbonate sheet slump from the Jubaila Formation, Saudi Arabia: Slope implications: *GeoArabia (Manama)*, v. 5, p. 144–145.
- Meyer, F. O., and R. C. Price, 1993, A new Arab-D depositional model, Ghawar field, Saudi Arabia: Society of Petroleum Engineers Middle East Oil Technical Conference and Exhibition, Bahrain, April 3–6, 1993, SPE Paper 25576, p. 465–474.
- Meyer, F. O., R. C. Price, I. A. Al-Ghamdi, I. M. Al-Goba, S. M. Al-Raimi, and J. C. Cole, 1996, Sequential stratigraphy of outcropping strata equivalent to Arab-D reservoir, Wadi Nisah, Saudi Arabia: *GeoArabia (Manama)*, v. 1, p. 435–456, doi:10.2118/25576-MS.
- Mitchell, J. C., P. J. Lehmann, D. L. Cantrell, I. A. Al-Jallal, M. A. R. Al-Thagafy, A. J. Lomando, and P. M. Harris, 1988, Lithofacies, diagenesis and depositional sequence: Arab-D Member, Ghawar field, Saudi Arabia: *SEPM Core Workshop* 12, p. 459–514.
- Montaggioni, L. F., 2005, History of Indo-Pacific coral reef systems since the last glaciation: Development patterns and controlling factors: *Earth-Science Reviews*, v. 71, p. 1–75, doi:10.1016/j.earscirev.2005.01.002.
- Moore, G. T., L. C. Sloan, D. N. Hayashida, and N. P. Umrigar, 1992, Paleoclimate of the Kimmeridgian/Tithonian (Late Jurassic) world: Part II. Sensitivity tests comparing three different paleotopographic settings: *Palaeogeography, Palaeoclimatology, Palaeoecology*, v. 95, p. 229–252, doi:10.1016/0031-0182(92)90143-S.
- Mouawad, J., 2010, China's growth shifts the geopolitics of oil: *New York Times*, p. B1: <http://www.nytimes.com/2010/03/20/business/energy> -

environment/20saudi.html?pagewanted=all&_r=0 (accessed January 29, 2013).

Murris, R. J., 1980, Middle East: Stratigraphic evolution and oil habitat: AAPG Bulletin, v. 64, p. 597–618.

Net Resources International, 2011, Saudi Aramco Khurais Mega Project, Khurais Saudi Arabia: <http://hydrocarbons-technology.com/projects/khurais> (accessed April 12, 2012).

Palmer, T. I. M., 1982, Cambrian to Cretaceous changes in hardground communities: Lethaia, v. 15, p. 309–323, doi:10.1111/j.1502-3931.1982.tb01696.x.

Pomar, L., and C. G. S. C. Kendall, 2008, Architecture of carbonate platforms: A response to hydrodynamics and evolving ecology: Society for Sedimentary Geology Special Publication 89, p. 187–216.

Powers, R. W., 1968, Lexique stratigraphique international: volume 3: Paris, France, Centre National de la Recherche Scientifiques, p. 177.

Powers, R.W., L. R. Ramirez, C. D. Redmond, and E. L. Elberg, 1966, Sedimentary geology of Saudi Arabia: Geology of the Arabian Peninsula: U.S. Geological Survey Professional Paper 150, p. 150.

Sellwood, B. W., P. J. Valdes, and G. D. Price, 2000, Geological evaluation of multiple general circulation model simulations of Late Jurassic paleoclimate: Palaeogeography, Palaeoclimatology, Palaeoecology, v. 156, p. 147–160, doi:10.1016/S0031-0182(99)00138-8.

Sorkhabi, R., 2008, The emergence of the Arabian oil industry: GeoExpro, v. 5, no. 6, http://www.geoexpro.com/article/The_Emergence_of_the_Arabian_Oil_Industry/d846be03.aspx (accessed January 29, 2013).

Stampfli, G. M., J. Mosar, P. Favre, A. Pillecuit, and J. C. Vannay, 2001, Permo-Mesozoic evolution of the western Tethys realm: The Neo-Tethys East Mediterranean basin connection: Peri-Tethys Memoir 6—Peri-Tethyan rift/wrench basins and passive margins: Paris (France), Museum National d'Histoire Naturelle, p. 51–108.

Toland, C., 1994, Late Mesozoic stromatoporoids: Their use as stratigraphic tools and paleoenvironmental indicators— Micropaleontology and hydrocarbon

- exploration in the Middle East: London, Chapman and Hall, p. 113–125.
- Walker, R. G., 1984, Channel-levee complexes and submarine fans: An example from Wheeler Gorge, California: SEPM Midyear Meeting Abstracts 1, p. 84-85.
- Walker, R. G., 1985a, Comparison of shelf environments and deep basin turbidite systems: SEPM Short Course Notes 13, p. 465–502.
- Walker, R. G., 1985b, Mudstones and thin-bedded turbidites associated with the Upper Cretaceous Wheeler Gorge conglomerates, California: A possible channel-levee complex: *Journal of Sedimentary Research*, v. 55, p. 279–290.
- Walker, R. G., 1992, Facies models: Response to sea level change: St. Johns, Newfoundland, Geological Association of Canada, p. 239–263.
- Wood, R. A., 1987, Biology and revised systematics of some late Mesozoic stromatoporoids: *Special Papers in Palaeontology*, November, 3789 p.
- Wood, R. A., 1995, The changing biology of reef building: *Palaios*, v. 10, p. 517–529, doi:10.2307/3515091.
- Wood, R. A., 1999, Reef evolution: Oxford, United Kingdom, Oxford University Press, 414 p.
- Wood, R. A., 2001, Are reefs and mud mounds really so different?: *Sedimentary Geology*, v. 145, p. 161–171, doi:10.1016/S0037-0738(01)00146-4.
- Ziegler, M. A., 2001, Late Permian to Holocene paleofacies evolution of the Arabian plate and its hydrocarbon occurrences: *GeoArabia (Manama)*, v. 6, p. 445–504.

Chapter 4: Stacked High Frequency Carbonate Reservoir Sequences in the Arab-D Reservoir, Khurais Field, Saudi Arabia²

4.1 Abstract

The Late Jurassic Arab Formation, the world's most prolific oil-bearing interval, is a succession of thickly interbedded carbonates and evaporites that are defined stratigraphically upsection as the Arab-D, Arab-C, Arab-B and Arab-A members. Each member of the Arab Formation forms a reservoir-bearing carbonate that is capped by a thick evaporite. The topmost evaporite overlying the Arab-A is the Hith Anhydrite.

High-resolution lithofacies analysis (10 cm-scaled) of the Arab-D reservoir led to the identification of the majority of a third-order composite sequence representing the Arab-D Member and the upper part of another third-order composite sequence representing the upper Jubaila Formation. In the example core used in this paper, there are six high-frequency, fourth-order sequences, with 12 parasequence and cycle sets; superimposed over these are 41 parasequences in the upper composite sequence and 123 parasequence-scale cycles in the lower composite sequence.

The high-resolution sequence-stratigraphic framework proposed in this study, together with our previously proposed depositional model of the Arab-D reservoir, should aid in a better understanding of the lithofacies distribution and flow and baffle units' geometric relationships within the reservoir in Khurais Field.

² This chapter has been submitted to *Marine and Petroleum Geology* and is currently under review.

4.2 Introduction

The Late Jurassic Arab Formation was discovered in Khurais Field—one of the Saudi kingdom's largest oil fields, in 1957 (Figure 4.1) (Al-Mulhim et al., 2010). The formation comprises four carbonate members: in ascending order, Arab-D, -C and -B (each capped by a sealing anhydrite), and Arab-A (capped by the Hith Formation anhydrite) (Figure 4.2) (Al-Husseini, 2009; Powers, 1968; Powers et al., 1966; Steineke & Bramkamp, 1952; Steineke et al., 1958). Khurais Field occupies a huge asymmetric NW-SE trending anticline, known as the Khurais-Burgan anticline that was formed during a Precambrian collision, which fused the Arabian Plate together (Figure 4.1) (Al-Afalge et al., 2002; Al-Husseini, 2000). In 2009, the Khurais Mega Project, the largest oil expansion project in history, brought significant production rates from Khurais and adjacent satellite fields (Al-Mulhim et al., 2010; hydrocarbons-technology.com, 2011; Mouawad, 2010).

Earlier studies on the Arab-D reservoir have primarily focused on Ghawar Field, the largest oil field in the world, and controversy over the age, stratigraphic framework and placement of units into specific system tracts is evident throughout the literature on the Arab, Jubaila and Hith Formations. The anhydrites of the Arab Formation have been included with their underlying carbonates in the same time-stratigraphic units by Powers et al. (1966), Al-Husseini (1997, 2009) and Le Nindre et al. (1990). On the other hand, sequence boundaries have been suggested to separate the Arab carbonates from their overlying anhydrites (Lindsay et al., 2006; McGuire et al., 1993). The exact extent of the sequence that spans the Arab-D reservoir and the placement of its maximum flooding surface has also been controversial (Al-Husseini, 1997, 2009; Handford et al., 2002; Hughes, 1996b; Hughes et al., 2004; Hughes, Varol, Hooker & Énay, 2008; Le Nindre et al., 1990; Lindsay et al., 2006; McGuire et al., 1993; Mitchell et al., 1988; Powers et al., 1966; Sharland et al., 2001). The work presented here, is the first to construct a high-resolution sequence-stratigraphic framework of Arab-D in Khurais Field. The recognition of repetitive motifs of reservoir lithofacies-stacking patterns in light of the depositional model presented in Al-Awwad and Collins (2013a) provide the

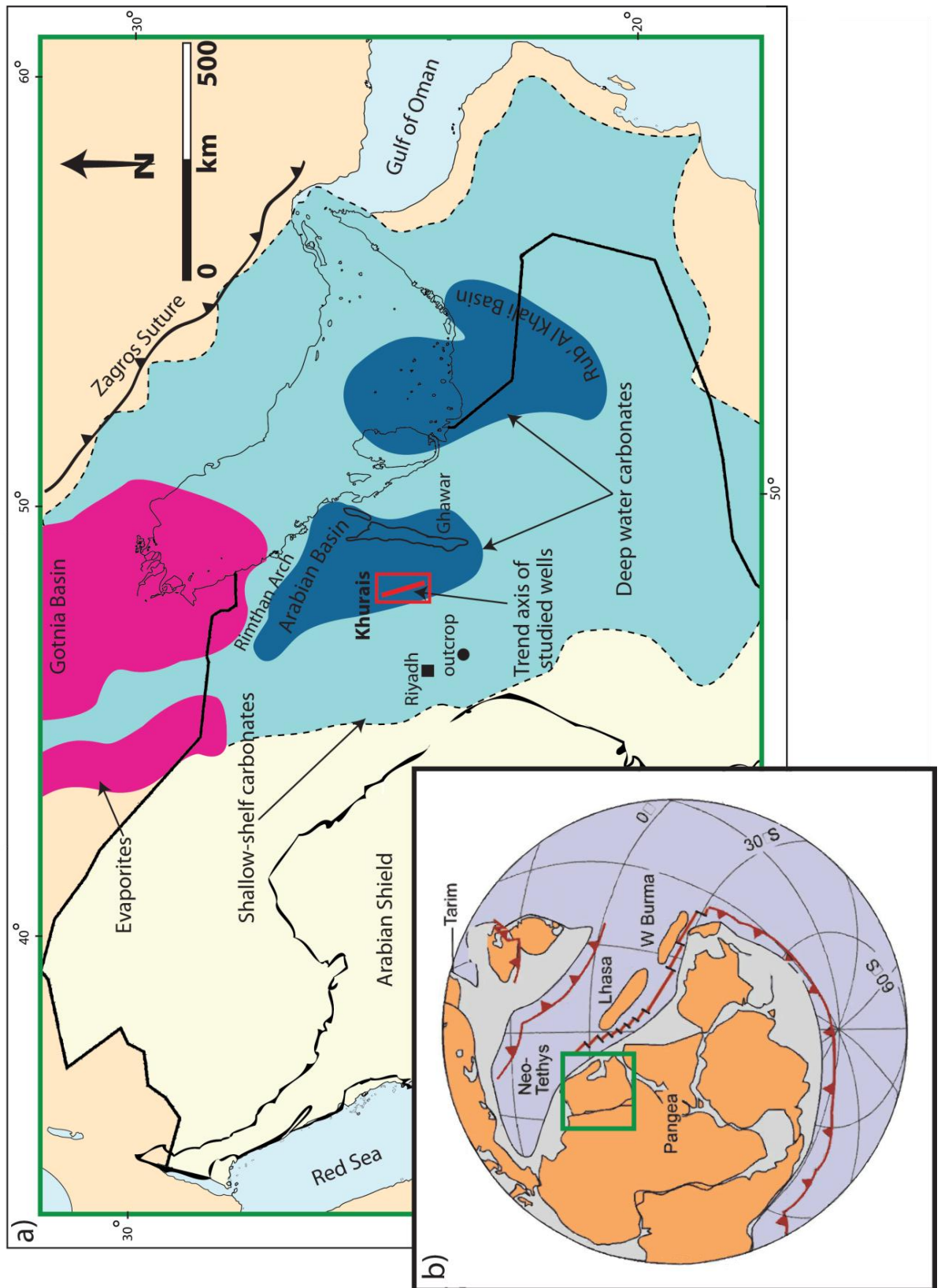


Figure 4.1: Location map of Khurais Field.

Notes: a) The red line depicts the trend axis of wells studied. Late Jurassic intrashelf basins where deposition of deep water carbonates took place are outlined as dark blue areas. Shallow-shelf carbonate deposition is highlighted as the light blue area. b) Li and Powell's paleogeographic configuration of the Jurassic. Orange, pale blue and purple colours depict emergent continents above present sea-level, oceanic areas and mafic volcanic rocks, respectively. The location of the paleo-equator is controversial (Golonka 2002; Stampfli et al. 2002).

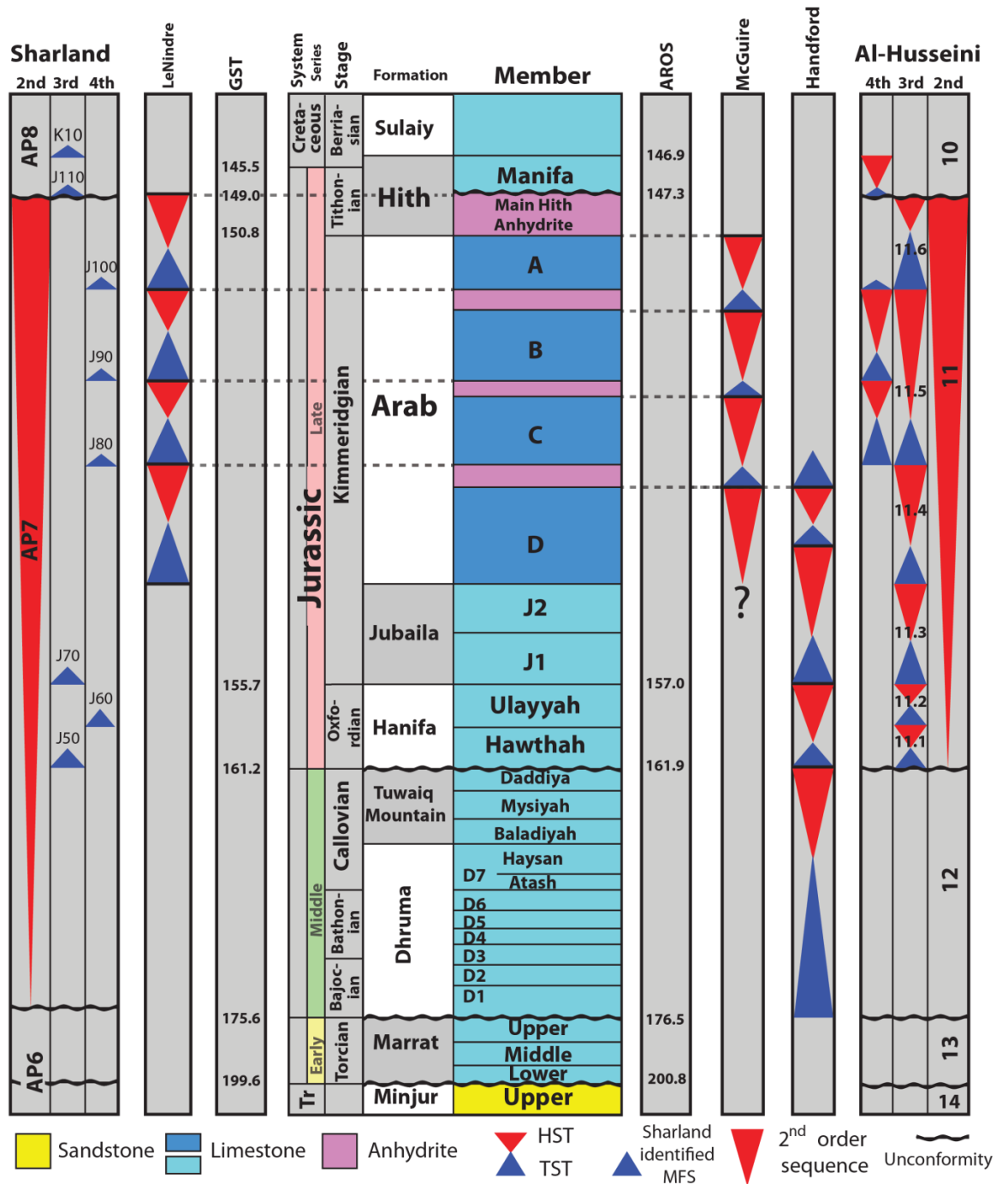


Figure 4.2: Saudi Arabia's Jurassic succession.

Notes: Figure 4.2 is not to scale to emphasise the stratigraphy of the upper Jurassic. Second-, third- and fourth-order sequences are illustrated from Al-Husseini (1997, 2009), and Sharland et al. (2001). Key ages are illustrated from both the GTS (Gradstein et al., 2004) and the Arabian Orbital Stratigraphy Project (Al-Husseini & Matthews, 2008). There is no biostratigraphic control on the age of the Arab and Hith Formations (Hughes, 2004a and b). The contrast between HST and TST definitions within the Arab and Hith are illustrated from McGuire et al. (1993), Le Nindre et al. (1990) and Handford et al. (2002). Note that the Hellangian, Sinemurian, Pliensbachian and Alenian are not represented in Saudi Arabia's succession. The Arab-D reservoir extends from the carbonates of the Arab-D Member of the Arab Formation to the upper part of the Jubaila Formation.

Source: Modified from Al-Husseini (2009), Sharland et al. (2001), Handford et al. (2002), McGuire et al. (1993) and Le Nindre et al. (1990)

basis for the new sequence-stratigraphic framework presented here. Detailed analysis of 32 Arab-D cored wells and more than 500 thin-sections from Khurais Field constitute the data set of this study, which was carried out in Saudi Aramco's Exploration Core Laboratories, Saudi Arabia, and Curtin University, Australia. This framework is presented through the example of the Arab-D core from Aramco HKHK Khurais well (coded name) due to its substantial vertical coverage and representative lithofacies-stacking patterns (Figure 4.3). The results of this study contribute to the understanding of the architectural heterogeneities within the Arab-D reservoir and the geometrical relationships among the different reservoir lithofacies.

4.3 Terminology

The smallest-scale base-level cycle that can be depicted from a set of genetically related, relatively conformable lithofacies and bound by marine flooding surfaces is a parasequence that forms the principal building blocks of this cyclic hierarchy scheme (Goldhammer, Dunn, & Hardie, 1990; Mitchum & Van Wagoner, 1991; Tinker, 1998; Van Wagoner, Mitchum, Posamentier & Vail, 1987). Commonly, each parasequence contains a deepening and a shallowing component represented by upright blue triangles and inverted red triangles, respectively (Tinker, 1998; Van Wagoner et al., 1988; see Figure 4.4). These parasequences are analogues in scale to fifth-order, 10–100 Kyr cycles (Goldhammer et al., 1990). Parasequences stacked in progradational, retrogradational or aggradational trends form parasequence sets that define highstand, transgressive and lowstand system tracts of a fourth-order, 100–400 Kyr, high-frequency sequence (Goldhammer et al., 1990; Harris, Kerans & Bebout, 1993; Kerans, Lucia & Senger, 1994; Mitchum & Van Wagoner, 1991). Several high frequency sequences can stack in prograding, retrograding or aggrading sets that comprise highstand transgressive and lowstand sets of a composite sequence analogous to a third-order cycle of 1–3 Myr (Goldhammer et al., 1990; Haq et al., 1987; Koerschner & Read, 1989; Mitchum & Van Wagoner, 1991; Vail, 1987).

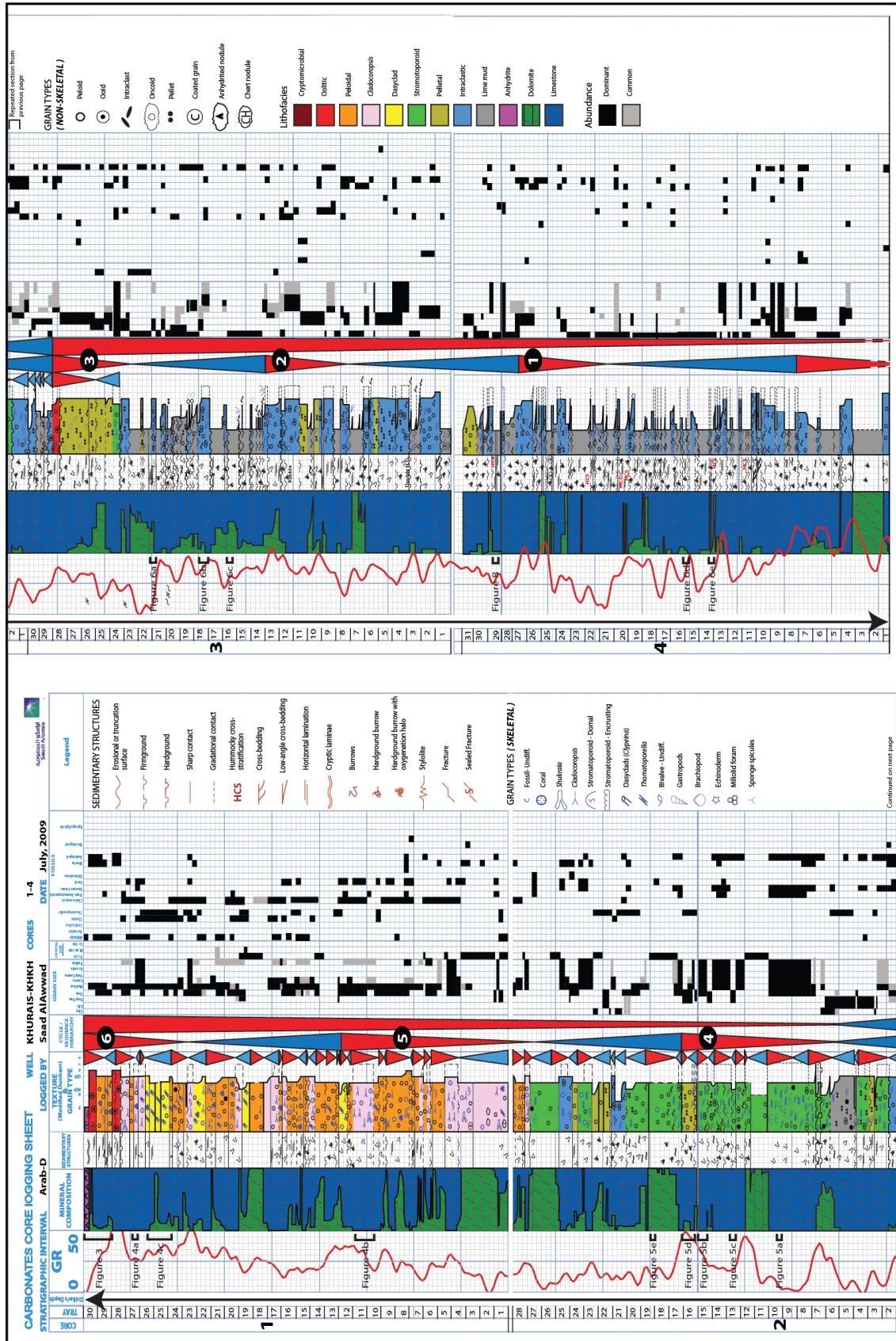


Figure 4.3: Characterisation of the Arab-D reservoir core, Aramco KKH Khurais.
 Notes: Only high-frequency sequences are picked in the monotonously interbedded lower part of the reservoir based on the upward thickness increase of the intraclastic beds (see Figure 4.11).
 High-frequency sequences are numbered in the black circles.

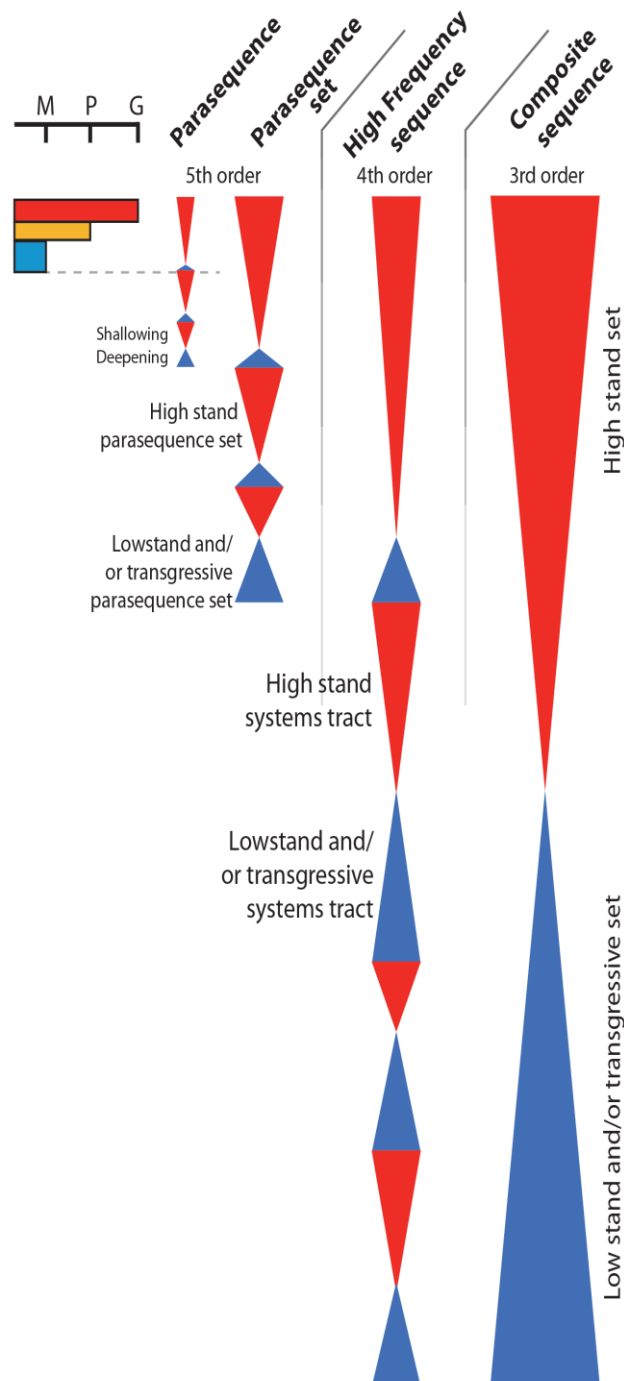


Figure 4.4: Sequence stratigraphic hierarchy.

Notes: A fifth-order parasequence represents the smallest-scale base-level cycle depicted in this study. Upright blue and inverted red triangles represent deepening and shallowing components of a parasequence, respectively. Parasequences stacked in progradational, retrogradational or aggradational trends form parasequence sets that define highstand transgressive and/or lowstand system tracts of a fourth-order high-frequency sequence. High-frequency sequences, in turn, stack in prograding, retrograding or aggrading sets that form highstand transgressive and/or lowstand sets of a third-order composite sequence.

4.4 Geologic and Stratigraphic Setting

The authors recently proposed an Arab-D depositional model of a gently prograding, shallow, reef-rimmed carbonate shelf. Arid climatic conditions prevailed on that shelf, and it was subjected to frequent storm activity that triggered turbidites (Al-Awwad & Collins, 2013a; see Figure 4.5). Progradation in the proposed model took place from the shallow Late Jurassic epeiric shelf into the relatively deep Arabian intrashelf basin (Leinfelder et al., 2005; M. A. Ziegler, 2001; see Figure 4.1). The present-day Arabian Gulf has a 10-m FWWB and 50-m SWB (Hughes, 2004; Lindsay et al., 2006), which can be taken, with caution, as a proxy for the

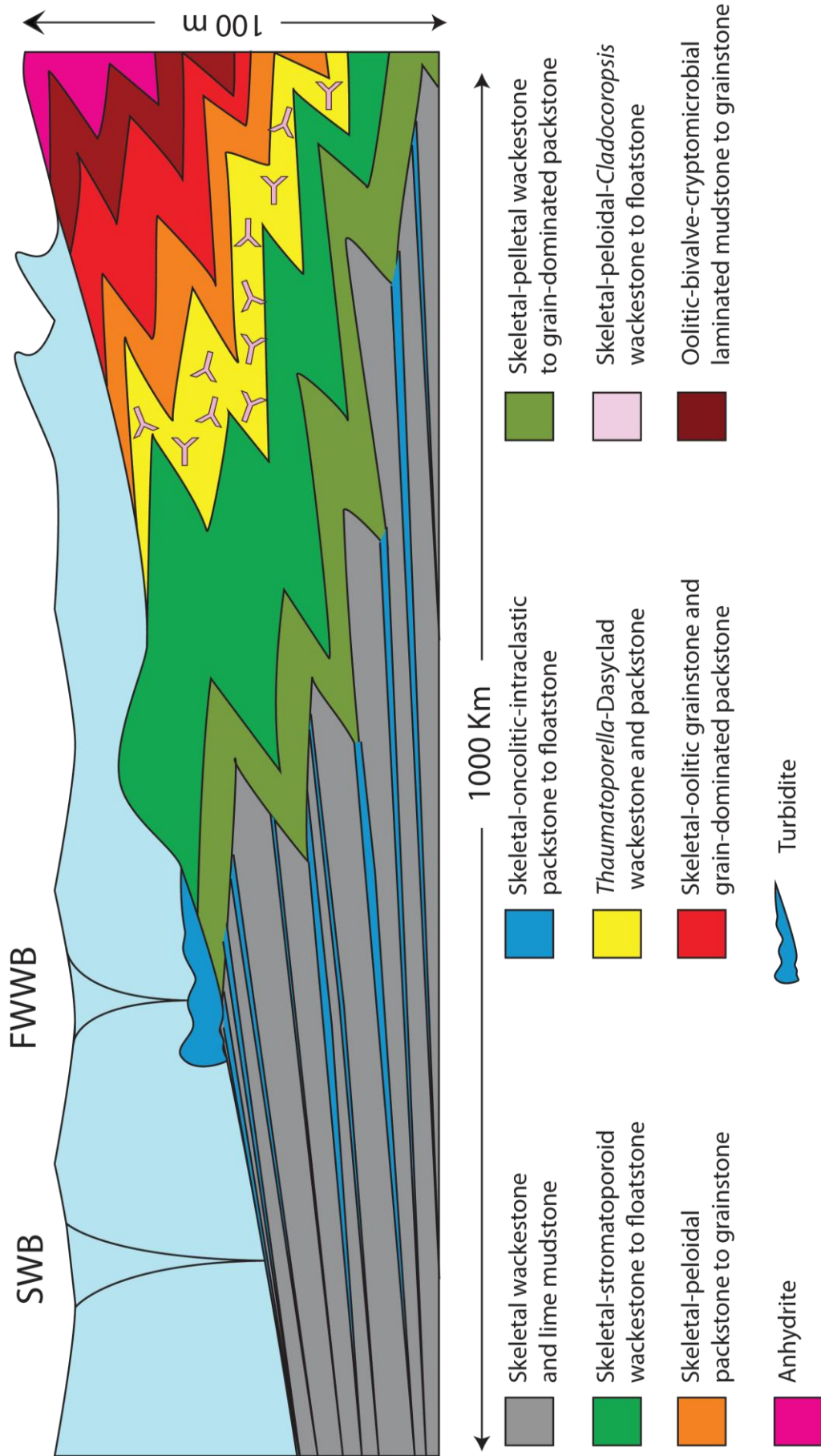


Figure 4.5 (previous page): A schematic depositional model of a prograding frequently storm-abraded, gently sloping, shallow, arid, stromatoporoid-reef-rimmed shelf

Notes: This model is not to scale. Salina and sabkha anhydrites are followed by peritidal stromatolites, and shallow subtidal ooids and peloids sand sheets basinward. These are followed by *Cladocoropsis* and a dasycladacean algae meadow that was protected in a lagoon by a rim of stromatoporoid reefs, which are followed by lower shoreface pelletal sands and silts. Reefs were reworked by storms yielding intraclastic turbidites. Lime muds either covered the turbidites as divisions E(t) and E(h) of Bouma Sequences and/or transgressed over the turbidites as pelagic rain. The platform was about 1,000-km wide (Figure 4.1); the vertical cored section (Figure 4.3) is about 100 m long. This figure is juxtaposed next to an idealised sequence-stratigraphic framework in Figure 4.9.

Source: Modified from L. Pomar, personal communication (2011), Leinfelder et al. (2005) and data from this study.

Arab-D-time conditions due to the striking resemblance between the two systems (Handford et al., 2002; Kinsman & Park, 1976; G. T. Moore et al., 1992; Sellwood et al., 2000). A detailed sedimentological characterisation of the different lithofacies recognised in Khurais's Arab-D cores and their deduced depositional environments (Table 4.1) has been fully discussed in Al-Awwad and Collins (2013a). These lithofacies, in ascending order, are: couplets of 1) lime mud and 2) intraclastic lithofacies representing basinal turbidites; 3) pelletal lithofacies representing lower shoreface sands and silts; 4) stromatoporoid lithofacies representing a reef; 5) *Cladocoropsis* and 6) dasycladacean algae lithofacies representing a lagoon; 7) peloidal and 8) oolitic lithofacies representing shallow subtidal shore-attached sand sheets; 9) cryptomicrobial lithofacies representing peritidal flats; 10) anhydrites representing sabkha then salina deposits; and 11) stratigraphically reoccurring dolomite.

The Khurais-Burgan anticline, which hosts the giant Khurais Field, formed together with three other N-oriented anticlines due to the EW-trending compressional stresses that propagated through the Arabian plate during the Amar collision that fused the plate together 640–620 Myr ago. (Al-Husseini, 2000; Brown et al., 1989; Stoesser & Camp, 1985). The collision was also responsible for an extensive network of faults that cut through the Precambrian basement, propagating movement through the Phanerozoic and breeding structural growth, subsidence and migration of hydrocarbons (Al-Husseini, 2000). The Carboniferous Hercynian orogeny rotated

the Arabian Plate 90° anticlockwise, uplifted and tilted central Arabia to the east and eroded several kilometres of its sediments (Al-Husseini, 2000; Haq & Al-Qahtani, 2005). The late Permian then witnessed the rifting and spreading of the Neo-Tethys, generating a passive margin to Arabia's east (Powers et al., 1966; M. A. Ziegler, 2001). Another passive margin occupied Arabia's northern edge as a result of the opening of the eastern Mediterranean in the Early Jurassic. This configuration yielded a vast shallow-marine shelf that inundated most of the Arabian Peninsula, and blanketed it with shallow-shelf carbonates and evaporite deposition (Énay, 1993; Le Nindre et al. 1987, 1990; Murriss, 1980; Pollastro et al., 1999).

In the Middle Jurassic, four intrashelf basins formed due to epeirogenic downwarp (Alsharhan & Kendall, 1986; Murriss, 1980; M. A. Ziegler, 2001; see Figure 4.1). These basins were the loci of the deposition of organic-rich, anoxic shales in the Hanifa and Tuwaiq Mountain formations (Figure 4.2), which later sourced the Arab Formation oils (Abdulrahman et al., 1986; Ayres et al., 1982; Droste, 1990; Murriss, 1980; M. A. Ziegler, 2001). As Central Arabia remained stable during the Late Jurassic, the Arab Formation carbonates progressively filled the intrashelf basins with repetitive shoaling-upward cycles surmounted by evaporitic flats (Haq & Al-Qahtani, 2005; M. A. Ziegler, 2001). During the same time, the Afro-Arabian and Indian plates rifted, generating another passive margin to the south of Arabia along Southern Oman (Abdulrahman et al., 1986; M. A. Ziegler, 2001). In the Late Cretaceous, the Neo-Tethys closing began due to the Arabian-Eurasian plates compression, which caused the obduction of the Oman ophiolites and the rise of the Zagros Mountains (Abdulrahman et al., 1986; Al-Husseini, 2000; Haq & Al-Qahtani, 2005; Wender, Bryant, Dickens, Neville & Al-Moqbel, 1998; M. A. Ziegler, 2001).

The Phanerozoic rock succession across the Arabian platform is neither complete nor accurately dated (Al-Husseini & Matthews, 2005a). Biostratigraphic and/or radiometric ages of Arabian sequence-stratigraphic surfaces and depositional sequences are ± 5 to 10 Myr, and ± 3 Myr at best, which highlights that caution must be exerted in chronostratigraphic correlations (Al-Husseini & Matthews, 2005a).

Table 4.1: Summary of Arab-D lithofacies and their deduced environmental setting.

Notes: For full discussion of the lithofacies, see Al-Awwad and Collins (2013a).

Lithofacies	Textures	Components	Sedimentary structures	Depositional environment	Porosity types
Lime mud	Wackestone and lime mudstone	lime mud, micritised pellets, bivalves, brachiopods, foraminifera (<i>Lenticulina spp.</i>), echinoderms, blackened and reddened peloids and pellets	Moderately sorted; phosphatised hardground or firmground caps; bioturbation; horizontal laminations; hardground burrows filled with grainier sediments; hummocky cross-stratification; Bouma sequence divisions C, D, E	Basin, offshore transition to offshore	Microporosity, mouldic, intraparticle
Intraclastic	Packstone to floatstones and rudstones	Intraclasts, oncrites, bivalves, reworked stromatoporoid, coral fragments, foraminifera, pellets, peloids	Extremely poorly sorted; phosphatised hardground or firmground bases; sharp to gradational upper contacts; Bouma sequence divisions A, B	Basin, offshore transition to offshore	Interparticle, intraparticle, microporosity
Pelletal	wackestone to grain-dominated packstone	Pellets, bivalve fragments, foraminifera, lime mud	Moderately sorted; gradational or firmground contacts; bioturbation; horizontal laminations	Sands and silts at FWWB, lower shoreface	Mouldic, microporosity
Stromatoporoid	Wackestone to floatstones and rudstones	Displaced domal and encrusting stromatoporoids, corals, microbial incrustations, foraminifera, bivalves, pellets, peloids, oncoids, intraclasts	Very poorly sorted; hardgrounds; firmgrounds; heavy bioturbation; borings	Reef, medium to upper shoreface	Vugular, mouldic, intraparticle
Cladocoropsis	Wackestone to floatstone and rudstones	nodular and dendroid <i>Cladocoropsis</i> , <i>Shuqraia</i> , foraminifera, corals, bivalves, peloids, <i>Clypeina</i> , <i>Thaumatoporella</i>	Poorly sorted; subrounded; firmgrounds; bioturbations; horizontal laminations	Lagoon, upper shoreface	Interparticle, intraparticle, mouldic, vugular
Dasycladacean algae	Wackestone and packstone	<i>Clypeina</i> , <i>Thaumatoporella</i> , miliolid, Kurnubia, bivalves, peloids	firmgrounds; bioturbation; wispy laminations	Lagoon, upper shoreface	mouldic, intraparticle
Peloidal	Packstone to grainstone	Peloids, bivalves, micritised <i>Cladocoropsis</i> , foraminifera	well-sorted; well-rounded to rounded; massive unstratified beds; horizontal lamination; low-angle cross-stratification; bioturbation; graded bedding	Sand sheet, foreshore	Interparticle, mouldic, intraparticle

continued on next page

Oolitic	Grainstone and grain-dominated packstone	Ooids, bivalves, foraminifera	very well-sorted; well-rounded; hardgrounds, firmgrounds; high-and low-angle cross-stratification; horizontal laminations	Sand sheet, foreshore	Interparticle, mouldic
Cryptomicrobial	Mudstone to grainstone	Cryptomicrobial laminates, ooids, cerithiid gastropods and bivalves	Undulated and/or domed mm-scale microbial laminae	Supratidal, backshore	Mouldic
Anhydrite	Vague	Anhydrite	Displasive nodules that increase upward into bedded nodular fabrics and ultimately become massive	Sabkha and Salina, backshore	None
Dolomite	Vague	Sucrosic, mosaic and saddle rhombs	Faint bioturbations	Stratigraphically reoccurring	Intercrystalline, mouldic

Haq and Al-Qahtani (2005) summarised the major hiatuses in the Arabian platform succession as follows:

1. A Carboniferous hiatus that lasted for about 25 Myr in which several kilometres of sediments were removed by the Hercynian Orogeny;
2. A latest Triassic through Early Jurassic hiatus that lasted for about 20 Myr and was caused by the separation of Arabia and Africa from India;
3. An Eocene hiatus caused by the major Antarctic ice cap buildup;
4. An Oligocene hiatus that lasted for about 10 Myr and was caused by the closure of the eastern extension of the Neo-Tethys Ocean.

In addition, Haq and Al-Qahtani (2005) divided the Arabian Phanerozoic succession into periods when eustasy was the dominant or subordinate controller of sedimentation by detecting similarities in cyclic-trends between the Arabian and global sea-level curves. The following divisions have been deduced:

1. From the Cambrian through early Silurian, eustasy was the likely controller of sedimentation, which is attributed to the gentle subsidence that prevailed at that time;
2. From the late Silurian to the Mississippian, little correspondence between the Arabian and global sea-level curves indicates dominance of active

tectonics;

3. From the late Permian to the Triassic, eustasy was the likely sedimentation controller as Arabia moved to equatorial latitudes during that period;
4. From Early Jurassic to early Palaeogene, global and local sea-level curves show agreement, indicating a eustatic control over sedimentation;
5. After the late Eocene, tectonics associated with the closure of the Tethys and emergence of the Zagros Mountains dominated the sedimentary record of the Arabian platform.

These findings of Haq and Al-Qahtani (2005) are supported by Bishop and Jones (1995), who concluded that relative tectonic stability dominated most of the Arabian Plate's Phanerozoic, and Al-Husseini and Matthews (2005a), who stated that most of the stratigraphic discontinuities separating Arabian Plate formations are interpreted as non-tectonic and extend for 100s to a 1,000 km.

In Oman, Immenhauser and Matthews (2004) combined the modelling of an orbital-forcing of the sea-level curve for the Albian with modelling of the sedimentation response to sea-level fluctuations and found a good match between the two, which supports a glacio-eustatic sea-level drive. They stated that as long as the Earth has ice sheets on continents, the stable 404-ky (fourth-order) cycles and 2.4 ± 0.4 Myr (third-order) cycles will be manifested on the relative time scales from Precambrian to Recent and can be utilised in correlation (Immenhauser & Matthews, 2004).

These findings are supported by the orbital-forcing numerical simulations work of Laskar et al. (2004), who highlighted the importance of the 1.2 and 2.4 Myr beats and concluded that Earth's eccentric orbit dominant periodicity is 405 kyr. They named it a straton and predicted it to be usable in providing absolute GTS back to 250 Myr because of its stability (Laskar et al., 2004). In addition, Boulila et al. (2011) examined the impact of long-period orbital modulation on eustasy during the icehouse and greenhouse of the Cenozoic and Mesozoic by applying statistical tests to the revised eustatic curve of Miller, Kominz, Browning et al. (2005) and by using several Cenozoic and Mesozoic sedimentary records. They found a correspondence between third-order sequences and long-period astronomical cyclicity, and

suggested a possible causal link between the two. This coupled with the fact that most of these third-order sequences appear to be globally preserved argues against tectonic-driven sea-level fluctuations (Boulila et al., 2011). They concluded that during the Cenozoic icehouse long-period, obliquity (1.2 Myr) is the major controller on the waning and waxing of polar ice sheets and expresses a strong signal on third-order depositional sequences (Boulila et al., 2011). During the Mesozoic greenhouse, however, long-period eccentricity (2.4 Myr) exerts a stronger control over sea level and is reflected in third-order depositional sequences (Boulila et al., 2011).

Al-Husseini and Matthews (2005a) used an orbital-forcing model, the Arabian Orbital Stratigraphy (AROS), as an alternative to the highly inaccurate, biostratigraphic-radiometric time scale and correlated it to Arabian rock successions from the Gulf of Suez to the United Arab Emirates. They predicted that sequence boundaries separating the modelled second-order depositional sequences should be reflected in the rock record as regional stratigraphic discontinuities (Al-Husseini & Matthews, 2005a, 2008). Their correlation between the regional stratigraphic discontinuities and the modelled second-order sequence boundaries was done mostly by stratigraphic positioning, within typical age range limits of more than ± 5 Myr (Al-Husseini & Matthews, 2005a). Their model yielded 38 second-order depositional sequences representing the Phanerozoic Eon; each sequence spanned 14.58 Myr, and 34 of them were matched to Arabian regional stratigraphic discontinuities (Al-Husseini & Matthews, 2005a). A complete second-order sequence is predicted by the model to comprise six third-order sequences of 2.43 ± 0.405 Myr, which in turn are each composed of six fourth-order sequences of 0.405 Myr (Al-Husseini & Matthews, 2005a).

4.5 Focusing on the Kimmeridgian of Saudi Arabia

Before addressing what our data mean for the sequence stratigraphy of the Arab-D reservoir, it is befitting to summarise published sequence-stratigraphic studies on the Jubaila and Arab formations. We refer to the work of Sharland et al. (2001), who

divided the Arabian Plate's late Precambrian and Phanerozoic into 11 tectonostratigraphic megasequences (TMS), reflecting the plate's tectonic evolution through time using the genetic stratigraphic sequences *sensu* Galloway (1989). Figure 4.2 shows Sharland et al.'s (2001) megasequence AP7 and the Late Jurassic MFS that they identified, dated and correlated, stating that they are likely eustatic in origin. We also refer to Al-Husseini and Matthews's (2005a, 2008) findings that the Late Jurassic, except for the late Tithonian, represents a complete modelled second-order sequence, DS² 11, which consists of the Hanifa, Jubaila, Arab Formations and the Hith Anhydrite beneath the Manifa reservoir (hereafter, the Main Hith Anhydrite) and spans *ca.* 14.6 Myr (Figure 4.2). The lower sequence boundary of DS² 11 implies the Callovian-Oxfordian polar glaciations, while the upper one implies the Tithonian glaciations (Al-Husseini, 2009; Dromart et al., 2003; Palike, Norris, Herrle & Wilson, 2006). The modelled DS² 11 has been divided into six third-order modelled sequences, referred to as DS³ 11.1 to DS³ 11.6 (Al-Husseini, 2009; Al-Husseini & Matthews, 2005b, 2008; see Figure 4.2).

4.5.1 Jubaila Formation

In outcrop, the lower part of the Jubaila Formation is marked by mudstones and intraclastic, peloidal packstones and wackestones, with a multitude of hardgrounds, while the upper part becomes increasingly rich in allocthonous sclerosponges and corals (Hughes, 2004a; Meyer et al., 2000). The 130 m thick Jubaila outcrop has been divided into two informal units: upper J2 and lower J1 (Bramkamp & Steineke, 1952; Énay et al., 1987; Manivit et al., 1985; Powers, 1968; Powers et al., 1966).

The Jubaila is interpreted as a complete separate third-order transgressive-regressive sequence (Al-Husseini, 2009; Sharland et al., 2001) and is dated as Kimmeridgian, based on nautiloids *Paracenoceras wepferi* and *P. ex gr. moreausum* (Tintant, 1987) and endemic ammonites *Perisphinctes jubailensis* (Al-Husseini, 2009; Arkell, 1952; Énay et al., 1987; J.-C. Fischer, Manivit & Vaslet, 2001; Hughes, 2004, 2006). The highest Jurassic global sea levels (Haq et al., 1988) led to the deposition of the controversially dated upper Kimmeridgian maximum flooding surface, 'MFS

J70' (Figure 4.2), within the Jubaila's lower unit, J1 *ca.* 152.25 Myr (Al-Husseini, 2009; Sharland et al., 2001; Simmons et al., 2007). Al-Husseini (2009) correlated the Jubaila to AROS 'DS³11.3' (Figure 4.2), which brackets it between 157.0 and 154.6 Myr, and puts the Jubaila MFS at *c.*155.8 Myr (Al-Husseini, 2009).

4.5.2 Arab Formation

After the deposition of the upper Jubaila, global sea-level decreased and the dominantly highstand Arab Formation was deposited (Sharland et al., 2001), which is around 54 m thick in outcrop and around 100–180 m thick in the subsurface. In most Saudi Arabian outcrops, these Arab Formation anhydrites are dissolved leading to brecciation and collapsing of the carbonates (Al-Husseini, 2009). The microfaunal assemblages of the Arab Formation were assessed to be Kimmeridgian to Tithonian (de Matos, 1995; J.-C. Fischer et al., 2001; Hughes, 1997, 2006; Hughes et al., 2004; Le Nindre et al., 1990).

Powers et al. (1966) stated that the anhydrite-carbonate boundaries of the Arab Members are probably diachronous and hence redefined time-stratigraphic units to include the capping anhydrites with their underlying carbonates in the Arab-D, -C and -B. Al-Husseini (1997, 2009) agreed with this interpretation, placing the Arab anhydrites and that of the Hith as late highstand deposits and the Arab carbonates as LST, TST and early HST deposits, although he stated that the exact assignment to the specific system tracts deserves more high-resolution modelling. Le Nindre et al. (1990) also interpreted the Arab members' anhydrites and that of the Hith as highstand deposits, assigning the Arab-D, -C, -B, and -A members together with the Hith to the Tithonian. Conversely, McGuire et al. (1993) assigned the Arab Formation to the Tithonian and the Hith Formation to Berriasian age. They placed the anhydrites of the Arab members as lowstand wedges and transgressive system tracts and the carbonates as highstand system tracts, separating the two by a sequence boundary (Figure 4.2). This notion is supported by the findings of Lindsay et al. (2006), who described brecciated surfaces that separated the Arab-D carbonate from its overlying anhydrite in multiple Ghawar Field cores and

interpreted them as sequence boundaries.

The Arab-D Member comprises the Arab-D carbonate and the overlying sealing anhydrite. Based on detection in surface and subsurface samples of benthic foraminifera *Alveosepta jaccardi*, *Kurnubia palastiniensis*, *Mangashtia viennoti*, *Trocholina palastiniensis*, *Everticyclammina hedbergi/virguliana* and *Pfenderina salernitana* and the absence of Redmondoides species, *Pfenderina trochoidea* and *Riyadhella regularis*, the Arab-D reservoir has been determined to be of undifferentiated Kimmeridgian age, as neither ammonites nor coccoliths were found (Hughes, 2006; Hughes et al., 2004a; Lindsay et al., 2006; Sharland et al., 2001). Micropalaeontologically, the base of the Arab-D Member is placed at consistent occurrences of *Clypeina* species and *Thaumatoporella parvovesiculifera* (as *Polygonella incrustata*) in the type section (Powers et al., 1966); in outcrop, the base is mapped at the uppermost occurrence of stromatoporoids (Hughes et al., 2004a).

Although Le Nindre et al. (1990) recognised the Arab-D as a third-order sequence with an undesignated MFS within its carbonate, the Arab-D does not have a regionally correlatable MFS according to Sharland et al.'s (2001) criteria. Al-Husseini (2009) placed a sequence boundary atop the Arab-D anhydrite and another subtle sequence boundary at the base of the Arab Formation, making a complete, separate transgressive-regressive third-order sequence out of the Arab-D Member. Hughes (1996b, 2004a) interpreted the Arab-D reservoir, which comprises the Arab-D Member carbonate and the upper part of Jubaila Formation, to reflect a transgression and a highstand based on biozone analysis; he interpreted the reservoir's capping anhydrite as a lowstand deposit. Al-Husseini (2009) correlated the Arab-D to the modelled DS³ 11.4 sequence (Figure 4.2), which brackets it between 154.6 and 152.2 Myr, and put an Arab-D Member MFS at 153.4 Myr.

4.6 Arab-D Reservoir Cyclic Hierarchy

Following the preview of the published sequence-stratigraphic framework of the Jubaila and Arab formations in Section 4.5, the focus here is on the cyclic hierarchy preserved in the lithofacies stacking patterns of the Arab-D reservoir. A long-term fall in eustatic sea level during the Late Jurassic (Handford et al., 2002; Haq & Al-Qahtani, 2005; Meyer & Price, 1993; Mitchell et al., 1988; Sharland et al., 2001) caused the overall shallowing-upward trend preserved in the stratigraphy of the Arab-D reservoir's lithofacies (Table 4.1). This sea-level-induced, upward-shallowing succession is punctuated by different scales of cycles (Figure 4.3); this is discussed in detail below.

4.6.1 Small-Scale Cycles

One hundred and fifty-six small-scale cycles (0.05 to 4.1 m) were identified in the example core, based on repetitive motifs in lithofacies stacking patterns (Figure 4.3). These cycles can be classified based on fining versus coarsening and/or shallowing versus deepening upward trends, which change in accordance with their relative position on the depositional platform. They can be categorised into five general types, discussed below in ascending order.

4.6.1.1. Basin Cycles

Starting at the bottom of the succession, a cyclic pattern is recognised, which reflects monotonously interbedded, graded cycles that fine upward from the intraclastic packstone to rudstone lithofacies to the bioturbated skeletal hardground-capped lime mudstone to wackestone lithofacies (Table 4.1 and Figure 4.6a). These lithofacies are interpreted as storm-triggered turbidite couplets due to the presence of hummocky cross stratification (HCS), swaley bedding, Bouma sequences and type-CCC turbidites (characterised by the presence of rip-up clasts, convolutions and climbing ripples) (Al-Awwad & Collins, 2013a). These cycles are present in the middle and lower parts of the Arab-D reservoir (Figure 4.5) and range

in scale from 0.5 to 2.1 m. The basin cycles do not represent a parasequence of genetically related beds bound by sea-level-fluctuation surfaces; rather, they represent Bouma sequence divisions A to E bound by hardground surfaces (Bouma, 1962).

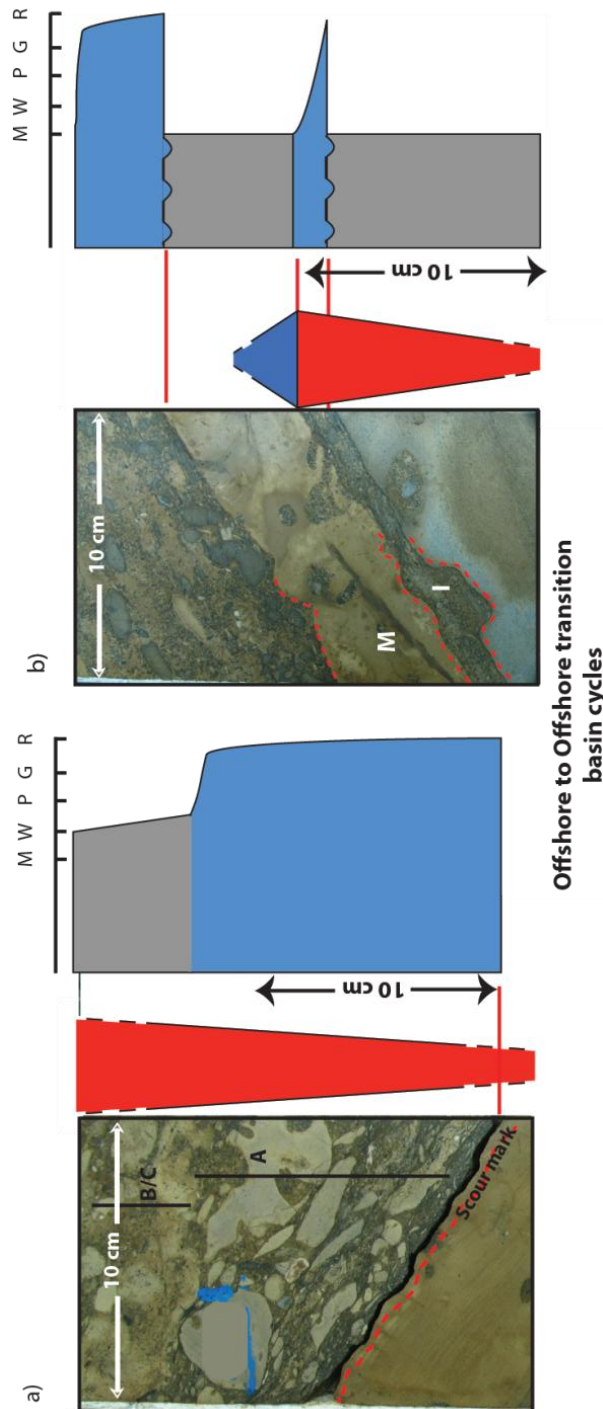


Figure 4.6: Offshore to offshore-transition basin cycles.

Notes: a) A gradational contact between an underlying intraclastic bed (division A of a Bouma sequence) and an overlying mud bed (division B or C of a Bouma sequence) is interpreted as a turbidite couplet, not indicative of sea-level fluctuations except in thickening upward sets of turbidites. b) A sharp contact between an underlying intraclastic bed (I) and an overlying mud bed (M) is interpreted as a transgression. Photographs are located or projected from correlated lithofacies onto the Aramco HKHK Khurais core description in Figure 4.3.

These bounding hardground surfaces are interpreted as surfaces cemented due to basin starvation, which were ripped up by subsequent avalanching turbidity currents. Less commonly, the transition between an underlying intraclastic bed and an overlying lime-mud bed is abrupt (Figure 4.6b), suggesting a sea-level rise that transgressed a lime-mud bed over an intraclastic bed. In such cases, the basin cycles are

interpreted as parasequences, where their deepening component is represented by the lime-mud bed and their shallowing component is represented by the intraclastic bed, and the two components are separated by the muddiest interval within a lime-mud bed (Figure 4.6b).

4.6.1.2. Reef Cycles

Another cyclic pattern tops the basin cycles and ranges in scale from 0.3 to 2.6 m.

These cycles are composed of bioturbated lime mudstones to wackestone, graded

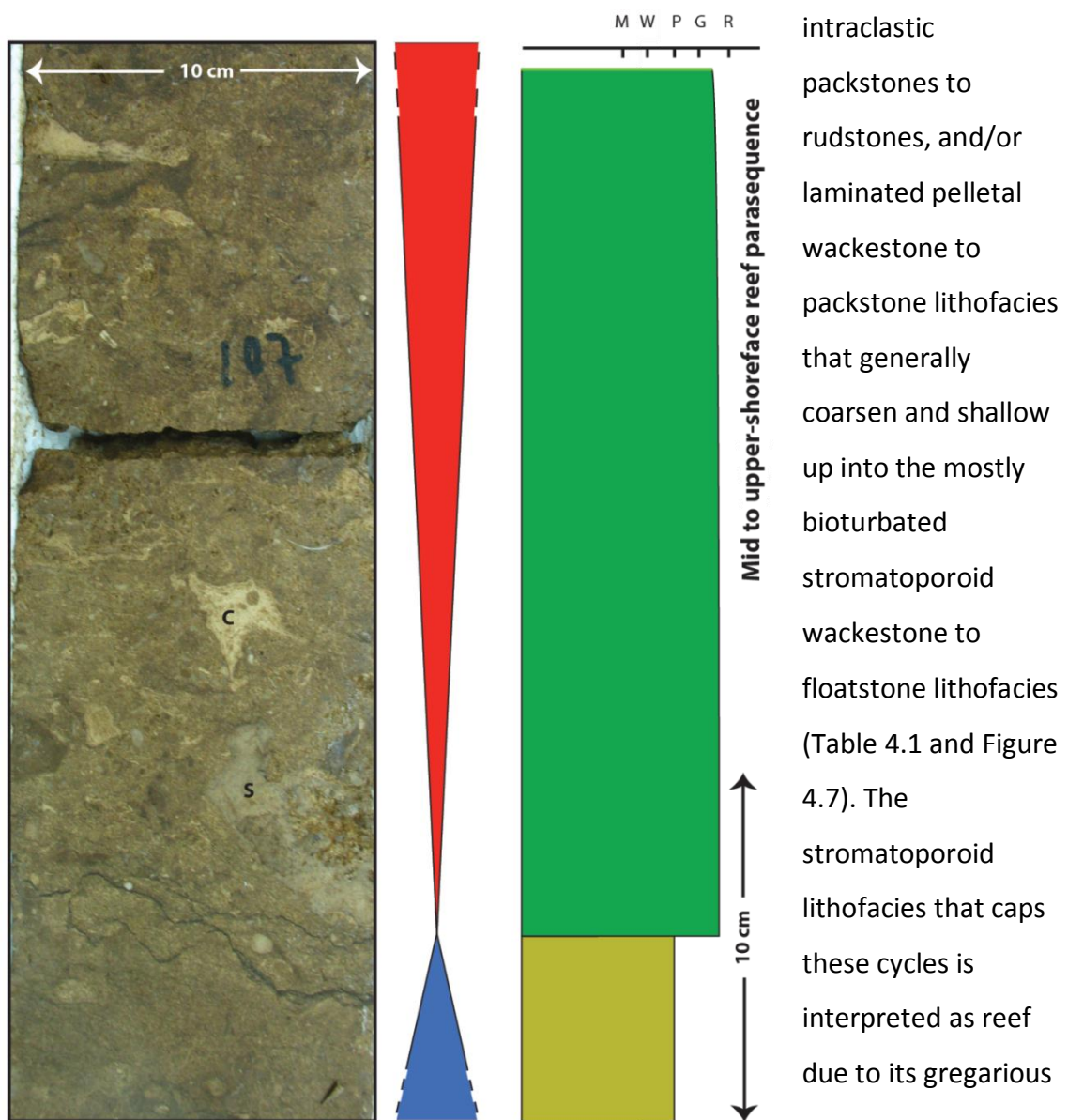


Figure 4.7: A reef parasequence that coarsens upward from the pelletal lithofacies to the stromatoporoid lithofacies.

Notes: Stylolitisation at interpreted maximum flooding surface. 'c' designates corals and 's' designate stromatoporoids. Photograph is located or projected from correlated lithofacies onto the Aramco HKHK Khurais core description in Figure 4.3.

laminar and domical growth forms and the presence of microbial encrustations, which coupled with its storm-reworked nature, suggest that the stromatoporoids were able to build wave-resistant structures. The reef cycles form a repetitive motif that is separated by sharp, erosive surfaces interpreted to represent marine floods that bring deeper over shallower lithofacies. Therefore, these cycles are interpreted as parasequences where the pelletal, lime mud and/or intraclastic lithofacies represent the deepening component and the stromatoporoid lithofacies represent the shallowing component, and both components are separated, in some cases, by firmgrounds or hardgrounds (Figure 4.7). These cycles occupy the area of the shelf between FWWB and mid-to-upper shoreface, that is, the transition from the Arabian intrashelf basin to the shelf (Al-Awwad & Collins, 2013a; see Figures 4.1 and 4.5).

4.6.1.3. Lagoon Cycles

Another cyclic pattern is preserved in the upper-shoreface of the lagoon behind the reef (Figure 4.5), and shows a fining-upward and shallowing-upward pattern in which the bioturbated stromatoporoid wackestone to floatstone transitions up into bioturbated *Cladocoropsis* and/or dasycladacean algae wackestone to floatstone lithofacies (Al-Awwad & Collins, 2013a; see Table 4.1 and Figure 4.8). The dasycladacean algae and *Cladocoropsis* lithofacies are interpreted to have been deposited in an upper-shoreface lagoon due to their lack of stratification, abundance of bioturbation and wispy lamination, which reflect a reduced energy setting where biologic rather than physical processes prevailed. In addition, the foraminiferal assemblages associated with these lithofacies are interpreted as lagoonal by Hughes (2004a). One cycle of this type is present in the example core; it is 1.7 m in scale and is separated by a sharp upper contact. The cycle is interpreted as a parasequence in which the *Cladocoropsis* and/or dasycladacean algae lithofacies represent the shallowing component and the stromatoporoid lithofacies represent the deepening component that is capped by a sharp contact or firmgrounds (Figure 4.8).

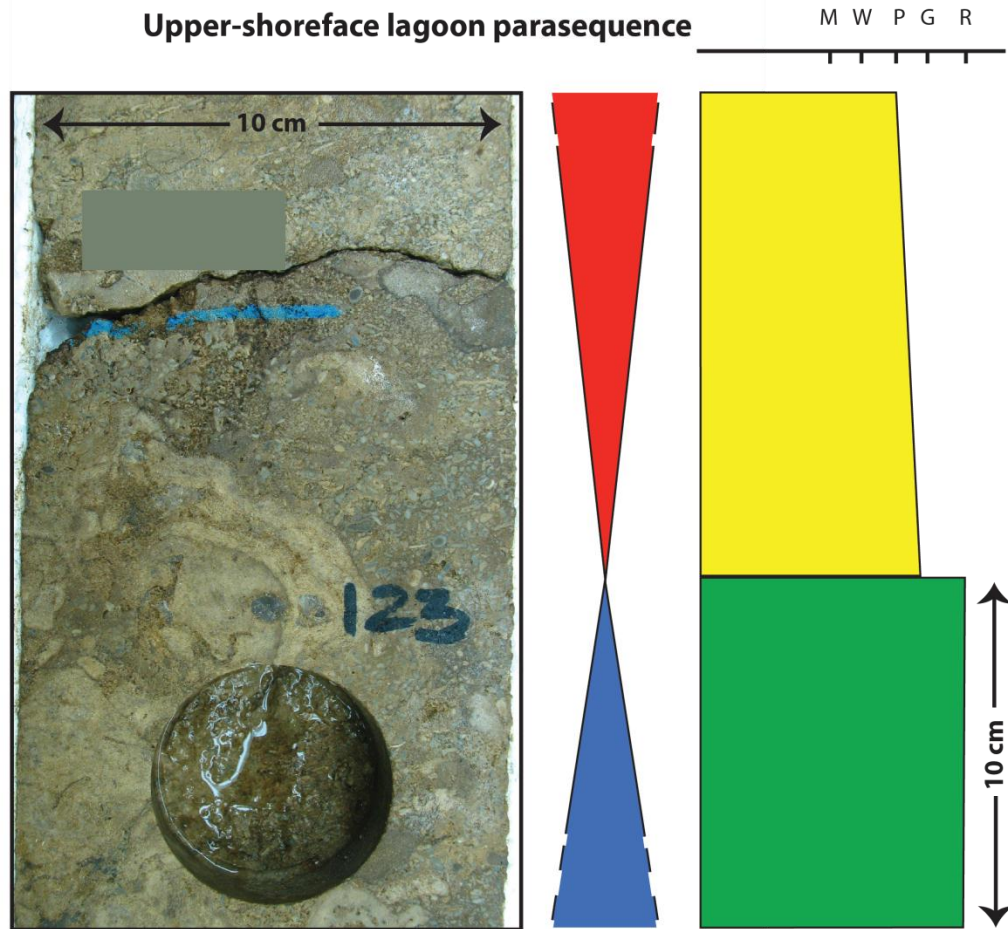


Figure 4.8: Upper shoreface lagoon parasequence.

Notes: A lagoon parasequence typically fines upward from the stromatoporoid lithofacies to the *Cladocoropsis* and/or dasycladacean algae lithofacies. Photograph is located or projected from correlated lithofacies onto the Aramco HKHK Khurais core description in Figure 4.3.

4.6.1.4. Sand-sheets Cycles

Another cyclic pattern is recognised in the foreshore area, where the lithofacies shallow from the *Cladocoropsis* and/or dasycladacean algae lithofacies to the peloidal and oolitic lithofacies (Al-Awwad & Collins, 2013a; see Figure 4.5, Table 4.1). The latter lithofacies are interpreted as sand sheets due to their cross-stratified structure and well-rounded, well-sorted, well-winnowed depositional textures, which indicate an increase in hydrodynamic energy and an increase in sorting and abrasion ability as the lithofacies belts continue shallowing towards the shoreline. These cycles are coarsening and shallowing upward, where the bioturbated wackestone to floatstone of the *Cladocoropsis* and/or dasycladacean algae lithofacies shallows up into the cross-bedded peloidal and/or oolitic

packstones to grainstones (Figure 4.9).

The cycles range from 0.2 to 2.9 m in thickness and are separated by sharp contacts that transgress deeper over shallower lithofacies. These cycles are interpreted as parasequences generated by small-scale sea-level changes. The deepening components of these parasequences are represented by the relatively deeper *Cladocoropsis* and/or dasycladacean algae lithofacies, and they culminate with increased muddiness. The shallowing components are represented by the relatively shallower peloidal and/or oolitic lithofacies. Storm activity in this part of the shelf is manifested by the winnowing of lagoonal sediments, transporting larger grains (*Cladocoropsis*) up-dip and concentrating them in thin sheets that were later capped by the peloidal lithofacies (Figure 4.3). This phenomenon yielded sporadic

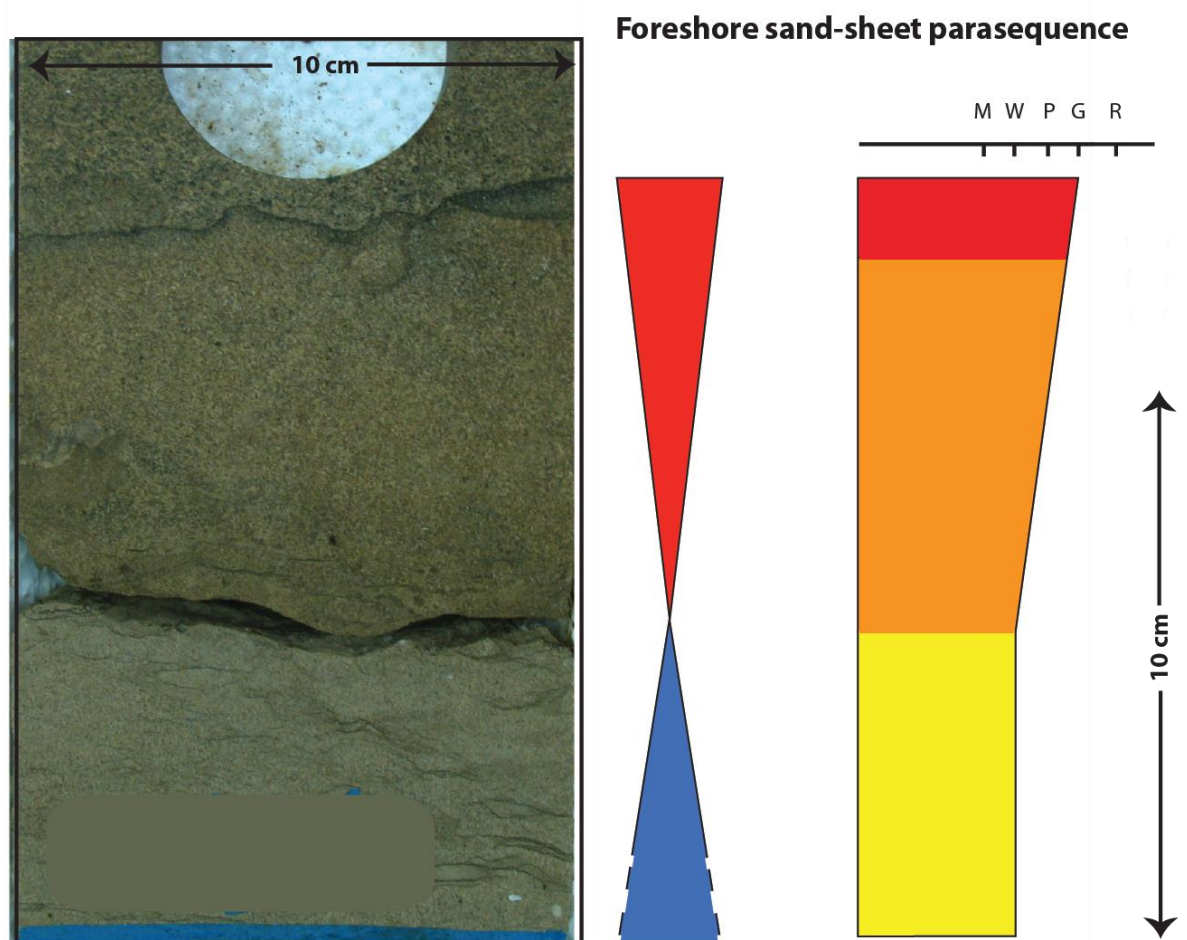


Figure 4.9: Foreshore sand-sheet parasequence.

Notes: The sand-sheet parasequence coarsens upward from *Cladocoropsis* and/or dasycladacean algae lithofacies to peloidal and oolitic lithofacies. Photograph is located or projected from correlated lithofacies onto the Aramco HKHK Khurais core description in Figure 4.3.

fining upward cycles with *Cladocoropsis* floatstone bases and peloidal packstone to grainstone caps in the foreshore area.

4.6.1.5. Peritidal Cycles

The peritidal cycles are the final capping cycles at the top of the succession and span the backshore area of the depositional platform, where the lithofacies shallow from the oolitic lithofacies to the cryptomicrobial and anhydrite lithofacies. The cryptomicrobial lithofacies is interpreted as hypersaline, peritidal stromatolites due to its microbial laminae, restricted fauna, dominated by cerithiid gastropods and stratigraphic position right below the anhydrites, which in turn are interpreted as sabkha type due to their chicken-wire fabrics and displasive nature. The anhydrites change up section from the chicken-wire fabric to bedded nodular and ultimately massive fabrics, suggesting a change from a sabkha to salina environment, with subaqueous evaporites production, and indicating a possible transgressive transition. The peritidal cycles also fine upward from the cross-bedded oolitic grain-dominated packstones to grainstones to the undulated cryptomicrobial mudstones to the grainstone and anhydrites of the backshore (Al-Awwad & Collins, 2013a; see Figure 4.5). One cycle of this type is preserved in the example core; it is slightly more than 0.9 m thick and is interpreted as a parasequence in which the oolitic lithofacies represent the deepening component, usually capped by sharp contact or hardground, brought from the foreshore area to the backshore area by a sea-level rise, and the cryptomicrobial and/or anhydrite lithofacies are interpreted as the shallowing component that caps the parasequence (Figure 4.10).

4.6.2 Cycle and Parasequence Sets, and High-Frequency Sequences

Progradational, aggradational and retrogradational stacking and upward thickening trends were utilised in bundling the cycles and parasequences described in Section 4.6.1 into 12 cycle and parasequence sets, which in turn are bundled into six high-frequency sequences (HFSs) that were successfully correlated both across Khurais

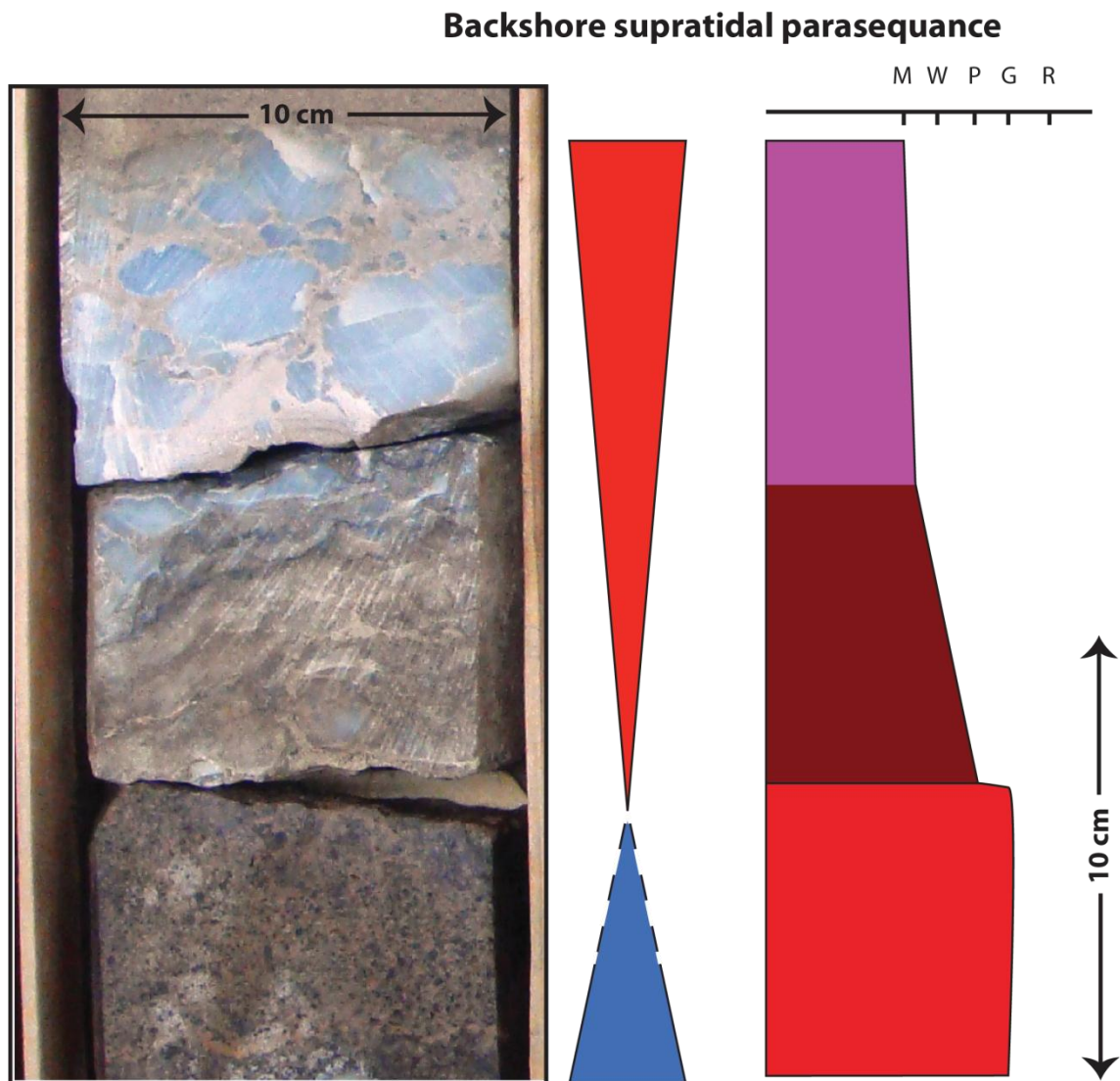


Figure 4.10: Backshore supratidal parasequence.

Notes: This backshore supratidal parasequence fines upward from oolitic lithofacies to cryptomicrobial and anhydrite lithofacies. Photograph is located or projected from correlated lithofacies onto Aramco HKHK Khurais core description, Figure 4.3.

Field and on a regional scale in an ongoing correlation study. These sets and HFSs can be categorised into basinal ones represented by the lower part of the Aramco HKHK Khurais core and numbered 1, 2 and 3 in Figure 4.3, and shelfal ones represented by the upper part of the core and numbered 4, 5, and 6 in Figure 4.3. Recognition of the shelfal parasequence sets and HFSs was based on the progressive upward appearance of shallower lithofacies, accompanied by progressive loss of deeper lithofacies that resulted in uniquely different HFSs, whereas progressive upward thickening of grainier lithofacies was the basis for recognising the basinal cycle sets and HFSs.

The vertical position of system tracts within a HFS, together with the progradational versus aggradational and retrogradational patterns preserved in the parasequence sets were the identification criteria for depicting system tracts of HFSs (Van Wagoner, Mitchum, Campion & Rahmanian, 1990).

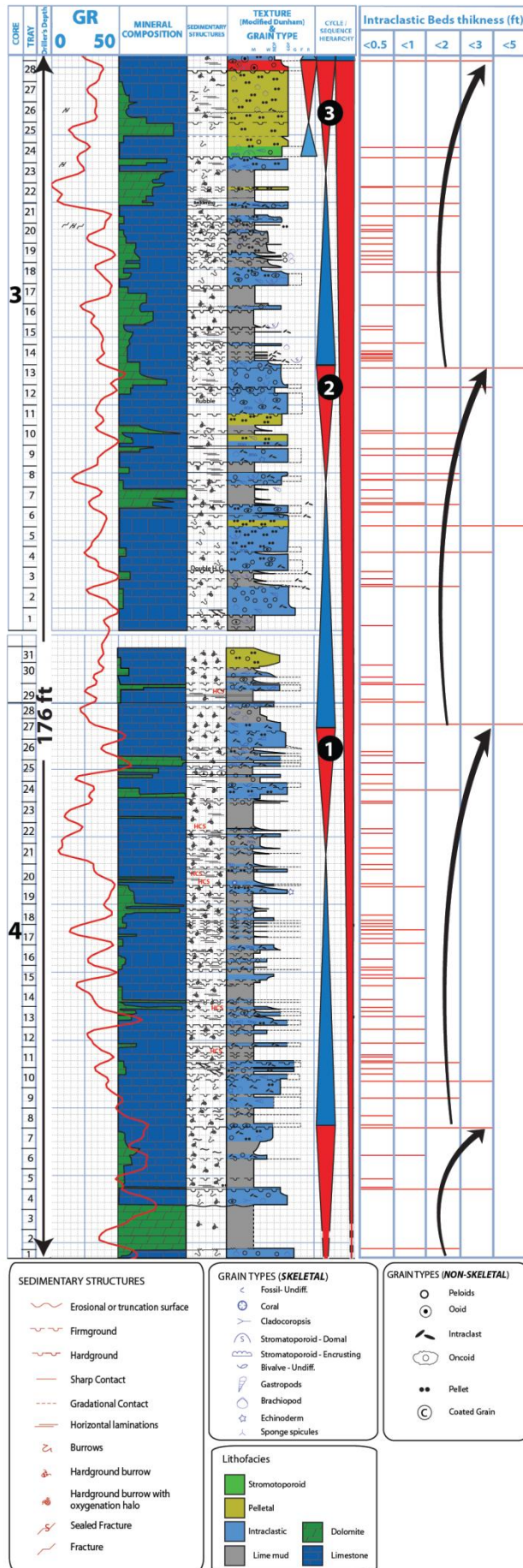
Depending on their respective position—either on the platform or basin—the composition of the TST and HST of each HFS varies in terms of the mud versus grain compositional dominance; yet generally, a TST is relatively muddier than its corresponding HST within a single HFS (Figure 4.3).

4.6.2.1. Basinal Cycle Sets and High Frequency Sequences

In the lower part of the reservoir, where the previously discussed basin cycles reside, lime mud dominated cycle sets ranging in thickness from 12.2 to 8.5 m alternate with intraclastic dominated cycle sets that are about 5.2 m. Every two basinal cycle sets can be bundled in 17.1 to 13.7 m-scaled HFSs that show a rhythmic pattern of upward coarsening and thickening of the intraclastic lithofacies (HFSs numbers 1–3 in Figures 4.3 and 4.11). It can be noted from Figure 4.3 that the lower-cycle set of each HFS represents a TST of a mud-rich interval, while the upper set represents an HST of a grainy, intraclast-rich interval. Progressively, up the lower part of the reservoir, the TSTs of the HFSs become less muddy and thinner and the HSTs become grainier and slightly thicker, as can be seen in Figure 4.3.

4.6.2.2. Shelfal Cycle Sets and High Frequency Sequences

The parasequences that span the upper part of the Arab-D reservoir, the shelf part of the depositional system, can be bundled into 12.5 to 5.5 m thick parasequence sets that reflect coupled retrogradational and progradational stacking patterns. Each parasequence-set couple can be grouped in a 22.3 to 15.8 m-scaled HFS that shows a progressive appearance of shallower lithofacies and a corresponding loss of deeper ones (HFS numbers 4, 5 and 6 in Figure 4.3).



These shelfal HFSs range from upward coarsening to upward fining depending on their respective locations on the platform; yet overall, their composing lithofacies reflect a gradual upward shallowing from stromatoporoid, *Cladocoropsis* and dasycladacean algae, peloidal, oolitic, to cryptomicrobial lithofacies and finally anhydrite (Al-Awwad & Collins, 2013a).

The lower parasequence set of each HFS represent a TST dominated by relatively deeper lithofacies—lime mud, intraclastic and pelletal lithofacies in HFS 4 stromatoporoid lithofacies in HFS5, and *Cladocoropsis*, dasycladacean algae and peloidal lithofacies in HFS 6 (Figure 4.3). Conversely, the upper

Figure 4.11: A plot of intraclastic bed thickness in the lower part of the reservoir shown against the core description and gamma log. Notes: The black arrows depict an increase in upward bed thickness and indicate a cyclic pattern that accords with the HFSs tops and increased gamma signal intervals.

parasequence sets represent HSTs, showing the dominance of relatively shallower lithofacies—stromatoporoid lithofacies in HFS 4, *Cladocoropsis*, dasycladacean algae and peloidal lithofacies in HFS 5, and oolitic, cryptomicrobial and anhydrite lithofacies in HFS 6 (Figure 4.3).

Inspection of the thickness variation of the shelfal HFSs, which are 15.8, 22.3, and 16.8 m thick in ascending order, shows that HFS 4 represents the reefal part of the platform (Figure 4.5) and reflects an increase in thickness compared to the basinal HFS beneath it (HFS 3). It is likely that this is caused by the biological buildup of the reef, which prograded towards an excess of accommodation space as it stepped into the intrashelf basin. The presence of the reefal framework above FWWB (Figure 4.5) and its resistance to wave energy (Al-Awwad & Collins, 2013a) allowed for ecologically-driven accommodation above the wave base 'razor' (Collins, 1988; Pomar & Kendall, 2008). This translated to thickening of HFS 5 compared to HFS 4, in an otherwise expected thinning-upward trend.

Following that, HFSs 6 show gradual decrease in thickness upward, which is likely to be the effect of the gradual diminution of accommodation as the lithofacies continued to shallow to sea level (Al-Awwad & Collins, 2013a).

The overall upward shallowing of the system in its shelf is manifested in the behaviour of the HSTs of the shelfal HFSs, which start out thin in HFS 4 and thicken upward, in HFS 5, then thin out in HFS6 due to accommodation expiration.

4.6.3 Composite Sequences

The Arab-D reservoir in the example core reflects long-term shallowing that preserved the majority of an upper, third-order composite sequence and a part of a lower, third-order composite sequence (1–3 Myr). The lower composite sequence represents the upper part of the Jubaila Formation, while the upper composite sequence represents the Arab-D Member of the Arab Formation (Figure 4.3). Overall shallowing in the lower composite sequence is evident by the appearance of

stromatoporoids at the top of it, which is followed by the flooding of lime mud and intraclastic lithofacies (Figures 4.3 and 4.12). Moreover, in outcrop, the boundary between these two composite sequences has been reported to contain 3 ft (1m) of sandstone (Steineke et al., 1958). In addition, Lindsay et al. (2006) reported eolian quartz silts from the subsurface of Ghawar Field and interpreted it to mark the boundary between the two composite sequences. Conversely, overall shallowing of the upper composite sequence is evident by lithofacies shallowing up to sabkha anhydrites (Figure 4.3, 12). In Khurais, the two composite sequences are punctuated by six fourth-order, high frequency sequences (0.1–0.4 Myr), superimposed on which are at least 12 parasequence sets. Superimposed on these are 41 fifth-order parasequences in the upper composite sequence and 123 parasequence-scale cycles in the lower composite sequence in the example core (Figures 4.3 and 4.12).

It is evident from the deposition and preservation of the foreshore oolitic sand sheet and the backshore cryptomicrobial laminites that Arab-D accommodation was completely filled to sea level. This accommodation filling would have dictated a seaward progradation leading to cutting off part of the shelf behind in which sabkha anhydrites were deposited during HST as the cutoff basin received an ever-diminishing marine recharge. If this scenario were true, then it is conceivable that the subsequent transgression caused a gradual increase in marine recharge that was not enough to keep up with the evaporation rate, leading consequently to subaqueous anhydrite deposition in a transgressive salina (Al-Awwad & Collins, 2013a). Therefore, the upper sequence boundary of the composite sequence is placed at the transition between the sabkha and massive subaqueous anhydrites (Figure 4.12), as the latter represent a sea-level transition from a fall to a rise. Along this line of reasoning, the dolomite stringers within the Arab-D anhydrite are interpreted to probably represent higher scale, fourth-order, maximum floods, where marine recharge was enough to switch the carbonate factory back on and deposit dolomite (note the fourth-order cyclicity in Figure 4.12). Finally, the lack of observable caliches or karst at the sequence boundaries of the composite sequences could be attributed to minimal rainfall due to climate aridity and/or minimal exposure time before subsequent transgressions.

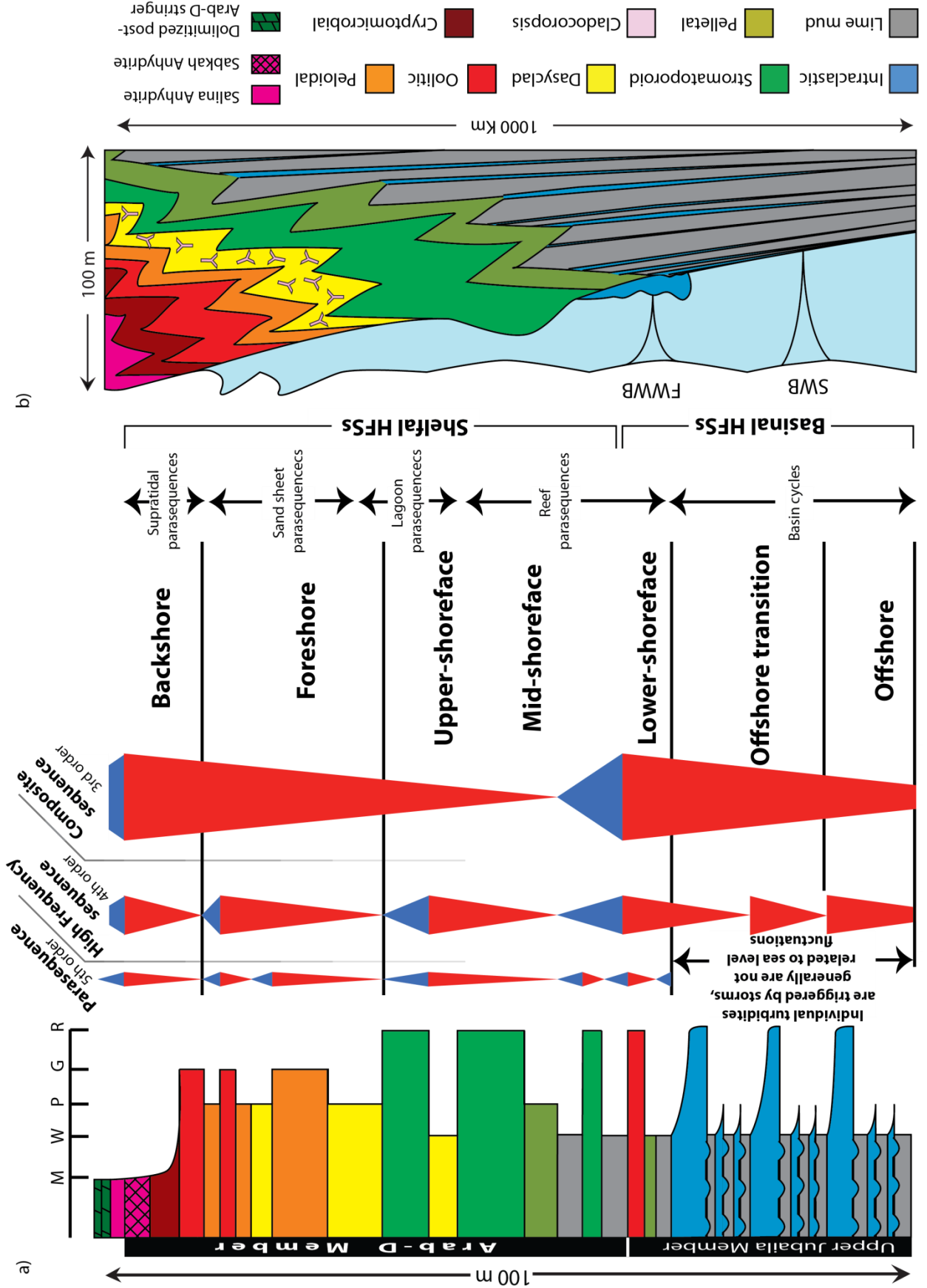


Figure 4.12 (previous page): An idealised Arab-D reservoir cored section and the interpreted sequence-stratigraphic framework.

Notes: On the composite sequence (third-order) scale, overall upward shallowing in the lower part of the core culminates with the deposition of thin units of stromatoporoids that mark a composite sequence boundary. This is followed by a marine flood represented by a thin interval of interbedded lime mud and intraclastic lithofacies, which is interpreted as a brief TST. The MFS of the upper composite sequence is picked at the highest occurrence of lime mud and or intraclastic lithofacies, which represents the maximum extent of deeper lithofacies landward. After the MFS, the lithofacies continue to shallow up to sabkha anhydrites (indicated by the chicken-wire pattern at the top of the section). A composite sequence boundary is interpreted at the transition from the sabkha anhydrites to the massive subaqueous anhydrites interpreted as early TST of a subsequent composite sequence. High-frequency sequences (fourth order) are picked based on vertical stacking patterns and each shows a unique lithofacies composition as the entire system continually shallows upward, except for the brief (third-order) flood that probably marks the contact between the Jubaila and Arab Formations. On the parasequence scale (fifth order), the individual basinal cycles are not taken to represent sea level fluctuations as they are interpreted as storm-triggered turbidites. Their respective cycle sets and HFSs reflect a stacking pattern that shows rhythmic thinning of the lime mud and ticking of the intraclastic intervals, which is interpreted to represent sea-level falls, as well as overall shallowing evident by the uppermost HFS being capped by stromatoporoids. Supratidal, sand-sheet, lagoon and reef parasequences are shown in their respective positions in the platform and are discussed in the text. A schematic depositional model of the Arab-D reservoir (not to scale) is juxtaposed next to the idealised sequence-stratigraphic framework for comparison.

The upper boundary of the upper composite sequence shows a vertical modulation in parasequence stacking pattern from progradation of foreshore and backshore carbonates, and sabkha anhydrites to aggradation in the salina anhydrites, which indicates that the sequence boundary is a Type II sequence boundary. The same conclusion could be drawn at the lower composite sequence boundary as it transitions from a progradation of offshore-transition lithofacies and shoreface reefal lithofacies to an aggradational pattern of offshore-transition basinal lithofacies (Vail, 1987; Van Wagoner et al., 1990).

Applying a Fischer plot (Fischer, 1964; Read & Goldhammer, 1988) to the Arab-D succession would have been useful in examining the suggested sequence-stratigraphic framework against the sea-level curve modelled by the plot. It is not possible to use the Fischer technique on this succession, however, because its cycles do not represent deposition at a fixed water depth; rather they show variant depositional depths that range from the basin, slope and rim to shelf (Sadler, Osleger & Montanez, 1993). Moreover, not all cycles in the succession aggrade to sea level; in fact, the majority of them are subtidal; hence their cumulative variable thicknesses do not model sea-level fluctuations (Boss & Rasmussen, 1995; Diecchio,

Boss & Rasmussen, 1995).

4.7 Discussion and Implications

Lindsay et al. (2006) identified all of the small-scale cycles depicted in the Arab-D reservoir as parasequences with transgressive mudstone, wackestone or packstone bases, deposited below fair-weather-wave base, capped by highstand cross-bedded grainstone, and/or mud-dominated to grain-dominated packstones, deposited within storm-wave base and/or fair-weather-wave base. A fundamental difference to this interpretation is introduced by differentiating the smallest-scale cycles into non-genetically related cycles (the basin cycles representing Bouma sequence) and genetically related parasequences (the reef, lagoon, sand-sheet, peritidal parasequences and the less-common basin parasequences).

On the HFS-scale the identification criterion of the shelfal cycle sets and HFSs concurs with that of Lindsay et al. (2006) as the HFSs show a characteristic progressive appearance of shallower lithofacies and a corresponding loss of deeper ones. Handford et al. (2002), however, identify their shelfal HFSs based on comparison to Hine and Neumann's (1997) model of the Little Bahama Bank; as such, they interpret the stromatoporoid reef to have formed during sea-level rise, back stepped landward and were then buried by seaward prograding grain shoals as the sea level fell. Consequently they interpret the lagoonal lithofacies (Table 4.1) situated shoreward of the reef to depict continuous deepening and eventually drowning of the reef, which discords with Hughes' (2004a) reporting of the lagoonal foraminiferal assemblages reflecting shallowing conditions.

On the basinal cycle sets and HFSs, the rhythmic pattern of the upward-coarsening and thickening intraclastic lithofacies is found to be telling in identifying the lower three HFSs. Handford et al. (2002) used similar criteria, but they recognised only one HFS in the lower part of the reservoir.

The large-scale rhythmic pattern of decreased muddiness of the TSTs and increased

graininess of the HSTs observed in the basinal HFSs is likely the result of sea-level fluctuations as sea-level falls would lower SWB, bringing higher levels of energy to the stromatoporoid reef and generating thicker intraclastic beds (i.e. division A of a Bouma sequence, Figure 4.6a). In addition, as sea level fell, higher order transgression probably deposited thinner mud beds due to increased hydrodynamic energy, as can be noted in the fading of the muddy beds up each large-scale cycle in Figures 4.12 and 4.3. Therefore, although sea-level fluctuations were not preserved in the small-scale basin cycles, they were preserved in the cyclicity of the larger-scale cycle sets and HFSs.

On the composite sequence scale, the recognition of two composite sequences divided by a sequence boundary that separates the Upper Jubaila Member from the overlying Arab-D Member generally agrees with Lindsay et al. (2006) and Mitchell et al. (1988). However, it disagrees with Meyer et al. (1996) and Meyer and Price (1993), who interpreted the reservoir as preserving one shallowing-upward genetic-depositional sequence with no intervening sequence boundaries. Handford et al. (2002) placed a composite sequence boundary within the Arab-D Member, combining the Jubaila Formation and the lower Arab-D Member in one composite sequence, and they placed the middle and upper parts of the Arab-D Member carbonates in another composite sequence based on their interpretation of the stromatoporoids' appearance as a transgressive event.

The interpretation presented here of the upper boundary of the upper composite sequence is more in line with McGuire et al. (1993) than with Le Nindre et al. (1990). McGuire et al. (1993) placed the Arab-D sequence boundary at maximum sea-level regressions that culminated with the carbonate deposition and considered the anhydrites to represent a transgressive system tract of the following sequence. This interpretation would have the anhydrites as onlapping transgressive deposits over the sequence boundary surfaces, as modelled by Sarg (1988) and Peebles, Suzuki & Shaner, (1995).

Conversely, Le Nindre et al. (1990) interpret the Arab anhydrites and that of the

Hith as highstand deposits, a notion with which Al-Husseini (1997, 2009) agrees (Figure 4.2). One problem with this interpretation, however, particularly in the Arab-D, is that if the Arab-D capping oolites and cryptomicrobial laminites represent deposition all the way up to sea-level, and hence represent complete consumption of accommodation, then it would be rather inconceivable for it to generate enough accommodation space within the same HST to deposit the entire Arab-D anhydrite, which averages 48 m across Khurais Field.

The high-resolution sequence-stratigraphic framework presented in this study represents the first model in Khurais Field and differs from published stratigraphic models on the Arab-D in Ghawar Field. Together with the previously proposed depositional model (Al-Awwad & Collins, 2013a), this sequence-stratigraphic framework establishes that the reservoir's facies are configured in a predictable prograding pattern. This interpretation is proving to be applicable and useful in an ongoing correlation study of the reservoir on a regional scale.

4.8 Conclusions

The Arab-D Member is established in the literature as a complete, separate third-order composite sequence bordered by a lower third-order composite sequence represented by the Jubaila Formation and upper sequences represented by the Arab-C and Arab-B Members (Al-Husseini, 2009; Le Nindre et al., 1990; McGuire et al., 1993; Sharland et al., 2001).

High-resolution lithofacies analysis of the Arab-D reservoir in Khurais Field led to the identification of a long-term shallowing trend that preserved the majority of a third-order composite sequence representing the Arab-D member and the upper part of another third-order composite sequence representing the upper part of the Jubaila Formation. Within these composite sequences lay six high-frequency sequences of the fourth order, superimposed on them are 12 parasequence and cycle sets, and superimposed over those are 41 fifth-order parasequences in the upper composite sequence and 123 parasequence-scale cycles in the lower composite sequence.

The upper parasequences represent deposition in the shallow-shelf part of the depositional system (above FWWB), while the lower cycles represent, for the most part, turbidite cycles deposited in the relatively deep basinal part of the system (sub-FWWB).

Identifying repetitive motifs in lithofacies stacking patterns allowed the recognition of *ca.* 1.4 m-scaled parasequences and *ca.* 0.4 m-scaled cycles, which can be classified based on fining versus coarsening and/or shallowing versus deepening upward trends into: 1) mostly upward fining basinal cycles comprised of the monotonously interbedded intraclastic and lime mudstone lithofacies representing the Bouma sequence; 2) upward-coarsening reefal parasequences comprising lime mudstone, intraclastic and/or pelletal lithofacies up into stromatoporoid lithofacies; 3) upward fining lagoonal parasequences comprising stromatoporoid up into *Cladocoropsis* and/or dasycladacean algae lithofacies; 4) upward-coarsening sand-sheet parasequences comprising *Cladocoropsis* and/or dasycladacean algae up into the peloidal and/or oolitic lithofacies; 5) upward fining peritidal parasequences comprising peloidal and/or oolitic up into cryptomicrobial and anhydrites lithofacies.

Vertical stacking patterns and thickening trends based the recognition of 12 *ca.* 8.5 m-scaled cycle and parasequence sets bundled into six *ca.* 16.8 m-scaled HFSs. In the basinal part of the depositional system, the cycle sets and HFSs show a rhythmic pattern of upward coarsening and thickening of the intraclastic lithofacies, which are interpreted to be caused by sea-level fluctuations bringing thicker turbidites during lowstands. In the shelf part of the depositional system, the parasequence sets reflect coupled retrogradational and progradational stacking patterns that represent the transgressive and highstand systems tract of progressively shallowing HFSs that shift in ascending order through the stromatoporoid, *Cladocoropsis* and dasycladacean algae, peloidal, oolitic, and cryptomicrobial to the anhydrite lithofacies.

Integration of this high-resolution sequence-stratigraphic framework with the depositional model of the Arab-D reservoir (Al-Awwad & Collins, 2013a) provides insights for characterising the spatial lithofacies distribution and geometric relationships of the Arab-D reservoir flow and baffle units in Khurais Field.

4.9 Acknowledgements

We are in debt to Aus Al-Tawil of Saudi Aramco for his unrelenting support, tenacity and commitment to this study. We would like to thank Saudi Aramco for granting permission to publish this study. Our appreciation is also extended to Luis Pomar, University de les Illes Balears, Spain, for his beneficial discussions and keen insights.

4.10 References

- Al-Afalge, N. I., Al-Garni, S., Rahmeh, B. & Al-Towailib, A. (2002). *Successful integration of sparsely distributed core and welltest derived permeability data in a viable model of a giant carbonate reservoir*. Paper presented at the SPE Annual Technical Conference and Exhibition, San Antonio, Texas.
- Al-Awwad, S. & Collins, L. B. (2013a). Arabian carbonate reservoirs: A depositional model of the Arab-D reservoir in Khurais Field, Saudi Arabia. *AAPG Bulletin*, 97(7), 1099–1119.
- Al-Husseini, M. I. (1997). Jurassic sequence stratigraphy of the western and southern Arabian Gulf. *GeoArabia (Manama)*, 2(4), 361–382.
- Al-Husseini, M. I. (2000). Origin of the Arabian Plate structures: Amara collision and Najd Rift. *GeoArabia (Manama)*, 5(4), 527–542.
- Al-Husseini, M. I. (2009). Update to Late Triassic-Jurassic stratigraphy of Saudi Arabia for the Middle East geologic time scale. *GeoArabia (Manama)*, 14(2), 145–186.
- Al-Husseini, M. I. & Matthews, R. K. (2005a). Arabian orbital stratigraphy: Periodic second-order sequence boundaries? *GeoArabia (Manama)*, 10(2), 165–168.
- Al-Husseini, M. I. & Matthews, R. K. (2005b). Stratigraphic note: Orbital-forcing calibration of the Late Cretaceous and Paleocene Aruma Formation, Saudi Arabia. *GeoArabia (Manama)*, 10(3), 173–176.
- Al-Husseini, M. I. & Matthews, R. K. (2008). Jurassic-Cretaceous Arabian orbital stratigraphy: The AROS-JK chart. *GeoArabia (Manama)*, 13(1), 89–94.
- Al-Mulhim, W. A., Al-Ajmi, F. A., Al-Shehab, M. A. & Pham, T. R. (2010). Khureis Complex; 1, Field development required best practices, leveraged technology. *Oil & Gas Journal*, 108(7), 37-38, 40-42.
- Alsharhan, A. S. & Kendall, C. G. S. C. (1986). Precambrian to Jurassic rocks of Arabian Gulf and adjacent areas: Their facies, depositional setting, and hydrocarbon habitat. *AAPG Bulletin*, 70(8), 977–1002.
- Alsharhan, A. S. & Sadooni, F. N. (2003). Eustatic overprints on the diagenetic evolution of Mesozoic platform carbonates from the Arabian Plate [Annual

- meeting expanded abstracts]. *American Association of Petroleum Geologists*, 12, 5.
- Arkell, W. J. (1952). Jurassic ammonites from Jebel Tuwaiq, central Arabia. *Philosophical Transactions of the Royal Society of London, Series B: Biological Sciences*, 236(633), 241-313.
- Ayres, M. G., Bilal, M., Jones, R. W., Slentz, L. W., Tartir, M. & Wilson, A. O. (1982). Hydrocarbon habitat in main producing areas, Saudi Arabia. *AAPG Bulletin*, 66(1), 1-9.
- Banner, F. T., Finch, E. M. & Simmons, M. D. (1990). On Lithocodium Elliott (calcareous algae); its palaeobiological and stratigraphical significance. *Journal of Micropalaeontology*, 9(1), 21-35.
- Barger, T. C. (1984). Birth of a Dream. *Saudi Aramco World*, 35.
- Blanchon, P., Jones, B. & Kalbfleisch, W. (1997). Anatomy of a fringing reef around Grand Cayman; storm rubble, not coral framework. *Journal of Sedimentary Research*, 67(1), 1-16. doi: 10.1306/d42684d7-2b26-11d7-8648000102c1865d
- Bodenbender, B. E., Wilson, M. A. & Palmer, T. J. (1989). Paleoecology of Sphenothallus on an Upper Ordovician hardground. *Lethaia*, 22(2), 217-225. doi: 10.1111/j.1502-3931.1989.tb01685.x
- Boss, S. K. & Rasmussen, K. A. (1995). Misuse of Fischer plots as sea-level curves. *Geology*, 23(3), 221-224. doi: 10.1130/0091-7613(1995)023<0221:mofpas>2.3.co;2
- Boulila, S., Galbrun, B., Miller, K. G., Pekar, S. F., Browning, J. V., Laskar, J. & Wright, J. D. (2011). On the origin of Cenozoic and Mesozoic 'third-order' eustatic sequences. *Earth-Science Reviews*, 109(3-4), 94-112. doi: 10.1016/j.earscirev.2011.09.003
- Bouma, A. H. (1962). *Sedimentology of some Flysch deposits; a graphic approach to facies interpretation*. Amsterdam; New York: Elsevier Pub. Co.
- Bramkamp, R. A. & Steineke, M. (1952). *Stratigraphical introduction*. Paper presented at the Royal Society of London Philosophical Transactions.
- Brown, G. F., Schmidt, D. L. & Huffman, A. C., Jr. (1989). *Geology of the Arabian Peninsula: Shield area of western Saudi Arabia* (US Geological Survey

- professional paper, A1–A188).
- Church, M., Coniglio, M., Hardie, L. A. & Longstaffe, F. J. (2003). Encyclopedia of sediments & sedimentary rocks. In G. V. Middleton (Ed.), *Encyclopedia of Earth Sciences Series* (p. 928). Dordrecht, The Netherlands: Springer.
- Collins, L. B. (1988). Sediments and history of the Rottneest Shelf, Southwest Australia; a swell-dominated, non-tropical carbonate margin. *Sedimentary Geology*, 60(1–4), 15–49.
- De Castro, P. (1990). Thaumatoporelle; conoscenze attuali e approccio all'interpretazione. *Bollettino della Societa Paleontologica Italiana*, 29(2), 179–206.
- de Matos, J. E. a. H., R. F. (1995). *Regional Characteristics and Depositional Sequences of the Oxfordian and Kimmeridgian*. Paper presented at the Middle East Petroleum Geosciences, Bahrain.
- Diecchio, R. J., Boss, S. K. & Rasmussen, K. A. (1995). Misuse of Fischer plots as sea-level curves; discussion and reply. *Geology (Boulder)*, 23(11), 1049–1050. doi: 10.1130/0091-7613(1995)023<1049:mofpas>2.3.co;2
- Dromart, G., Garcia, J. P., Picard, S., Atrops, F., Lecuyer, C. & Sheppard, S. M. F. (2003). Ice age at the Middle-Late Jurassic transition? *Earth and Planetary Science Letters*, 213(3–4), 205–220. doi: 10.1016/s0012-821x(03)00287-5
- Droste, H. (1990). Depositional cycles and source rock development in an epeiric intra-platform basin: The Hanifa Formation of the Arabian Peninsula. *Sedimentary Geology*, 69(3–4), 281–296.
- Énay, R. (1993). Les apports sud-tethysiens parmi les faunes jurassiques nord-ouest europeennes: Interpretation paleobiogeographique. *Comptes Rendus de l'Academie des Sciences, Serie 2, Mecanique, Physique, Chimie, Sciences de l'Univers, Sciences de la Terre*, 317(1), 115–21.
- Énay, R., Le Nindre, Y. M., Mangold, C., Manivit, J. & Vaslet, D. (1987). Le Jurassique d'Arabie Saoudite central: Nouvelles donnees sur la lithostratigraphie, les paleoenvironnements, les faunes d'ammonites, les ages et les correlations [The Jurassic of central Saudi Arabia: New data on lithostratigraphy, paleoenvironments, ammonite fauna, ages and correlations]. *Geobios, Memoire Special*, 9, 13–65.

- Fischer, A. G. (1964). The Lofer cyclothems of the Alpine Triassic. (Vol. 1, pp. 107-149).
- Fischer, J.-C., Manivit, J. & Vaslet, D. (2001). Jurassic gastropod faunas of central Saudi Arabia. *GeoArabia (Manama)*, 6(1), 63-100.
- Goldhammer, R. K., Dunn, P. A. & Hardie, L. A. (1990). Depositional cycles, composite sea-level changes, cycle stacking patterns, and the hierarchy of stratigraphic forcing; examples from Alpine Triassic platform carbonates. *Geological Society of America Bulletin*, 102(5), 535-562. doi: 10.1130/0016-7606(1990)102<0535:dccslc>2.3.co;2
- Gradstein, F. M., Ogg, J. G., Smith, A. G., Agterberg, F. P., Bleeker, W., Cooper, R. A., . . . Wilson, D. (2004). A geological time scale 2004 [Miscellaneous Report]. *Geological Survey of Canada* (0068–7642).
- Handford, C. R., Cantrell, D. L. & Keith, T. H. (2002). Regional facies relationships and sequence stratigraphy of a super-giant reservoir (Arab-D member), Saudi Arabia [Program and abstracts]. *Society of Economic Paleontologists (Gulf Coast Section) Research Conference*, 22, 539–563.
- Haq, B. U. & Al-Qahtani, A. M. (2005). Phanerozoic cycles of sea-level change on the Arabian Platform. *GeoArabia (Manama)*, 10(2), 127–160.
- Haq, B. U., Hardenbol, J. & Vail, P. R. (1987). Chronology of fluctuating sea levels since the Triassic. *Science*, 235(4793), 1156–1167.
- Haq, B. U., Hardenbol, J. & Vail, P. R. (1988, September 1988). Mesozoic and Cenozoic chronostratigraphy and cycles of sea-level change *Society of Economic Paleontologists and Mineralogists*, 42, 72–108.
- Harris, P. M., Kerans, C. & Bebout, D. G. (1993). Ancient outcrop and modern examples of platform carbonate cycles; implications for subsurface correlation and understanding reservoir heterogeneity. *AAPG Memoir*, 57, 475-492.
- Hine, A.C., and A.C. Neumann, 1977, Shallow carbonate-bank-margin growth and structure, Little Bahama Bank, Bahamas: AAPG Bull., v. 61, p. 376-406.
- Hubbard, D. K. (1992). Hurricane-induced sediment transport in open-shelf tropical systems; an example from St. Croix, U.S. Virgin Islands. *Journal of Sedimentary Research*, 62(6), 946-960. doi: 10.1306/d4267a23-2b26-11d7-

8648000102c1865d

- Hubbard, D. K., Miller, A. I. & Scaturro, D. (1990). Production and cycling of calcium carbonate in a shelf-edge reef system (St. Croix, U.S. Virgin Islands); applications to the nature of reef systems in the fossil record. *Journal of Sedimentary Research*, 60(3), 335-360. doi: 10.1306/212f9197-2b24-11d7-8648000102c1865d
- Hughes, G. W. (1996). Environmentally-induced biofacies events in the Arab-D reservoir of Saudi Arabia. *GeoArabia (Manama)*, 1(1), 150.
- Hughes, G. W. (1997). The Great Pearl Bank Barrier of the Arabian Gulf as a possible Shu'aiba analogue. *GeoArabia (Manama)*, 2(3), 279–304.
- Hughes, G. W. (2004). Middle to Upper Jurassic Saudi Arabian carbonate petroleum reservoirs; biostratigraphy, micropalaeontology and palaeoenvironments. *GeoArabia (Manama)*, 9(3), 79–114.
- Hughes, G. W. (2006). *Biostratigraphy, biofacies, palaeoenvironments, lithostratigraphy and reservoir implications for the Shaqra Group (Jurassic) of Saudi Arabia*. Paper presented at the 7th Middle East Geosciences Conference and Exhibition (GEO 2006).
- Hughes, G. W., Dhubeeb, A. G., Varol, O., Lindsay, R. F. & Mueller, H. (2004). The Arab-D biofacies of Saudi Arabia: Their paleoenvironment and new biozonation. *GeoArabia (Manama)*, 9(1), 79–80.
- Hughes, G. W., Varol, O. & Al-Dhubeeb, A. (2004). *Biofacies and palaeoenvironments of Late Jurassic carbonates of Saudi Arabia*. Paper presented at the 32nd International Geological Congress.
- Hughes, G. W., Varol, O., Hooker, N. P. & Énay, R. (2008). New aspects of Saudi Arabian Jurassic biostratigraphy. *GeoArabia (Manama)*, 13(1), 174.
- hydrocarbons-technology.com. (2011). *Saudi Aramco Khurais Mega Project, Khurais*. Retrieved from <http://www.hydrocarbons-technology.com/projects/khurais/>
- Immenhauser, A. & Matthews, R. K. (2004). Albian sea-level cycles in Oman; the 'Rosetta Stone' approach. *GeoArabia (Manama)*, 9(3), 11-46.
- Kerans, C., Lucia, F. J. & Senger, R. K. (1994). Integrated characterization of carbonate ramp reservoirs using Permian San Andres Formation outcrop

- analogs. *AAPG Bulletin*, 78(2), 181–216. doi: 10.1306/bdff905a-1718-11d7-8645000102c1865d
- Kinsman, D. J. J. & Park, R. K. (1976). *Algal belt and coastal sabkha evolution, Trucial Coast, Persian Gulf*. Amsterdam, The Netherlands: Elsevier.
- Koerschner, W. F., III & Read, J. F. (1989). Field and modelling studies of Cambrian carbonate cycles, Virginia, Appalachians. *Journal of Sedimentary Petrology*, 59(5), 654-687. doi: 10.1306/212f9048-2b24-11d7-8648000102c1865d
- Konert, G., Afifi, A. M., Al-Hajri, S. A., de Groot, K., Al Naim, A. A. & Droste, H. J. (2001). Paleozoic stratigraphy and hydrocarbon habitat of the Arabian Plate. *AAPG Memoir*, 74, 483-515.
- Laskar, J., Robutel, P., Joutel, F., Gastineau, M., Correia, A. C. M. & Levrard, B. (2004). A long-term numerical solution for the insolation quantities of the Earth. *Astronomy & Astrophysics*, 428(1), 261-285. doi: 10.1051/0004-6361:20041335
- Leeder, M. (2011). *Sedimentology and sedimentary basins: from turbulence to tectonics* (2nd ed.). Oxford, UK: Wiley-Blackwell.
- Leinfelder, R. R., Schlagintweit, F., Werner, W., Ebli, O., Nose, M., Schmid, D. U. & Hughes, G. W. (2005). Significance of stromatoporoids in Jurassic reefs and carbonate platforms—concepts and implications. *Facies*, 51(1-4), 288-326. doi: 10.1007/s10347-005-0055-8
- Le Nindre, Y.-M., Manivit, J. & Vaslet, D. (1987). *Histoire geologique de la bordure occidentale de la plate-forme arabe du Paleozoique inferieur au Jurassique superieur* (Unpublished doctoral dissertation). University Pierre and Marie Curie, Paris.
- Le Nindre, Y.-M., Manivit, J. & Vaslet, D. (1990). Stratigraphie sequentielle du Jurassique et du cretace en Arabie Saoudite. *Bulletin, Societe Geologique de France, Paris*, 6, 1025–35.
- Lindsay, R. F., Cantrell, D. L., Hughes, G. W., Keith, T. H., Mueller, H. W., III & Russell, S. D. (2006). Ghawar Arab-D reservoir: Widespread porosity in shoaling-upward carbonate cycles, Saudi Arabia. *AAPG Memoir*, 88, 97-138.
- Manivit, J., Pellaton, C., Vaslet, D., Le Nindre, Y.-M., Brosse, J.-M. & Fourniguet, J. (1985). Explanatory notes to the geologic map of the Wadi al Mulayh

- Quadrangle, Sheet 22 H, Kingdom of Saudi Arabia (Vol. GM-92C, pp. 32-32, 31 sheet). Saudi Arabia (SAU): Kingdom of Saudi Arabia, Ministry of Petroleum and Mineral Resources, Jiddah, Saudi Arabia (SAU).
- McGuire, M. D., Koepnick, R. B., Markello, J. R., Stockton, M. L., Waite, L. E., Kompanik, G. S., . . . Al-Amoudi, M. O. (1993). *Importance of sequence stratigraphic concepts in development of reservoir architecture in Upper Jurassic grainstones, Hadriya and Hanifa Reservoirs, Saudi Arabia*. Paper presented at the Middle East Oil Show.
- Mey, J. L. (2008). The uranium series diagenesis and the morphology of drowned Barbadian paleo-reefs. (Doctoral dissertation, no. 3312925), City University of New York, United States.
- Meyer, F. O., Hughes, G. W. & Al-Ghamdi, I. (2000). Jubaila Formation, Tuwaiq Mountain escarpment, Saudi Arabia: Window to lower Arab-D reservoir faunal assemblages and bedding geometry. *GeoArabia (Manama)*, 5(1), 143.
- Meyer, F. O. & Price, R. C. (1993). *A new Arab-D depositional model, Ghawar Field, Saudi Arabia*. Paper presented at the Middle East Oil Show, Bahrain.
- Meyer, F. O., Price, R. C., Al-Ghamdi, I. A., Al-Goba, I. M., Al-Raimi, S. M. & Cole, J. C. (1996a). Outcropping strata equivalent to Arab-D reservoir, Wadi Nisah, Saudi Arabia. *GeoArabia (Manama)*, 1(1), 171–2.
- Meyer, F. O., Price, R. C., Al-Ghamdi, I. A., Al-Goba, I. M., Al-Raimi, S. M. & Cole, J. C. (1996b). Sequential stratigraphy of outcropping strata equivalent to Arab-D reservoir, Wadi Nisah, Saudi Arabia. *GeoArabia (Manama)*, 1(3), 435–56.
- Miller, K. G., Kominz, M. A., Browning, J. V., Wright, J. D., Mountain, G. S., Katz, M. E.,... Pekar, S. F. (2005). The Phanerozoic record of global sea-level change. *Science*, 310(5752), 1293-1298. doi: 10.1126/science.1116412
- Mitchell, J. C., Lehmann, P. J., Cantrell, D. L., Al-Jallal, I. A. & Al-Thagafy, M. A. R. (1988). Lithofacies, diagenesis and depositional sequence: Arab-D Member, Ghawar Field, Saudi Arabia. *SEPM Core Workshop*, 12, 459–514.
- Mitchum, R. M., Jr & Van Wagoner, J. C. (1991). High-frequency sequences and their stacking patterns: sequence-stratigraphic evidence of high-frequency eustatic cycles. *Sedimentary Geology*, 70(2–4), 131-160. doi: 10.1016/0037-0738(91)90139-5

- Montaggioni. (2005). History of Indo-Pacific coral reef systems since the last glaciation; development patterns and controlling factors. *Earth-Science Reviews*, 71(1-2), 1-75.
- Moore, G. T., Sloan, L. C., Hayashida, D. N. & Umrigar, N. P. (1992). Paleoclimate of the Kimmeridgian/Tithonian (Late Jurassic) world: II. Sensitivity tests comparing three different paleotopographic settings. *Palaeogeography, Palaeoclimatology, Palaeoecology*, 95(3-4), 229-252. doi: 10.1016/0031-0182(92)90143-s
- Moore, J. M., Allen, P., Wells, M. K. & Howland, A. F. (1979). Tectonics of the Najd transcurrent fault system, Saudi Arabia. *Journal of the Geological Society of London*, 136, Part 4, 441-454.
- Mouawad, J. (2010, March, 19). China's growth shifts the geopolitics of oil, *The New York Times*. Retrieved from <http://www.nytimes.com/2010/03/20/business/energy-environment/20saudi.html?pagewanted=1>
- Murris, R. J. (1980). Middle East: Stratigraphic evolution and oil habitat. *AAPG Bulletin*, 64(5), 597-618.
- Palike, H., Norris, R. D., Herrle, J. O. & Wilson, P. A. (2006). The heartbeat of the oligocene climate system. *Science (Washington)*, 314(5807), 1894-1898.
- Palmer, T. I. M. (1982). Cambrian to Cretaceous changes in hardground communities. *Lethaia*, 15(4), 309-323. doi: 10.1111/j.1502-3931.1982.tb01696.x
- Peebles, R. G., Suzuki, M., and Shaner, M. (1995). The effects of long-term, shallow-burial diagenesis on carbonate – evaporite successions. Selected Middle East Papers from Geo 94, the Middle East Geoscience Conference, April, 1994. Gulf Petrolink, Bahrain.
- Pollastro, R. M., Karshbaum, A. S. & Viger, R. J. (1999). *Map showing geology, oil and gas fields, and geologic provinces of the Arabian Peninsula* (US Geological Survey open-file report). Denver, CO: US Department of the Interior.
- Pomar, L. & Kendall, C. G. S. C. (2008). Architecture of carbonate platforms; a response to hydrodynamics and evolving ecology. *Special Publication -*

Society for Sedimentary Geology, 89, 187-216.

Powers, R. W. (1968). Saudi Arabia. In *Lexique stratigraphique international* [International stratigraphic lexicon]: Vol. 3, Asia, p. 177.

Powers, R. W., Ramirez, L. F., Redmond, C. D. & Elberg, E. L., Jr. (1966). *Sedimentary geology of Saudi Arabia: Geology of the Arabian Peninsula* (US Geological Survey professional paper, 150).

Read, J. F. & Goldhammer, R. K. (1988). Use of Fischer plots to define third-order sea-level curves in Ordovician peritidal cyclic carbonates, Appalachians. *Geology (Boulder), 16(10), 895-899.* doi: 10.1130/0091-7613(1988)016<0895:uofptd>2.3.co;2

A red line, a new kingdom, America, and oil. (2007, 20 February) Retrieved April, 2011, from <http://www.aramcoexpats.com/articles/category/in-search-of-oil/page/25/>

Sadler, P. M., Osleger, D. A. & Montanez, I. P. (1993). On the labeling, length, and objective basis of Fischer plots. *Journal of Sedimentary Research, 63(3), 360-368.* doi: 10.1306/d4267aff-2b26-11d7-8648000102c1865d

Sellwood, B. W., Valdes, P. J. & Price, G. D. (2000). Geological evaluation of multiple general circulation model simulations of Late Jurassic palaeoclimate. *Palaeogeography, Palaeoclimatology, Palaeoecology, 156(1-2), 147-160.*

Sharland, P. R., Archer, R., Casey, D. M., Davies, R. B., Hall, S. H., Heward, A.P., . . . Simmons, M. D. (2001). Arabian plate sequence stratigraphy. *GeoArabia Special Publication No. 2.*

Simmons, M., Casey, D., Davies, R., Holmes, S., Schulze, F., Sharland, P., . . . Anonymous. (2007, 2007). *Arabian Plate sequence stratigraphy; potential consequences for global chronostratigraphy*, Bahrain (BHR).

Sorkhabi, R. (2008). The emergence of the Arabian oil industry. *GeoExpro, 5(6).*

Stegner, W. E. (2007). *Discovery! The Search for Arabian Oil* (First ed.). Portola St. Vista: Selwa Press.

Steineke, M. & Bramkamp, R. A. (1952). Mesozoic rocks of eastern Saudi Arabia. *Bulletin of the American Association of Petroleum Geologists, 36(5), 909.*

Steineke, M., Bramkamp, R. A. & Sander, N. J. (1958). Stratigraphic relations of Arabian Jurassic oil. In L. G. Weeks (Ed.), *Habitat of oil: A symposium* (pp.

- 1294–1329). Tulsa, OK: American Association of Petroleum Geologists.
- Stoeser, D. & Camp, V. E. (1985). Pan-African microplate accretion of the Arabian Shield. *Geological Society of America Bulletin*, 96(7), 817.
- Tinker, S. W. (1998). Shelf-to-basin facies distributions and sequence stratigraphy of a steep-rimmed carbonate margin; Capitan depositional system, McKittrick Canyon, New Mexico and Texas. *Journal of Sedimentary Research*, 68(6), 1146–1174. doi: 10.1306/d4268923-2b26-11d7-8648000102c1865d
- Tintant, H. (1987). Les nautilus du Jurassique d'Arabie Saoudite. Jurassic nautiloids of Saudi Arabia. *Geobios, Memoire Special*, 9(0293-843X, 0293-843X), 67–159.
- Toland, C. (1994). Late Mesozoic stromatoporoids; their use as stratigraphic tools and palaeoenvironmental indicators. London: Chapman and Hall.
- Vail, P. R. (1987). Seismic stratigraphy interpretation using sequence stratigraphy; Part 1, Seismic stratigraphy interpretation procedure. *AAPG Studies in Geology*, 27(1), 1–10.
- Walker, R. G. (1985a). Comparison of shelf environments and deep basin turbidite systems. *SEPM Short Course*, 13, 465–02.
- Walker, R. G. (1985b). Mudstones and thin-bedded turbidites associated with the Upper Cretaceous Wheeler Gorge conglomerates, California; a possible channel-levee complex. *Journal of Sedimentary Research*, 55(2), 279–290. doi: 10.1306/212f869d-2b24-11d7-8648000102c1865d
- Walker, R. G. & Noel, P. (1992). St. Johns, NL: Geological Association of Canada.
- Wender, L. E., Bryant, J. W., Dickens, M. F., Neville, A. S. & Al-Moqbel, A. M. (1998). Pre-Khuff (Permian) hydrocarbon geology of the Ghawar area, eastern Saudi Arabia. *GeoArabia (Manama)*, 3(1), 167–8.
- Wood, R. A. (1987). *Special papers in palaeontology*, 37.
- Wood, R. A. (1995). The changing biology of reef-building. *Palaeos*, 10(6), 517–529.
- Wood, R. A. (2001). Are reefs and mud mounds really so different? *Sedimentary Geology*, 145(3-4), 161–171. doi: 10.1016/s0037-0738(01)00146-4
- Worth, R. F. (2008, July 1, 2008). Khurais oil field journal: Saudi oil project brings skepticism to the surface, *NY Times*. Retrieved from <http://www.nytimes.com/2008/07/01/world/middleeast/01saudi.html?pag>

ewanted=all

Ziegler, M. A. (2001). Late Permian to Holocene paleofacies evolution of the Arabian Plate and its hydrocarbon occurrences. *GeoArabia (Manama)*, 6(3), 445–504.

Chapter 5: Carbonate-Platform Scale Correlation of Stacked High-Frequency Sequences in the Arab-D Reservoir, Saudi Arabia³

5.1 Abstract

The Late Jurassic Arab Formation contains a number of hydrocarbon-bearing carbonates, the most important of which is the lowermost Arab-D reservoir. The reservoir's lithofacies in Khurais Field are: couplets of 1) Lime mud and 2) Intraclastic lithofacies representing basinal turbidites; 3) Pelletal lithofacies representing FWWB sands and silts; 4) Stromatoporoid lithofacies representing a reef; 5) *Cladocoropsis* and 6) Dasycladacean algae lithofacies representing a lagoon; 7) Peloidal and 8) Oolitic lithofacies representing shore-attached sand sheets; 9) Cryptomicrobial lithofacies representing supratidal flats; 10) Anhydrites representing sabkha and salina deposits; and 11) stratigraphically reoccurring Dolomite.

These lithofacies are arranged in a third-order sequence representing the Arab-D Member and the upper part of another third-order sequence representing the upper Jubaila Formation. Within these sequences lie six fourth-order high-frequency sequences, on which are superimposed fifth-order parasequences and parasequence-scale cycles.

The preserved upward shallowing trend of the Arab-D reservoir is manifested laterally by a regional eastward thickening interpreted to be the result of eastward progradation across the shallow Late Jurassic epeiric shelf and into the relatively deep Arabian intrashelf basin.

³ This chapter has been published in *Sedimentary Geology*, Volume 294, 15 August 2013, Pages 205–218. See appendices D and E for further details and permissions.

This study presents a correlation model that explains the drastic thickening and downward climb of the reservoir lithofacies that is observed between the outcrops south of Riyadh and the subsurface in Ghawar Field.

This model is different from the one currently used and predicts an eastward porosity improvement in the upper part of the reservoir accompanied by a porosity reduction in the lower part, assuming null diagenetic modifications effect.

5.2 Introduction

The Late Jurassic Arab Formation contains a number of remarkable reservoir-quality carbonates, each capped by a nonpermeable anhydrite layer, where the upper most carbonate member, Arab-A, is capped by the thick Hith Formation anhydrite (Figure 5.1). The Arab Formation first produced oil in Khurais Field, a giant Saudi Arabian oil field discovered via surface and gravity mapping (Figure 5.2), in 1957 (Al-Mulhim et al., 2010).

Based on detailed analysis of 32 Arab-D cores and hundreds of thin-sections from Khurais Field, we recently proposed an Arab-D depositional model of a prograding, gently sloping shallow, arid, reef-rimmed carbonate shelf (Al-Awwad & Collins, 2013a) and established a high-resolution sequence-stratigraphic framework of the reservoir (Al-Awwad & Collins, in-review). The Arab-D lithofacies recognised in Khurais Field are summarised in Table 5.1; these lithofacies start at the bottom of the succession with monotonously interbedded couplets of Lime-mud and Intraclastic lithofacies representing basinal turbidites, followed by Pelletal lithofacies that represent FWFB sands and silts, followed by Stromatoporoid lithofacies, which formed a shelf-fringing reef. The reef protected a lagoon behind it where a meadow of *Cladocoropsis* and Dasycladacean algae lithofacies resided. Then the succession goes up into Peloidal and Oolitic lithofacies that represent shore-attached sand sheets that are capped by Cryptomicrobial lithofacies representing supratidal flats. Finally, the reservoir units are sealed by Anhydrite

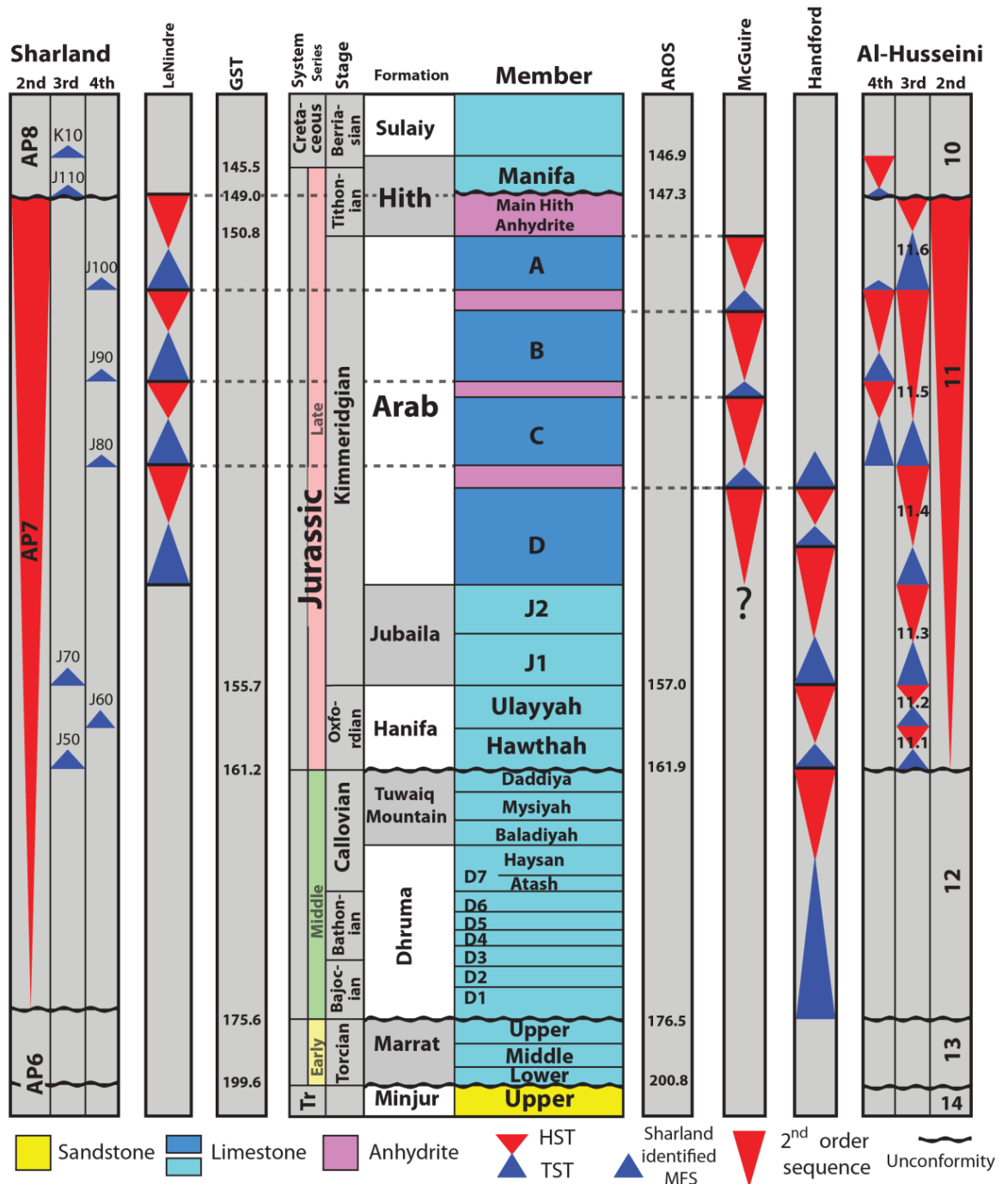


Figure 5.1: Jurassic succession of Saudi Arabia.

Notes: Second-, third- and fourth-order sequences are shown from Al-Husseini (1997, 2009) and Sharland et al. (2001). Key ages are illustrated from both the Geological Time Scale (GTS, Gradstein et al., 2004) and the Arabian Orbital Stratigraphy Project (AROS, Al-Husseini & Matthews, 2008). Lack of biostratigraphic control on the age of the Arab and Hith Formations has been highlighted by Hughes (2004a). The positioning and identification criteria of HST and TST within the Arab and Hith Formations differ among McGuire et al. (1993), Le Nindre et al. (1990) and Handford et al. (2002). Note that the Arab-D reservoir extends from the carbonates of the Arab-D Member of the Arab Formation to the upper part of Jubaila Formation. The Hellangian, Sinemurian, Pliensbachian and Alenian are not represented in Saudi Arabia's succession. The section is not drawn to scale in order to emphasise the stratigraphy of the Upper Jurassic.

Source: Modified from Al-Husseini (2009), Handford et al. (2002), McGuire et al. (1993), Le Nindre et al. (1990) and Sharland et al. (2001)

lithofacies, which reflect deposition in a sabkha followed by deposition in a salina. The reservoir is also characterised by the presence of stratigraphically reoccurring Dolomite.

The high-resolution sequence-stratigraphic framework is of a third-order composite sequence representing the Arab-D Member atop the upper part of another third-order composite sequence representing the upper part of the Jubaila Formation. Within these are six fourth-order, high-frequency sequences; superimposed on them are 12 parasequence and cycle sets, which contain 33 fifth-order parasequences in the upper composite sequence and 123 parasequence-scale cycles in the lower composite sequence. This study explores the degree of connectivity or lack thereof of Khurais Field to the broad Arabian platform by regionally correlating the Arab-D reservoir outside the field boundaries, using the proposed depositional environment model and sequence-stratigraphic framework of the reservoir. The results suggest that sequence analysis is key in understanding the architectural heterogeneities of the reservoir and their bearing on the porosity zonation and distribution of flow and baffle units; thus, a different model is proposed to the present one in use. Two cross-sections are presented, a W-E cross-section that extends from the Arab-D outcrops south of the Saudi capital Riyadh to Ghawar Field across a distance of 413 km, and a N-S cross-section that extends from the Safaniya area down to south Khurais along a 397 km line of section (Figure 5.2).

Examining the cores from Khurais Field offered an excellent opportunity to formulate a regional perspective of the reservoir's configuration and bridge the correlational gap between the Arab-D in outcrop and in Ghawar, which has been tentatively attempted before by Leinfelder et al. (2005). Another regional correlation was done by Handford et al. (2002), but it did not account for the area west of Ghawar, which has a significant role in the understanding of the regional configuration of the reservoir and in interlacing the outcrop to the subsurface.

5.3 Regional and Structural Settings

The Arabian plate formed by terrane accretion to the northeastern edge of the African plate. Figure 5.2c shows the Midyan, Hijaz, and Asir Terranes, which were accreted to the northeastern edge of the African plate before 715 Myr and were separated from the Afif Terrane by the Nabitah Sea (Stoeser & Camp, 1985).

Between 680–640 Myr, the Nabitah collision between the Afif Terrane on one side and Midyan, Hijaz, and Asir Terranes on the other consumed the Nabitah Sea into the Nabitah Suture. An east-dipping subduction commenced below the Amar Arc 670 Myr ago, consuming the Amar Sea, and culminated with the fusion of the Rayn Terrane, which comprises eastern and central Arabia, and the Afif Terrane. This fusion, known as the Amar collision, took place between 640–620 Myr ago and yielded the obducted N-trending thrust slices of ophiolites known as the Amar Suture (Al-Husseini, 2000; Stoeser & Camp, 1985; see Figure 5.2c). The Amar collision also generated EW-trending compressional stresses that propagated through the Arabian plate and formed uniformly aligned, N-oriented anticlines: the En Nala Anticline, the Khurais-Burgan Anticline, the Summan Platform and the Qatar Arch (Figure 5.2), (Al-Husseini, 2000; Brown et al., 1989; Stoeser & Camp, 1985).

The Ghawar and Safaniya fields are situated on the 500 km-long En Nala Anticline, and the Khurais and Burgan fields are situated on the 500 km-long Khurais-Burgan Anticline (Al-Husseini, 2000). The collision also yielded the NE-trending Wadi Batin Fault and NW-trending Abu Jifan Fault, which are two orthogonal, strike-slip faults that bind the Rayn anticlines and intersect near the Amar Suture (Figure 5.2). In addition, an extensive network of faults trending N, NW and NE cut through the Precambrian basement, forming rigid unstable basement blocks that propagated movement upward through the Phanerozoic succession, causing structural growth, subsidence and hydrocarbon migration (Al-Husseini, 2000). Subsequent to the Amar collision, between 620 and 530 Myr ago, the collapse of the Arabian-Nubian Shield took place; the cause of this collapse has been contributed to post-collisional gravitational instability associated with lithospheric over thickening (Blasband et al., 2000; Genna et al., 2000; Husseini, 1987, 1988; Husseini & Husseini, 1990). It is

thought that the post-Amar-collision extension peaked by the formation of the extensive, 570 to 530 Myr, sinistral Najd Fault system and its associated rift basins. The Najd Fault system (Figure 5.2) comprises three parallel fault zones that collectively extend over 1,100 km of length and 300 km of width, and individually are five to 10 km wide (Brown, 1972; Brown & Jackson, 1960; Brown et al., 1989; Howland, 1979). The Najd Fault system dislocated the 680–640 Myr N-trending Nabitah Suture laterally by c. 300 km (Brown, 1972; Brown & Jackson, 1960; Brown et al., 1989; Howland, 1979; G. T. Moore et al., 1979).

This extensional rifting phase caused the Rayn anticlines to become uplifted horsts bounded by normal faults and subsiding grabens (Al-Husseini, 2000). Reactivation of the Ryan anticlines first occurred during the 570 to 530 Myr Najd Rift System. Then, the Carboniferous Hercynian Orogeny rotated the Arabian Plate, uplifted and tilted central Arabia towards the east, eroded several kilometres of sediments, creating a hiatus and uplifting the Rayn anticlines (Al-Husseini, 2000; Haq & Al-Qahtani, 2005). Subsequently, the Permo-Triassic Neo-Tethys rifting and spreading along the present-day Zagros Suture and Gulf of Oman (Figure 5.2) created a passive margin east of Arabia and activated the Rayan anticlines (Al-Husseini, 2000; Powers et al., 1966; M. A. Ziegler, 2001). The opening of the eastern Mediterranean followed in the Early Jurassic, creating another passive margin along the plate's northern edge, which yielded a vast, shallow-marine shelf that occupied most of the Arabian Peninsula and blanketed it with shallow-shelf carbonate and evaporite deposition (Énay, 1993; Le Nindre et al., 1987, 1990; Murriss, 1980; Pollastro et al., 1999).

Organic-rich, anoxic shales (Hanifa and Tuwaiq Mountain formations; Figure 5.1) that later sourced the oils of the Arab reservoirs were deposited in the intrashelf basins (Figure 5.2) that developed as a result of epeirogenic downwarp during the Middle Jurassic (Alsharhan & Kendall, 1986; Ayres et al., 1982; Droste, 1990; Murriss, 1980; M. A. Ziegler, 2001). Carbonates of the Arab Formation progressively filled the intrashelf basins with repetitive shoaling-upward carbonate cycles that were capped with evaporitic flats, during the Late Jurassic, as Central Arabia remained stable (Haq & Al-Qahtani, 2005; M. A. Ziegler, 2001). These Arab Formation

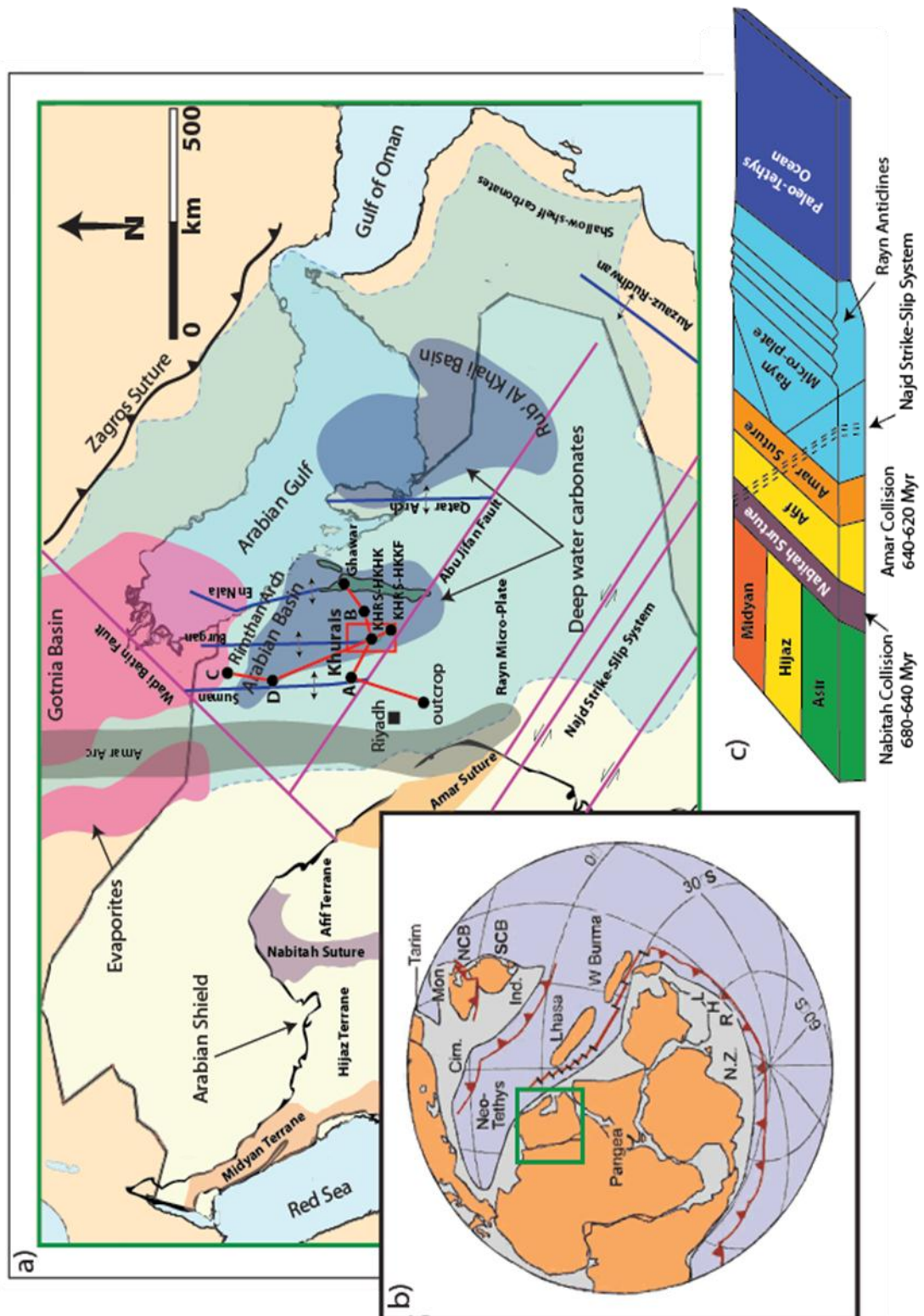


Figure 5.2: Location map of Khurais Field and schematic structural model.

Notes: a) The red rectangle shows the location of Khurais Field. Dark blue areas outline Late Jurassic intrashelf basins where deposition of deep-water carbonates took place. The extent of shallow-shelf carbonate deposition is highlighted by the light blue area. b) Li and Powell's palaeogeographic configuration during the Jurassic, with the Arabian Plate position enclosed in the green square. Note that the location of the palaeoequator is controversial (Golonka, 2002; Stampfli et al., 2001). c) Schematic model of the Precambrian Nabitah and Amar collisions that accreted the Arabian plate.

Source: Modified from M. A. Ziegler (2001), Li and Powell (2001) and Al-Husseini (2000).

members maintain a uniform fabric and thickness across the 250 km wide Arabian Basin (M. A. Ziegler, 2001). Finally, the Ryan anticlines were reactivated during the Neo-Tethys closing due to the Arabian-Eurasian plates' compression. This compression commenced in the Late Cretaceous, and caused the obduction of the Oman ophiolites and emergence of the Zagros Mountains (Al-Husseini, 2000; Alsharhan & Kendall, 1986; Haq & Al-Qahtani, 2005; Wender et al., 1998; M. A. Ziegler, 2001).

5.4 Methodology

Lithofacies components, repetitive motifs in lithofacies stacking patterns, recognition of retrogradational, aggradational and progradational modulations, vertical thickening versus thinning trends, upward fining versus coarsening and/or shallowing versus deepening trends (Van Wagoner et al., 1990) coupled with gamma-log calibrations have been utilised in this correlation study. The gamma-log calibration worked exceptionally well in the monotonous, turbidity-dominated basinal part of the Arab-D reservoir, where gamma values showed regional consistency and conspicuous rhythmicity that accords with the turbidites' HFS. A question of the Arab-D's gamma signal being a reflection of diagenetic fluids mobilisation, which could cause disequilibrium of parent/daughter activity ratios in uranium and thorium decay series, has been raised (see Ivanovich & Harmon, 1992; Mey, 2008). While that could very well be true, the data presented herein argues against excluding a depositional causality for the following reasons. First, the gamma signal shows a consistent, characteristic upward increase of a scale that accords with the reservoir's HFS scale established by the lithofacies stacking patterns (Al-Awwad & Collins, in-review). Second, the gamma trends, as illustrated in this study, are consistent on a regional scale, hundreds of kilometres across; diagenetic trends, on the other hand, are expected to be less extensive. Third, diagenetic effects, such as dolomitisation, dissolution, and cementation, could distort a depositional signal that is already there, but that does not necessitate them being the only or determinant cause of it. Fourth, the correlation presented here is based on a sequence-stratigraphic framework that is entirely reliant on

sedimentary trends (Al-Awwad & Collins, in-review), and its drastic, regional-scaled agreement with the preserved gamma signal can hardly be attributed to mere coincidence.

5.5 Regional Correlation

It has been established that the Arab-D reservoir reflects a long-term shallowing event, which preserved an upper, 1–3 Myr, third-order composite sequence that represents the Arab-D Member (Al-Husseini, 2009; Le Nindre et al., 1990; McGuire et al., 1993; Sharland et al., 2001), and where deposition took place on the shallow-marine shelf, rimmed by a reef, above FWWB (Al-Awwad & Collins, in press, in-review). The lower part of the reservoir preserved the upper part of another 1–3 Myr, third-order composite sequence that represents the upper part of the Jubaila Formation (Al-Husseini, 2009; Le Nindre et al., 1990; McGuire et al., 1993; Sharland et al., 2001), where, for the most part, turbidite couplets were deposited in a relatively deep basinal sub-FWWB setting (Figure 5.3). This notion is supported by Alsharhan and Kendall (1986), who stated that the transition from Jubaila Formation into Arab-D Member in the Arabian intrashelf basin marks a shallowing-upward cycle from deep subtidal facies into shallow intertidal facies and ultimately into supratidal sabkha anhydrites. These composite sequences are punctuated by six 0.1–0.4 Myr, fourth-order high-frequency sequences, superimposed on which are at least 12 parasequence sets, and multiple parasequences and small-scale cycles (Al-Awwad & Collins, in-review).

The upper boundary of the Arab-D composite sequence is interpreted as a type II sequence boundary, dated by Al-Husseini and Matthews' (2008) orbital-forcing model at 153.4 Myr (Al-Husseini, 2009). It is placed at the transition from the sabkha anhydrites to the massive subaqueous anhydrites, as they represent a sea-level transition from a fall to a rise (Figure 5.3). The lower boundary of the Arab-D composite sequence is also a type II sequence boundary, dated by Al-Husseini and Matthews' (2008) orbital-forcing model at 154.6 Myr (Al-Husseini, 2009). It is placed at the base of a thoroughgoing transgressive interval. This interval tops an extensive

stromatoporoid-reef layer that contains reworked oolitic and/or coated grains (coloured in red in the cross-sections) and caps the basinal interbedded Intraclastic and Lime-mud lithofacies of the upper Jubaila Member (Figure 5.3).

Figure 5.4 shows a west-east regional correlation across 413 Km. The cross-section starts on the Arab-D outcrop sections described by Meyer et al. (1996), where the capping anhydrites are dissolved and brecciated and all of the reservoir's lithostratigraphic zones are present, except for the *Cladocoropsis* and the Oolitic lithofacies. The section then extends east towards Well A, KHRS-HKHK (Al-Awwad & Collins, 2013a), Well B, and finally to a well in Ghawar Field described by Lindsay et al. (2006). Figure 5.5 shows a north-south regional correlation that extends for 397 Km across Well C, Well D, Khurais HKHK (Al-Awwad & Collins, 2013a) and Khurais HKKF described by the main author. The two cross-sections intersect in the KHRS-HKHK well and are illustrated in a fence diagram in 3D in Figure 5.6.

The authors' previous sedimentologic and stratigraphic work (Al-Awwad & Collins, 2013a, in-review) has been used as a common denominator to unify the reservoir characterisations by other authors who have worked in the area. Fourth-order high-frequency sequences identified in Khurais are numbered and correlated to the other outcrop and subsurface sections (Figures 5.4 and 5.5). The boundaries of the Arab-D composite sequence are marked by thick red lines, both sections are datumed from the upper Arab-D sequence boundary, and the boundaries are correlated across both cross-sections (Figures 5.4 and 5.5) using the above highlighted criteria. Figure 5.4 shows that the Arab-D composite sequence increases in thickness from 50 ft (15.2 m) in the outcrop section to 153 ft (46.6 m) in Khurais and finally 164 ft (50.0 m) in Ghawar, as its lower boundary significantly shifts downward from west to east. Figure 5.5, however, illustrates that the Arab-D composite sequence, except at Well D, maintains more or less the same thickness across the 397 km of cross-section, as its lower boundary remains at the same elevation. It is difficult to depict with certainty whether the Jubaila composite sequence is thickening or thinning in any of the sections, as its lower boundary is not penetrated by the cores or exposed in the outcrop.

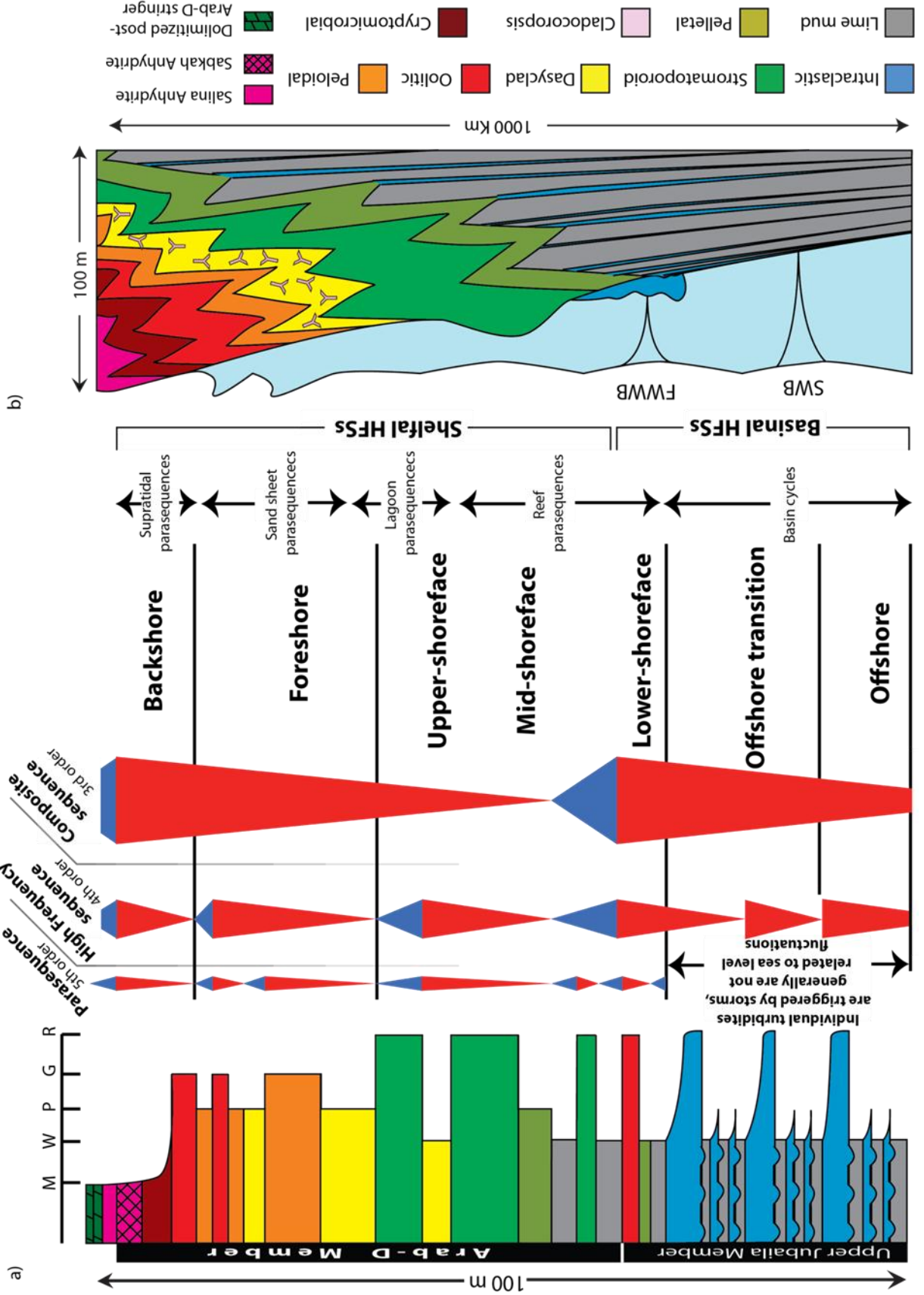


Figure 5.3 (previous page): An idealised Arab-D reservoir core with the interpreted sequence-stratigraphic framework and a schematic depositional model.

Notes: On the composite-sequence scale in Figure 5.3a), the lower part's overall upward shallowing culminates with deposition of thin units of stromatoporoids characterised by reworked oolitic and/or coated grains (coloured in red) that mark a lower composite sequence boundary. This is followed by a marine flood represented by a thin interval of interbedded Lime mud and Intraclastic lithofacies and is interpreted as a brief transgressive set that probably marks the contact between the Jubaila and Arab Formations. The MFS of the upper composite sequence is picked at the highest occurrence of Lime mud and or Intraclastic lithofacies, which represents maximum extent of deeper lithofacies landward. After the MFS, the lithofacies continue to shallow up to sabkha anhydrites (indicated by the chicken wire pattern at the top of the section). The upper composite sequence boundary is placed at the transition from the sabkha anhydrites to the massive subaqueous anhydrites interpreted as early TST of a subsequent composite sequence. High frequency sequences (4th order) are picked based on vertical stacking patterns and each shows a unique lithofacies composition as the system shallows upward. On the parasequence scale (5th order), the individual basinal cycles represent storm triggered turbidites and hence do not represent sea-level fluctuations. Their respective cycle sets and HFSs reflect a stacking pattern that shows rhythmic thinning of the Lime mud and thickening of the Intraclastic lithofacies which is interpreted to represent sea-level falls. Supratidal, sand-sheet, lagoon, and reef parasequences are shown in their respective positions of the platform and are discussed in detail in Al-Awwad and Collins (in-review). b) The schematic depositional model (not to scale) is of a prograding frequently storm-abraded, gently sloping, shallow, arid, stromatoporoid-reef-rimmed shelf of the Arab-D reservoir (Al-Awwad & Collins, 2013a). Salina and sabkha anhydrites are followed by stromatolites, ooids and peloids sand sheets, and a *Cladocoropsis* and Dasycladacean algae meadow that was protected by a rim densely populated by small-scale stromatoporoid reefs toed by near FWWB pelletal silts. Storms mainly reworked the reefs generating Intraclastic turbidites. The depositional model is juxtaposed next to the idealised sequence-stratigraphic framework for comparison.

5.5.1 Shelfal Lithofacies Correlated from West to East

Focusing on the W-E cross-section, the shelfal lithofacies (HFSs 4, 5 and 6) almost triple in thickness from the outcrop to Khurais, continue thickening slightly to Ghawar, and correspondingly show a significant downward shift in elevation (Figure 5.4). The upper part of the reservoir (Figure 5.4) is comprised of thick supratidal cryptomicrobial laminites in the outcrop that quickly diminish eastward, except for very thin slivers below the anhydrites. Within HFS 6, the oolitic sand sheet is absent in the outcrop, appears in well A, thickens and splits into two cycles in Khurais, and becomes thickest in Ghawar. The peloidal sand-sheet, lagoonal and reefal lithofacies in HFSs 4, 5 and 6, show consistent thickening to the east. HFSs 6 and 5 condense into one HFS west of well A (Figure 5.4). The oolitic sand sheet seems to

dominate in the HST of HSF 6, whereas the peloidal sand sheet dominates its TST. In HFS 5, the peloidal sand sheet and the lagoonal lithofacies dominate the HST, whereas the reefal lithofacies dominate the TST. This reefal lithofacies preserves two muddier intervals, coloured in pale green, that considerably thin or pinch out towards the outcrop. The lower of these muddier intervals caps HFS 4 and seems to be much more extensive laterally than the upper. The HST of HFS 4 is dominated by reefal lithofacies while its TST is dominated by the basinal turbidites.

5.5.2 Basinal Lithofacies Correlated from West to East

Correlation of individual storm beds has been shown to extend from 3 up to 15 miles in various outcrop studies (Aigner, 1985; Elrick & Read, 1991). The storm triggered turbidite couplets of the lower part of the Arab-D reservoir are correlated across hundreds of kilometres based on the thickening upward packages of the Intraclastic lithofacies rather than individual beds. This high-frequency-sequence-scaled thickening has been attributed to eustatic fluctuations, that probably lowered storm wave base allowing higher levels of energy, to generate upward thickening turbidites (Al-Awwad & Collins, 2013a, in-review).

From W to E (Figure 5.4), this thickening trend seems to hold true again for the basinal part of the reservoir (HFSs 1, 2 and 3). At least for HFS 3, which is correlatable all the way through to the outcrop, and drastically thickens from 5 ft (1.5 m) in outcrop, to 39 ft (12 m) in Khurais. Both the Lime mud and particularly the Intraclastic lithofacies in HFS 1, 2 and 3 drastically thicken and downstep from the outcrop to Khurais and then slightly thin away from Khurais towards Ghawar (Figure 5.4). Finally, the hardgrounds separating the Lime mud from the Intraclastic lithofacies are 4" (10 cm) apart in outcrop, 6" (15 cm) apart in Khurais, and 2–3' (0.6–0.9 m) apart in Ghawar (Lindsay et al., 2006).

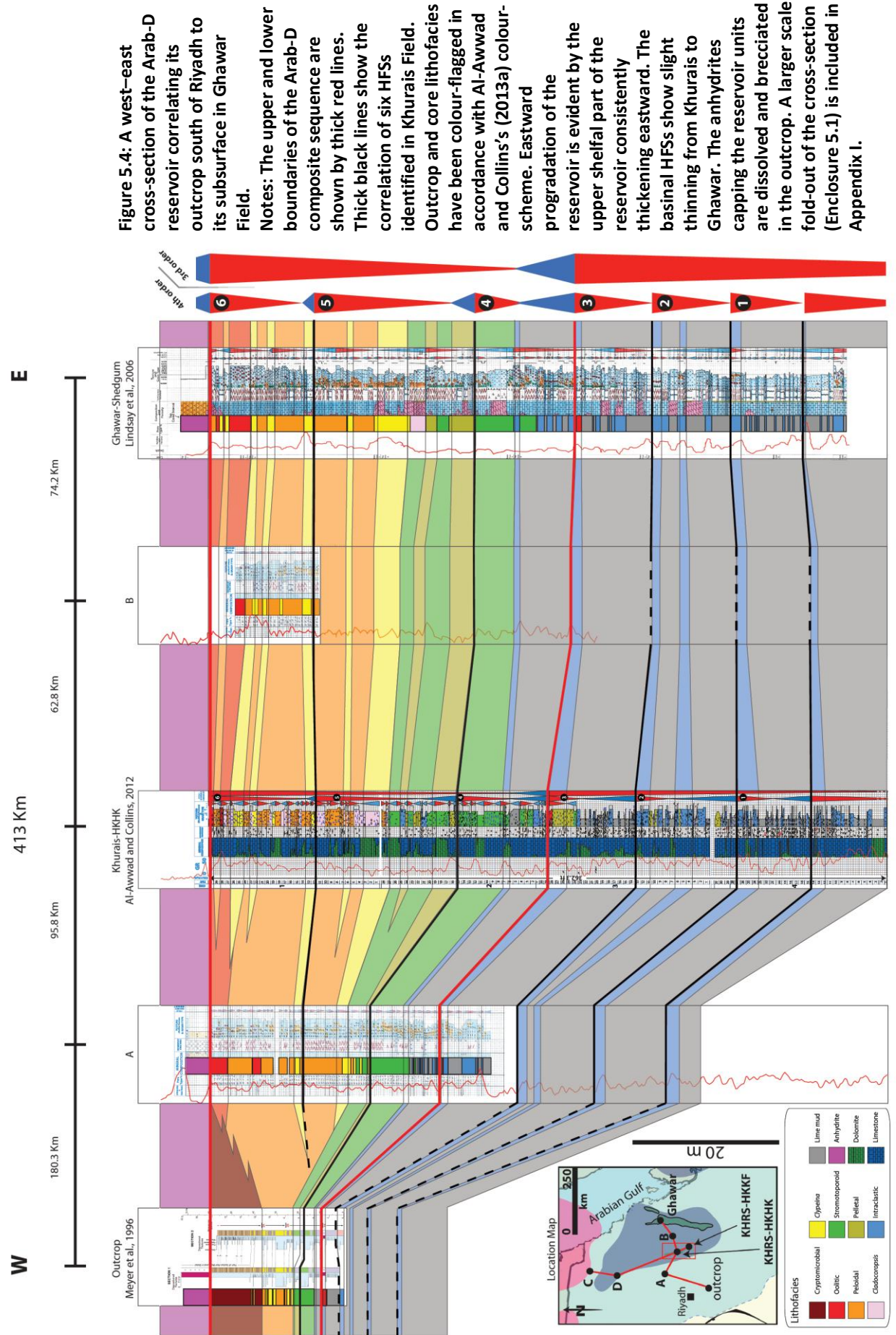


Figure 5.4: A west-east cross-section of the Arab-D reservoir correlating its outcrop south of Riyadh to its subsurface in Ghawar Field.

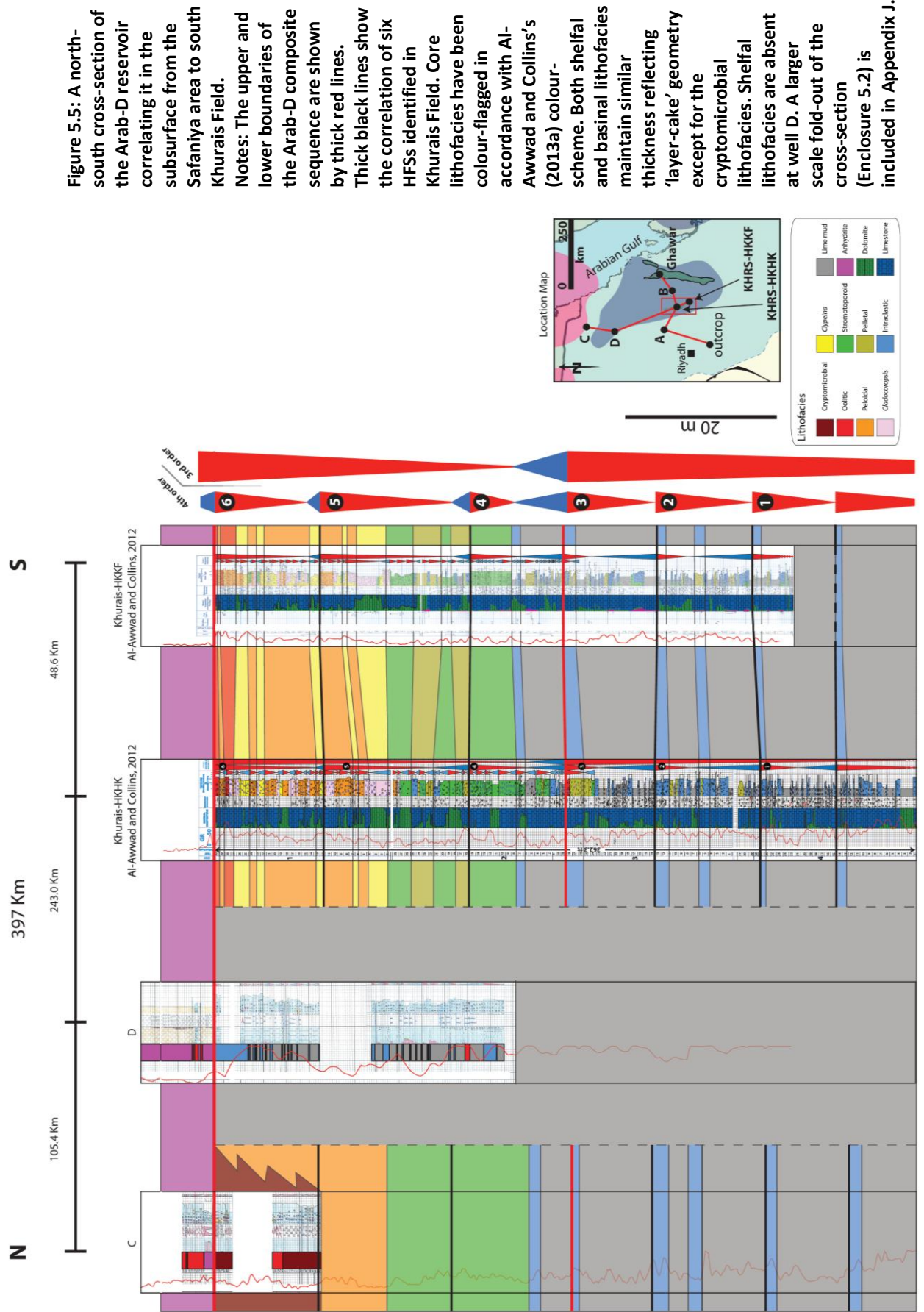
Notes: The upper and lower boundaries of the Arab-D composite sequence are shown by thick red lines. Thick black lines show the correlation of six HFSS identified in Khurais Field. Outcrop and core lithofacies have been colour-flagged in accordance with Al-Awwad and Collins's (2013a) colour-scheme. Eastward progradation of the reservoir is evident by the upper shelfal part of the reservoir consistently thickening eastward. The basal HFSS show slight thinning from Khurais to Ghawar. The anhydrites capping the reservoir units are dissolved and brecciated in the outcrop. A larger scale fold-out of the cross-section (Enclosure 5.1) is included in Appendix I.

5.5.3 North to South Correlation

From N-S, Figure 5.5 illustrates that the shelfal and basinal lithofacies continue more or less with the same thickness, showing a layer-cake geometry except for the Cryptomicrobial lithofacies which pinches out somewhere between well C (where a major collapsed breccia surface appears beneath the Anhydrites) and Khurais HKHK. The shelfal lithofacies are completely absent at well D and another well located 93.2 km to the east of it (not included in the cross-section). They show basinal lithofacies directly beneath the Arab-D anhydrite without passing through the shelfal lithofacies.

5.6 Discussion

The major collapsed breccia surface, which appears beneath the Anhydrites in well C in the north (Figure 5.5), indicates a likely sea-level drop and exposure. This substantiates the placement of the upper boundary of the Arab-D composite sequence at the transition from the sabkha anhydrites and the massive subaqueous salina anhydrites, which represent a sea-level fall followed by a rise (Figure 5.3), (Al-Awwad & Collins, in-review). This boundary's identification criteria, which places the boundary within the anhydrites, is stratigraphically close, but not quite identical to the criteria established by Lindsay et al. (2006), Mitchell et al. (1988) and McGuire et al. (1993). They placed the upper composite sequence boundary at the transition between the reservoir's carbonates and its sealing anhydrites, considering all of the anhydrites as transgressive salina deposits deposited during the subsequent composite sequence transgression. This interpretation suggests that the subaqueous salina anhydrites are onlapping transgressive deposits over the sequence boundary surfaces, as modelled by Sarg (1988), which caps the sabkha anhydrides. This interpretation is similar to what Meyer and Price (1993) concluded; that the anhydrites represent the peak of the reservoir shallowing, though the authors did not specifically elaborate on the sequence boundary's particular position. Using different boundary identification criteria, Le Nindre et al. (1990) and Al-Husseini (1997, 2009), interpret the Arab anhydrites, including the one atop the



Arab-D, as highstand deposits (Figure 5.1). One problem with this interpretation, at least in the Arab-D case, is that it does not explain how the extra accommodation was created within the same composite sequence HST to house the capping anhydrites, at a time when up-to-sea-level oolites and supratidal cryptomicrobial laminites culminated the reservoir deposition. It appears rather inconceivable to generate enough accommodation within the same HST to deposit the entire Arab-D anhydrite, which averages a 157.5 ft (48.0 m) in Khurais Field, when deposition had already reached sea level.

The criteria adopted here for identifying the lower boundary of the Arab-D composite sequence generally agrees with Lindsay et al. (2006) and Mitchell et al.'s (1988) criteria in Ghawar Field. Lindsay et al. (2006) stated that although identifying the boundary has proven to be difficult due to the incompleteness of the subsurface section compared to the outcrop, the upward decrease in stromatoporoids coupled with the increase in *Cladocoropsis* has been used for its identification. More specifically, the lower boundary is identified to be at the base of the laterally extensive transgressive interval that caps the first laterally extensive reef interval, which is characterised by reworked ooids and/or coated grains. This lower boundary identification criteria, though, disagrees with Meyer and Price (1993) who stated that the entire reservoir with both its lower (basinal) and upper (shelfal) parts represent a single genetic depositional sequence with no boundary separating them.

The upward-shallowing trend, reflected vertically in the reservoir lithofacies (Al-Awwad and Collins, 2013 a), is translated laterally as a regional thickening interpreted as a progradational trend from W to E (Figure 5.4). The reservoir's lithofacies thicken and downstep eastward indicating that the Late Jurassic basin was to the east, and that the palaeoshoreline was trending in a N-S direction, relatively close to the current Arabian Gulf's shoreline trend. This interpretation of the basin and shoreline positions agrees with Meyer et al. (1996) work on the Arab-D outcrop in Wadi Nisah, where they measured strike directions of symmetrical carbonate sand ripples whose wavelengths are 80 cm, heights are 5–7 cm and crests trended N5°W

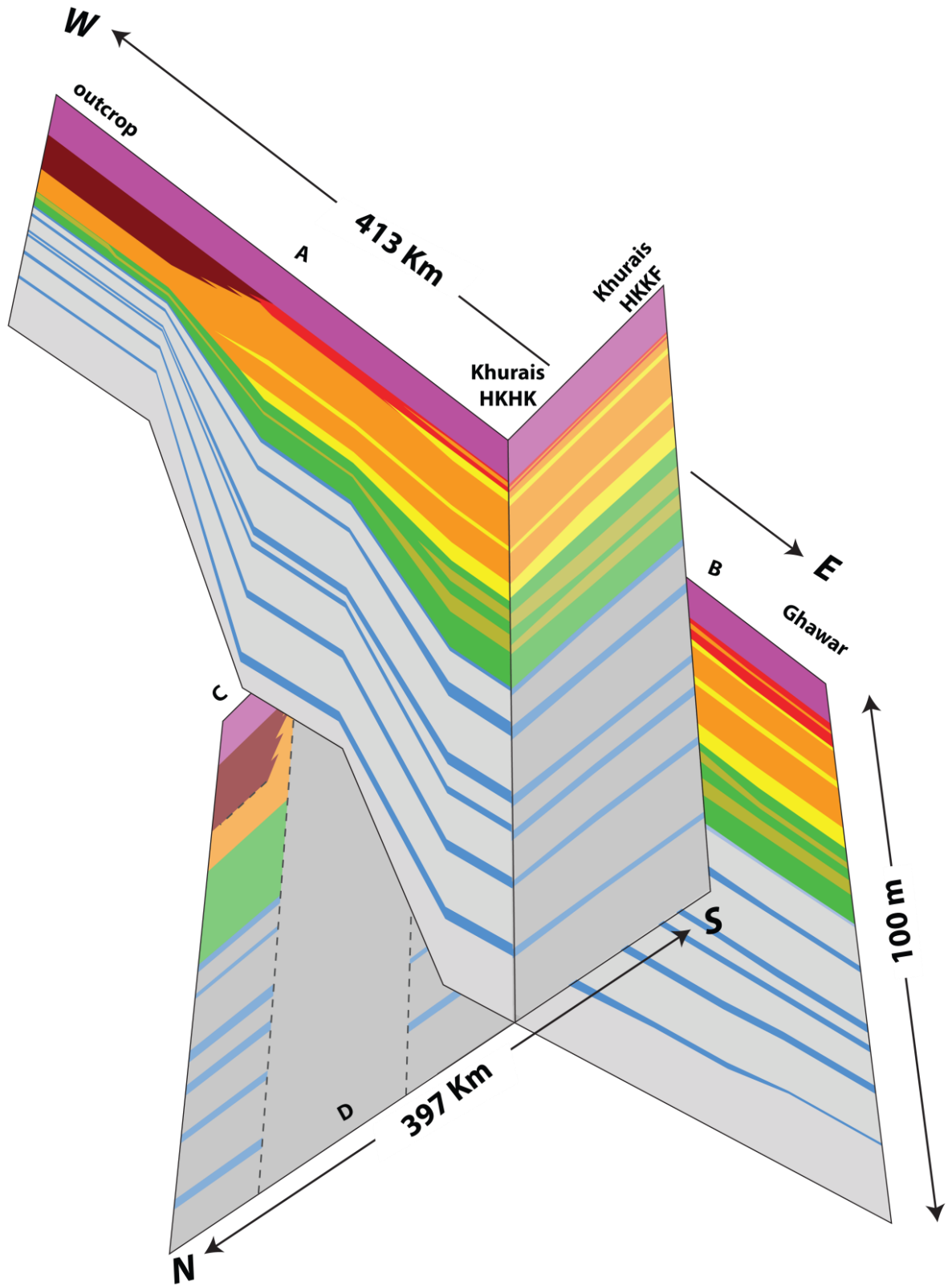


Figure 5.6: A fence diagram showing the intersection of Figures 5.4 and 5.5 at Khurais HKHK.
Notes: The colour scheme is similar to the one used in figures 5.4 and 5.5.

indicating that the palaeoshoreline trended in the same direction. Perpendicular to these, they measured east-dipping imbricated flat-pebble conglomerates confirming a westward onshore (Meyer et al., 1996). In addition, Meyer and Price (1993) concluded an eastward basin based on local correlation of the Arab-D reservoir across Ghawar field. This conclusion is also in accordance with the palaeogeographic reconstructions of the Arabian Plate's Jurassic intrashelf basins and its margin with the Neo-Tethys (Figure 5.2), (Li & Powell, 2001; M. A. Ziegler, 2001).

Previous studies have suggested that a grain shoal formed on the Rimthan Arch, framed the Arabian intrashelf basin, and prograded southward to fill it (Handford et al., 2002). This reasoning is based on regional top Arab-D anhydrite thickening to the south, which has been interpreted as Salina deposits of a subsequent transgression (Handford et al., 2002; Lindsay et al., 2006). Had this been the case, then it would be inexplicable that the Arab-D grainy lithofacies are present to the west of Ghawar in Khurais, and as far west as the outcrop. Others suggested the progradation to be trending to the north based on carbonate thickening in that direction, explaining the evaporites as coeval sabkha deposits thinning out to the north (Meyer & Price, 1993; Mitchell et al., 1988). To the contrary, Al-Silwadi et al. 1996; de Matos & Hulstrand, 1995; and Simmons, 1994 recorded a pinch out of the Arab-D carbonate and the top Arab-D anhydrite to the east of Ruwais, located west of Abu Dhabi, which supports an eastward situated basin and progradation direction. Moreover, Azer and Peebles (1995) showed considerable thinning and pinch out of the Hith Anhydrite and the Arab-C member in the area offshore of Abu Dhabi, from west to east. Other workers have proposed that the intrashelf basins were completely filled by the Kimmeridgian, and interpret the Arab-D to show a broad layer-cake aggradation (Ayres et al., 1982; A. O. Wilson, 1985). Contrastingly, M. A. Ziegler (2001) concluded that shelf marginal carbonates of the Hanifa, Jubaila, Arab and Manifa formations wedged out and downlapped onto the Arabian and Rub' Al-Khali intrashelf basins. The Arab-D regional correlation presented in this study addresses both the N-S and W-E lateral variations of the reservoir, and does so at a more extensive scale than previous studies. It also concurs with Sharland et al.'s

(2001), M. A. Ziegler's (2001), Meyer and Price's (1993) and Meyer et al.'s (1996) views. We also agree that the majority of the top Arab-D anhydrite was deposited in a salina setting, but that could mean that the anhydrite's thickening trends are simply indicative of depression positions along the Arabian shelf, rather than indicating progradation trends of the reservoir.

In the W-E cross-section (Figure 5.4) Peloidal, Dasycladacean algae, *Cladocoropsis* and Stromatoporoid lithofacies in HFSs 4, 5 and 6 almost triple in thickness from the outcrop to Khurais, indicating that the accommodation increased to the East allowing for progradation and thickening of the upper lithofacies belts. This accords with Meyer et al. (1996) findings of slight eastward increase in thickness of these lithofacies in their correlations of the Arab-D outcrop measured sections. The thickness increase being most dramatic west of Khurais suggests that Khurais, Well B and Ghawar occupied localities more proximal to the intrashelf depocenter, which probably was further east. In addition, the capping anhydrites dissolution and brecciation in outcrop suggests that it was closer to the shoreline and hence was subjected to exposure, as compared to the eastward localities that preserved the anhydrites.

This thickening trend is accompanied by the appearance of the oolitic lithofacies to the east of the outcrop and its eastward thickening and splitting trend, which opposes the cryptomicrobial lithofacies eastward diminishing trend. This indicates a progradational trend from west to east in which relatively shallower lithofacies thin and pinch out giving way to the thickening of relatively deeper lithofacies in the upper part of the reservoir (HFSs 6 and 5, Figure 5.4).

This progradation trend is further supported by the thinning of HFS 4 and condensation of HFS 6 and 5 in the outcrop section towards the palaeoshoreline (Figure 5.4). In the TST of HFS 5, the reef's overall eastward increase in thickness, in addition to its two muddier intervals, is interpreted to represent flooding events, thinning or pinching out westward, and further supports locating the basin and the progradational direction to the East. The lower of the reef's floods caps, HFS4,

seems to be the result of a major sea-level rise that yielded a much more extended, mud-rich deposition across the platform towards the west.

The Intraclastic and Lime mud lithofacies in HFSs 1, 2 and 3 also drastically thicken and downstep from the outcrop to Khurais (Figure 5.4) indicating a progradational trend towards the east. This thickening trend also suggests that well A and the outcrop are more proximal to the intrashelf basin margin, where limited accommodation restricted deposition.

The fact that hardgrounds are most abundant in outcrop, less in Khurais, and least in Ghawar (Lindsay et al., 2006), first suggests that all three localities were probably within the Arabian intrashelf basin, hence the presence of the hardground-capped, basinal turbidite couplets in all of them. And second, this difference in hardground abundance suggests that the three localities progress respectively from the basin's westward edge towards its centre. In other words, the outcrop position at the margin would be subjected to more storm triggered turbidity avalanches; only bigger, fewer turbidites would reach deeper to Khurais further east; and even fewer and bigger ones would reach deeper to Ghawar, hence the progressively larger spacing among the hardgrounds eastward.

The previously proposed depositional model (Al-Awwad & Collins, 2013a) predicts that the basinal turbidites would thin in the progradation direction, which is observed in the slight thinning from Khurais to Ghawar, especially in the Intraclastic lithofacies (Figure 5.4). In addition, the thinning of HFS 1, 2 and 3 from Khurais to Ghawar suggests that the Lime mud lithofacies represent, for the most part, divisions C, D and E of Bouma sequences (Al-Awwad & Collins, 2013a), rather than flooding coming from the intrashelf basin from the East towards the west. It appears that as a result of progressive filling of the accommodation to the east, the slopes of the lithofacies boundaries decreased gradually from the bottom part of the reservoir (HFS 1, 2 and 3) to the upper part of the reservoir (HFS 4, 5 and 6).

The N-S regional correlation section (Figure 5.5) illustrates that the Arab-D and

upper Jubaila lithofacies continue more or less with the same thickness across the 378 km of section. This coupled with the fact that the correlation lines connecting the HFSs boundaries across the section are parallel to the lithofacies boundaries suggests that this section runs along regional strike. The lower sequence boundaries of the Arab-D composite sequence and the regional flood that caps HFS 3 are clearly present, easily correlatable throughout and show no variation in elevation. The exception to this interpretation occurs at well D (Figure 5.5), which shows basinal lithofacies directly beneath the Arab-D anhydrite. A similar trend continues on another well located 93.2 km to the east of it. The juxtaposition of basinal lithofacies in these two wells, right below the anhydrites, is anomalous in comparison to the hundreds of wells drilled in the study area. This anomaly could be explained by a regional trough where only basinal lithofacies were deposited and later were draped by the top Arab-D anhydrite; or it could indicate an uplift and erosion of the Arab-D shelfal lithofacies in that area. Unfortunately, the data available for this study are insufficient to verify any of these hypotheses.

5.7 The Timelines Dilemma

Correlating timelines within the Arab-D is problematic due to the lack of biostratigraphic age control (Hughes et al., 2004), which inopportunely coalesces with lack of exposure surfaces or sedimentary markers. In light of the authors' proposed depositional model (Figure 5.3 b), the correlation lines, tying the HFSs (Figures 5.4 and 5.5), separate relatively deeper lithofacies, interpreted to be deposited during eustatic rises, from relatively shallower ones, interpreted to be deposited during eustatic falls. Hence, these correlation lines are presented here as stratigraphic-marker horizons, in their respective locations (i.e., in the one dimensional sense of the well-bore or the outcrop section). It should be underlined here that these stratigraphic-marker horizons are not actual timelines.

The gentle slope (Meyer, 2000) of the depositional shelf is expected to cause the observed lithofacies lateral extensity, and consequently, cause the stratigraphic-marker horizons to follow the facies boundaries. Nevertheless, at a basin margin,

the bathymetric gradient is expected to control a light-penetration gradient that would dictate the geographic distribution of photosynthetic producers, and accordingly, impact the distribution of benthic consumers (Flügel, 2004). Additionally, the bathymetric gradient would impose a wave-energy gradient that would bear upon the platform's ecology (Flügel, 2004). Therefore, it is hypothesized here that these dynamics would mandate much-less-laterally-extensive timelines than the stratigraphic-marker horizons correlated in Figures 4. These timelines would also transcend the lithofacies boundaries at a much steeper geometry than that shown by the correlated stratigraphic-marker horizons. Thus, it is tempting to correlate each stratigraphic-marker horizon to the one sequentially above it as illustrated by Figure 5.7, which shows hypothetical time lines (the thick black lines) superimposed on the dip section. These proposed hypothetical timelines transcend the facies boundaries and top lap against and down lap on the composite sequence boundaries (Figure 5.7). With the lack of biostratigraphic constraint, pinning down the geographic location at which a link between a stratigraphic-marker horizon should be made to the one sequentially above it remains uncertain.

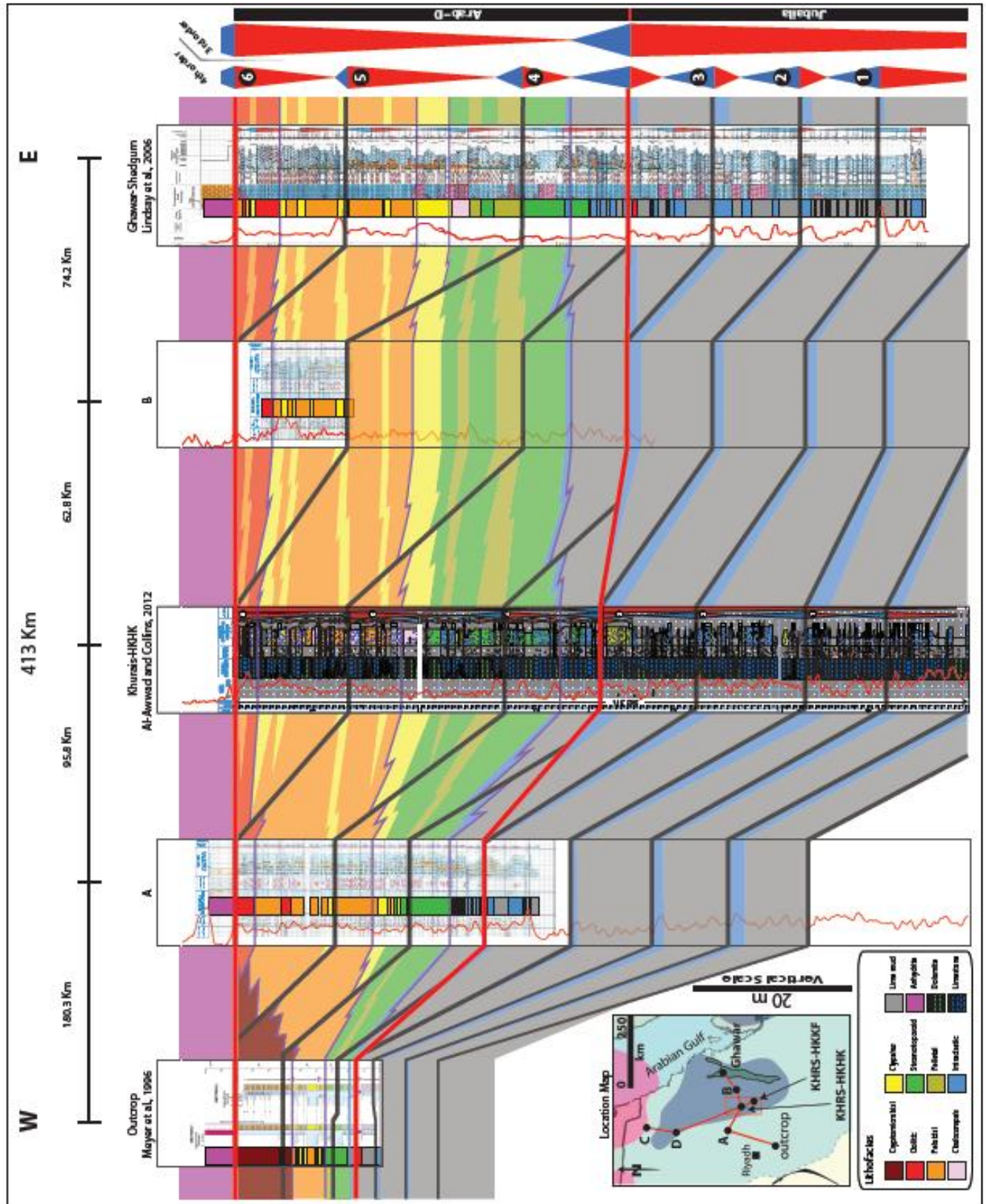


Figure 5.7:
 Hypothesised
 timelines
 superimposed on
 dip section
 presented in Figure
 5.4.
 Notes: These
 timelines are
 based on expected
 wave-energy and
 light-penetration
 variance and their
 impact on ecology
 and facies
 distribution at a
 shelf margin.

5.8 Reservoir Quality

Based on local W-E correlation of the Arab-D across Ghawar Field, Meyer and Price (1993) concluded that reservoir quality improves eastward across Ghawar in the upper part of the reservoir, and decreases in the lower part. Data presented in this study agrees with their conclusion and extrapolate it regionally (Figure 5.8). The shelfal reservoir lithofacies in HFSs 4, 5 and 6 possess better reservoir qualities in Ghawar, as compared to Khurais, based on their regional progradational thickening eastward (Figure 5.4). In the basinal part of the reservoir, the intraclastic floatstone and rudstone beds possess better porosity qualities than the lime mud beds. Regional correlation shows the intraclastic floatstone and rudstones in HFSs 1, 2 and 3 thicken from outcrop to Khurais, and then thin from Khurais to Ghawar (Figure 5.4).

A corresponding reservoir quality enhancement, followed by reduction in the same direction is expected. In addition, HFSs 1, 2 and 3 thinning from Khurais to Ghawar and the hardgrounds frequency decrease eastward suggests a decrease and possible pinch out of the turbidites, which could trap oil in the floatstones and rudstones, if the mudstones are sufficient to form permeability barriers. Vertically, in the lower part of the reservoir, the reservoir quality is predicted to improve at the HFSs scale, 3 - 6 m (10 - 20 ft), as the intraclastic rudstones and floatstones' thickness increases up each of the basinal HFSs (HFS1, 2 and 3). The above reservoir-quality improvement deductions are based on reservoir facies thickening trends and could only be true provided no significant diagenetic overprint has negatively altered the reservoir porosity and/or permeability

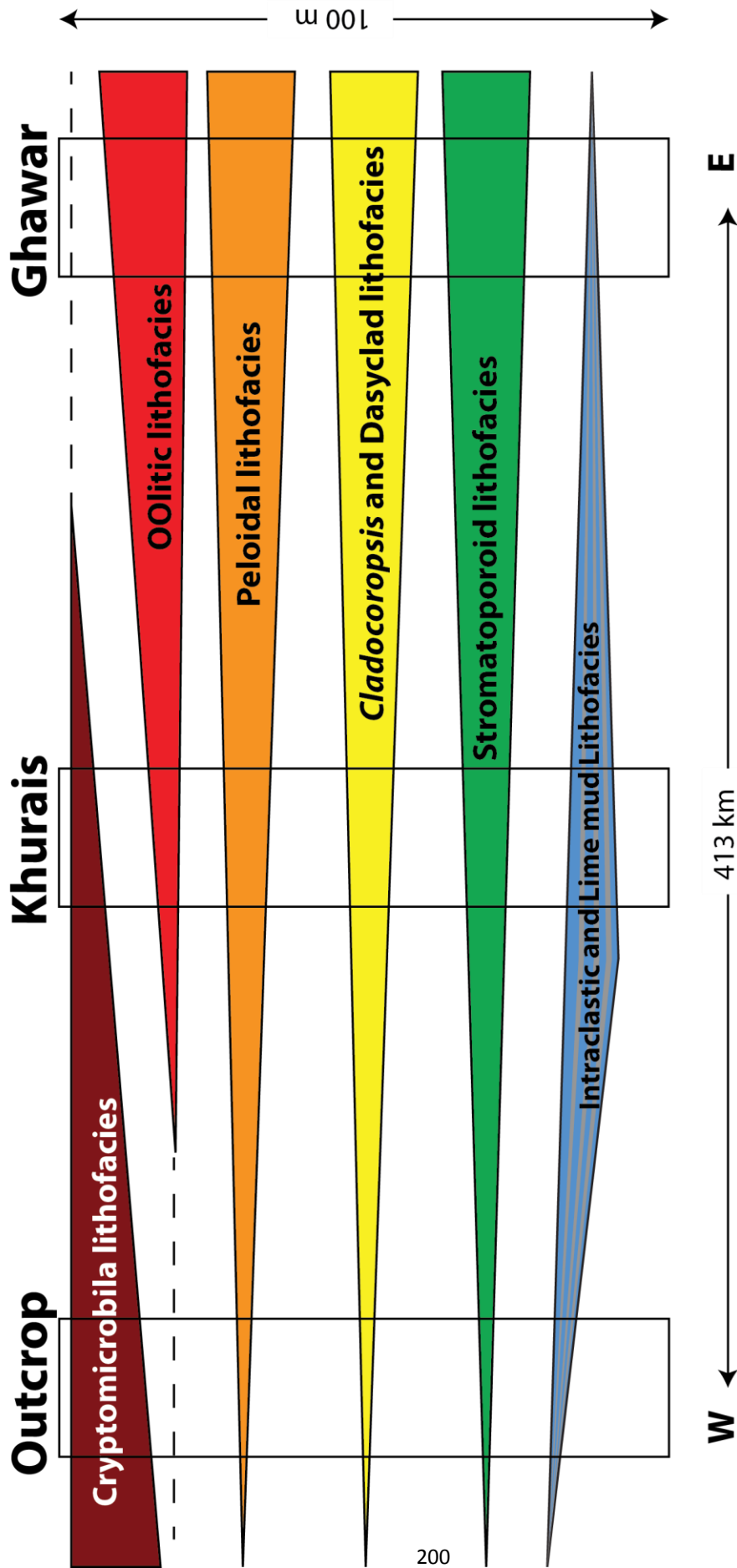


Figure 5.8: Stratigraphic thickness model.

Note: This model shows the regional thickness variance of major Arab-D reservoir lithofacies from west to east and depicts regional eastward porosity improvement in the upper part of the reservoir coupled with a porosity decrease in the lower part of the reservoir east of Khurais.

5.9 Conclusions

The preserved upward-shallowing trend of the Arab-D reservoir across Khurais Field is manifested by an eastward progradational trend. This is demonstrably supported by the 'layer-cake' stratigraphic trends preserved in the reservoir in the N-S strike section. This line of reasoning is in agreement with the notion that progradation of the Arab-D reservoir took place across the shallow Late Jurassic epeiric shelf and into the relatively deep Arabian intrashelf basin after the deposition of the Hanifa source rock, which caused the Jurassic carbonates to downlap and change to argillaceous deep-water carbonates (Alsharhan & Kendall, 1986; Leinfelder et al., 2005; Meyer & Price, 1993; M. A. Ziegler, 2001).

Data introduced in this study suggest that the outcrop, Khurais and Ghawar were all located within the Arabian intrashelf basin, where the outcrop was proximal to the intrashelf margin and Ghawar was distal to it.

The authors previously proposed model of a reef-rimmed shelf subjected to storm activity explains the thickening and downward climb of the shelfal and basinal lithofacies observed in the dip-section (Figure 5.4). Furthermore, the proposed model and correlation predicts a regional eastward porosity improvement in the upper part of the reservoir and a reduction in the lower part of the reservoir. In addition, the regional correlation model suggests a vertical reservoir-quality improvement at the scale of the HFSs in the lower part of the reservoir. These predictions assume null diagenetic effect.

5.10 Acknowledgments

We thank Aus Al-Tawil of Saudi Aramco for his unrelenting support and commitment to this study. We would like to thank Saudi Aramco for granting permission to publish this study. Our appreciation is also extended to Luis Pomar, University de les Illes Balears, Spain, for his beneficial discussions and keen insights.

5.11 References

- Aigner, T. (1985). Storm depositional systems: dynamic stratigraphy in modern and ancient shallow-marine sequences. *Lecture notes in earth sciences series Vol. 3*. Berlin, Germany: Springer Verlag.
- Al-Awwad, S. & Collins, L. B. (2013a). Arabian carbonate reservoirs: A depositional model of the Arab-D reservoir in Khurais Field, Saudi Arabia. *AAPG Bulletin*, 97(7), 1099–1119.
- Al-Awwad, S. & Collins, L. B. (in-review). Stacked high-frequency carbonate reservoir sequences in the Arab-D, Khurais Field, Saudi Arabia. *Marine and Petroleum Geology*.
- Al-Husseini, M. I. (1997). Jurassic sequence stratigraphy of the western and southern Arabian Gulf. *GeoArabia (Manama)*, 2(4), 361–382.
- Al-Husseini, M. I. (2000). Origin of the Arabian Plate structures: Amar collision and Najd Rift. *GeoArabia (Manama)*, 5(4), 527–542.
- Al-Husseini, M. I. (2009). Update to Late Triassic-Jurassic stratigraphy of Saudi Arabia for the Middle East geologic time scale. *GeoArabia (Manama)*, 14(2), 145–186.
- Al-Husseini, M. I. & Matthews, R. K. (2008). Jurassic-Cretaceous Arabian orbital stratigraphy: The AROS-JK chart. *GeoArabia (Manama)*, 13(1), 89–94.
- Al-Mulhim, W. A., Al-Ajmi, F. A., Al-Shehab, M. A. & Pham, T. R. (2010). Khureis Complex: 1, Field development required best practices, leveraged technology. *Oil & Gas Journal*, 108(7), 37–8, 40–2.
- Alsharhan, A. S. & Kendall, C. G. S. C. (1986). Precambrian to Jurassic rocks of Arabian Gulf and adjacent areas: Their facies, depositional setting, and hydrocarbon habitat. *AAPG Bulletin*, 70(8), 977–1002.
- Al-Silwadi, M. S., Kirkham, A., Simmons, M. D. & Twombly, B. N. (1996). New insights into regional correlation and sedimentology, Arab Formation (Upper Jurassic), offshore Abu Dhabi. *GeoArabia (Manama)*, 1(1), 6–27.
- Ayres, M. G., Bilal, M., Jones, R. W., Slentz, L. W., Tartir, M. & Wilson, A. O. (1982). Hydrocarbon habitat in main producing areas, Saudi Arabia. *AAPG Bulletin*,

66(1), 1–9.

- Azer, S. R. & Peebles, R. G. (1995). *Sequence stratigraphy of the Hith/Upper Arab Formations offshore Abu Dhabi, UAE*. Paper presented at the Middle East Oil Show, Bahrain.
- Blasband, B., White, S., Brooijmans, P., DE Boorder, H. & Visser, W. (2000). Late Proterozoic extensional collapse in the Arabian-Nubian Shield. *Journal of the Geological Society*, 157(3), 615–28. doi: 10.1144/jgs.157.3.615
- Brown, G. F. (1972). *Tectonic map of the Arabian Peninsula*. (US Geological Survey open-file report).
- Brown, G. F. & Jackson, R. O. (1960). The Arabian Shield. *Proceedings of the 21st International Geological Congress, Copenhagen, 9*, 69–77.
- Brown, G. F., Schmidt, D. L. & Huffman, A. C., Jr. (1989). *Geology of the Arabian Peninsula: Shield area of western Saudi Arabia* (US Geological Survey professional paper, A1–A188).
- de Matos, J. E. & Hulstrand, R. F. (1995). Regional characteristics and depositional sequences of the Oxfordian and Kimmeridgian, Abu Dhabi. In *Middle East Geosciences Conference, GEO* (Vol. 94, pp. 346–56).
- Droste, H. (1990). Depositional cycles and source rock development in an epeiric intra-platform basin: The Hanifa Formation of the Arabian Peninsula. *Sedimentary Geology*, 69(3–4), 281–96.
- Elrick, M. & Read, J. F. (1991). Cyclic ramp-to-basin carbonate deposits, Lower Mississippian, Wyoming and Montana: A combined field and computer modeling study. *Journal of Sedimentary Petrology*, 61(7), 1194–224. doi: 10.1306/d4267866-2b26-11d7-8648000102c1865d
- Énay, R. (1993). Les apports sud-tethysiens parmi les faunes jurassiques nord-ouest europeennes: Interpretation paleobiogeographique. *Comptes Rendus de l'Academie des Sciences, Serie 2, Mecanique, Physique, Chimie, Sciences de l'Univers, Sciences de la Terre*, 317(1), 115–21.
- Genna, A., Vaslet, D., Janjou, D., Le Metour, J. & Halawani, M. (2000). Rifting of the Arabian Platform during the Proterozoic-to-Phanerozoic interval. *GeoArabia (Manama)*, 5(1), 94–5.
- Golonka, J. (2002). Plate-tectonic maps of the Phanerozoic [Special Publication].

Society for Sedimentary Geology, 72, 21–75.

- Gradstein, F. M., Ogg, J. G., Smith, A. G., Agterberg, F. P., Bleeker, W., Cooper, R. A., . . . Wilson, D. (2004). A geological time scale 2004 [Miscellaneous Report]. *Geological Survey of Canada* (0068–7642).
- Handford, C. R., Cantrell, D. L. & Keith, T. H. (2002). Regional facies relationships and sequence stratigraphy of a super-giant reservoir (Arab-D member), Saudi Arabia [Program and abstracts]. *Society of Economic Paleontologists (Gulf Coast Section), Research Conference*, 22, 539–63.
- Haq, B. U. & Al-Qahtani, A. M. (2005). Phanerozoic cycles of sea-level change on the Arabian Platform. *GeoArabia (Manama)*, 10(2), 12760.
- Howland, A. F. (1979). Tectonics of the Najd transcurrent fault system, Saudi Arabia. *Journal of the Geological Society of London*, 136(4), 441–54.
- Hughes, G. W., Varol, O. & Al-Dhubeeb, A. (2004). *Biofacies and palaeoenvironments of Late Jurassic carbonates of Saudi Arabia*. Paper presented at the 32nd International Geological Congress, Italy.
- Husseini, M. I. (1988). The Arabian Infracambrian extensional system. *Tectonophysics*, 148(1–2), 93–103.
- Husseini, M. I. (1989). Tectonic and deposition model of late Precambrian-Cambrian Arabian and adjoining plates. *AAPG Bulletin*, 73(9), 1117–31.
- Husseini, M. I. & Husseini, S. I. (1990). Origin of the Infracambrian salt basins of the Middle East. *Geological Society Special Publications*, 50, 279–92.
- Ivanovich, M. & Harmon, R. S. (1992). *Uranium-series disequilibrium: Applications to earth, marine, and environmental sciences*. Oxford, Clarendon Press.
- Kinsman, D. J. J. & Park, R. K. (1976). *Algal belt and coastal sabkha evolution, Trucial Coast, Persian Gulf*. Amsterdam: Elsevier.
- Leinfelder, R. R., Schlagintweit, F., Werner, W., Ebli, O., Nose, M., Schmid, D. U. & Hughes, G. W. (2005). Significance of stromatoporoids in Jurassic reefs and carbonate platforms: Concepts and implications. *Facies*, 51(1–4), 288–326. doi: 10.1007/s10347-005-0055-8
- Le Nindre, Y.-M., Manivit, J. & Vaslet, D. (1987). *Histoire géologique de la bordure occidentale de la plate-forme arabe du Paléozoïque inférieur au Jurassique supérieur* (Unpublished doctoral dissertation). University Pierre and Marie

Curie, Paris.

- Le Nindre, Y.-M., Manivit, J. & Vaslet, D. (1990). Stratigraphie sequentielle du Jurassique et du cretace en Arabie Saoudite. *Bulletin, Societe Geologique de France, Paris, 6*, 1025–35.
- Li, Z.-X. & Powell, C. M. (2001). An outline of the palaeogeographic evolution of the Australasian region since the beginning of the Neoproterozoic. *Earth-Science Reviews, 53*(3–4), 237–77.
- Lindsay, R. F., Cantrell, D. L., Hughes, G. W., Keith, T. H., Mueller, H. W., III & Russell, D. (2006). Ghawar Arab-D reservoir: Widespread porosity in shoaling-upward carbonate cycles, Saudi Arabia. *AAPG Memoir, 88*, 97–138.
- McGuire, M. D., Koepnick, R. B., Markello, J. R., Stockton, M. L., Waite, L. E., Kompanik, G. S., . . . Al-Amoudi, M. O. (1993). *Importance of sequence stratigraphic concepts in development of reservoir architecture in Upper Jurassic grainstones, Hadriya and Hanifa Reservoirs, Saudi Arabia*. Paper presented at the Middle East Oil Show.
- Mey, J. L. (2008). *The uranium series diagenesis and the morphology of drowned Barbadian paleo-reefs* (Doctoral dissertation, no. 3312925). City University of New York, United States.
- Meyer, F. O. (2000). Carbonate sheet slump from the Jubaila Formation, Saudi Arabia: Slope implications. *GeoArabia (Manama), 5*(1), 144–5.
- Meyer, F. O. & Price, R. C. (1993). *A new Arab-D depositional model, Ghawar Field, Saudi Arabia*. Paper presented at the Middle East Oil Show, Bahrain.
- Meyer, F. O., Price, R. C., Al-Ghamdi, I. A., Al-Goba, I. M., Al-Raimi, S. M. & Cole, J. C. (1996). Sequential stratigraphy of outcropping strata equivalent to Arab-D Reservoir, Wadi Nisah, Saudi Arabia. *GeoArabia (Manama), 1*(3), 435–56.
- Mitchell, J. C., Lehmann, P. J., Cantrell, D. L., Al-Jallal, I. A. & Al-Thagafy, M. A. R. (1988). Lithofacies, diagenesis and depositional sequence: Arab-D Member, Ghawar Field, Saudi Arabia. *SEPM Core Workshop, 12*, 459–514.
- Moore, J. M., Allen, P., Wells, M. K. & Howland, A. F. (1979). Tectonics of the Najd transcurrent fault system, Saudi Arabia. *Journal of the Geological Society of London, 136, Part 4*, 441–454.
- Murris, R. J. (1980). Middle East: Stratigraphic evolution and oil habitat. *AAPG*

- Bulletin*, 64(5), 597–618.
- Pollastro, R. M., Karshbaum, A. S. & Viger, R. J. (1999). *Map showing geology, oil and gas fields, and geologic provinces of the Arabian Peninsula* (US Geological Survey open-file report). Denver, CO: US Department of the Interior.
- Powers, R. W., Ramirez, L. F., Redmond, C. D. & Elberg, E. L., Jr. (1966). *Sedimentary geology of Saudi Arabia: Geology of the Arabian Peninsula* (US Geological Survey professional paper, 150).
- Sarg, J. F. (1988). Carbonate sequence stratigraphy. In *Sea Level Changes: An Integrated Approach*. Society of Economic Paleontologists and Mineralogists Special Publication, 42, 155–81.
- Sellwood, B. W., Valdes, P. J. & Price, G. D. (2000). Geological evaluation of multiple general circulation model simulations of Late Jurassic palaeoclimate. *Palaeogeography, Palaeoclimatology, Palaeoecology*, 156(1–2), 147–60.
- Sharland, P. R., Archer, R., Casey, D. M., Davies, R. B., Hall, S. H., Heward, A.P., . . . Simmons, M. D. (2001). Arabian plate sequence stratigraphy. *GeoArabia Special Publication No. 2*. 371 p.
- Simmons, M. D. (1994). Micropalaeontological biozonation of the Khamah Group (Early Cretaceous), Central Oman Mountains. In M. D. Simmons (Ed.), *Micropalaeontology and Hydrocarbon Exploration in the Middle East*. London, UK: Chapman and Hall.
- Stampfli, G. M., Mosar, J., Favre, P., Pillecuit, A. & Vannay, J.-C. (2001). Permo-Mesozoic evolution of the western Tethys realm: The Neo-Tethys East Mediterranean Basin connection. *Memoires du Museum National d'Histoire Naturelle*, 186, 51–108.
- Stoeser, D. & Camp, V. E. (1985). Pan-African microplate accretion of the Arabian Shield. *Geological Society of America Bulletin*, 96(7), 817.
- Van Wagoner, J. C., Mitchum, R. M., Campion, K. M. & Rahmanian, V. D. (1990). Siliciclastic sequence stratigraphy in well logs, cores, and outcrops: Concepts for high-resolution correlation of time and facies. *Methods in Exploration Series*, 7, 55.
- Wender, L. E., Bryant, J. W., Dickens, M. F., Neville, A. S. & Al-Moqbel, A. M. (1998).

Pre-Khuff (Permian) hydrocarbon geology of the Ghawar area, eastern Saudi Arabia. *GeoArabia (Manama)*, 3(1), 167–8.

Wilson, A. O. (1985). *Depositional and diagenetic facies in the Jurassic Arab-C and -D reservoirs, Qatif Field, Saudi Arabia*. New York, NY: Springer-Verlag.

Ziegler, M. A. (2001). Late Permian to Holocene paleofacies evolution of the Arabian Plate and its hydrocarbon occurrences. *GeoArabia (Manama)*, 6(3), 445–504.

Conclusions

Saudi Arabia has been blessed with astounding oil resources, which, combined with its phenomenal production and exportation capacities, has led to its undisputed position in the global oil market. Oil was discovered in Saudi Arabia in the Upper Jurassic Arab Formation, the world's most prolific oil-bearing interval, in multiple giant and super-giant fields that stretch for millions of acres across the kingdom. This thesis investigated the most prolific of the Arab Formation reservoirs, the Arab-D reservoir, which was discovered in one of the biggest oil fields in the world, Khurais Field, in 1957. The thesis commenced with a comprehensive overview of the evolutionary processes responsible for the development of the reservoir's facies and their spatial stacking patterns. This was done under the broad umbrella of the Jurassic Period on the scale of Khurais Field and regionally across the Arabian platform. The thesis then proposed a reservoir's architectural depositional model and high-resolution sequence stratigraphic model, examined them in detail, and employed these models in a correlation study that characterized the reservoir's geometry, lithofacies heterogeneities and quality on a regional scale.

Detailed (10 cm-scaled) analysis of the Arab-D cores from 32 Khurais wells led to classification of the reservoir as monotonously interbedded units of intraclastic floatstone and rudstone that abruptly overlie hardground-capped skeletal wackestone and lime mudstone. These are overlain by pelletal wackestone and packstone units that pass up into stromatoporoid wackestone, packstone and floatstone units. Overlying these are *Cladocoropsis* wackestone, packstone and floatstone, dasycladacean algae wackestone and packstone, and peloidal packstone and grainstone units. Ooid grainstone units cap the succession and are in turn capped by cryptomicrobial laminites and ultimately evaporites. These lithofacies are interpreted to have been deposited in the following ascending cored environments: submarine turbidity fans shallowing up into lower shoreface pelletal silts and sands, stromatoporoid reefs, *Cladocoropsis* and *Clypeina* lagoon, peloidal and oolitic sand

sheets, supratidal stromatolites, and finally evaporitic flats and salina. The Arab-D's shallowing-upward succession reflects a prograding, shallow, epeiric, arid carbonate and evaporite-rimmed shelf, where frequent storms 'shaved' the rim, depositing turbidites.

In addition, analysis of the reservoir's lithofacies identified the majority of a third-order composite sequence representing the Arab-D Member of the Arab Formation and the upper part of another third-order composite sequence representing the upper part of the Jubaila Formation. Within these composite sequences lay six high-frequency sequences of the fourth order; superimposed on them are 12 parasequence and cycle sets. The upper composite sequence is punctuated by multiple fifth-order parasequences that represent deposition on the shallow shelf (above FWWB). From bottom to top, and based on repetitive motifs in lithofacies stacking patterns and fining versus coarsening and/or shallowing versus deepening upward trends, these parasequences can be classified into the following types: upward-coarsening reefal parasequences comprising lime mudstone, intraclastic and/or pelletal lithofacies up into stromatoporoid lithofacies; upward fining lagoonal parasequences comprising stromatoporoid up into *Cladocoropsis* and/or dasycladacean algae lithofacies; upward-coarsening sand-sheet parasequences comprising *Cladocoropsis* and/or dasycladacean algae up into the peloidal and/or oolitic lithofacies; and upward fining peritidal parasequences comprising peloidal and/or oolitic up into cryptomicrobial and anhydrites lithofacies. The lower composite sequence represents the relatively deep basinal part of the depositional system (sub-FWWB). It is punctuated by many parasequence-scale cycles, which mostly represent upward fining basinal Bouma sequences comprising the monotonously interbedded intraclastic and lime mudstone lithofacies.

Based on vertical stacking patterns and thickening trends, 12 cycle and parasequence sets were recognised and bundled into six HFS. In the basinal part of the depositional system, the cycle sets and HFSs show rhythmic upward coarsening and thickening of the intraclastic lithofacies. This reflects sea-level fluctuations bringing thicker turbidites during lowstands. In the shelf part of the depositional

system, the parasequence sets reflect both retrogradational and progradational stacking patterns that represent the transgressive and highstand systems tract of progressively shallowing HFSs that shift through the stromatoporoid, *Cladocoropsis* and dasycladacean algae, peloidal, oolitic, cryptomicrobial and anhydrite lithofacies, in ascending order.

The Arab-D reservoir's upward-shallowing trend is manifested as an eastward progradational trend regionally. Progradation of the Arab-D reservoir took place across the shallow Late Jurassic epeiric shelf and into the relatively deep Arabian intrashelf basin, causing the Jurassic carbonates to downlap and change to argillaceous deep-water carbonates. The data of this study further suggest that the Arab-D outcrop section, Khurais and Ghawar, were all located within the Arabian intrashelf basin; the outcrop section was probably close to the basin's edge and Ghawar was probably closer to the basin's centre.

The conclusions reached in this research address the long-standing, Arab-D controversy in a way that honours both the palaeontologic data and the lack of progradational trends, in a north-south direction, observed in previous studies. This study concludes that the reservoir prograded in a west-to-east direction, from the Arabian platform to the Arabian intrashelf basin. This progradation explains the different biotic components of the upper and lower parts of the reservoir as coeval temporally. Consequently, this study found that the reservoir cyclicity at the finest scale can be divided into a) shelfal shallowing-upward parasequences and b) basinal non-genetically related cycles as illustrated in figures 5 and 6.

In terms of regional reservoir-quality trends, the proposed models and correlation predict a regional eastward porosity improvement in the upper part of the reservoir and a reduction in the lower part of the reservoir. In addition, the models and correlation suggest a vertical reservoir-quality improvement at the scale of the HFSs in the lower part of the reservoir. This conclusion is of utmost importance and has profound applicability that could guide and impact future exploration activities in the region.

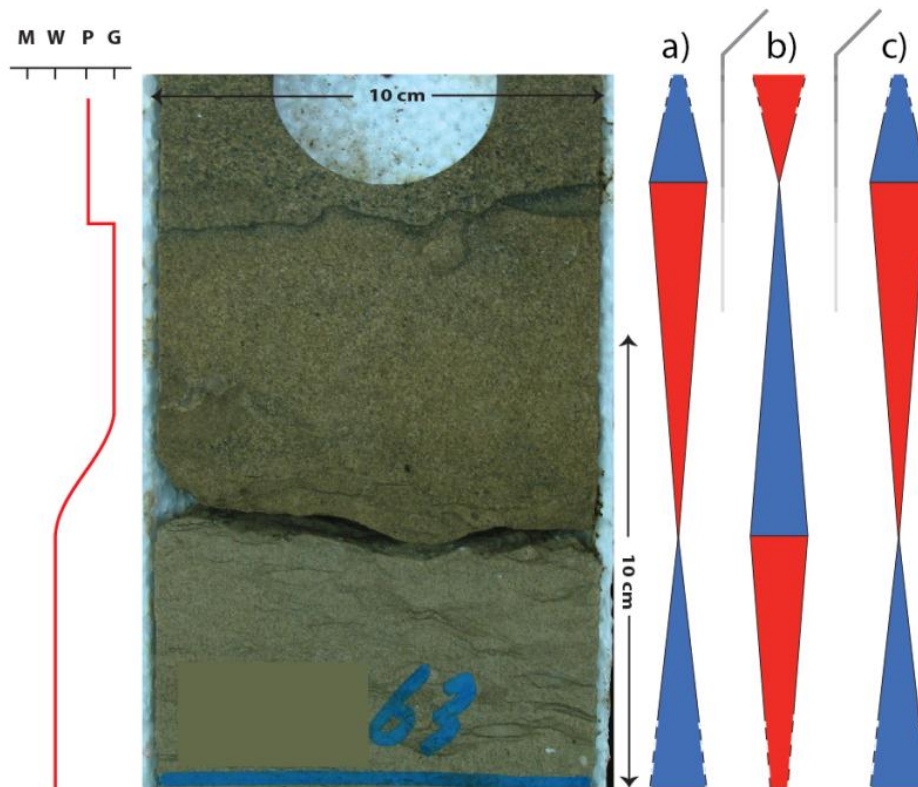


Figure 5: A typical coarsening-upward cycle from the upper part of the reservoir.
a) The cyclicity interpretation adopted by a hypothesized progradational scenario in an open shelf. b) The cyclicity interpretation adopted by a hypothesized aggradational scenario in a silled platform. c) The cyclicity interpretation concluded in this study, which interprets the cycles in the upper part of the reservoir to reflect upward shallowing with repetitive motifs of progressive appearance of shallower over deeper lithofacies.

Finally, distributing the reservoir facies into high-resolution sequence stratigraphic framework, which was achieved in this research, paves the way for future integration with diagenetic characterization of the classified and mapped facies, calibration of porosity and permeability values and incorporation of structural elements in the region. The potential of such integration could profoundly improve the management and production of Khurais Field, and other fields in the region.

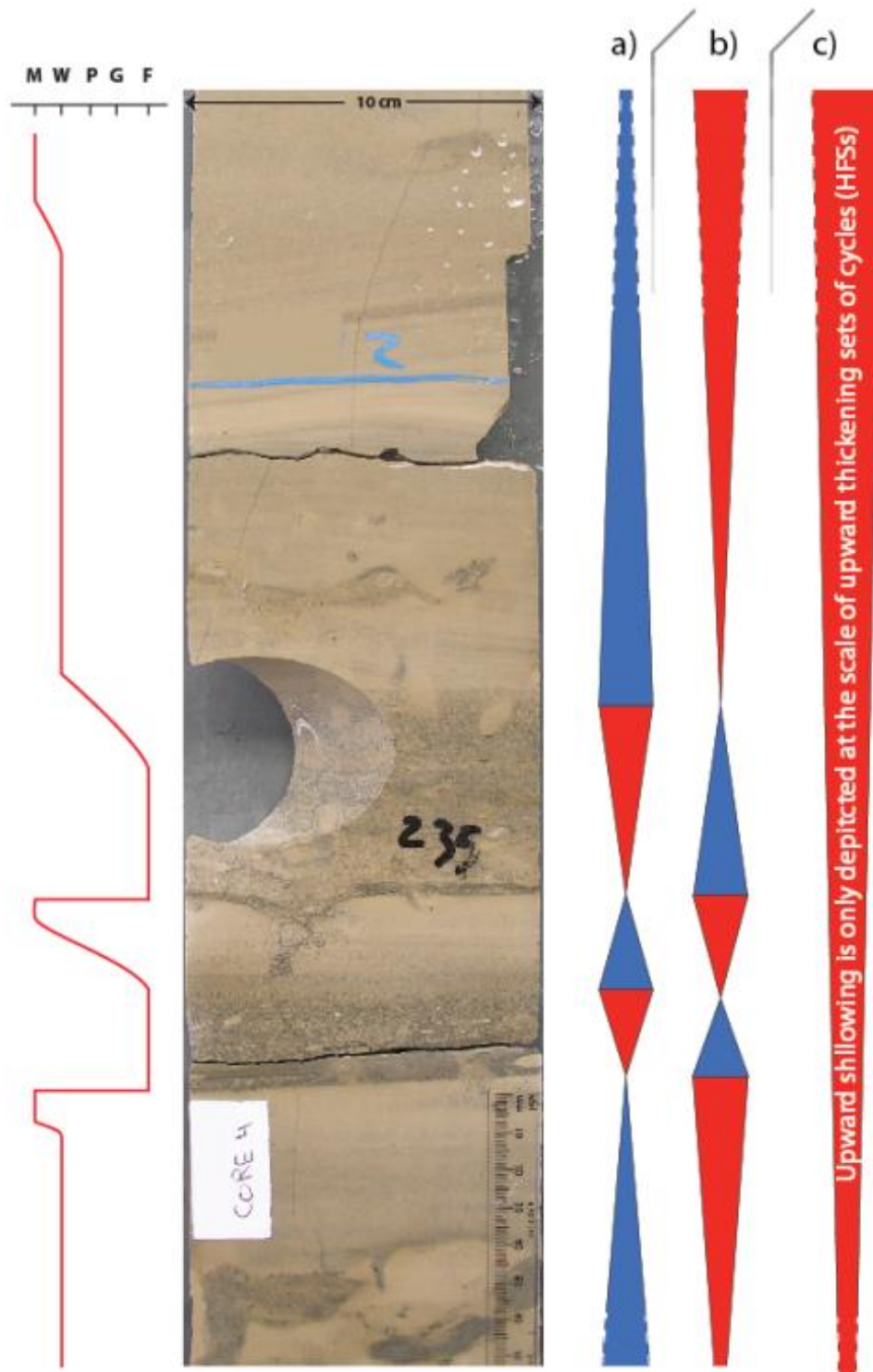


Figure 1: Typical fining-upward cycles from the lower part of the reservoir.
a) The cyclicity interpretation adopted by a hypothesized progradational scenario in an open shelf. b) The cyclicity interpretation adopted by a hypothesized aggradational scenario in a silled platform. c) The cyclicity interpretation concluded in this study, which interprets the cycles in the lower part of the reservoir as non-genetically related Bouma sequences and depicts sea-level fluctuations only at the scale of thickening upward packages of cycles (HFSs).

Bibliography

- Abdel-Rahman, A. M. (1995). Tectonic-magmatic stages of shield evolution: The Pan-African belt in northeastern Egypt. *Tectonophysics*, 242(3–4), 223–40. doi: [http://dx.doi.org/10.1016/0040-1951\(94\)00171-5](http://dx.doi.org/10.1016/0040-1951(94)00171-5)
- Abdelsalam, M. G. & Dawoud, A. S. (1991). The Kabus ophiolitic melange, Sudan, and its bearing on the western boundary of the Nubian Shield. *Journal of the Geological Society*, 148(1), 83–92. doi: <http://dx.doi.org/10.1144/gsjgs.148.1.0083>
- Abu-Ali, M. A., Al-Shamsi, A. S., Bin-Afif, T. A. & Grover, G. A. (1996). Characterization of the upper Arab-D reservoir, Abqaiq Field, Saudi Arabia. *GeoArabia (Manama)*, 1(1), 97.
- Acharyya, S. K. (2000). Break up of Australia–India–Madagascar block, opening of the Indian Ocean and Continental accretion in Southeast Asia with special reference to the characteristics of the peri-Indian collision zones. *Gondwana Research*, 3(4), 425–443. doi: [http://dx.doi.org/10.1016/S1342-937X\(05\)70753-X](http://dx.doi.org/10.1016/S1342-937X(05)70753-X)
- Aigner, T. (1985). Storm depositional systems: dynamic stratigraphy in modern and ancient shallow-marine sequences. *Lecture Notes in Earth Sciences Series Vol.3*. Berlin, Germany: Springer Verlag.
- Al-Afalge, N. I., Al-Garni, S., Rahmeh, B. & Al-Towailib, A. (2002). *Successful integration of sparsely distributed core and welltest derived permeability data in a viable model of a giant carbonate reservoir*. Paper presented at the SPE Annual Technical Conference and Exhibition, San Antonio, Texas.
- Al-Awwad, S., Al Temimi, K., Smith, L. B., Hughes, G. W. & Read, J. F. (2008). Comparative sequence development of Arab-D reservoir from three fields, Saudi Arabia. [Annual meeting abstracts]. *American Association of Petroleum Geologists*.
- Al-Awwad, S. & Collins, L. B. (2013a). Arabian carbonate reservoirs: A depositional model of the Arab-D reservoir in Khurais Field, Saudi Arabia. *AAPG Bulletin*,

97(7), 1099–1119.

Al-Awwad, S. & Collins, L. B. (in-review). Stacked high-frequency carbonate reservoir sequences in the Arab-D, Khurais Field, Saudi Arabia. *Marine and Petroleum Geology*.

Al-Awwad, S. & Collins, L. B. (2013b). Carbonate platform scale correlation of stacked high frequency sequences in the Arab-D Reservoir, Saudi Arabia. *Sedimentary Geology*, 294, 205–2018.

Al-Awwad, S., Al-Tawil, A., Read, F., Al-Temimi, K., Mousa, Y. & Smith, L. (2009). Carbonate/evaporite sequence stratigraphy of the subsurface late Jurassic Arab-D Formation from three fields, Saudi Arabia. [Annual meeting abstracts]. *American Association of Petroleum Geologists*.

Al-Dhubbeeb, A. G. (2003). Late Jurassic Foraminifera and their palaeoenvironmental significance in the Arab-D Reservoir of the Ghawar Oilfield. *Palynology*, 27, 252.

Al-Ghamdi, A., Tello, R., Al-Bain, F. & Swadi, M. (2008). *Collaboration breeds success in the Khurais Mega-Project in Saudi Arabia*. Paper presented at the 2008 SPE Saudi Arabia Section Technical Symposium on the Ultimate Challenge: Unlocking Hydrocarbons through Optimum Exploitation Strategies, Al Khobar, Saudi Arabia.

Al-Goba, I. & Kamal, R. (2000). A new technique to predictively map occurrences of abnormally high permeabilities in the Arab-D Reservoir, Ghawar Field, Saudi Arabia. *GeoArabia (Manama)*, 5(1), 22.

Al-Husseini, M. I. (1997). Jurassic sequence stratigraphy of the western and southern Arabian Gulf. *GeoArabia (Manama)*, 2(4), 361–82.

Al-Husseini, M. I. (2000). Origin of the Arabian Plate structures: Amar collision and Najd Rift. *GeoArabia (Manama)*, 5(4), 527–42.

Al-Husseini, M. I. (2007). Stratigraphic note: Revised ages (Ma) and accuracy of Arabian Plate maximum flooding surfaces. *GeoArabia*, 12 (4), 167–70.

Al-Husseini, M. I. (2009). Update to Late Triassic-Jurassic stratigraphy of Saudi Arabia for the Middle East geologic time scale. *GeoArabia (Manama)*, 14(2), 145–186.

Al-Husseini, M. I. & Matthews, R. K. (2005a). Arabian orbital stratigraphy: Periodic

- second-order sequence boundaries? *GeoArabia (Manama)*, 10(2), 165–8.
- Al-Husseini, M. I. & Matthews, R. K. (2005b). Stratigraphic note: Orbital-forcing calibration of the Late Cretaceous and Paleocene Aruma Formation, Saudi Arabia. *GeoArabia (Manama)*, 10(3), 173–6.
- Al-Husseini, M. I. & Matthews, R. K. (2006). Orbital calibration of the Arabian Jurassic second-order sequence stratigraphy. *GeoArabia (Manama)*, 11(3), 161–70.
- Al-Husseini, M. I. & Matthews, R. K. (2008). Jurassic-Cretaceous Arabian orbital stratigraphy: The AROS-JK chart. *GeoArabia (Manama)*, 13(1), 89–94.
- Al-Husseini, M. I., Matthews, R. K. & Mattner, J. (2006). Stratigraphic note: Orbital forcing calibration of the Late Jurassic (Oxfordian–early Kimmeridgian) Hanifa Formation, Saudi Arabia. *GeoArabia (Manama)*, 11(1), 145–9.
- Al-Mansoori, A., Strohmenger, C. J., El-Agrab, A. F., Khouri, A. A. & Al-Aiderous, A. (2008). *Sequence stratigraphy and sedimentology of the Upper Jurassic Arab and Hith Formations with emphasis on anhydrite deposits, Abu Dhabi and United Arab Emirates*. Paper presented at the Eighth Middle East Geoscience Conference and Exhibition.
- Al-Mulhim, W. A., Al-Ajmi, F. A., Al-Shehab, M. A. & Pham, T. R. (2010). Khureis Complex: 1, Field development required best practices, leveraged technology. *Oil & Gas Journal*, 108(7), 37–8, 40–2.
- Al-Mulhim, W. A., Hussain A. F., Al-Shehab, M. A. & Al-Shamrani, S. S. (2010). Mega I-Field application in the world's Largest Oil Increment Development. Paper presented at the SPE Intelligent Energy Conference and Exhibition, Utrecht, The Netherlands.
- Al-Saad, H. & Ibrahim, M. I. A. (2005). Facies and palynofacies characteristics of the Upper Jurassic Arab D reservoir in Qatar. *Revue de Paleobiologie*, 24(1), 255–241.
- Al-Saad, H. & Sadooni, F. (2001). A new depositional model and sequence stratigraphic interpretation for the Upper Jurassic Arab 'D' Reservoir in Qatar. *Journal of Petroleum Geology*, 24(3), 243–64.
- Alsharhan, A. S. (1989). Petroleum geology of the United Arab Emirates. *Journal of Petroleum Geology*, 12(3), 253–288.

- Alsharhan, A. S. (1993). *The Jurassic of the Arabian Gulf basin: Their facies, depositional setting and hydrocarbon habitat*. Paper presented at the Carboniferous to Jurassic Pangea First International Symposium, Calgary, Canada.
- Alsharhan, A. S. & Kendall, C. G. S. C. (1986). Precambrian to Jurassic rocks of Arabian Gulf and adjacent areas: Their facies, depositional setting, and hydrocarbon habitat. *AAPG Bulletin*, 70(8), 977–1002.
- Alsharhan, A. S. & Kendall, C. G. S. C. (1994). Depositional setting of the Upper Jurassic Hith Anhydrite of the Arabian Gulf: An analog to Holocene evaporites of the United Arab Emirates and Lake MacLeod of Western Australia. *AAPG Bulletin*, 78(7), 1075–1096.
- Alsharhan, A. S. & Kendall, C. G. S. C. (2003). Holocene coastal carbonates and evaporites of the southern Arabian Gulf and their ancient analogues. *Earth-Science Reviews*, 61(3), 191–243.
- Alsharhan, A. S. & Magara, K. (1994). The Jurassic of the Arabian Gulf basin: Facies, depositional setting and hydrocarbon habitat. *Memoir—Canadian Society of Petroleum Geologists*, 17, 397–412.
- Alsharhan, A. S. & Magara, K. (1995). Nature and distribution of porosity and permeability in Jurassic carbonate reservoirs of the Arabian Gulf basin. *Facies*, 32(1), 237–54.
- Alsharhan, A. S., & Nairn, A. E. M. (1993). Geology and hydrocarbon habitat in the Arabian Basin: the Mesozoic of the State of Qatar. *Geologie en Mijnbouw*, 72, 265-265.
- Alsharhan, A. S. & Sadooni, F. N. (2003). Eustatic overprints on the diagenetic evolution of Mesozoic platform carbonates from the Arabian Plate. [Annual meeting expanded abstracts]. *American Association of Petroleum Geologists*, 12, 5.
- Alsharhan, A. S. & Scott, R. W. (2000). Hydrocarbon potential of Mesozoic carbonate platform-basin systems, UAE [Special publication]. *Society of Sedimentary Geology* 69, 335–58.
- Alsharhan, A. S., & Whittle, G. L. (1995). Chronostratigraphy and hydrocarbon habitat associated with the Jurassic carbonates of Abu Dhabi, United Arab

- Emirates. AAPG Bulletin, 79(CONF-950995--).
- Alsharhan, A. S., Whittle, G. L., Clerke, E. A. & Buiting, J. J. (1995). Carbonate-evaporite sequences of the Late Jurassic, southern and southwestern Arabian Gulf: Multiple discrete pore systems in Arab D limestone. *AAPG Bulletin*, 79(11), 1608–30.
- Al-Siddiqi, A. & Dawe, R. (1999). Qatar's oil and gasfields: A review. *Journal of Petroleum Geology*, 22(4), 417–36.
- Al-Silwadi, M. S., Kirkham, A., Simmons, M. D. & Twombly, B. N. (1996). New insights into regional correlation and sedimentology, Arab Formation (Upper Jurassic), offshore Abu Dhabi. *GeoArabia (Manama)*, 1(1), 6–27.
- Al-Suwaidi, A. & Aziz, S. (1998). *Regional basin modelling: An approach to understand sheifal carbonate reservoirs of the Oxfordian and Kimmeridgian in offshore Abu Dhabi*. Paper presented at the Abu Dhabi International Petroleum Exhibition and Conference, Abu Dhabi, United Arab Emirates.
- Anderson, L., Abbott, M. B. & Finney, B. P. (2001). Holocene climate inferred from oxygen isotope ratios in lake sediments, central Brooks Range, Alaska. *Quaternary Research*, 55(3), 313–21.
- Anderson, T., Popp, B., Williams, A., Ho, L. Z. & Hudson, J. (1994). The stable isotopic records of fossils from the Peterborough Member, Oxford Clay Formation (Jurassic), UK: Palaeoenvironmental implications. *Journal of the Geological Society*, 151(1), 125–38.
- Anthes, R. A. (1982). Tropical cyclones, their evolution, structure and effects. *Meteorological Monographs*, 19.
- Arkell, W. J. (1952). Jurassic ammonites from Jebel Tuwaiq, central Arabia. *Philosophical Transactions of the Royal Society of London, Series B: Biological Sciences*, 236(633), 241–313.
- Ayres, M. G., Bilal, M., Jones, R. W., Slentz, L. W., Tartir, M. & Wilson, A. O. (1982). Hydrocarbon habitat in main producing areas, Saudi Arabia. *AAPG Bulletin*, 66(1), 1–9.
- Azer, S. R. (1989). *Preliminary investigations into possible stratigraphic traps, offshore Abu Dhabi*. Paper presented at the Middle East Oil Show, Bahrain.
- Azer, S. R. & Peebles, R. G. (1995). *Sequence stratigraphy of the Hith/Upper Arab*

- Formations offshore Abu Dhabi, UAE*. Paper presented at the Middle East Oil Show, Bahrain.
- Badenas, B. & Aurell, M. (2001). Proximal-distal facies relationships and sedimentary processes in a storm dominated carbonate ramp (Kimmeridgian, northwest of the Iberian Ranges, Spain). *Sedimentary Geology*, 139(3–4), 319–40.
- Banner, F. T., Finch, E. M. & Simmons, M. D. (1990). On Lithocodium Elliott (calcareous algae): its palaeobiological and stratigraphical significance. *Journal of Micropalaeontology*, 9(1), 21–35.
- Barger, T. C. (1984, May/June). Birth of a dream. *Saudi Aramco World*, 35, 34–41.
- Barger, T. C. (2000). *Out in the blue: Letters from Arabia 1937 to 1940*. Vista, CA: Selwa Press.
- Barker, C. & Dickey, P. A. (1984). Hydrocarbon habitat in main producing areas, Saudi Arabia: Discussion. *AAPG Bulletin*, 68(1), 108–9.
- Barnard, P. D. W. (1973). Mesozoic floras. In N. F. Hughes (Ed.), *Organsims and Continents Through Time* (Vol. 12, pp. 175–188). London, UK: Paleontological Society of London.
- Barron, E. J., Hay, W. W. & Thompson, S. (1989). The hydrologic cycle: A major variable during Earth history. *Global and Planetary Change*, 1(3), 157–74.
- Bates, B. S. (1973). Oscar for an oilfield. *Saudi Aramco World*, 24(6), 14–15.
- Benninghoff, W. S. (1992). Earth Science: Jurassic and Cretaceous floras and climates of the Earth by V. A. Vakhrameev, J. V. Litinov (Trans.) and N. F. Hughes (Ed.). *Choice*, 30(1), 155.
- Berger, W. H. & Crowell, J. C. (1982). *Climate in Earth history*. [Final report]. Presented at the American Geophysical Union, Toronto.
- Berner, R. (1990). Atmospheric carbon dioxide levels over Phanerozoic time. *Science*, 249(4975), 1382–6.
- Beydoun, Z. R. (1988). *The Middle East: Regional Geology and Petroleum Resources*. Scientific Press, Beaconfield, UK.
- Beydoun, Z. R. (1991). Arabian Plate hydrocarbon geology and potential: A plate tectonic approach. *AAPG Studies in Geology*, 33, 77.
- Beydoun, Z. R. (1991). Middle East hydrocarbon reserves enhancement, 1975–1990:

- Significant developments and implications for potential future large increases. *Journal of Petroleum Geology*, 14(1), ii–iv.
- Beydoun, Z. R. (1991). The Red Sea/Gulf of Aden hydrocarbon potential reassessment. *AAPG Bulletin*, 75(8), 1406.
- Bierhals, E., Preiss, A., Ziegler-Schmidt, A. & Pilgrim, B. (2001). Leitfaden Landschaftsplan: Landschaftsplan fuer eine lebenswerte Gemeinde. *Informationsdienst Naturschutz Niedersachsen*, 21(2), 71–120.
- Billo, S. M. (1989). Petroleum production in Saudi Arabia. [Conference]. *AAPG Bulletin*, 73(9), 1142.
- Bishop, R. S. & Jones, T. W. (1995). The maturation history of the Paleozoic hydrocarbon system of the Arabian Platform. *AAPG Bulletin*, 79(8), 1198.
- Blanchon, P., Jones, B. & Kalbfleisch, W. (1997). Anatomy of a fringing reef around Grand Cayman: Storm rubble, not coral framework. *Journal of Sedimentary Research*, 67(1), 1–16. doi: 10.1306/d42684d7-2b26-11d7-8648000102c1865d
- Blasband, B. (2009). Neoproterozoic tectonics of the Arabian-Nubian Shield. [Abstracts]. *Israel Geological Society, Annual Meeting*, 33.
- Blasband, B., White, S., Brooijmans, P., DE Boorder, H. & Visser, W. (2000). Late Proterozoic extensional collapse in the Arabian-Nubian Shield. *Journal of the Geological Society*, 157(3), 615–28. doi: 10.1144/jgs.157.3.615
- Bodenbender, B. E., Wilson, M. A. & Palmer, T. J. (1989). Paleoecology of Sphenothallus on an Upper Ordovician hardground. *Lethaia*, 22(2), 217–25. doi: 10.1111/j.1502-3931.1989.tb01685.x
- Boss, S. K & Rasmussen, K. A. (1995). Misuse of Fischer plots as sea-level curves. *Geology*, 23(3), 221–4. doi: 10.1130/0091-7613(1995)023<0221:mofpas>2.3.co;2
- Boulila, S., Galbrun, B., Miller, K. G., Pekar, S. F., Browning, J. V., Laskar, J. & Wright, J. D. (2011). On the origin of Cenozoic and Mesozoic ‘third-order’ eustatic sequences. *Earth-Science Reviews*, 109(3–4), 94–112. doi: 10.1016/j.earscirev.2011.09.003
- Bouma, A. H. (1962). *Sedimentology of some Flysch deposits: A graphic approach to facies interpretation*. Amsterdam: Elsevier.

- Bourdon, B. (Ed.). (2003). *Uranium-series geochemistry* (Vol. 52). Mineralogical Society of America.
- Bouroulllec, J., & Meyer, A. (1995). Sedimentological and diagenetic model of the Arab Formation (Qatar): Reservoir implications. *The Middle East Petroleum Geosciences*, 1, 236-246.
- Bramkamp, R. A. & Powers, R. W. (1958). Classification of Arabian carbonate rocks. *Geological Society of America Bulletin*, 69(10), 1305–18. doi: 10.1130/0016-7606(1958)69[1305:coacr]2.0.co;2
- Bramkamp, R. A. & Steineke, M. (1952). *Stratigraphical introduction*. Paper presented at the Royal Society of London Philosophical Transactions.
- Brasier, M., Anderson, M. & Corfield, R. (1992). Oxygen and carbon isotope stratigraphy of early Cambrian carbonates in southeastern Newfoundland and England. *Geological Magazine*, 129(3), 265–79.
- Brown, G. F. (1972). *Tectonic map of the Arabian Peninsula*. (US Geological Survey open-file report).
- Brown, G. F. & Jackson, R. O. (1960). The Arabian Shield. *Proceedings of the 21st International Geological Congress, Copenhagen, 9*, 69–77.
- Brown, G. F., Schmidt, D. L. & Huffman, A. C., Jr. (1989). *Geology of the Arabian Peninsula: Shield area of western Saudi Arabia* (US Geological Survey professional paper, A1–A188).
- Budyko, M. I., Ronov, A. B., & Ianshin, A. L. (1985). The history of the atmosphere. *Leningrad Gidrometeoizdat*, 1.
- Cantrell, D., Swart, P. & Hagerty, R. (2004). Genesis and characterization of dolomite, Arab-D Reservoir, Ghawar Field, Saudi Arabia. *GeoArabia (Manama)*, 9(2), 11–36.
- Cantrell, D., Swart, P., Westphal, H., Handford, C. R. & Kendall, C. G. S. C. (2000). Origin of dolomite from the Ghawar Field, Saudi Arabia. *GeoArabia (Manama)*, 5(1), 65–6.
- Cantrell, D. L. (2006). Cortical fabrics of Upper Jurassic ooids, Arab Formation, Saudi Arabia: Implications for original carbonate mineralogy. *Sedimentary Geology*, 186(3–4), 157–70.
- Cantrell, D. L., Alsharhan, A. S., Kendall, C. G. S. C. & Al-Suwaidi, A. S. (2008).

- Significance of dolomite in a large evaporite-carbonate cycle: Arab-D Reservoir, Saudi Arabia. *GeoArabia (Manama)*, 13(2), 147.
- Cantrell, D. L. & Swart, P. K. (2004). Enhanced porosity development in the Arab-D as a result of alteration by hydrothermal fluids. [Annual meeting expanded abstracts]. *American Association of Petroleum Geologists*, 13, 21.
- Cantrell, D. L., Swart, P. K., Handford, C. R., Kendall, C. G. & Westphal, H. (2001). Geology and production significance of dolomite, Arab-D Reservoir, Ghawar Field, Saudi Arabia. *GeoArabia (Manama)*, 6(1), 45–60.
- Cavazza, W., Roure, F., Spakman, W., Stampfli, G. M. & Ziegler, P. A. (2004). The TRANSMED Atlas: Geological-geophysical fabric of the Mediterranean region. *Episodes*, 27(4), 244–54.
- Charig, A. J. (1973). Kurten's theory of ordinal variety and the number of continents. In D. H. Tarlin & a. R. S. K. (Eds.), *Implication of continental drift to the earth sciences* (Vol. 1, pp. 229–46). London, UK: Academic Press.
- Choquette, P. W., & Pray, L. C. (1970). Geologic nomenclature and classification of porosity in sedimentary carbonates. *AAPG bulletin*, 54(2), 207-244.
- Christian, L. (1997). Cretaceous subsurface geology of the Middle East region. *GeoArabia*, 2(3), 239.
- Christie-Blick, N. (1982). Pre-Pleistocene glaciation on Earth: Implications for climatic history of Mars. *Icarus*, 50(2), 423–43.
- Christie-Blick, N., Grotzinger, J. P. & Von der Borch, C. (1988). Sequence stratigraphy in Proterozoic successions. *Geology*, 16(2), 100–4.
- Church, M., Coniglio, M., Hardie, L. A. & Longstaffe, F. J. (2003). Encyclopedia of Sediments & Sedimentary Rocks. In G. V. Middleton (Ed.), *Encyclopedia of Earth Sciences Series* (1st ed.), p. 928 . Dordrcchi, Netherlands: Springer.
- Clerke, E. A. (2007). The Rosetta Stone Project: II, Spectral analysis of the pore geometries and their relationships to reservoir properties for the Arab D limestones. *GeoArabia (Manama)*, 12(1), 157.
- Clerke, E. A. (2009). Permeability, relative permeability, microscopic displacement efficiency, and pore geometry of M_1 bimodal pore systems in Arab D Limestone. *SPE Journal*, 14(3), 524–31.
- Clerke, E. A. (2004). Beyond porosity-permeability relationships: Determining pore

- network parameters for the Ghawar Arab-D using the Thomeer method. *GeoArabia (Manama)*, 9(1), 55.
- Clerke, E. A. & Buiting, J. J. (2008). Multiple discrete pore systems in Arab D limestone. [Annual meeting abstracts]. *American Association of Petroleum Geologists*.
- Clerke, E. A. & Mueller, H. W. (2007). The Rosetta Stone Project: I, Spectral analysis of pore geometries and their relationships to depositional facies for the Arab D limestones. *GeoArabia (Manama)*, 12(1), 157.
- Colbert, E. H. (1964). Climatic zonation and terrestrial faunas. In A. E. M. Narin (Ed.), *Problem of palaeoclimatology* (pp. 617–37). New York: Wiley.
- Cole, G. A., Carrigan, W. J., Colling, E. L., Halpern, H. I., Alkhadrawi, M. R. & Jones, P. J. (1993, August 1). *Jurassic source rocks and their associated oil distribution in the Eastern Province of Saudi Arabia*. Paper presented at the Carboniferous to Jurassic Pangea First International Symposium, Calgary, Canada.
- Cole, J. C. & Hedge, C. E. (1986). *Geochronologic investigation of late Proterozoic rocks in the northeastern shield of Saudi Arabia* (p. 42): Saudi Arabian Deputy Ministry for Mineral Resources Technical Record USGS-TR-.
- Collins, L. B. (1988). Sediments and history of the Rottneest Shelf, Southwest Australia: A swell-dominated, non-tropical carbonate margin. *Sedimentary Geology*, 60(1–4), 15–49.
- Corbett, P. W. M., Jensen, J. L., Cantrell, D. L., Alsharhan, A. S., Kendall, C. G. S. C. & Al-Suwaidi, A. S. (2000). Lithological and zonal porosity-permeability distributions in the Arab-D Reservoir, Uthmaniyah Field, Saudi Arabia: Discussion. *AAPG bulletin*, 84(9), 1365-1367.
- Creber, G. & Chaloner, W. G. (1984). Influence of environmental factors on the wood structure of living and fossil trees. *The Botanical Review*, 50(4), 357–448.
- Crowell, J. C. & Frakes, L. A. (1970). Phanerozoic glaciation and the causes of ice ages. *American Journal of Science*, 268(3), 193–224.
- Crowell, J. C. & Frakes, L. A. (1971). Late Paleozoic glaciation: Part IV, Australia. *Geological Society of America Bulletin*, 82(9), 2515–40.

- Crowley, T. J., & North, G. R. (1991). *Paleoclimatology* (Vol. 57). Oxford University Press, NY, United States. 339 p.
- Davis, R., Fontanilla, J., Biswas, P. & Saha, S. (1997, March). *Lithology, lithofacies, and permeability estimation in Ghawar Arab-D reservoir*. Paper presented at the Middle East Oil Show and Conference.
- Davies, G. R. & Smith, L. B. (2006). Structurally controlled hydrothermal dolomite reservoir facies: An overview. *AAPG Bulletin*, 90(11), 1641–90.
- De Castro, P. (1990). Thaumatoporella: conoscenze attuali e approccio all'interpretazione. *Bollettino della Societa Paleontologica Italiana*, 29(2), 179–206.
- de Matos, J. E. (1977). *Stratigraphy, sedimentation and oil potential of the Lower Jurassic to Kimmeridgian of United Arab Emirates: Outcrop and subsurface compared*. (Unpublished doctoral dissertation). University of Aberdeen, Scotland.
- de Matos, J. E. (1994). Upper Jurassic-Lower Cretaceous stratigraphy: The Arab, Hith and Rayda Formations in Abu Dhabi. London, UK: Chapman and Hall.
- de Matos, J. E. & Hulstrand, R. F. (1995). Regional characteristics and depositional sequences of the Oxfordian and Kimmeridgian, Abu Dhabi. In *Middle East Geosciences Conference, GEO* (Vol. 94, pp. 346–56).
- de Matos, J. E. & Walkden, G. M. (2000). Stratigraphy and sedimentation of the Middle Jurassic [UAE Special Publication]. *Society for Sedimentary Geology*, 69, 21–35.
- Dercourt, J., Cotiereau, N. & Vrielynck, B. (1993, April 25–28). *Reconstruction of Tethys from Permian to Recent: Implications for sedimentary facies distribution and oceanic circulation* [Annual meeting expanded abstracts]. American Association of Petroleum Geologists Annual Convention, New Orleans, 91.
- Dezes, P. (1999). Tectonic and metamorphic evolution of the central Himalayan domain in Southeast Zaskar (Kashmir, India). *Memoires de Geologie Lausanne*, 32, 152.
- Dickson, J. A. D. (1966). Carbonate identification and genesis as revealed by staining. *Journal of Sedimentary Research*, 36(2), 491-505.

- Diecchio, R. J., Boss, S. K. & Rasmussen, K. A. (1995). Misuse of Fischer plots as sea-level curves: Discussion and reply. *Geology (Boulder)*, 23(11), 1049–50. doi: 10.1130/0091-7613(1995)023<1049:mofpas>2.3.co;2
- Douglas, J. L. (1996). Geostatistical model for the Arab-D Reservoir, North 'Ain Dar Pilot, Ghawar Field, Saudi Arabia: An improved reservoir simulation model. *GeoArabia (Manama)*, 1(2), 267–84.
- Dromart, G., Garcia, J. P., Picard, S., Atrops, F., Lecuyer, C. & Sheppard, S. M. F. (2003). Ice age at the Middle-Late Jurassic transition? *Earth and Planetary Science Letters*, 213(3–4), 205–20. doi: 10.1016/s0012-821x(03)00287-5
- Droste, H. (1990). Depositional cycles and source rock development in an epeiric intra-platform basin: The Hanifa Formation of the Arabian Peninsula. *Sedimentary Geology*, 69(3–4), 281–96.
- Droste, H. (2010). High-resolution seismic stratigraphy of the Shu'aiba and Natih Formations in the Sultanate of Oman: Implications for Cretaceous epeiric carbonate platform systems. In F. S. P. Van Buchem, K. D. Gerdes & M. Esteban (Eds.), *Mesozoic and Cenozoic carbonate systems of the Mediterranean and the Middle East: Stratigraphic and diagenetic reference models*. Geological Society, London, Special Publications, 239, 145–62. doi: 10.1144/sp329.7
- Dunham, R. J. (1962). Classification of carbonate rocks according to depositional texture. *Memoir–American Association of Petroleum Geologists*, 108–21.
- Dunham, R. J. (1970). Stratigraphic reefs versus ecologic reefs. *Bulletin of the American Association of Petroleum Geologists*, 54(10), 1931.
- Durham, L. S. (2005). Saudi Arabia's Ghawar Field: The elephant of all elephants. *AAPG Explorer*, 26(1), 4–7.
- Edgell, H. S. (1996). Salt tectonism in the Persian Gulf Basin. *Geological Society Special Publications*, 100, 129–51.
- Ehrenberg, S., Nadeau, P. & Aqrabi, A. (2007). A comparison of Khuff and Arab reservoir potential throughout the Middle East. *AAPG Bulletin*, 91(3), 275–86.
- Elrick, M. & Read, J. F. (1991). Cyclic ramp-to-basin carbonate deposits, Lower Mississippian, Wyoming and Montana: A combined field and computer

- modeling study. *Journal of Sedimentary Petrology*, 61(7), 1194–224. doi: 10.1306/d4267866-2b26-11d7-8648000102c1865d
- Emadi, A. A. M. A., Jorry, S., Chautru, J.-M., Caline, B., Blum, M.-S., Jedaan, N. M. R., . . . Fraise, C. (2009). *3D modeling of the Arab Formation (Maydan Mahzam Field, offshore Qatar): An integrated approach*. Paper presented at the International Petroleum Technology Conference, Doha, Qatar.
- Embry, A. F., III & Klovan, J. E. (1971). A late Devonian reef tract on northeastern Banks Island N.W.T. *Bulletin of Canadian Petroleum Geology*, 19(4), 730–81.
- Énay, R. (1993). Les apports sud-tethysiens parmi les faunes jurassiques nord-ouest europeennes: Interpretation paleobiogeographique. *Comptes Rendus de l'Academie des Sciences, Serie 2, Mecanique, Physique, Chimie, Sciences de l'Univers, Sciences de la Terre*, 317(1), 115–21.
- Énay, R., Le Nindre, Y. M., Mangold, C., Manivit, J. & Vaslet, D. (1987). Le Jurassique d'Arabie Saoudite central: Nouvelles donnees sur la lithostratigraphie, les paleoenvironnements, les faunes d'ammonites, les ages et les correlations [The Jurassic of central Saudi Arabia: New data on lithostratigraphy, paleoenvironments, ammonite fauna, ages and correlations]. *Geobios, Memoire Special*, 9, 13–65.
- Epshteyn, O. (1978). Mesozoic-Cenozoic climates of northern Asia and glacial-marine deposits. *International Geology Review*, 20(1), 49–58.
- Favre, P. & Stampfli, G. M. (1992). From rifting to passive margin: The examples of the Red Sea, central Atlantic and Alpine Tethys. *Tectonophysics*, 215(1–2), 69–97.
- Fischbuch, B. & Soremi, Y. (2008). Ghawar's magnificent five. *Saudi Arabia Oil and Gas Magazine*, 2.
- Fischer, A. (1964). The Lofer cyclothems of the Alpine Triassic. *Symposium*, 169(1), 10749.
- Fischer, A. G. (1982). Long-term climatic oscillations recorded in stratigraphy. *Climate in Earth history*, 97-104.
- Fischer, J.-C., Manivit, J. & Vaslet, D. (2001). Jurassic gastropod faunas of central Saudi Arabia. *GeoArabia (Manama)*, 6(1), 63–100.
- Fluegel, E. & Kiessling, W. (2002). Patterns of Phanerozoic reef crises. [Special

- publication]. *Society for Sedimentary Geology*, 72, 691–733.
- Flügel, E. & Flügel-Kahler, E. (1992). Phanerozoic reef evolution: Basic questions and data base. *Facies*, 26(1), 167–277.
- Ford, D. & Golonka, J. (2003). Phanerozoic paleogeography, paleoenvironment and lithofacies maps of the circum-Atlantic margins. *Marine and Petroleum Geology*, 20(3), 249–285.
- Frakes, L. A. (1979). *Climates throughout geologic time*. Amsterdam: Elsevier.
- Frakes, L. A., Francis, J. E. & Syktus, J. I. (1992). *Climate modes of the Phanerozoic: The history of the Earth's climate over the past 600 million years*. New York, NY: Cambridge University Press.
- Frakes, L. A., Francis, J. E. & Syktus, J. I. (2005). *Climate modes of the Phanerozoic*. New York, NY: Cambridge University Press.
- Frakes, L. A., Kemp, E. M. & Crowell, J. C. (1975). Late Paleozoic Glaciation: Part VI, Asia. *Geological Society of America Bulletin*, 86(4), 454–64.
- Friedman, G. M., Gebelein, C. D. & Sanders, J. E. (1971). Micritic envelopes of carbonate grains are not exclusively of photosynthetic algal origin. *Sedimentology*, 16(1–2), 89–96.
- Frizon de Lamotte, D., Raulin, C., Mouchot, N., Wrobel-Daveau, J.-C., Blanpied, C. & Ringenbach, J.-C. (2011). The southernmost margin of the Tethys realm during the Mesozoic and Cenozoic; initial geometry and timing of the inversion processes. *Tectonics*, 30(3), TC3002.
- Galloway, W. E. (1989). Genetic stratigraphic sequences in basin analysis: I, Architecture and genesis of flooding-surface bounded depositional units. *AAPG Bulletin*, 73(2), 125–142. doi: 10.1306/703c9af5-1707-11d7-8645000102c1865d
- Gary, J. H., William, D., Sarah, J. D., John, A. H. & Keith, R. A. (2005). Use of spectral gamma-ray data to refine subsurface fluvial stratigraphy: Late Cretaceous strata in the Book Cliffs, Utah, USA. *Journal of the Geological Society*, 162, 603–621.
- Genna, A., Vaslet, D., Janjou, D., Le Metour, J. & Halawani, M. (2000). Rifting of the Arabian Platform during the Proterozoic-to-Phanerozoic interval. *GeoArabia (Manama)*, 5(1), 94–5.

- Ghawar oil field, Saudi Arabia. (1959). *Bulletin of the American Association of Petroleum Geologists*, 43(2), 434–54.
- Giant of the sea. (1962, December). *Saudi Aramco World*, 13(3).
- Glennie, K. W. (2000). Cretaceous tectonic evolution of Arabia's eastern plate margin: A tale of two oceans. [Special publication]. *Society for Sedimentary Geology*, 69, 9–20.
- Glennie, K. W. (2001, January). *Neo-tethys 1 & neo-tethys 2: Successive Permian to Cenozoic oceans that flanked NE Arabia*. Paper presented at the International Conference on Geology of Oman, Muscat, Sultanate (Oman).
- Goldberg, K., Grunt, T., Lenova T., McGowan A., Morgans H., Naugolnykh, S.,... Ziegler, A. (2002). *The Paleogeographic Atla Project*. Retrieved from <http://www.geo.arizona.edu/~rees/PGAPhome.html>
- Goldhammer, R. K., Dunn, P. A. & Hardie, L. A. (1990). Depositional cycles, composite sea-level changes, cycle stacking patterns, and the hierarchy of stratigraphic forcing; examples from Alpine Triassic platform carbonates. *Geological Society of America Bulletin*, 102(5), 535–62. doi: 10.1130/0016-7606(1990)102<0535:dccslc>2.3.co;2
- Goldring, R., Taylor, A. M. & Hughes, G. W. (2005). The application of ichnofabrics towards bridging the dichotomy between siliciclastic and carbonate shelf facies: Examples from the Upper Jurassic Fulmar Formation (UK) and the Jubaila Formation (Saudi Arabia). *Proceedings of the Geologists' Association*, 116(3–4), 235–49.
- Golonka, J. (2002). Plate-tectonic maps of the Phanerozoic [Special Publication]. *Society for Sedimentary Geology*, 72, 21–75.
- Golonka, J. (2004). Plate tectonic evolution of the southern margin of Eurasia in the Mesozoic and Cenozoic. *Tectonophysics*, 381(1–4), 235–73.
- Golonka, J. & Bocharova, N. Y. (2000). Hot spot activity and the break-up of Pangea. *Palaeogeography, Palaeoclimatology, Palaeoecology*, 161(1–2), 49–69.
- Golonka, J., Ross, M. I. & Scotese, C. R. (1994). Phanerozoic paleogeographic and paleoclimatic modeling maps. *Memoir—Canadian Society of Petroleum Geologists*, 17, 1–47.
- Gordon, W. A. (1975). Distribution by latitude of Phanerozoic evaporite deposits.

- Journal of Geology*, 671–84.
- Grabowski, G. J., Jr. & Norton, I. O. (1995). Tectonic controls on the stratigraphic architecture and hydrocarbon systems of the Arabian Plate. *SEG Annual Meeting Expanded Technical Program Abstracts with Biographies*, 65, 857.
- Gradstein, F. M., Ogg, J. G., Smith, A. G., Agterberg, F. P., Bleeker, W., Cooper, R. A., . . . Wilson, D. (2004). A geological time scale 2004 [Miscellaneous Report]. *Geological Survey of Canada* (0068–7642).
- Grant, N. K. (1969). The Late Precambrian to Early Paleozoic Pan-African Orogeny in Ghana, Togo, Dahomey, and Nigeria. *Geological Society of America Bulletin*, 80(1), 45–56. doi: 10.1130/0016-7606(1969)80[45:tlptep]2.0.co;2
- Guiraud, R. & Bellion, Y. (1996). *Late Carboniferous to recent geodynamic evolution of the West Gondwanian cratonic Tethyan margins*. New York, NY: Plenum Press.
- Habicht, J. (1979). *Paleoclimate, paleomagnetism, and continental drift*. American Association of Petroleum Geologists.
- Hallam, A. (1978). Eustatic cycles in the Jurassic. *Palaeogeography, Palaeoclimatology, Palaeoecology* 23(1/2), 1–32.
- Hallam, A. (1982). Jurassic climate. National Research Council, Commission on Physical Sciences, Mathematics, and Resources, Geophysics Research Board, Geophysics Study Committee, Climate in Earth history, Washington, DC, National Academy Press, 1982, 159–163.
- Hallam, A. (1984). Continental humid and arid zones during the Jurassic and Cretaceous. *Palaeogeography, Palaeoclimatology, Palaeoecology*, 47(3–4), 195–223.
- Hallam, A. (1985). A review of Mesozoic climates. *Journal of the Geological Society*, 142(3), 433–45.
- Hallam, A. (1986). Role of climate in affecting Late Jurassic and Early Cretaceous sedimentation in the North Atlantic. *Geological Society Special Publications*, 21, 277–81.
- Hallam, A. (1988). A reevaluation of Jurassic eustasy in the light of new data and the revised Exxon curve. [Special Publication]. *Society of Economic Paleontologists and Mineralogists*, 42, 261–73.

- Hallam, A. (1994). Jurassic climates as inferred from the sedimentary and fossil record. In J. R. L. Allen, [B. J. Hoskins](#), [P. J. Valdes](#), [B. W. Sellwood](#) & [R. Spicer](#) (Eds.), *Palaeoclimates and their modelling: With special reference to the Mesozoic era* (pp. 7988). London, UK: Chapman & Hall.
- Hallam, A. (1996). *Major bio-events in the Triassic and Jurassic*. Berlin, Germany: Springer.
- Hallam, A. (1998). The determination of Jurassic environments using palaeoecological methods. *Bulletin de la Societe Geologique de France*, 169(5), 681–7.
- Hallam, A. (1999). Evidence of sea-level fall in sequence stratigraphy: Examples from the Jurassic. *Geology*, 27(4), 343–6.
- Hallam, A., Crame, J., Mancenido, M., Francis, J. & Parrish, J. (1993). Jurassic climates as inferred from the sedimentary and fossil record [and discussion]. *Philosophical Transactions of the Royal Society of London, Series B: Biological Sciences*, 341(1297), 287–96.
- Halpern, H., Jones, P., Tobey, M., Carrigan, W. & Al-Amoudi, M. (2000). A study of reservoir connectivity in the Khurais and Qirdi fields using geochemical techniques. *GeoArabia (Manama)*, 5(1), 102.
- Handford, C. R., Cantrell, D. L. & Keith, T. H. (2002). Regional facies relationships and sequence stratigraphy of a super-giant reservoir (Arab-D member), Saudi Arabia [Program and abstracts]. *Society of Economic Paleontologists (Gulf Coast Section), Research Conference*, 22, 539–63.
- Handford, C. R., Cantrell, D. L. & Kendall, C. (2000). Depositional facies and sequence stratigraphy of the Arab-D carbonates, Haradh area, Ghawar Field, Saudi Arabia. *GeoArabia (Manama)*, 5(1), 102–3.
- Handford, C. R., Keith, T. H., Mueller, H. W. & Dommissie, R. (2003). Sequence stratigraphic framework and depositional systems of the Arab-D reservoir in Ghawar Field, Saudi Arabia [Annual meeting expanded abstracts]. *American Association of Petroleum Geologists*, 12, 70.
- Handford, C. R. & Loucks, R. G. (1994). Carbonate depositional sequences and systems tracts-responses of carbonate platforms to relative sea-level changes. *Houston Geological Society Bulletin*, 37(4), 10.

- Haq, B. U. & Al-Qahtani, A. M. (2005). Phanerozoic cycles of sea-level change on the Arabian Platform. *GeoArabia (Manama)*, 10(2), 12760.
- Haq, B. U., Hardenbol, J. & Vail, P. R. (1987). Chronology of fluctuating sea levels since the Triassic. *Science*, 235(4793), 1156–67.
- Haq, B. U., Hardenbol, J. & Vail, P. R. (1988). Mesozoic and Cenozoic chronostratigraphy and cycles of sea-level change [Special publication]. *Society of Economic Paleontologists and Mineralogists*, 42, 72–108.
- Harris, P. M., Kerans, C. & Bebout, D. G. (1993). Ancient outcrop and modern examples of platform carbonate cycles: Implications for subsurface correlation and understanding reservoir heterogeneity. *AAPG Memoir*, 57, 475–92.
- Hayes, J. D. & Pitman W. C. (1973). Lithospheric plate motion, sea level changes and climatic and ecological consequences. *Nature*, 246, 18-22.
- Hine, A.C., and A.C. Neumann, 1977, Shallow carbonate-bank-margin growth and structure, Little Bahama Bank, Bahamas: AAPG Bull., v. 61, p. 376-406.
- Homke, S., Verges, J., Serra-Kiel, J., Bernaola, G., Sharp, I., Garces, M.,... Goodarzi, M. H. (2009). Late Cretaceous-Paleocene formation of the proto-Zagros foreland basin, Lurestan Province, SW Iran. *Bulletin of the Geological Society of America*, 121(7–8), 963–78.
- Hook, J. E., Golubic, S. & Milliman, J. D. (1984). Micritic cement in microborings is not necessarily a shallow-water indicator. *Journal of Sedimentary Research*, 54(2), 425–31. doi: 10.1306/212f8431-2b24-11d7-8648000102c1865d
- Howland, A. F. (1979). Tectonics of the Najd transcurrent fault system, Saudi Arabia. *Journal of the Geological Society of London*, 136(4), 441–54.
- Hubbard, D. K. (1992). Hurricane-induced sediment transport in open-shelf tropical systems: An example from St. Croix, US Virgin Islands. *Journal of Sedimentary Research*, 62(6), 946–60. doi: 10.1306/d4267a23-2b26-11d7-8648000102c1865d
- Hubbard, D. K., Miller, A. I. & Scaturro, D. (1990). Production and cycling of calcium carbonate in a shelf-edge reef system (St. Croix, US Virgin Islands): Applications to the nature of reef systems in the fossil record. *Journal of Sedimentary Research*, 60(3), 335–60. doi: 10.1306/212f9197-2b24-11d7-

8648000102c1865d

- Huber, B. T., MacLeod, K. G. & Wing, S. L. (1999). *Warm climates in earth history*. Cambridge University Press.
- Hughes, G. W. (1996a). Environmentally-induced biofacies events in the Arab-D Reservoir of Saudi Arabia. *GeoArabia (Manama)*, 1(1), 150.
- Hughes, G. W. (1996b). A new bioevent stratigraphy of Late Jurassic Arab-D carbonates of Saudi Arabia. *GeoArabia (Manama)*, 1(3), 417–34.
- Hughes, G. W. (1997). The Great Pearl Bank Barrier of the Arabian Gulf as a possible Shu'aiba analogue. *GeoArabia (Manama)*, 2(3), 279–304.
- Hughes, G. W. (2004a). Middle to Late Jurassic biofacies of Saudi Arabia. *Rivista Italiana di Paleontologia e Stratigrafia*, 110(1), 173–9.
- Hughes, G. W. (2004b). Middle to Upper Jurassic Saudi Arabian carbonate petroleum reservoirs: Biostratigraphy, micropalaeontology and palaeoenvironments. *GeoArabia (Manama)*, 9(3), 79–114.
- Hughes, G. W. (2006). *Biostratigraphy, biofacies, palaeoenvironments, lithostratigraphy and reservoir implications for the Shaqra Group (Jurassic) of Saudi Arabia*. Paper presented at the Seventh Middle East Geosciences Conference and Exhibition.
- Hughes, G. W. (2009). Using Jurassic micropaleontology to determine Saudi Arabian carbonate palaeoenvironments [special publication]. *Society for Sedimentary Geology*, 93, 127–52.
- Hughes, G. W., Dhubeeb, A. G., Varol, O., Lindsay, R. F. & Mueller, H. (2004). The Arab-D biofacies of Saudi Arabia: Their palaeoenvironment and new biozonation. *GeoArabia (Manama)*, 9(1), 79–80.
- Hughes, G. W. & Naji, N. (2008). Sedimentological and micropalaeontological evidence to elucidate post-evaporitic carbonate palaeoenvironments of the Saudi Arabian latest Jurassic. *Volumina Jurassica*, 6(6), 61–73.
- Hughes, G. W., Varol, O. & Al-Dhubeeb, A. (2004). *Biofacies and palaeoenvironments of Late Jurassic carbonates of Saudi Arabia*. Paper presented at the 32nd International Geological Congress, Italy.
- Hughes, G. W., Varol, O., Hooker, N. P. & Énay, R. (2008). New aspects of Saudi Arabian Jurassic biostratigraphy. *GeoArabia (Manama)*, 13(1), 174.

- Hsü, K. J. (1975). Paleooceanography of the Mesozoic Alpine Tethys. *Geology*, 3(6), 347–8. doi: 10.1130/0091-7613(1975)3<347:potmat>2.0.co;2
- Husinec, A., Basch, D., Rose, B. & Read, J. F. (2008). Fischerplots: An Excel spreadsheet for computing Fischer plots of accommodation change in cyclic carbonate successions in both the time and depth domains. *Computers & Geosciences*, 34(3), 269–77. doi: 10.1016/j.cageo.2007.02.004
- Husseini, M. I. (1988). The Arabian Infracambrian extensional system. *Tectonophysics*, 148(1–2), 93–103.
- Husseini, M. I. (1989). Tectonic and deposition model of late Precambrian-Cambrian Arabian and adjoining plates. *AAPG Bulletin*, 73(9), 1117–31.
- Husseini, M. I. (1991). Tectonic and depositional model of the Arabian and adjoining plates during the Silurian-Devonian. *AAPG Bulletin*, 75(1), 108–20.
- Husseini, M. I. & Hussein, S. I. (1990). Origin of the Infracambrian salt basins of the Middle East. *Geological Society Special Publications*, 50, 279–92.
- hydrocarbons-technology.com. (2011). *Saudi Aramco Khurais Mega Project, Khurais*. Retrieved from <http://www.hydrocarbons-technology.com/projects/khurais/>
- Ibe, A. C. (1985). In situ formation of petroleum in oolites: II, A case study of the Arab Formation oolite reservoirs. *Journal of Petroleum Geology*, 8(3), 331–41.
- Immenhauser, A. & Matthews, R. K. (2004). Albian sea-level cycles in Oman: The 'Rosetta Stone' approach. *GeoArabia (Manama)*, 9(3), 11–46.
- Insalaco, E., Boisseau, T., Glover, S., Vieban, F. & Walgenwitz, F. (2004). The Upper Arab Formation: Is the present really the key to the past? *GeoArabia (Manama)*, 9(1), 81.
- Ivanovich, M. & Harmon, R. S. (Eds.). (1982). *Uranium series disequilibrium: Applications to environmental problems*. New York, NY: Oxford University Press.
- Ivanovich, M. & Harmon, R. S. (1992). *Uranium-series disequilibrium: Applications to earth, marine, and environmental sciences*. Oxford, UK: Clarendon Press.
- James, N. P. (1984). Shallowing-upward sequences in carbonates. *Facies models*, 1.
- Javaux, C., Cochet, F., Gauthier, B., Prinnet, C., haven, L. T. & Herriou, M. (2000). 3D

- geological model to reservoir simulation of the Lower Arab Formation—Abu Al Bukhoosh (ABK) Field, offshore Abu Dhabi.* Paper presented at the Abu Dhabi International Petroleum Exhibition and Conference, Abu Dhabi, United Arab Emirates.
- Johnson, P. R. & Stewart, I. C. F. (1995). Magnetically inferred basement structure in central Saudi Arabia. *Tectonophysics*, 245(1–2), 37–52.
- Kawaguchi, K.-I. (1991). *Geological controls on reservoir quality of Arab Formation in Satah Field.* Paper presented at the Middle East Oil Show, Bahrain.
- Keith, T., Cole, J. C., Mattner, J. E., Ozkaya, S. I. & Waak, K. A. (1998). A conceptual model for super permeability in Uthmaniyah Field. *GeoArabia (Manama)*, 3(1), 108.
- Keith, T. H. (2005). Finding the super-giant: The discovery of Ghawar Field. *GeoFrontier*, 2.
- Kennedy, W. (1964). The structural differentiation of Africa in the Pan-African (± 500 my) tectonic episode. *Leeds Univ. Res. Inst. Afr. Geol. Annu. Rep.*, 8, 48–9.
- Kerans, C., Lucia, F. J. & Senger, R. K. (1994). Integrated characterisation of carbonate ramp reservoirs using Permian San Andres Formation outcrop analogs. *AAPG Bulletin*, 78(2), 181–216. doi: 10.1306/bdff905a-1718-11d7-8645000102c1865d
- Kinsman, D. J. J. & Park, R. K. (1976). *Algal belt and coastal sabkha evolution, Trucial Coast, Persian Gulf.* Amsterdam: Elsevier.
- Kirkham, A. (2004). Patterned dolomites: Microbial origins and clues to vanished evaporites in the Arab Formation, Upper Jurassic, Arabian Gulf. *Geological Society Special Publications*, 235, 301–8.
- Koerschner, W. F., III & Read, J. F. (1989). Field and modelling studies of Cambrian carbonate cycles, Virginia, Appalachians. *Journal of Sedimentary Petrology*, 59(5), 654–87. doi: 10.1306/212f9048-2b24-11d7-8648000102c1865d
- Konert, G., Afifi, A. M., Al-Hajri, S. A., de Groot, K., Al Naim, A. A. & Droste, H. J. (2001). Paleozoic stratigraphy and hydrocarbon habitat of the Arabian Plate. *AAPG Memoir*, 74, 483–515.
- Konyuhov, A. & Maleki, B. (2006). The Persian Gulf Basin: Geological history, sedimentary formations, and petroleum potential. *Lithology and Mineral*

- Resources*, 41(4), 344–61.
- Kroener, A. & Stern, R. J. (2005). *Africa: Pan-African Orogeny*. Oxford, UK: Elsevier.
- Kusky, T. M., Abdelsalam, M., Tucker, R. D., & Stern, R. J. (2003). Evolution of the East African and related orogens, and the assembly of Gondwana. *Precambrian Research*, 123(2-4), 81-85.
- Kutzbach, J., Gallimore, R., Harrison, S., Behling, P., Selin, R. & Laarif, F. (1998). Climate and biome simulations for the past 21,000 years. *Quaternary Science Reviews*, 17(6), 473–506.
- Laing, J. E. (1991). Geologic constraints to fluid flow in the Jurassic Arab-D Reservoir, eastern Saudi Arabia. *AAPG Bulletin*, 75(8), 1415.
- Lambert, L., Durlet, C., Loreau, J.-P. & Marnier, G. (2006). Burial dissolution of micrite in Middle East carbonate reservoirs (Jurassic–Cretaceous): Keys for recognition and timing. *Marine and Petroleum Geology*, 23(1), 79–92. doi: 10.1016/j.marpetgeo.2005.04.003
- Laskar, J., Robutel, P., Joutel, F., Gastineau, M., Correia, A. C. M. & Levrard, B. (2004). A long-term numerical solution for the insolation quantities of the Earth. *Astronomy & Astrophysics*, 428(1), 261–85. doi: 10.1051/0004-6361:20041335
- Lea, D. W., Bijma, J., Spero, H. J., & Archer, D. (1999). Implications of a carbonate ion effect on shell carbon and oxygen isotopes for glacial ocean conditions. In *Use of Proxies in Paleoceanography* (pp. 513-522). Springer Berlin Heidelberg.
- Leeder, M. (2011). *Sedimentology and sedimentary basins: From turbulence to tectonics* (2nd ed.). Oxford, UK: Wiley-Blackwell.
- Leeder, M. R., & Zeidan, R. (1977). Giant late Jurassic sabkhas of Arabian Tethys. [10.1038/268042a0]. *Nature*, 268(5615), 42-44.
- Lehmann, C. T., Ibrahim, K., Bu-Hindi, H., Al-Kassawneh, R., Cobb, D. & Al-Hendi, A. (2008). High-resolution sequence-stratigraphic interpretation of the Upper Jurassic Arab Formation on new field development, offshore Abu Dhabi. [Annual meeting abstracts]. *American Association of Petroleum Geologists*.
- Leinfelder, R. R. (1994). *Distribution of Jurassic reef types: A mirror of structural and environmental changes during breakup of Pangea*.

- Leinfelder, R. R., Schlagintweit, F., Werner, W., Ebli, O., Nose, M., Schmid, D. U. & Hughes, G. W. (2005). Significance of stromatoporoids in Jurassic reefs and carbonate platforms: Concepts and implications. *Facies*, 51(1–4), 288–326. doi: 10.1007/s10347-005-0055-8
- Le Nindre, Y.-M., Manivit, J. & Vaslet, D. (1987). *Histoire géologique de la bordure occidentale de la plate-forme arabe du Paléozoïque inférieur au Jurassique supérieur* (Unpublished doctoral dissertation). University Pierre and Marie Curie, Paris.
- Le Nindre, Y.-M., Manivit, J. & Vaslet, D. (1990). Stratigraphie séquentielle du Jurassique et du Crétacé en Arabie Saoudite. *Bulletin, Société Géologique de France, Paris*, 6, 1025–35.
- Le Nindre, Y.-M., Manivit, J., Vaslet, D. & Manivit, H. (1991). *Sequential stratigraphy of Jurassic and Cretaceous in the central Saudi Arabian platform*. *Geobyte*; (United States), 75(CONF-910978--).
- Le Nindre Y.-M, Vaslet, D., Maddah, S. S. & Al-Husseini, M. I. (2008). Stratigraphy of the Valanginian? to Early Paleocene succession in central Saudi Arabia outcrops: Implications for regional Arabian sequence stratigraphy. *GeoArabia*, 13(2), 51–86.
- Leveridge, B. E. & Hartley, A. J. (2006). *The Variscan Orogeny: The development and deformation of Devonian/Carboniferous basins in SW England and south Wales*. London, UK: The Geological Society.
- Leyrer, K., Meyer, F. O. & Peterhaensel, A. (2008). The role of evaporites in a holistic investigation of Arab sequence stratigraphy and the related depositional sequences in the northern part of the eastern province, Saudi Arabia. *GeoArabia (Manama)*, 13(1), 190–192.
- Li, Z.-X. & Powell, C. M. (2001). An outline of the palaeogeographic evolution of the Australasian region since the beginning of the Neoproterozoic. *Earth-Science Reviews*, 53(3–4), 237–77.
- Lindholm, R. C., & Finkelman, R. B. (1972). Calcite staining; semiquantitative determination of ferrous iron. *Journal of Sedimentary Research*, 42(1), 239–242.
- Lindsay, R. F., Cantrell, D. L., Hughes, G. W., Keith, T. H., Mueller, H. W., III & Russell,

- D. (2006). Ghawar Arab-D reservoir: Widespread porosity in shoaling-upward carbonate cycles, Saudi Arabia. *AAPG Memoir*, 88, 97–138.
- Little, M. G., Schneider, R. R., Kroon, D., Price, B., Summerhayes, C. P. & Segl, M. (1997). Trade wind forcing of upwelling, seasonality, and Heinrich events as a response to sub-Milankovitch climate variability. *Paleoceanography*, 12, 568–76.
- Lomando, A. J. & Harris, P. M., eds. (1988). *Giant oil and gas fields: A core workshop*. [Society of Economic Paleontologists and Mineralogists](#) core workshop, 12, vol. 2.
- Loucks, R. G. & Sarg, J. F. (1993). Carbonate sequence stratigraphy: Recent developments and applications. *American Association of Petroleum Geologists*.
- Loucks, R. G., Kerans, C., Janson, X. & Marhx, A. (2006). Origin and organization of mass-transported carbonate debris in the Lower Cretaceous (Albian) Tamabra Formation, Poza Rica Field area, Mexico, United States. [Annual meeting abstracts]. *American Association of Petroleum Geologists*, 15, 66.
- Lucia, F. J. (1995). Rock-fabric/petrophysical classification of carbonate pore space for reservoir characterization. *AAPG Bulletin-American Association of Petroleum Geologists*, 79(9), 1275-1300.
- Lucia, F. J. (2004). Origin and petrophysics of dolostone pore space. *Geological Society Special Publications*, 235, 141–55.
- Magara, K., Khan, M. S., Sharief, F. A. & Al-Khatib, H. N. (1993). Log-derived reservoir properties and porosity preservation of Upper Jurassic Arab Formation in Saudi Arabia. *Marine and Petroleum Geology*, 10(4), 352–63. doi: 10.1016/0264-8172(93)90080-c
- Manabe, S., & Bryan, K. (1985). CO₂-induced change in a coupled ocean-atmosphere model and its paleoclimatic implications. *Journal of Geophysical Research: Oceans* (1978–2012), 90(C6), 11689-11707.
- Manabe, S. & Wetherald, R. T. (1980). On the distribution of climate change resulting from an increase in CO₂ content of the atmosphere. *Journal of the Atmospheric Sciences*, 37(1), 99–118.
- Manivit, J., Le Nindre, Y. M. & Vaslet, D. (1990). Histoire géologique de la bordure

- occidentale de la plate-forme arabe. (Geologic history of the western border of the Arabian Platform Documents). Bureau de recherches géologiques et minières . 4, 60.
- Manivit, J., Pellaton, C., Vaslet, D., Le Nindre, Y. M., Brosse, J.-M. & Fourniguet, J. (1985). *Explanatory notes to the geologic map of the Wadi al Mulayh Quadrangle* (Sheet 22H, Vol. GM-92C, pp. 32). Jiddah, Saudia Arabia: Ministry of Petroleum and Mineral Resources.
- Mattner, J. & Al-Husseini, M. (2002). Applied cyclo-stratigraphy for the Middle East E&P industry. *GeoArabia (Manama)*, 7(4), 734–44.
- Max Steineke. (1952, 23 April). *Aramco ExPats*. Retrieved from <http://www.aramcoexpats.com/obituaries/1952/04/max-steineke.aspx>
- McGuire, M. D., Koepnick, R. B., Markello, J. R., Stockton, M. L., Waite, L. E., Kompanik, G. S., . . . Al-Amoudi, M. O. (1993). *Importance of sequence stratigraphic concepts in development of reservoir architecture in Upper Jurassic grainstones, Hadriya and Hanifa Reservoirs, Saudi Arabia*. Paper presented at the Middle East Oil Show.
- Mesozoic and Cenozoic sea level cycles: Towards a complete stratigraphic documentation. (1986). [Abstracts with programs]. *Geological Society of America*, 18(6), 628.
- Mey, J. L. (2008). The uranium series diagenesis and the morphology of drowned Barbadian paleo-reefs. (Doctoral dissertation, 3312925), City University of New York, United States.
- Meyer, F. O. (2000). Carbonate sheet slump from the Jubaila Formation, Saudi Arabia: Slope implications. *GeoArabia (Manama)*, 5(1), 144–5.
- Meyer, F. O. & Cantrell, D. (2000). Porous Arab-D dolomite rhombs: A question of leached or arrested crystal growth. *GeoArabia (Manama)*, 5(1), 144.
- Meyer, F. O. & Hughes, G. W. (2000). *A multidisciplinary integration of selected Saudi Arabian carbonate unconformities*. Paper presented at the Middle East Oil Show, Bahrain.
- Meyer, F. O., Hughes, G. W. & Al-Ghamdi, I. (2000). Jubaila Formation, Tuwaiq Mountain escarpment, Saudi Arabia: Window to lower Arab-D Reservoir faunal assemblages and bedding geometry. *GeoArabia (Manama)*, 5(1), 143.

- Meyer, F. O. & Price, R. C. (1993). *A new Arab-D depositional model, Ghawar Field, Saudi Arabia*. Paper presented at the Middle East Oil Show, Bahrain.
- Meyer, F. O., Price, R. C., Al-Ghamdi, I. A., Al-Goba, I. M., Al-Raimi, S. M. & Cole, J. C. (1996a). Outcropping strata equivalent to Arab-D reservoir, Wadi Nisah, Saudi Arabia. *GeoArabia (Manama)*, 1(1), 171–2.
- Meyer, F. O., Price, R. C., Al-Ghamdi, I. A., Al-Goba, I. M., Al-Raimi, S. M. & Cole, J. C. (1996b). Sequential stratigraphy of outcropping strata equivalent to Arab-D Reservoir, Wadi Nisah, Saudi Arabia. *GeoArabia (Manama)*, 1(3), 435–56.
- Meyer, F. O., Price, R. C. & Al-Raimi, S. M. (2000). Stratigraphic and petrophysical characteristics of cored Arab-D super-k intervals, Hawiyah area, Ghawar Field, Saudi Arabia. *GeoArabia (Manama)*, 5(3), 355–84.
- Miller, K. G., Kominz, M. A., Browning, J. V., Wright, J. D., Mountain, G. S., Katz, M. E., . . . Pekar, S. F. (2005). The Phanerozoic record of global sea-level change. *Science*, 310(5752), 1293–8. doi: 10.1126/science.1116412
- Mitchell, J. C., Lehmann, P. J., Cantrell, D. L., Al-Jallal, I. A. & Al-Thagafy, M. A. R. (1988). Lithofacies, diagenesis and depositional sequence: Arab-D Member, Ghawar Field, Saudi Arabia. *SEPM Core Workshop*, 12, 459–514.
- Mitchum, R. M., Jr & Van Wagoner, J. C. (1991). High-frequency sequences and their stacking patterns: Sequence-stratigraphic evidence of high-frequency eustatic cycles. *Sedimentary Geology*, 70(2–4), 131–60. doi: 10.1016/0037-0738(91)90139-5
- Montaggioni. (2005). History of Indo-Pacific coral reef systems since the last glaciation: Development patterns and controlling factors. *Earth-Science Reviews*, 71(1–2), 1–75.
- Montanez, I. P. & Osleger, D. A. (1993). Parasequence stacking patterns, third-order accommodation events, and sequence stratigraphy of Middle to Upper Cambrian platform carbonates, Bonanza King Formation, southern Great Basin. *AAPG Memoir*, 57(0271–8529, 0271–8529), 305–26.
- Moore, G. T., Hayashida, D. N., Ross, C. A. & Jacobson, S. (1992). Paleoclimate of the Kimmeridgian/Tithonian (Late Jurassic) world: I. Results using a general circulation model. *Palaeogeography, Palaeoclimatology, Palaeoecology*, 93(1–2), 113–50.

- Moore, G. T., Hayashida, D. N., Ross, C. A. & Jacobson, S. (1993). Late Jurassic paleoclimate of Pangea based on results from a general circulation model. In R. Oremland (Ed.), *Biogeochemistry of global change* (pp. 61–79). New York, NY: Springer.
- Moore, G. T., Sloan, L. C., Hayashida, D. N. & Umrigar, N. P. (1992). Paleoclimate of the Kimmeridgian/Tithonian (Late Jurassic) world: II. Sensitivity tests comparing three different paleotopographic settings. *Palaeogeography, Palaeoclimatology, Palaeoecology*, *95*(3–4), 229–52. doi: 10.1016/0031-0182(92)90143-s
- Moore, J. M., Allen, P., Wells, M. K. & Howland, A. F. (1979). Tectonics of the Najd transcurrent fault system, Saudi Arabia. *Journal of the Geological Society of London*, *136*, Part 4, 441–54.
- Mouawad, J. (2010, March 19). China's growth shifts the geopolitics of oil. *The New York Times*.
- Muller, R., Dutkiewicz, A., Seton, M. & Gaina, C. (2010). *Jurassic to present seawater chemistry and climate: Links with the history of seafloor spreading and subduction*. Paper presented at the European Geosciences Union General Assembly 2010.
- Murris, R. J. (1980). Middle East: Stratigraphic evolution and oil habitat. *AAPG Bulletin*, *64*(5), 597–618.
- Nairn, A. E. M., & Alsharhan, A. S. (1997). Sedimentary basins and petroleum geology of the Middle East. Elsevier Science, Amsterdam, 843 pp.
- Nicholson, P. (2000). Compressional fault-related folds and Saudi Arabia's major hydrocarbon fields. *GeoArabia (Manama)*, *5*(1), 152–3.
- Nicholson, P. G., Carney, S., Miller, M. A. & Melvin, J. (2002). Depositional framework and reservoir potential of the Silurian Qusaiba Member, eastern and central Saudi Arabia. [Abstract]. *American Association of Petroleum Geologists International Conference Abstracts*.
- Nicholson, P. G. & Groshong, R. H. (2006). A structural model for typical hydrocarbon traps in Saudi Arabia. [Abstracts with programs]. *Geological Society of America*, *38*(7), 543.
- Norton, M. (1988, May). Well done, Well Seven. *Saudi Aramco World*, *39*, 7.

- Oil pioneer: A suicide. (1917, July 31). *The New York Times*. Retrieved from <http://query.nytimes.com/mem/archive-free/pdf?res=F20D11FC3B5F157A93C3AA178CD85F438185F9>
- Okla, S. M. (1959). Ghawar oil field, Saudi Arabia: Microfacies of the Jubaila Limestone (Upper Jurassic) in central Tuwaiq Mountains. *AAPG Bulletin*, 43(2), 434–54.
- Okla, S. M. (1986). Litho- and microfacies of Upper Jurassic carbonate rocks outcropping in central Saudi Arabia. *Journal of Petroleum Geology*, 9(2), 195–206.
- Okla, S. M. (1987). Algal microfacies in upper Tuwaiq Mountain Limestone (Upper Jurassic) near Riyadh, Saudi Arabia. *Palaeogeography, Palaeoclimatology, Palaeoecology*, 58(2), 55–61.
- Ooyama, K. V. (1982). Conceptual evolution of the theory and modelling of the tropical cyclone. *Journal of the Meteorological Society of Japan*, 60(1), 369–380.
- Our company, 2013. Retrieved January 5, 2013 from <http://www.saudiaramco.com/en/home.html#our-company%257C%252Fen%252Fhome%252Four-company.baseajax.html>
- Palike, H., Norris, R. D., Herrle, J. O. & Wilson, P. A. (2006). The heartbeat of the Oligocene climate system. *Science (Washington)*, 314(5807), 1894–98.
- Palmer, T. I. M. (1982). Cambrian to Cretaceous changes in hardground communities. *Lethaia*, 15(4), 309–23. doi: 10.1111/j.1502-3931.1982.tb01696.x
- Parrish, J. T. (1985). *Latitudinal distribution of land and shelf and absorbed solar radiation during the Phanerozoic* (US Geological Survey open-file report, 85–31). Denver, CO: US Department of the Interior, Geologic Survey.
- Parrish, J. T. (1992). Jurassic climate and oceanography of the Pacific region. *World and Regional Geology*, 3, 365–79.
- Parrish, J. T. (1993). Climate of the supercontinent Pangea. *Journal of Geology*, 101(2), 215.
- Parrish, J. T., Ziegler, A. & Scotese, C. R. (1982). Rainfall patterns and the distribution of coals and evaporites in the Mesozoic and Cenozoic. *Palaeogeography*,

- Palaeoclimatology, Palaeoecology*, 40(1), 67–101.
- Patterson, R. & Kinsman, D. (1981). Hydrologic framework of a sabkha along Arabian Gulf. *AAPG Bulletin*, 65(8), 1457.
- Pearson, P. N., Ditchfield, P. W., Singano, J., Harcourt-Brown, K. G., Nicholas, C. J., Olsson, R. K.,... Hall, M. A. (2001). Warm tropical sea surface temperatures in the Late Cretaceous and Eocene epochs. *Nature*, 413(6855), 481–7.
- Pearson, P. N., van Dongen, B. E., Nicholas, C. J., Pancost, R. D., Schouten, S., Singano, J. M. & Wade, B. S. (2007). Stable warm tropical climate through the Eocene Epoch. *Geology*, 35(3), 211–14.
- Peebles, R. G. (1999). Stable isotope analyses and dating of the Miocene of the Emirate of Abu Dhabi, United Arab Emirates. Fossil Vertebrates of Arabia: With Emphasis on Late Miocene Faunas, Geology, and Palaeoenvironments of the Emirate of Abu Dhabi, United Arab Emirates.
- Peebles, R. G., Suzuki, M., and Shaner, M. (1995). The effects of long-term, shallow-burial diagenesis on carbonate – evaporite successions. Selected Middle East Papers from Geo 94, the Middle East Geoscience Conference, April, 1994. Gulf Petrolink, Bahrain.
- Pemberton, S. G., Gingras, M. K., Hussain, M., Raza, M. J. & Anonymous. (2005). Classification and characterisations of biogenically enhanced permeability source beds for the Mesozoic and younger oils in Saudi Arabia: Constraints of biomarker applications. *AAPG Bulletin*, 89(11), 1493–1517. doi: 10.1306/07050504121
- Perincek, D., Saner, S., Al-Ghamdi, A., Cole, J. & Kamal, R. (2000). Surface to subsurface data integration for an improved understanding of the structural history of the Ghawar Field, Saudi Arabia. *GeoArabia (Manama)*, 5(1), 159.
- Pitman, W. C. (1978). Relationship between eustacy and stratigraphic sequences of passive margins. *Geological Society of America Bulletin*, 89(9), 1389–1403.
- Pollastro, R. M. (2003). Total petroleum systems of the Paleozoic and Jurassic, Greater Ghawar Uplift and adjoining provinces of Central Saudi Arabia and Northern Arabian-Persian Gulf. *US Geological Survey Bulletin* 2202-H. Retrieved from <http://pubs.usgs.gov/bul/b2202-h/>
- Pollastro, R. M., Karshbaum, A. S. & Viger, R. J. (1999). *Map showing geology, oil*

- and gas fields, and geologic provinces of the Arabian Peninsula* (US Geological Survey open-file report). Denver, CO: US Department of the Interior.
- Pomar, L. & Kendall, C. G. S. C. (2008). Architecture of carbonate platforms: A response to hydrodynamics and evolving ecology. [Special Publication]. *Society for Sedimentary Geology*, 89, 187–216.
- Pomar, L. & Ward, W. C. (1995). Sea-level changes, carbonate production and platform architecture: The Lluçmajor Platform, Mallorca, Spain. *Sequence stratigraphy and depositional response to eustatic, tectonic and climatic forcing*, 87–112.
- Powers, R. W. (1962). Arabian Upper Jurassic carbonate reservoir rocks. *Classification of carbonate rocks: AAPG Memoir*, 1, 122-192.
- Powers, R. W. (1968). Saudi Arabia. In *Lexique stratigraphique internationale* [International stratigraphic lexicon]: Vol. 3. Asia, p. 177.
- Powers, R. W., Ramirez, L. F., Redmond, C. D. & Elberg, E. L., Jr. (1966). *Sedimentary geology of Saudi Arabia: Geology of the Arabian Peninsula* (US Geological Survey professional paper, 150).
- Prelude to discovery. (2007, February 19). *Aramco ExPats*. Retrieved from <http://www.aramcoexpats.com/articles/category/in-search-of-oil/page/25/>
- Rakus, M. (1988). Evolution of the northern margin of Tethys: The results of IGCP Project 198, Volume 1. *Occasional Publications ESRI, New Series*, 3, 244.
- Rakús, M., Dercourt, J., Nairn, A. E. M. & 198, I. P. (1988). *Evolution of the northern margin of Tethys: The results of IGCP Project 198*. University of South Carolina, US: Earth Sciences and Resources Institute.
- Read, J. F. (1998). Phanerozoic carbonate ramps from greenhouse, transitional and ice-house worlds: Clues from field and modelling studies. *Geological Society Special Publications*, 149, 107–35.
- Read, J. F. & Goldhammer, R. K. (1988). Use of Fischer plots to define third-order sea-level curves in Ordovician peritidal cyclic carbonates, Appalachians. *Geology (Boulder)*, 16(10), 895–9. doi: 10.1130/0091-7613(1988)016<0895:uofptd>2.3.co;2
- Read, J. F., Kerans, C., Weber, L. J., Sarg, J. F. & Wright, F. M. (1995). Overview of

- carbonate platform sequences, cycle stratigraphy and reservoirs in greenhouse and icehouse worlds. *SEPM Short Course Notes*, 35, 102.
- A red line, a new kingdom, America, and oil. (2007, February 20). *Aramco ExPats*. Retrieved from <http://www.aramcoexpats.com/articles/category/in-search-of-oil/page/25/>
- Rees P. M., Noto C. R., Parrish J. M. & Parrish J. T. (2004). Late Jurassic climates, vegetation, and dinosaur distributions. *Journal of Geology*, 112(6), 643.
- Rees, P. M.; Ziegler, A. M.; and Valdes, P. J. 2000. Jurassic phytogeography and climates: new data and model comparison. In Huber, B. T.; Macleod, K. G.; and Wing, S. L., eds. *Warm climates in earth history*. Cambridge, Cambridge University Press, p. 297–318.
- Robertson, A. (1987). The transition from a passive margin to an Upper Cretaceous foreland basin related to ophiolite emplacement in the Oman Mountains. *Geological Society of America Bulletin*, 99(5), 633–53. doi: 10.1130/0016-7606(1987)99<633:ttfapm>2.0.co;2
- Robertson, A. H. F., Searle, M. P. & Ries, A. C. (1990). International discussion meeting: The geology and tectonics of the Oman region. *Geological Society Special Publications*, 49, 846.
- Roehl Perry, O. and Choquette, P. W. (1985). *Carbonate petroleum reservoirs*. New York, NY: Springer-Verlag.
- Ross, C. A. & Ross, J. R. P. (1983). Late Paleozoic accreted terranes of western North America. In C. H. Stevens (Ed.), *Pre-Jurassic rocks in western North American suspect terranes*. Society of Economic Paleontologists and Mineralogists, Pacific Section.
- Rousseau, M., Dromart, G., Garcia, J. P., Atrops, F. & Guillocheau, F. (2005). Jurassic evolution of the Arabian carbonate platform edge in the central Oman Mountains. *Journal of the Geological Society*, 162(2), 349–62.
- Rowley, D. B. (1996). Age of initiation of collision between India and Asia: A review of stratigraphic data. *Earth and Planetary Science Letters*, 145(1), 1–13.
- Rowley, D. B., Ziegler, A. M., Hulver, M., Markwick, P. J., Lottes, A. L. & Nie, S. Y. (1993, 8–12 August). *Paleogeographic reconstructions of the Mesozoic*. Paper presented at the SEPM meeting—Stratigraphic record of global

- change, Penn State University Campus, US.
- Ruzyla, K., & Jezek, D. I. (1987). Staining method for recognition of pore space in thin and polished sections. *Journal of Sedimentary Research*, 57(4), 777-778.
- Sadler, P. M., Osleger, D. A. & Montanez, I. P. (1993). On the labeling, length, and objective basis of Fischer plots. *Journal of Sedimentary Research*, 63(3), 360–8. doi: 10.1306/d4267aff-2b26-11d7-8648000102c1865d
- Sail, I. A. & Magara, K. (1988). Petroleum generation and maturation of the Arabian Gulf region. *Journal of King Abdulaziz University: Earth Sciences*, 1, 27–60.
- Saner, S., & Sahin, A. (1999). Lithological and zonal porosity-permeability distributions in the Arab-D reservoir, Uthmaniyah Field, Saudi Arabia. *AAPG bulletin*, 83(2), 230-243.
- Saner, S. & Sahin, A. (2000). Lithological and zonal porosity-permeability distributions in the Arab-D Reservoir, Uthmaniyah Field, Saudi Arabia: Reply. *AAPG Bulletin*, 84(9), 1368–1370. doi: 10.1306/022700841368
- Sarg, J. F. (1988). Carbonate sequence stratigraphy. In *Sea Level Changes: An Integrated Approach*. Society of Economic Paleontologists and Mineralogists Special Publication, 42, 155–81.
- Sarg, J. F. (1995). *Carbonate sequence architecture and sea-level records*. US.
- Sarg, J. F. (2001). The sequence stratigraphy, sedimentology, and economic importance of evaporite-carbonate transitions: A review. *Sedimentary Geology*, 140(1–2), 9–42.
- Sarg, J. F. (2003). Carbonate sequence stratigraphy: Future directions for exploration and development. *AAPG Bulletin*, 87(7), 1249–50.
- Saudi Aramco: 80 years in photographs. (2013). Retrieved from http://www.saudiaramco.com/ar_sa/home.html#%25D8%25A7%25D9%2584%25D8%25A3%25D8%25AE%25D8%25A8%25D8%25A7%25D8%25B1%257Chttp%253A%252F%252Fwww.saudiaramco.com%252F%252Fwww.saudiaramco.com%252F%252Fnews%252Fpublications-and-reports%252Fbooks0%252F80YearsinPhotographs.baseajax.html
- Saudi Aramco by the numbers. (2008, May/June). *Saudi Aramco World*, 59(3).
- Saudi Aramco lets contract for Khurais Field development. (2005, August 1). *Oil & Gas Journal*, 103(29), 30.

- Saudi's Khurais field on verge of supergiant status. (1973). *Oil & Gas Journal*, 71(14), 137.
- Schaeffer, B. & Scott, G. (1971). *The braincase of the holostean fish Macrepistius, with comments on neurocranial ossification in the Actinopterygii*. (American Museum Novitates, No. 2459). New York, NY: American Museum of Natural History.
- Scotese, C.R. (2000). Paleomap Project. Available at <http://www.scotese.com>
- Scotese, C. R. (2004). A continental drift flipbook. *Journal of Geology*, 112(6), 729–41.
- Scotese, C. R. & Golonka, J. (1992). *PALEOMAP paleogeographic atlas*. Arlington, TX: University of Texas at Arlington.
- Sellwood, B. W., Price, G. D. & Valdest, P. J. (1994). Cooler estimates of Cretaceous temperatures. *Nature*, 370, 453–55. doi: 10.1038/370453a0
- Sellwood, B. W. & Valdes, P. J. (2006). Mesozoic climates: General circulation models and the rock record. *Sedimentary Geology*, 190(1), 26987.
- Sellwood, B. W. & Valdes, P. J. (2008). Jurassic climates. *Proceedings of the Geologists' Association*, 119(1), 5–17.
- Sellwood, B. W., Valdes, P. J. & Price, G. D. (2000). Geological evaluation of multiple general circulation model simulations of Late Jurassic palaeoclimate. *Palaeogeography, Palaeoclimatology, Palaeoecology*, 156(1–2), 147–60.
- Sengor, A. M. C. (1979). Mid-Mesozoic closure of Permo-Triassic Tethys and its implications. *Nature (London)*, 279(5714), 590–3.
- Sengor, A. M. C. & Natal'in, B. A. (1996). Paleotectonics of Asia: Fragments of a synthesis. *World and Regional Geology*, 9, 486–640.
- Sharland, P. R., Archer, R., Casey, D. M., Davies, R. B., Hall, S. H., Heward, A.P., . . . Simmons, M. D. (2001). Arabian plate sequence stratigraphy. *GeoArabia Special Publication No. 2*.
- Shirley, K. (2008, May). Geologists made their marks. *AAPG Explorer*, 29. Retrieved from <http://www.aapg.org/explorer/2008/05may/marks.cfm>
- Significance of dolomite in a large evaporite-carbonate cycle: Arab-D Reservoir, Saudi Arabia. *AAPG Bulletin*, 84(9), 1365–7. doi: 10.1306/a9673eaa-1738-11d7-8645000102c1865d

- Simmons, M. D. (1994). Micropalaeontological biozonation of the Khamah Group (Early Cretaceous), Central Oman Mountains. In M. D. Simmons (Ed.), *Micropalaeontology and Hydrocarbon Exploration in the Middle East*. London, UK: Chapman and Hall.
- Simmons, M. D., Sharland, P. R., Casey, D. M., Davies, R. B. & Sutcliffe, O. E. (2007). Arabian Plate sequence stratigraphy: Potential implications for global chronostratigraphy. *Geoarabia (Manama)*, 12(4), 101.
- Sloan, L. C. & Barron, E. J. (1990). 'Equable' climates during Earth history? *Geology*, 18(6), 489–92.
- Sorkhabi, R. (2008). The emergence of the Arabian oil industry. *GeoExpro*, 5(6).
- Sorkhabi, R. (2010). The king of giant fields. *GeoExpro*, 7(4).
- Sorkhabi, R. (2011, June). Finding Ghawar: Elephant hid in desert. *AAPG Explorer*, 32, 2.
- Sprague, A. R., Sullivan, M. D., Campion, K. M., Jensen, G. N., Goulding, F. J., Garfield, T. R. (2002, March). *The physical stratigraphy of deep-water strata: A hierarchical approach to the analysis of genetically related stratigraphic elements for improved reservoir prediction*. Paper presented at the Annual meetings abstracts—American Association of Petroleum Geologists and Society of Economic Paleontologists and Mineralogists, US.
- Stampfli, G. M. & Borel, G. D. (2002). A plate-tectonic model for the Paleozoic and Mesozoic constrained by dynamic plate boundaries and restored synthetic oceanic isochrons. *Earth and Planetary Science Letters*, 196(1–2), 17–33.
- Stampfli, G. M. & Borel, G. D. (2004). The TRANSMED Atlas: Geological-geophysical fabric of the Mediterranean region. *Episodes*, 27(4), 244–54.
- Stampfli, G. M., Borel, G. D., Cavazza, W., Mosar, J. & Ziegler, P. A. (2001). *Paleotectonic atlas of the PeriTethyan domain*. [CD-ROM].
- Stampfli, G. M., Borel, G. D., Cavazza, W., Mosar, J. & Ziegler, P. A. (2001). Palaeotectonic and palaeogeographic evolution of the western Tethys and PeriTethyan domain (IGCP Project 369). *Episodes*, 24(4), 222–7.
- Stampfli, G., Marcoux, J., & Baud, A. (1991). Tethyan margins in space and time. *Palaeogeography, Palaeoclimatology, Palaeoecology*, 87(1), 373–409.
- Stampfli, G. M., Mosar, J., Favre, P., Pilleveit, A. & Vannay, J.-C. (2001). Permo-

- Mesozoic evolution of the western Tethys realm: The Neo-Tethys East Mediterranean Basin connection. *Memoires du Museum National d'Histoire Naturelle*, 186, 51–108.
- Stegner, W. E. (2007). *Discovery! The Search for Arabian Oil*. Portola St. Vista: Selwa Press.
- Steineke, M. & Bramkamp, R. A. (1952). Mesozoic rocks of eastern Saudi Arabia. *Bulletin of the American Association of Petroleum Geologists*, 36(5), 909.
- Steineke, M., Bramkamp, R. A. & Sander, N. J. (1958). Stratigraphic relations of Arabian Jurassic oil. In L. G. Weeks (Ed.), *Habitat of oil: A symposium* (pp. 1294–1329). Tulsa, OK: American Association of Petroleum Geologists.
- Stephens, N., Puls, D., Albotrous, H., Al-Ansi, H. & Fahad, A. T. (2009). *Sequence stratigraphic framework of the Arab Formation reservoirs, Dukhan Field, Qatar*. Paper presented at the International Petroleum Technology Conference.
- Stocklin, J. (1974). *Possible ancient continental margins in Iran*. New York, NY: Springer-Verlag.
- Stoeser, D. & Camp, V. E. (1985). Pan-African microplate accretion of the Arabian Shield. *Geological Society of America Bulletin*, 96(7), 817.
- Stoeser, D. B. & Frost, C. D. (2006). Nd, Pb, Sr, and O isotopic characterisation of Saudi Arabian Shield terranes. *Chemical Geology*, 226(3–4), 163–88. doi: <http://dx.doi.org/10.1016/j.chemgeo.2005.09.019>
- Swart, P. K., Cantrell, D. L., Westphal, H., Handford, C. R., Kendall, C. G., Cantrell, D. L. & Hagerty, R. M. (2005). Origin of Dolomite in the Arab-D Reservoir from the Ghawar Field, Saudi Arabia. *Journal of Sedimentary Research*, 75(3), 476–91. doi: 10.2110/jsr.2005.037
- Terry, R. D., & Chilingar, G. V. (1955). Summary of " Concerning some additional aids in studying sedimentary formations," by MS Shvetsov. *Journal of Sedimentary Research*, 25(3), 229-234.
- Tinker, S. W. (1998). Shelf-to-basin facies distributions and sequence stratigraphy of a steep-rimmed carbonate margin: Capitan depositional system, McKittrick Canyon, New Mexico and Texas. *Journal of Sedimentary Research*, 68(6), 1146–174. doi: 10.1306/d4268923-2b26-11d7-8648000102c1865d

- Tintant, H. (1987). Les nautilus du Jurassique d'Arabie Saoudite. (Jurassic nautiloids of Saudi Arabia). *Geobios, Memoire Special*, 9(0293–843X), 67–159.
- Toland, C. (1994). *Late Mesozoic stromatoporoids: Their use as stratigraphic tools and palaeoenvironmental indicators*. London, UK: Chapman and Hall.
- Trabelsi, A., Ekamba, B., Jameson, J., Schnacke, A., Jamieson, H. & Sykes, M. (2009). *Reservoir rock type classification and variation of reservoir quality in the Arab Formation, Dukhan Field, Qatar*. Paper presented at the International Petroleum Technology Conference, Doha, Qatar.
<http://www.onepetro.org/mslib/app/Preview.do?paperNumber=IPTC-13628-MS&societyCode=IPTC>
- Tracy, W. (1984). Khamis: 'The guide of guides'. *Saudi Aramco World*, 35, 7.
- Haq, B. U., (1988). Fluctuating Mesozoic and Cenozoic sea levels and implications for stratigraphy. [Meeting abstract]. *AAPG Bulletin*, 72(12), 1521.
- Vail, J. R. (1988). Tectonics and evolution of the Proterozoic basement of northeastern Africa. Braunschweig, Germany: Friedrich Vieweg & Sohn.
- Vail, P. R. (1987). Seismic stratigraphy interpretation using sequence stratigraphy: Part 1, Seismic stratigraphy interpretation procedure. *AAPG Studies in Geology*, 27(1), 1–10.
- Vakhrameev, V. A. (1964). *Jurassic and early Cretaceous floras of Eurasia and paleofloristic provinces of this period*. Moscow, Russia: Tr. Geological Institute of Moscow.
- Vakhrameev, V. A. (1987). Climates and the distribution of some gymnosperms in Asia during the Jurassic and Cretaceous. *Review of Palaeobotany and Palynology*, 51(1–3), 205–12. doi: [http://dx.doi.org/10.1016/0034-6667\(87\)90030-3](http://dx.doi.org/10.1016/0034-6667(87)90030-3)
- Vakhrameev, V. A. (1991). *Jurassic and Cretaceous floras and climates of the Earth*. Cambridge, UK: Cambridge University Press.
- Vakhrameev, V. A. (1992). Jurassic and Cretaceous floras and climates of the Earth (English ed.). [Short reviews]. *The Journal of Ecology*, 80(1), 188.
- Valdes, P. J., & Sellwood, B. W. (1992). A palaeoclimate model for the Kimmeridgian. *Palaeogeography, Palaeoclimatology, Palaeoecology*, 95(1), 47-72.

- Valentine, J. W. & Moores, E. M. (1972). Global tectonics and the fossil record. *Journal of Geology*, 167–84.
- Van Buchem, F. S. P., Simmons, M. D., Droste, H. J. & Davies, R. B. (2011). Late Aptian to Turonian stratigraphy of the eastern Arabian Plate: Depositional sequences and lithostratigraphic nomenclature. *Petroleum Geoscience*, 17(3), 211–22. doi: 10.1144/1354-079310-061
- Van Wagoner, J. C. (1995). Overview of sequence stratigraphy of foreland basin deposits: Terminology, summary of papers, and glossary of sequence stratigraphy. *AAPG Memoir*, 64, ix–xxi.
- Van Wagoner, J. C., Mitchum, R. M., Campion, K. M. & Rahmanian, V. D. (1990). Siliciclastic sequence stratigraphy in well logs, cores, and outcrops: Concepts for high-resolution correlation of time and facies. *Methods in Exploration Series*, 7, 55.
- Van Wagoner, J. C., Mitchum, R. M., Jr., Posamentier, H. W. & Vail, P. R. (1987). Seismic stratigraphy interpretation using sequence stratigraphy: Part 2, Key definitions of sequence stratigraphy. *AAPG Studies in Geology*, 27(1), 11–14.
- Van Wagoner, J. C., Posamentier, H. W., Mitchum, R. M., Jr., Vail, P. R., Sarg, J. F., Loutit, T. S. & Hardenbol, J. (1988, September). *An overview of the fundamentals of sequence stratigraphy and key definitions*. Paper presented at the Sea-level Changes: An Integrated Approach, US.
- Vaslet, D. (1990). *Histoire géologique de la bordure occidentale de la plate-forme arabe: Vol. 1, Le Paléozoïque (Anté-Permien supérieur) d'Arabie Saoudite*. (Document, (191), 210). Orléans: Bureau de Recherches Géologiques et Minières.
- Vaslet, D., Al-Muallem, M. S., Maddah, S. S., Brosse, J.-M., Fourniguet, J., Breton, J.-P. and Le Nidre, Y.-M. (Cartographer). (1991). *Explanatory note to the geologic map of the Ar Riyadh Quadrangel, Kingdom of Saudi Arabia*. [Geoscience map GM-121, sheet 24I].
- Voelker, J. (2005). *A reservoir characterisation of Arab-D super-k as a discrete fracture network flow system, Ghawar Field, Saudi Arabia*. (Doctoral dissertation). Stanford University, Stanford, US.
- Von Raumer, J. F. & Stampfli, G. M. (2001). Early Paleozoic events at the Gondwana

- margin. [Abstracts with programs]. *Geological Society of America*, 33(6), 206.
- Walkden, G. M. & de Matos, J. E. (2000). 'Tuning' high-frequency cyclic carbonate platform successions using omission surfaces: Lower Jurassic of the UAE and Oman. [Special publication]. *Society for Sedimentary Geology*, 69, 37–52.
- Walker, R. G. (1984). Channel-levee complexes and submarine fans: An example from Wheeler Gorge, California. [Abstracts]. *SEPM Midyear Meeting*, 1, 84–5.
- Walker, R. G. (1985a). Comparison of shelf environments and deep basin turbidite systems. *SEPM Short Course*, 13, 465–502.
- Walker, R. G. (1985b). Mudstones and thin-bedded turbidites associated with the Upper Cretaceous Wheeler Gorge conglomerates, California: A possible channel-levee complex. *Journal of Sedimentary Research*, 55(2), 279–290. doi: 10.1306/212f869d-2b24-11d7-8648000102c1865d
- Walker, R. G. & James, N. P. (1992). *Facies models: Response to sea level change*. St. Johns, Newfoundland: Geological Association of Canada.
- Weber, L.J., S.J. Albertin, D. J. Lehrmann, 1997, Sequence stratigraphic zonation of the Arab-D: pilot study, northern Hawiyah, Ghawar Field, Saudi Arabia, Project EPR-96-5.
- Weidlich, O. & Bernecker, M. (2003). Supersequence and composite sequence carbonate platform growth: Permian and Triassic outcrop data of the Arabian platform and Neo-Tethys. *Sedimentary Geology*, 158(1–2), 87.
- Weissert, H. & Erba, E. (2004). Volcanism, CO₂ and palaeoclimate: A Late Jurassic–Early Cretaceous carbon and oxygen isotope record. *Journal of the Geological Society*, 161(4), 695–702.
- Weissert, H. & Mohr, H. (1996). Late Jurassic climate and its impact on carbon cycling. *Palaeogeography, Palaeoclimatology, Palaeoecology*, 122(1–4), 27–43.
- Wender, L. E., Bryant, J. W., Dickens, M. F., Neville, A. S. & Al-Moqbel, A. M. (1998). Pre-Khuff (Permian) hydrocarbon geology of the Ghawar area, eastern Saudi Arabia. *GeoArabia (Manama)*, 3(1), 167–8.
- Wilhelms, A., Carpentier, B. & Huc, A. Y. (1994). New methods to detect tar mats in petroleum reservoirs. *Journal of Petroleum Science and Engineering*, 12(2),

147–55. doi: 10.1016/0920-4105(94)90014-0

- Williams, M., Haywood, A. M., Taylor, S. P., Valdes, P. J., Sellwood, B. W. & Hillenbrand, C. D. (2005). Evaluating the efficacy of planktonic foraminifer calcite $\delta^{18}\text{O}$ data for sea surface temperature reconstruction for the Late Miocene. *Geobios*, 38(6), 843–63.
- Wilson, A. O. (1981, January 1). *Jurassic Arab-C and -D carbonate petroleum reservoirs, Qatif Field, Saudi Arabia*. Paper presented at the Proceedings of the Society of Petroleum Engineers Middle East Technical Conference, Dallas, US.
- Wilson, A. O. (1985). *Depositional and diagenetic facies in the Jurassic Arab-C and -D reservoirs, Qatif Field, Saudi Arabia*. New York, NY: Springer-Verlag.
- Wilson, A. O. (1987). In-situ formation of petroleum in oolites—II: A case study of the Arab Formation oolite reservoirs: Discussion. *Journal of Petroleum Geology*, 10(2), 227–8.
- Wilson, E. N. & Sahikh Ali, M. S. (1991). Evaluation of Jurassic Arab-D reservoir quality in low-relief traps in Qatar. *Proceedings of the Middle East Oil Show*, 7, 925–32.
- Wilson, J. (1975). *Carbonate facies in geologic history*. New York: Springer-Verlag.
- Wood, R. (2008). The evolution of reefs. [Abstract]. *International Geological Congress Abstracts*, 33.
- Wood, R. A. (1987). Biology and revised systematics of some late Mesozoic stromatoporoids. *Special Papers in Palaeontology*, 37, 3789.
- Wood, R. A. (1995). The changing biology of reef-building. *Palaios*, 10(6), 517–29.
- Wood, R. A. (1999). *Reef Evolution*. Oxford, UK: Oxford University Press.
- Wood, R. A. (2001). Are reefs and mud mounds really so different? *Sedimentary Geology*, 145(3–4), 161–71. doi: 10.1016/s0037-0738(01)00146-4
- Wood, R. A. (2007). Microbes and Reefs. [Annual meeting abstracts]. *American Association of Petroleum Geologists*, 151.
- Worth, R. F. (2008, July 1). Khurais oil field journal: Saudi oil project brings skepticism to the surface. *The New York Times*.
- Xiao, H.-B., Payne, B. A., Neville, A. & Gregory, G. (2003). An overview of Ghawar structure as revealed by Ghawar SuperCube. [Annual meeting expanded

- abstracts]. *American Association of Petroleum Geologists*, 12, 185.
- Yao, J. (1992). Global Jurassic floras and climate. [Special Publication]. *The Paleontological Society*, 6, 320.
- Zeidan, R. H. (1994, January 1). *Dolomitization and the development of secondary porosity in Arabian carbonate rocks*. Paper presented at the Middle East Geoscience Conference, Manama, Bahrain.
- Ziegler, A. D., Sheffield, J., Maurer, E. P., Nijssen, B., Wood, E. F., Lettenmaier, D. P. (2003). Detection of intensification in global- and continental-scale hydrological cycles: Temporal scale of evaluation. *Journal of Climate*, 16(3), 535-547.
- Ziegler, A. M., Eshel, G., Rees, P. M. A., Rothfus, T., Rowley, D. & Sunderlin, D. (2007). Tracing the tropics across land and sea: Permian to present. *Lethaia*, 36(3), 227–54.
- Ziegler, A. M., Raymond, A. L., Gierlowski, T. C., Horrell, M. A., Rowley, D. B. & Lottes, A. L. (1987). Coal, climate and terrestrial productivity: The present and Early Cretaceous compared. In A. C. Scott (Ed.), *Coal and coal-bearing strata: Recent advances*. Geological Society, London, Special Publications, 32, 25–49.
- Ziegler, A. M., & Rowley, D. B. In Crowley T., Burke K. (Eds.), *The vanishing record of epeiric seas, with emphasis on the late cretaceous "hudson seaway"* Oxford University Press, Inc., 2001 Evans Rd. Cary NC 27513 USA, URL:<http://www.oup-usa.org>].
- Ziegler, M. A. (1982). *Saudi Aramco miscellaneous report* (Unpublished). Dhahran, Saudi Arabia.
- Ziegler, M. A. (2001). Late Permian to Holocene paleofacies evolution of the Arabian Plate and its hydrocarbon occurrences. *GeoArabia (Manama)*, 6(3), 445–504.
- Ziegler, P. A. (1988). Evolution of the Arctic-North Atlantic and the Western Tethys: A visual presentation of a series of paleogeographic-paleotectonic maps. *American Association of Petroleum Geologists Memoir 43*, 164–96.

Every reasonable effort has been made to acknowledge the owners of copyright material. I would be pleased to hear from any copyright owner who has been omitted or incorrectly acknowledged.

Appendices

Appendix A: Supervisor and Co-author Statement

To whom it may concern,

I, Lindsay B. Collins have contributed as supervisor, technical advisor and mentor to the three research papers listed below as part of a PhD thesis prepared by Saad Fahd Al-Awwad for Curtin University of Technology. I am listed as co-author of these papers in my capacity as a PhD supervisor.

List of papers:

Al-Awwad, S. & Collins, L. B. (2013a). Arabian carbonate reservoirs: A depositional model of the Arab-D reservoir in Khurais Field, Saudi Arabia. *AAPG Bulletin*, 97(7), 1099–1119.

Al-Awwad, S. & Collins, L. B. (in-review). Stacked high-frequency carbonate reservoir sequences in the Arab-D, Khurais Field, Saudi Arabia. *Marine and Petroleum Geology*.

Al-Awwad, S. & Collins, L. B. (2013b). Carbonate platform scale correlation of stacked high frequency sequences in the Arab-D Reservoir, Saudi Arabia. *Sedimentary Geology*, 294, 205–2018.

The papers constitute part of the PhD thesis and the main author is Saad Fahd Al-Awwad.

Supervisor and Co-author Signature:

Professor Lindsay B. Collins

Candidate Signature:

Saad F. Al-Awwad

Appendix B: AAPG Bulletin Permission to Reprint “Arabian Carbonate Reservoirs: A Depositional Model of the Arab-D Reservoir in Khurais Field, Saudi Arabia”

PERMISSION TO USE COPYRIGHT MATERIAL AS SPECIFIED BELOW:

Arabian Carbonate Reservoirs: A Depositional Model of the Arab-D, Khurais Field, Saudi Arabia

by Saad F. AlAwwad and Lindsay B. Collins

in the BLTN12-103 AAPG Bulletin

I hereby give permission for Saad Fahd A. AlAwwad to include the above-mentioned material(s) in his/her higher degree thesis for the Curtin University of Technology, and to communicate this material via the Australasian Digital Thesis Program. This permission is granted on a non-exclusive basis and for an indefinite period.

I confirm that I am the copyright owner of the specified material.

Signed: *Andrea Sharrer*

Name: *Andrea Sharrer*

Position: *AAPG Bulletin Technical Editor*

Date: *4/1/13*

Please return signed form to

Saad A-Awwad
Saad.shamary@gmail.com
30 A Sussex St.
East Victoria Park
Perth, WA, 6101
Australia

**Appendix C: Arabian Carbonate Reservoirs: A Depositional Model of
the Arab-D Reservoir in Khurais Field, Saudi Arabia**

Arabian carbonate reservoirs: A depositional model of the Arab-D reservoir in Khurais field, Saudi Arabia

Saad F. Al-Awwad and Lindsay B. Collins

ABSTRACT

The Upper Jurassic Arab Formation in the Arabian Peninsula, the most prolific oil-bearing interval of the world, is a succession of interbedded thick carbonates and evaporites that are defined stratigraphically upsection as the Arab-D, Arab-C, Arab-B, and Arab-A. The Arab-D reservoir is the main reservoir in Khurais field, one of the largest onshore oil fields of the Kingdom of Saudi Arabia.

In Khurais field, the Arab-D reservoir is composed of the overlying evaporitic Arab-D Member of the Arab Formation and the underlying upper part of the Jubaila Formation. It contains 11 lithofacies, listed from deepest to shallowest: (1) hardground-capped skeletal wackestone and lime mudstone; (2) intraclast floatstone and rudstone; (3) pelletal wackestone and packstone; (4) stromatoporoid wackestone, packstone, and floatstone; (5) *Cladocoropsis* wackestone, packstone, and floatstone; (6) *Clypeina* and *Thaumatoporella* wackestone and packstone; (7) peloidal packstone and grainstone; (8) ooid grainstone; (9) crypt-microbial laminites; (10) evaporites; and (11) stratigraphically reoccurring dolomite.

The Arab-D reservoir lithofacies succession represents shallowing-upward deposition, which, from deepest to shallowest, reflects the following depositional environments: offshore submarine turbidity fans (lithofacies 1 and 2); lower shoreface settings (lithofacies 3); stromatoporoid reef (lithofacies 4); lagoon (lithofacies 5 and 6); shallow subtidal settings (lithofacies 7 and 8); peritidal settings (lithofacies 9); and sabkhas and salinas (lithofacies 10). The depositional succession of the reservoir represents a prograding, shallow-marine,

AUTHORS

SAAD F. AL-AWWAD ~ Saudi Aramco, Dhahran, Saudi Arabia; present address: Curtin University of Technology, Perth, Western Australia, 6845 Australia; saad.shamary@gmail.com

Saad Al-Awwad has been with Saudi Aramco since 2003 where he has worked as a reserves geologist specializing in carbonate sedimentology and stratigraphy. Al-Awwad's work involves reservoir characterization and sequence stratigraphy studies in various carbonate reservoirs in Saudi Arabia. He has a B.Sc. degree in geology from the University of Kansas, Lawrence, Kansas.

LINDSAY B. COLLINS ~ Curtin University of Technology, Perth, Western Australia, Australia; l.collins@curtin.edu.au

Lindsay Collins has worked in petroleum exploration specializing in carbonate sedimentation of both warm and cool water carbonates. His recently published work is on stromatolite systems and fabrics in Shark Bay. He has been chief scientist aboard the *RV Franklin*, a national research vessel. He is a member of the Australia–New Zealand Science Council for the Integrated Ocean Drilling Program.

ACKNOWLEDGEMENTS

We thank Saudi Aramco for granting permission to publish this study. We also thank Aus Al Tawil of Saudi Aramco for his continuous support and tireless commitment. We thank Luis Pomar, University de les Illes Balears, Spain; Robert Lindsay and Wyn Hughes of Saudi Aramco; Langhorne Smith, New York State Museum, United States; and Jerry Lucia, University of Texas at Austin, United States, for the comments and critique that were as insightful as they were essential.

The AAPG Editor thanks the following reviewers for their work on this paper: Robert F. Lindsay and Jerry Lucia.

DATASHARE 48

An unbroken version of Figure 3 is available as Datashare 48 at www.aapg.org/datashare.

Copyright ©2013. The American Association of Petroleum Geologists. All rights reserved.

Manuscript received June 29, 2012; provisional acceptance October 5, 2012; revised manuscript received October 12, 2012; final acceptance November 5, 2012.

DOI:10.1306/11051212103

reef-rimmed carbonate shelf that was subjected to common storm abrasion, which triggered turbidites.

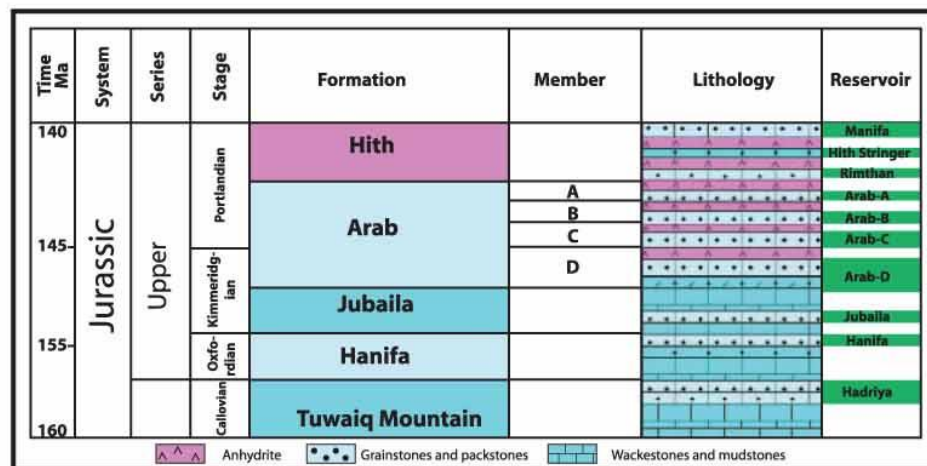
INTRODUCTION AND HISTORY

The Upper Jurassic Arab Formation, the most prolific oil-bearing interval of the world (Barger, 1984; Sorkhabi, 2008), is composed of a series of excellent reservoir quality carbonates, namely the Arab-D, C, B, and A members. Each member is capped by a nonpermeable anhydrite layer, whereas the uppermost member is capped by the Hith Formation anhydrite (Figure 1). Previous work done on the Arab-D reservoir focused primarily on Ghawar field, and different depositional models were developed. Mitchell et al. (1988) divided the Arab-D carbonates into skeletal-oolitic limestones and dolomites, *Cladocoropsis* limestones and dolomites, stromatoporoid–red algae–coral limestones, bivalve-coated grain-intraclast limestones, micritic limestones and dolomites, and diagenetic dolomite, in addition to the sealing anhydrite. Lindsay et al. (2006) used the same classification scheme of Mitchell et al. (1988). Meyer and Price (1993) slightly modified Mitchell et al.’s (1988) lithofacies and listed the following types: micritic, bivalve-coated grain-intraclast, stromatoporoid, burrowed skeletal-peloidal, *Cladocoropsis*, fragmented *Cladocoropsis*, foraminiferal, mixed skeletal-peloidal, oolite, and anhydrite. Handford et al. (2002) modified

Mitchell et al.’s (1988) classification scheme using Dunham’s (1962) and Embry and Klovan’s (1971) textures and listed the following lithofacies: lime mudstone-wackestone, burrowed skeletal-peloidal wackestone-packstone, intraclast rudstone and oncoid rudstone, coral stromatoporoid wackestone-packstone to boundstone and floatstone, burrowed to stratified *Cladocoropsis* wackestone grainstone and boundstone (bafflestone), stratified foraminiferal-peloid packstone-grainstone, ooid-coated–grain packstone and grainstone, evaporite association of peloidal-ostracod dolowackestone-packstone gastropod dolopackstone and dolomudstone, paleosol breccias and rooted wackestones, bedded nodular to massive anhydrite.

In 1957, the Arab-D oil was discovered in the second largest onshore oil field of Saudi Arabia, Khurais field, using surface and gravity mapping (Figure 2A) (Al-Mulhim et al., 2010). Further delineation drilling proved that the Qirdi field, discovered south of Khurais in 1973, is also part of the huge Khurais oil accumulation. The field occupies an asymmetric northwest-southeast–trending anticline with 2° of dip on its eastern flank and 8.7° of dip on its western flank (Figure 2A) (Al-Afalge et al., 2002; Net Resources International, 2011). In the summer of 2009, Saudi Aramco successfully completed the largest oil expansion project in history, bringing to production a nationally significant rate from Khurais and adjacent satellite fields in what became known as the Khurais Mega Project (Al-Mulhim et al., 2010; Mouawad, 2010).

Figure 1. Jurassic reservoir stratigraphy and lithology of Saudi Arabia. No biostratigraphic control on the age of the Arab and Hith Formations exists (Hughes, 2004). Note that the Arab-D reservoir extends from the carbonates of the Arab-D Member of the Arab Formation to the upper part of Jubaila Formation (modified from Powers, 1968).



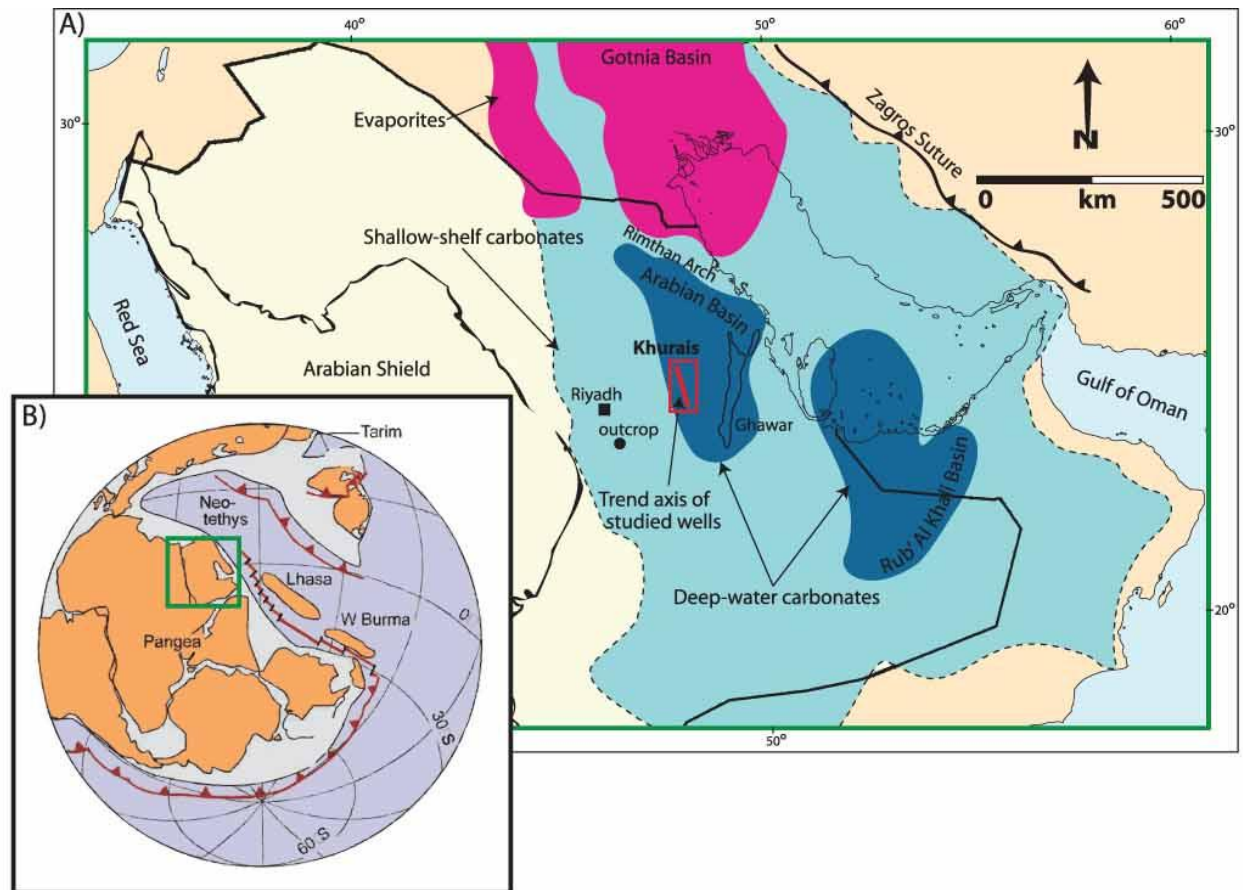


Figure 2. (A) Location map of Khurais field. The trend axis of studied Arab-D cores is shown by the red line. The dark blue areas depict intrashelf basins where deposition of deep-water carbonates occurred in the Late Jurassic. The outlined light blue area depicts shallow-shelf carbonate deposition. Note the location of Upper Jurassic outcrops south of the capital Riyadh. (B) Image shows Li and Powell's (2001) paleogeographic configuration during the Jurassic, with the Arabian plate position enclosed in the green square. Orange, pale blue, and purple depict emergent continents above the present sea level, oceanic areas, and mafic volcanic rocks, respectively. Note that the location of the paleoequator is controversial (Stampfli et al., 2001; Golonka 2002). Modified from Ziegler (2001), and Li and Powell (2001).

This article is the first to address the sedimentology of the Arab-D in the Khurais field. The article focuses on the analysis of 32 cored Khurais wells and more than 500 thin sections and proposes a different depositional model to currently accepted models. The study was conducted at Saudi Aramco's Exploration Core Laboratories and Curtin University. The core from the Aramco HKHK Khurais well (coded name) has been chosen as a representative example because of its substantial vertical coverage (Figure 3) and the continuity of its lithofacies across the field. The results of this study provide evidence that the Arab-D is a prograding, upward-shallowing reservoir, and this article presents a

new depositional model that can be used in predicting the architectural heterogeneities of the reservoir lithofacies.

REGIONAL SETTING

Approximately 640 to 620 Ma, the Amar collision between the Rayn plate and the Arabian-Nubian craton created a north-trending horst-graben system on the Precambrian basement east of the Arabian Shield (a complex of Precambrian igneous and metamorphic rocks; Figure 2A; Blasband et al., 2000). This fault system acted as an architectural

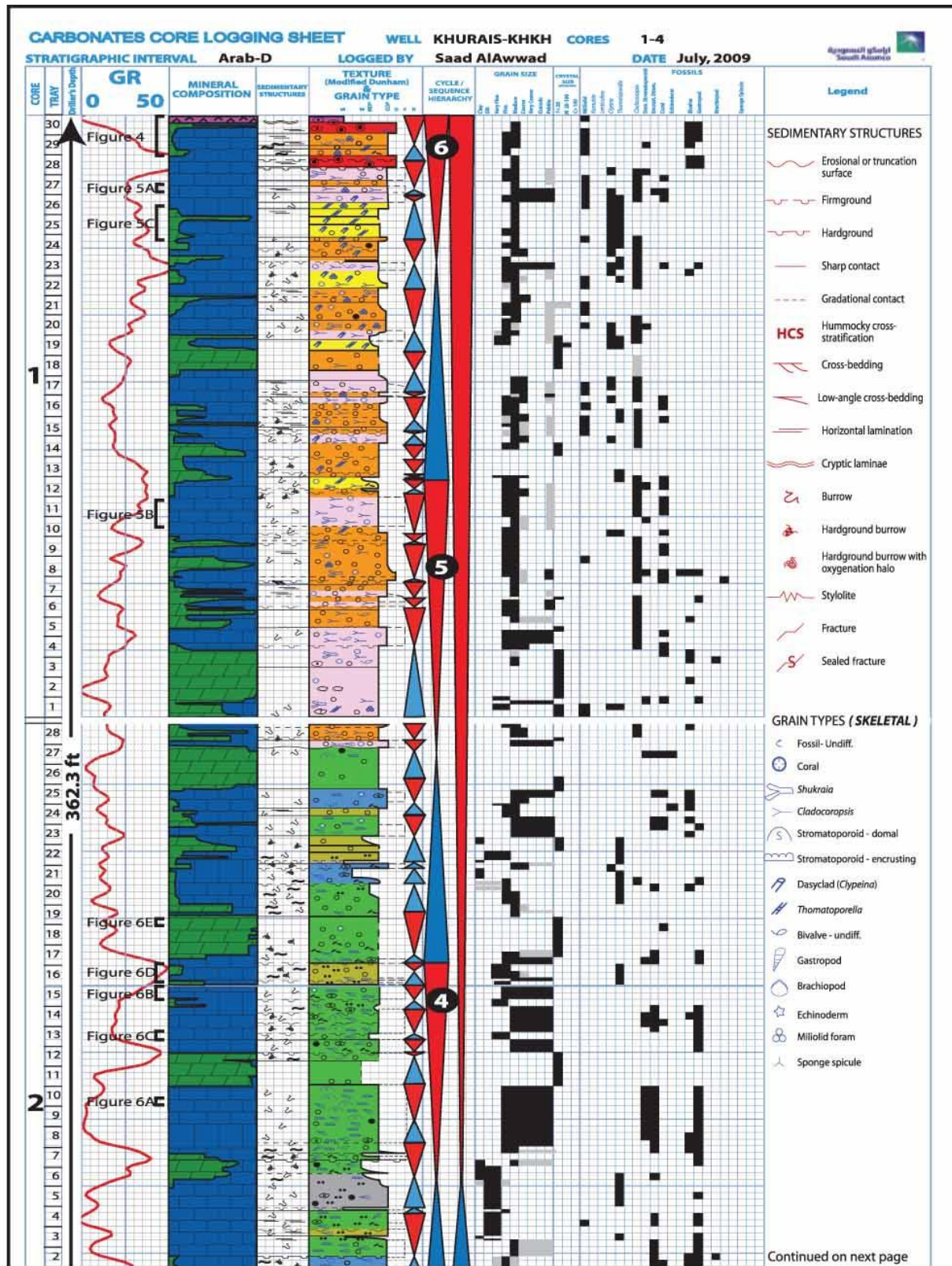
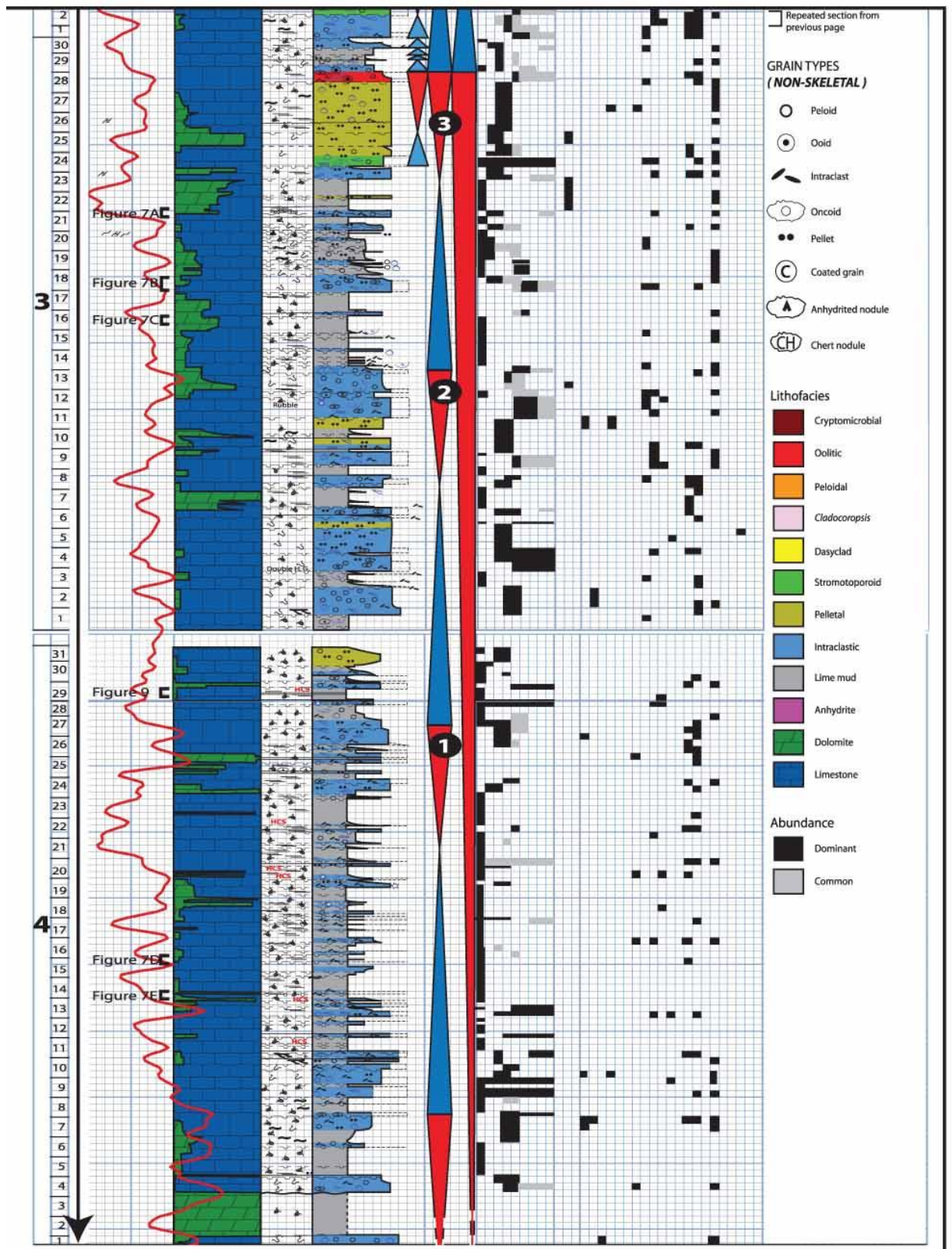


Figure 3. Characterization of Arab-D reservoir core, Aramco KHKH Khurais, Kurais field. Note that only high frequency sequences are picked in the monotonously interbedded lower part of the reservoir based on upward thickness increase of the intraclastic beds (see text for more details).

S



mold that controlled subsequent deposition and shaped subsequent structures, including the Khurais field anticline (Figure 2A) (Ayres et al., 1982; Al-Husseini, 2000; Konert et al., 2001; Al-Mulhim et al., 2010). During the late Paleozoic, the Hercynian orogeny event rotated the Arabian plate 90° counterclockwise, uplifted central Arabia, tilted it toward the east, and eroded it. Following the Hercynian orogeny event, the Neotethys commenced rifting and spreading during the Late Permian along the Zagros suture and Gulf of Oman (Figure 2A, B), creating a passive margin with Arabia (Powers et al., 1966; Ziegler, 2001). The Early Jurassic witnessed the opening of the eastern Mediterranean, which resulted in another passive margin development along the northern edge of Arabia. As a result of this Early Jurassic development, a vast shallow-marine shelf occupied most of the Arabian Peninsula, possibly extending all the way to the present-day Arabian Shield, and dominated the plate with shallow shelf carbonate and evaporite deposition (Murriss, 1980; Le Nindre et al., 1990; Enay, 1993). Epeirogenic downwarp during the Middle Jurassic led to the development of four intrashelf basins on the Arabian craton, namely, the Rub' Al-Khali, the Ras al Khaimah, the Arabian, and the Gotnia Basins, the latter two separated by the Rimthan arch (Figure 2A) (Murriss, 1980; Alsharhan and Kendall, 1986; Ziegler, 2001). Organic rich, anoxic shales (Hanifa and Tuwaiq Mountain Formations; Figure 1) were deposited in the intrashelf basins and later sourced the oils of the Arab reservoirs (Ayres et al., 1982; Droste, 1990; Ziegler, 2001). The intrashelf basins provided antecedent paleotopography that dictated the later deposition of the Jubaila, Arab, and Hith Formations, as evident in changes in lithofacies, thickness, and composition of these formations over the intrashelf basins (Ziegler, 2001; Lindsay et al., 2006). The source-reservoir-seal enclosure requirements are spectacularly met in these intrashelf basins, and the Arabian oil fields are concentrated around them (Ziegler, 2001; Lindsay et al., 2006). During the Late Jurassic, central Arabia remained stable, and carbonates progressively filled the intrashelf basins with repetitive cycles of shoaling-upward carbonate sediments that were capped with evaporitic flat fa-

cies, whereas the African-Arabian and Indian plates rifted along southern Oman, creating another passive margin to the south of Arabia. The Neotethys closing did not commence until the Late Cretaceous, causing the obduction of the Oman ophiolites during the Arabian-Eurasian plates compression (Alsharhan and Kendall, 1986; Ziegler, 2001).

LITHOFACIES

Detailed (4-in. [10-cm]–scaled) analysis of the Arab-D reservoir from 32 Khurais cores has resulted in recognition of the following 11 lithofacies (Figure 3):

1. Anhydrite lithofacies
2. Oolitic-skeletal-cryptomicrobial laminated wackestones to grainstones (referred to as cryptomicrobial lithofacies hereafter)
3. Skeletal-oolitic grainstones and grain-dominated packstone (oolitic lithofacies)
4. Skeletal-peloidal mud-dominated packstones to grainstones (peloidal lithofacies)
5. *Thaumatoporella*–*Clypeina* wackestones and mud-dominated packstones (dasyclad lithofacies)
6. Skeletal-peloidal-*Cladocoropsis* wackestones to floatstones (*Cladocoropsis* lithofacies)
7. Skeletal-stromatoporoid wackestones to floatstones (stromatoporoid lithofacies)
8. Skeletal-pelletal wackestones to grain-dominated packstones (pelletal lithofacies)
9. Skeletal-oncolitic-intraclastic mud-dominated packstones to floatstones (intraclastic lithofacies)
10. Skeletal wackestones and lime mudstones (lime mud lithofacies)
11. Dolomite lithofacies

Anhydrite Lithofacies

The anhydrite lithofacies (Figure 4A, B) provides the nonporous vertical seal for the Arab-D reservoir, and although rarely cored, it can be easily identified from its conspicuous log character. The anhydrite contact with underlying carbonates varies from gradational to sharp. Typically, at gradational

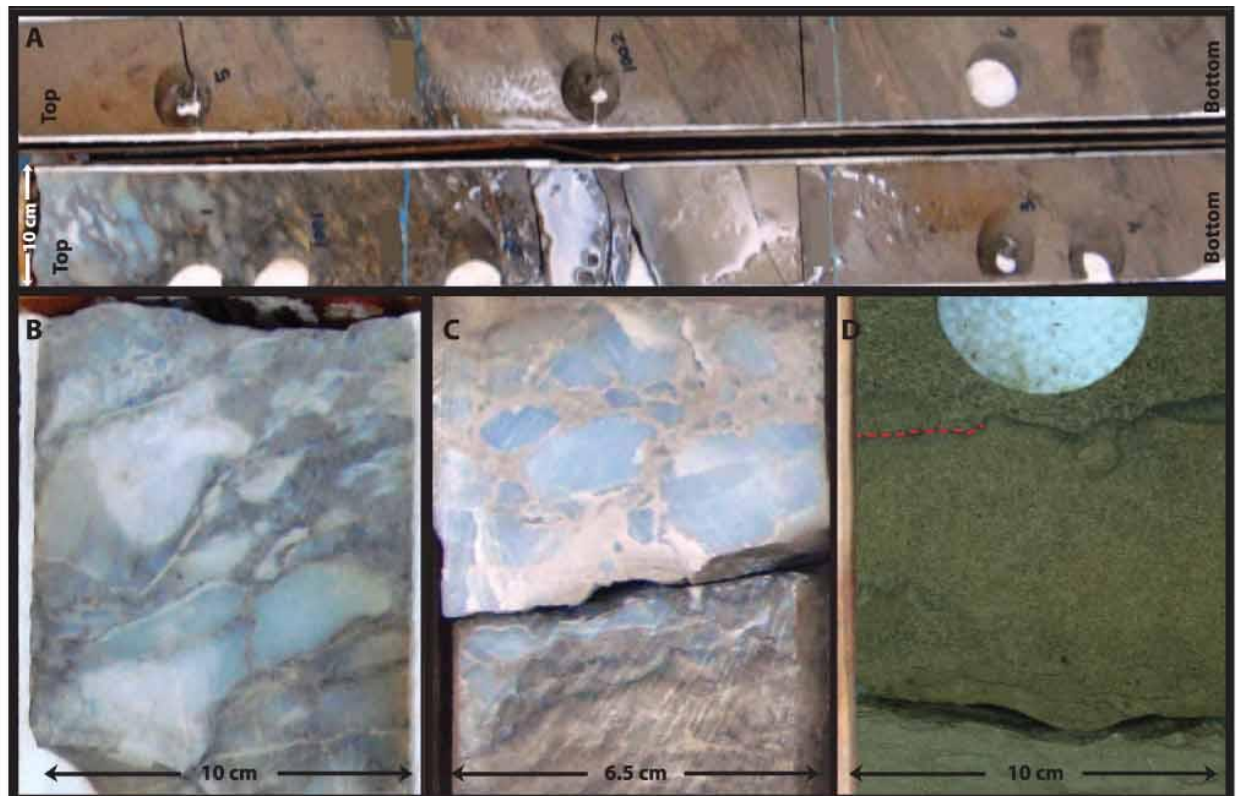


Figure 4. (A) The upper two trays of Aramco HKHK Khurais core, showing a continuum through the anhydrite, cryptomicrobial, and oolitic lithofacies. (B) Anhydrite. (C) Millimeter-scale cryptomicrobial laminae below the anhydrite. (D) Oolitic lithofacies with well-sorted and well-rounded ooids and a hardground marked in red. Photographs are located on the Aramco HKHK Khurais core description, Figure 3.

boundaries, anhydrites start out as displacive nodules that grow at the expense of the limestone and dolomites, increase upward into bedded nodular fabrics, and ultimately become (apparently) massive.

The anhydrite lithofacies is interbedded with several dolomite stringers, where the lowermost of these, which was described in a few Khurais cores, ranges in thickness from 1 to 4 ft (0.3–1.2 m) and contains fabric-mimetic to semimimetic dolomites of what appears to have been originally oolitic grainstones.

A substantial thickness of anhydrite covers the Arab-D reservoir in Khurais field and provides an excellent vertical seal.

Cryptomicrobial Lithofacies

The oolitic-bivalve-cryptomicrobial laminated mudstone to grainstone, the cryptomicrobial lithofacies

(Figure 4C), caps the reservoir just below the anhydrite seal. The faunal composition is restricted and consists of cerithiid gastropods and bivalves. Beds are thin, approximately 1 ft (0.3 m) thick, commonly with gradational upper and lower contacts. The microbial laminae are millimeters in scale and are undulatory and/or domed. Moldic porosity is the most common porosity type in this lithofacies.

Oolitic Lithofacies

The skeletal-oolitic grainstone and grain-dominated packstone, the oolitic lithofacies (Figure 4D), is present in the upper part of the reservoir and is composed of very well-sorted, well-rounded, medium-grained ooids, bivalves, and foraminifera. The beds are commonly 0.5 to 1 ft (0.2–0.3 m) thick and amalgamate into 2- to 3-ft (0.6–1-m)-thick intervals below the cryptomicrobial lithofacies. Sharp

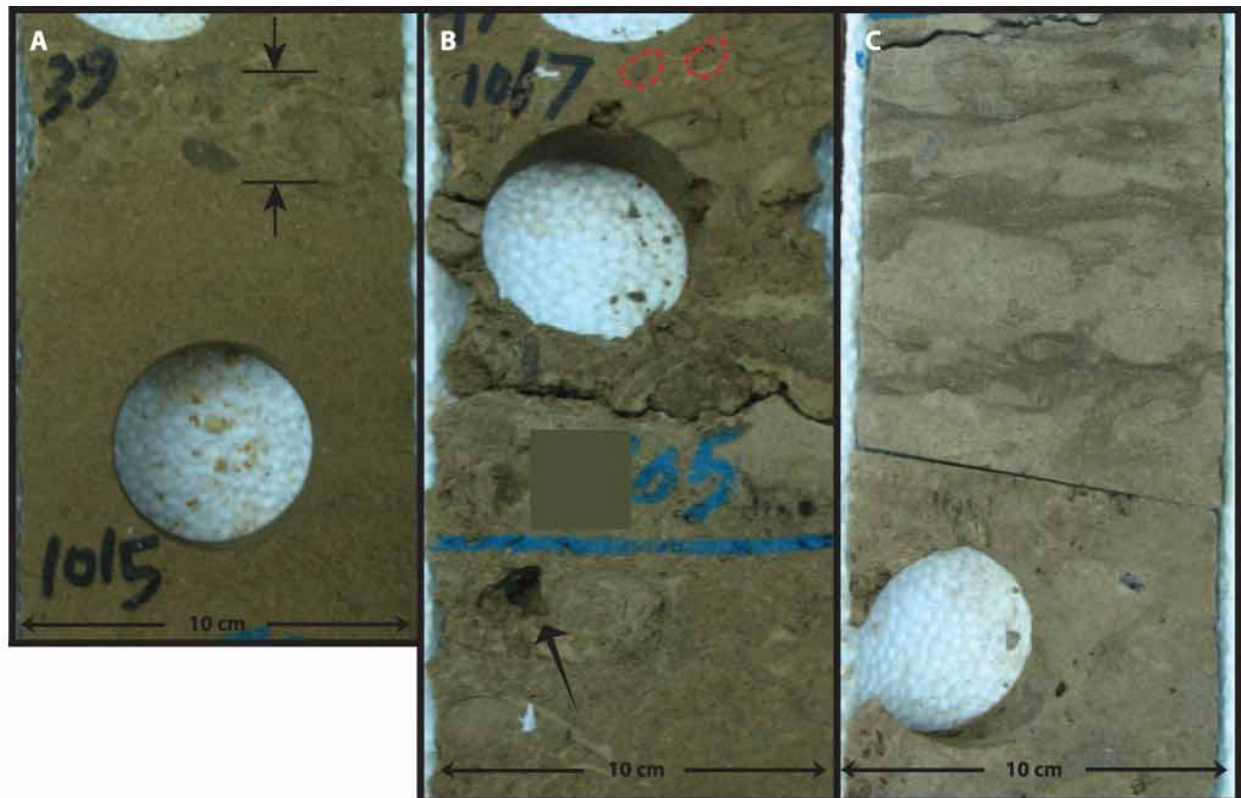


Figure 5. (A) Peloidal lithofacies. The two arrows bracket an interbedded *Cladocoropsis* rudstone; Aramco HKKF Khurais (coded name). (B) *Cladocoropsis* lithofacies. Cross sectional cuts of *Cladocoropsis* stems are enclosed in dashed red ovals. Note the poor sorting and coral dissolution causing vugular porosity (black arrow); Aramco HKKF Khurais. (C) Dasyclad lithofacies. Note the heavy bioturbation; Aramco HKKF Khurais. Photographs are projected from correlated lithofacies onto the Aramco HKHK Khurais core description, Figure 3.

hardground or firmground contacts characterize this lithofacies. High- and low-angle cross-stratification and horizontal laminations are the dominant sedimentary structures present. Porosity types are mostly interparticle and moldic.

Peloidal Lithofacies

The peloidal lithofacies (Figure 5A) is located in the upper part of the reservoir, stratigraphically beneath the oolitic lithofacies, and is composed of well-sorted, well-rounded to rounded, fine to medium-grained skeletal-peloidal mud-dominated packstone, grain-dominated packstone, and grainstone. Bivalve fragments, fragmented micritized *Cladocoropsis*, and foraminifera are among the components present in this lithofacies. Bed thickness ranges from 1 to

6 ft (0.3–1.8 m) with both sharp and gradational boundaries. In addition to massive unstratified beds, horizontal lamination, low-angle cross-stratification, bioturbation, and graded bedding with muddier caps characterize this lithofacies. Porosity is mostly interparticle with some moldic and intraparticle pores.

Cladocoropsis Lithofacies

The skeletal-peloidal-*Cladocoropsis* wackestone to floatstone, the *Cladocoropsis* lithofacies (Figure 5B), is present in the upper part of the Arab-D reservoir. It is located below, and mixed with, the peloidal lithofacies. It is composed of nodular and dendroid *Cladocoropsis* (calcified sponge) mud-dominated packstones and wackestones in addition to floatstones

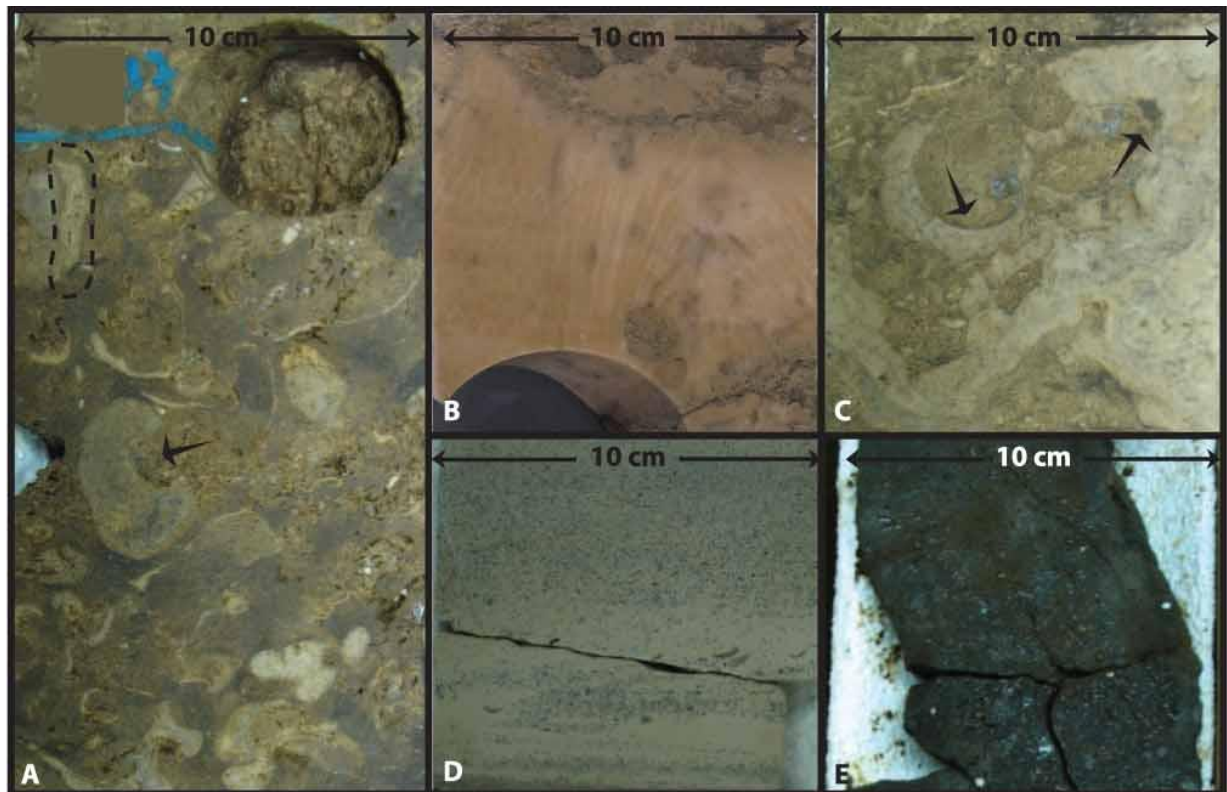


Figure 6. (A) Stromatoporoid lithofacies, domal (arrow) and laminar (oval) forms. Note the leaching mostly of corals, making vugular porosity (shown by the rugged breakage surface of the plug cut (upper right corner); Aramco HKHK Khurais. (B) Coral in stromatoporoid lithofacies; Aramco NAN Khurais (coded name). (C) Gastropods encrusted by stromatoporoids (arrows) in stromatoporoid lithofacies; Aramco HKHK Khurais. (D) Pelletal lithofacies showing dark-colored silt and very fine sand pellets; Aramco HKKF Khurais. (E) Dolomite lithofacies, black because of oil staining; Aramco HKHK Khurais. Photographs are located or projected from correlated lithofacies onto the Aramco HKHK Khurais core description, Figure 3.

and rudstones with mud-dominated packstone to grain-dominated packstone matrices. Bed thickness ranges from 1 to 5 ft (0.3–1.5 m), and contacts can be gradational or sharp. The components of this lithofacies are poorly sorted and subrounded and consist of *Cladocoropsis* stems (broken but unfragmented; Figure 5B), *Cladocoropsis* fragments (see description of the peloidal lithofacies above), *Shuqraia* (a *Cladocoropsis* relative), foraminifera, corals (Figure 5B), bivalves, peloids, *Clypeina* (dasyclad alga), and *Thaumatoporella* (considered to be related to the calcareous green algae by de Castro [1990]). Bioturbation, horizontal laminations, and firmgrounds are the dominant sedimentary structures present in this lithofacies. Porosity types in order of abundance are interparticle, intraparticle, moldic, and vugular.

Dasyclad Lithofacies

The *Thaumatoporella-Clypeina* wackestone and mud-dominated packstone, the dasyclad lithofacies (Figure 5C), is intermixed with the *Cladocoropsis* and the peloidal lithofacies but is limited stratigraphically to the interval above the stromatoporoid lithofacies. Components present in this lithofacies are *Clypeina*, predominantly miliolid foraminifera, *Kurnubia*, *Thaumatoporella*, bivalves, and peloids. This lithofacies forms 1- to 3-ft (0.3–0.9-m)-thick beds, gradationally caps the stromatoporoid and *Cladocoropsis* lithofacies, and is capped by sharp or gradational upper contacts. Sedimentary structures present in this lithofacies include bioturbation, wispy laminations, and some firmgrounds that, when present, commonly cap this

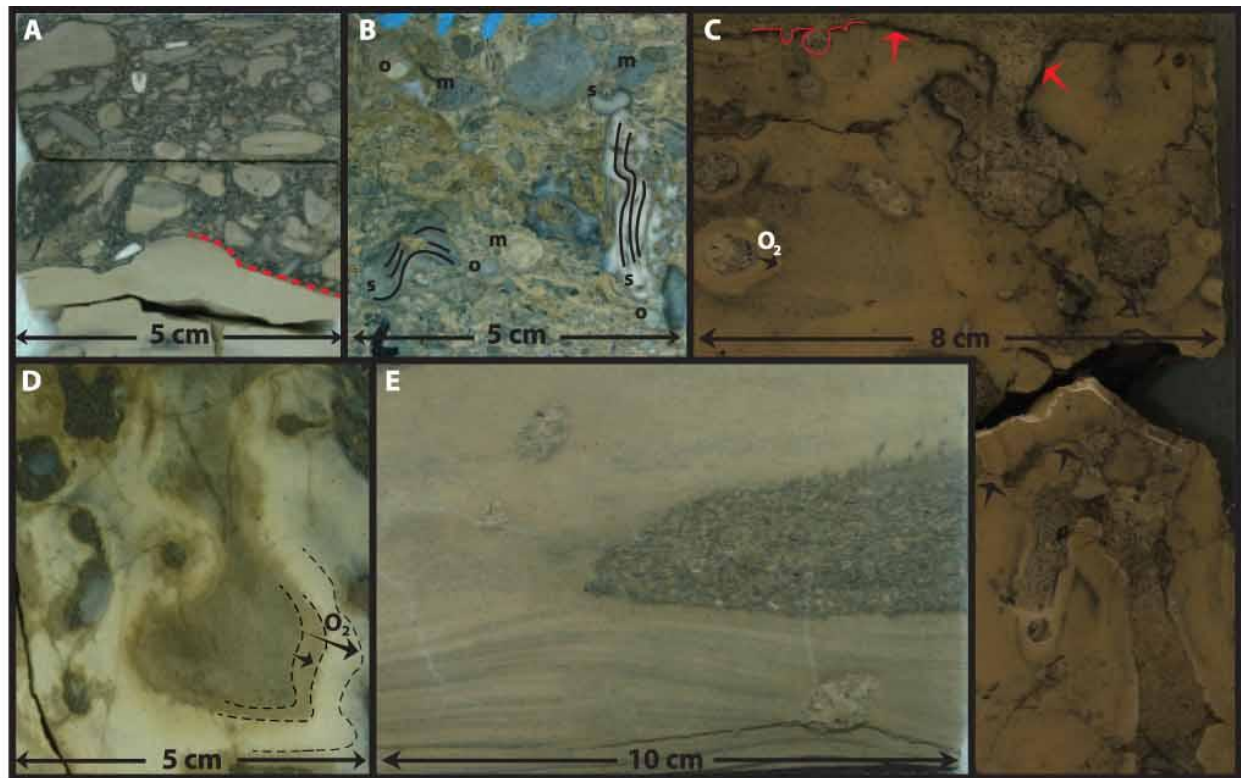


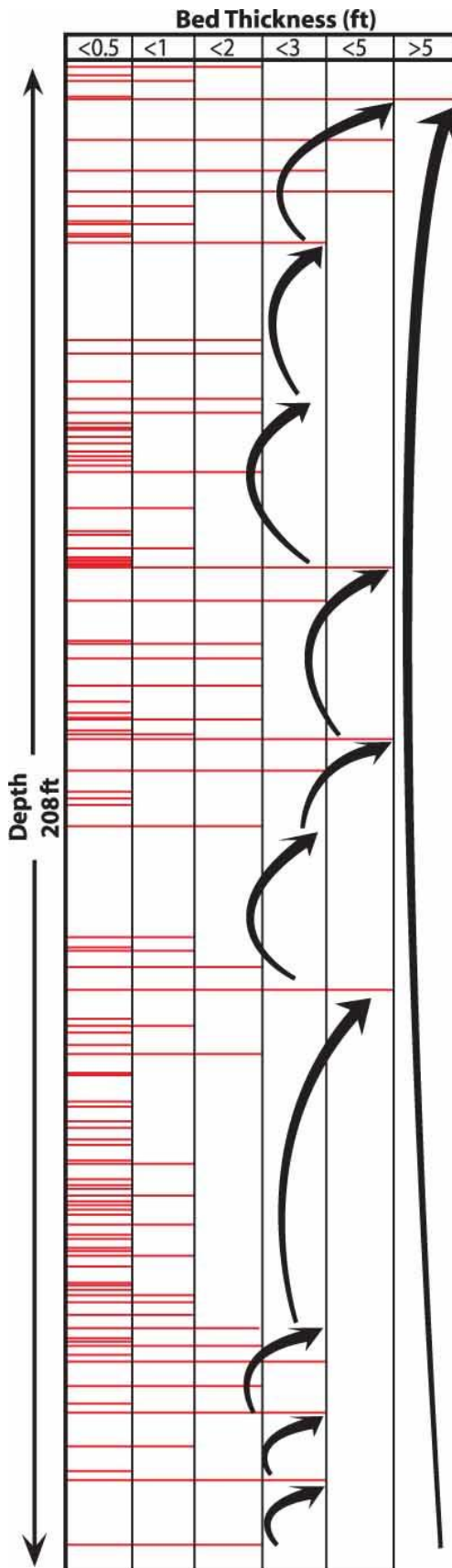
Figure 7. (A) Intraclastic and lime mud lithofacies separated by a scour mark (red line); Aramco HKKF Khurais. (B) Different components of the intraclastic lithofacies, stromatoporoids (s)—black lines mark internal lamina—mixed with mudclasts (m) and oncoids (o); Aramco HKKF Khurais. (C) Hardground with organic marks separating a lower lime mud bed from an upper intraclastic bed. Note the borings (red line) and phosphatization at hardground surface (red arrows), oxygenation halos (O_2), and fractures connecting burrows (black arrows); Aramco NAN Khurais. (D) Oil staining spreading out from hardground burrows. Note staining in interconnecting fractures, oxygenation halos (long arrow; O_2), and dolomitization in and around burrows (short arrow); Aramco HCHK Khurais. (E) Hummocky cross-stratification in lime mud; Aramco HKKF Khurais. Photographs are located or projected from correlated lithofacies onto Aramco HCHK Khurais core description, Figure 3.

lithofacies. Porosity types include moldic and intraparticle porosities.

Stromatoporoid Lithofacies

The skeletal-stromatoporoid (calcified sponge) wackestone to floatstone, the stromatoporoid lithofacies (Figure 6A), is present in the middle part of the Arab-D reservoir and is composed of floatstones and rudstones with matrix textures ranging from wackestone to grain-dominated packstone. The components of this lithofacies are very poorly sorted, with a wide range of grain sizes ranging from fine sands to pebbles. The components include mostly displaced domal and encrusting stromatoporoids, a few centimeters to a decimeter across (Figure 6A);

corals, a few centimeters to a decimeter across (Figure 6B); microbial encrustations; foraminifera; bivalves (including as much as 2-in. [5-cm]-wide gastropods; Figure 6C); pellets; peloids; oncoids; and intraclasts. Thick bedding, as much as 9 ft (2.7 m) in the illustrated Khurais core (Figure 3) and as much as 18 ft (5.5 m) in another Khurais core, characterizes this lithofacies. This latter bed may have had its boundaries obliterated by diagenesis. Sharp bases, commonly hardgrounds or firmgrounds, and gradational upper contacts into the pelletal lithofacies discussed below mark this lithofacies. Heavy bioturbation is very common in addition to borings, occurring mostly on the stromatoporoids. Vugular (because of dissolution of aragonitic corals; Figure 6A), moldic, and intraparticle porosities are the dominant pore types.



Pelletal Lithofacies

The skeletal-pelletal wackestone to grain-dominated packstone, the pelletal lithofacies (Figure 6D), is present in the middle part of the Arab-D reservoir. The components of this lithofacies range in size from clay to very fine sand and are moderately sorted pellets, bivalve fragments, foraminifera, and lime mud. The beds are 0.5 to 4 ft (0.2–1.2 m) thick and have sharp firmground contacts with the underlying lime mud lithofacies. The upper contacts of this lithofacies can be gradational or sharp with the overlying stromatoporoid lithofacies. Bioturbation, horizontal laminations, firmgrounds, and hardgrounds are the common sedimentary structures characterizing this lithofacies. Mostly moldic porosity and microporosity types are present.

Intraclastic Lithofacies

The skeletal-oncolitic-intraclastic mud-dominated packstone to floatstone, the intraclastic lithofacies (Figure 7A, upper bed, and B), is present in the middle and lower parts of the Arab-D reservoir and is composed of oncolitic and/or intraclastic rudstones and floatstones with matrix textures ranging from wackestone to grain-dominated packstone. The components in this lithofacies are extremely poorly sorted and include angular to subrounded intraclasts, oncoids (marked by coating development around intraclasts and skeletal fragments), bivalves, reworked stromatoporoid and coral fragments (Figure 7B), foraminifera, pellets, peloids, and rare *Cladocoropsis* fragments. Bed thickness ranges from 0.1 to 4 ft (0.03–1.2 m) with sharp hardground or firmground bases that were commonly scoured and sharp to gradational upper contacts. These beds are numerous, as much as one bed every 2 in. (5 cm) in the lower part of the reservoir (Figure 8). The hardgrounds that underline almost every single intraclastic bed correlate one for one

Figure 8. The thicknesses of 110 described intraclastic beds are plotted against their occurrence depth in the lower part of the Arab-D reservoir core, Aramco HKHK Khurais. Cyclicity is indicated by the thick curved arrows and is depicted by bed thickness increase up each cycle. Note the overall thickness increase up the entire interval (large curved arrow).

with a conspicuous increase in (hot) gamma-log spikes that mark the lower Arab-D reservoir.

Hardgrounds are marked by color alteration and/or blackening, possibly attributed to phosphatization (Palmer, 1982; Bodenbender et al., 1989) that extends down from the hardground surface and/or borings (Figure 7C). The firmgrounds are characterized by color alterations and terminated burrow tops against the firmground surface. Angular to subangular mudclasts rest on top of the hardgrounds (Figure 7A), whereas subrounded ones sometimes cap firmgrounds. Scour marks (made by a scouring current; Figure 7A) and organic marks (made by burrowing organisms and filled with the intraclastic lithofacies; Figure 7C) characterize the hardgrounds and firmgrounds underlying this lithofacies. Other sedimentary structures include burrowing, graded bedding, horizontal laminations, and rare hummocky and/or swaley cross-stratifications. The porosity types present in this lithofacies are interparticle, intraparticle, and microporosity.

Lime Mud Lithofacies

The skeletal wackestone and lime mudstone, the lime mud lithofacies (Figure 7A, lower bed, and E), is present in the lower part of the Arab-D reservoir. In addition to lime mud, the components of this lithofacies include micritized pellets; bivalves; brachiopods; foraminifera, particularly *Lenticulina spp.*; echinoderms; and rare blackened and/or reddened peloids and/or pellets.

Bed thickness ranges from 0.2 to 4 ft (0.06–1.2 m) with mostly sharp hardground or firmground caps (these make up the base of the intraclastic lithofacies as discussed above) and transitional bases. This lithofacies is characterized by heavy bioturbation that, generally, churns the sediment and becomes more distinct, filled with grainier sediment infills, and preferentially dolomitized toward the hardground caps (Figure 7C). These distinct burrows, associated with hardgrounds, are subsequently referred to as hardground burrows.

The hardground burrows are sometimes outlined with oxygenation halos and occasionally are dolomitized and/or have dolomitized outer rims

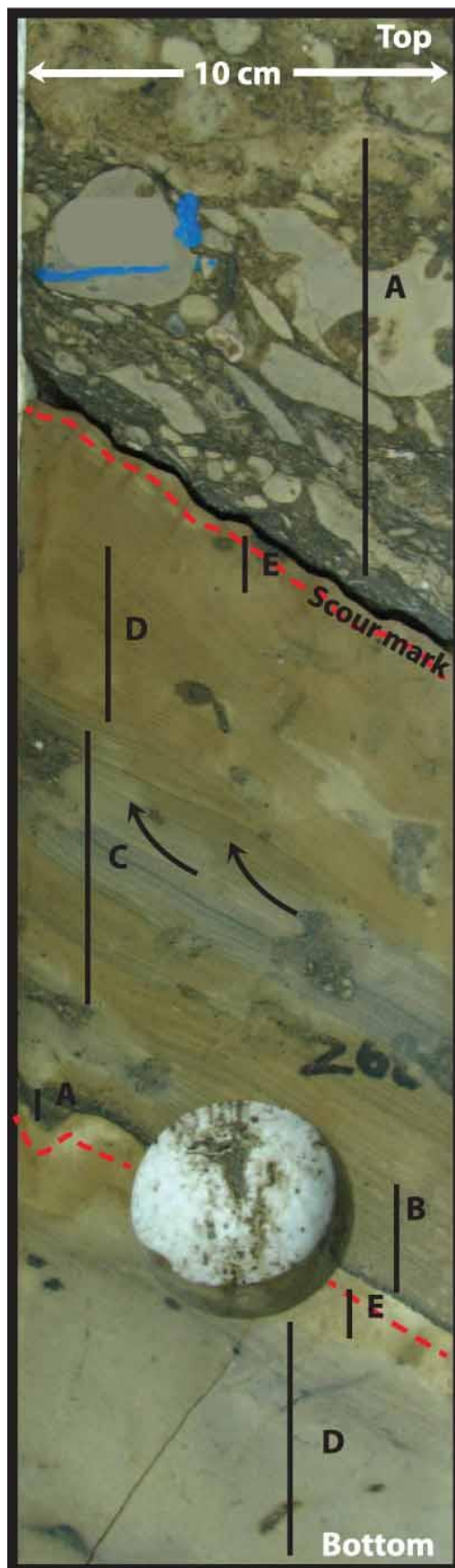
(Figure 7C, D). Commonly, oil staining intensifies around the hardground burrows (Figure 7D). When this lithofacies is not interrupted by bioturbation, original horizontal to slightly inclined to undulated laminations, commonly attributed to the size difference between mud and micropellets, are preserved. Rare hummocky cross-stratification (HCS) to swaley bedding marks this lithofacies (Figure 7E), in addition to rare slumps. Fractures commonly interconnect these hardground burrows, fracture the overlying mudclasts of the intraclastic lithofacies, and range from completely sealed with blocky calcite cement to partially open to completely open, in addition to solution-enhanced fractures (Figure 7C).

The pore types are mostly micropores and, to a lesser extent, moldic and intraparticle pores. Some interparticle and intercrystal porosity can be observed in the grainy infills of the hardground burrows and commonly contain higher porosities than the surrounding lime muds. Figure 9 shows a typical continuum through the intraclastic and lime mud lithofacies in the lower part of the Arab-D reservoir. The following observations can be made:

1. The lower Arab-D is composed of monotonous interbedded couplets of these two lithofacies.
2. The bases of the intraclastic lithofacies separating it from the underlying lime mud lithofacies are almost always sharp.
3. These sharp bases are always marked with scour marks or organic marks (Figure 9; 7A, C) as previously discussed.
4. The couplets show preserved Bouma sequences, sometimes with all divisions A, B, C, D, and E (Figure 9).

Dolomite Lithofacies

The dolomite lithofacies (Figure 6E) is composed of sucrosic or mosaic, fine to medium-size dolomite crystals that occur as distinctive beds, commonly with sharp top and bottom boundaries, ranging in thickness from 0.2 to 8 ft (0.06–2.4 m). These beds are not specific to any of the aforementioned lithofacies and occur throughout the reservoir, commonly obliterating original fabrics.



Porosity types are mostly intercrystal and, to a lesser extent, moldic.

DEPOSITIONAL MODEL

Figure 10 illustrates our proposed depositional model of the Arab-D reservoir in the Khurais field. This model was constructed by defining the recognized lithofacies components, their stratigraphic positions in core, the nature of their boundaries and sedimentary structures, their bedding thickness trends, in addition to being integrated with Hughes' (2004, 2009) published micropaleontological analysis of Arab-D samples. This model is of a prograding, gently sloping, arid, shallow, rimmed carbonate shelf, which was subjected to common storm shaving that triggered turbidites. The following points summarize key aspects pertaining to the model:

- Progradation occurred from the shallow epeiric shelf into the relatively deep Arabian intrashelf basin (Figure 2) (Ziegler, 2001; Leinfelder et al., 2005).
- The epeiric sea waters were probably overheated as suggested by paleoclimatic modeling (Moore et al., 1992; Sellwood et al., 2000; Alsharhan and Sadooni, 2003).

Figure 9. Typical type-CCC turbidite, indicative of deposition on a submarine channel levee and distinguished by the presence of climbing-ripple laminations, convolutions, and rip-up clasts (Walker, 1992) with a full Bouma sequence (Bouma, 1962) preserved. Division A of the sequence above the scour marks is structureless, consists of clasts up to 5 cm (2 in.) across, and represents the highest energy conditions. Division A grades up into the horizontally laminated sands of division B, which represent current energy fall to upper flow regime. Then follows the current ripples of division C that form climbing ripples (indicated by curved arrows) as more sediments deposit from suspension. These are followed by the parallel-laminated silts and muds of division D. Finally, pellets and muds of division E are deposited, and they represent the final decay of the current energy. Eh muds and pellets, if present, are hemipelagic sediments sourced from the turbidity current but deposited directly from the sea water, that is, no current movement is involved; Aramco HKHK Khurais; position marked on Figure 3. Vertical scale is same as horizontal scale.

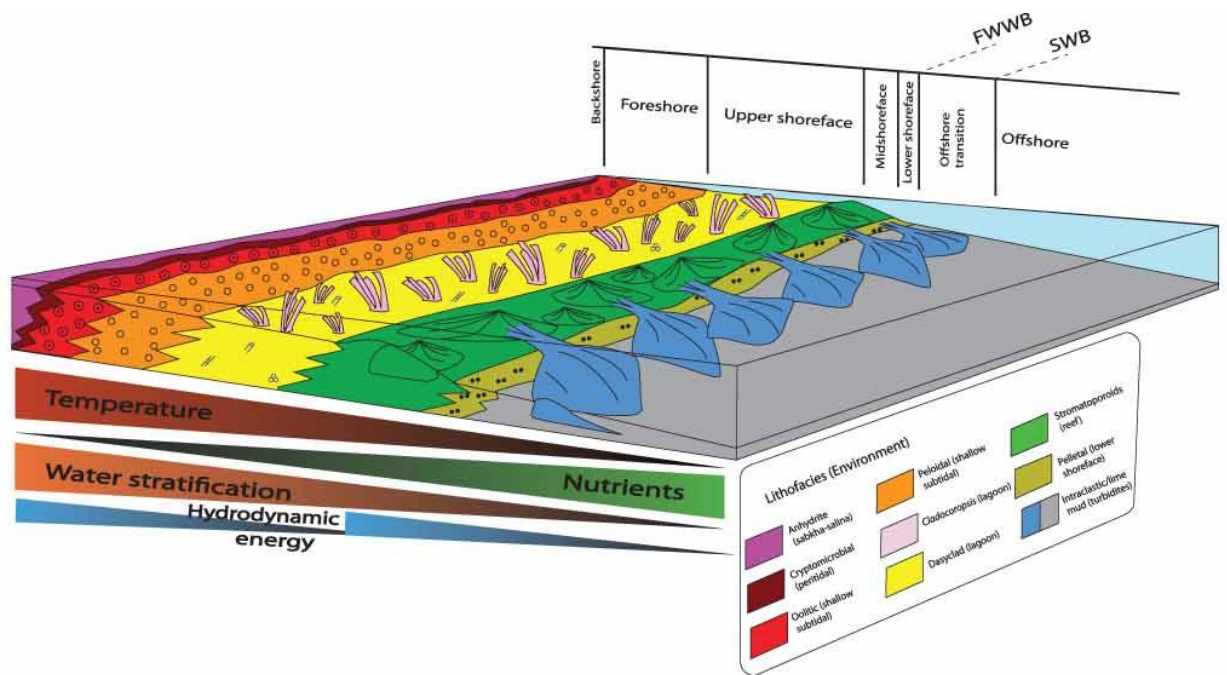


Figure 10. Schematic depositional model (not to scale). The model is of a prograding, commonly storm-abraded, gently sloping, shallow, arid stromatoporoid reef-rimmed shelf. The climate aridity probably overheated the nearshore waters as shown by the temperature gradient. This overheating inflicted a corresponding vertical water stratification gradient. The enormous width and shallow depth of the shelf probably cut off water circulation with the Neotethys and caused nutrients to decrease landward. The hydrodynamic energy increased up to the reef, decreased by reef resistance to waves in the lagoon, and increased back up to the shoreface. The salina and sabkha environment was followed basinward by peritidal settings, with stromatolites, and shallow subtidal settings, with ooids and peloids deposited as shore-attached sand sheets. These were followed by a *Cladocoropsis* and dasyclad lagoon that was protected by a rim densely populated by small-scale stromatoporoid reefs. These were succeeded by lower shoreface environment characterized by pelletal sands and silts at or near the fair weather-wave base (FWWB). Storms mainly reworked the reefs generating turbidites, which are shown (cross sectional view) to represent wedging out basinward. Finally, lime muds draped the turbidites (Et) and (Eh) divisions of Bouma sequence and/or transgressed over the turbidites as pelagic rain. SWB is storm-wave base. The entire platform was approximately 1000 km (621 mi) wide (Figure 1); the vertical cored section (Figure 3) is approximately 100 m (328 ft) long (modified from L. Pomar, 2011, personal communication; Leinfelder et al., 2005), and data from this study.

- Paleogeographic reconstruction and proximity to paleoequator (Figure 2) (Li and Powell, 2001) also suggest overheating of the waters.
- Richness in evaporites that cap the succession and the presence of miliolid foraminifera and *Clypeina* suggest water shallowness.
- The water probably cooled and inflicted a vertical water stratification toward the intrashelf basin (Figure 10).
- The enormous width and shallow depth of the shelf (Ziegler, 2001) probably led to cutting the water circulation off with the Neotethys and yielded a decrease in nutrient supply landward (Figure 10) (Leinfelder et al., 2005).
- The present-day bathymetry of the gulf of 33-ft (10-m) fair weather-wave base (FWWB) and 164-ft (50-m) storm-wave base (SWB) (Hughes et al., 2004b; Lindsay et al., 2006), can be thought of, with caution, as a proxy for the Arab-D-time conditions because of the striking resemblance between the two systems (Kinsman and Park, 1976; Moore et al., 1992; Sellwood et al., 2000; Handford et al., 2002).

The stratigraphic position of the recognized lithofacies represent an overall upward-shallowing succession (see discussion below) that is punctuated by parasequences and parasequence sets

(Figure 3) caused by high-frequency eustatic changes. This interpretation is in agreement with the micro-paleontological tiering observed by Hughes (2004), where he deduced that upward tiering faunal assemblages on the scale of 10 ft (3 m) represent sea level shallowing of possibly 66 ft (20 m).

Intraclastic and Lime Mud Lithofacies

Starting at the bottom of Aramco HKHK Khurais core (Figure 3), the complexity of the lower intraclastic and lime mud lithofacies dictates that we reiterate some of the pertinent facts associated with them. First, these two lithofacies occur monotonously interbedded. Second, both lithofacies are characterized by the presence of HCS, swaley bedding, Bouma sequences, and type-CCC turbidites characterized by the presence of rip-up clasts, convolutions, and climbing ripples (Figures 7E, 9) (Bouma, 1962; Walker, 1985b). Third, the contact between a lime mud bed and an overlying intraclastic bed is almost always marked by a sharp hardground or firmground. Fourth, the lime muds show oxygenation halos around hardground burrows. Fifth, the lime mud lithofacies is interpreted to represent the deepest Arab-D lithofacies by Hughes (1996, 2004), who described the foraminifera *Lenticulina spp.* in this lithofacies, which, together with monaxon and tetraxon sponge spicules and juvenile costate brachiopods, represent normal marine conditions. This succession in the outcrop uniquely contains ammonites and deep-marine trace fossils (G. W. Hughes, 2011, personal communication). Sixth, plotting the thickness of the intraclastic beds against their occurrence depth (Figure 8) shows a cyclic pattern that bundles the beds in thickening-upward sets and depicts an overall increase in thickness throughout the lower part of the reservoir.

With the above facts in mind, we think that separating the lime mud lithofacies genetically from the intraclastic lithofacies is not always warranted. Close attention must be paid to the nature of the transition from an intraclastic bed and an overlying lime mud bed. In less common cases where the transitions are abrupt, it is most likely that the lime muds represent transgression of deep pelagic muds

over the intraclastic lithofacies. More commonly, however, the transitions are gradational and exhibit Bouma sequences, indicating that the two lithofacies are genetically related, which leads to interpreting them as turbidite couplets, placing them by definition below the FWWB (Figure 10; Walker, 1984). In these latter cases, it is conceivable that the turbidity currents avalanched down the slope and into the basin (see stromatoporoids discussion below), scoured surfaces, ripped up clasts, and arranged sediments into Bouma sequences. Thus, the lime mud blankets that gradually drape the intraclastic beds are mere Et divisions of Bouma (settled down as the energy of the turbidity current dwindled to null) and Eh divisions (turbidity-sourced, hemipelagic muds deposited directly from sea water, where no current movement is involved) (Figure 9) (Walker, 1992; Church et al., 2003). This deduction explains the apparent coincidence of the intraclastic beds always being situated on hardgrounds that cap the lime mud beds. Had the lime mud been deposited by continuous, slow, deep-water-sourced pelagic rain, it would be inexplicable to assume that the pelagic rain stopped conveniently before every turbidity commencement to allow for the lime muds to cement up and form hardgrounds. The more likely scenario is that every intraclastic and lime mud couplet represents a geologic instant of time when a turbidity current avalanched. All of the remaining time subsequent to the turbidity instant had probably been consumed in cementing up the deposits and forming a hardground that would be scoured and ripped up by the next turbidity current. Meyer and Price (1993) used this geologic instant concept of the turbidites to correlate across Ghawar field as further discussed below.

The HCS that sometimes marks the couplets points out a storm origin and a specific bathymetry between the FWWB and the SWB (Walker, 1992). This, coupled with the cyclicity depicted in Figure 8, eliminates tectonic-driven seismic activities as the triggering mechanism of the turbidites. Instead, we interpret the turbidites to be triggered by common storms because their wave bases are affected by the cyclic fluctuations of sea level. As sea level dropped, it lowered the SWB, allowing higher levels of energy

to strike the reef (see stromatoporoids discussion below) and generating thicker turbidites.

In cases where the turbidites were deposited between the FWWB and the SWB, the upper divisions of their Bouma sequences (divisions C, D, and E) were likely reworked by storm waves into HCS, whereas full preservation of Bouma sequences was probably attained when the turbidites were deposited below the SWB. In the latter case, submarine fans would have been likely to form where channel levee complexes would develop in their suprafans yielding type-CCC turbidites, like the one shown in Figure 9 (Walker, 1985a).

Thus, the preserved vertical succession of the turbidite couplets represents shallowing upward from thin incomplete Bouma sequences deposited below the SWB in the lower fan to thicker type-CCC turbidites deposited below the SWB in the midfan to even thicker—and probably amalgamated—HCS to swaley-bedded stratified couplets deposited between the FWWB and the SWB. Finally, the oxygenation halos marking the hardground burrows in the lime muds suggest that they were deposited in anoxic conditions, a phenomenon known to happen in basins separated from the open ocean by shallow sills (Leeder, 2011), which is the case of the Arabian intrashelf basin being separated from the Neotethys (Ziegler, 2001).

Pelletal Lithofacies

Landward from the interpreted turbidites, the pelletal lithofacies is characterized by silt and very fine sand-size particles, moderate sorting, bioturbation, and horizontal lamination. These features represent a low-energy environment where physical processes are still in play; because of this, we position this lithofacies in the lower shoreface, above or near the FWWB (Figure 10).

Stromatoporoid Lithofacies

Further landward the stromatoporoid lithofacies is deposited. The observed gregarious laminar and domical stromatoporoid growth forms and the presence of microbial encrustations in this lithofacies are interpreted as a reef (Figure 10) in the

sense of Wood (1999, p. 5): “a discrete carbonate structure formed by in situ or bound organic components that develops topographic relief upon the sea floor.” The reworked nature of the stromatoporoids in this lithofacies is taken in light of Hubbard et al. (1990), Hubbard (1992), Wood (1995, 2001), Blanchon et al. (1997), and Montaggioni (2005), who concluded that the interlocked in-place framework requirements in the literature for defining reefs are difficult to demonstrate in modern and ancient examples. In fact, Hubbard goes as far as describing the term “framework” in reefs’ definition as “troublesome,” as he demonstrates that as much as 90% of his studied reefs are composed of detritus (reworked reef components and bioeroded sediments that were re-incorporated in reef accretion) and voids (Hubbard et al., 1990; Hubbard, 1992; Wood, 2001). Moreover, we think that Arab-D stromatoporoid reefs were probably kept from being overwhelmed by detrital sediments by the storm reworking, as was demonstrated by the results of Hubbard et al. (1990) and Hubbard (1992). Leinfelder et al. (2005), documented that approximately 20% of the Upper Jurassic reefs have significant stromatoporoids with corals, and another 10% are dominated by stromatoporoids, especially in the southern Neotethys and intra-Neotethys areas.

Based on the stratigraphic position of life assemblages of the stromatoporoids in beach-capped, shoaling-up sequences, they have been determined to live in mid-to-upper shoreface environments at paleowater depths of less than 10 m (33 ft) (see Toland, 1994). Stromatoporoids are also absent from *Lithocodium*-dominated facies, which have an estimated paleowater depth of 15 to 60 m (49–197 ft) (Wood, 1987; Banner et al., 1990; Toland, 1994). This, coupled with the reworked nature of stromatoporoid, suggests that they were able to build wave-resistant reefs because their reworking and displacement is highly unlikely to be the result of fair-weather waves, but instead of storm waves. With this in mind, interpreting the stromatoporoid lithofacies as reefs explains the apparent discrepancy between the heterogeneous muddy nature of its matrix and the high energy of its hydrodynamic position in the mid-to-upper shoreface, simply by

reef resistance to wave energy. This conclusion contrasts with Meyer and Price (1993), who positioned the stromatoporoids at the FWWB and attributed the matrix muddiness to low hydrodynamic energy.

The stromatoporoids' stratigraphical limitation to the middle interval of the Arab-D reservoir (Figure 3) suggest a paleoenvironmental control on their ecological niches. Salinity could be a control because they are absent from the hypersaline waters that are transational to the deposition of the anhydrite caps; yet, stromatoporoids are tolerant to slight hypersalinity because they dominate in echinoderm-free intervals of the Arab-D (Leinfelder et al., 2005). However, the absence of stromatoporoids in *Lithocodium*-dominated sediments and their limitation to pure carbonates (as opposed to argillaceous carbonates or siliciclastics) suggests a dependence on well-lit waters, which could be explained by a bacterial-photosymbiotic feeding habit in addition to their filter-feeding one (Leinfelder et al., 2005). The well-lit, slightly hypersaline water requirements for stromatoporoids were likely only met at the rims of the intrashelf basins, hence limiting stromatoporoids to this narrow geographic niche; this conforms with the conclusions of Le Nindre et al. (1990) and Powers et al. (1966). The position of the stromatoporoid reefs at the intrashelf basin rims probably increased the slope into the basin and thus gave more momentum to the interpreted turbidity currents (see discussion above). This deduction is supported by Meyer and Price (1993), who used the turbidites to correlate across Ghawar field and showed that the stromatoporoid and shallower lithofacies dip at a gentler angle than the intraclastic and lime mud lithofacies.

Although the stromatoporoid reefal buildups were insignificant in height, 10 to 16 ft (3–5 m) high and 98 ft (30 m) wide (Meyer et al., 1996a, b; Hughes, 2004; Hughes et al., 2004a, b), their relief would have been accentuated by the gentle nature of the shelf behind them (Meyer, 2000). This configuration probably contributed to the composition of the interpreted turbidites in two ways. First, although the carbonate factory of the shelf extended from the stromatoporoid reef all the way

upslope to the cryptomicrobial lithofacies, for the most part, only the reefs sourced sediments to the turbidites because they were the highest points facing abrasion by storms coming toward the shoreline. Second, the reefs, being elevated barriers, prevented storm transportation of sediments from the back-reefal area downslope. Both of these interpretations are supported by the reworked stromatoporoids that contribute substantially to the makeup of the lower turbidites (Figure 7F) and the paucity of shallower-than-stromatoporoid components in the turbidites. Last, based on our preliminary stratigraphic correlation of several cores across the Khurais field and on the outcrop observation of Meyer et al. (1996) and Hughes (2004), we think that these stromatoporoid reefs were not laterally continuous; yet, they were probably abundant in the mid-to-upper shoreface of the Arab-D shelf, as illustrated in Figure 10.

Dasyclad Lithofacies

The stromatoporoid reefal buildups, as interpreted above, would have facilitated the deposition of mud-dominated textures in the upper shoreface, in a lagoon behind the stromatoporoid reef, by hindering wave energy. The dasyclad lithofacies is interpreted as being deposited in this upper-shoreface lagoon (Figure 10). This interpretation accords with the lack of stratification, abundance of bioturbation, and wispy lamination in the dasyclad lithofacies, which reflects a reduced energy setting where biologic instead of physical processes are the determinant factor. This interpretation is also in line with Hughes' (2004) interpretation of the foraminiferal assemblages associated with this lithofacies as lagoonal.

Cladocoropsis Lithofacies

The *Cladocoropsis* lithofacies is stratigraphically mixed with the dasyclad lithofacies. This suggests that it probably existed as bushlike aggregates or a meadow within the lagoon (Figure 10). In fact, the *Cladocoropsis* presence behind the reef could have further reduced energy and enhanced mud deposition as its dendroid form would have baffled

wave energy. Storm activity in the lagoon is manifested in the *Cladocoropsis* dendritic or branching form, which is a morphologic adaptation known to flourish in abrasive settings, as it is capable of substantial sediment shedding that is beneficial in keeping up with high sedimentation rates (Toland, 1994). Storm activity is also evident by the common reworking of the *Cladocoropsis*, which generally never leaves them in growth position. Note that the *Cladocoropsis* floatstones and rudstones that base the peloidal lithofacies in the fining-upward sequences (Figure 3, upper part of Figure 5A), suggest that the *Cladocoropsis* were transported updip, probably by storms. When storms struck, they probably winnowed the lagoonal sediments from the muds, carried the bigger grains (the *Cladocoropsis* stems) updip, and concentrated them in thin sheets that were later capped by the peloidal lithofacies. Last, the *Cladocoropsis* and dasyclad lithofacies that intermix and variably overlie the stromatoporoid lithofacies suggest a random distribution of the *Cladocoropsis* within the lagoon instead of its existence in a specific zone or belt as suggested by Hughes (2004) and Lindsay et al. (2006).

Peloidal Lithofacies

Further landward the low-angle cross-stratifications, rounded, sorted, and winnowed components that are characteristics of the peloidal lithofacies indicate an increase in hydrodynamic energy and an increase in sorting and abrasion ability as the lithofacies belts continue shallowing toward the shoreline. Therefore, we interpret this lithofacies as a peloidal sand sheet in the wave-dominated foreshore area (Figure 10).

Oolitic Lithofacies

The well-rounded, well-sorted, well-winnowed depositional texture of oolitic lithofacies and its cross-bedded structure suggests a further increase in hydrodynamic energy, as the lithofacies belts continue shallowing to agitated water conditions. Because of the absence of muddy lagoonal sediments separating the oolitic lithofacies from the overlying

cryptomicrobial lithofacies, we interpret it as a foreshore oolitic sand sheet fringing the Arab-D-time shoreline (Figure 10), as opposed to an oolitic shoal as suggested by Lindsay et al. (2006).

Cryptomicrobial Lithofacies

The microbial laminae in the cryptomicrobial lithofacies together with its restricted fauna, dominated by cerithiid gastropods, and stratigraphic position right below the anhydrites represent hypersaline peritidal stromatolites deposited in the backshore area (Figure 10). This conclusion is in line with the microfaunal assemblage recognized by Hughes (2004) in this lithofacies.

Anhydrite Lithofacies

Further backshore, the anhydrite lithofacies represents deposition in a sabkha-type environment, at least in its lower interval. This is evident with the chicken wire fabrics that characterize the lower interval of the anhydrites and its displacive nature, together with its stratigraphic position right above the cryptomicrobial lithofacies. The change from the chicken wire fabric to the bedded nodular and ultimately massive fabrics could be interpreted as a change from a sabkha to a salina environment, where evaporites were produced subaqueously, allowing accommodation space for the deposition of the thick (164 ft [50 m]) anhydrite seal and indicating a possible transgressive expansion of the salina.

Accommodation Space and Physical Versus Ecological Processes

The whole Arab-D succession can be divided in terms of dominance of physical and ecological processes into three realms. The first realm spans from the peloidal sand sheet upward, plus the pelletal lithofacies (Figure 3). Fair-weather waves are the dominant controller of sorting, sediment dispersal, and sedimentary structures in this shallow realm, except for the storm wave-affected, normally graded, shallowing upward cycles of *Cladocoropsis* bases and peloidal caps (Figure 3, Figure 5A). The second

realm is the reef and the lagoon protected by it, where ecological processes, namely, stromatoporoid-reef resistance and *Cladocoropsis* baffling to wave energy, control sediment size, sorting, and dispersal. The third realm represents the intrashelf basin and includes the intraclastic and lime mud lithofacies, where storm abrasion and reworking and turbidity currents are the controlling factors on the sorting; grain size, shape, and composition; sediment dispersal; and sedimentary structures. In terms of accommodation space, the presence of the reefal framework above the FWWB, and its resistance to wave energy, allowed for ecologically driven accommodation above the wave base razor (Figure 10) (Pomar and Kendall, 2008).

CONCLUSIONS

The largest oil reservoir of the world, Arab-D, is present in one of the largest onshore oil fields of Saudi Arabia, Khurais. Detailed (4-in. [10-cm]-scaled) core analysis of the Arab-D reservoir in the Khurais field led to the recognition of 11 lithofacies that begin with, at the bottom of the reservoir, monotonously interbedded units of intraclastic floatstone and rudstone that abruptly overlies hardground-capped skeletal wackestone and lime mudstone. These lower lithofacies are overlain by pelletal wackestone and packstone units that pass up into stromatoporoid wackestone, packstone, and floatstone units. Overlying these are *Cladocoropsis* wackestone, packstone, and floatstone; dasyclad wackestone and packstone; and peloidal packstone and grainstone units. Ooid grainstone units cap the succession and are, in turn, capped by cryptomicrobial laminites and, ultimately, by evaporites.

This depositional succession represents shallow epeiric carbonate and evaporite lithofacies that prograded across the Late Jurassic Arabian shelf and into the relatively deep Arabian intrashelf basin.

The depositional model interpreted here is of a gently sloping, shallow, arid, reef-rimmed carbonate shelf, which was subjected to common storm shaving that triggered turbidite avalanches.

The lithofacies are interpreted to have been deposited in the following environment in ascending order: submarine turbidity fans shallowing up into FWWB pelletal silts and sands, stromatoporoid reefs, *Cladocoropsis* and *Clypeina* lagoons, peloidal and oolitic sand sheets, supratidal stromatolites, and, finally, evaporitic flats and salinas.

REFERENCES CITED

- Al-Afalge, N. I., S. Al-Garni, B. Rahmeh, and A. Al-Towailib, 2002, Successful integration of sparsely distributed core and well test derived permeability data in a viable model of a giant carbonate reservoir: Society of Petroleum Engineers Annual Technical Conference and Exhibition, San Antonio, Texas, SPE Paper 77743, 8 p., doi:10.2118/77743-MS.
- Al-Husseini, M. I., 2000, Origin of the Arabian plate structures: Amar collision and Najd rift: *GeoArabia* (Manama), v. 5, p. 527–542.
- Al-Mulhim, W. A., F. A. Al-Ajmi, M. A. Al-Shehab, and T. R. Pham, 2010, Khureis complex: Part 1. Field development required best practices, leveraged technology: *Oil & Gas Journal*, v. 108, p. 37–38, 40–42.
- Alsharhan, A. S., and C. G. S. C. Kendall, 1986, Precambrian to Jurassic rocks of Arabian Gulf and adjacent areas: Their facies, depositional setting, and hydrocarbon habitat: *AAPG Bulletin*, v. 70, p. 977–1002.
- Alsharhan, A. S., and F. N. Sadooni, 2003, Eustatic overprints on the diagenetic evolution of Mesozoic platform carbonates from the Arabian plate: *AAPG Annual Meeting Expanded Abstracts*, v. 12, p. 5.
- Ayres, M. G., M. Bilal, R. W. Jones, L. W. Slentz, M. Tartir, and A. O. Wilson, 1982, Hydrocarbon habitat in main producing areas, Saudi Arabia: *AAPG Bulletin*, v. 66, p. 1–9.
- Banner, F. T., E. M. Finch, and M. D. Simmons, 1990, On *LithocodiumElliott* (calcareous algae): Its paleobiological and stratigraphical significance: *Journal of Micropalaeontology*, v. 9, p. 21–35, doi:10.1144/jm.9.1.21.
- Barger, T. C., 1984, Birth of a dream: Saudi Aramco World, May/June 1984, p. 34–41.
- Blanchon, P., B. Jones, and W. Kalbfleisch, 1997, Anatomy of a fringing reef around Grand Cayman: Storm rubble, not coral framework: *Journal of Sedimentary Research*, v. 67, p. 1–16.
- Blasband, B., S. White, P. Brooijmans, H. De Boorder, and W. Visser, 2000, Late Proterozoic extensional collapse in the Arabian-Nubian shield: *Journal of the Geological Society*, v. 157, p. 615–628, doi:10.1144/jgs.157.3.615.
- Bodenbender, B. E., M. A. Wilson, and T. J. Palmer, 1989, Paleocology of *Sphenothallus* on an Upper Ordovician hardground: *Lethaia*, v. 22, p. 217–225, doi:10.1111/j.1502-3931.1989.tb01685.x.
- Bouma, A. H., 1962, Sedimentology of some flysch deposits:

- A graphic approach to facies interpretation: Amsterdam, Elsevier Publishing Company, 168 p.
- Church, M., M. Coniglio, L. A. Hardie, and F. J. Longstaffe, 2003, Encyclopedia of sediments and sedimentary rocks, in G. V. Middleton, ed., Encyclopedia of Earth sciences series: Dordrecht, Netherlands, Springer, p. 928.
- De Castro, P., 1990, Thaumapoporelle: Conoscenze attuali e approccio all'interpretazione: Bollettino della Societa Paleontologica Italiana, v. 29, p. 179–206.
- Droste, H., 1990, Depositional cycles and source rock development in an epeiric intraplatform basin: The Hanifa Formation of the Arabian Peninsula: Sedimentary Geology, v. 69, p. 281–296, doi:10.1016/0037-0738(90)90054-W.
- Dunham, R. J., 1962, Classification of carbonate rocks according to depositional texture, in W. E. Ham, ed., Classification of carbonate rocks: AAPG Memoir 1, p. 108–121.
- Embry, A. F. III, and J. E. Klovan, 1971, A late Devonian reef tract on northeastern Banks Island, N.W.T: Bulletin of Canadian Petroleum Geology, v. 19, p. 730–781.
- Enay, R., 1993, Les apports sud-Tethysiens parmi les faunes jurassiques Nord-Ouest Europeennes: Interpretation paleobiogeographique: Comptes Rendus de l'Academie des Sciences Serie 2, v. 317, p. 115–121.
- Golonka, J., 2002, Plate-tectonic maps of the Phanerozoic: Society for Sedimentary Geology Special Publication 72, p. 21–75.
- Handford, C. R., D. L. Cantrell, and T. H. Keith, 2002, Regional facies relationships and sequence stratigraphy of a super-giant reservoir (Arab-D Member), Saudi Arabia: Society of Economic Paleontologists Gulf Coast Section Research Conference Program and Abstracts 22, p. 539–563.
- Hubbard, D. K., 1992, Hurricane-induced sediment transport in open-shelf tropical systems: An example from St. Croix, U.S. Virgin Islands: Journal of Sedimentary Research, v. 62, p. 946–960.
- Hubbard, D. K., A. I. Miller, and D. Scaturro, 1990, Production and cycling of calcium carbonate in a shelf-edge reef system (St. Croix, U.S. Virgin Islands): Applications to the nature of reef systems in the fossil record: Journal of Sedimentary Research, v. 60, p. 335–360.
- Hughes, G. W., 1996, A new bioevent stratigraphy of Late Jurassic Arab-D carbonates of Saudi Arabia: GeoArabia (Manama), v. 1, p. 417–434.
- Hughes, G. W. A. G., 2004, Middle to Upper Jurassic Saudi Arabian carbonate petroleum reservoirs: Biostratigraphy, micropaleontology and paleoenvironments: GeoArabia (Manama), v. 9, p. 79–114.
- Hughes, G. W. A. G., 2009, Using Jurassic micropaleontology to determine Saudi Arabian carbonate paleoenvironments: Society for Sedimentary Geology Special Publication 93, p. 127–152.
- Hughes, G. W., A. G. Dhubeeb, O. Varol, R. F. Lindsay, H. Mueller, and Anonymous, 2004a, The Arab-D biofacies of Saudi Arabia: Their paleoenvironment and new biozonation: GeoArabia (Manama), v. 9, p. 79–80.
- Hughes, G. W., O. Varol, A. Al-Dhubeeb, and Anonymous, 2004b, Biofacies and paleoenvironments of Late Jurassic carbonates of Saudi Arabia: Congres Geologique International Resumes, v. 32, part 2, p. 893.
- Kinsman, D. J. J., and R. K. Park, 1976, Algal belt and coastal sabkha evolution, Trucial Coast, Persian Gulf: Stromatolites: Amsterdam, Elsevier Science Publishing Company, p. 421–433.
- Konert, G., A. M. Afifi, S. A. Al-Hajri, K. de Groot, A. A. Al Naim, and H. J. Droste, 2001, Paleozoic stratigraphy and hydrocarbon habitat of the Arabian plate: AAPG Memoir 74, p. 483–515.
- Leeder, M., 2011, Sedimentology and sedimentary basins: From turbulence to tectonics: Oxford, United Kingdom, Wiley-Blackwell, 768 p.
- Leinfelder, R. R., F. Schlagintweit, W. Werner, O. Ebli, M. Nose, D. U. Schmid, and G. W. Hughes, 2005, Significance of stromatoporoids in Jurassic reefs and carbonate platforms: Concepts and implications: Facies, v. 51, p. 299–337, doi:10.1007/s10347-005-0055-8.
- Le Nindre, Y. M., J. Manivit, and D. Vaslet, 1990, Stratigraphie sequentielle du Jurassique et du cretace en Arabie Saoudite: Societe Geologique de France Bulletin, Paris, v. 6, p. 1025–1035.
- Li, Z.-X., and C. M. Powell, 2001, An outline of the paleogeographic evolution of the Australasian region since the beginning of the Neoproterozoic: Earth-Science Reviews, v. 53, p. 237–277, doi:10.1016/S0012-8252(00)00021-0.
- Lindsay, R. F., D. L. Cantrell, G. W. Hughes, T. H. Keith, H. W. Mueller III, and D. Russell, 2006, Ghawar Arab-D reservoir: Widespread porosity in shoaling-upward carbonate cycles, Saudi Arabia: AAPG Memoir 88, p. 97–138.
- Meyer, F., 2000, Carbonate sheet slump from the Jubaila Formation, Saudi Arabia: Slope implications: GeoArabia (Manama), v. 5, p. 144–145.
- Meyer, F. O., and R. C. Price, 1993, A new Arab-D depositional model, Ghawar field, Saudi Arabia: Society of Petroleum Engineers Middle East Oil Technical Conference and Exhibition, Bahrain, April 3–6, 1993, SPE Paper 25576, p. 465–474, doi:10.2118/25576-MS.
- Meyer, F. O., R. C. Price, I. A. Al-Ghamdi, I. M. Al-Goba, S. M. Al-Raimi, and J. C. Cole, 1996, Sequential stratigraphy of outcropping strata equivalent to Arab-D reservoir, Wadi Nisah, Saudi Arabia: GeoArabia (Manama), v. 1, p. 435–456, doi:10.2118/25576-MS.
- Mitchell, J. C., P. J. Lehmann, D. L. Cantrell, I. A. Al-Jallal, M. A. R. Al-Thagafy, A. J. Lomando, and P. M. Harris, 1988, Lithofacies, diagenesis and depositional sequence: Arab-D Member, Ghawar field, Saudi Arabia: SEPM Core Workshop 12, p. 459–514.
- Montaggioni, L. F., 2005, History of Indo-Pacific coral reef systems since the last glaciation: Development patterns and controlling factors: Earth-Science Reviews, v. 71, p. 1–75, doi:10.1016/j.earscirev.2005.01.002.
- Moore, G. T., L. C. Sloan, D. N. Hayashida, and N. P. Umrigar, 1992, Paleoclimate of the Kimmeridgian/Tithonian (Late Jurassic) world: Part II. Sensitivity tests comparing three different paleotopographic settings: Palaeogeography, Palaeoclimatology, Palaeoecology, v. 95, p. 229–252, doi:10.1016/0031-0182(92)90143-S.
- Mouawad, J., 2010, China's growth shifts the geopolitics of oil: New York, The New York Times, p. B1: accessed January 29, 2013, <http://www.nytimes.com/2010/03/20/business/energy-environment/20saudi.html?pagewanted=all&r=0>.

- Murris, R. J., 1980, Middle East: Stratigraphic evolution and oil habitat: AAPG Bulletin, v. 64, p. 597–618.
- Net Resources International, 2011, Saudi Aramco Khurais Mega Project, Khurais Saudi Arabia: accessed April 12, 2012, <http://hydrocarbons-technology.com/projects/khurais>.
- Palmer, T. I. M., 1982, Cambrian to Cretaceous changes in hardground communities: *Lethaia*, v. 15, p. 309–323, doi:10.1111/j.1502-3931.1982.tb01696.x.
- Pomar, L., and C. G. S. C. Kendall, 2008, Architecture of carbonate platforms: A response to hydrodynamics and evolving ecology: Society for Sedimentary Geology Special Publication 89, p. 187–216.
- Powers, R. W., 1968, *Lexique stratigraphique international*: volume 3: Paris, France, Centre National de la Recherche Scientifiques, p. 177.
- Powers, R. W., L. R. Ramirez, C. D. Redmond, and E. L. Elberg, 1966, Sedimentary geology of Saudi Arabia: Geology of the Arabian Peninsula: U.S. Geological Survey Professional Paper 150, p. 150.
- Sellwood, B. W., P. J. Valdes, and G. D. Price, 2000, Geological evaluation of multiple general circulation model simulations of Late Jurassic paleoclimate: *Palaeogeography, Palaeoclimatology, Palaeoecology*, v. 156, p. 147–160, doi:10.1016/S0031-0182(99)00138-8.
- Sorkhabi, R., 2008, The emergence of the Arabian oil industry: *GeoExpro*, accessed January 29, 2013, http://www.geoexpro.com/article/The_Emergence_of_the_Arabian_Oil_Industry/d846be03.aspx, v. 5, no. 6.
- Stampfli, G. M., J. Mosar, P. Favre, A. Pilleveit, and J. C. Vannay, 2001, Permo-Mesozoic evolution of the western Tethys realm: The Neo-Tethys East Mediterranean basin connection: *Peri-Tethys Memoir 6—Peri-Tethyan rift/wrench basins and passive margins*: Paris (France), Museum National d'Histoire Naturelle, p. 51–108.
- Toland, C., 1994, Late Mesozoic stromatoporoids: Their use as stratigraphic tools and paleoenvironmental indicators—Micropaleontology and hydrocarbon exploration in the Middle East: London, Chapman and Hall, p. 113–125.
- Walker, R. G., 1984, Channel-levee complexes and submarine fans: An example from Wheeler Gorge, California: SEPM Midyear Meeting Abstracts 1, p. 84–85.
- Walker, R. G., 1985a, Comparison of shelf environments and deep basin turbidite systems: SEPM Short Course Notes 13, p. 465–502.
- Walker, R. G., 1985b, Mudstones and thin-bedded turbidites associated with the Upper Cretaceous Wheeler Gorge conglomerates, California: A possible channel-levee complex: *Journal of Sedimentary Research*, v. 55, p. 279–290.
- Walker, R. G., 1992, Facies models: Response to sea level change: St. Johns, Newfoundland, Geological Association of Canada, p. 239–263.
- Wood, R. A., 1987, Biology and revised systematics of some late Mesozoic stromatoporoids: *Special Papers in Palaeontology*, November, 3789 p.
- Wood, R. A., 1995, The changing biology of reef building: *Palaios*, v. 10, p. 517–529, doi:10.2307/3515091.
- Wood, R. A., 1999, *Reef evolution*: Oxford, United Kingdom, Oxford University Press, 414 p.
- Wood, R. A., 2001, Are reefs and mud mounds really so different?: *Sedimentary Geology*, v. 145, p. 161–171, doi:10.1016/S0037-0738(01)00146-4.
- Ziegler, M. A., 2001, Late Permian to Holocene paleofacies evolution of the Arabian plate and its hydrocarbon occurrences: *GeoArabia (Manama)*, v. 6, p. 445–504.

Appendix D: Sedimentary Geology Permission to Reprint “Carbonate-platform scale correlation of stacked high-frequency sequences in the Arab-D reservoir, Saudi Arabia”

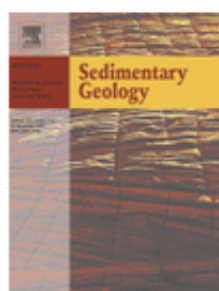


RightsLink®

Home

Account
Info

Help



Title: Carbonate-platform scale correlation of stacked high-frequency sequences in the Arab-D reservoir, Saudi Arabia

Author: Saad F. Al-Awwad, Lindsay B. Collins

Publication: Sedimentary Geology

Publisher: Elsevier

Date: 15 August 2013

Copyright © 2013, Elsevier

Logged in as:
Saad Al

LOGOUT

Order Completed

Thank you very much for your order.

This is a License Agreement between Saad Al-Awwad ("You") and Elsevier ("Elsevier"). The license consists of your order details, the terms and conditions provided by Elsevier, and the [payment terms and conditions](#).

[Get the printable license.](#)

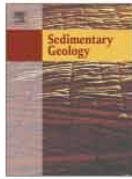
License Number	3194591046991
License date	Jul 23, 2013
Licensed content publisher	Elsevier
Licensed content publication	Sedimentary Geology
Licensed content title	Carbonate-platform scale correlation of stacked high-frequency sequences in the Arab-D reservoir, Saudi Arabia
Licensed content author	Saad F. Al-Awwad, Lindsay B. Collins
Licensed content date	15 August 2013
Licensed content volume number	294
Number of pages	14
Type of Use	reuse in a thesis/dissertation
Portion	full article
Format	both print and electronic
Are you the author of this Elsevier article?	Yes
Will you be translating?	No
Order reference number	
Title of your thesis/dissertation	High-resolution Sequence Stratigraphy of the Arab-D Reservoir, Khurais Field, Saudi Arabia
Expected completion date	Dec 2013
Elsevier VAT number	GB 494 6272 12
Permissions price	0.00 USD
VAT/Local Sales Tax	0.00 USD
Total	0.00 USD

ORDER MORE...

CLOSE WINDOW

Copyright © 2013 [Copyright Clearance Center, Inc.](#) All Rights Reserved. [Privacy statement.](#)
Comments? We would like to hear from you. E-mail us at customer care@copyright.com

Appendix E: Carbonate-platform scale correlation of stacked high-frequency sequences in the Arab-D reservoir, Saudi Arabia



Carbonate-platform scale correlation of stacked high-frequency sequences in the Arab-D reservoir, Saudi Arabia



Saad F. Al-Awwad^{a,b,*}, Lindsay B. Collins^b

^a Saudi Aramco, Dhahran, Saudi Arabia

^b Curtin University of Technology, Perth, WA, Australia

ARTICLE INFO

Article history:

Received 15 November 2012

Received in revised form 21 May 2013

Accepted 28 May 2013

Available online 10 June 2013

Editor: B. Jones

Keywords:

High-frequency sequence correlation

Arab-D reservoir

Late Jurassic

Khurais Field

Carbonates

Reservoir quality

ABSTRACT

The Late Jurassic Arab Formation contains a number of hydrocarbon-bearing carbonates, the most important of which is the lowermost Arab-D reservoir. The reservoir lithofacies in Khurais Field are: couplets of 1) lime mud and 2) intraclastic lithofacies representing basinal turbidites; 3) pelletal lithofacies representing lower shoreface sands and silts; 4) stromatoporoid lithofacies representing a reef; 5) *Cladocoropsis* and 6) dasyclad lithofacies representing a lagoon; 7) peloidal and 8) oolitic lithofacies representing shore-attached sand sheets; 9) cryptomicrobial lithofacies representing supratidal flats; 10) anhydrites representing sabkha followed by salina deposits; and 11) stratigraphically reoccurring dolomite.

These are arranged in two, partially preserved, third-order sequences, the upper of which represents the Arab-D Member and the lower of which represents the upper Jubaila Formation. Within these sequences lie six fourth-order high frequency sequences, composed of fifth-order parasequences and parasequence-scale cycles. The preserved upward shallowing trend of the Arab-D reservoir is manifested laterally by a regional eastward thickening interpreted to be the result of an eastward progradation across the shallow Late Jurassic epeiric shelf and into the relatively deep Arabian intrashelf basin.

This study presents a correlation model that explains the drastic thickening and downward climb of the reservoir lithofacies that is observed between the outcrops south of Riyadh and the subsurface in Ghawar Field.

This model is different from the one currently used and predicts an eastward porosity improvement in the upper part of the reservoir accompanied by a porosity reduction in the lower part, assuming a null diagenetic modification effect.

© 2013 Elsevier B.V. All rights reserved.

1. Introduction

Predicting the existence of a facies, and harder still its extent and geometry, in the subsurface posits a defying task to the stratigrapher. This task becomes even more daunting in the realm of carbonate sequence stratigraphy owing to the in situ nature of carbonate sedimentation. The matter becomes further complicated when stratigraphic analysis is conducted in a regional, shelf-to-basin, scale since complete, shelf-to-basin, platform transects are less common in outcrops (Goldhammer et al., 1990; Mitchum and Van Wagoner, 1991; Handford and Loucks, 1994; Tinker, 1998). Yet, regional stratigraphic analysis is key in comprehending lateral and vertical facies changes and predicting intra-reservoir geometric relationships, which together with diagenesis and fracturing shape the porosity–permeability schemes of carbonate reservoirs. Thus, platform-scaled correlation, if this could be conducted at the high-frequency-sequence scale, can

contribute in resolving reservoirs' architectural heterogeneities and pin down fluid-flow patterns.

This paper presents the results of a detailed sequence stratigraphic analysis of one of the world's most prolific reservoirs, the Arab-D reservoir, in Saudi Arabia. The Arab-D is one of four carbonate reservoirs of the Upper Jurassic Arab Formation. Each of these carbonate reservoirs possesses remarkable porosity and permeability, and each is capped by a nonpermeable anhydrite unit (Fig. 1). The Arab Formation reservoirs are sandwiched between the organic-rich mudstones of the Hanifa and Tuwaiq Mountain formations below and the tight anhydrites of the Arab and Hith formations above (Fig. 1). Giant expansive structural traps, such as the anticlines of Ghawar and Khurais fields (Fig. 2), proficiently harvest the Arab Formation oils from the extensive source rocks that lay across the Arabian Peninsula. In 2009, Saudi Aramco successfully completed the largest oil expansion project in the earth's history, known as the Khurais Mega Project bringing to production nationally significant rates from Khurais and adjacent satellite fields mainly from the 100-m-thick Arab-D reservoir (Al-Ghamdi et al., 2008; Al-Mulhim et al., 2010; Mouawad, 2010).

This paper details the stratal patterns of the high-frequency sequences that compose the reservoir, discusses the sequences' characteristics and

* Corresponding author at: Curtin University of Technology, Perth WA, Australia.
E-mail address: saad.shamary@gmail.com (S.F. Al-Awwad).

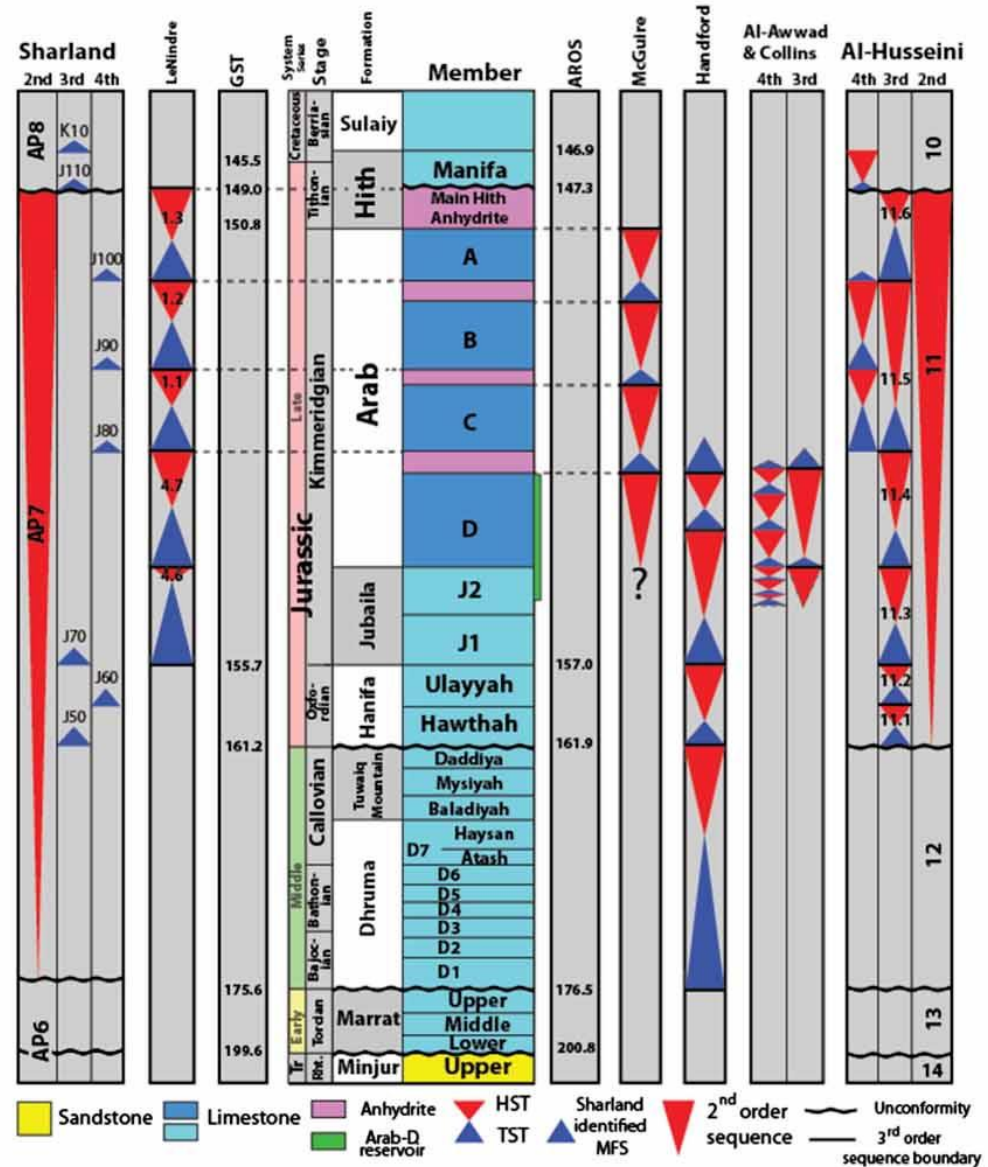


Fig. 1. Jurassic succession of Saudi Arabia. 2nd, 3rd and 4th order sequences are shown from Al-Husseini (1997, 2009) and Sharland et al. (2001). Key ages are illustrated from both the Geological Time Scale (Gradstein et al., 2004) and the Arabian Orbital Stratigraphy Project (Al-Husseini and Matthews, 2008). Lack of biostratigraphic control on the age of the Arab and Hith formations has been highlighted by Hughes (2004). Different positioning and identification criteria of HST and TST within the Arab and Hith formations are contrasted between McGuire et al. (1993), Le Nindre et al. (1990), Handford et al. (2002) and Al-Awwad and Collins (in review). Note that the Arab-D reservoir extends from the carbonates of the Arab-D Member of the Arab Formation to the upper part of Jubaila Formation. The Hellangian, Sinemurian, Pliensbachian and Alenian are not represented in Saudi Arabia's succession. The section is drawn not-to-scale to put the emphasis on the stratigraphy of the upper Jurassic. Modified from Al-Awwad and Collins (in review), Al-Husseini (2009), Handford et al. (2002), Le Nindre et al. (1990), McGuire et al. (1993), and Sharland et al. (2001).

identification criteria and correlates them on a platform-wide, shelf-to-basin, scale. The study also addresses the long-standing controversy surrounding the progradational direction of the reservoir, which has been suggested to be prograding in virtually all directions – north, south, east and west (Mitchell et al., 1988; Meyer and Price, 1993; Al-Saad and Sadooni, 2001; Handford et al., 2002; Lindsay et al., 2006; Stephens et al., 2009). To address this controversy, the study uses an extensive, never previously used data set of 32 cored wells described meticulously at a 10-cm scale and 500 thin sections. Working at such high-resolution enables the detection of subtle lithofacies

variations and deciphers what they disclose in terms of key geologic factors, their relative significance, and how they interplayed to control the paleoenvironments of deposition. The study also manifests the benefits of expanding the scope of geologic observations to a broader, trans-political-boarders sense, as it makes use of reported observation on the regional thinning and pinches out trends of the Arab and Hith formation carbonates and anhydrites in the United Arab Emirates, as discussed in Section 5.

Examining the cores from Khurais Field offered an excellent opportunity to formulate a regional perspective of the reservoir's configuration

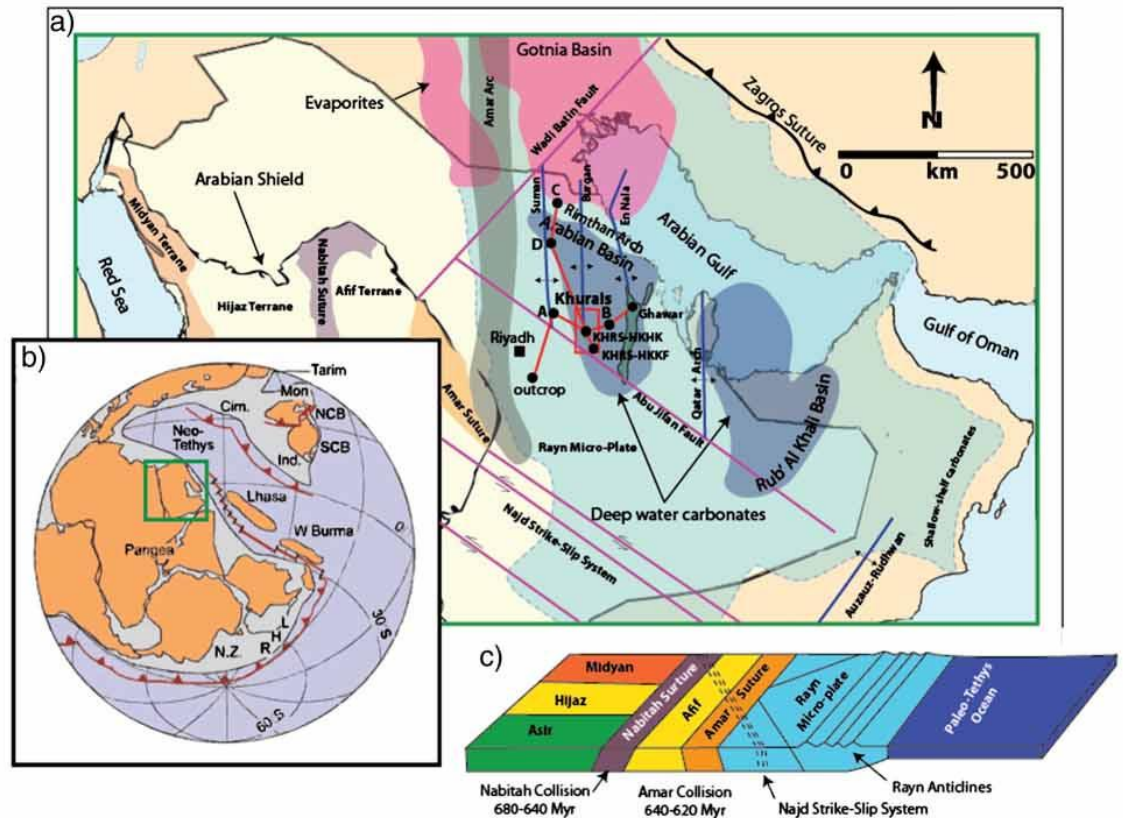


Fig. 2. a) Location map of the Khurais Field (red rectangle). Dark blue areas outline Late Jurassic intrashelf basins where deposition of deep water carbonates took place. The extent of shallow-shelf carbonate deposition is highlighted by the light blue area. b) Li and Powell's (2001) paleogeographic configuration during the Jurassic, with the Arabian plate position enclosed in the green square. Note that the location of the paleoequator is controversial (Stampfli et al., 2001; Golonka, 2002). c) Schematic model of the Precambrian Nabitah and Amar collisions that accreted the Arabian plate. Modified from Ziegler (2001), Li and Powell (2001) and Al-Husseini (2000).

and bridge, for the first time, the correlational gap between the Arab-D outcrop in Wadi Nisah, south of the Saudi capital, Riyadh, and the subsurface beneath Ghawar Field (Fig. 2). Two cross-sections are presented, a W–E one that extends from the Arab-D outcrop to Ghawar Field across a distance of 413 km; and a N–S cross-section that extends from the Safaniya area down to the southern tip of Khurais Field along a 397 km line of section (Fig. 2).

The concluded correlation model differs from the one presently in use and relies on the authors' previously proposed depositional environments' model and sequence stratigraphic framework of the reservoir (Al-Awwad and Collins, in press, in review). This model is able to predict lateral and vertical heterogeneities and architectural arrangements of the reservoir facies regionally. This could potentially guide future modeling of three-dimensional-spatial distribution of porosity, permeability, diagenetic, structural and other petrophysical parameters within the reservoir and depict how they dictate the architecture of fluid-flow and -baffle units.

2. Depositional model and sequence stratigraphic framework

The Arab-D lithofacies recognized in the Khurais Field are detailed in Al-Awwad and Collin's (in press) paper and summarized in Table 1; these lithofacies start at the bottom of the succession with monotonously interbedded couplets of lime mud and intraclastic lithofacies representing offshore basinal turbidites, followed by pelletal lithofacies that represent lower shoreface sands and silts, and then by stromatoporoid lithofacies which formed a shelf fringing reef. The reef protected a lagoon behind it where a meadow of

Cladocoropsis and dasyclad lithofacies were deposited. Then the succession goes up into peloidal and oolitic lithofacies that represent shore-attached, shallow subtidal sand sheets that are capped by cryptomicrobial lithofacies representing supratidal flats. Finally the reservoir units are sealed by the anhydrite lithofacies which reflect deposition in a sabkha followed by deposition in a salina. The reservoir is also characterized by the presence of stratigraphically reoccurring dolomite.

These facies are interpreted to have been deposited in a prograding, gently sloping shallow, arid, reef-rimmed carbonate shelf (Fig. 3b) (Al-Awwad and Collins, in press). The reef (sensu Hubbard, 1992; Blanchon et al., 1997; Wood, 1999; Montaggioni, 2005) was composed of mid-to-upper-shoreface, mostly reworked gregarious laminar (sensu Toland, 1994) and domical stromatoporoids and microbial encrustations. These are interpreted to have formed a discontinuous, but abundantly populated rim of reefal buildups that were, 3–5 m (10–16 ft) high, with their relief accentuated by the gentle nature of the shelf behind them (Meyer, 2000; Al-Awwad and Collins, in press).

The reservoir facies are stacked in a third-order composite sequence representing the Arab-D Member atop the upper part of another third-order composite sequence representing the upper part of the Jubaila Formation (Al-Awwad and Collins, in review).

Within these are six, fourth-order, high-frequency sequences, which are regionally correlated in this study; stacked in these are 12 parasequence-sets and cycle-sets, which contain multiple, fifth-order, parasequences in the upper composite sequence and parasequence-scaled cycles in the lower composite sequence (Al-Awwad and Collins, in review).

Table 1
Summary of Arab-D lithofacies and their deduced environmental settings.

Lithofacies	Textures	Components	Sedimentary structures	Depositional environment	Porosity types
Lime mud	Wackestone and lime mudstone	Lime mud, micritized pellets, bivalves, brachiopods, foraminifera (<i>Lenticulina</i> spp.), echinoderms, blackened and reddened peloids and pellets	Moderately sorted, phosphatized hardground or firmground caps; bioturbation; horizontal laminations; hardground burrows filled with grainier sediments; hummocky cross stratification; Bouma sequence divisions C, D, and E	Basin, offshore transition to offshore	Microporosity, moldic, intraparticle
Intra-clastic	Packstone to floatstones and rudstones	Intraclasts, oncolites, bivalves, reworked stromatoporoid, coral fragments, foraminifera, pellets, peloids	Extremely poorly sorted; phosphatized hardground or firmground bases; sharp to gradational upper contacts; Bouma sequence divisions A and B	Basin, offshore transition to offshore	Interparticle, intraparticle, microporosity
Pelletal	Wackestone to grain-dominated packstone	Pellets, bivalve fragments, foraminifera, lime mud	Moderately sorted, gradational or firmground contacts, bioturbation, horizontal laminations	Sands and silts at FWWB, lower shoreface	Moldic and microporosity
Stromatoporoid	Wackestone to floatstones and rudstones	Displaced domal and encrusting stromatoporoids, corals, microbial incrustations, foraminifera, bivalves, pellets, peloids, oncoids, intraclasts	Very poorly sorted, hardgrounds, firmgrounds, heavy bioturbation, borings	Reef, medium to upper shoreface	Vugular, moldic, intraparticle
<i>Cladocoropsis</i>	Wackestone to floatstone and rudstones	Nodular and dendroid <i>Cladocoropsis</i> , <i>Shuqraia</i> , foraminifera, corals, bivalves, peloids, <i>Clypeina</i> , <i>Thaumatoporella</i>	Poorly sorted; subrounded; firmgrounds; bioturbations; horizontal laminations	Lagoon, upper shoreface	Interparticle, intraparticle, moldic, vugular
Dasyclad	Wackestone and packstone	<i>Clypeina</i> , <i>Thaumatoporella</i> , miliolid, <i>Kurnubia</i> , bivalves and peloids	Firmgrounds; bioturbation; wispy laminations	Lagoon, upper shoreface	Moldic, intraparticle
Peloidal	Packstone to grainstone	Peloids, bivalves, micritized <i>Cladocoropsis</i> , foraminifera	Well sorted, well rounded to rounded, massive unstratified beds, horizontal lamination, low angle cross stratification, bioturbation, graded bedding	Sand sheet, foreshore	Interparticle, moldic, intraparticle
Oolitic	Grainstone and grain-dominated packstone	Ooids, bivalves, foraminifera	Very well sorted, well rounded, hardgrounds, firmgrounds; high and low angle cross stratification, horizontal laminations	Sand sheet, foreshore	Interparticle, moldic
Crypto-microbial	Mudstone to grainstone	Cryptomicrobial laminates, ooids, and cerithid gastropods and bivalves	Undulated and/or domed mm-scale microbial laminae	Supratidal, backshore	Moldic
Anhydrite	Vague	Anhydrite	Displasive nodules that increase upward into bedded nodular fabrics and ultimately become massive	Sabkha and Salina, backshore	None
Dolomite	Vague	Sucrosic, mosaic and saddle rhombs	Faint bioturbations	Stratigraphically reoccurring	Intercrystalline, moldic

3. Regional and structural settings

The Arabian plate formed by the accretion of the Midyan, Hijaz, and Asir terranes (Fig. 2c) to northeastern Africa before 715 Myr (Stoeser and Camp, 1985). After that, the Afif Terrane was accreted between 680 and 640 Myr, forming the Nabitah Suture. The Rayn Terrane, which is comprised of eastern and central Arabia fused with the Afif Terrane in what is known as the Amar collision, which took place between 640 and 620 Myr and yielded the Amar Suture, an obducted N-trending thrust slices of ophiolites (Fig. 2c) (Stoeser and Camp, 1985; Al-Husseini, 2000).

The Amar collision also generated EW-trending compressional stresses that propagated through the Arabian plate and formed uniformly aligned, N-oriented anticlines, namely the En Nala Anticline, the Khurais–Burgan Anticline, the Summan Platform and the Qatar Arch (Fig. 2a) (Stoeser and Camp, 1985; Brown et al., 1989; Al-Husseini, 2000). The Ghawar and Safaniya fields are situated on the 500 km long, En Nala Anticline; and the Khurais and Burgan fields are situated on the 500-km-long Khurais–Burgan Anticline (Al-Husseini, 2000). The collision also yielded two orthogonal, strike-slip faults that bind the Rayn anticlines, the NE-trending Wadi Batin Fault and NW-trending Abu Jifan

Fault (Fig. 2a). In addition, an extensive network of N, NW and NE trending faults cut through the Precambrian basement and propagated upward movement causing structural growth, subsidence and hydrocarbon migration throughout the Phanerozoic (Al-Husseini, 2000).

Subsequent to the Amar collision, between 530 and 620 Myr, the collapse of the Arabian–Nubian Shield took place (Husseini, 1988, 1989; Husseini and Husseini, 1990; Blasband et al., 2000; Genna et al., 2000). This event peaked by the formation of the extensive, 570 to 530 Myr, sinistral Najd Fault system and its associated rift basins (Fig. 2a, c). This extensional rifting phase caused the Rayn anticlines to become uplifted horsts bounded by normal faults and subsiding grabens (Al-Husseini, 2000; Brown, 1972; Brown and Jackson, 1960; Howland, 1979; Moore et al., 1979). Reactivation of the Ryan anticlines first occurred during the formation of the Najd Rift system. Subsequently, the Rayn anticlines were uplifted during the Carboniferous Hercynian Orogeny (Al-Husseini, 2000; Haq and Al-Qahtani, 2005). After that, the Rayn anticlines were reactivated during the Permo-Triassic Neo-Tethys rifting and spreading along the present day Zagros Suture and Gulf of Oman (Fig. 2b), which created a passive margin east of Arabia (Powers et al., 1966; Al-Husseini, 2000; Ziegler, 2001). Following that, the Neo-Tethys branched to the southwest

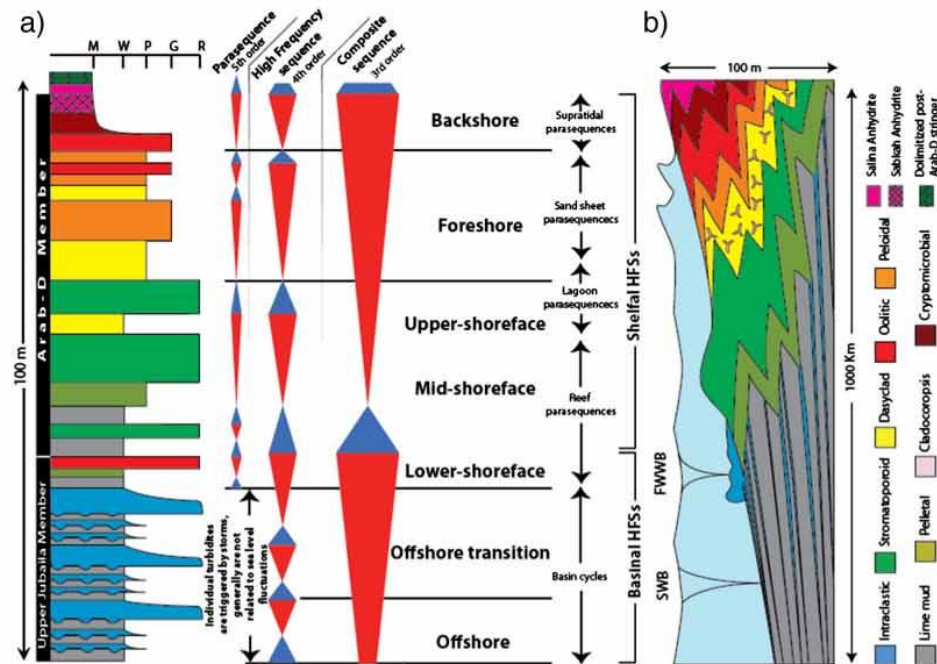


Fig. 3. a) An idealized Arab-D reservoir core with the interpreted sequence stratigraphic frame work. On the composite-sequence scale, the lower part's overall upward shallowing culminates with deposition of thin units of stromatoporoids characterized by reworked oolitic and/or coated grains (colored in red) that mark a lower composite sequence boundary. This is followed by a marine flood represented by a thin interval of interbedded lime mud and intraclastic lithofacies and is interpreted as a brief transgressive set that probably marks the contact between the Jubaila and Arab formations. The MFS of the upper composite sequence is picked at the highest occurrence of lime mud and or intraclastic lithofacies, which represents maximum extent of deeper lithofacies landward. After the MFS, the lithofacies continue to shallow up to sabkha anhydrites (indicated by the chicken wire pattern at the top of the section). The upper composite sequence boundary is placed at the transition from the sabkha anhydrites to the massive subaqueous anhydrites interpreted as early TST of a subsequent composite sequence. High frequency sequences (4th order) are picked based on vertical stacking patterns and each shows a unique lithofacies composition as the system shallows upward. On the parasequence scale (5th order), the individual basinal cycles represent storm triggered turbidites and hence do not represent sea level fluctuations. Their respective cycle sets and HFS reflect a stacking pattern that shows rhythmic thinning of the lime mud and thickening of the intraclastic lithofacies which is interpreted to represent sea level falls. Supratidal, sand-sheet, lagoon, and reef parasequences are shown in their respective positions of the platform and are discussed in detail in Al-Awwad and Collins (in review). b) A schematic depositional model of a prograding frequently storm-abraded, gently sloping, shallow, arid, stromatoporoid-reef-rimmed shelf of the Arab-D reservoir, not to scale (Al-Awwad and Collins, in press; Moore et al., 1992; Sellwood et al., 2000). Salina and sabkha anhydrites are followed by stromatolite, ooid and peloid sand sheets, and a *Cladocoropsis* and dasyclad meadow that were protected by a rim densely populated by small-scale stromatoporoid reefs toed by near fair-weather-wave-base (FWWB) pelletal silts. Storms mainly reworked the reefs generating intraclastic turbidites. The depositional model is juxtaposed next to the idealized sequence stratigraphic framework for comparison.

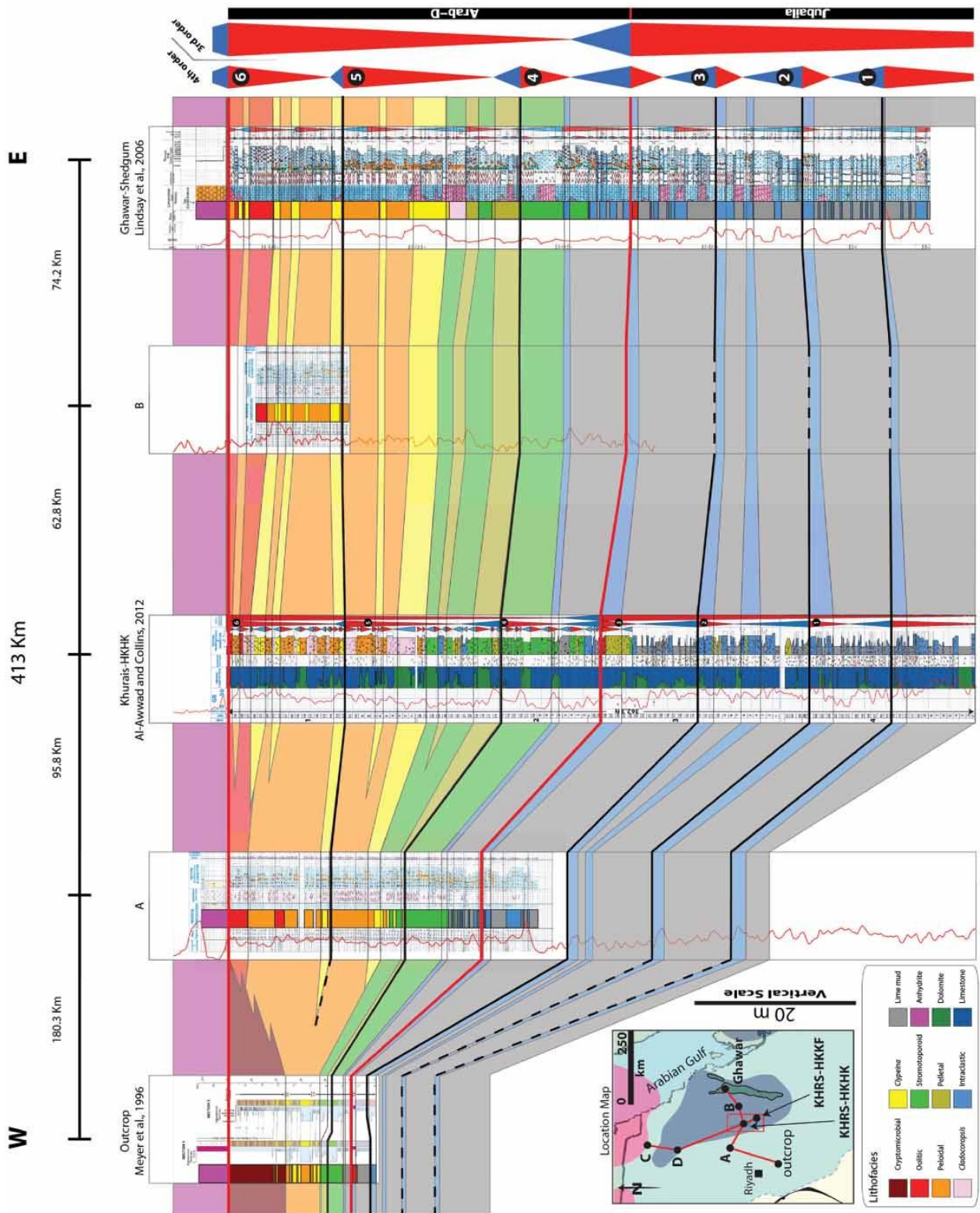
connecting with the Alpine Tethys and creating another passive margin along the plate's northern edge. This configuration yielded a vast shallow-marine shelf that occupied most of the Arabian Peninsula, and blanketed it with shallow shelf carbonate and evaporite deposition (Murriss, 1980; Le Nindre et al., 1987, 1990; Enay, 1993; Pollastro et al., 1999).

Organic rich, anoxic shales and lime muds (Hanifa and Tuwaiq Mountain formations; Fig. 1) that later sourced the oils of the Arab reservoirs were deposited in the intrashelf basins (Fig. 2a) that developed as a result of epirogenic downwarp during the Middle Jurassic (Murriss, 1980; Ayres et al., 1982; Alsharhan and Kendall, 1986; Droste, 1990; Ziegler, 2001).

Haq and Al-Qahtani (2005) concluded that the Arabian plate was tectonically stable leading to a dominance of eustatic control on sedimentation from middle Jurassic through Paleogene, as the global sea-level curve shows general agreement with the Arabian plate regional curve over that period (Le Nindre et al., 1990). Thus, in the Late Jurassic, carbonates of the Arab Formation progressively filled the intrashelf basins with successive shoaling-upward carbonate cycles that exhibit uniformity in fabric and thickness and were capped by evaporitic flats (Ziegler, 2001; Haq and Al-Qahtani, 2005). Finally the Ryan anticlines were reactivated coevally to the Neo-Tethys closure due to the Arabian-Eurasian plate collision, which commenced in the Late Cretaceous, and caused the obduction of the Oman ophiolites and emergence of the Zagros Mountains (Alsharhan and Kendall, 1986; Wender et al., 1998; Al-Husseini, 2000; Ziegler, 2001; Haq and Al-Qahtani, 2005).

4. Methodology

One dimensional sequence stratigraphic analysis was initially conducted on 32 cored wells in Khurais and presented in Al-Awwad and Collins's (in review) paper (Fig. 3a). Lithofacies components, repetitive motifs of lithofacies stacking patterns, recognition of retrogradational, aggradational and progradational modulations, vertical thickening versus thinning trends, upward fining versus coarsening and/or shallowing versus deepening trends (Van Wagoner et al., 1990) coupled with gamma log calibrations have been utilized in this correlation study. Third-order sequence boundaries were identified based on evidence of exposure and stacking pattern modulations. Candidate fourth-order flooding surfaces were identified and utilized in the correlation based on the interpretation of depositional environments. The gamma log calibration worked exceptionally well in the monotonous, turbidity-dominated basinal part of the Arab-D reservoir, where gamma values showed regional consistency and conspicuous rhythmicity that accords with the turbidites' high-frequency-sequences (HFSs). A question of the Arab-D's gamma signal being a reflection of diagenetic fluids mobilization, which could cause disequilibrium of parent/daughter activity ratios in uranium and thorium decay series, has been raised (cf. Ivanovich and Harmon, 1992; Mey, 2008). While that could very well be true, the data presented herein argues against excluding a depositional causality due to the following reasons. First, the gamma signal shows a consistent, characteristic upward increase of a scale that



accords with the reservoir's HFS scale established by the lithofacies stacking patterns (Al-Awwad and Collins, in review). Second, the gamma trends, as illustrated in this study, are consistent on a regional-scale, hundreds of kilometers across; diagenetic trends, on the other hand, are expected to be less extensive. Third, diagenetic effects, such as dolomitization, dissolution, and cementation, could distort a depositional signal that is already there, but that does not necessitate them being the only or determinant cause of it. Fourth, the correlation presented here is based on a sequence stratigraphic framework that is entirely reliant on sedimentary trends (Al-Awwad and Collins, in review) and it would be rather inexplicable to attribute its drastic, regional-scaled agreement with the preserved gamma signal to mere coincidence.

5. Regional correlation

Bridging the correlational gap between the Arab-D outcrop and the subsurface in Ghawar Field has only been tentatively attempted before by Leinfelder et al. (2005). Another regional correlation was attempted by Handford et al. (2002), but it did not account for the area west of Ghawar, which, in light of this study, has a significant role in understanding the regional configuration of the reservoir and interlacing the outcrop to the subsurface (Al-Saad and Sadooni, 2001).

It has been established that the upper part of the Arab-D reservoir reflects a long term shallowing event that preserved an upper, 1 to 3 Myr, third-order, composite sequence that represents the Arab-D Member (Le Nindre et al., 1990; McGuire et al., 1993; Sharland et al., 2001; Al-Husseini, 2009) where deposition took place on the shallow marine shelf, rimmed by a reef, above fair-weather-wave-base (FWWB) (Al-Awwad and Collins, in press, in review).

The lower part of the reservoir preserved the upper part of another 1 to 3 Myr, third-order, composite sequence that represents the upper part of the Jubaila Formation (Le Nindre et al., 1990; Sharland et al., 2001; Al-Husseini, 2009) where, for the most part, turbidite couplets characterized by the presence of Bouma sequences (Bouma, 1962; Walker, 1985) were deposited in a relatively deep basinal sub FWWB setting (Fig. 3b). This notion is supported by Alsharhan and Kendall (1986) who stated that the transition from Jubaila Formation into Arab-D Member in the Arabian intrashelf basin marks a shallowing upward cycle from deep subtidal facies into shallow intertidal and ultimately into supratidal sabkha anhydrites. These composite sequences are punctuated by six, 0.1 to 0.4 Myr, fourth-order, high frequency sequences, which contain at least 12 parasequence sets, and multiple parasequences and small scale cycles (Al-Awwad and Collins, in review).

The upper boundary of the Arab-D composite sequence is interpreted as a type II sequence boundary, tentatively dated by placement to Al-Husseini and Matthews' (2008) orbital forcing model at 153.4 Myr (Al-Husseini, 2009), and placed at the transition from the sabkha anhydrites to the massive subaqueous anhydrites, as they represent a sea-level transition from a fall to a rise (Fig. 3a). The lower boundary of the Arab-D composite sequence is also a type II sequence boundary, tentatively dated by placement to Al-Husseini and Matthews' (2008) orbital forcing model at 154.6 Myr (Al-Husseini, 2009), and is placed at the base of a thoroughgoing transgressive interval. This interval tops an extensive stromatoporoid reef layer that contains reworked oolitic and/or coated grains (colored in red in the cross-sections) and caps the basinal interbedded intraclastic and lime mud lithofacies of the upper Jubaila Member (Fig. 3a).

Fig. 4 shows a W–E regional correlation across 413 km. The cross-section starts on the Arab-D outcrop sections, described by Meyer et al. (1996), where the capping anhydrites were dissolved,

carbonates were brecciated and the reservoir's lithostratigraphic zones are present, except for the *Cladocoropsis* and the oolitic lithofacies. The section then extends east towards well A, KHRS-HKHK (coded well name), well B, and finally to a well in the Ghawar Field described by Lindsay et al. (2006). Fig. 5 shows a N–S regional correlation that extends for 397 km across well C, well D, Khurais HKHK, and Khurais HKKF (coded well name). The two cross-sections' intersection in the KHRS-HKHK well and a fence diagram showing the two sections in 3D is illustrated in Fig. 6. The authors' previous sedimentologic and stratigraphic work (Al-Awwad and Collins, in press, in review) has been used as a common denominator to unify the reservoir characterization done by other authors (Meyer et al., 1996; Lindsay et al., 2006) who worked in the area. Fourth order high frequency sequences identified in Khurais are numbered and correlated to the other outcrop and subsurface sections (Figs. 4, 5). The boundaries of the Arab-D composite sequence are marked by thick red lines; both sections are datumed from the upper Arab-D sequence boundary; and the boundaries were correlated across both cross-sections using the above highlighted criteria (Figs. 4, 5). Fig. 4 shows that the Arab-D composite sequence increases in thickness from 15.2 m (50 ft) in the outcrop section to 46.6 m (153 ft) in Khurais and finally to 50.0 m (164 ft) in Ghawar, as its lower boundary significantly shifts downward from W to E. Fig. 5, however, illustrates that the Arab-D composite sequence, except at the location of well D, maintains, more or less, the same thickness across the 397 km of cross-section as its lower boundary remains at the same elevation. It is difficult to depict with certainty whether the Jubaila composite sequence is thickening or thinning in any of the sections as its lower boundary is not penetrated by the cores or exposed in the outcrop.

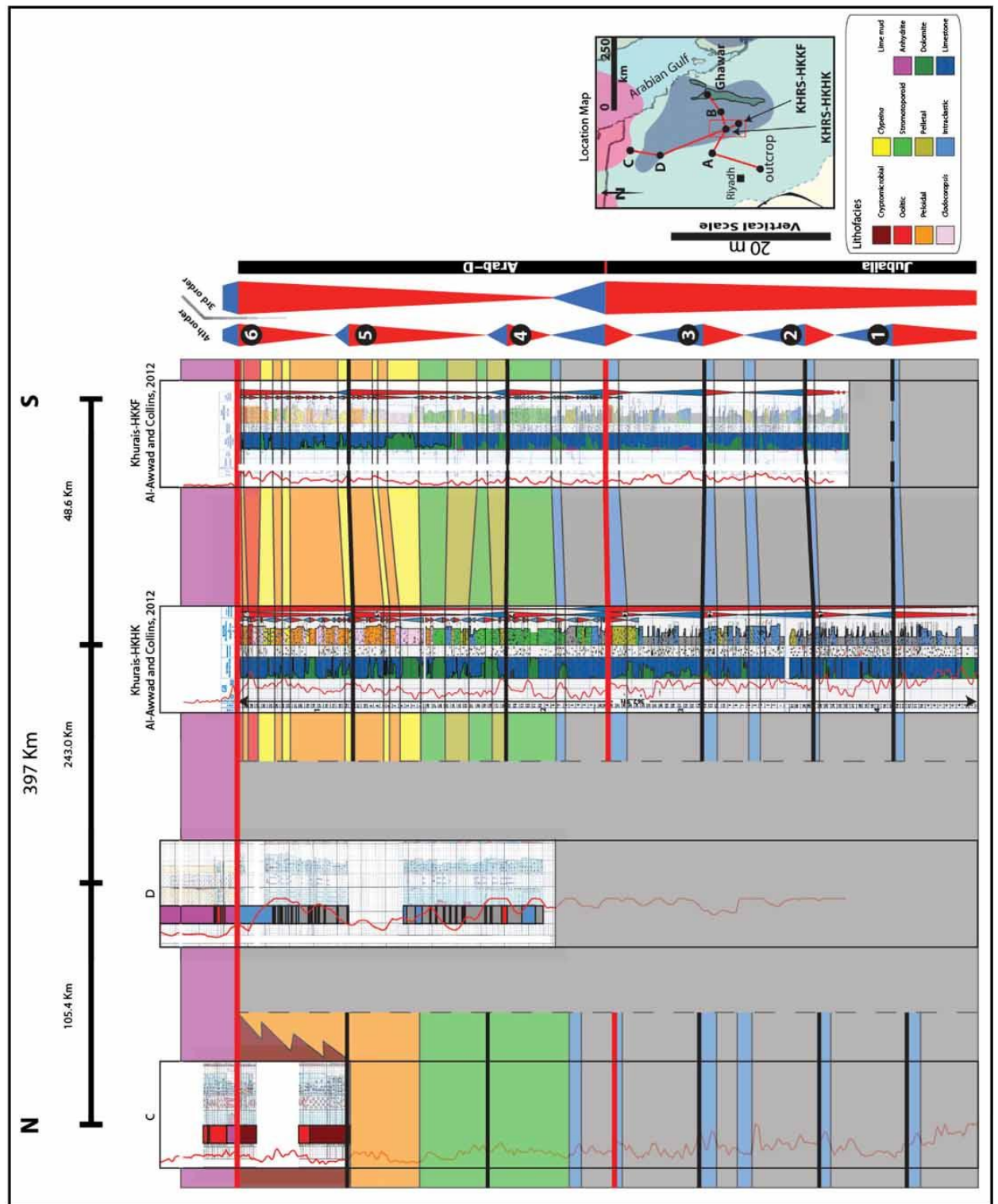
5.1. Shelfal lithofacies correlated from W to E

Focusing on the W–E cross-section, the shelfal lithofacies (HFS 4, 5 and 6) almost triple in thickness from the outcrop to Khurais, continue thickening slightly to Ghawar, and correspondingly show a significant downward shift in elevation (Fig. 4). The upper carbonates of the Arab-D Member (Fig. 4) are composed of thick supratidal cryptomicrobial laminites in the outcrop that quickly diminish eastward, except for very thin slivers below the anhydrites. Within HFS 6, the oolitic lithofacies is absent in the outcrop, appears in well A, thickens and splits into two cycles in Khurais, and becomes thickest in Ghawar. The peloidal, lagoonal and reefal lithofacies in HFS 4, 5 and 6, show consistent thickening to the east. HFS 6 and 5 condense into one HFS west of well A (Fig. 4). The oolitic lithofacies seems to dominate in the highstand system tract, HST, of HFS 6, whereas the peloidal sand sheet dominates its transgressive system tract, TST. In HFS 5, the peloidal and the lagoonal lithofacies dominate the HST, whereas the reefal lithofacies dominate the TST. The HST of HFS 4 is dominated by reefal lithofacies while its TST is dominated by the basinal turbidites.

5.2. Basinal lithofacies correlated from W to E

Correlation of individual storm beds has been shown to extend from 5 up to 28 km (3 to 15 miles) in various outcrop studies (Aigner, 1985; Elrick and Read, 1991). The storm triggered turbidite couplets of the lower part of the Arab-D reservoir are correlated across hundreds of kilometers here based on their thickening upward packages rather than individual beds. These packages have been attributed to eustatic fluctuations that probably lowered storm-wave base allowing higher levels of energy to generate upward thickening turbidites (Al-Awwad and

Fig. 4. A west–east cross-section of the Arab-D reservoir correlating its outcrop south of Riyadh to its subsurface in the Ghawar Field. The Upper and lower boundaries of the Arab-D composite sequence are shown by thick red lines. Thick black lines show the correlation of six HFS identified in the Khurais Field. Outcrop and core lithofacies have been color-flagged in accordance with Al-Awwad and Collins (in press) color-scheme. Eastward progradation of the reservoir is evident by the upper shelfal part of the reservoir consistently thickening eastward. The basinal HFS show slight thinning from Khurais to Ghawar. The anhydrites capping the reservoir units are dissolved and brecciated in the outcrop.



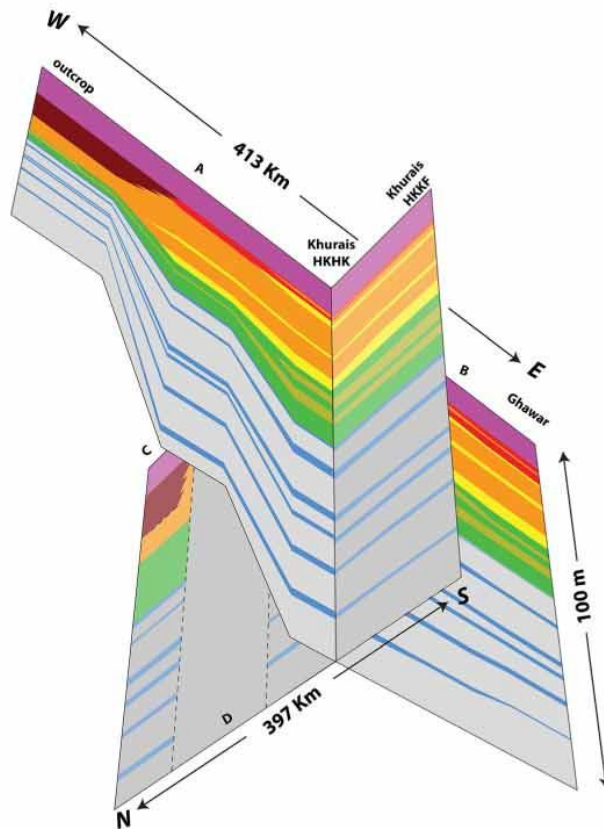


Fig. 6. A fence diagram showing the intersection of Figs. 4 and 5 at Khurais HKHK.

Collins, in press). Hence these upward thickening packages have also been used to identify high-frequency-sequence in the lower part of the reservoir (Al-Awwad and Collins, in review).

From W to E (Fig. 4), this thickening trend seems to hold true again for the basal part of the reservoir (HFS 1, 2 and 3), at least for HFS 3, which is correlatable, top to bottom, all the way through to the outcrop, and drastically thickens from 1.5 m (5 ft) in the outcrop, to 12 m (39 ft) in Khurais. Both the lime mud and particularly the intraclastic lithofacies in HFS 1, 2 and 3 drastically thicken and downstep from the outcrop to Khurais and then slightly thin away from Khurais towards Ghawar (Fig. 4). Finally, the hardgrounds separating the lime mud from the intraclastic lithofacies are 10 cm (4 in.) apart in the outcrop, 15 cm (6 in.) apart in the Khurais Field, and 0.6–0.9 m (2–3 ft) apart in the Ghawar Field (Lindsay et al., 2006).

5.3. N to S correlation

From N–S, Fig. 5 illustrates that the shelfal and basal lithofacies have approximately similar thicknesses, showing a “layer-cake” geometry except for the cryptomicrobial lithofacies which pinches out somewhere between well C (where a major collapsed breccia surface appears beneath the anhydrites) and Khurais HKHK. The shelfal lithofacies are completely absent at well D and in another well located 93.2 km to the east of it (not included in the cross-section). In both of these anomalous wells, the basal lithofacies are situated directly

beneath the Arab-D anhydrite without passing through the shelfal lithofacies.

6. Discussion

6.1. Composite sequence boundaries

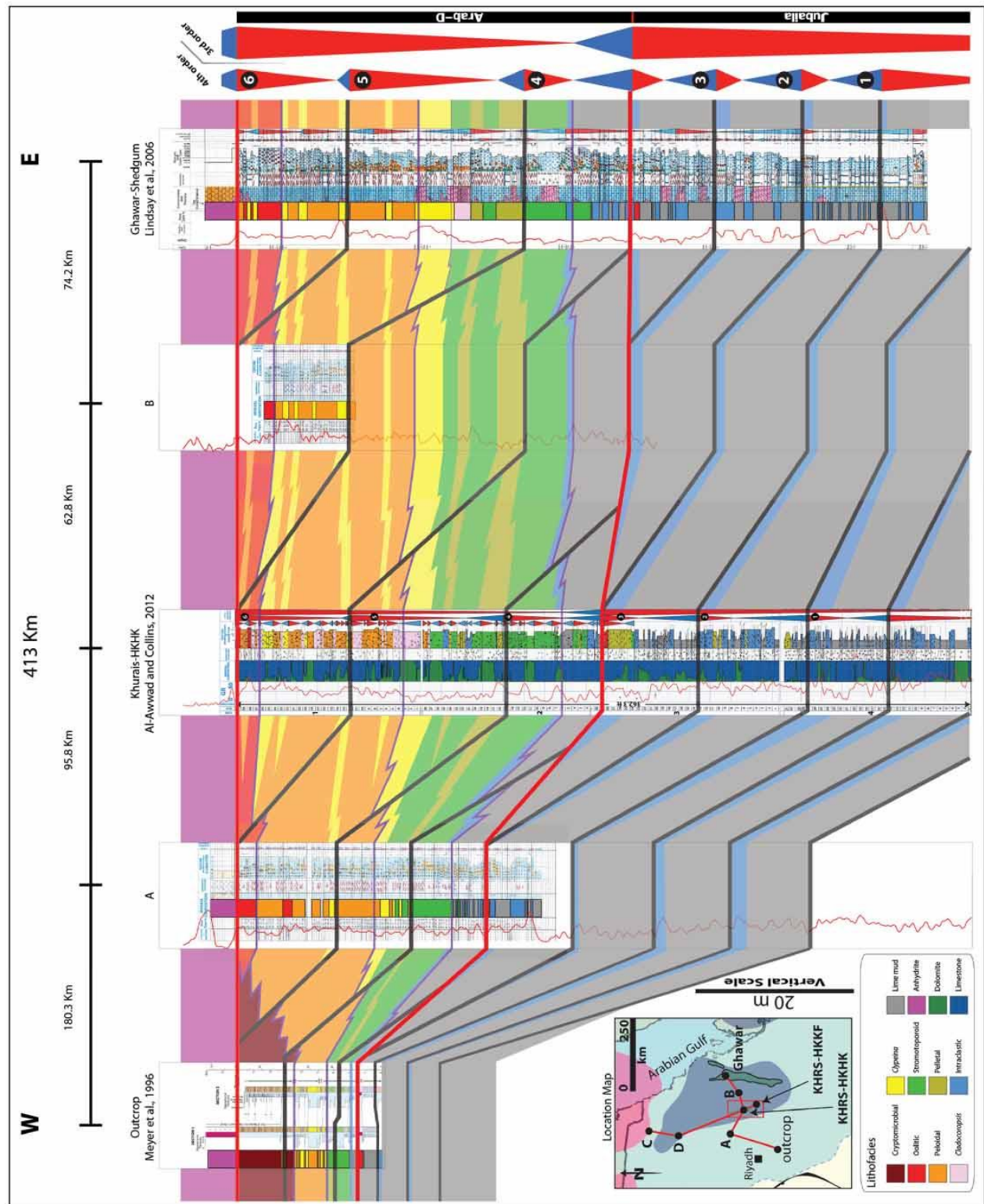
The different sequence stratigraphic interpretations concluded by different authors who worked on the Arab Formation, as presented in Fig. 1, are imputed to the inherent difficulties of the succession represented by the inaccuracies of the biostratigraphic–radiometric timing that marks the entire Phanerozoic of the Arabian platform (Al-Husseini and Matthews, 2005, 2008). This combines with the Arab Formation’s lack of biostratigraphic age control (Hughes, 2004) and lack of observable caliches or karst surfaces makes working with this succession even more difficult.

The placement of the upper boundary of the Arab-D composite sequence at the transition from the sabkha anhydrites to the massive subaqueous salina anhydrites has been interpreted to represent a sea-level fall followed by a rise (Fig. 3a) (Al-Awwad and Collins, in review). This boundary’s identification criteria is substantiated by the major collapsed breccia surface, which appears beneath the anhydrites in well C in the north (Fig. 5), as it indicates a likely sea level drop and exposure. Placing the boundary within the anhydrites, as done here, is stratigraphically close, but not quite identical to the criteria established by Lindsay et al. (2006), Mitchell et al. (1988) and McGuire et al. (1993). These authors placed the upper composite sequence boundary at the transition between the reservoir’s carbonates and its sealing anhydrites, considering all of the anhydrites as transgressive salina deposits, accumulated during the subsequent composite sequence transgression. This study suggests that the subaqueous salina anhydrites are onlapping transgressive deposits over the sequence boundary surface, which caps the sabkha anhydrites, as modeled by Sarg (1988). This interpretation is similar to what Meyer and Price (1993) concluded, that the anhydrites represent the peak of the sea-level shallowing, though these authors did not specifically elaborate on the sequence boundary’s particular position.

Using different boundary identification criteria, Le Nindre et al. (1990) and Al-Husseini (1997, 2009), interpret the Arab anhydrites, including the one atop Arab-D, as highstand deposits (Fig. 1). One problem with this interpretation, at least in the Arab-D case, is that it does not explain how the extra accommodation was created. If deposition of the oolites, supratidal cryptomicrobial laminites, and sabkha anhydrites that cap the reservoir neared or reached sea-level, then how could extra accommodation be created within the same composite sequence’s HST to contain the capping anhydrites? In other words, it appears rather inconceivable to generate enough accommodation within the same HST to deposit the entire Arab-D anhydrite, which averages a 48.0 m (157.5 ft) in the Khurais Field, when deposition had already neared or reached sea-level.

The lower composite sequence boundary marks the contact between the Arab and Jubaila formations and has been reported to contain 1 m (3 ft) of sandstone in the outcrop (Steineke et al., 1958) and coincides with reported eolian quartz silts from the subsurface of the Ghawar Field at the same interval (Lindsay et al., 2006). The criteria adopted here for identifying this boundary relied on the overall shallowing observed in the lower composite sequence marked by stromatoporoid appearance at the top of it. More specifically, the lower boundary is placed at the base of a laterally continuous transgressive interval that caps the first laterally extensive reef interval, which is characterized by reworked ooids and/or coated grains, and colored in

Fig. 5. A north–south cross-section of the Arab-D reservoir correlating it in the subsurface from the Safaniya area to south of the Khurais Field. The upper and lower boundaries of the Arab-D composite sequence are shown by thick red lines. Thick black lines show the correlation of six HFS identified in the Khurais Field. Core lithofacies have been color-flagged in accordance with Al-Awwad and Collins (in press) color-scheme. Both shelfal and basal lithofacies maintain similar thickness reflecting a layer-cake geometry except for the cryptomicrobial lithofacies. Shelfal lithofacies are absent at well D.



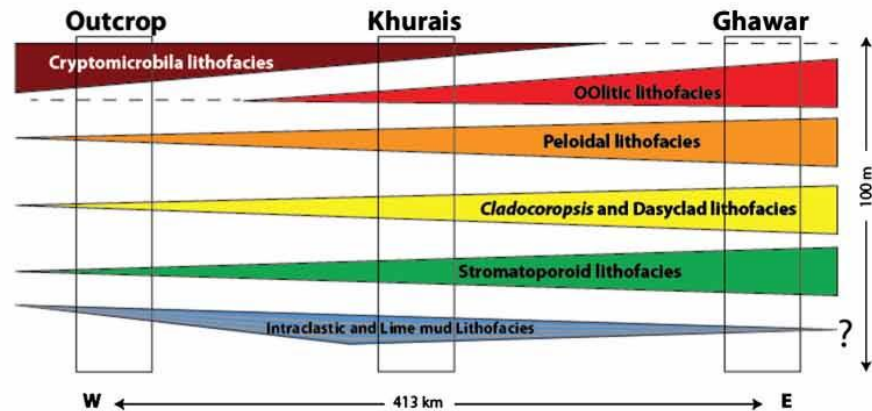


Fig. 8. Stratigraphic thickness model shows the regional thickness variance of major Arab-D reservoir lithofacies from the west to the east and depicts regional eastward porosity improvement in the upper part of the reservoir coupled with a porosity decrease in the lower part of the reservoir east of Khurais.

red in the cross-sections. These lower boundary identification criteria disagree with Meyer and Price (1993) who stated that the entire reservoir with both its lower (basinal) and upper (shelfal) parts represents a single genetic depositional sequence with no boundary separating them.

6.2. Regional progradation trends

It has been proposed that the intrashelf basins on the Arabian shelf were completely filled by the Kimmeridgian, and that led to interpreting the Arab-D reservoir to show a broad “layer-cake” aggradation (Ayres et al., 1982; Wilson, 1985). Contrastingly, Ziegler (2001) concluded that shelf marginal carbonates of the Hanifa, Jubaila, Arab and Manifa formations wedged out and downlapped onto the Arabian and Rub’ Al-Khali intrashelf basins. This study shows that the upward shallowing trend reflected vertically in the Arab-D reservoir lithofacies (Table 1) is translated laterally as a regional thickening interpreted as a progradational trend from W to E (Fig. 4). The reservoir’s lithofacies thicken and downstep eastward indicating that the late Jurassic basin was to the east, and that the paleoshoreline was trending in a N–S direction, relatively close to the current Arabian Gulf’s shoreline trend. This interpretation of the basin and shoreline positions agrees with Meyer et al. (1996) work on the Arab-D outcrop in Wadi Nisah, where they measured strike directions of symmetrical carbonate sand ripples whose wavelengths are 80 cm, heights are 5–7 cm and crests trended N5°W indicating that the paleoshoreline trended in the same direction. Perpendicular to these, Meyer et al. (1996) measured east-dipping imbricated flat-pebble conglomerates confirming a westward onshore. In addition, Meyer and Price (1993) concluded an eastward basin based on local correlation of the Arab-D reservoir across the Ghawar Field. This conclusion is also in accordance with the paleogeographic reconstructions of the Arabian Plate’s Jurassic intrashelf basins and its margin with the Neo-Tethys (Fig. 2b) (Li and Powell, 2001; Ziegler, 2001).

Previous studies have suggested that a grain shoal formed on the Rimthan Arch framed the Arabian intrashelf basin and prograded southward to fill it (Handford et al., 2002). This reasoning is based on regional top Arab-D anhydrite thickening to the south, which has been interpreted as salina deposits of a subsequent transgression (Handford et al., 2002; Lindsay et al., 2006). Had this been the case, then it would be inexplicable that the Arab-D grainy lithofacies are present to the west of Ghawar in Khurais, and as far as west of the

outcrop, as shown in this study. On the contrary, Meyer and Price (1993) and Mitchell et al. (1988) suggested the progradation to be trending to the north based on carbonate thickening in that direction, explaining the evaporites as coeval sabkha deposits thinning out to the north. Yet, the above conclusions are based on local anhydrite and carbonate thinning trends, and take no heed of the regional Arab-D carbonate and top Arab-D anhydrite trends, which have been reported to pinch out to the east of Ruwais, located west of Abu Dhabi, in the United Arab Emirates (Simmons, 1994; de Matos and Hulstrand, 1995; Al-Silwadi et al., 1996). Moreover, Azer and Peebles (1995) showed considerable west to east thinning and pinch out of the Hith anhydrite and the Arab-C member in the area offshore of Abu Dhabi. These trans-political-boarder trends support the conclusion presented here of an eastward situated basin and progradation direction. This study agrees that the majority of the top Arab-D anhydrite was deposited in a salina setting; this could mean that the local anhydrite’s thickening trends are simply indicative of depressions’ positions along the Arabian shelf, rather than indicating progradation trends of the reservoir.

6.3. High-frequency sequence correlation

In the W–E cross-section (Fig. 4), peloidal, dasyclad, *Cladocoropsis*, and stromatoporoid lithofacies in HFS 4, 5 and 6 almost triple in thickness from the outcrop to Khurais, indicating that the accommodation space increased to the east allowing progradation and thickening of the upper lithofacies belts. This accords with Meyer et al. (1996) findings of slight eastward increase in thickness of these lithofacies in their correlations of the Arab-D outcrop measured sections. The thickness increase being most dramatic west of Khurais suggests that Khurais, well B and Ghawar occupied localities more proximal to the intrashelf depocenter, which probably was further east as suggested by the pinch out of the Arab-D and -C members in the United Arab Emirates (Simmons, 1994; Azer and Peebles, 1995). In addition, the capping anhydrites’ dissolution and brecciation in the outcrop suggest that these were closer to the shoreline and hence were subjected to exposure, as compared to the eastward localities that preserved the anhydrites. This thickening trend is accompanied by the appearance of the oolitic lithofacies to the east of the outcrop and its eastward thickening and splitting trend, which opposes the cryptomicrobial lithofacies eastward diminishing trend. This indicates a progradational trend from the west to the east in

Fig. 7. Hypothesized timelines superimposed on the dip section presented in Fig. 4. These timelines are based on expected impact of wave-energy and light-penetration variance on ecology and facies distribution at a shelf margin.

which relatively shallower lithofacies thin and pinch out giving way to the thickening of relatively deeper lithofacies in the upper part of the reservoir (HFS 6 and 5, Fig. 4). This progradation trend is further supported by the thinning of HFS 4 and condensation of HFS 6 and 5 in the outcrop section towards the paleoshoreline (Fig. 4).

The intraclastic and lime mud lithofacies in HFS 1, 2 and 3 also drastically thicken and downstep from the outcrop to Khurais (Fig. 4) indicating a progradational trend towards the east. This thickening trend also suggests that well A and the outcrop are more proximal to the intrashelf basin margin, where limited accommodation restricted deposition. The fact that hardgrounds are most frequent in the outcrop, less in Khurais, and least in Ghawar (Lindsay et al., 2006), first suggests that all three localities were probably within the Arabian intrashelf basin, hence the presence of the hardground-capped, basinal turbidity couplets in all of them. Second, this hardground frequency variance indicates that the three localities progress respectively from the basin's westward edge towards its center. In other words, the outcrop position at the margin would be subjected to more storm triggered turbidity avalanches; only bigger, fewer turbidites would reach deeper to Khurais further east; and even fewer and bigger ones would reach deeper to Ghawar, hence the progressively larger spacing among the hardgrounds eastward.

A previously proposed depositional model (Al-Awwad and Collins, *in press*) predicts that the basinal turbidites would thin in the progradation direction, which is observed in the slight thinning from Khurais to Ghawar, especially in the intraclastic lithofacies (Fig. 4). In addition, the thinning of HFS 1, 2 and 3 from Khurais to Ghawar suggests that the lime mud lithofacies represent, for the most part, divisions C, D and E of the Bouma sequences (Al-Awwad and Collins, *in press*), rather than flooding coming from the intrashelf basin from the east towards the west. It appears that as a result of progressive filling of the accommodation space to the east, the slopes of the lithofacies boundaries decreased gradually from the bottom part of the reservoir (HFS 1, 2 and 3) to the upper part of the reservoir (HFS 4, 5 and 6).

The N–S regional correlation section (Fig. 5) illustrates that the Arab-D and upper Jubaila lithofacies continue more or less with the same thickness across the 378 km of section. This coupled with the fact that the correlation lines connecting the HFS boundaries across the section are parallel to the lithofacies boundaries suggests that this section runs along regional strike, and that the strike direction does not change, at least along the 378 km line of section. The lower sequence boundaries of the Arab-D composite sequence and the regional flood that caps HFS 3 are clearly present, easily correlatable throughout and show no variation in elevation. The exception to this interpretation occurs at well D (Fig. 5), which shows basinal lithofacies directly beneath the Arab-D anhydrite. A similar trend continues on another well located 93.2 km to the east of it. The juxtaposition of basinal lithofacies in these two wells, right below the anhydrites, is anomalous in comparison to the hundreds of wells drilled in the study area. This anomaly could be explained by a regional trough where only basinal lithofacies were deposited and later were draped by the top Arab-D anhydrite; or it could indicate an uplift and erosion of the Arab-D shelfal lithofacies in that area. Unfortunately, the data available for this study are insufficient to verify any of these hypotheses.

6.4. The timeline dilemma

Correlating timelines within the Arab-D reservoir is problematic due to the lack of biostratigraphic age control (Hughes, 2004), which inopportunely coalesces with lack of exposure surfaces or sedimentary markers. In light of the authors' proposed depositional model (Fig. 3b), the correlation lines, tying the HFS (Figs. 4, 5), separate relatively deeper lithofacies, interpreted to be deposited during eustatic rises, from relatively shallower ones, interpreted to be deposited during eustatic falls. Hence, these correlation lines are presented here as stratigraphic-marker horizons, in their respective locations (i.e., in the

one dimensional sense of the well-bore or the outcrop section). It should be underlined here that these stratigraphic-marker horizons are not actual timelines.

The gentle slope (Meyer, 2000) of the depositional shelf is expected to cause the observed lithofacies lateral extensity, and consequently, cause the stratigraphic-marker horizons to follow the facies boundaries. Nevertheless, at a basin margin, the bathymetric gradient is expected to control a light-penetration gradient that would dictate the geographic distribution of photosynthetic producers, and accordingly, impact the distribution of benthonic consumers (Flügel, 2004). Additionally, the bathymetric gradient would impose a wave-energy gradient that would bear upon the platform's ecology (Flügel, 2004). Therefore, it is hypothesized here that these dynamics would mandate much-less-laterally-extensive timelines than the stratigraphic-marker horizons correlated in Fig. 4. These timelines would also transcend the lithofacies boundaries at a much steeper geometry than the geometry shown by the correlated stratigraphic marker horizons (Fig. 4). Thus, it is tempting to correlate each stratigraphic-marker horizon to the one sequentially above it as illustrated by Fig. 7, which shows hypothetical timelines (the thick black lines) superimposed on the dip section. These proposed hypothetical timelines transcend the facies boundaries and top lap against and downlap on the composite sequence boundaries (Fig. 7). With the lack of biostratigraphic constraint, pinning down the geographic location at which a link between a stratigraphic-marker horizon should be made to the one sequentially above it remains uncertain.

6.5. Reservoir quality

Based on local W–E correlation of the Arab-D reservoir across the Ghawar Field, Meyer and Price (1993) concluded that the reservoir quality improves eastward across Ghawar in the upper part reservoir, and decreases in the lower part. Data presented in this study agrees with their conclusion and extrapolate it regionally (Fig. 8). The shelfal reservoir lithofacies in HFS 4, 5 and 6 possess better reservoir qualities in Ghawar, as compared to Khurais, based on their regional progradational thickening eastward (Fig. 4). In the basinal part of the reservoir, the intraclastic floatstone and rudstone beds possess better porosity qualities than the lime mud beds. Regional correlation shows that the intraclastic floatstone and rudstones in HFS 1, 2 and 3 thicken from the outcrop to Khurais, and then thin from Khurais to Ghawar (Fig. 4).

A corresponding reservoir quality enhancement, followed by reduction in the same direction is expected. In addition, HFS 1, 2 and 3 thinning from Khurais to Ghawar and the hardground frequency decrease eastward suggest a decrease and possible pinch out of the turbidites, which could trap oil in the floatstones and rudstones, if the mudstones are sufficient to form permeability barriers. Vertically, in the lower part of the reservoir, the reservoir quality is predicted to improve at the HFS scale, 3–6 m (10–20 ft), as the intraclastic rudstones and floatstones' thickness increases up each of the basinal HFS (HFS 1, 2 and 3). The above reservoir-quality improvement deductions are based on reservoir facies thickening trends and could only be true provided no significant diagenetic overprint has negatively altered the reservoir porosity and/or permeability.

7. Conclusions

Predicting lateral and vertical heterogeneities and architectural arrangements of carbonates in the subsurface are a challenging task. High-frequency-sequence scaled stratigraphic analysis and correlation is crucial in tackling this task and is presented here through the analysis of one of the world's most significant reservoirs, the Arab-D reservoir.

The preserved upward shallowing trend of the Arab-D reservoir across the Khurais Field is manifested by an eastward progradational trend. This is demonstrably supported by the "layer-cake" stratigraphic

trends preserved in the reservoir in the N–S strike section. This line of reasoning is in agreement with the notion that progradation of the Arab-D reservoir took place across the shallow Late Jurassic epeiric shelf, and into the relatively deep Arabian intrashelf basin, which caused the Jurassic carbonates to downlap and change to argillaceous deep water carbonates (Alsharhan and Kendall, 1986; Meyer and Price, 1993; Ziegler, 2001; Leinfelder et al., 2005).

The data introduced in this study suggest that the outcrop, the Khurais Field and Ghawar Field were all located within the Arabian intrashelf basin, where the outcrop was proximal to the basin margin and the Ghawar Field was distal to it. The authors' previously proposed model of a storm "shaved" reef rimmed carbonate shelf for the reservoir explains the thickening and downward climb of the shelfal and basinal lithofacies observed in the dip-section (Fig. 4). Furthermore, the proposed model and correlation predict a regional eastward porosity improvement in the upper part of the reservoir and a reduction in the lower part of the reservoir, in addition to a vertical reservoir quality improvement at the scale of the HFS in the lower part of the reservoir, assuming a null diagenetic effect. This model, once integrated with petrophysical and structural data could predict fluid flow patterns in the reservoir.

Acknowledgments

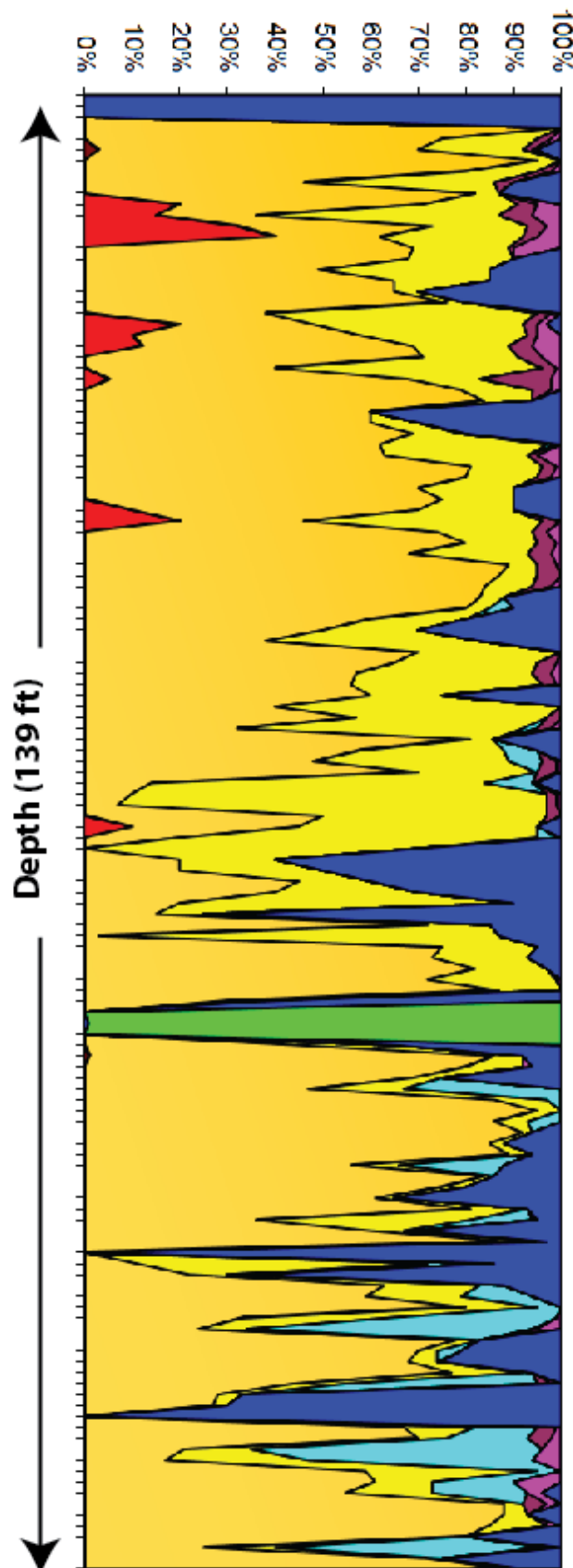
We thank Aus Al-Tawil of Saudi Aramco for his unremitting support and commitment to this study. We would like to thank Saudi Aramco for granting permission to publish this study. Our appreciation is also extended to Luis Pomar, University de les Illes Balears, Spain for his beneficial discussions and keen insights.

References

- Aigner, T., 1985. Storm depositional systems: dynamic stratigraphy in modern and ancient shallow-marine sequences: Storm depositional systems: dynamic stratigraphy in modern and ancient shallow-marine sequences: Berlin, Federal Republic of Germany (DEU). Springer Verlag, Berlin, 174 pp.
- Al-Awwad, S., Collins, L.B., 2013. Arabian carbonate reservoirs – a depositional model of the Arab-D reservoir in Khurais field, Saudi Arabia. AAPG Bulletin (in press) <http://dx.doi.org/10.1306/11051212103>.
- Al-Awwad, S., Collins, L.B., 2013w. Stacked high frequency carbonate reservoir sequences in the Arab-D, Khurais field, Saudi Arabia. Marine and Petroleum Geology (in review).
- Al-Ghamdi, A., Tello, R., Al-Bain, F., Swadi, M., 2008. Collaboration breeds success in the Khurais Mega-Project in Saudi Arabia. Paper presented at the 2008 SPE Saudi Arabia cSection Technical Symposium on the Ultimate Challenge: Unlocking Hydrocarbons Through Optimum Exploitation Strategies, Al Khobar, Saudi Arabia.
- Al-Husseini, M.I., 1997. Jurassic sequence stratigraphy of the western and southern Arabian Gulf. *GeoArabia (Manama)* 2, 361–382.
- Al-Husseini, M.I., 2000. Origin of the Arabian Plate structures; Amar collision and Najd rift. *GeoArabia (Manama)* 5, 527–542.
- Al-Husseini, M., 2009. Update to Late Triassic–Jurassic stratigraphy of Saudi Arabia for the Middle East geologic time scale. *GeoArabia (Manama)* 14, 145–150 (155–156, 159–162, 167–168, 171–172, 175–178, 181–182, 185–186).
- Al-Husseini, M.I., Matthews, R.K., 2005. Arabian orbital stratigraphy: Periodic second-order sequence boundaries? *GeoArabia (Manama)* 10 (2), 165–168.
- Al-Husseini, M., Matthews, R.K., 2008. Jurassic–Cretaceous Arabian orbital stratigraphy: the AROS–JK chart. *GeoArabia (Manama)* 13, 89–94 (1 sheet).
- Al-Mulhim, W.A., Al-Ajmi, F.A., Al-Shehab, M.A., Pham, T.R., 2010. Khurais complex; 1. field development required best practices, leveraged technology. *Oil & Gas Journal* 108, 37–38 (40–42).
- Al-Saad, H., Sadooni, F., 2001. A new depositional model and sequence stratigraphic interpretation for the Upper Jurassic Arab 'D' reservoir in Qatar. *Journal of Petroleum Geology* 24 (3), 243–264.
- Alsharhan, A.S., Kendall, C.G.S.C., 1986. Precambrian to Jurassic rocks of Arabian Gulf and adjacent areas: their facies, depositional setting, and hydrocarbon habitat. AAPG Bulletin 70, 977–1002.
- Al-Silwadi, M.S., Kirkham, A., Simmons, M.D., Twombly, B.N., 1996. New insights into regional correlation and sedimentology, Arab Formation (Upper Jurassic), offshore Abu Dhabi. *GeoArabia (Manama)* 1 (1), 6–27.
- Ayres, M.G., Bilal, M., Jones, R.W., Slentz, L.W., Tartir, M., Wilson, A.O., 1982. Hydrocarbon habitat in main producing areas, Saudi Arabia. AAPG Bulletin 66, 1–9.
- Azer, S.R., Peebles, R.G., 1995. Sequence stratigraphy of the Hith/Upper Arab Formations offshore Abu Dhabi, UAE. Paper presented at the Middle East Oil Show, Bahrain.
- Blanchon, P., Jones, B., Kalbfleisch, W., 1997. Anatomy of a fringing reef around Grand Cayman: storm rubble, not coral framework. *Journal of Sedimentary Research* 67 (1), 1–16. <http://dx.doi.org/10.1306/d42684d7-2b26-11d7-8648000102c1865d>.
- Blasband, B., White, S., Broojmans, P., De Boorder, H., Visser, W., 2000. Late Proterozoic extensional collapse in the Arabian–Nubian Shield. *Journal of the Geological Society* 157, 615–628.
- Bouma, A.H., 1962. *Sedimentology of Some Flysch Deposits: A Graphic Approach to Facies Interpretation*. Elsevier, Amsterdam.
- Brown, G.F., 1972. Tectonic map of the Arabian Peninsula. Open-File Report – U.S. Geological Survey, p. 1 (sheet).
- Brown, G.F., Jackson, R.O., 1960. The Arabian Shield. Proceedings of the 21st International Geological Congress. Copenhagen 9, 69–77.
- Brown, G.F., Schmidt, D.L., Huffman Jr., A.C., 1989. Geology of the Arabian Peninsula; shield area of western Saudi Arabia. United States Geological Survey Professional Paper A1–A188.
- de Matos, J.E., Hulstrand, R.F., 1995. Regional characteristics and depositional sequences of the Oxfordian and Kimmeridgian, Abu Dhabi. Middle East Geosciences Conference: GEO, vol. 94, pp. 346–356.
- Droste, H., 1990. Depositional cycles and source rock development in an epeiric intra-platform basin; the Hanifa Formation of the Arabian Peninsula. *Sedimentary Geology* 69, 281–296.
- Elrick, M., Read, J.F., 1991. Cyclic ramp-to-basin carbonate deposits, Lower Mississippian, Wyoming and Montana; a combined field and computer modeling study. *Journal of Sedimentary Petrology* 61, 1194–1224.
- Enay, R., 1993. Les Apports sud-téthysiens parmi les faunes jurassiques nord-ouest européennes; interpretation paleobiogéographique. Comptes Rendus de l'Académie des Sciences, Serie 2, Mécanique, Physique, Chimie, Sciences de l'Univers, Sciences de la Terre, vol. 317, pp. 115–121.
- Flügel, E., 2004. *Microfacies of Carbonate Rocks: Analysis, Interpretation and Application*. Springer Verlag.
- Genna, A., Vaslet, D., Janjou, D., Le Metour, J., Halawani, M., 2000. Rifting of the Arabian Platform during the Proterozoic-to-Phanerozoic interval. *GeoArabia (Manama)* 5, 94–95.
- Goldhammer, R.K., Dunn, P.A., Hardie, L.A., 1990. Depositional cycles, composite sea-level changes, cycle stacking patterns, and the hierarchy of stratigraphic forcing: examples from Alpine Triassic platform carbonates. *Geological Society of America Bulletin* 102 (5), 535–562. [http://dx.doi.org/10.1130/0016-7606\(1990\)102<0535:dcclsc>2.3.co;2](http://dx.doi.org/10.1130/0016-7606(1990)102<0535:dcclsc>2.3.co;2).
- Golonka, J., 2002. Plate-tectonic maps of the Phanerozoic. Special Publication – Society for Sedimentary Geology 72, 21–75.
- Gradstein, F.M., Ogg, J.G., Smith, A.G., Agterberg, F.P., Bleeker, W., Cooper, R.A., Davydov, V., Gibbard, P., Hinnov, L., House, M.R., Lourens, L., Luterbacher, H.P., McArthur, J., Melchin, M.J., Robb, L.J., Shergold, J., Villeneuve, M., Wardlaw, B.R., Ali, J., Brinkhuis, H., Hilgen, F.J., Hooker, J., Howarth, R.J., Knoll, A.H., Laskar, J., Monechi, S., Plumb, K.A., Powell, J., Raffi, I., Roehl, U., Sanfilippo, A., Schmitz, B., Shackleton, N.J., Shields, G.A., Strauss, H., van Dam, J., van Kollfshoten, T., Veizer, J., Wilson, D., 2004. A geological time scale 2004. Miscellaneous Report – Geological Survey of Canada. 1 (sheet-1 sheet).
- Handford, C.R., Loucks, R.G., 1994. Carbonate depositional sequences and systems tracts-responses of carbonate platforms to relative sea-level changes. *Houston Geological Society Bulletin* 37 (4), 10.
- Handford, C.R., Cantrell, D.L., Keith, T.H., 2002. Regional facies relationships and sequence stratigraphy of a super-giant reservoir (Arab-D Member), Saudi Arabia. Program and Abstracts – Society of Economic Paleontologists. Gulf Coast Section. Research Conference, vol. 22 539–563.
- Haq, B.U., Al-Qahtani, A.M., 2005. Phanerozoic cycles of sea-level change on the Arabian Platform. *GeoArabia (Manama)* 10, 127–160.
- Howland, A.F., 1979. Tectonics of the Najd transcurrent fault system, Saudi Arabia. *Journal of the Geological Society of London* 136, 441–454 (Part 4).
- Hubbard, D.K., 1992. Hurricane-induced sediment transport in open-shelf tropical systems: an example from St. Croix, US Virgin Islands. *Journal of Sedimentary Research* 62 (6), 946–960. <http://dx.doi.org/10.1306/d4267a23-2b26-11d7-8648000102c1865d>.
- Hughes, G.W., 2004. Middle to Upper Jurassic Saudi Arabian carbonate petroleum reservoirs: Biostratigraphy, micropalaeontology and palaeoenvironments. *GeoArabia (Manama)* 9 (3), 79–114.
- Husseini, M.I., 1988. The Arabian Infracambrian extensional system. *Tectonophysics* 148, 93–103.
- Husseini, M.I., 1989. Tectonic and deposition model of late Precambrian–Cambrian Arabian and adjoining plates. AAPG Bulletin 73, 1117–1131.
- Husseini, M.I., Husseini, S.I., 1990. Origin of the Infracambrian salt basins of the Middle East. *Geological Society Special Publications* 50, 279–292.
- Ivanovich, M., Harmon, R.S., 1992. Uranium-series Disequilibrium: Applications to Earth, Marine, and Environmental Sciences. Clarendon Press, Oxford.
- Le Nindre, Y.M., Manivit, J., Vaslet, D., 1987. Histoire géologique de la bordure occidentale de la plate-forme arabe du Paléozoïque inférieur au Jurassique supérieur. University Pierre et Marie Curie, Paris.
- Le Nindre, Y.M., Manivit, J., Vaslet, D., 1990. Stratigraphie séquentielle du Jurassique et du crétacé en Arabie Saoudite. Bulletin, Société Géologique de France, Paris 6, 1025–1035.
- Leinfelder, R.R., Schlagintweit, F., Werner, W., Ebl, O., Nose, M., Schmid, D.U., Hughes, G.W., 2005. Significance of stromatoporoids in Jurassic reefs and carbonate platforms – concepts and implications. *Facies* 51, 288–326.
- Li, Z.-X., Powell, C.M., 2001. An outline of the palaeogeographic evolution of the Australasian region since the beginning of the Neoproterozoic. *Earth-Science Reviews* 53, 237–277.
- Lindsay, R.F., Cantrell, D.L., Hughes, G.W., Keith, T.H., Mueller, H.W., Russell, S.D., Anonymous, 2006. Ghawar Arab-D: widespread porosity in shoaling-upward carbonate cycles, Saudi Arabia. Abstracts: Annual Meeting – American Association of Petroleum Geologists, 15, p. 64.
- McCuire, M.D., Koepnick, R.B., Markello, J.R., Stockton, M.L., Waite, L.E., Kompanik, G.S., Al-Shammery, M.J., Al-Amoudi, M.O., 1993. Importance of Sequence Stratigraphic

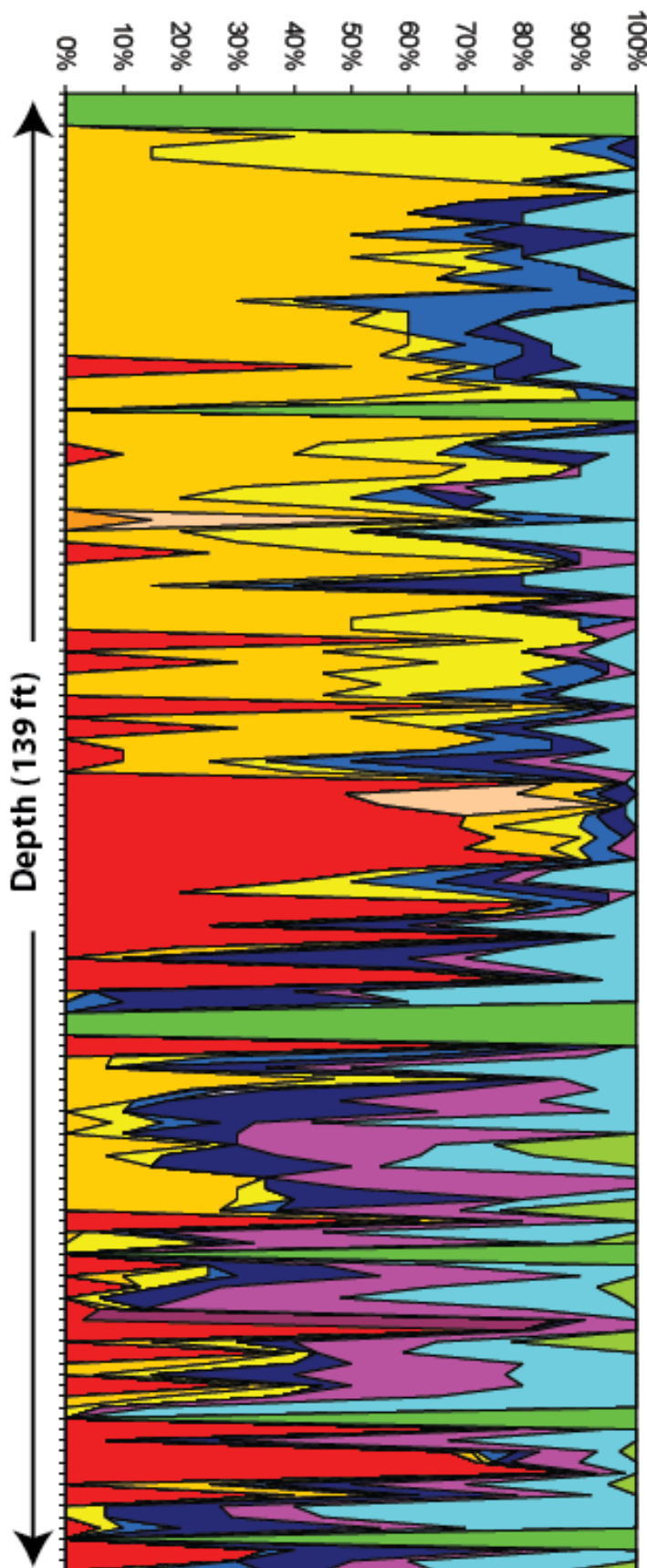
- Concept in Development of Reservoir Architecture in Upper Jurassic Grainstones, Hadiya and Hanifa Reservoirs, Saudi Arabia. L489–L499.
- Mey, J.L., 2008. The Uranium Series Diagenesis and the Morphology of Drowned Barbadian Paleo-reefs: 3312925. Thesis City University of New York, United States — New York.
- Meyer, F., 2000. Carbonate sheet slump from the Jubaila Formation, Saudi Arabia; slope implications. *GeoArabia* (Manama) 5, 144–145.
- Meyer, F.O., Price, R.C., 1993. A new Arab-D depositional model, Ghawar Field, Saudi Arabia. Middle East Oil Show, Bahrain.
- Meyer, F.O., Price, R.C., Al-Ghamdi, I.A., Al-Goba, I.M., Al-Raimi, S.M., Cole, J.C., 1996. Sequential stratigraphy of outcropping strata equivalent to Arab-D Reservoir, Wadi Nisah, Saudi Arabia. *GeoArabia* (Manama) 1, 435–456.
- Mitchell, J.C., Lehmann, P.J., Cantrell, D.L., Al-Jallal, I.A., Al-Thagafy, M.A.R., Lomando, A.J., Harris, P.M., 1988. Lithofacies, diagenesis and depositional sequence. Arab-D Member, Ghawar Field, Saudi Arabia. SEPM Core Workshop, vol. 12 459–514.
- Mitchum Jr., R.M., Van Wagoner, J.C., 1991. High-frequency sequences and their stacking patterns: sequence-stratigraphic evidence of high-frequency eustatic cycles. *Sedimentary Geology* 70 (2–4), 131–160. [http://dx.doi.org/10.1016/0037-0738\(91\)90139-5](http://dx.doi.org/10.1016/0037-0738(91)90139-5).
- Montaggioni, 2005. History of Indo-Pacific coral reef systems since the last glaciation: development patterns and controlling factors. *Earth-Science Reviews* 71 (1–2), 1–75.
- Moore, J.M., Allen, P., Wells, M.K., Howland, A.F., 1979. Tectonics of the Najd transcurent fault system, Saudi Arabia. *Journal of the Geological Society of London* 136, 441–454 (Part 4).
- Moore, G.T., Sloan, L.C., Hayashida, D.N., Umrigar, N.P., 1992. Paleoclimate of the Kimmeridgian/Tithonian (Late Jurassic) world: II. Sensitivity tests comparing three different paleotopographic settings. *Palaeogeography, Palaeoclimatology, Palaeoecology* 95, 229–252.
- Mouawad, J., (2010, March 19). China's growth shifts the geopolitics of oil. *The New York Times*.
- Murris, R.J., 1980. Middle East: stratigraphic evolution and oil habitat. *AAPG Bulletin* 64, 597–618.
- Pollastro, R.M., Karshbaum, A.S., Viger, R.J., 1999. Map showing geology, oil and gas fields, and geologic provinces of the Arabian Peninsula. Open-File Report — U.S. Geological Survey, p. 1 (disc).
- Powers, R.W., Ramirez, L.R., Redmond, C.D., Elberg, E.L., 1966. Sedimentary geology of Saudi Arabia: geology of the Arabian Peninsula. United States Geological Survey Professional Paper 150, 150.
- Sarg, J.F., 1988. Carbonate sequence stratigraphy. In sea level changes: an integrated approach. Society of Economic Paleontologists and Mineralogists Special Publication 42, 155–181.
- Sellwood, B.W., Valdes, P.J., Price, G.D., 2000. Geological evaluation of multiple general circulation model simulations of Late Jurassic palaeoclimate. *Palaeogeography, Palaeoclimatology, Palaeoecology* 156, 147–160.
- Sharland, P.R., Archer, R., Casey, D.M., Davies, R.B., Hall, S.H., Heward, A.P., Horbury, A.D., Simmons, M.D., 2001. Arabian plate sequence stratigraphy. *GeoArabia Special Publication No. 2*.
- Simmons, M.D., 1994. Micropalaeontological biozonation of the Khamah Group (Early Cretaceous), Central Oman Mountains. In: Simmons, M.D. (Ed.), *Micropalaeontology and Hydrocarbon Exploration in the Middle East*. Chapman and Hall, London, UK.
- Stampfli, G.M., Mosar, J., Favre, P., Pilleveit, A., Vannay, J.C., 2001. Permo-Mesozoic evolution of the western Tethys realm: the Neo-Tethys East Mediterranean basin connection: Peri-Tethys Memoir 6. Peri-Tethyan Rift/Wrench Basins and Passive Margins. *Museum national d'Histoire naturelle, Paris* (France) (51–108 pp.).
- Steineke, M., Bramkamp, R.A., Sander, N.J., 1958. Stratigraphic relations of Arabian Jurassic oil. In: Weeks, L.G. (Ed.), *Habitat of oil: A symposium*. American Association of Petroleum Geologists, Tulsa, OK, pp. 1294–1329.
- Stephens, N., Puls, D., Albotrous, H., Al-Ansi, H., Fahad, A.T., 2009. Sequence stratigraphic framework of the Arab Formation reservoirs, Dukhan Field, Qatar. Paper Presented at the International Petroleum Technology Conference.
- Stoeser, D., Camp, V.E., 1985. Pan-African microplate accretion of the Arabian Shield. *Geological Society of America Bulletin* 96, 817.
- Tinker, S.W., 1998. Shelf-to-basin facies distributions and sequence stratigraphy of a steep-rimmed carbonate margin: Capitan depositional system, McKittrick Canyon, New Mexico and Texas. *Journal of Sedimentary Research* 68 (6), 1146–1174. <http://dx.doi.org/10.1306/d4268923-2b26-11d7-8648000102c1865d>.
- Toland, C., 1994. Late Mesozoic Stromatoporoids: Their Use as Stratigraphic Tools and Palaeoenvironmental Indicators. Chapman and Hall, London, UK.
- Van Wagoner, J.C., Mitchum, R.M., Campion, K.M., Rahmanian, V.D., 1990. Siliciclastic sequence stratigraphy in well logs, cores, and outcrops: concepts for high-resolution correlation of time and facies. *Methods in Exploration Series*, vol. 7 55.
- Walker, R.G., 1985. Comparison of shelf environments and deep basin turbidite systems. *SEPM Short Course*, 13, pp. 465–502.
- Wender, L.E., Bryant, J.W., Dickens, M.F., Neville, A.S., Al-Moqbel, A.M., 1998. Pre-Khuff (Permian) hydrocarbon geology of the Ghawar area, eastern Saudi Arabia. *GeoArabia* (Manama) 3, 167–168.
- Wilson, A.O., 1985. Depositional and diagenetic facies in the Jurassic Arab-C and -D reservoirs, Qatif Field, Saudi Arabia. *Carbonate Petroleum Reservoirs*. Springer-Verlag, New York, NY 319–340.
- Wood, R.A., 1999. Reef Evolution. Oxford University Press, Oxford, UK.
- Ziegler, M.A., 2001. Late Permian to Holocene paleofacies evolution of the Arabian Plate and its hydrocarbon occurrences. *GeoArabia* (Manama) 6, 445–504.

Appendix F: Sample of semi-quantitative petrography data from Arab-D reservoir, Khurais Field

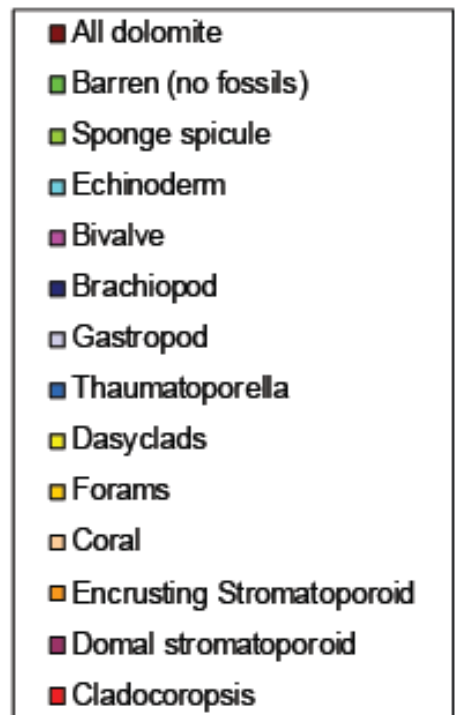


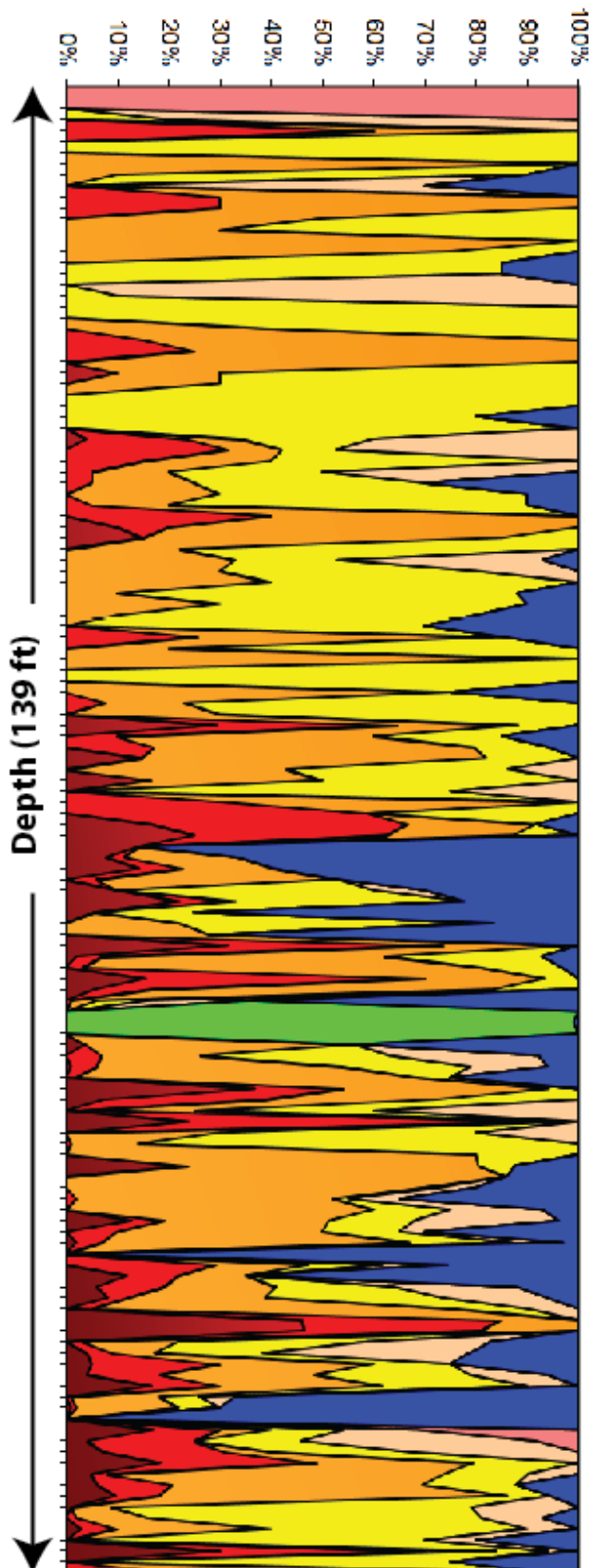
Thin-sections semi-quantitative petrography (1 thin section per foot) of abiotic constituents determined by comparison to visual percentage estimation charts (Terry and Chilingar, 1955) and plotted against thin-sections' depths. From cored well Khurais-HU.

- Dolomite (only if all dolomite)
- Mud
- Pellets
- saddle dolomite
- Blocky calcie cement
- Isopchous rim cement
- Oncolites (>2mm)
- Intraclasts (>2mm)
- Skeletal
- Peloids
- Coated grains
- Ooids

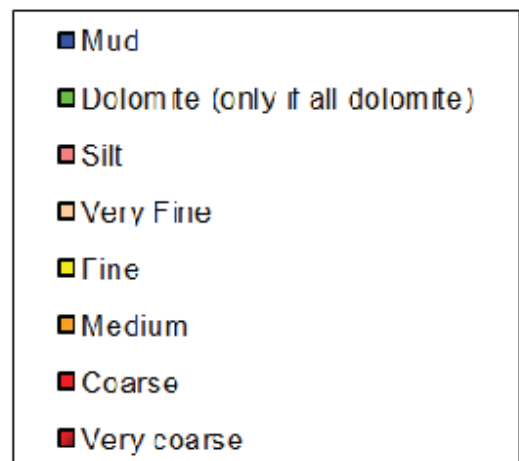


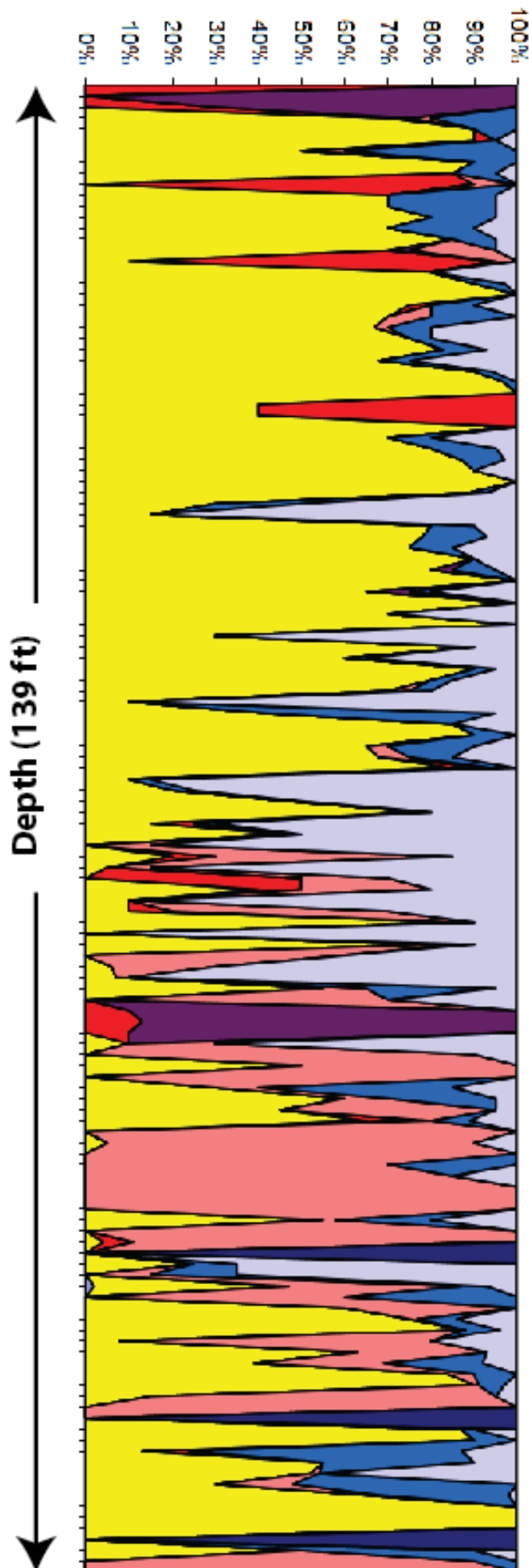
Thin-sections semi-quantitative petrography (1 thin section per foot) of biotic constituents determined by comparison to visual percentage estimation charts (Terry and Chilingar, 1955) and plotted against thin-sections' depths. From cored well Khurais-HU.



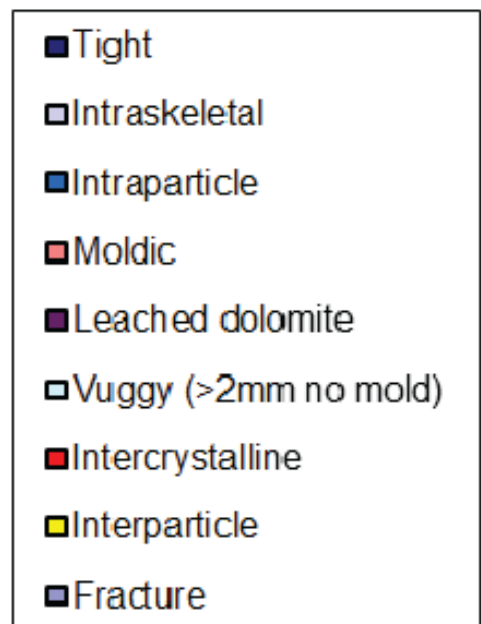


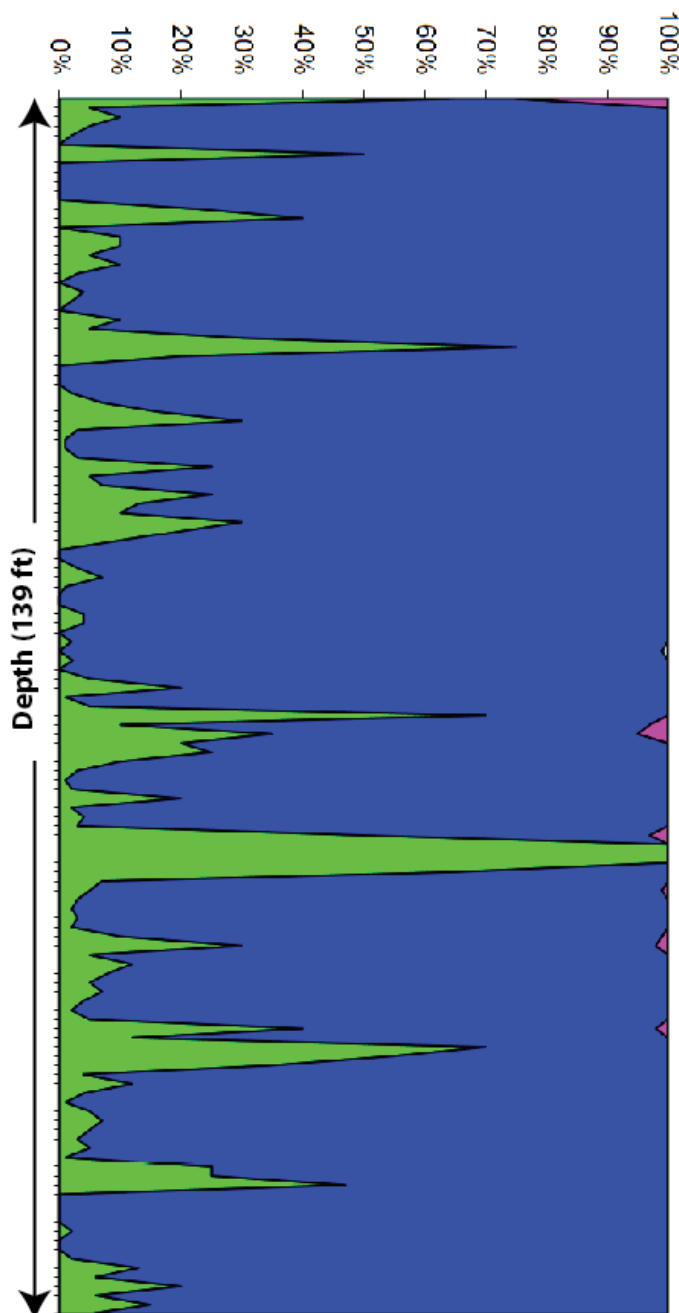
Thin-sections semi-quantitative petrography (1 thin section per foot) of grain sizes determined by comparison to visual percentage estimation charts (Terry and Chilingar, 1955) and plotted against thin-sections' depths. From cored well Khurais-HU.



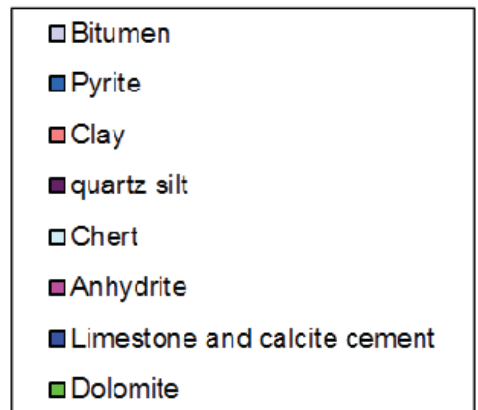


Thin-sections semi-quantitative petrography (1 thin section per foot) of porosity types determined by comparison to visual percentage estimation charts (Terry and Chilingar, 1955) and plotted against thin-sections' depths. From cored well Khurais-HU.

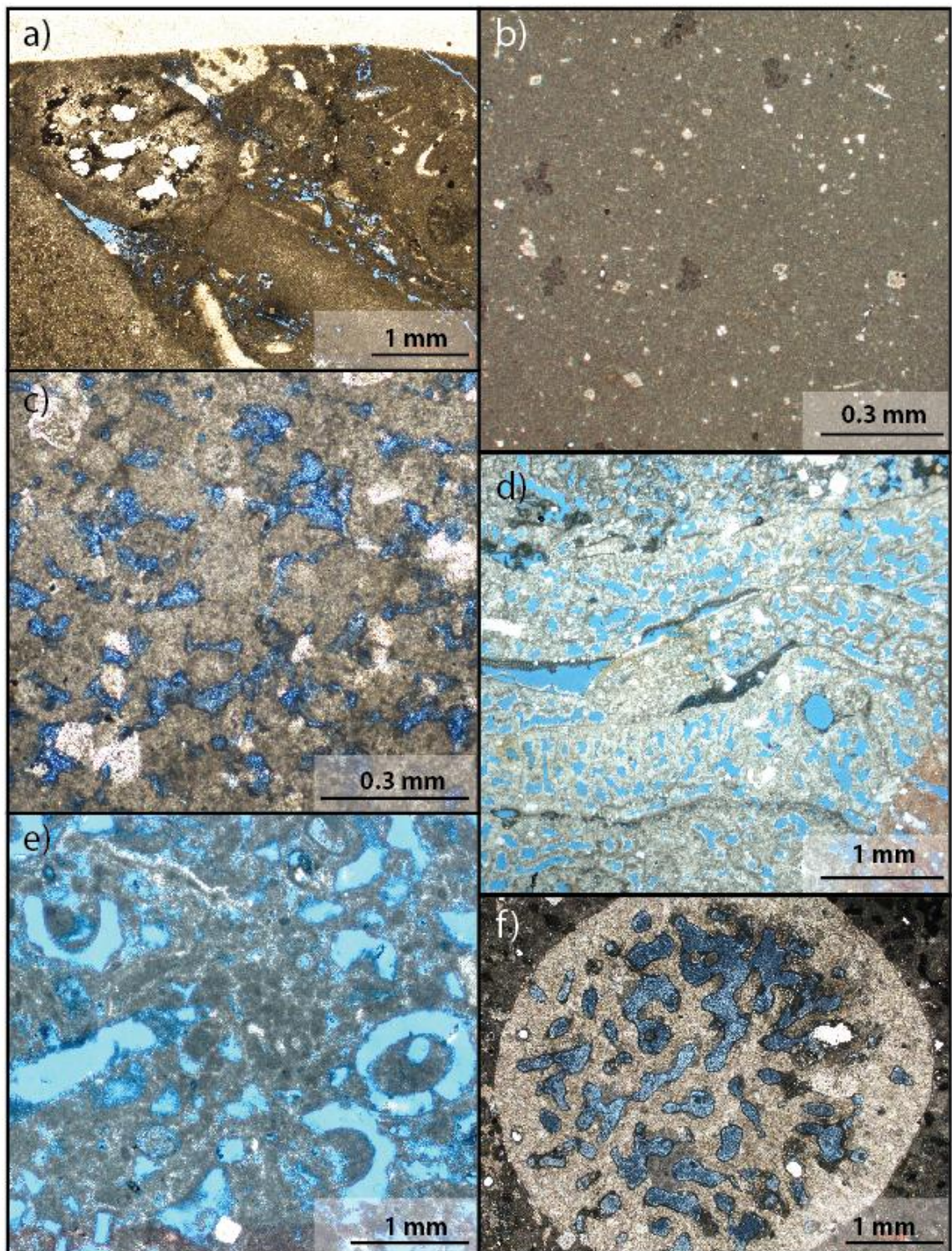




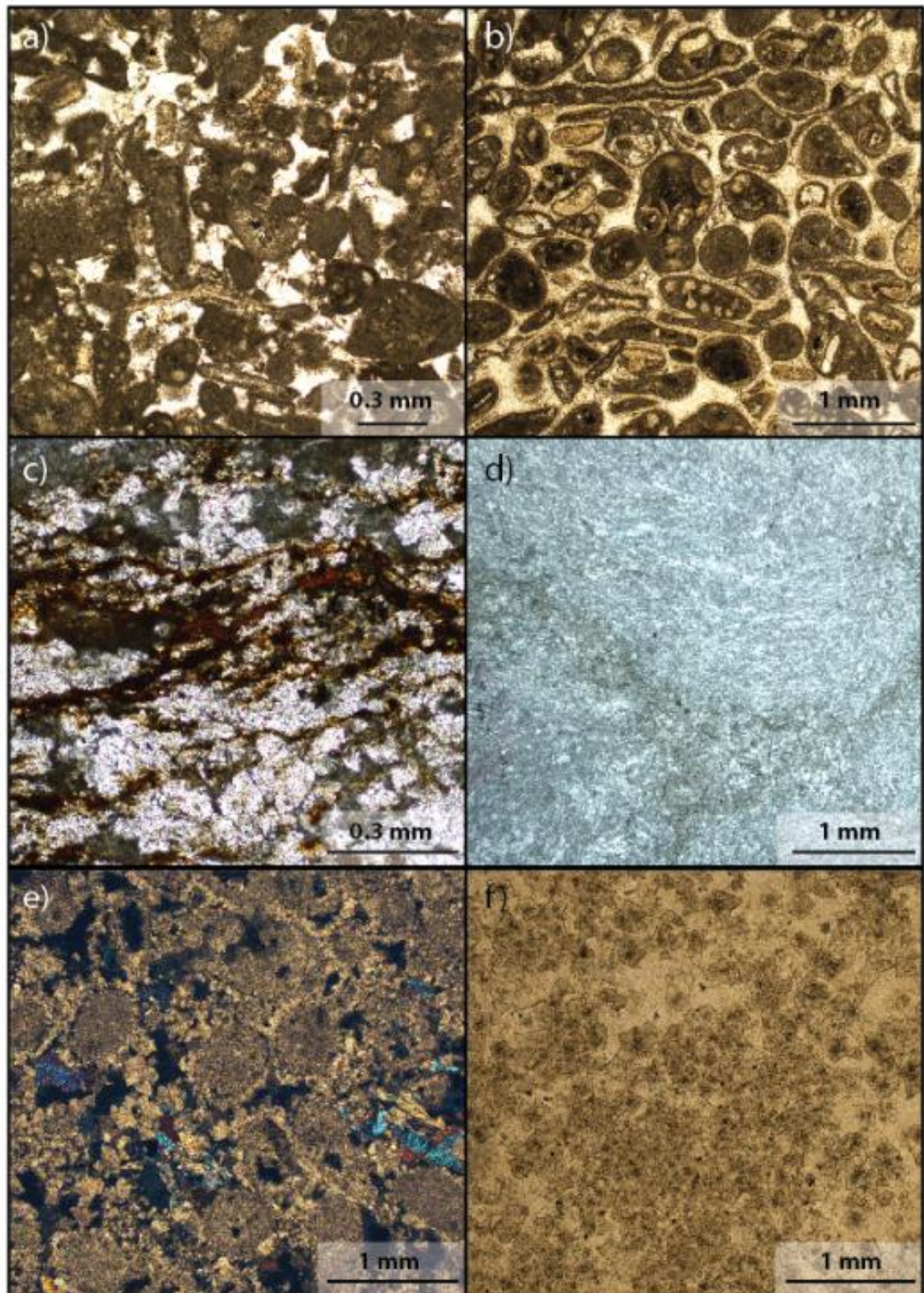
Thin-sections semi-quantitative petrography (1 thin section per foot) of mineral composition determined by comparison to visual percentage estimation charts (Terry and Chilingar, 1955) and plotted against thin-sections' depths. From cored well Khurais-HU.



Appendix G: Representative Photomicrographs of the Arab-D reservoir lithofacies from Khurais Field

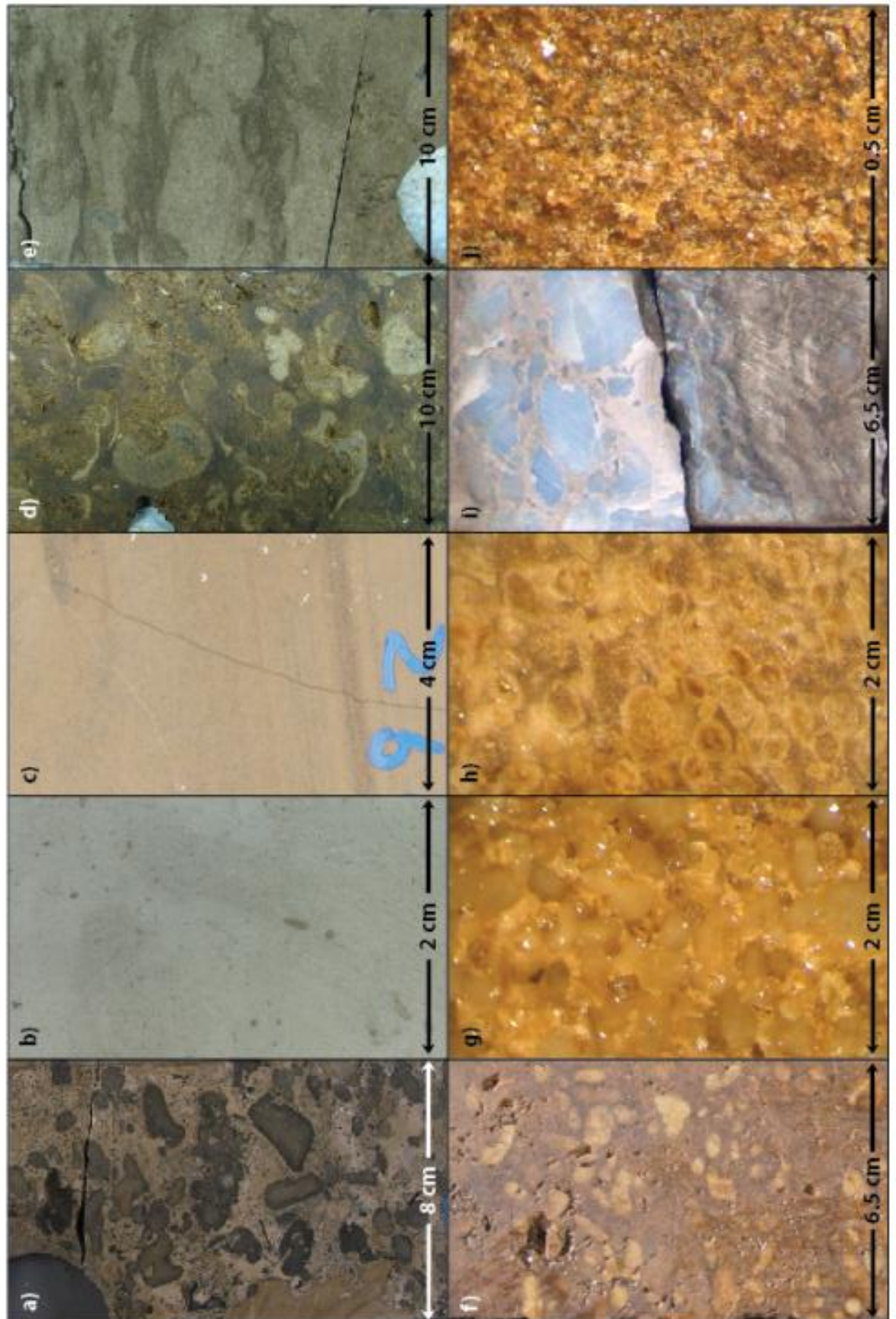


Representative photomicrographs of the Arab-D reservoir lithofacies, in an ascending order: a) intraclastic lithofacies, plug # 173 from Khurais-HKKF; b) lime mud lithofacies, plug #152 from Khurais-HKKF; c) pelletal lithofacies, plug #155 from Khurais HKKF; d) stromatoporoid lithofacies, plug #99 from Khurais-HF; e) dasycladacean algae lithofacies, plug #3 from Khurais-HF; f) *Cladocoropsis* lithofacies, plug # 24 from Khurais HKKF.



Representative photomicrographs of the Arab-D reservoir lithofacies, in an ascending order: a) peloidal lithofacies, plug # 6 from Khurais-HKKF; b) oolitic lithofacies, plug #5 from Khurais-HKKF; c) cryptomicrobial lithofacies, plug #3 from Khurais HKKF; d) anhydrite lithofacies, plug #1 from Khurais-HU; e) dolomitized oolitic grainstone from the post Arab-D stringer, plug #1 from Khurais-HKKF; f) dolomite lithofacies, plug # 11 from Khurais HKKF.

Appendix H: Representative Core Photographs of the Arab-D reservoir lithofacies from Khurais Field



Representative core photographs of the Arab-D reservoir lithofacies, in ascending order: a) intraclastic; b) lime mud, c) pelletal; d) stromatoporoid; e) dasycladacean algae; f) *Cladocoropsis*; g) peloidal; h) oolitic; i) cryptomicrobial and anhydrite; j) dolomite.

Appendix I: Foldout of Enclosure 3.1

Enclosure 3.1: Characterisation of Arab-D reservoir core, Aramco KHKH Khurais, Khurais Field.

Appendix J: Foldouts of Enclosures 5.1 and 5.2

Enclosure 5.1: A west–east cross-section of the Arab-D reservoir correlating its outcrop south of Riyadh to its subsurface in Ghawar Field.

Enclosure 5.2: A north-south cross-section of the Arab-D reservoir correlating it in the subsurface from the Safaniya area to south Khurais Field.